IAEA TECDOC SERIES

IAEA-TECDOC-1912

Challenges for Coolants in Fast Neutron Spectrum Systems

IAEA
International Atomic Energy Agency

IAEA SAFETY STANDARDS AND RELATED PUBLICATIONS

IAEA SAFETY STANDARDS

Under the terms of Article III of its Statute, the IAEA is authorized to establish or adopt standards of safety for protection of health and minimization of danger to life and property, and to provide for the application of these standards.

The publications by means of which the IAEA establishes standards are issued in the **IAEA Safety Standards Series**. This series covers nuclear safety, radiation safety, transport safety and waste safety. The publication categories in the series are **Safety Fundamentals**, **Safety Requirements** and **Safety Guides**.

Information on the IAEA's safety standards programme is available on the IAEA Internet site

http://www-ns.iaea.org/standards/

The site provides the texts in English of published and draft safety standards. The texts of safety standards issued in Arabic, Chinese, French, Russian and Spanish, the IAEA Safety Glossary and a status report for safety standards under development are also available. For further information, please contact the IAEA at: Vienna International Centre, PO Box 100, 1400 Vienna, Austria.

All users of IAEA safety standards are invited to inform the IAEA of experience in their use (e.g. as a basis for national regulations, for safety reviews and for training courses) for the purpose of ensuring that they continue to meet users' needs. Information may be provided via the IAEA Internet site or by post, as above, or by email to Official.Mail@iaea.org.

RELATED PUBLICATIONS

The IAEA provides for the application of the standards and, under the terms of Articles III and VIII.C of its Statute, makes available and fosters the exchange of information relating to peaceful nuclear activities and serves as an intermediary among its Member States for this purpose.

Reports on safety in nuclear activities are issued as **Safety Reports**, which provide practical examples and detailed methods that can be used in support of the safety standards.

Other safety related IAEA publications are issued as **Emergency Preparedness and Response** publications, **Radiological Assessment Reports**, the International Nuclear Safety Group's **INSAG Reports**, **Technical Reports** and **TECDOCs**. The IAEA also issues reports on radiological accidents, training manuals and practical manuals, and other special safety related publications.

Security related publications are issued in the **IAEA Nuclear Security Series**.

The **IAEA Nuclear Energy Series** comprises informational publications to encourage and assist research on, and the development and practical application of, nuclear energy for peaceful purposes. It includes reports and guides on the status of and advances in technology, and on experience, good practices and practical examples in the areas of nuclear power, the nuclear fuel cycle, radioactive waste management and decommissioning.

CHALLENGES FOR COOLANTS IN FAST NEUTRON SPECTRUM SYSTEMS

The following States are Members of the International Atomic Energy Agency:

AFGHANISTAN
ALBANIA
ALGERIA
ANGOLA
ANTIGUA AND BARBUDA
ARGENTINA
ARMENIA
AUSTRALIA
AUSTRIA
AZERBAIJAN
BAHAMAS
BAHRAIN
BANGLADESH
BARBADOS
BELARUS
BELGIUM
BELIZE
BENIN
BOLIVIA, PLURINATIONAL STATE OF
BOSNIA AND HERZEGOVINA
BOTSWANA
BRAZIL
BRUNEI DARUSSALAM
BULGARIA
BURKINA FASO
BURUNDI
CAMBODIA
CAMEROON
CANADA
CENTRAL AFRICAN REPUBLIC
CHAD
CHILE
CHINA
COLOMBIA
CONGO
COSTA RICA
CÔTE D'IVOIRE
CROATIA
CUBA
CYPRUS
CZECH REPUBLIC
DEMOCRATIC REPUBLIC OF THE CONGO
DENMARK
DJIBOUTI
DOMINICA
DOMINICAN REPUBLIC
ECUADOR
EGYPT
EL SALVADOR
ERITREA
ESTONIA
ESWATINI
ETHIOPIA
FIJI
FINLAND
FRANCE
GABON
GEORGIA
GERMANY
GHANA
GREECE
GRENADA
GUATEMALA
GUYANA
HAITI
HOLY SEE
HONDURAS
HUNGARY
ICELAND
INDIA
INDONESIA
IRAN, ISLAMIC REPUBLIC OF
IRAQ
IRELAND
ISRAEL
ITALY
JAMAICA
JAPAN
JORDAN
KAZAKHSTAN
KENYA
KOREA, REPUBLIC OF
KUWAIT
KYRGYZSTAN
LAO PEOPLE'S DEMOCRATIC REPUBLIC
LATVIA
LEBANON
LESOTHO
LIBERIA
LIBYA
LIECHTENSTEIN
LITHUANIA
LUXEMBOURG
MADAGASCAR
MALAWI
MALAYSIA
MALI
MALTA
MARSHALL ISLANDS
MAURITANIA
MAURITIUS
MEXICO
MONACO
MONGOLIA
MONTENEGRO
MOROCCO
MOZAMBIQUE
MYANMAR
NAMIBIA
NEPAL
NETHERLANDS
NEW ZEALAND
NICARAGUA
NIGER
NIGERIA
NORTH MACEDONIA
NORWAY
OMAN
PAKISTAN
PALAU
PANAMA
PAPUA NEW GUINEA
PARAGUAY
PERU
PHILIPPINES
POLAND
PORTUGAL
QATAR
REPUBLIC OF MOLDOVA
ROMANIA
RUSSIAN FEDERATION
RWANDA
SAINT LUCIA
SAINT VINCENT AND THE GRENADINES
SAN MARINO
SAUDI ARABIA
SENEGAL
SERBIA
SEYCHELLES
SIERRA LEONE
SINGAPORE
SLOVAKIA
SLOVENIA
SOUTH AFRICA
SPAIN
SRI LANKA
SUDAN
SWEDEN
SWITZERLAND
SYRIAN ARAB REPUBLIC
TAJIKISTAN
THAILAND
TOGO
TRINIDAD AND TOBAGO
TUNISIA
TURKEY
TURKMENISTAN
UGANDA
UKRAINE
UNITED ARAB EMIRATES
UNITED KINGDOM OF GREAT BRITAIN AND NORTHERN IRELAND
UNITED REPUBLIC OF TANZANIA
UNITED STATES OF AMERICA
URUGUAY
UZBEKISTAN
VANUATU
VENEZUELA, BOLIVARIAN REPUBLIC OF
VIET NAM
YEMEN
ZAMBIA
ZIMBABWE

The Agency's Statute was approved on 23 October 1956 by the Conference on the Statute of the IAEA held at United Nations Headquarters, New York; it entered into force on 29 July 1957. The Headquarters of the Agency are situated in Vienna. Its principal objective is "to accelerate and enlarge the contribution of atomic energy to peace, health and prosperity throughout the world''.

IAEA-TECDOC-1912

CHALLENGES FOR COOLANTS IN FAST NEUTRON SPECTRUM SYSTEMS

INTERNATIONAL ATOMIC ENERGY AGENCY
VIENNA, 2020

COPYRIGHT NOTICE

For further information on this publication, please contact:

Physics Section
International Atomic Energy Agency
Vienna International Centre
PO Box 100
1400 Vienna, Austria
Email: Official.Mail@iaea.org

Printed by the IAEA in Austria
May 2020

IAEA Library Cataloguing in Publication Data

Names: International Atomic Energy Agency.
Title: Challenges for coolants in fast neutron spectrum systems / International Atomic Energy Agency.
Description: Vienna : International Atomic Energy Agency, 2020. | Series: IAEA TECDOC series, ISSN 1011–4289 ; no. 1912 | Includes bibliographical references.
Identifiers: IAEAL 20-01316 | ISBN 978–92–0–107820–9 (paperback : alk. paper) |
ISBN 978–92–0–107920–6 (pdf)
Subjects: LCSH: Nuclear reactors — Cooling. | Fast reactors. | Accelerator-driven systems. | Fusion reactors. | Fast neutrons.

FOREWORD

Nuclear applications with a fast neutron spectrum (i.e. fusion, fission and accelerators) pose many challenges to coolants, such as material damage by irradiation, modifications by nuclear reactions and interaction of the coolant and the structure material. This is because of the neutrons' high power densities and/or heat loads.

To evaluate the different coolant options for nuclear applications with a fast neutron spectra, this publication compiles models, simulations, methods, benchmarked procedures/approaches and experiences as well as best practices from the fusion, fission and accelerator/spallation communities to create a knowledge base on coolants, identify the gaps and formulate near term R&D activities to overcome them.

This publication is the outcome of two IAEA sponsored meetings: the First IAEA Workshop on Challenges for Coolants in Fast Neutron Spectrum Systems: Chemistry and Materials, held 5–7 July 2017 in Vienna, and a consultancy meeting on the topic held 2–4 July 2018 in Vienna. These meetings brought together representatives from the fusion, fission and accelerator/spallation communities to compile the current state of knowledge and to address research needs identified in experiments and in operation in the area of coolant behaviour in fast neutron spectra.

The IAEA gratefully acknowledges the contributions of numerous experts to the preparation of this publication, in particular R. Stieglitz (Germany), L. El-Guebaly (United States of America), Y. Dai (Switzerland) and J. Konys (Germany). The IAEA officers responsible for this publication were M. Barbarino and S.M. Gonzalez de Vicente of the Division of Physical and Chemical Sciences.

EDITORIAL NOTE

This publication has been prepared from the original material as submitted by the contributors and has not been edited by the editorial staff of the IAEA. The views expressed remain the responsibility of the contributors and do not necessarily represent the views of the IAEA or its Member States.

Neither the IAEA nor its Member States assume any responsibility for consequences which may arise from the use of this publication. This publication does not address questions of responsibility, legal or otherwise, for acts or omissions on the part of any person.

The use of particular designations of countries or territories does not imply any judgement by the publisher, the IAEA, as to the legal status of such countries or territories, of their authorities and institutions or of the delimitation of their boundaries.

The mention of names of specific companies or products (whether or not indicated as registered) does not imply any intention to infringe proprietary rights, nor should it be construed as an endorsement or recommendation on the part of the IAEA.

The authors are responsible for having obtained the necessary permission for the IAEA to reproduce, translate or use material from sources already protected by copyrights.

The IAEA has no responsibility for the persistence or accuracy of URLs for external or third party Internet web sites referred to in this publication and does not guarantee that any content on such web sites is, or will remain, accurate or appropriate.

CONTENTS

SUMMARY

Fast neutrons interact with coolants and coolant confining structures and components, causing also synergetic effects which cause challenges to the design and licensing of different nuclear systems. To elaborate similarities, but also differences in view of different fast neutron applications, this publication is structured around the following topics:

— Impact of coolant choice on design and performance of fast neutron systems;
— Coolant characteristics under irradiation;
— Cooling confining structures;
— Interfaces;
— Safety and operational aspects.

In general, substantial progress has been achieved in the individual topics mentioned above, mainly through enhanced computing and simulation capabilities, which have provided a deeper insight not only in fundamental physics, but also on the engineering level by tackling multi-physics and multi-scale problems. A detailed subject-related analysis of the central progress, including the gaps and research activities derived from them, can be found at the beginning of each section.

The major objectives of this publication are to:

— Facilitate exchange of information, practises and procedures across different science communities as well as gathering available information and expertise about coolants and their challenges.
— Foster cross fertilization of operational know-how, challenges and R&D gaps with respect to coolants and coolant confining structures from a fundamental to a system level, not aiming at a comparing coolants nor design concepts.
— Discuss the progress related to coolant aspects across the different science and technology communities (fusion, fission and spallation sources and accelerator applications).

In summary, this publication shows that across all sections one major hurdle is the lack of experimental data and facilities providing neutrons in the relevant spectral range, either with respect to single effect studies but also to study synergistic effects, allowing for technology qualification to establish procedures or to conduct the safety assessment to demonstrate their validity for compliance with established regulatory or design criteria. Thus, mainly code-to-code comparisons or single effect studies are conducted for validation and verification or upscaling. To what degree such an approach is realistic or encompasses the reality is not well understood. Hence, future R&D programs will need to address the following points indispensable to operate fast neutron spectrum nuclear systems:

— Complement experimental and/or numerical verification and validation processes;
— Formulate integral experimental studies to develop predictive multi-physics and multi-scale tools, allowing for enveloping technology and procedure development.

1. INTRODUCTION

1.1. BACKGROUND

Fast neutrons cover a wide range of nuclear applications from pure science-based missions, such as are realized in accelerators, to energy production, for example in fission or fusion reactors. The major challenges posed to coolants are associated with the neutrons high power densities and/or heat loads, which can cause:

— Material damage by irradiation (e.g. defects, transmutation products);
— Coolant modifications by nuclear reactions (e.g. radiolysis, activation, spallation products, etc.);
— Mutual interaction of the coolant with the structure material (e.g. irradiation assisted stress corrosion cracking).

Hence, there is a large set of coolants compatible for fast neutron applications according to their nuclear properties (mainly their cross-sections), such as:

a) Gas (helium, CO_2);
b) Water;
c) Liquid metals (sodium, lithium, lead and its alloys, Hg);
d) Molten salts (e.g. halogen containing binary and ternary salt mixtures).

1.2. OBJECTIVE

The objective of this publication is to evaluate the different coolant options considered for nuclear applications with fast neutron spectrum (i.e. fusion, fission and accelerators), as well as to compile the current state of knowledge and to address research needs identified in experiments and in operation. In this study, systems cooled by light and heavy liquid metals, molten salts, as well as gas and water choices are analysed and discussed.

In brief, this TECDOC aims to document present state of know-how in the area of fusion, fission and accelerators applications, and the major progress made in the past years in terms of observations, methods, experimental findings and operational experience. Moreover, this publication targets formulating knowledge gaps and thereby addressing near term R&D efforts required to overcome them.

1.3. SCOPE

The scope of this publication is to compile a general state of the art methods used in practice and a basic description of the physics and modelling tools and design approaches adopted, rather than to provide a detailed description of each of models or design aspects. For the latter, the devoted reader may use the references cited in the individual contributions.

This publication avoids comparing different coolants in the context of an individual application and does not analyse or judge the credibility of technical designs, and it is not intended to be a comprehensive textbook.

1.4. STRUCTURE

The TECDOC is divided into five standalone but interrelated sections consisting of individual contributions in the following topics:

— Impact of coolant choice on design and performance of fast neutron systems;
— Coolant characteristics under irradiation:
  (i) Radiation chemistry radiolysis;

(ii) Activation, species production and computational models;
(iii) Coolant processing and handling procedures.

— Cooling confining structures:
(i) Coolant-confining structures: tackling impact of operating conditions and compatibility;
(ii) Irradiation damage;
(iii) He and H embrittlement of structure.

— Interface:
(i) Interfaces covering erosion, corrosion and diffusion;
(ii) Barriers / Coatings for structure.

— Safety and operational aspects:
(i) Safety and operational aspects dealing with inventory control and accountancy;
(ii) Qualification procedures;
(iii) Enveloping system analysis.

At the beginning of each section, a summary on the most relevant results and achievements is provided. Any identified knowledge gaps are addressed therein, from which near term R&D activities are derived. Additionally, some examples of currently ongoing R&D projects are provided.

2. SUMMARY OF IMPACT OF COOLANT CHOICE ON DESIGN AND PERFORMANCE OF FAST NEUTRON SYSTEMS

R. Stieglitz (Karlsruhe Institute of Technology, Germany)

This section describes the reasons for the challenges in fast neutron spectrum systems, which are set out in more detail in the subsequent article.

Regardless of the fast neutron production mode (accelerator, fission or fusion), the neutrons interact with matter characterized by nuclear reactions (e.g. absorption, scattering, transmutation dependent on their cross-section) associated with radiation and heat release. In contrast to thermal neutrons the energy of fast neutrons exceeds the binding energy of most molecules and causes thereby an interaction with the coolant itself, expressed either in form of radical formation, tritium or helium generation or transmutation. Except for helium, this leads to an immediate direct activation of the coolant, which requires a specific control during the operation of the nuclear facility, since the coolant usually remains for the lifetime of a component or a reactor within the control area. This long residence time allows also for permeation of impurities through the interfaces, leading also to coolant activation.

Not only the coolant is affected by neutron irradiation but also the coolant confining structure materials. Because of nuclear reactions, the structural material properties change depending on irradiation intensity, neutron energy and irradiation time and temperature. Prominent examples of these changes are for example hardening, embrittlement but also the incorporation of transmutation products such as helium or hydrogen gas production. It must be emphasized that each fast neutron application exhibits a specific damage characteristics, e.g. He/dpa ratio, for which in many cases the experimental database is, due to the absence of prototypical irradiation sources, rather sparse. The present state of the knowledge and potential options for material optimization to comply with technical requirements are sketched, and these are further elaborated in Section 4 of this publication.

Both material damage and coolant modification are interlinked through the interface of coolant and structural material not just through state variables (e.g. pressure and temperature), prescribing the mechanical integrity but also the (electro-)chemical interaction. The coolant choice is an essential aspect since it is circulated not only through the core environment, but it also poses the interface to the non-nuclear environment (e.g. spallation target). Independently if a power production plant or an accelerator application is considered, the coolant undergoes, during the loop circulation, a permanent change of its thermodynamic state, which is associated with transport processes causing possible effects like erosion, corrosion, dissolution attack, limiting the durability and thereby the lifetime. Some of these are subsequently briefly sketched and further elaborated in Section 5 of this publication.

In summary, requirements arising from both neutron energy spectrum and the power density together with the coolant choice decisively determine the basic design of the nuclear component/reactor, as shown by the examples for fast reactors and accelerator applications. Also, the safety architecture in case of a loss of the coolant confining structure by whatsoever event/malfunction is strongly coolant dependent. This refers not only to the potential radioactive release and the release paths of the coolant but also to the chemical and potential energies, as well as the thermal energies stored within the coolant. All these aspects require fundamentally different coolant dependent measures, which are expressed by different plant architectures, and are described by the examples of fast reactor and accelerator application.

OVERVIEW ON IMPACT OF COOLANT CHOICE ON DESIGN AND PERFORMANCE OF FAST NEUTRON SYSTEMS

R. STIEGLITZ, A. MÖSLANG
Karlsruhe Institute of Technology,
Eggenstein, Germany

S.M. GONZALEZ DE VICENTE
International Atomic Energy Agency,
Vienna

Abstract

This overview article describes at first the specific aspects of different coolants potentially to be utilized in fast neutron spectrum applications. Based on those the general environment and the boundary conditions for nuclear systems are elaborated. Next, the impact of the coolant choice on various fast reactor designs is illustrated by some examples. Then, phenomena as coolant poisoning, corrosion are explained to translate them into the material challenges to be mastered for fast spectrum nuclear applications. Herein, mainly the different effects are outlined which need to consider in the design of coolant confining structures with and without irradiation and typical temperature ranges and material damage rates for the different applications are provided. Since coolant choice and material selection define the operational regime of a nuclear system both enter synergistic into the safety performance, for which some technical design examples are shown for the decay heat removal systems of fast reactors. A second example shows how the coolant choice impacts the set-up of a technical design for an accelerator application.

1. INTRODUCTION

Assigning fast neutron spectrum systems according to their typical neutron energy, the triad reads to fission, fusion, and finally spallation covering an energy spectrum from some tenth of keV up to the GeV-range. Irrespective of the mission of these systems — ranging from fundamental science to energy production — their realization faces increasingly stricter safety regulations, associated procedures and waste disposal quality/quantities. Simultaneously they have to meet their scientific and/or economic target in terms of higher particle yields, better fuel utilization or higher thermal efficiency. Simplified arguments yield to more compact technical designs, which in turn translate into power loads/densities often beyond the limit of presently licensed and operated nuclear installations.

The key role in this context plays the choice of the structural material/coolant combination, which not only prescribes the operational temperature by its thermo-physical properties. It moreover defines kinetic parameters like flow velocity, volumetric and/or surface power. Once this decision has been taken it impacts not only the primary heat removal systems/components but also propagates through the entire technical set-up determining their dimensioning, efficiency, recirculating power and moreover the safety demonstration, as well as the normal/abnormal state. Intrinsically, the coolant choice also defines largely the material selection of the coolant confining structures and consequently the operable temperature window. Depending on neutron fluence and energy and mode of operation, the structural material has to withstand a combination of irradiation damage and creep-fatigue load over the entire component lifetime. Finally, metallic or ceramic thin coatings may be needed to reduce significantly the susceptibilities to corrosion/erosion and to so called stress corrosion cracking.

In that context the overview sketches the impacts of the coolant and material choice on the technical design and the safety performance by two examples addressing the lower end of the neutron energy spectrum covered by fast fission reactors and the upper end provided by accelerator applications.

Four different lines of Fast Reactors (FR) are being developed [1] scoping coolants as pressurized helium, i.e. Gas-Cooled Fast Reactors (GFR), Molten Salts Fast Reactors (MSFR), Sodium-Cooled Fast Reactors (SFR) and heavy liquid metals, i.e. Lead-Cooled Fast Reactors (LFR) [1]. Despite their quite similar neutronics performance and the related comparable yield of transmutation products like tritium or helium, the coolant choice almost fully dictates their design mainly due to safety aspects. Albeit GFRs based on helium as coolant allow a large freedom in material selection, the postulate to demonstrate even in case of a Loss of Coolant Accident (LOCA) in a depressurized state limits considerably the power density to economically unattractive values and, moreover, poses large burdens on the containment. Adversely, salts or liquid metals coolants allow for an almost depressurized operation, but, due to their high-power density a closed safety demonstration pose significant challenge. Especially qualified structural materials with high thermal conductivity capable to withstand > 100 dpa with superior

corrosion/erosion resistance are in the designers wish lists. However, each of the liquid coolants necessitates its own coolant chemistry, structural material class and barrier development to attain a mature licensable design.

On the high energy end of the neutron energy spectrum (>600 MeV) novel spallation source projects like ESS are aiming high particle yields associated with a high helium and displacement damage production in the coolant confining structures. Simple surface to volume considerations for spallation material and coolant set-ups have shown that for conventional coolants as water safety limits are by far exceeded. This led in turn to the development of homogeneous liquid metal targets or heterogeneous design options as solid gas cooled targets. For liquid metal cooled types, the corrosion of the coolant confining structures is in the focus of the R&D, while for gas cooled options the material erosion due to high fluid velocities, the transport of erosion products, the permeation of tritium through structures formulates R&D challenges. That is, for both pathways at the limits of structural and functional material and dictates the entire system architecture. Finally, the confinement of the flea circus of radioactive spallation products and the safe cooling formulates for both lines a pre-requisite.

2. NEUTRONIC AND THERMAL PROPERTIES OF COOLANTS EMBEDDED IN FAST SPECTRUM SYSTEMS

Modern nuclear systems are aiming at high volumetric efficiencies either if this related to the electric power production in nuclear reactors or by the generation of secondary particles utilized for fundamental physics experiments or diagnostic purposes. These higher volumetric efficiencies are achieved by several means such as enriched fuel compositions, dedicated target materials, reduced leakage and adequate structural material choice as well as higher incident particle fluxes. Especially the latter immediately translates into higher volumetric power densities to be generated either in the nuclear fuel or in the target material, which in turn have to be removed by the coolant in such a manner that the confining structures do not exceed material sustainable limits both at nominal operation or in accidental transients.

Therefore, at best the coolant shall not interact with the neutrons/protons meaning that it needs to be as almost transparent to the in order not to deteriorate the functionality and performance of the reactor or accelerator application.

Naturally, in any continuum elementary particles interact with matter housed in the elementary cell leading to collisions and thereby to a slowing down. Applying momentum and energy conservation one can compute the energy of the scattered particles in the simplest approach to $\alpha = [(A-1)/(A+1)]^2$, where A is the atomic number of the nucleus. Technically, it is more useful to work with logarithmic quantities and therefore one defines the logarithmic energy decrement per collision ξ which describes the mean logarithmic reduction of neutron energy per collision, which also depends only on the atomic mass A of the nucleus. It is given by:

$$\xi = 1+\frac{(A-1)^2}{2A}\ln\frac{A-1}{A+1} \quad (1)$$

Aside from the elastic scattering there is quite large set of nuclear reactions occurring in a technical system such as inelastic scattering, absorption, α-, β-emissions, fission, leakage etc., necessitating complex deterministic or Monte-Carlo based computations to evaluate for the technical configurations consisting of coolant, structural material, and fuel the energy released therein, the reaction products produced (nuclide vector) and the activation (excited states) at any power level and time of operation.

Considering, at first the moderation aspect of the Slowing Down Power being comprised of the product (ξ-Σ_s), where Σ_s denotes the macroscopic scattering cross-section, the data of several structure and coolant elements/molecules are listed in Table 1.

From the table it becomes clear that lead provides hardly any moderation, while light nuclei favour moderation, with water or hydrogen being most efficient. But also, intermediate weight nuclei like oxygen, silicon and nitrogen contribute in the sense of moderation shifting an initially fast spectrum, comprised of incident neutrons/protons having more than 2 MeV, to lower energies and thereby creating a low energy tail. The next striking aspect is that Zr or, better, zirconium provides less slowing down power than iron, which serves zirconium being a favourable fuel cladding material housing the nuclear fuel in Light Water Reactors (LWR). Classical liquid metal FR concepts, however, use Fe-based cladding materials or SiC structures as in gas cooled FRs. Why is this feasible? This is devoted to the smaller nuclear cross-sections of iron at higher incident neutron energies , expressed by substantially declining cross-sections for rising neutron energies.

TABLE 1. MACROSCOPIC SLOWING DOWN POWER OF SELECTED ELEMENTS RELEVANT IN NUCLEAR ENGINEERING

	$(\xi\text{-}\Sigma_s)$ [cm^{-1}]
Zr	0.00046
Fe	0.0023
Na	0.0027
Pb	0.00013
H_2O	1.36
He	0.00024
C	0.06
O	0.0058

A deeper look into the spectral cross-section distribution of potential coolants (Fig. 1) shows immediately that the cross-section of hydrogen remains even at high incident energies at a large level providing too much moderation. Lead or lead alloys exhibit still higher values than sodium, however, they do not have strong broad band resonances as sodium and moreover provide good reflection properties. With respect to this neutronic aspect, helium is an ideal coolant.

The prior task of a coolant is to effectively remove the heat. This sets a number of pre-requisites. Ideally the thermal heat conductivity of the fluid needs to be high in order to reduce the temperature gradients across the coolant confining structures, which minimizes the thermal stresses.

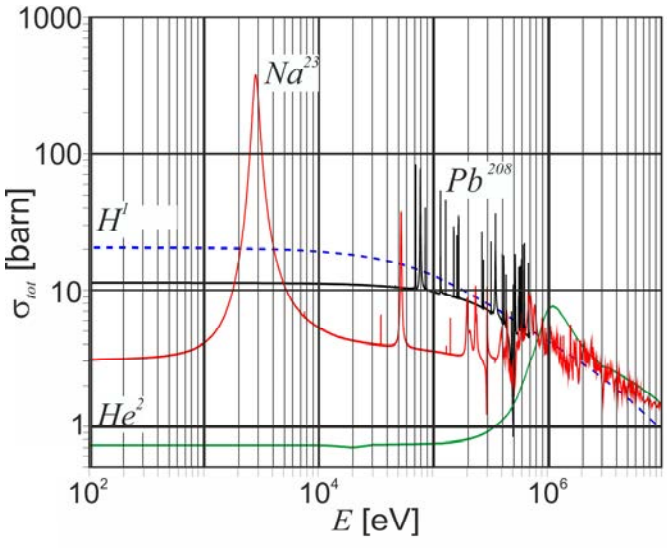

FIG. 1. Total cross-section $\boldsymbol{\sigma_{tot}}$ of fast spectrum coolants as function of neutron energy in eV [2].

This favours liquid metals, which exhibit an excellent heat conductivity compared to water, salts or gaseous fluids and do not require a pressurization of the coolant confining structures. On the other hand, the volumetric heat capacity given as the product of the specific density and the heat capacity describes the thermal inertia of system. High values are in this context desired to provide large grace times for operation. Virtually, here pressurized water exhibits an outstanding high thermal inertia and is therefore often termed as optimal coolant solution for high power density applications. But, it has to be stated that the thermal inertia is only one part of the truth, the other is spanned by the operational temperature threshold for power extraction and the capability to transfer the heat from the interface to the bulk. Here, water exhibits a strong limitation given by its boiling curve in the region of 330°C. Here, pressurized gases pose practically no limitations except for the coolant confining structures. Liquid metals as well as salts also serve a quite large operational temperature range before the onset of boiling, however some

constraints are provided by the high melting points e.g. for lead or the salts requiring auxiliary heating systems. Finally, also some words need to be spent to the thermal expansion, which influences the capability to remove the natural convection heat. Here a high value in combination with a high heat capacity of the liquid would be pleasant for a good safety performance. Liquid salts provide for both quantities a reasonably high value compared to liquid metals and especially the gaseous coolants. Table 2 provides an overview of the thermo-physical properties of different fluids considered for fast neutron spectrum applications.

Aside from the thermal properties also the kinematic properties are of relevance, since they describe technological effort to transport the coolant through the structures. Naturally incompressible fluids necessitate no compression work and thereby exhibits by several orders of magnitude lower pumping power. On the other hand, the dynamic viscosity μ, being the product of density and kinematic viscosity υ, describes the friction exerted on the structure for a given flow velocity. The friction is globally expressed by the pressure drop scaling proportional with the square of the mean flow velocity u in the circuit to be generated by a pump. But, friction also defines the shear stress τ acting on the coolant confining material, which is given by $\tau = \mu\,(\partial u/\partial y)$ with $(\partial u/\partial y)$ the wall normal velocity gradient. Both aspects have to be considered so that although gases have a small viscosity they require high flow velocities immediately translating to higher pressure drops and wall shear stresses favouring structural material erosion. Most favourable in that context are water and the light alkali metals while liquid salts show a considerable viscosity.

TABLE 2. THERMO-PHYSICAL PROPERTIES OF REACTOR COOLANTS AT WITHIN THEIR TYPICAL TEMPERATURE OPERATION DOMAIN

	H_2O [4] [300°C, 15MPa]	*Li [5]* [500°C]	*Na [6]* [500°C]	*Hg [7]* [20°C]	*Pb [8]* [500°C]	*$Pb^{45}Bi^{55}$* [8] [500°C]	*Salt [9]* *NaCl-KCl-$MgCl_2$* [600°C]	*He [10]* [500° C, 6MPa]	*CO_2* [11] [500°C 2MPa]
ρ [kg/m^3]	725	475	857	1353	10724	9660	1800	3.7	13.5
c_p [J/(kg·K)]	5475	4169	1262	140	145	145	1004	5190	1170
$(\rho \cdot c_p)$ [MJ / (m^3· K)]	3.97	1.98	1.081	1.89	1.555	1.401	1.807	0.19	0.158
λ [W/(mK)]	0.561	49.7	66.3	8.3	15	11	0.39	0.303	0.056
ν [(m^2/s)·10^{-7}]	1.2	7.16	2.6	1.1	1.5	1.1	0.138	0.9	0.25
T_{melt} [°C]	-0.4	180	98	-39	327	126	396	-	-58
$T_{boiling}$ [°C]	334	1317	883	356	1737	1533	2500	-	-78

Up to now, in the considerations, we have linked the neutronics as well as the thermal-hydraulics to both the coolant and its confining structural material housing the functional material. Those may be for example a nuclear fuel, a breeding material, or a spallation material. Also, this structural material is affected by the nuclei matter interaction expressed by nuclear reactions and dependent on the energy level of the nuclei, the operational temperature as well as the design of the component. These effects may lead to irradiation degradation including the formation of transmutation products, swelling, creep, loss of ductility and fracture toughness deterioration. Simultaneously, at the fluid structure interface, mass transport processes occur in both directions from the coolant to the structure and vice versa. Responsible for these transport processes are gradients of the temperature and concentration scalars. Dependent on the gradient sign either transmutation products generated in the coolant may be transferred into the structure or alloy constituents of the structure are dissolved in the coolant. All these effects are driven by thermo-electric forces and provoke irradiation enhanced corrosion, stress-corrosion cracking or embrittlement.

Hence, in the simplest form a nuclear system can be reduced to a sketch as depicted in Fig. 2 consisting of nuclear island, in which the functionality is obtained, where structure material houses the functional materials and coolant(s). Dependent on the application within the active part of the nuclear island in fast spectrum systems enormous neutron fluxes of 10^{15} (FR) and up to 10^{17} (high current accelerators) per cm^2 and per second appear with mean neutron energies from 2 MeV (FR) up to 5 GeV causing the above-mentioned interactions. These fluxes are one to several orders of magnitude larger than in pressurized light water reactors (PWR). It is obvious that this poses a significant technological challenge not only in terms of activation of the associated materials, but also with respect to the lifetime and structural integrity. The latter also impacts the safety demonstration ensuring the confinement of the activated materials for any anticipated internal and external event within a defined containment.

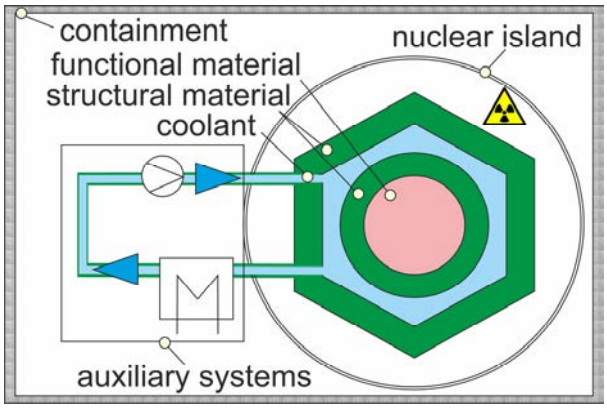

FIG. 2. Simplified sketch of a general nuclear system.

Limiting the discussion on the coolant choice to two classes of applications the FR and the accelerator applications, the coolant choice seems to be more or less straightforward from the pure nuclear physics point of view. However, once the coolant choice has been decided, it affects immediately the overall structure of the entire nuclear system architecture.

Irrespective of the type of application considered, any nuclear installation is determined by main three actors composed of customer, operator and overarching a societal contract, as depicted in Fig. 3. The boundary conditions for operation system are prescribed in form of regulations embedded mainly within an international framework, which is in the nuclear context spanned by the IAEA. The top priority to be respected is related to the safety in its various forms. While the operator accompanies the system from planning via built and operation to decommissioning the customer is only involved within the design life time, which may scope durations of 60 years for e.g. FRs.

In order to start and successfully complete a licensing procedure a credible knowledge on coolant and coolant confining structures formulates a pre-requisite, which is in the case of fast spectrum nuclear system is not based on a broad material, coolant and operational experiences depicted either in codes and standards or international reports. A wider deployment is mainly limited hindered by a rather sparse validated data base for structural and structure/coolant interaction phenomena especially for high damage rates and the large accumulated fluences. Hence, for these types of applications often coolant and material choices are conducted in a conservative approach by justified extrapolations wherever possible. Responsible for this are both a lack of experimental facilities but also challenging numerical and modelling access of these strongly interdependent phenomena, as e.g. life-time predictions of Helium/dp ratio. However, in terms of a licensing procedure a safe operation has to be demonstrated along the entire operational time and even for disposal. Here, it has to be mentioned that the licensing procedure spans from birth of the nuclear installation on paper to death in the repository, which is almost a generation contract. Therefore, this contribution tries to synthesize knowledge of coolant behaviour obtained by the three nuclear communities being involved in fast spectrum systems, but also aims to elucidate potential knowledge gaps or experimental/modelling efforts to overcome currently existing deficits with the focus on:

- Coolant characteristics under irradiation;
- Coolant confining structures;
- Interfaces;
- Safety and operational aspects.

Subsequently, examples for fast reactors as well as accelerator applications are sketched to depict the challenging complexity designers and operators need to focus for a successful project.

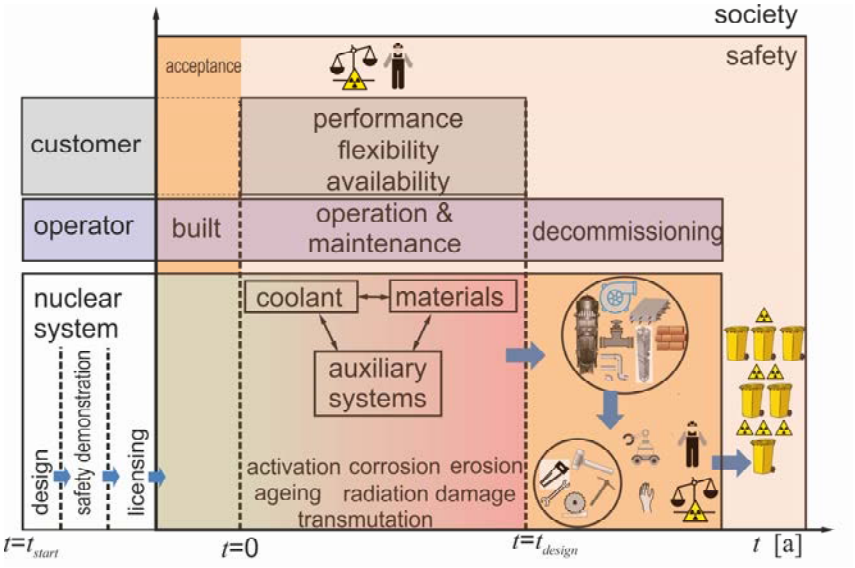

FIG. 3. Schematic interrelation of the stakeholders of a nuclear installation at different stages of its lifetime t, t=0 start-up of power operation, t_{design}=tentative design life time.

3. IMPACT OF COOLANT ON FAST REACTOR DESIGNS AND MATERIAL CHOICE

3.1. Fast reactor concepts and their boundary conditions

Within the generation IV international forum, a set of six nuclear systems have been selected for further development, for more details see Ref. [1]. Among those are the Gas-cooled Fast Reactor (GFR), Lead-cooled Fast Reactor (LFR), Sodium-cooled Fast Reactor (SFR), Molten Salt Reactor (MSR), Supercritical Water cooled Reactor (SCWR) and Very High Temperature Reactor (VHTR), for which only the latter two have a epi-thermal or a thermal spectrum. One of the reason for these types have been the following criteria:

— Sustainability:
  (i) Improved fuel utilization – capacity of breeding
  (ii) Minimization of waste – recycling (capability of Minor Actinide (MA) recycling with minor impact on core safety parameters, homogeneous core configuration or Minor Actinide Breeding Blanket (MABB) option).
— Economics:
  (i) Comparable to other energy sources (reactor & fuel cycle);
  (ii) Long cycle lengths – high loading factors (low reactivity swing, steady power shape);
  (iii) Improved lifetimes for fuel & absorbing elements (material performance, optimized fuel pin, absorbing materials with low efficiency);
  (iv) Compact core size.
— Safety:
  (i) High level of safety and operational reliability;
  (ii) Very low probability of core damage accidents (CDA);
  (iii) Practical elimination of need for off-site emergency response.
— Proliferation resistance:
  (i) Low susceptibility to diversion & physical protection against deliberate aggression.

Figs 4(a)-(d) show three fast reactor concepts compared to a pressurized light water reactor (PWR). Most striking is that for all fast reactor concepts the coolant fraction is substantially smaller than in a PWR, which is devoted to the maximum utilization of the fission neutrons and the nuclear cores are more compact.

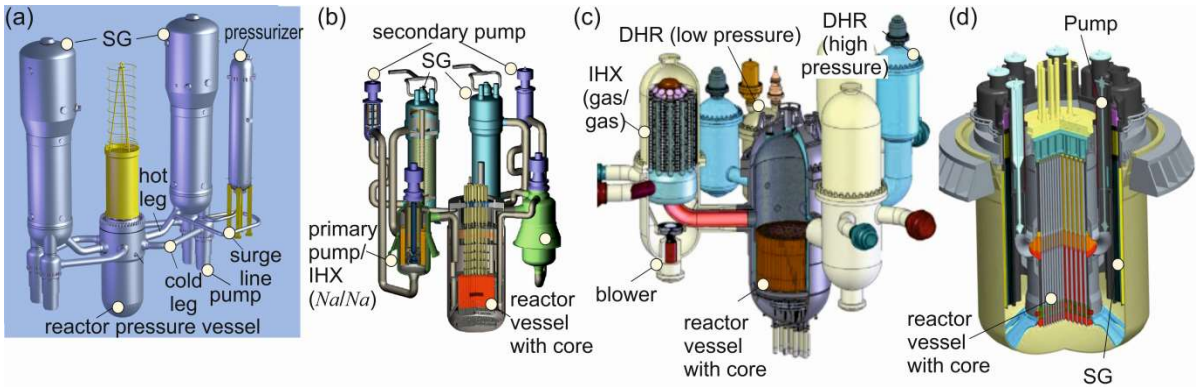

FIG. 4. (a) Sketch of a pressurized water reactor in AP1000 design [13]; (b) loop type sodium-cooled fast reactor (SFR) [13]; (c) gas-cooled fast reactor (GFR) [15]; (d) pool type lead cooled fast reactor (LFR) [16].

The coolant channels are smaller than in the PWR design. Additionally, the combination of increased fission/absorption and higher number of neutrons per fission yields more excess neutrons from ^{239}Pu and allows breeding or transmutation. The Generation-IV fast systems have similar characteristics and exhibit nuclear cross sections which are considerably smaller in than in the thermal spectrum. The ratio of the Pu-239 fission to U-238 capture cross-section in fast reactor is at least one order of magnitude lower and thus fast reactors requires a higher enrichment to achieve criticality. On the other hand the parasitic capture cross section of fission products and iron based structures are much smaller in a fast neutron spectrum than in a thermal one allowing iron based alloys as as cladding. But, due to the reduced absorption of all materials the mean neutron diffusion length is a factor 10 larger than in PWR, where they are in a range of 2 cm. This yields higher neutron leakage of 20% compared to 3.5% in a PWR and reflectors (top/bottom and circumferential) are important.

But, dependent on the coolant choice one can identify through Fig. 4 also substantial differences. While liquid metal systems provide both pool or loop type design options, for a gas cooled system a pool type configuration is impractical, because it would require enormous dimensions. Also, the volumetric power densities vary considerably from about 100 MW/m^3 for a GFR which is comparable to a pressure water reactor to about 250MW/m^3 for a SFR, while lead and molten salt fast reactors are somewhere in between. Aside from the volumetric core power density, which is mainly pre-scribed by the thermal and kinetic fluid properties also the heat transfer and power flow configurations are very different.

The choice of coolants exhibiting large boiling temperatures has not only been triggered by attaining high thermodynamic efficiencies attainable compared to LWR, but it is rather based on neutronic aspects. While coolant voiding leads in under-moderated LWRs to a negative reactivity insertion and hence to a rapid power decline, in FRs such an event can cause essential reactivity insertion that can result in prompt power excursions, unless dedicated design measures regarding neutronic reflectors, blankets and fuel arrangement are undertaken. Therefore, large coolant density gradients, as caused by coolant boling or steam ingress have to be avoided. Nevertheless, the higher outlet temperatures attainable with FR make it extremely attractive. from the thermodynamic cycle point of view.

Fig. 5 shows the typical data of the pressure and temperature scalars as well as fuel and cladding type of the above-mentioned FRs in comparison to a PWR. Also, here, except for the SFR, all FRs rely on an eight-shaped loop. In the SFR a sodium intermediate loop is interconnected for safety reasons even though in an advanced concept as for the French ASTRID project [17] a gas driven power conversion system is adopted. Except for this similarity even all reactor types differ for several reasons. The liquid metal operated reactors operate at nearly the same temperature levels, use similar fuel types and rely at a first glance on steel based cladding materials. For the latter, however, they deviate substantially.

While SFR can use stainless steel even accepting irradiation hardening of the steel and volumetric swelling of some percent, see e.g. displayed in Fig. 6, thanks to the excellent heat transfer properties of sodium and its low

chemical activity with respect to the steel alloy constituents, LFR concepts have to rely either on ferritic martensitic steel using dedicated barriers to prevent steel alloy dissolution within the coolant or even oxide dispersed steel (ODS) also benefitting from its higher thermal conductivity. From a design point of view, the structural materials and their behaviour limit the design of LFR and SFR reactors rather than the coolant properties.However, especially large efforts in the international R&D are undertaken to qualify metal based structural materials for generation-IV applications as the EU-FP7 Program GETMAT [19].

Relying in the design on ceramic as structural material extends considerably the thermal efficiencies and also minimizes the systems vulnerability to short time scale events as reactivity transients. On the other hand, only their integration into the design allows GFRs to build them within competitive dimensions in order to attain an economic design. The drawbacks of ceramics as structural material are attributed so several aspects such as point defect swelling and amorphization (<0.3 T_M, < 5 dpa) and radiation induced thermal conductivity decline (<0.4 T_M, < 5 dpa) at low dose rates and similar to metals volumetric swelling from void formation and irradiation creep at high dose rates (>5 dpa). Although a significant progress has been attained in the recent years by extensive irradiation campaigns and advanced modelling, applicable codes and standards allowing for a closed design in terms of a licensing procedure are still in their infancies.

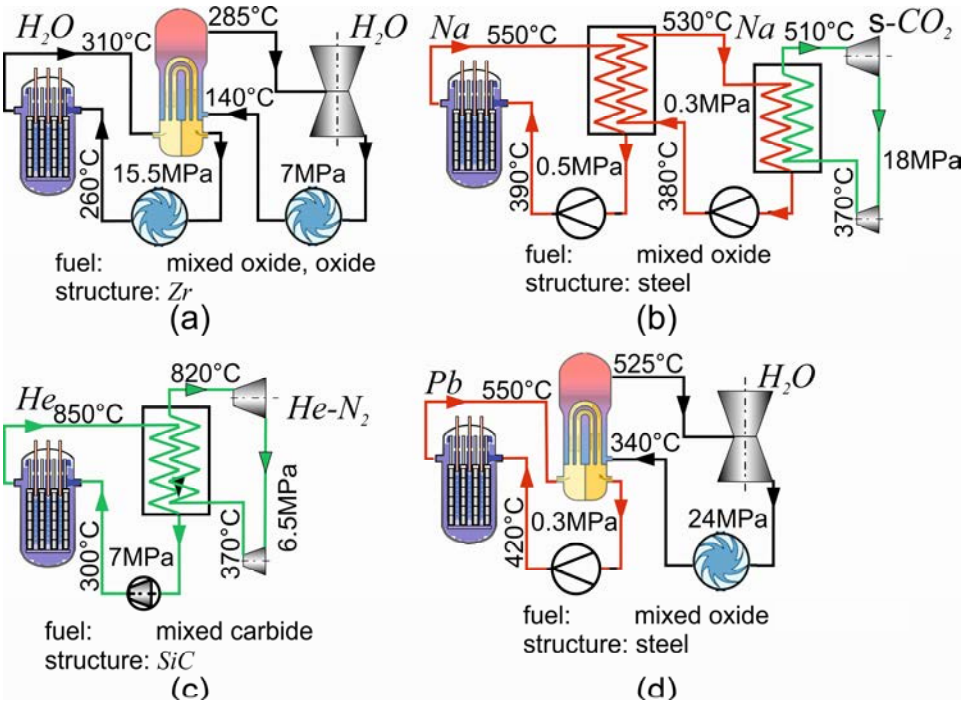

FIG. 5. Thermodynamic cycle concept of a PWR (a) compared to a SFR (b), GFR (c) and LFR (d) associated with typical pressure and temperature data, as well as fuels and coolant materials.

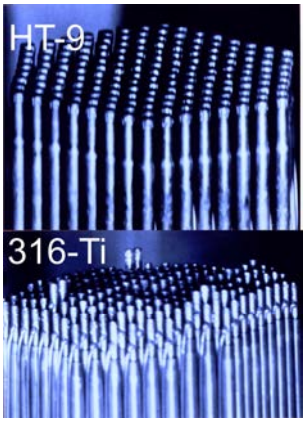

FIG. 6. Irradiation swelling of HT-9 and 316-Ti steel in a SFR at ~60 dpa [19].

3.2. Coolant poisoning/conditioning/handling

At first, aside from cladding also the coolant is subject of nuclear reactions with the neutrons generated by fission, which in turn leads to the formation of radioisotopes, as depicted in Table 3.

Hence, for SFR operation, without fuel rod failures, requires after shutting down about 50–60 years to use sodium again in any way or to return it in the environment without additional measures. Because of the 209Bi activity of bismuth, lead-bismuth coolant needs to be classified and treated as radioactive waste practically forever, while the situation for lead is not so unequivocal as for lead-bismuth, but its repeated utilization only in radioactive-dangerous technologies or final disposal are the most possible decisions for natural lead coolant. The activation of the coolant is only one of many questions. Since the coolant, in contrast to the structure, travels along the entire reactor system exposed to significant temperatures it is an optimal sink for transmutation and corrosion products being spread over the system. Fig.7 shows the H, He, D production cross-section in iron (54Fe) in correspondence of the neutron flux as a function of the neutron energy for different typical high flux reactors. Although a minor fraction of the fission neutrons has energies exceeding 2 MeV, gas is produced, which can diffuse through the structure into the coolant.

TABLE 3. NUCLEAR REACTIONS OF POTENTIAL COOLANTS IN SFR AND LFR REACTORS

isotope	formation channel	$T_{1/2}$ [a]	decay type	decay energy [MeV]
^{22}Na	$^{23}Na(n,2n)^{22}Na$	2.6	β	2.85
^{24}Na	$^{23}Na(n,\gamma)^{24}Na$	1.7×10^{-3}	β	5.51
^{205}Pb	$^{204}Pb(n,\gamma)^{205}Pb$	1.5×10^{-7}	β	0.05
^{208}Bi	$^{209}Bi(n,2n)^{208}Bi$	3.7×10^{5}	β	2.88
^{210}Bi	$^{209}Bi(n,\gamma)^{210}Bi$	3.6×10^{6}	α	4.96
^{210}Po	$^{210}Bi\ (\beta)\rightarrow{}^{210}Po$	0.38	α	5.41

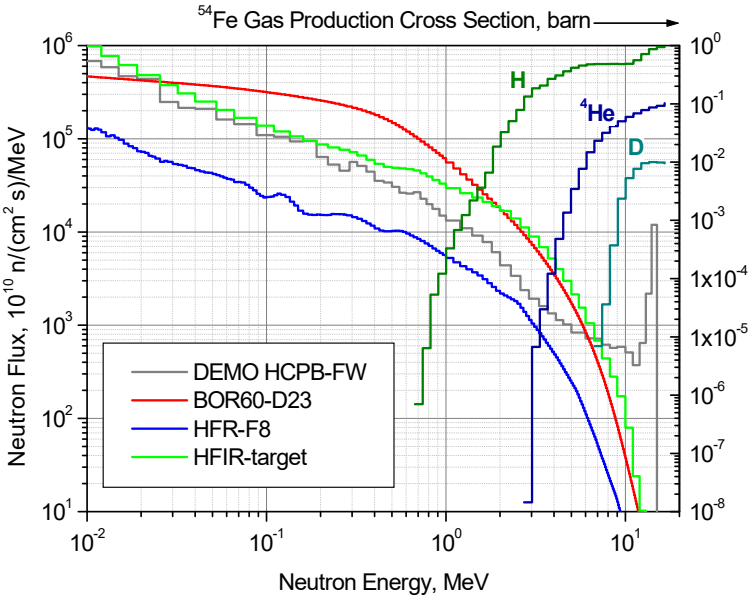

FIG. 7. Normalized neutron flux and gas production in iron as a function of the neutron energy for different test reactors compared to a DEMO fusion reactor [22].

More important in that context is, that transmutation products generated by the nuclear reactions in the fuel such as tritium can, in the pre-damaged structural material, readily diffuse through the cladding and enter the coolant. In SFRs this tritium is removed by the primary cold traps to a large fraction. But, due to the anticipated long operation time still a part diffuses through the intermediate heat exchanger into the secondary side and precipitates in the cold traps of the secondary side. Oxide coating on the atmosphere side of the stainless-steel piping provide an efficient barrier to rapid release through the reactor piping [18]. Another measure is to keep the tritium in the secondary side is to increase the hydrogen partial pressure on the ternary side to a level higher than on the secondary side to impose a negative gradient.

Except for the economical characteristics calling for an inexpensive and easily available coolant, the environmental aspects play a substantial role. Of course, a low toxicity and an environmentally harmless behaviour are mostly needed in conventional systems. The boundary conditions for fast reactors pose here more stringent constraints requring the leading order for a low chemical activity and a low physic-chemical potential ensuring long term integrity of the structural material. Sodium exhibits among the three FR coolants a high chemical activity with water and air, requiring dedicated measures for fire and explosion protection, as well as procedures for extraction and purification, which may be taken from [17] and the literature cited therein. But, a long term operational experience of more than 500 full power reactor years has been obtained. It also serves a low oxygen (Noden law) and hydrogen (Whittingham law) solubility close to its melting point, so that sodium can be purified by cooling, leading to crystallization of oxigen and hydrogen as Na_2O and NaH in a "cold trap".

In contrast to this, lead cooled reactor systems demand an active coolant control, in which the oxygen concentration must be high enough to create and stabilize protective oxide layers on steel and counteracting this oxygen concentration must not exceed values at which PbO is formed. This requires knowledge of the oxygen solubility for the control of oxygen concentration in the liquid metal. Unfortunately, this limits the operational threshold of the maximum allowable coolant temperature difference if steel based piping are considered or require dedicated coatings preventing steel corrosion, see Fig.8.

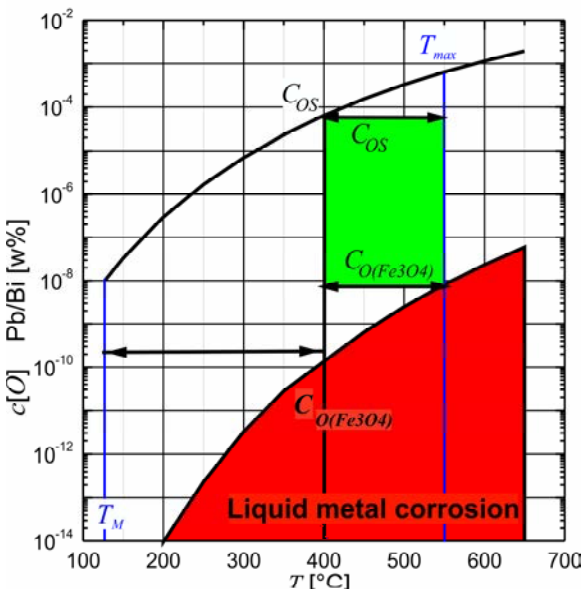

FIG. 8. Operational temperature threshold (green) of a LBE cooled reactor to prevent coolant oxidation and structure corrosion [23].

Also, despite being chemically inert, helium cooled reactors require a coolant control. Similar to SFR, tritium can migrate through the SiC structures and is naturally further transported to sites where the temperature is lowest, which is obviously the heat exchanger. Additionally, due to the substantially higher coolant velocities, the shear stresses τ acting on the surface are higher causing material erosion, which products are transported through the piping system demanding dedicated filter systems.

3.3. Coolant Confining structures

So far, the discussion focussed more or less on the coolant aspect. But, as already seen for the oxygen control aspect in lead only adequate paring of coolant and coolant confining structure ensures the performance of the nuclear system.

Similar to the traditional thermal power engineering plants, the structural materials need to satisfy criteria with respect to tensile strength, fracture toughness, high/low cycle fatigue behaviour, creep, ageing. FRs pose in terms of further constraints mainly associated with the irradiation of the structure materials. Mostly affected are the cladding materials, Fig. 9 compares different currently developed fast reactor concepts with typical generation II-III PWRs as well as fusion and accelerator applications. The graph illustrates that the demands in terms of material damage for all these are by a factor 2–3 larger in FRs and moreover, they are occurring at higher temperatures.

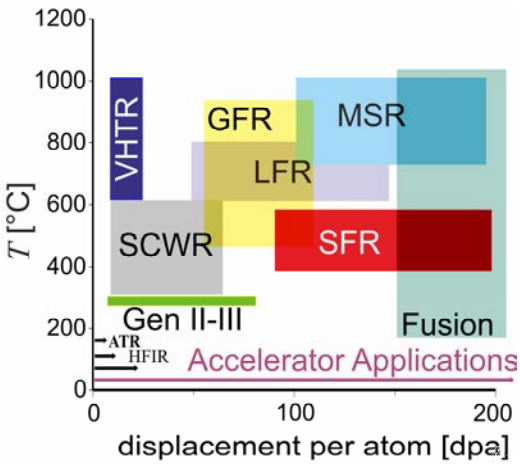

FIG. 9. Irradiation damage of several reactor types and accelerator applications at typical operation temperatures in comparison to test reactors.

Especially, the irradiation causes significant constraints to the material performance. Fundamentally, it causes radiation induced growth on an atomic scale and segregation of atoms in the lattice, which are diffusion controlled and thereby for each chemical element dependent on temperature. As consequence for most reactor materials, radiation induced growth is observed. The swelling of the material depends on several parameters:

— Temperature (peaks at intermediate temperature);
— Dose (increases with dose after "incubation" period);
— Dose rate (increases with decreasing dose rate for same dose);
— Stress state (hydrostatic tensile stress enhances swelling);
— Composition;
— Presence of helium (helps nucleate voids and bubbles).

The radiation damage affects the mechanical properties of the material by irradiation hardening and localized deformation, fracture behaviour and embrittlement, and irradiation creep either by creep, swelling interaction or creep growth interaction. Unfortunately, irradiation cannot be considered independently but correlates with corrosion and stress state of the material. At high neutron fluxes and mean particle energies there are five issues with respect to the radiation damage in metal based materials:

— Radiation hardening & embrittlement (<0.4 T_M, > 0.1 dpa);
— Phase instabilities from radiation-induced precipitation (0.3–0.6 T_M, > 10 dpa);
— High temperature He embrittlement (>0.5 T_M, > 10 dpa);
— Volumetric swelling from void formation (0.3–0.6 T_M, > 10 dpa);
— Irradiation creep (<0.45 T_M, > 10 dpa).

where T_M denotes the melting temperature and dpa is the displacement per atom. Independent of the irradiation aspect, corrosion of the structure poses a significant challenge due to the difference in the chemical potentials. While for helium this aspect is almost negligible, water and liquid metal affect the structure significantly by corrosion. Typical corrosion mechanisms are:

— Dissolution of alloying elements into the liquid metal (W << Fe, Cr < Ni);
— Mass transport of structural materials in liquid due to temperature gradients yielding a dissolution in hot areas and to precipitation in colder regions (heat exchanger, cooler, pumps etc.) causing fouling or even potentially blocking of pipes and channels;
— Exchange of non-metals (O, N, C) between structural materials and the liquid deteriorating protection layers and enhancing diffusion transport;
— Erosion of structural materials in dynamic (fast flowing) systems;
— Embrittlement at low temperatures (with and without irradiation).

While corrosion as such depends on the chemical potential, it can lead together with irradiation to enhanced oxidation or pick-up of hydrogen. Together with those effects the swelling of the material leads to an increased stress state, which can enhance so called irradiation assisted stress corrosion cracking (IASCC). But also, the neutron spectrum itself can substantially affect the mechanical properties. From Fig. 7 gas production rates normalized to displacement damage can be derived. Compared to typical fission reactor neutrons, fusion neutrons have ~ 20 times higher He production per dpa and spallation neutrons yield even ~70 times higher ones as shown in Fig. 10.

While instrumented tensile tests after neutron irradiation to ~ 16 dpa show above ~ 420°C no visible effect on fission reactor irradiation, at least up to about 415 appm helium in ferritic martensitic 9CrWTaV steels like EUROFER [42, 43], spallation neutrons produce at the same irradiation temperature substantial irradiation hardening and ductility loss [44], as Fig. 11. shows. The reason is attributed mainly to the production of a large variety of spallation isotopes - which are not created during fission or fusion neutron irradiation - rather than to the increased helium concentration. This example also shows that spallation neutron sources are not suitable to create e.g. a materials database for e.g. nuclear fusion and vice versa.

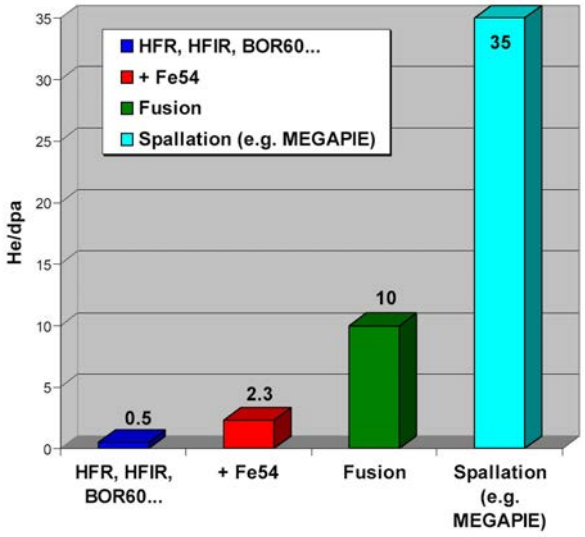

FIG. 10. Helium production rates in He-appm per dpa for different neutron spectra. Isotopic tailoring with Fe54 would increase in steels the He production in fission reactor as well [22].

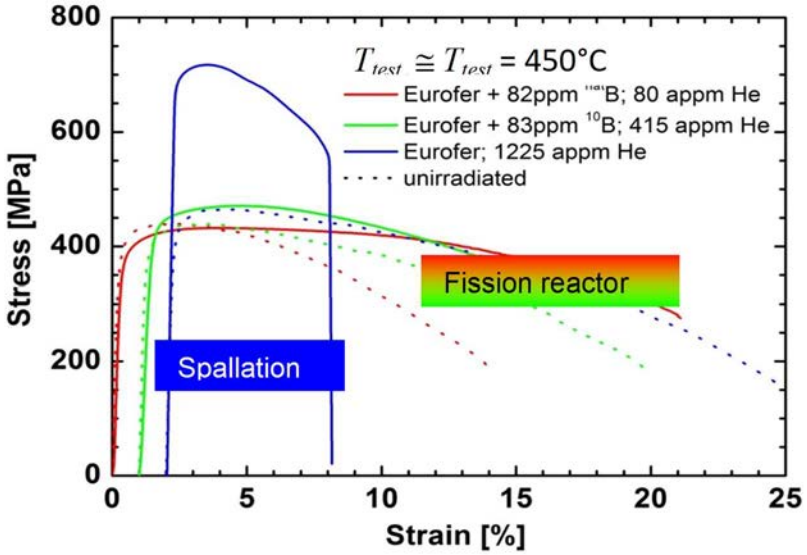

FIG. 11. Fission reactor neutrons show above ~ 420°C no visible effect of irradiation (~16 dpa) and Helium (below ~ 415 appm) on tensile properties while spallation neutron show substantial irradiation effects, compiled from Refs [42–44].

The operational-temperature range for ferritic martensitic steels is presently 300–550°C (105 hours creep rupture time at 100 MPa). Enhancement of the operational temperature to above 700°C could be realized with nanostructured oxide-dispersion-strengthened (ODS) steels where embrittlement is mitigated by dispersed Y-O or Y-Ti-O particles (e.g. Y_2O_3 or $Y_2Ti_2O_7$) that become effective sinks for trapping point defects and helium atoms, preventing their migration and coalescence. Such nanoscale ODS steels are not only very irradiation tolerant and aging resistant, they also show after neutron irradiation less irradiation hardening and unprecedented uniform elongation compared to their conventional counterparts (Figs 12 (a)–(b)). The exceptional irradiation tolerance of nanoscale steels is based on the tailored powder-metallurgical production routes and the related microstructures, providing new and neutron spectra-independent design solutions under exceptional harsh environments.

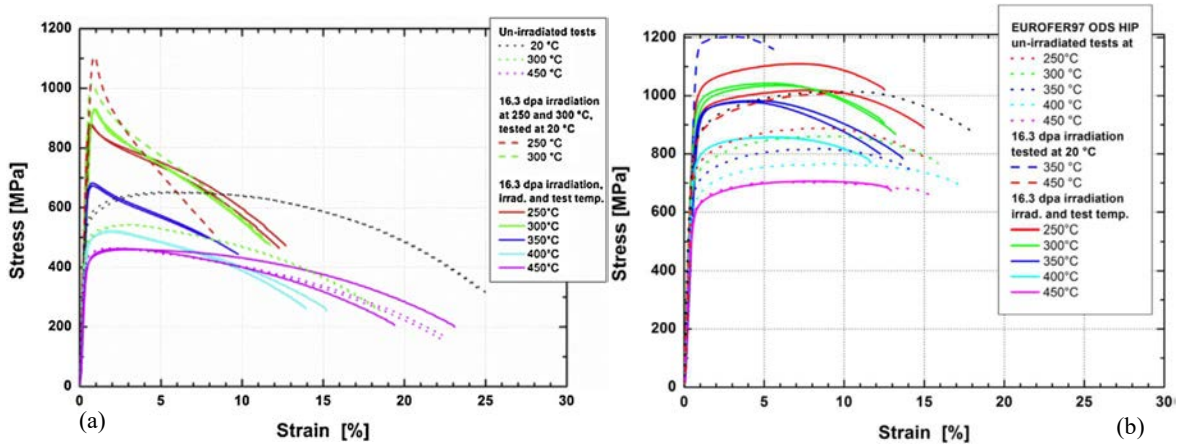

FIG. 12. (a) Stress-strain diagrams for EUROFER steel showing early strain localization for T_{irr}≤350°C (left); (b) stress-strain diagrams for EUROFER ODS steel showing superior uniform elongation after neutron irradiation in a wide temperature window (right) [42].

While the few examples of neutron irradiation effects on steels may have shown the potential and attractiveness of tailored materials science but also their sensitivity on neutron spectrum, it is also clear that huge resources are needed also in future to provide complete databases and their implementation in design codes and rules. This means in view of the limited resources in all parties that the major strategy element to close the knowledge gaps can likely only be the intensification of harmonized international crosscutting activities.

Major elements of such cross-cutting activities must include:

— Intensified coordination of common R&D activities by International Agencies (e.g. IAEA, IEA) and related formation of strategic alliances for accelerated development and cost reduction;
— In the field “Small Specimen Test Technology”, a strongly coordinated top-down approach towards near-term international licensing;
— In the area “fission reactor irradiations”, a harmonization of test matrixes for effective use and cost sharing.

The availability of dedicated and intensive neutron sources with instrumented facilities or test modules is essential for the development of materials and their qualification.They are at the critical path as their results are indispensable for the creation of reliable databases necessary for design, efficient and safe operation as well as for a long lifetime of strongly neutron irradiated core structures. Without dedicated intense neutron sources it would not be possible to achieve Technology Readiness Level (TRL) [46] beyond 5 or even 6.

4. SAFETY ASPECTS

For fast reactors in the past years especially within the European Commission R&D framework programs, several programs have been carried out analysing the safety behaviour of individual reactor types [24–29] or of cross cutting nature enhancing model development and validation [30–33]. With respect to the enveloping safety analysis the following accident sequences have been mentioned as the most relevant ones for the fast reactor types:

— GFR: decay heat removal (DHR) in depressurized conditions;
— SFR: sodium chemical activity causing fires, positive void reacivity effect (caused by unprotected loss of flow or loss of heat sink accidents), decay heat removal (DHR);
— LFR: degradation of the core materials in normal operation, formation of radioactive polonium, seismic stability of containment, decay heat removal (DHR).

Strikingly, the plant safety limiting scenarios differ from that of a PWR, where a LOCA or a reactivity initiated accident (RIA) for high burnup fuel are considered to be most relevant. The designers of all fast reactor types therefore need to develop their own strategies and engineering measures to cope with those sequences.

Due to the high-power densities envisaged for the FRs, the decay heat removal poses a significant challenge. Comparing the decay heat removal (DHR) systems of a LWR with a FR the prior strategy in a FR is to keep the coolant level in case of boundary break whatever happens. To some extent this is also done in a LWR using the Emergency Core Cooling Systems (ECCS) but for FR's this is of vital nature. In principle also, FRs rely on natural convection as the ultimate heat sink in case of a station black-out. The general scheme followed by all reactor types is depicted in Fig. 13. In contrast to LWR, where water is also the primary core coolant, the mixing of primary and secondary heat removal coolants is not allowed. Most challenging is the heat removal in a GFR, where a certain pressure needs to be assured in a containment to allow for a sufficient coolant density to guarantee a safe decay heat removal. Therefore, the entire primary and secondary systems are housed in a containment allowing to be pressurized to several bars. The decay heat removal is assured by two means, a high-pressure system (battery buffered to work at 7 MPa) and a low-pressure system (also supplied by an emergency power supply operating at about 0.4 MPa). Thhe heat sink is as in all other DHR system located outside the containment. For SFRs the situation is also challenging due to the high chemical activity of sodium with water, preventing a direct dip-cooling by water in the primary coolant pool. The weakest challenge is posed for the LFR in terms of the DHR. Here, dip-coolers can be directly immersed in the pool and connected to the heat sink, provided either by blowers (active), chimneys (passive) or a water pool (natural circulation).

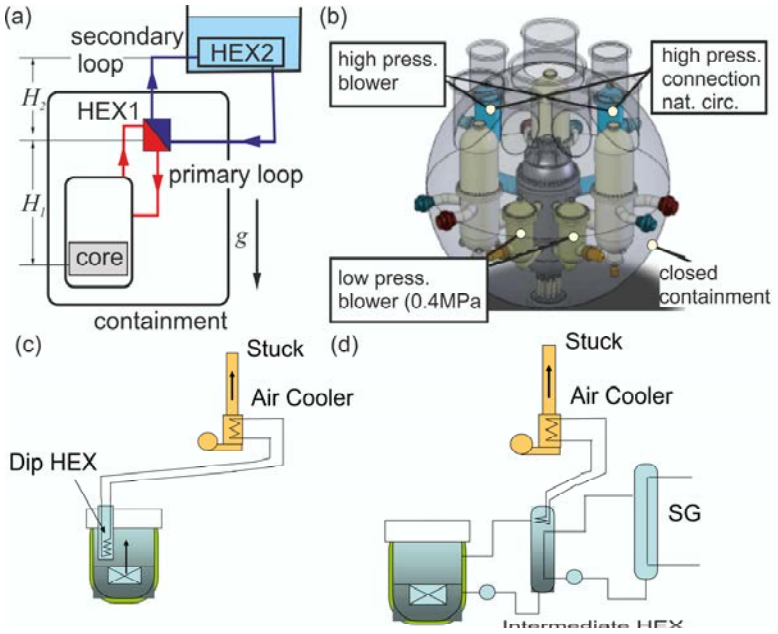

FIG. 13. (a) Physical principle of a decay heat removal system (DHR); (b) technical realization in a GFR [15]; (c) sketch of realization in a LFR; (d) sketch of realization in a SFR.

5. COOLANT CHALLENGES IN ACCELERATOR APPLICATIONS

In accelerator applications the incident particle energies and their flux constitute the largest challenge. By the interaction of primary nuclei with a target material, secondary particles — so called spallation products — are produced. Dependent on the incident nuclei energy a wide range of the periodic table is then present in the target system. The number of secondary particles can be at high incident primary particle energies of the order of 10 or

more and are emitted in a sharper spectrum than that provided by a fast reactor and yields even higher material damages, although the incident particles are charged.

Especially for the high power target the volumetric power released in the target material exceeds the capability to be safely removed by water, prominent examples in that context are the liquid metal operated target for the spallation neutron Source SNS [34], the MEGAPIE target [35] or the concepts for the IFMIF target [36]. Those liquid metal operated targets are called homogeneous targets, because the liquid metals act both as functional material to provide the neutrons but also as a coolant. Such target types facilitate simple and robust designs. They are thinkable either as window-designs in which the beam line transporting the primary beam is separated by a thin structure from the liquid target fluid or as windowless option in which the target fluid is directly facing the proton beam.

The heterogeneous target option uses a solid target material acting as functional material whereas the heat deposited by the beam is removed by a gaseous coolant. Both options have been developed in the context of the currently erected European Spallation Source (ESS). The ESS beam has a mean energy of 2.5 GeV and a beam current of 50 mA pulsed with 14 Hz having beam dimension of 6 cm × 16 cm, which translates to a mean average beam power of 5 MW, for more details see e.g. [37].

In order to illustrate the main differences arising simply by the coolant choice, both designs are briefly sketched. Fig. 14 shows the developed free surface target operated with PbBi as spallation material. The fundamental design idea of this METAL:LIC concept is based on housing of the spallation material entirely in a service room underneath the facility, allowing for an emergency draining by gravity only and thereby minimizing the coolant inventory. Also decay heat removal is easily obtained by a water evaporation cooling within the bunker.

The utilization of PbBi as coolant and spallation material limits the radiation induced material damage to that of the coolant confining ducts, where it stays at a low value of below 50 dpa for a five-year operation [38]. Moreover, even in case of beam transients or unintended beam focussing the liquid temperature remains at levels substantially below its boiling temperature and also the coolant confining structures are considerably far under the material limits, although the volumetric power release in the Bragg peak accumulates to almost 2 GW/m3 including photon heating by the adjacent structures [39]. This is attained even for mean flow velocities not exceeding 2m/s. Moreover, the design profits from abstaining of any activated fluid piping leaving the target station.

Despite, these quite favourable qualities of the windowless target option it exhibited some drawbacks. At first, the pulsed beam operation caused pressure oscillations modifying the surface shape. Although by designs, these fluctuations could be minimized the operational threshold of the target design is limited. Another disadvantage are start-up and shut-down operations of the target causing droplets to be ejected from the surface. In addition, high power operation produces mercury (195Hg) similarly to the MEGAPIE target[40], which has a high vapour pressure. This requires specific measures for its sepearation and removal within the beam tube. Finally, the coolant activation requires a dedicated treatment at end of life similar as in a Lead Bismuth Eutectic (LBE) cooled reactor.

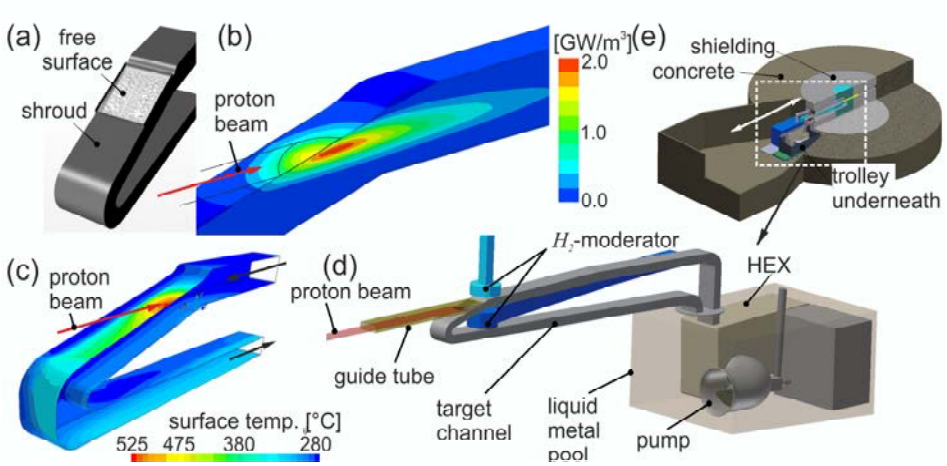

FIG. 14. (a) Sketch of the windowless METAL:LIC target (a); (b) temperature distribution in the spallation liquid PbBi at nominal power; (c) corresponding structure temperatures; (d) set-up of the integrated target concepts; (e) integration in the target station.

Therefore, it has been decided to realize a forced convection, helium cooled rotating tungsten target, as illustrated in Fig. 15, reducing the development risk considerably to a few aspects, which can be treated separately.

Due to the high beam energy the wheel has an outer wheel diameter of approximately 2.5 m, bared in a 0.5 m diameter shaft, which is rotating at 25 rpm. Within the shaft the helium is guided within the wheel in-/outward to the auxiliary systems composed of filters, heat exchangers and the pump. This about 19 tons heavy target assembly is assembled from the top into the target station and more actual design data may be taken from [41].

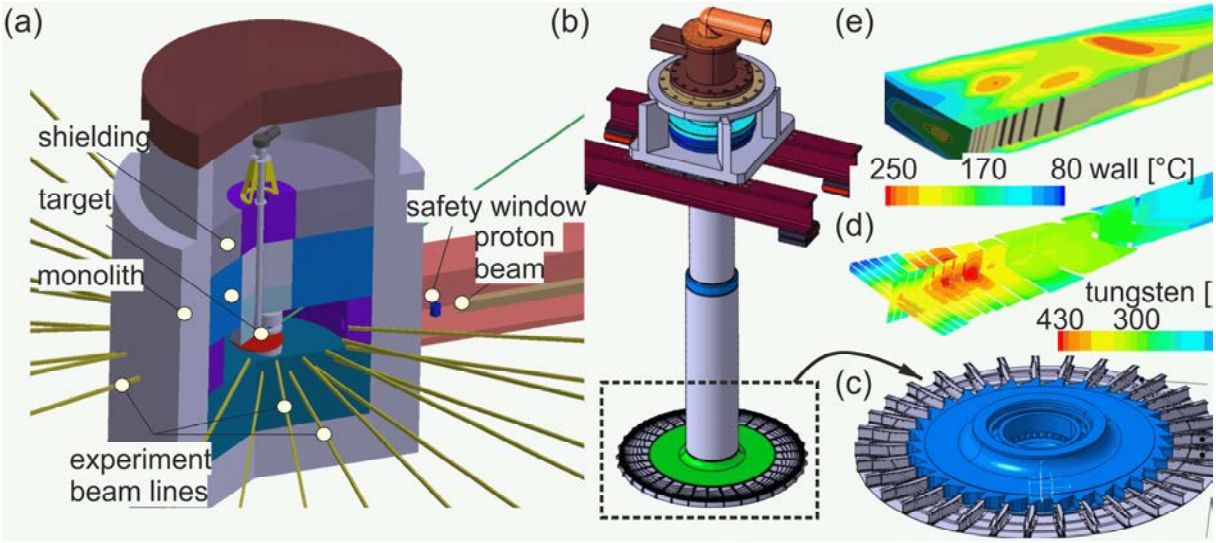

FIG. 15. (a) Sketch of the ESS target station; (b)a rotating helium cooled tungsten target; (c) where in the wheel tungsten blocks are form fitted; (d) the computed distribution of temperature field in the tungsten blocks; (e) the wall at nominal flow conditions.

6. SYNOPSIS

This article tries to elucidate the dependence of the coolant choice on the performance of the fast neutron spectrum reactor. Thereby, it became obvious that neutronics, thermo-physics and thermo-chemistry of both coolant and its confining structures are strongly interconnected.

While thermo-physical properties largely determine dimensioning of components and active systems, the interaction of material and coolant under irradiation poses a challenging non-linear multi-physics and multi-scale problem up to now not closed accessible by numerical means. However, the predictive prognosis of the material-coolant behaviour on all scales, especially under irradiation, is the basic prerequisite for the start of a licensing procedure, which requires the provision of a validated database, certified calculation methods as well as standards for the planned operating regime of the nuclear plant. In the view of the long licensing procedures and the anticipated increased operational times the importance of providing a comprehensive database becomes of vital importance for a timely realization. This in turn means that, especially against the background of newly developed materials and innovative manufacturing technologies, these must first be verified and tested in infrastructures with the right neutron spectrum before any licensing procedure can be considered at all. Unfortunately, the number of irradiation facilities is very manageable.

The absence of a validated database is also a major obstacle that makes a comprehensive safety demonstration very difficult. Despite progress in inventory control and technology qualification, there is often a lack of evidence in medium-sized experimental facilities that would allow reactor scaling. However, these types of test facilities are indispensable in order to enable a closed safety analysis in case of design basis accidents.

In the case of beyond design basis accidents, many calculation procedures cannot simply be transferred to other coolants. This refers not only to the individual coolant or material parameters, but also to substantially different process paths, failure scenarios or interaction phenomena due to the design. This problem also affects reactor types that have already been implemented, such as the SFR. Although in the past severe accident codes were developed and verified by complementary experiments, the new reactor concepts enter parameter ranges which exceed the

validation range of the methods developed in the past. In the absence of experimental facilities, code-to-code comparisons are now mainly used to verify the safety codes. The extent to which these models can, however, represent real conditions or take all effects into account is at least questionable. Therefore, numerical and experimental efforts at the international level are necessary for the future, supported by a closed V&V approach in the form of benchmark exercises[45].

REFERENCES

[1] Gen-IV International Forum, 2014, Technology Roadmap Update for Generation IV Nuclear Energy Systems.
[2] Evaluated Nuclear Data File (ENDF), IAEA (2017).
[3] Petersen, The Properties of Helium: Density, Specific Heats. Viscosity, and Thermal Conductivity at Pressures from 1to 100 bar and from Room Temperature to about 1800 K, Rise Report No. 224 (1970).
[4] IAPWS, 2007, R4-84 (2007).
[5] ADDISON, C., The chemistry of the liquid alkali metals, Wiley, Chichester (1984).
[6] FOUST (Ed.), O.J., Sodium-NaK engineering Handbook, Gordon & Breach, New York (1976).
[7] FAGHRI, A., ZHANG, Y., HOWELL, J., Advanced Heat and Mass Transfer, Global Digital Press, Columbia, MO (2010).
[8] Nuclear Energy Agency, 2007. Handbook on Lead-bismuth Eutectic Alloy and Lead Properties, Materials Compatibility, Thermal-hydraulics and Technologies. OECD/NEA Nuclear Science Committee Working Party on Scientific Issues of the Fuel Cycle Working Group on Lead-bismuth Eutectic.
[9] HEJZLAR, et al., Cross-comparison of fast reactor concepts with various coolants, Nuclear Engineering and Design **239** (2009) 2672–2691.
[10] Petersen, The Properties of Helium: Density, Specific Heats, Viscosity, and Thermal Conductivity at Pressures from 1 to 100 bar and from Room Temperature to about 1800 K, Riso Report No. 224 (1970).
[11] SPAN, R.; WAGNER, W., A New Equation of State for Carbon Dioxide Covering the Fluid Region from the Triple-Point Temperature to 1100 K at Pressures up to 800 MPa, J. Phys. Chem. Ref. Data **25** (1996) 1509–1596.
[12] LOCATELLI, G., MANCINI, M., TODESCHINI, N., Generation IV nuclear reactors: Current status and future prospects, Energy Policy **61** (2013) 1503–1520.
[13] CUMMINS, W.E., CORLETTI, M.M., SCHULZ, T.L., Westinghouse AP1000 Advanced Passive Plant (Proc. Int. Cong. on Adv. in Nuclear Power Plants, ICAPP 2003, Cordoba, Spain, Paper No. 3235) (2003).
[14] KATOH, A., et al., Design features and cost reduction potential of JSFR, Nuclear Engineering and Design **280** (2014) 586–597.
[15] POETTE, P., "Gas Cooled Fast Reactors: recent advances and prospects, presentation", Int. Conf. on Fast Reactors and Related Fuel Cycles: Safe Technologies and Sustainable Scenarios, 2013, Paris (2013).
[16] PONCIROLI, R, et al., A preliminary approach to the ALFRED reactor control strategy, Progr. in Nuclear Energy **73**, (2014) 113–128.
[17] GUIDEZ, J., Sodium cooled fast reactors, DEN Monographs, 2016.
[18] BORGSTEDT, H. U., Material Behavior and Physical Chemistry in Liquid Metal Systems, Springer-Verlag, (1982).
[19] GETMAT- Testing metals for nuclear reactors FP7-EURATOM-FISSION , Project ID: 212175, European commission (2009).
[20] F.A. GARNER, F., Radiation Damage in Austenitic Steels, Comprehensive Nuclear Materials **4** (2012) 33–95.
[21] SNEAD, L., Limits on irradiation-induced thermal conductivity and electrical resistivity in silicon carbide materials, J. Nucl. Mat. **329** Part A, (2004) 524–529.
[22] FISCHER, U., PERESLAVTSEV, P., MÖSLANG, A, RIETH, M., Transmutation and activation analysis for divertor materials in a HCLL-type fusion power reactor, J. Nucl. Mat. **386–388** (2009) 789–792.
[23] SCHROER, C., et al, Gas/liquid oxygen-transfer to flowing lead alloys, Nuc. Engng Des. **241** (2011) 1310–1318.
[24] EURATOM FP6 ELSY Project, Contract N° FI6W-2006-036439, February 2007.
[25] LEADER, Lead-cooled European Advanced DEmonstration Reactor, FP7- EURATOM-FISSION, Project Reference 249668.
[26] GOFASTR (European gas cooled fast reactor), FP7-EURATOM-FISSION Project ID: 249678 (2010).
[27] Collaborative Project on European Sodium Fast Reactor (CP-ESFR) (2007).
[28] JASMIN – Joint Advanced Severe Accidents Modelling and Integration for Na-cooled fast neutron reactors.
[29] SAMOFAR, A Paradigm Shift in Reactor Safety with the Molten Salt Fast Reactor, Project ID: 661891 (2015).
[30] SARGEN-IV – Harmonized European methodology for the Safety Assessment of innovative GEN-IV reactors.
[31] ESNII plus, 2013, strategic approach to advanced fission systems in Europe in support of the European Sustainable Industrial Initiative (ESNII) within the SET -Plan. Project number 605172.
[32] SESAME, 2014, Thermal hydraulics Simulations and Experiments for the Safety Assessment of MEtal cooled reactors, Horizon 2020 Framework Programme Activity: NFRP -01-2014.
[33] THINS, 2010, Thermal-hydraulics of Innovative Nuclear Systems, FP7-EURATOM-FISSION , Project ID: 249337.
[34] WENDEL, M., Measurements of Bubbles in Liquid Mercury for SNS Target Applications, 3rd international Workshop on Measuring Techniques for Liquid Metal Flows (MTLM 2015) April 14-17, 2015.
[35] GRÖSCHEL, F., Das Megapie-Experiment – Zahlen & Fakten, PSI Nachrichten (2007).
[36] GORDEEV, S., HEINZEL, V., STIEGLITZ, R., Fusion Engineering and Design **87** (2012) 569–574.
[37] PEGGS, S., Conceptual design report (2012).

[38] WEINHORST, B. et al, Radiation damage analysis for the liquid metal target METAL:LIC, J. Nuc. Mat. **450** (2014) 219–224.
[39] FETZER, J. et al, Design measures to counteract pressure wave effects in the liquid metal target METAL:LIC, J. Nuc. Mat. **450** (2014) 212–218.
[40] NEUHAUSEN, J., Investigations on the release of mercury from liquid eutectic lead–bismuth alloy under different gas atmospheres, Nuclear Instruments and Methods in Physics Research Section **A562** (2006) 702–705.
[41] HAINES, J. et al., Spallation neutron source target station design, development, and commissioning, Nuclear Instruments and Methods in Physics Research Section A **764** (2014) 94–115.
[42] MATERNA-MORRIS, E., LINDAU, R., SCHNEIDER, H.-C., MÖSLANG, A., Tensile behaviour of EUROFER ODS steel after neutron irradiation up to16.3 dpa between 250 and 450◦C, Fus. Eng. Des. **98-99** (2015) 2038–2041.
[43] KLIMENKOV, M., et al, J. Nucl. Mater. **462** (2015) 280–288.
[44] TONG, Z., DAI, Y., The microstructure and tensile properties of ferritic/martensitic steels T91, Eurofer-97 and F82H irradiated up to 20 dpa in STIP-III. J. Nuc. Mater. **398** (2010) 43–48.
[45] INTERNATIONAL ATOMIC ENERGY AGENCY, Integrated Approach to Safety Classification of Mechanical Components for Fusion Applications, IAEA-TECDOC-1851, IAEA, Vienna (2018).

3. SUMMARY OF COOLANT CHARACTERISTICS UNDER IRRADIATION

L. El-Guabaly (University of Wisconsin, USA)

During the First IAEA Workshop on Challenges for Coolants in Fast Neutron Spectrum Systems, 5–7 July 2017, IAEA Headquarters, Vienna, Austria, participants from many countries covered the topic of coolant characteristics under irradiation for three nuclear systems: (i) water, helium, PbLi, and Flibe/Flinabe coolants for the fusion system; (ii) sodium, lead, MS fluoride mixtures, helium, and water for the fission system; (iii) helium and Pb-Bi for the accelerator/spallation system. Since the choice of coolant defines the coolant confining structure, operating temperature window, flow velocity, corrosion/erosion products, and variety of activation by-products, the specific subtopics included: (i) radiation chemistry and radiolysis; (ii) activation, species production, and computational models/tools; (iii) coolant processing and handling procedures. Tables 3, 4, and 6 of this section document the critical issues, challenges, major achievements, experimental verifications, and R&D needs for each coolant employed in the three nuclear systems: fusion, fission, and accelerator/spallation. Based on the 10 orals and 6 posters presented at the above mentioned workshop, the key challenges and takeaways are:

— The lack of 14 MeV neutron source presents a major hurdle for fusion material development and validation of numerical tools.
— The behaviour of all coolants under synergistic effects (14 MeV neutrons, high operating temperature, strong magnetic field, flowing coolants, etc.) is not well understood and requires extensive R&D programs.
— Fusion generates tritium in large quantity (~100 kg/y for 2 GW fusion power plant vs. e.g. ~ 2 g/y for SFR (SuperPhenix) and ~ 4 g/y in ITER). Tritium is also an issue for accelerator/spallation applications even though the annual quantity produced is significantly below fusion but exceeding those of fast rectors. Tritium tends to permeate through the coolant-confining structure and reach the He and/or water coolants, raising safety concerns related to worker exposure and tritium release to the environment, and mandating the development of efficient tritium extraction systems for all coolants/ breeders/neutron multipliers and for disposal of radioactive materials.
— A challenging task facing fusion is the accurate evaluation of the coolant radioactive inventory as the coolant flows in/out the fusion power core with multiple residence times, flow rates, irradiation loads, neutron spectra, mixing patterns, and purification level in the outer loop. This scopes also the diffusion of tritium through irradiated/unirradiated materials which constitute substantial part of the inventory.
— For fast neutron systems, very limited database exists for water corrosion and radiolysis under irradiation conditions (see Section 6).
— High level of fidelity in computational results could be achieved by further developing the interface that couples the CAD with 3-D neutronics codes and subsequently with multi-physics codes (such as fluid dynamic, stress, and activation codes). The validation with experiments (such as JET in the UK) is essential for the credibility of such software.
— Heavy liquid metals and molten salts get contaminated by their own radioactive by-products, presenting a major concern for occupational exposure during operation and releases during accidents, calling for continuous processing, filtering, and purifying of coolants.
— For heavy liquid metals, it is necessary to develop protective coating or improved materials with regards liquid metal embrittlement and corrosion as well as an efficient oxygen control process. In addition, other important functions for those coating materials such as barrier for avoiding Tritium permeation and acting as electrical insulator to avoid or mitigate Magnetohydrodynamic (MHD) effect are to be considered (see Section 5).
— For alkaline liquid metals (such as sodium and lithium), dedicated research is required to improve models to simulate fires and liquid metal fragmentation that has a strong influence on the thermal power absorbed by the reactor's internal structures. Also, continuous coolant purification and its monitoring pose challenges.
— The sodium fast reactors utilities have to take care of material susceptibility to different corrosion mechanisms during maintenance operation.

— The presence of many spallation products requires the development of knowledge related to their physical and radio-chemical behaviour in Pb-Bi and He coolants of the spallation system. A special focus is requested for ^{210}Po in Pb-Bi cooled reactors/targets and ^{195}Hg in spallation targets and also for mobile activated materials (e.g., activated steel in He cooled targets).
— For all coolants, it is necessary to:
  (i) Develop an efficient strategy to remove the coolant and decontaminate it during maintenance phases or reactor dismantling.
  (ii) Implement a reliable in-service inspection strategy related to the development of upgraded instrumentation able to operate at high temperature.

At the present time, several ongoing or planned projects intend to address and overcome the knowledge gaps in order to meet the near-term R&D needs for many coolants. Some examples of ongoing/planned projects include:

— Fusion-relevant neutron sources are planned to be built worldwide in the US, Europe, Japan, and China for materials testing, validation of nuclear data and numerical tools, blanket testing. In particular, EU is working within EUROfusion/PPPT (Power Plant Physics and Technology) on the accelerator-based neutron source International Fusion Materials Irradiation Facility-DEMO Oriented Neutron Source (IFMIF-DONES) to provide the irradiation data for the qualification of materials for the EU DEMO.
— An ongoing study at CEA simulates the pulsed mode using the OSCAR-Fusion code. The validation of the OSCAR-Na code against operating experience with SFRs and experimental loops is also ongoing at CEA to further the qualification of OSCAR-Na.
— An experiment is being conducted at the Kyushu University and NIFS in Japan to extract tritium from Flibe or Flinabe molten salt coolants.
— Technologies for tritium removal from He and PbLi are under development and testing on various experimental facilities under EUROfusion (e.g. at KIT, Germany).
— Further development of the software that couples CAD with 3-D MCNP code is ongoing worldwide (e.g. in the US, EU, and China) with planned effort to couple it with multi-physics codes for fluid dynamic, stress, and activation analyses.
— Within the framework of the EUROfusion consortium, the UNED group in Spain is currently developing advanced methodology to reliably predict the PbLi activation in loops of EU DEMO.
— The ÚJV group (in Czech Republic) and CEA are conducting further R&D activity on gas-cooled fast reactor issues related to the helium coolant.

OVERVIEW OF COOLANT CHARACTERISTICS UNDER IRRADIATION: RADIATION-CHEMISTRY, RADIOLYSIS, ACTIVATION, AND THEIR CONSEQUENCES ON OPERATION, MAINTENANCE, AND DECOMMISSIONING

L. EL-GUEBALY
University of Wisconsin,
Madison, WI, USA

C. LATGÉ, F. DACQUAIT
French Atomic and Alternative Energies Commission,
Cadarache, France

A. AERTS
Belgian Nuclear Research Center,
Mol, Belgium

A. BARON-WIECHEC
Centre for Fusion Energy,
Culham, UK

A. BOJANOWSKA
Institute of Nuclear Chemistry and Technology,
Warsaw, Poland

I. CRISTESCU, U. FISCHER
Karlsruhe Institute of Technology,
Karlsruhe, Germany

S. FUKADA
Kyushu University, NIFS; Tohoku University,
Tohoku, Japan

M. GARCIA
UNED, Dept. of Energy Engineering,
Madrid, Spain

V. IGNATIEV
National Research Center, Kurchatov Institute,
Moscow, Russia

U. ODEN
European Spallation Source,
Lund, Sweden

I. RICAPITO
Fusion for Energy; European Commission,
Barcelona, Spain

M. SOUKUPOVA
UJV Rez, Husinec; UCT,
Prague, Czech Republic

M. UTILI
ENEA FSN-ING,
Brasimone, Italy

Abstract

The nuclear community continues its search efforts for the most promising coolants for nuclear applications: fission, fusion, and accelerator/spallation-driven systems. Water has been extensively used for fission reactors around the world and accumulated a wealth of operating experience. For years, the search for the ultimate goal of safer, more efficient cooling system with high performance has stimulated worldwide research on liquid metal (LM), molten salt (MS), and gas coolants: PbLi, lithium, LiSn, Flibe/Flinabe, and helium for the fusion system, and sodium, lead, lead-bismuth eutectic (LBE), MS fluoride mixtures, and helium for fission and spallation systems. Design and material issues, concerns, and challenges emerge with the use of each coolant. This paper provides a brief overview of the characteristics of selected coolants under typical operating environment in fast spectrum systems. It also addresses our current understanding of coolant-related challenges facing nuclear systems, identifies the knowledge gaps and research and development (R&D) needs, along with strategies to elaborate scientific and technological solutions related to radiation chemistry, radiolysis, activation, and their consequences on operation, maintenance, and decommissioning of nuclear facilities.

1. INTRODUCTION

At the First IAEA Workshop on Challenges for Coolants in Fast Neutron Spectrum Systems, 5–7 July 2017, IAEA Headquarters, Vienna, Austria, 10 oral presentations were presented during Session 1 titled "Coolant Characteristics under Irradiation." Invited and contributed presentations covered numerous coolants for three nuclear systems: water, helium, PbLi, and Flibe/Flinabe coolants for the fusion system; sodium, lead, MS fluoride mixtures, helium, and water for the fission system; helium and Pb-Bi for the spallation system. Some topics could not be entirely presented during the oral session, but required complementary input from other experts, which is conducted in the form of posters. Table 1 lists the oral and poster presentations for Session 1 with assigned oral or poster numbers at the beginning (e.g., O-9 or P-5) that will be referred to throughout the text and to their corresponding companion papers in this TECDOC.

TABLE 1. CONTRIBUTIONS IN SESSION COOLANT CHARACTERISTICS UNDER IRRADIATION

10 Orals:

O-2: L. El-Guebaly and C. Latgé, "Overview of Coolant Characteristics Under Irradiation: Radiation-Chemistry, Radiolysis, Activation, and their Consequences on Operation, Maintenance, and Decommissioning."

O-3: M. Utili, "Challenges and R&D Needs for PbLi Coolant for Fusion Applications."

O-4: A. Baron-Wiechec, I. Ricapito et al., "Water and pressurized Helium as coolants of fusion reactor breeding blankets: chemistry issues and purification technologies."

O-5: V. Ignatiev, "Molten Salts Characteristics under Irradiation in Fission Related Systems."

O-6: F. Dacquait, "Modelling the contamination transfer in nuclear reactors: The OSCAR code - Application to SFR and ITER."

O-7: A. Aerts, "Modelling the Release of Radionuclides from Irradiated LBE."

O-8: U. Fischer, I. Cristescu et al., "Activation Characteristics of Fusion Power Plant Coolants (He, water, Pb-Li) and Aspects of Related Tritium Extract Techniques."

O-9: S. Fukada et al., "Our Recent Experimental Challenges on Flibe or Flinabe Coolant for Fusion Applications and Related Japanese Researches."

O-10: C. Latge, "Sodium coolant: Activation, Species production Coolant processing and handling procedures."

O-11: M. Soukupova, P. Nilsson, U. Odén, "ALLEGRO Gas-Cooled Fast Reactor Helium Management & European Spallation Source ERIC – Target Helium Cooling."

6 Posters:

P-1: A. Bojanowska-Czajka et al., "Study of processes occurring under regular operation of water circulation systems in nuclear power plants with suggested actions aimed at upgrade of nuclear safety."

P-2: I. Cristescu, "Tritium Transfer and Extraction from Water, He, and PbLi Coolants."

P-3: M. García et al., "Development of methodology to determine LiPb activation in DEMO Breeding Blankets."

P-4: E. Gugiu, "Evaluations and Analysis of the Lead-coolant of ALFRED Demonstrator – Challenges, Needs and Gaps."

P-5: A. Baron-Wiechec et al., "Water chemistry challenges and R&D guidelines for water cooled systems of DEMO Pb-Li Breeder Blanket."

P-6: I. Ricapito et al., "Pressurized Helium as coolant of fusion reactor breeding blankets: focus on the Purification Technologies."

The choice of coolant defines the coolant-confining structure, operating temperature window, flow velocity, corrosion/erosion products, and variety of activation by products. In that context, the specific topics addressed during Session 1 included:

— Radiation chemistry and radiolysis;
— Activation, Species production, and Computational models/tools;
— Coolant processing and handling procedures.

Since the workshop main mission was to depict the current state-of-the-art and formulate challenges to be overcomed and solved in the near future, the above topics scoped i) the limiting constraints and range of use for coolants under irradiation; ii) present state of knowledge and experimental verification; lacking evidence, major issues, deficits and gaps that require R&D efforts; iii) major difficulties with existing processing and handling procedures along with new approaches that offer potential for improvements. The summary tables at the end of the following fusion, fission, and spallation sections outline and document in great details such crucial points for all coolants under consideration.

2. THE FUSION SYSTEM

2.1. Background

Since the early 1950s, researchers around the globe have been sharing results and discussing challenges of magnetic fusion to more fully understand and advance the physics and technology of fusion energy. More than 60 large-scale conceptual DEMO and power plant studies [1], > 100 operational experiments built in the US, Japan, Russia, UK, S. Korea, China, France, India, and other countries, impressive international collaboration in all areas of research materialized in designing and constructing the international fusion experiment ITER [2] in France. The large body of accumulated knowledge has led to the current wealth of fusion information and understanding with an opportunity for fusion to join the energy mix in the 21st century.

2.2. Fusion Concepts

Three magnetic confinement fusion concepts were pursued internationally (tokamak, stellarator, and spherical torus) and experienced substantial modifications over the past 60 years [1]. Most of the studies and experiments are currently devoted to the D-T fuel cycle, since it is the least demanding to reach ignition. Internationally, the tokamak concept is regarded as the most viable candidate to demonstrate fusion energy generation. All fusion talks presented at the workshop were tokamak-related, except O-9 on the stellarator concept.

2.3. Tritium Breeding Blankets

The transition from ITER to fusion DEMO and power plant requires developing tritium breeding blanket to generate tritium (T) in unprecedented large quantities to sustain the plasma operation: 55.6 kg of T per GW of fusion power, per full power year of operation (vs. 4 g/y in ITER and 2 g/y in Sodium Fast Reactor). Thus, fusion devices generating substantial fusion power and consuming 10s - 100s kg of T annually must breed their own T in a blanket surrounding the plasma, as external supply of large amount of T does not exist. A variety of liquid and ceramic breeder blanket concepts have been developed since the 1970s, suggesting several coolants, liquid metals, and molten salts for fusion [3]. For instance, in the US, the dual-coolant PbLi (DCLL) blanket [4] is the preferred concept for future fusion devices [5-9]; Europeans developed ceramic breeder blanket and PbLi-based blanket, both concepts could be cooled with either He or water [10-15]; Japan prefers molten salt (Flibe/Flinabe), water cooled ceramic breeder, and PbLi blankets [16,17]; and China developed DCLL and ceramic breeder blankets [18,19].

An appreciable amount of the tritium permeates through the coolant-confining structures and eventually reaches the helium and water coolants, raising safety concerns related to worker exposure and T release to the environment. Developing efficient T extraction systems represents a challenging task for fusion designers. Different schemes have been developed as the T concentration and partial pressure are orders of magnitude higher for HCLL and WCLL blankets compared to the DCLL blanket. The vacuum permeator seems promising for the DCLL blanket [20-22] while the He-bubble tower and droplet rains offer advantages for the HCLL and WCLL blankets [23] (see also P-2, O-8, O-9 in Table 1).

2.4. Neutron Spectrum

The fusion, fission, and spallation neutron spectra differ greatly with energies ranging from thermal to GeV. Such widely varying spectra impact the choice of coolant and the damage to the coolant-confining structure in terms of He/dpa ratio (see Table 2) and H/dpa ratio. Figure 1 compares the three spectra. The fusion spectrum peaks at 14 MeV and is quite sensitive to the blanket concept, as illustrated in Fig. 2, with notable impact on the FW radiation damage, service lifetime, and transmutation products [26,27].

TABLE 2. HE/DPA RATIO FOR TESTING IN EXISTING AND PROPOSED NEUTRON SOURCES [24]

Irradiation Facilities	**Fusion Nuclear Science Facility (FSNF)**	**High Flux Isotope Reactor (HFIR)**	**Spallation Neutron Source (SNS; sample @ 3 cm)**	**IFMIF/DONES[1] (high flux text module)**
% of neutron with E>0.1 MeV	~75%	~24%	~65%	~96%
RAFM alloys	10	0.3 (low)	74 (high)	13
Tungsten	0.6	0.0008 (low)	—	4 (high)
SiC	95	1.7 (low)	98	150 (high)

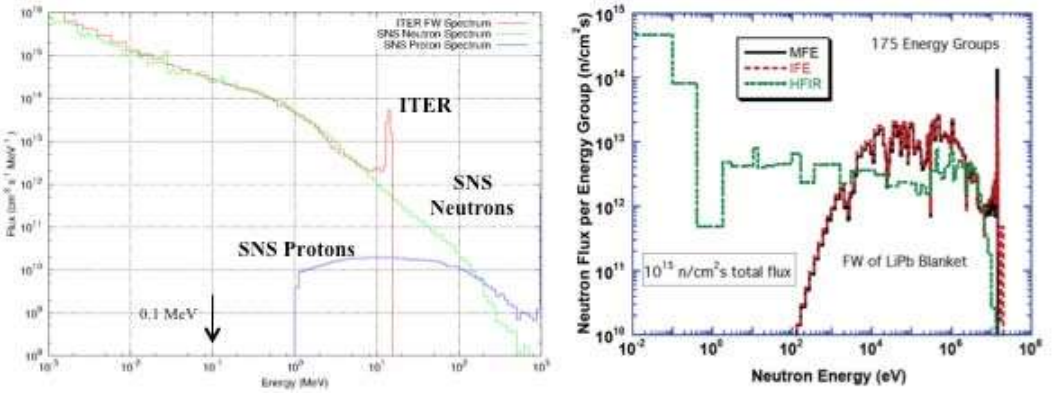

FIG. 1. Comparison of SNS-ITER spectra. Courtesy of A. Davis (UW-Madison) and Fission-Fusion spectra [25].

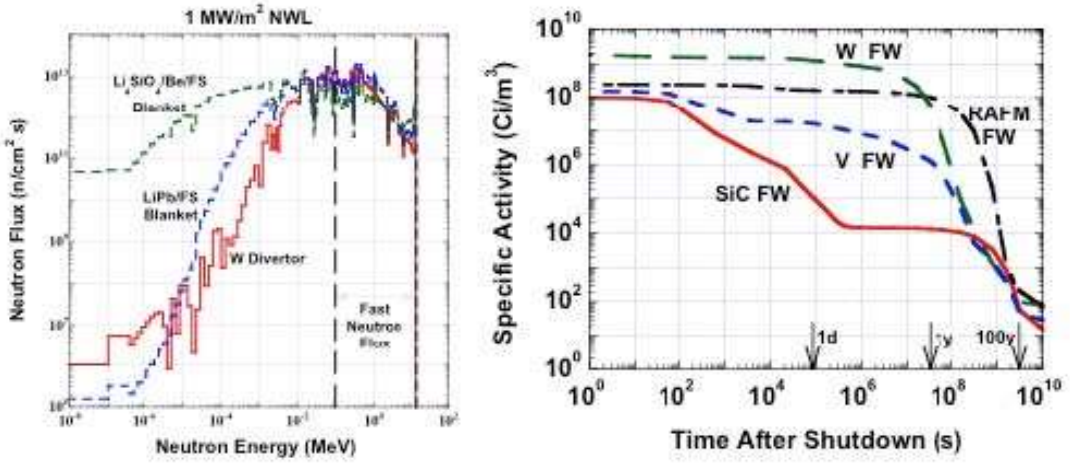

FIG. 2. First wall spectrum [27] and structure activation for US power plant designs (ARIES-RS, -ACT1, and -ACT2).

[1] International Fusion Materials Irradiation Facility (IFMIF) and European DEMO-Oriented Neutron Source (DONES).

2.5. Activation of Coolant and Structure

Fusion designers have the freedom to select low activation structural materials (reduced activation ferritic/martensitic (RAFM) steels [5–10], vanadium alloys [16,28], tungsten alloys [27], and SiC/SiC composites [29,7]), but impurities (Nb, Mo, Ag, Al, Re, etc.) must be controlled to very low level (wppm or wppb). Such coolant confining structures activate differently in fusion environment (refer to Fig. 2). The widely used structural RAFM steel will be further developed to withstand high radiation damage (150-200 dpa) with acceptable corrosion resistant characteristics. Each coolant exhibits unique activation property during operation (O-8, P-3). Several design parameters could impact the coolant chemistry and corrosion behaviour in the presence of strong magnetic field, not only during normal operation, but also during transients (O-3, O-4, O-9, P-5). PbLi and Flibe/Flinabe in particular are contaminated by their own radioactive by products (O-8, P-3, O-9). Moreover, the activated corrosion products (ACP) present a major concern for occupational exposure during operation and releases to the environment in the case of accident (O-6). For these reasons, it is necessary to continuously process, filter, and purify all coolants in order to control their quality, avoid contaminating sub-systems, and assure safe operation (O-3,O-4,O-9,P-5,P-6).

There is a severe corrosion issue with the release of free fluorine after tritium is bred, as fluorine forms a tritiated hydrofluoric acid, which is highly corrosive to all steel-based structural materials. To reduce the T permeation through the heat exchanger, mixing hydrogen-absorption metal powders (e.g., Ti, Zr, or V) with Flibe was proposed [16, O-9]. To widen the operating temperature window to 305-700°C, the FFHR study suggested the use of vanadium alloy (that offers higher operating temperature (700°C) than steel) along with the Flinabe breeder (that has lower melting point (305°C) than Flibe).

The activation of coolants and liquid breeders are more complex than that of structural components. All coolants circulate in and out of the neutron radiation field in several separate coolant flow paths through the device [30–31] (see also P-3 in Table 1). It is essential to consider realistic residence times and various neutron spectra within the blanket as the coolant/breeder circulate through the system. For example, coolant irradiated for few minutes inside the blanket, followed by > 5 minutes outside the irradiation zone where the coolant mix in various sub-systems (for heat transfer, chemistry control, T removal, etc.) [30–31] (see also P-3 in Table 1). Simplistic modelling for coolant activation at or near the first wall (O-8) overestimates the coolant activity and radioactive inventory by orders of magnitude.

2.6. Computational Models and Tools

Modelling the complex fusion geometry is a challenging task for 3-D neutronics, shielding, and activation analyses. In recent decades, state-of-the-art neutronics codes were developed in Germany (McCAD by KIT [32], O-8), US (DAGMC by UW [33]), China (MCAM by FDS team [34]) and other countries to model the fine details of the fusion power core. Such tools couple the CAD geometry directly with the 3-D MCNP code [35] to diminish the uncertainty attributed to approximations in modelling. The UW DAGMC [33] is the only code that accurately models the non-planar stellarator geometry. Coupling such CAD based codes with activation codes [FISPACT (KIT, Germany) [36, O-8], ALARA (UW, USA) [37], ACAB (UNED, Spain) [38, P-3] could provide full 3-D mapping of radiation environment and shutdown doses. Other computational codes include:

— R2S/R2Smesh system (KIT, Germany) [39] for activation and shutdown dose rate calculations, linking MCNP transport to FISPACT [36], ALARA [37], and ACAB [38, P-3] inventory calculations;
— OSCAR-Fusion (CEA, France) for ACP transfer in water (O-6);
— OTIS (UW, USA) for water activation in various loops [40].

2.7. Summary of coolants for fusion system

The following points briefly summarize some observations from the fusion presentations while Table 3 compiles the limiting constraints, major issues, experimental verifications, and R&D needs for fusion coolants: water, PbLi, He, and Flibe/Flinabe:

— PbLi is the most popular liquid metal breeder worldwide. Most PbLi-based blankets are supplemented with water or helium coolant, as in WCLL, HCLL, and DCLL blankets.
— Sparse database exits for Molten Salts (Flibe/Flinabe). Only Japan is currently pursuing self-cooled MS designs.
— Breeders generate tritium in large quantity (~100 kg/y vs. ~2g/y for SFR (SuperPhenix) and ~4g/y in ITER). Small fraction of T permeates through the structure and eventually reaches He and water coolants,

mandating online extraction of T from all coolants, along with developing T barriers and corrosion resistant coolant-confining structures.

— All coolants corrode structures and carry activated corrosion products (ACP). LMs and MSs generate their own radioactive by-products that could, along with ACPs, contaminate IHX, pumps, etc., unless filtered and purified online.
— The use of helium coolant offers unique advantage compared to other coolants due to the absence of activation concerns.
— 3-D CAD-based neutronics and activation codes are essential tools to assess radiation environment, activation, heat loads, and T source term for complex fusion geometry with high fidelity.
— For coolant activation, it is essential to consider realistic residence times and various neutron spectra within the blanket as the coolant circulate through the system.
— Water chemistry and corrosion behaviour during start up/shutdown, transients, and normal operation (in presence of magnetic field) are not well understood and require R&D program.

TABLE 3. SUMMARY OF FUSION LIMITING CONSTRAINTS, RANGE OF USE FOR COOLANTS UNDER IRRADIATION, EXPERIMENTAL VERIFICATION, MAJOR ISSUES AND CHALLENGES, ACHIEVEMENTS, AND R&D NEEDS

Coolant or Topic	**Application**	**Limits of Use and Radiation Effects**	**Research Details, Major Issues, and Challenges**	**Achievements**	**R&D Needs**
Water (O-4, P-5)	EU DEMO	**Constraints**: high velocity water, fast burn-up and dwell cycle, temp. Range 285-325° C, compatibility with Eurofer, presence of 14 MeV neutron flux and magnetic field. **Main Radiation Effects**: Water radiolysis at 14MeV neutron flux, activation of corrosion products	Program review, computation and experimental experiences. **Major Issues and Challenges**: Very limited database of experimental results to validate computational codes. Lack of facilities producing fusion range of neutrons to validate materials integrity and asses water radiolysis.	Review of current water chemistry program -Identification of water chemistry requirements for DEMO WCLL BB	Determination of the optimum pHT control in order to minimise corrosion of Eurofer-97 – Determination of the SCC susceptibility of Eurofer-97 under various concentrations of oxygen and aggressive species – Development and validation of corrosion and water radiolysis modelling codes and more!

TABLE 3. CONTINUED

Coolant or Topic	Application	Limits of Use and Radiation Effects	Research Details, Major Issues, and Challenges	Achievements	R&D Needs
Liquid Metal (PbLi) (O-3)	ITER and EU DEMO	Constraints: Temperature window: 234°C – 550°C; compatibility with materials; high Ni solubility in PbLi; stainless steel show high corrosion	-Conceptual design of LiPb breeder loops concepts auxiliary systems: Thermohydraulic numerical analysis (RELAP5-3D) and procedure to be adopted for normal and abnormal operations (LOCA and LOFA in/ex Vessel); §Integration PbLi loops in tokamak building; **-Investigation on corrosion** of EUROFER with LiPb and development of protection coatings (anti-corrosion and Antipermeation coatings); **-Investigation of MHD** issues and performing of related R&D (modelling and experimental activity), taking into account also tritium transport, buoyancy effect, etc; **-Irradiation** behaviour of PbLi/EUROFER/coating under irradiation; - **Control/Purification** of LiPb from radioactive transmutation products.	- Optimization antipermeation/ corrosion barrier - Development of code for MHD analysis and PbLi/Water interaction - Design and Integration of PbLi systems	– Characterisation Antipermeation/corrosion barrier under relevant neutron flux – 3D MHD effect in DCLL/HCLL/WCLL BB – Safety analysis: water/PbLi interaction – Thermohydraulic characterisation

TABLE 3. CONTINUED

Coolant or Topic	Application	Limits of Use and Radiation Effects	Research Details, Major Issues, and Challenges	Achievements	R&D Needs
Molten Salt (Flibe (Li2BeF4) or Flinabe (LiF+NaF+BeF2)) (O-9)	Self-cooled tritium breeder and coolant for Stellarator design	470-700°C for Flibe or 350-700°C for Flinabe, no irradiation limits, corrosive TF is generated and converted to T2 by Be redox control. Corrosive TF formation by neutron irradiation.	Experimental proof and T diffusion analysis. T leak due to high permeability; use of Ti particles mixed with Flibe or Flinabe; Lack of sufficient experiment.	– Suppress T permeation by use of Ti particles – Tritium recovery from neutron irradiated Flibe – Redox control of Flibe by Be rod	– Detailed physical or chemical properties of Flinabe – T absorption and desorption in Flinabe mixed with Ti
Activation of coolants (He, water, and PbLi) (O-8)	EU DEMO (Coolants at/near outboard first wall)	**Limitations** governed by selected structural material (Eurofer RAFM steel). **Main Radiation Effects**: Activation of coolant constituents, impurities and corrosion products affecting safety during plant operation and maintenance.	Computational simulations of produced activation with 3D DEMO models and specified irradiation scenario. **Major Issues and Challenges**: -T generated in or permeating to coolant, corrosion products, hazardous radionuclides (16,17N in water, ^{210}Po in PbLi) -Detritriation, water circulation (shielding of pipes due to 16,17N activity)	Assessment of coolant activity inventories & resulting radiation hazards	– Water, PbLi: Corrosion products, T permeation – PbLi: 210Po generation, Bi/Po extraction – Water: Radiolysis, chemistry
ACAB Code for PbLi Activation (P-3)	PbLi moving through various loops in EU DEMO	Long computational times (may be weeks for lifetime of DEMO) when the systems are very detailed; solutions are being explored	Computational Simulation for Activation of the PbLi flowing in DCLL breeder and loops. Computational simulation experiences putting together transport and activation codes with specific dedicated scripts	More realistic simulation of the PbLi activation in the DEMO fusion reactor breeder and loops	Computational: Improvement in order to reduce computational time
Tritium extraction from coolants (He, water, and PbLi) (O-8, P-2)	EU DEMO	**Main Radiation Effects:** Due to water radiolysis, hydrogen will be generated in the cooling loops. Negligible amount of tritium will be generated due to radiation	**Issues**: Calculations concerning the required capacity (flow rates) of the cooling purification system versus the reasonable tritium concentration in the coolants are on-going **Challenges**: Definition of the allowable tritium concentration in the coolant and the quantification of the tritium released in the steam generation loops based on experimental data. Designing and qualifying High tritium extraction and removal system from PbLi based on PAV and VST technologies.	Water detritiation technologies are well advanced and the processing capacity depends on allowable tritium concentration in the cooling loops. The technologies for tritium removal from He and PbLi are under development and testing on various experimental rigs.	– Benchmark the modelling tools concerning tritium permeation from the breeders in the coolants against experimental data in similar conditions as expected in DEMO. – Development & qualification of tritium permeation barriers at interface between the coolant and the steam

3. THE FISSION SYSTEM

3.1. Background

The future of mankind is confronted with increasing energy demands, the gradual exhaustion of fossil fuels, and the pressure to reduce greenhouse gas emissions. This is why more and more countries are considering nuclear energy as a viable element of their energy mix. Up to now, most of the nuclear energy (Total: 441 Units, 382 855 MWe by end of 2015) [41] is provided, thanks to systems based on thermal neutrons, cooled by water: Pressurized Water Reactors (PWR: 282 Units 263705 MWe , Boiling Water Reactors (BWR: 78 Units 75 208 MWe) and in a less extend by Light Water cooled Graphite moderated Reactor (LWGR: 15 Units 10 219 MWe). By end of 2015, 68 units are under construction among them 58 PWR and 4 BWR. Currently the Fast Neutron Systems, connected to the grid, represents only 1369 MWe, with 3 Units (BN600, BN800 in Russia and FBTR in India). Three additional BFRs are in operation: CEFR in China, JOYO in Japan and BOR-60 in Russia) (1 369 MWe). One FBR is under commissioning: PFBR in India. All of them are cooled by sodium.

3.2. Fast Neutron Systems

A policy to preserve these natural uranium stocks needs therefore to be developed to sustain this renaissance. This is one of the main challenges facing Generation IV Fast Neutron Reactors and it will be the keystone on which the future of nuclear energy can be built.

This fourth generation will focus on fast reactors which are capable of converting a large majority of uranium-238 into plutonium-239 while producing electricity. In this way, it will become possible to exploit more than 90% of natural uranium to generate electricity, rather than only 0.5 to 1% in light water reactors. The large quantities of depleted and reprocessed uranium available in France could be used to maintain the current electricity production for several thousand years. The worldwide availability of primary fissile resources could thus be multiplied by more than 50. The construction of fast reactors will also open the door to unlimited plutonium recycling (multi-recycling) by taking advantage of its energy potential.

Radioactive waste management is yet another challenge facing Generation IV reactors which involves reducing the volume and the inherent long term radioactivity of final waste. These reactors may in fact be capable of burning some of the long lived radioactive elements contained in radioactive waste: minor actinides (americium, neptunium, curium, etc.).

Several main objectives have been defined to characterise the future reactor systems that must be: sustainability, safety and reliability, proliferation resistant, ability to resist to external hazards, cost effectiveness.

Generation IV forum [42] has selected six concepts, among them four Fast Neutron Spectrum Systems are deeply investigated, each of them being mainly characterized by its coolant: Sodium, Heavy Liquid Metal (Lead or Lead-Bismuth Eutectic), helium and molten salts. At the European level, three technologies are considered, related to sodium, heavy liquid metal and gas; SFR are considered as the reference option (Fig.3). During the forties, two other coolants were also considered: mercury (Hg) and sodium-potassium eutectic (Na-K). Each coolant is considered, due to its claimed attractive properties, which will be underlined in this paper, but the choice of a coolant induces challenges facing nuclear systems, related to design, operation, maintenance and decommissioning phase particularly due to radiation-chemistry, radiolysis, activation, and their consequences on operation, maintenance, and decommissioning of nuclear facilities.

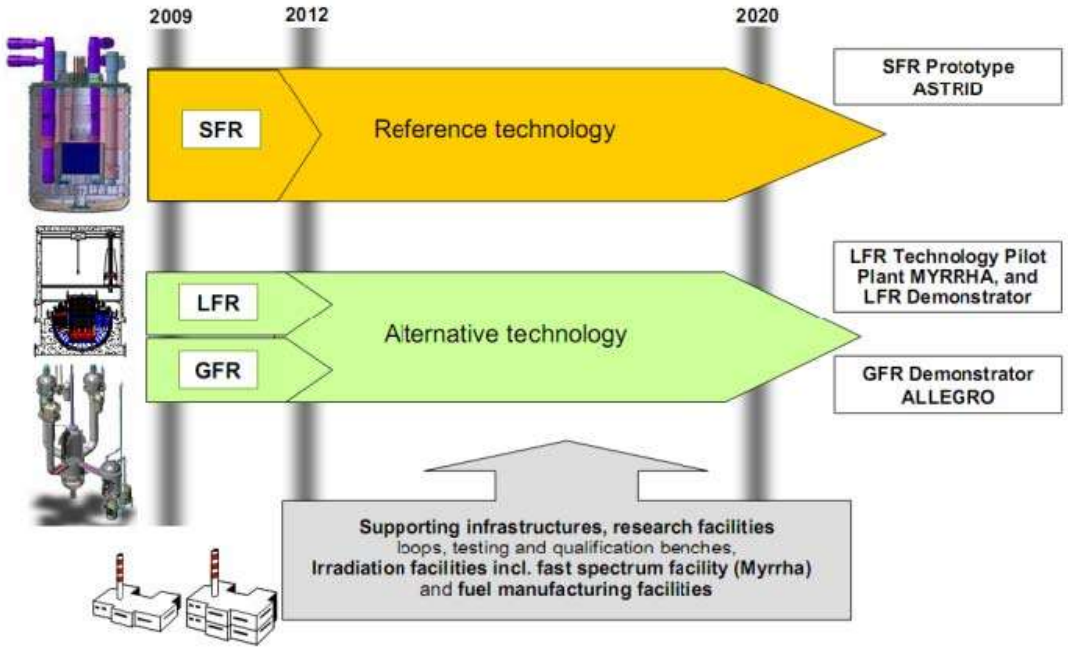

FIG. 3. European strategy for Fast Reactors [50].

3.3. Neutron spectrum

The most fundamental technological difference between nuclear fission reactors concerns the means by which the problem of sustaining a chain reaction is achieved. One solution is to slow down neutrons to so-called "thermal" energies (around 0.025 eV) by using a « moderator ». This has the advantage of allowing a chain reaction to be sustained using natural or slightly enriched uranium. The disadvantage of this approach is that only 0.7% of uranium produces useful energy. This can be overcome by increasing the proportion of fissile atoms by enrichment, or by using plutonium, and by constructing the reactor without a moderator. In this case the average energy of the neutrons in the core is much greater than in thermal reactors (they are known as "fast" neutrons). In Light Water Reactors (LWR), most of the fissions occur in the 0.1eV thermal peak (Fig 4) [43]. In Fast Neutron Reactors (FNR), moderation is avoided: there are no “thermal” neutrons. The comparison of fast neutron spectra for sodium, lead and gas in shown in Fig. 5 [43].

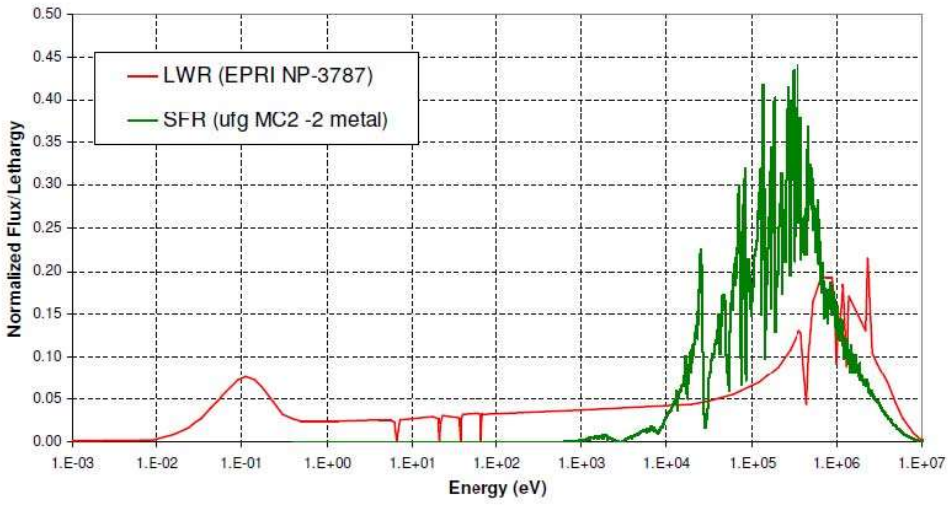

FIG 4. Comparison of LWR and SFR neutron spectra.

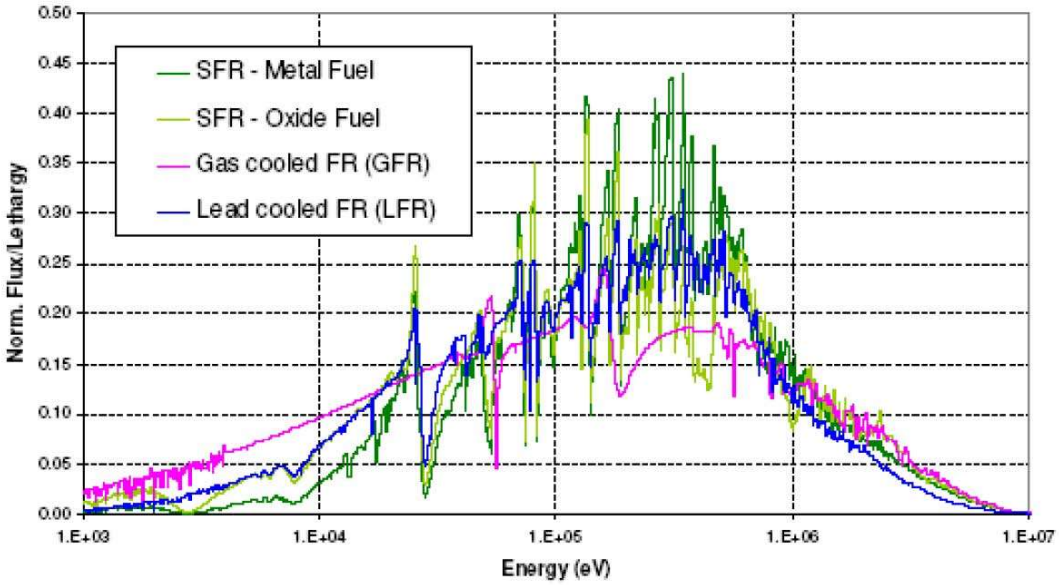

FIG 5. Comparison of fast neutron spectra for sodium (SFR), lead (LFR) and gas (GFR) cooled reactors.

3.4. Activation and contamination of coolant and structures

Environmental conditions and factors can affect materials behaviour relevant for the structural integrity of confinement barriers and components. These include the impact on mechanical properties from the environment such as local thermal hydraulic (such as flow distribution and mixing, temperatures distribution, stratification and instabilities, pressure variations, coolant structure interactions, etc.), but also liquid metal embrittlement as well as environmental assisted property effects, like corrosion and irradiation effects.

For the design of FNRs, it is mandatory to analyse the potential impact of the previous environmental effects and to bring design solutions to master their consequences, demonstrating the life duration of the reactor, i.e. 60 years, in safe operating conditions. Coolant can be also activated and/or contaminated by activated impurities already present in the coolant or generated during operation of the reactor or by fuel-cladding ruptures. Coolant radio-contamination and mass transfer created in the system, interaction between bulk and cover gas for liquid coolants induces issues relevant for radiological impact assessment, operation, including maintenance, inspection and handling, etc. The occurrence of activated corrosion products (ACP) generates the need of a mass transfer model able to predict the distribution of radio-activated species and to estimate dosimetry and requirements for cleaning and decontamination processes, required prior to inspection and repair or decommissioning. It is possible to control corrosion in liquid metal systems thanks to O control by appropriate processes (O-7, O10) (O-26 by Kharitonova).

Tritium is also a key issue for all fission systems, due to its ability to permeation through structural walls at high temperature (namely >400°C): in order to satisfy the release authorizations, it is necessary to mitigate the diffusion towards environment by appropriate means (O-5, O-10, O-11) i.e. cold trapping or diffusion barriers. For molten salts, soluble fission products are expected of course to appear in the coolant and have to be removed (O-5) i.e. 131I (O-5). For helium cooled systems (Gas Fast Reactors), it is necessary to control the corrosion and consequently the contamination by helium quality control, including O2, H2O, CO… Noble gases (Xe and Kr) and fission products, contaminated dust particles need also to be removed by adsorption and filtration (O-11).

3.5. Computational models and tools

Several tools to model ACPs mass transfer (O-10) have been developed in the recent years i.e. OSCAR in France for LWR, SFRs and even Fusion Systems (O6); tools for similar objectives for SFRs have been also developed in Russia, Japan or India. Tritium behaviour can be also modelled with TTT code (Japan) or KUTIM (France) (O-10), used also for other liquid metal systems. For Lead Bismuth Eutectic, used in Myrrha project (O-7), a global approach to predict radionuclide release/chemistry in LBE has been developed, based on the “MYrrha

THermochemical model" (MYTH), which allows to predict the dissolved, gas and condensed, and more particularly the polonium behaviour.

3.6. Consequences of coolant on operation, maintenance and decommissioning of nuclear facilities

Coolants are selected, due to their claimed attractive properties, which are underlined in the various presentations done during the seminar (O-5, O-7, O-10, O-11) but their behaviour is very different versus corrosion, mass transfer and consequently various processes need to be implemented. The choice of a coolant induces challenges facing nuclear systems, related to design, operation, maintenance and decommissioning phase particularly due to radiation-chemistry, radiolysis, activation, and their consequences on operation, maintenance, and decommissioning of nuclear facilities. For instance, each isotope exhibits unique activation properties during operation. It is essential to purify the coolant in order to control its quality and guaranty a safe operation. Cleaning and decontamination phases are required during maintenance or decommissioning. These steps are necessary prior to inspection, repair or removal of components and such operations produce effluents.

3.7. Summary of Coolants for Fission System

The following points briefly summarize some observations from the fission presentations:

— Sodium is considered the most mature liquid metal coolant worldwide;
— In addition to radio-activated impurities, LMs and MSs generate their own radioactive by-products;
— All coolants deal with corrosion and subsequent activated corrosion products (ACP), and more particularly heavy liquid metals, inducing the necessity to provide an efficient oxygen control process and the development of protective coating for different systems (except Na with stainless steels). These ACP contaminates structural material, and thus it is necessary to develop efficient and safe cleaning and decontamination processes, prior to in-service inspection and repair (ISIR) for components.
— The SFR's operational feedback has also highlighted that utilities have to take care of material susceptibility to different corrosion mechanisms (Stress Corrosion Cracking induced by caustic solution) during maintenance operation. These events are currently mitigated, thanks to appropriate operating procedures.
— Tritium, (produced by B4C, plutonium by ternary fissions, and even Pb-Bi itself by spallation) even if the output is very low compared to fusion, needs to be trapped with regards to environmental impact, inducing the necessity to develop efficient strategies to control it and associated mass transfer models to support their validation.
— For all coolants, it is necessary to develop efficient purification systems, well adapted to various impurities (O, H and T, ACP, fission products, dust in gas phase or particles in liquid phase…). For Pb-Bi, salts, more attention has to be paid to ^{210}Po, ^{233}Pa.
— For all coolants, it is necessary to develop an efficient strategy to remove the coolant and decontaminate it during maintenance phases or reactor dismantling.

TABLE 4. SUMMARY OF FISSION LIMITING CONSTRAINTS, RANGE OF USE FOR COOLANTS UNDER IRRADIATION, EXPERIMENTAL VERIFICATION, MAJOR ISSUES AND CHALLENGES, ACHIEVEMENTS, AND R&D NEEDS.

Coolant or Topic	Application	Limits of Use and Radiation Effects	Research Details, Major Issues, and Challenges	Achievements	R&D Needs
Liquid Metal (Na) (O-10)	6 reactors in operation (BOR-60, BN600, BN800, CEFR, FBTR, Joyo), and Gen-IV projects: BN1200, CFR600, FBR1-2, JSFR , ASTRID, PGSFR. (chemistry, dynamo, solar…)	97.8°C < *T* < ~600°C (governed by material behaviour), limited generalized corrosion, but potential SCC with aqueous NaOH after repair, chemical reactivity & related confinement. Na purification & treatment well mastered. **Main Radiation Effects**: Activation very limited (22Na (2.6y) and 24Na (15h) but necessity to use "nuclear grade" Na. Activated corrosion products (ACP) from the core: 54Mn, 60Co, 58Co… Fission products after pin rupture: 137Cs…	Very large reactors operational feedback (500+ reactor-years) (current ones, EBR2, FFTF, Phenix, SPX, KNK2, PFR, FBTR, BN350, JOYO). Experimental-theoretical studies: EU projects: CP-ESFR, ESNII+, SESAME, MATER… OECD-NEA Expert Group on LM, IAEA TECDOCs, CRP NAPRO, GIF. **Challenges related to the Topic**: ACP mass transfer modelling, tritium release control, Na leak detection, mitigation of Na fire, Na-H2O-air event	-ACP mass transfer models (PSYCHE, OSCAR-Na, and IPPE, IGCAR models…) -3H mass transfer models: KUTIM, TTT -Na-H2O models in various conditions - Na-fire models, - Atmospheric dispersion models including Na hydroxide aerosols carbonation - Development of efficient mitigation strategies at design stage of the reactors.	-Mechanistic corrosion models - Mass transfer models (i.e. OSCAR-Na) Codes: Metal oxides solubilities / Diffusion coefficients in steel / Particles production -Assessment of 3H source (B4C, Fuel) - Efficiency of RVC Cs trap models at very low concentrations - Chemical instrumentation /O,C - Na fragmentation phenomenological model to be included in Na fire models
Heavy Liquid Metal (Pb and Pb-Bi) (O-7)	In USSR, submarines with Pb-Bi. New projects: Pb: BREST300, BREST 1200, ALFRED (Italy & Romania), CLEAR (China), Pb-Bi: MRRHA, SVBR-100.	Pb: 325°C< T<500°C Pb-Bi: 124°C<T<400°C (governed by material behaviour), generalized corrosion, liquid metal embrittlement, Coolant velocity: < 2m.s-1 to avoid erosion. Necessity to use "nuclear grade" Pb, Pb-Bi. **Main radiation effects**: 210Po issue in Pb-Bi Activated corrosion products (ACP) from the structures and the core. Fission products after pin rupture	LFR technology cannot rely on the same large experimental database as SFR, except USSR Pb-Bi cooled submarines. Experimental-theoretical studies: EU projects: TECLA, HELIMNET, EUROTRANS, LEADER, GETMAT, ESNII+, SESAME, MATER, ARCADIA, MATISSE, SILER, FREYA…OECDNEA Expert Group on LM, IAEA TECDOCs, GIF. **Challenges**: -Predicting radionuclide release from LBE: – Very complex system: tens of interacting chemical elements → limited experimental verification – Currently, basic understanding release mechanisms only – Quantification release several safety-critical nuclides not yet possible, especially in accident conditions, which is in conflict with licensing large ADS, such as MYRRHA.	First global description of equilibrium chemistry in primary system of ADS (MRRHA) O control systems and dedicated instrumentation (Ometer) to control chemistry	– fundamental chemistry data of radionuclide chemical species – non-equilibrium release mechanisms – mapping uncertainties – chemistry system code development

TABLE 4. CONTINUED

Coolant or Topic	Application	Limits of Use and Radiation Effects	Research Details, Major Issues, and Challenges	Achievements	R&D Needs
Salt Fluoride Mixtures (O-5)	pSSC: EU MSFR, RF MOSART, US-FHR In most cases the base-line fuel / coolant salt is LiF, BeF2 and / or ThF4 based salt as it has best properties.	fuel salt in the primary circuit made of special Ni-alloy is mainly limited by Te IGC depending on salt Redox potential (750-800°C). Min temperature of fuel salt is determining its melting point and the AnF3 solubility (550-600°C). **Main Radiation Effects:** In reactor tests strongly suggested that the F2 generation had at the high temperature not occurred (gas was generating mainly via reaction 6Li(n,α)T), but had occurred by radiolysis of the mixture in the solid state. F2 evolution at 35°C corresponded to about 0,02 mol. per 100 eV absorbed, could be completely stopped by heating to 100°C or above, and could be reduced by chilling to -70°C.	tritium to diffuse through hot metals will permit a large fraction of the 3H2 to penetrate the primary heat exchanger to enter the secondary coolant.	removal by the sparging of Xe, Kr; addition of U and TRUs to replace that lost by burnup; in situ production of UF3 to keep the Redox potential of the fuel at the desired level; recycling of all An's, removal of rare earths; isolating 233 Pa; removal of inadvertent oxide contaminants from the fuel; addition of ThF4 and removal of a portion of the insoluble noble FP's.	necessary to establish what fraction of the uranium may be present as UF3 without deleterious chemical reactions of the UF3 with other materials within the fuel circuit (2) Details of behaviour of the noble and semi-noble FP's are still poorly known (3) The technology necessary to limit to acceptable levels the rate at which tritium is released from MSR is required.
Helium (O-11)	ALLEGRO – helium cooled experimental fast reactor	• Membrane separation of helium from Guard vessel atmosphere. Limits of Use: dependent on the chosen membrane • **Helium purification** Limits of Use: governed by selected materials in technological steps • **Material testing** Limits of Use: Temperature: 25900°C; Pressure: 37MPa; impure helium atmosphere	– Simulation of membrane separation system in the large scale. The proposed helium/nitrogen gas mixture with flow rate 200L/min. – Development of borosilicate membrane module. – Determination of helium content on Guard vessel which will be an economic advantage for helium regeneration in order to state the efficient operational regimes. – Improved seal testing and certification. – Continuation of material testing in HTHL loop.	Mastering the purification methods for helium and start up of preparation for HTHL integral tests. Development of improved He flange joint seal.	Development of borosilicate membrane module.
Water (P-1)	Nuclear Power Plants	High concentration of boric acid (about 12g/l) in the primary cooling system must be removed prior to analysis of selected radionuclides (Sr-90, Tc-99).	Experimental experiences. 1. Evaluation of the fuel rod tightness based on analysis of fission products in fuel 2. Determination of the possibility of reducing the radiation dose received by power plant personnel from the corrosion products of primary circuit materials	Analytical methods were developed for monitoring radionuclides in primary cooling system (including corrosion products).	1. Selective radionuclides extraction methods from water of primary cooling system and fuel storage tanks 2.Determination of radionuclides transfer coefficients in the ecosystem.

TABLE 4. CONTINUED

Coolant or Topic	Application	Limits of Use and Radiation Effects	Research Details, Major Issues, and Challenges	Achievements	R&D Needs
Water (P-1)	Nuclear Power Plants	High concentration of boric acid (about 12g/l) in the primary cooling system must be removed prior to analysis of selected radionuclides (Sr-90, Tc-99).	Experimental experiences. 1. Evaluation of the fuel rod tightness based on analysis of fission products in fuel 2. Determination of the possibility of reducing the radiation dose received by power plant personnel from the corrosion products of primary circuit materials 3. Development of improved technologies for decontamination of devices of primary cooling system 4. Evaluation of the efficiency of ion exchangers for the purification of cooling water.	Analytical methods were developed for monitoring radionuclides in primary cooling system (including corrosion products).	1. Selective radionuclides extraction methods from water of primary cooling system and fuel storage tanks 2. Determination of radionuclides transfer coefficients in the ecosystem.
OSCAR Code for ACP of Na	• Fusion reactor cooling water	1.Formation of ACPs under neutron flux 2.Contamination of	• OSCAR-Fusion: Cu alloy added • OSCAR-Na: Specific	Adaptation of OSCAR (modular code) to different	• **Fusion**: Simulation of pulsed mode / Corrosion of Cu

4. THE SPALLATION SYSTEM

4.1. Background

Spallation targets are developed and implemented to produce fast neutrons, used for basic research or nuclear wastes transmutation (see Table 5) [45]. Partitioning and Transmutation (P&T) techniques could contribute to reduce the radioactive inventory and its associated radio-toxicity. Sub-critical Accelerator Driven Systems (ADS) are potential candidates as dedicated transmutation systems, and thus their development is a relevant Research and Development topic in Europe. A key component is the spallation target, which produces fast neutrons, able to transmute long-live nuclear wastes i.e. minor actinides produced in Light Water reactors. A key experiment in the ADS roadmap, the MEGAwatt PIlot Experiment (MEGAPIE) (1 MW) was initiated in 1999 and supported by an international group of research institutions in order to design and build a liquid lead-bismuth spallation target, then to operate it into the Swiss spallation neutron facility SINQ at Paul Scherrer Institute (PSI) [46];

Several targets have been developed and are in operation: SNS (ORNL-USA), JSNS (JAEA-Japan), SINQ (PSI-Switzerland), ISIS (RAL-UK) cooled by Hg, Pb-Bi, H2O (Figs. 6) see Fig. 7 [45]. New sources are currently being built: ESS (ESS-SWEDEN Denmark and Europe) cooled by He, and CSNS (China) cooled by Pb-Bi. More recently (O-29byRamos) in CERN, new projects intend to use Na or NaF:LiF eutectic (39:61 mol.%) as potential coolants for a tungsten solid target.

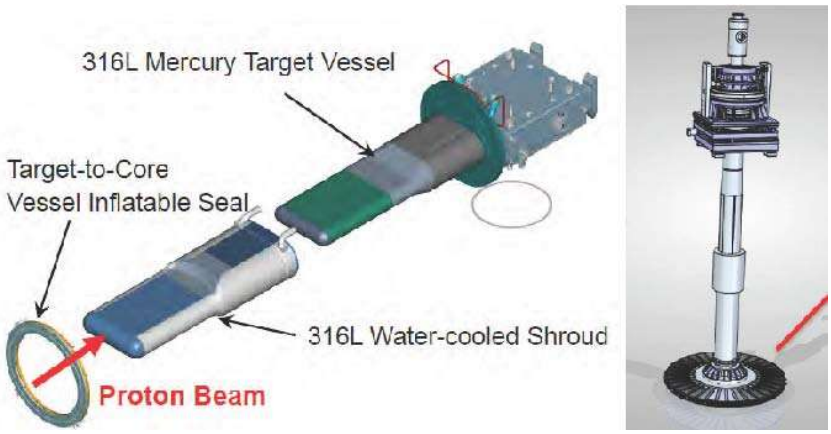

FIG 6. SNS Target (Courtesy of ORNL). ESS Target (Courtesy of ESS).

Facility	Status / rep. rate	Energy	Target Type / Time structure	Coolant	Power Level [kW]	Additional Information
IPNS (ANL)	decom. 30 Hz	0.450	Solid SP	H_2O	7	Depl. U / W
ISIS TS 1 (RAL)	running 50 Hz	0.800	Solid SP	H_2O	100 - 200	Depl. U / Ta / W-Ta clad
ISIS TS 2 (RAL)	running 10 Hz	0.800	Solid SP	H_2O	48	W-Ta clad
Lujan Center (LANL)	running 20 Hz	0.800	Solid SP	H_2O	100	W
KENS (KEK)	decom. 20 Hz	0.500	Solid SP	H_2O	3	W-Ta clad
SINQ (PSI)	running 51 MHz	0.575	solid/liquid CW	D_2O/LBE	800 – 1000	Zr / Pb-SS clad / Pb-Zr clad / LBE
SNS (ORNL)	running 60 Hz	1.000	Liquid SP	Hg	1000	1.4 MW design
JSNS (J-PARC)	running 25 Hz	3.000	Liquid SP	Hg	1000	1.0 MW design

Thorium Energy Conference 2013 (ThEC13), 27 – 31 October 2013, CERN, Switzerland

FIG.7. Spallation Targets Producing Fast Neutrons [45].

4.2. Neutron spectrum

As an example, in Fig 8 related to MEGAPIE Target (O-7), the neutron spectrum measured by different means is described in [47,48].

4.3. Activation and contamination of coolant and structures:

As in fission systems, environmental conditions and factors can affect materials behaviour relevant for the structural integrity of confinement barriers and components, and coolant can be also activated and/or contaminated (O-7, O-11). Chemical analyses of the integral MEGAPIE experiment remain the most important experience feedback to qualitatively check model predictions and also to contribute to the definition and preparation of the decommissioning and waste management procedure [46, 49].

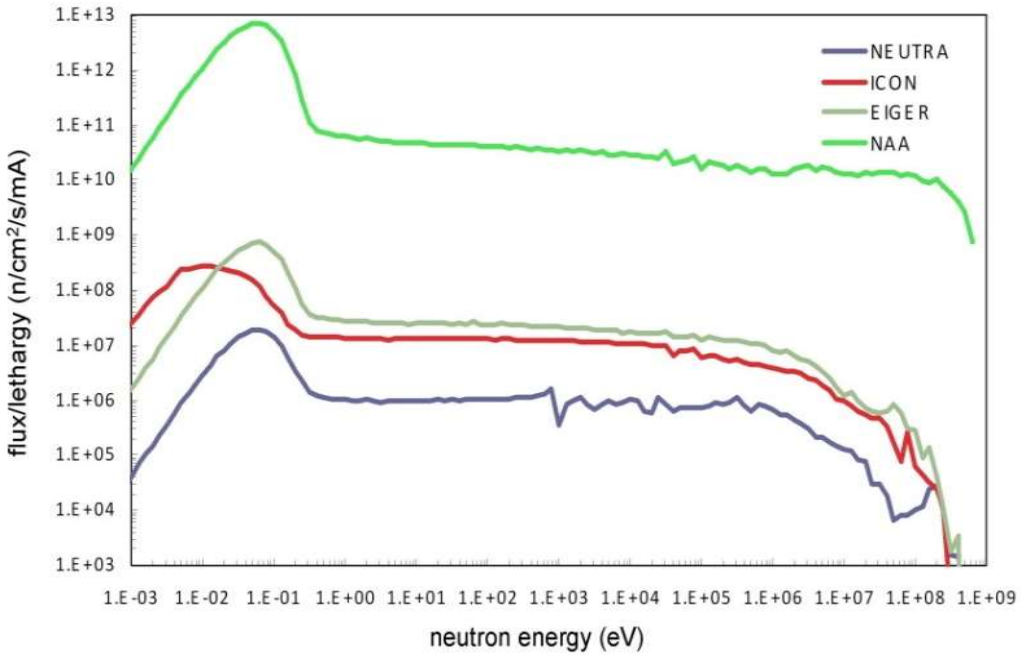

FIG 8. MEGAPIE Target Mapping of the neutron flux in its different ranges (thermal, epithermal, fast) in the SINQ facility around the target.

4.4. Computational models and tools:

"MYrrha THermochemical model" (MYTH) allows to predict the dissolved, gas and condensed, and more particularly the Polonium behaviour in Pb-Bi liquid coolant of the target. A Chemistry system code, able to support the design of O-control and Pb-Bi purification is missing and needs to be developed.

4.5. Summary of Coolants for Spallation System

The following points briefly summarize some observations from the spallation presentations:

— All fission points are also relevant for spallation system.
— Additionally, it is mandatory to address the key issues induced by the presence of many spallation products and to develop the knowledge related to their physical and radiochemical behaviour in the coolant (Pb-Bi, He).
— A special focus is requested for ^{210}Po (Pb-Bi cooled targets) and dust (He cooled targets).
— Experiments showed that tungsten oxide layer is resistant to He-flow (share stress < 100Pa) and will not produce tungsten oxide particles.

4.6. Concluding Remarks

Efforts of researchers in the U.S., Europe, Russian Federation, Japan, China, Canada, India, and other countries were significant in recent decades and crucial to all nuclear systems. Innovative designs have been developed, identifying knowledge gaps for numerous coolants, launching R&D activities, and outlining strategies to achieve technological solutions that satisfy the design requirements. Such impressive efforts will continue worldwide in the future to overcome challenges identified (see Table 5) for the prominent coolant of each nuclear system.

TABLE 5. SUMMARY OF SPALLATION LIMITING CONSTRAINTS, RANGE OF USE FOR COOLANTS UNDER IRRADIATION, EXPERIMENTAL VERIFICATION, MAJOR ISSUES AND CHALLENGES, ACHIEVEMENTS, AND R&D NEEDS.

Coolant or Topic	**Application**	**Limits of Use and Radiation Effects**	**Research Details, Major Issues, and Challenges**	**Achievements**	**R&D Needs**
Helium (O-11)	European Spallation Source ERIC Target System	Spallation Material – Tungsten max 500°C Cooling Media – Helium 40°-240°C 11 bar **Main Radiation Effects** (unmitigated/mitigated) : Pipe rupture: -Workers 250 / 2.8 mSv - Public 0.05 / 0.05 mSv LOCA: -Workers 579 **Sv** / 0 mSv - Public 75 / 0.05 mSv	No tungsten oxide erosion in lab with Target System operation conditions **Challenges**: First of its kind – tungsten spallation source/helium cooling facility	Coolant Processing and Handling: Helium 11 bar 3 kg/s. No tungsten oxide erosion within the Target System conditions	– Design of helium filter equipment
Pb-Bi (O-7)	MEGAPIE, TEF-T; MYRRHA & CLEAR ADS	**Constraints**: 125°C (solidification) < *T* < ~400°C (material compatibility), activation. **Main Radiation Effects:** Coolant activation and related safety issues	Experimental-theoretical. MYRRHA R&D+ EU projects EUROTRANS, SEARCH, MYRTE; MEGAPIE; IPPE, JAEA studies. **Major Issues and Challenges** Predicting radionuclide release from LBE: – Very complex system:	First global description of equilibrium chemistry in primary system of ADS.	– Fundamental chemistry data of radionuclide chemical species – Non-equilibrium release mechanisms – Mapping uncertainties – Chemistry system code

REFERENCES

[1] EL-GUEBALY, L., "History and Evolution of Fusion Power Plant Studies: Past, Present, and Future Prospects." Chapter 6 in book: Nuclear Reactors, Nuclear Fusion and Fusion Engineering. A. Aasen and P. Olsson Editors. NOVA Science Publishers, Inc.: Hauppauge, New York, USA. ISBN: 978-1-60692-508-9 (2009) 217–271.

[2] ITER, https://www.iter.org

[3] EL-GUEBALY, L., BOCCACCINI, L.V., KURTZ, R.J., WAGANER, L.M., Technology-Related Challenges Facing Fusion Power Plants," Chapter in book: Fusion Energy and Power: Applications, Technologies and Challenges. NOVA Science Publishers, Inc.: Hauppauge, New York, USA. (2015).

[4] MALANG, S., et al., Development of the lead lithium (DCLL) blanket concept, Fusion Science and Technology **60** (2011) 249.

[5] NAJMABADI, F. and THE ARIES TEAM, Spherical torus concept as power plants – the ARIES-ST study, Fusion Engineering and Design **65** (2003) 143–164.

[6] RAFFRAY, R. A., EL-GUEBALY, L., et al., 'Engineering Design and Analysis of the ARIES-CS Power Plant, Fusion Science and Technology **54** 725 (2008).

[7] KESSEL, C., et al., The ARIES Advanced and Conservative Tokamak (ACT) Power Plant Study, Fusion Science and Technology **67** (2015) 1–21.

[8] KESSEL, C., BLANCHARD, J.P., DAVIS, A., EL-GUEBALY, L., et al., The Fusion Nuclear Science Facility (FNSF), the Critical Step in the Pathway to Fusion Energy, Fusion Science and Technology **68** (2015) 225–236.

[9] MENARD, J., BROWN, T., EL-GUEBALY L., et al., Fusion Nuclear Science Facility and Pilot Plants Based on the Spherical Tokamak, Nuclear Fusion **56** (2016) 106023.

[10] FEDERICI, G., et al., Overview of the design approach and prioritization of R&D activities towards EU DEMO, Fusion Engineering and Design **109–111** (2016) 1464–1474.
[11] BOCCACCINI, L.V., et al., Objectives and status of EUROfusion DEMO blanket studies, Fusion Engineering and Design **109–111** (2016) 1199–1206.
[12] AUBERT, J., et al., Development of water cooled lithium lead blanket for DEMO, Fusion Engineering and Design **89** (2014) 1386–1391.
[13] SARDAIN, P., et al., The European power plant conceptual study: helium cooled lithium lead reactor concept," Fusion Engineering and Design **81** (2006) 2673–2678.
[14] AIELLO, G., et al., HCLL TBM design status and development, Fusion Engineering and Design **86** (2011) 1444–1450.
[15] AIELLO, G., et al., Development of helium cooled lithium lead blanket for DEMO, Fusion Engineering and Design, 89 (2014) 2129–2134.
[16] SAGARA, A., et al., Helical reactor design FFHR-d1 and c1 for steady-state DEMO, Fusion Engineering and Design **89** (2014) 2114–2120.
[17] ENOEDA, M., TANIGAWA, H., HIROSE, T., NAKAJIMA, M., SATO, S., et al., R&D status on water cooled ceramic breeder blanket technology, Fusion Engineering and Design **89** (2014) 1131–1136.
[18] WU, Y., Overview of liquid lithium lead breeder blanket program in China, Fusion Engineering and Design **86** (2011) 2343–2346.
[19] FENG, K.M., ZHANG, G.S., HU, G., CHEN, Y.J., FENG, Y.J., et al., New progress on design and R&D for solid breeder test blanket module in China, Fusion Engineering and Design **89** (2014) 1119–1125.
[20] MALANG, S., et al., An example pathway to a fusion power plant system based on lead– lithium breeder: Comparison of the dual-coolant lead–lithium (DCLL) blanket with the helium cooled lead–lithium (HCLL) concept as initial step, Fusion Engineering and Design **84** (2014) 2145–2157.
[21] HUMRICKHOUSE P.W., MERRILL, B.J., Vacuum permeator analysis for extraction of tritium from DCLL blankets, Fusion Science and Technology **68** (2015) 295–302.
[22] GARCINUÑO B., et al., Design of a Permeator Against Vacuum for Tritium Extraction from Eutectic Lithium-Lead in a DCLL DEMO, Fusion Engineering and Design **117** (2017) 226–231.
[23] OKINO F., et al., Feasibility Analysis of Vacuum Sieve Tray for Tritium Extraction in the HCLL Test Blanket System, Fusion Engineering and Design **109–111** (2016) 1748–1753.
[24] EL-GUEBALY, L., ROWCLIFFE, A., MENARD, J., BROWN, T., TBM/MTM for HTS-FNSF: An Innovative Testing Strategy to Qualify/Validate Fusion Technologies for U.S. DEMO, Energies **9** (2016) 632.
[25] SAWAN, M., Damage Parameters of Structural Materials in Fusion Environment Compared to Fission Reactor Irradiation, Fusion Engineering and Design **87** (2012) 551–555.
[26] ROBINSON, A., EL-GUEBALY, L., HENDERSON, D., W-Based Alloys for Advanced Divertor Designs: Detailed Activation and Radiation Damage Analyses, University of Wisconsin Fusion Technology Institute Report, UWFDM-1378 (2010).
[27] EL-GUEBALY, L., KURTZ, R., RIETH, M., KURISHITA, H., ROBINSON, A., W-Based Alloys for Advanced Divertor Designs: Options and Environmental Impact of State-of-the-Art Alloys, Fusion Science and Technology **60** (2011) 185–189.
[28] NAJMABADI, F., et al., Overview of ARIES-RS reversed shear power plant study, Fusion Engineering and Design **38** (1997) 3–25.
[29] NAJMABADI, F., et al., The ARIES-AT Advanced Tokamak, Advanced Technology Fusion Power Plant, Fusion Engineering and Design **80** (2006) 3–23.
[30] HENDERSON, D., EL-GUEBALY, L., WILSON, P., ABDOU, A., Activation, Decay Heat, and Waste Disposal Analysis for ARIES-AT Power Plant, Fusion Technology **39** 444 (2001).
[31] PETTI, D., MERRILL, B., MOORE, R., LONGHURST, G., EL-GUEBALY, L., et al., Safety and Environment Assessment of ARIES-AT, Fusion Technology **39** (2001) 449–457.
[32] McCAD code by KIT, https://github.com/McCadKIT/McCad
[33] DAGMC Users Guide, University of Wisconsin-Madison Fusion Technology Institute (2008), http://svalinn.github.io/DAGMC/usersguide/
[34] MCAM code by FDS team, http://www.fds.org.cn/en/software/mcam_1.asp

[35] MCNP X-5 MONTE CARLO TEAM, MCNP–A General Monte Carlo N-Particle Transport Code, Version 5, Volume I: Overview and Theory, LA-UR-03-1987; Volume II: User's Guide, LA-CP-03-0245; Volume III: Developer's Guide, LA-CP-03-0284, Los Alamos National Laboratory (2005).
[36] FORREST, R.A., "FISPACT 2007: User Manual", UKAEA FUS 534 (2007).
[37] WILSON, P., HENDERSON, D., ALARA: Analytic and Laplacian Adaptive Radioactivity Analysis: A Complete Package for Analysis of Induced Activation, University of Wisconsin Fusion Technology Institute Report. Volume I - UWFDM-1070, Volume II - UWFDM-1071 (1998).
[38] The ACAB Code, http://www.oecd-nea.org/tools/abstract/detail/nea-1839/
[39] MAJERLE, M., et al., Verification and Validation of the R2Smesh Approach for the Calculation of High Resolution Shutdown Dose Rate Distribution, Fusion Engineering and Design **87** (2012) 443–447.
[40] DAVIS, A., SAWAN, M., MARRIOTT, E., WILSON, P., Final Report on Tokamak Cooling Water System Water Activation, UD ITER report (2017).
[41] ELECTRONUC Nuclear Power Plants in the world Edition, CEA (2016).
[42] ABONNEAU, T., et al., "French GEN IV program: an overview of the situation and the next steps", FR17 Conference (Proc. Int. Conf. Yekaterinburg, 2017).
[43] SALVATORES, M., "Education & Training Seminar on Fast Reactor Science and Technology", IAEA Consultancy Meeting, ITESM Mexico (2015)
[44] GENIN, J.B., BRISSONNEAU, L., "Validation Against Sodium Loop Experiments of Corrosion Product Contamination Code OSCAR-Na", FR17 Conference (Proc. Int. Conf. Yekaterinburg, 2017).
[45] RIEMER, B., WOHLMUTHER, M., et al., "Spallation target developments", ThEC13 Conference (Proc. Int. Conf. Geneva, 2013).
[46] LATGE, C., WOHLMUTHER, M., et al., "MEGAPIE: the world's first high-power liquid metal spallation neutron source", ThEC13 Conference (Proc. Int. Conf. Geneva, 2013).
[47] PANEBIANCO, S., "Neutronic performances of the MEGAPIE target", International Conference on Nuclear Data for Science and Technology (Proc. Int. Conf. Nice, 2007).
[48] ZANINI, L., et al., Experience from the Post-Test Analysis of MEGAPIE, J. Nucl. Mater. **415** (2011)
[49] HAMMER, B., SCHUMANN, D., NEUHAUSEN, J., WOHLMUTHER, M., TÜRLER, A., Radiochemical determination of polonium in liquid metal spallation targets, Nucl. Data Sheets **119** (2014) 280–283.
[50] European Sustainable Nuclear Industrial Initiative, http://www.snetp.eu/esnii/

CHALLENGES AND R&D NEEDS FOR PB-LI COOLANT FOR FUSION APPLICATIONS

M. UTILI, A. TINCANI, M. TARANTINO
ENEA FSN-ING C.R.,
Camugnano (BO)

D. MARTELLI, G. BARONE, A. VENTURINI
University of Pisa, Dipartimento di Ingegneria Civile e Industriale,
Pisa

F. DIFONZO
Nano2Energy Laboratory Centre for Nanoscience and Technology Polimi Istituto Italiano di Tecnologia,
Milano

Italy

T. HERNANDEZ
CIEMAT, Fusion Technology Division,
Madrid, Spain

M. KORDAC, L. KOSEK, L. VALA, T. MELICHAR
Centrum výzkumu Řež,
Husinec-Řež, Czech Republic

C. MISTRANGELO, L. BUEHLER, J. KONYS
Karlsruhe Institute of Technology,
Karlsruhe, Germany

Abstract

The Lead Lithium Eutectic (LLE) alloy, Pb–16Li enriched at 90% in 6Li, is the candidate Tritium breeder and carrier of three out of four Breeding Blanket (BB) concepts proposed for DEMO Thermonuclear Tokamak Reactor: WCLL (Water Cooled Lithium Lead), DCLL (Dual Coolant Lithium Lead) and HCLL (Helium Cooled Lithium Lead) BBs. In the case of DCLL BB the LLE is used also as a coolant. The other main functions of LLE systems are: (i) to circulate the liquid LLE through the blanket; (ii) to extract the Tritium produced inside the breeder modules from LLE (this function is shared with the Tritium Extraction System); (iii) to control LLE chemistry and to remove accumulated impurities; and (iv) to avoid Tritium permeation into primary coolant. Several technological issues are still open in the design of LLE loops, such as the corrosion of structural materials, magnetohydrodynamic (MHD) effect, buoyancy effect, design of pumping system, heat exchanger and Tritium Removal System, chemistry management and integration of all the systems in the tokamak building. Moreover, due to the melting point of LLE (234°C), corrosion/erosion characteristic, opacity and high density, the conventional instrumentation cannot be used to measure pressure, mass flow rate, velocity, level, temperature and to control the chemistry. In ITER Research Reactor a LLE BB concept will be qualified: a HCLL Test Blanket Module, with LLE loop, instrumentations and auxiliary systems, will be characterized with the support of European infrastructures. However, even if ITER will play a crucial role in the qualification of some LLE components and systems, some crucial aspects will not be investigated and therefore R&D activities are requested to solve LLE technical issues. The present work aims to analyse the challenges and R&D needs for LLE coolant and breeder for DEMO reactors, describing the actual status of technologies and activities performed in the European roadmap.

1. INTRODUCTION

Fusion reaction is commonly considered as one of the most promising sources of clean, safe and abundant energy. Among several possible reactions, the reaction between Deuterium and Tritium is the most practical from a physical point of view [1]: it has the highest cross section and its maximum is at the lowest energy (and thus plasma temperature) among all fusion reactions. Nevertheless, Tritium does not exist in nature and it has to be created by inducing reactions of neutron capture in a Li-containing material (breeder material) [1]. One of the most suitable choice as breeder material is the eutectic alloy Lead Lithium (LLE), in which Li is enriched at 90% in ^{6}Li. This liquid alloy has been proposed as breeder material in 3 concepts of Breeding Blanket for DEMO reactor: Helium Cooled Lithium Lead (HCLL) [2], Water Cooled Lithium Lead (WCLL) [3] and Dual Coolant Lithium Lead (DCLL) [4]. The last concept adopts LLE also as coolant material, with Helium as additional coolant. Table 1 presents the operative conditions of these BB concepts.

Using LLE as coolant leads to several technological issues: material compatibility, particularly corrosion issues [5], and removal of corrosion products [6], magnetohydrodynamic issues [7], Tritium related issues, e.g., mass transfer characteristic parameter [8] and inventory in the materials [9,10], removal of irradiation products (He generated by neutron capture in Li [11] and corrosion activated products [6]), PbLi-water interaction [12] (only in WCLL BB) and development of mitigation strategies such as anti-corrosion and permeation coatings [13,14]. Moreover, the conventional instrumentation cannot be used in flowing PbLi as a consequence of the combination of PbLi features: high melting point (234°C [15]), high density (about 9850 kg/m3 at 300°C [16]), corrosion/erosion characteristics and opacity.

This section describes technology issues and R&D needs, presenting the actual status of technologies and activities performed in the European roadmap.

TABLE 1. OPERATIVE CONDITIONS OF THE THREE BBS THAT ADOPT PBLI AS BREEDER AND/OR COOLANT

Parameters	DCLL BB	WCLL BB	HCLL BB
BB total volume [m^3]	891	844	743
Total LLE mass flow rate [kg/s]	26466	956	894
Recirculation/day	265	10	11
LLE velocity [m/s]	0.005-0.17	0.005-0.01	0.005-0.01
LLE outlet temperature [°C]	530/550	326	300
Max T at LLE/EUROFER interface [°C]	530/550	350-450	540
HT pressure [Pa]	<0.1	40-60	~30
LLE operative pressure [MPa]	0.3-3.0	0.3-3.0	0.3-3.0
Corrosion rate [µm/y]	~ 240 (at 540°C, 0.17m/s)	1.58 (at 330°C)	0.95 (at 300°C)
BB lifetime [y]	5	5	5

2. LLE TECHNOLOGY

The circulation of the LLE in the BB concepts is provided by inboard and outboard loops. The preliminary design of LLE loops layout as well as their integration in the tokamak building is still an on-going activity. The project is based on the following main functional requirements:

— To remove the nuclear heating generated into the BB (DCLL);
— To convey outside the Tritium generated inside the breeder modules (DCLL, HCLL, WCLL);
— To control the coolant chemistry and remove accumulated impurities (DCLL, HCLL, WCLL);
— To ensure gravitational draining of the BB modules and of the LLE loop (DCLL, HCLL, WCLL);
— To mitigate potential overpressures of the liquid metal (DCLL, HCLL, WCLL).

The preliminary design of DCLL, HCLL, and WCLL LLE loops (status 2016) was proposed in [17,18]. The foreseen LLE average temperature is 417.3°C for the DCLL and 300°C for the WCLL and HCLL concepts. In Fig. 1 the DCLL preliminary P&ID is reported. Considering the 2015 DCLL BB design (18 sectors), 12 LLE loops are foreseen (9 for the outboard BB and 3 for the inboard BB).

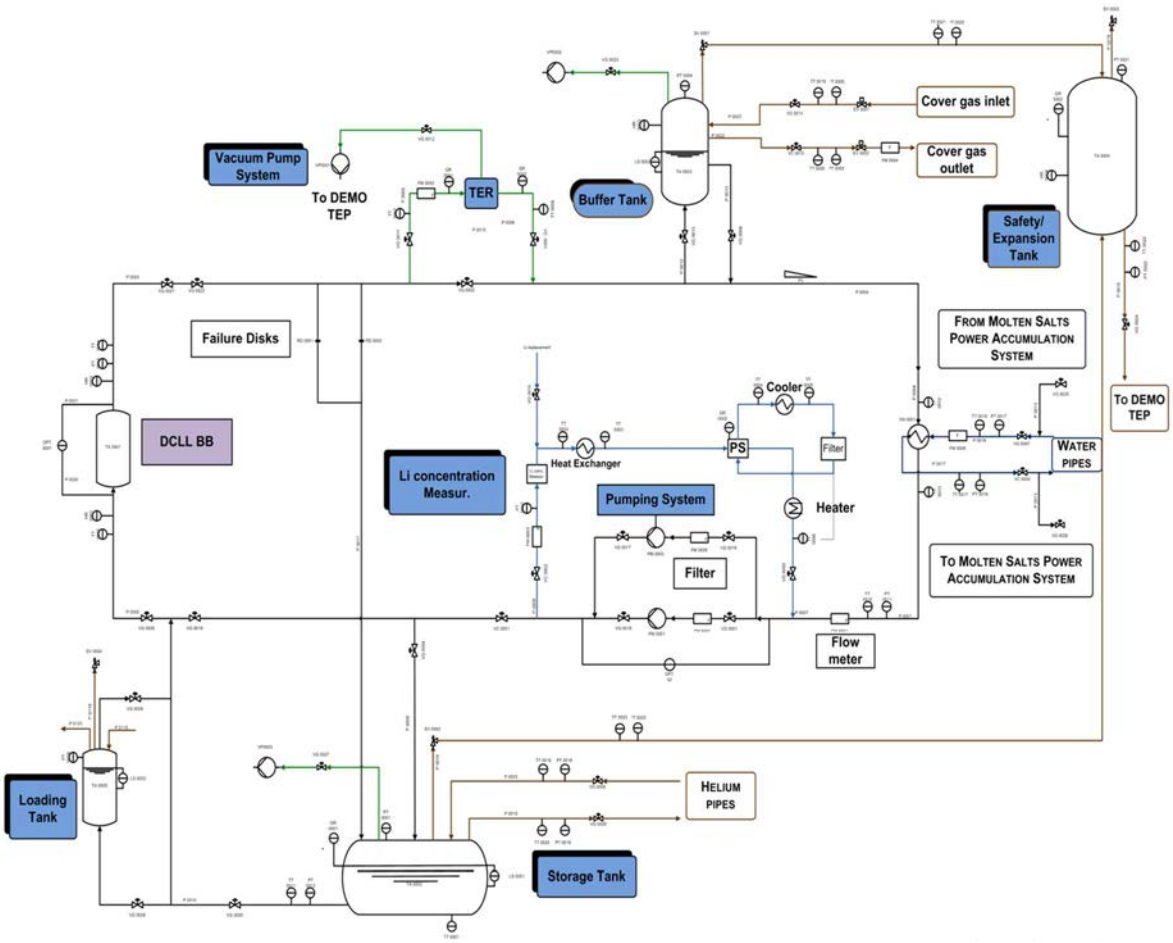

FIG. 1. DCLL Preliminary layout.

During normal operation of the system, the LLE returns from the BB to the LLE loop and is conveyed towards the Tritium Extraction and removal System (TES) [19] placed in the hot part of the loop. As a primary assumption, the LLE mass flow rate managed by the TES is the 100% in order to maximize the Tritium extracted. Nevertheless, control valves are foreseen allowing modulating the LLE flow rate towards the TES. Downstream the TES the LLE passes through the expansion vessel in order to discharge the helium bubbles produced inside the BB. The velocity in the buffer tank has to be reduced in the range of 10-100 mm/s to maximize the release of He. Then, LLE is cooled down to about 300°C [17] (286°C [18]) for the DCLL concept.

The mechanical pump is positioned in the cold part of the loops of the 3 BB concepts. Instead, the LLE Purification System (PS) is foreseen as a by-pass line of the pumping system and the adjustment of the amount of liquid metal sent to the PS is performed by regulation valves.

During non-operational phases the LLE is stored in dedicated storage tanks located in the lower part of the circuit. Each tank is connected to the piping of the loop through two separated lines, one dedicated to normal draining operation (draining of the system by gravity) and the other dedicated to fast drainage procedure. This line is equipped with failure disks that allow the draining of the circuit in the case of an accidental scenario (e.g. BB-LOCA).

3. MHD EFFECT

When an electrically conducting fluid, such as LLE, flows inside a strong magnetic field, such as the one that is used to confine plasma in the fusion reaction [20], currents are induced in the fluid. These currents, in turn, induce a magnetic field. As a consequence, several magnetohydrodynamic effects arise [21]. The induced Lorentz force has globally an opposite direction with respect to the flow leading to MHD pressure drops, which are dependent on flow velocity and intensity of the magnetic field. Pressure drops affect the design of PbLi loop and, in particular, of the pumping system. Moreover, the Lorentz force has a different direction in the centre of the pipe and near the pipe wall. This, in combination with the buoyancy effect generated by the heat transfer, causes a change in the velocity profile and therefore of the corrosion rate. The magnetic field modifies the turbulence and, therefore, mass and heat transfer. Also, T permeation is strongly dependent on the velocity profile, with different transport models towards the secondary fluid and the vacuum vessel.

A better comprehension of these MHD phenomena is necessary to achieve a better design of the LLE loop and of the auxiliary systems. 3D CFD analyses and experimental studies on BB mock-ups are being carried out, using also more sophisticated mathematical models, with the aim to fulfil this goal. Figure 2 shows some examples of the analysis methods used in this task. However, a 3D Multiphysics tool which can analyses the combination of MHD, heat transfer, tritium permeation is mandatory in order to predict the pressure drops, LLE velocity profiles and Tritium permeation into BB. A benchmark of the code with experimental results will be required in order to validate the code. Examples of analyses performed experimentally and with 3D CFD codes are in Figs 2–4.

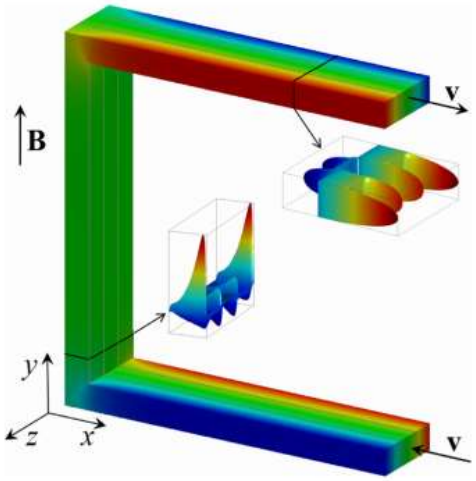

FIG. 2. 3D CFD modelling of velocity profile with Electro-magnetic flow coupling [22].

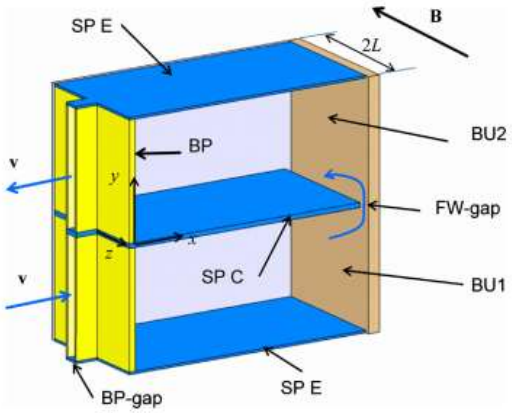

FIG. 3. Scheme of the breeding units of a HCLL BB mock-up [23].

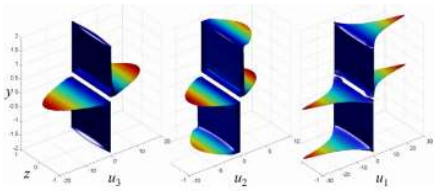

FIG. 4. Profiles of radial velocity u (x), u (x) and u (x) at three positions [23].

4. LLE CORROSION

The use of LLE and RAFM steels in fusion applications requires a better understanding of material compatibility related to physical/chemical interaction in the required temperature range. In steel/LLE system, the associated corrosion phenomenon is known as a “liquid metal attack”. Experimental and theoretical studies [19, 24-27] of corrosion of structural materials performed in the last thirty years have revealed various deterioration mechanisms related to the liquid metal attack including dissolution of the main steel constituents, formation of intermetallic compounds, penetration of liquid metal along grain boundaries and leaching of particular steel constituents. Due to the high solubility of Nickel in Pb-16Li is not possible to use AISI 316 as structural materials for piping and main components. Chromium steel or compatible material with lead lithium must be used, which required post-welding treatment. Operative working window of RAFM and SS is shown in Fig. 5. In the case of RAFM/LLE (e.g., EUROFER), the key mechanism is the uniform dissolution of Iron and Chromium in the flowing LLE.

The impact of corrosion includes deterioration of the mechanical integrity of the structural material due to the wall thinning, as well as serious concerns associated with the transport of corrosion products throughout the liquid metal loop. The activated corrosion products transported by the flowing LLE can precipitate in localized regions where corrosion concentration exceeds the solubility level giving rise to plugging phenomena.

Available experimental data on the mass loss for ferritic/martensitic steels in the flowing LLE vary over a wide range, predicting possible wall thinning at temperatures higher than 450°C from 5 m/yr to values up to a few hundred m/yr [28] due to the chemistry in LLE and velocity profile. To fill the gap experimental activities related to the investigation of the corrosion rate on EUROFER material are carried out at ENEA Brasimone (LIFUS II [6]) and at KIT (PICOLO [29]). In the next experimental campaign on LIFUS II, coated and bare EUROFER samples will be tested at three different velocities (0.01, 0.1, 1 m/s) at a temperature of 550°C. The corrosion rate is also influenced by MHD effect, which changes the velocity profile, flow regime and heat transfer effect. Characterization of BB mock-up at relevant conditions will allow analysing the corrosion rate of RAFM steels.

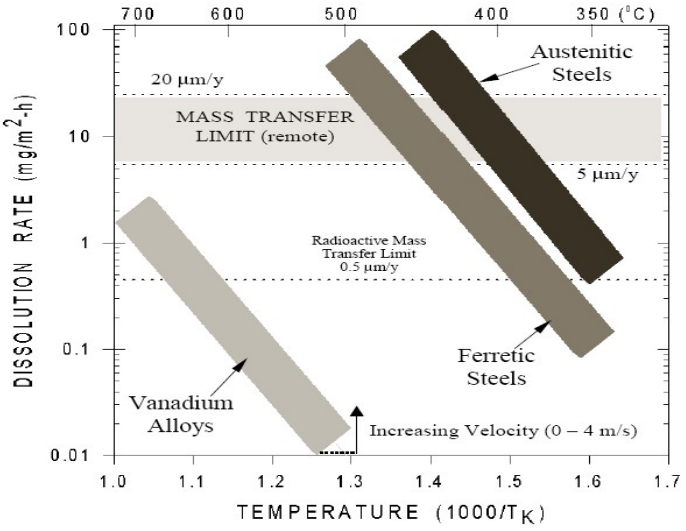

FIG. 5 Dissolution rate of Ferritic steel, Austenitic steel, and Vanadium alloy in PbLi.

5. ANTI-CORROSION AND ANTI-PERMEATION COATINGS

Coating materials have to fulfil three main requirements: avoid Tritium permeation (high Permeation Reduction Factor), protect structural material from corrosion (dissolution of elements in LLE (Cr, Ni, Fe, etc.)) and act as electrical insulator in order to avoid MHD effect.

In a LLE liquid blanket system, the liquid breeder carries the bred Tritium directly to the T extraction system. Due to low solubility of Tritium in LLE, T increases equilibrium dissociation pressure and consequently increases T permeation. Hence, the development of T permeation barrier with good compatibility with LLE is necessary. Anti-permeation coatings have to be qualified at least for 16.000 h in order to demonstrate their performances (no detachment, no cracking, and no LLE penetration in the bulk material or substrate). Presently, two kinds of coating are under evaluation in EU BB project:

— Al-based corrosion barriers-electrochemical ECX process, based on ionic liquids developed at KIT [30];
— Al_2O_3 coating developed by Pulsed Laser Deposition (PLD) (IIT-ENEA) [13-14].

The ECX process is based on the electrodeposition of aluminium from an ionic liquid for the fabrication of Fe-Al barriers. Al is diffused gradually into the EUROFER. The main drawback of this process is the high-roughness of the external surface (Fig. 6 (*a*)).

In the Pulsed Laser Deposition (PLD) technique, a high-power pulsed laser beam is focused inside a vacuum chamber to strike a target of the material that has to be deposited. Al is vaporized from the target and, as a result, a high homogeneous layer of alumina is deposited on the EUROFER. The interphase is well defined and the external surface is smooth (Figure 6 (*b*)). PLD coatings are also electrical insulators, as their electrical conductivity is between 10^{-13} and 10^{-11} S/m.

Tritium permeation barriers are developed for BBs by coating LLE side. Permeation tests were carried out at ENEA Brasimone and at CIEMAT to evaluate the values of Permeation Rate Factor (PRF) without irradiation and with electron and gamma rays and measuring Tritium permeation with Van De Graff accelerator. Results of the tests showed a PRF in the range 100–1000. This process proved its feasibility and effectiveness, but further optimization is needed to address the impact of irradiation, neutron damage will be investigated in LLE capsule in Fission reactor LVR-15 (at CVR).

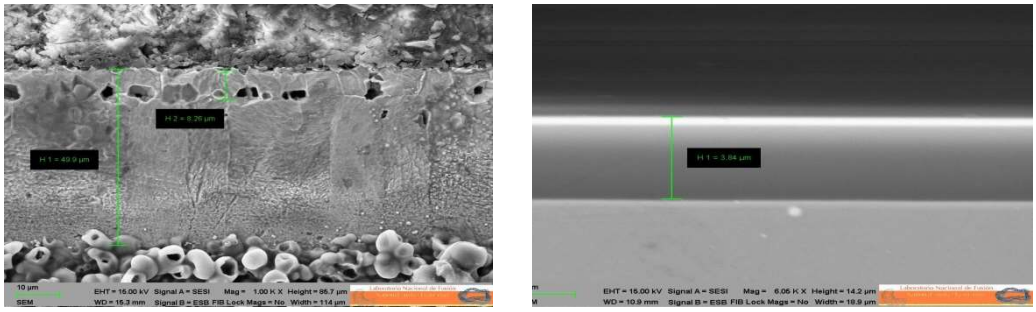

(*a*) (*b*)

FIG. 6 (a) ECX Alumina as-coated; (b) PLD Alumina as-coated [32,33].

6. LLE IRRADIATION, HE PRODUCTION AND OTHER IRRADIATION PRODUCTS

He is, together with T, a product of the reactions between a neutron and a nucleus of ^{6}Li (or ^{7}Li). Daily a relatively large amount of He will be produced. In fact, to produce 1 g of T, 2.33 g of ^{6}Li will be consumed and 1.33g of He will be released. These values lead to a daily production of more than 500 g. It is important to avoid He nucleation and accumulation inside BB as it would cause problems to T inventory and neutron shielding. Depending from PbLi mass flow rate, temperature, pressure, Helium will leave the module as dissolved gas or, if the solubility limit is exceeded, as a gas bubble. (Fig. 7).

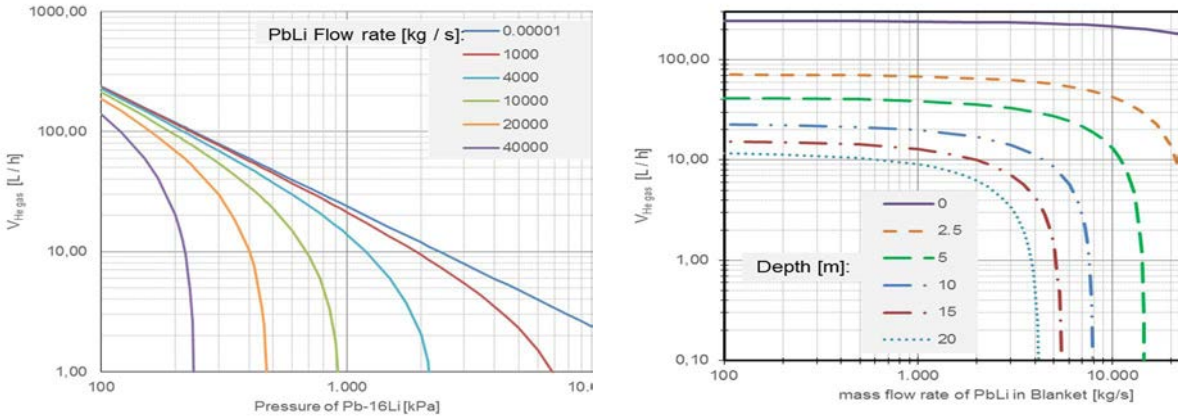

FIG 7: Effect of mass flow rate (right) and of depth (left) on He build-up.

DCLL BB is characterized by high mass flow rates of LLE, as LLE is used also as coolant. For this reason, all He needs to be entirely solubilized, but there is the possibility that He can build-up in zones where velocity is lower because of BB geometry. The proposed solution to remove He solubilized in LLE is to use the expansion tank as release tank. All LLE has to be managed inside the tank with enough residual time to remove all He solubilized, or He bubbles inside LLE. Moreover, the system developed to remove the irradiation products generated into LLE due to neutron flux, gas saturator together with cold traps, can be used to remove a part of solubilized He. In table 2 shows the irradiation products generated in LLE with reaction and the calculation of the specific activities after 2.5y of irradiation, together with the reactions that generate them, their halftimes and specific activities. Mercury and Polonium are the two most abundant elements among activated product, with a vapor pressure 1012 or 108 times higher than that of Tl.

TABLE 2. IRRADIATION PRODUCTS WITH REACTIONS, HALFTIMES AND SPECIFIC ACTIVITIES AFTER 2.5 Y OF IRRADIATION [31]

Reactant	**Reaction type**	**Products**
^{6}Li	n, T	T, α
^{7}Li	n, 2n	^{6}Li
^{7}Li	n, γ	^{8}Li
^{7}Li	n, d	^{6}He
^{204}Pb	n, n'	^{204m} Pb
^{204}Pb	n, 2n	^{203}Pb
^{204}Pb	n, p	^{204}Tl
^{206}Pb	n, T	^{204}Tl
^{206}Pb	n, α	^{203}Hg
^{206}Pb	n, γ	^{207}Bi
^{208}Pb	n, γ	^{209}Bi
^{208}Pb	n, 2n+α	^{203}Hg

Species	Half time	Specific activity after irradiation [Bq/kg]
^{3}H	12.32 y	8.89 10^{12}
^{203}Hg	46.6 d	2.41 10^{10}
^{204}Tl	3.78 y	6.91 10^{9}
^{202}Tl	122.2 d	1.16 10^{9}
^{210}Po	138 d	5.49 10^{8}
^{203}Pb	51.9 h	2.37 10^{7}
^{210}Bi	5.01 d	5.86 10^{6}
^{205}Pb	1.5 10^{7} y	4.61 10^{6}
^{207}Bi	32.2 y	6.95 10^{5}
^{208}Bi	3.7 10^{5} y	3.79 10^{4}
^{210}Pb	22.3 y	6.92 10^{3}
^{209}Po	102 y	5.14 10^{3}
^{206}Bi	6.24 d	1.53 10^{3}

R&D activities in this field are focused on two main areas: verification of the neutron spectrum produced by a D–T reaction using a dedicated neutron generator at high energy (e.g., GRADEL: 14MeV neutron generator) and calculation of the reaction rates for activated products.

7. CONCLUSION

The selection of LLE for thermonuclear fusion applications guarantee significant benefits related to the achievements of the self-sustainability goal. The use of Lead as neutron multiplier and 6Li as breeder material ensure relatively high Tritium Breeding Ratios (TBR) and higher thermal efficiency compared to solid breeder blankets. Nevertheless, several issues still need R&D activities. LLE compatibility with structural material leads to the development of new materials such as the Reduced Activation Ferritic/Martensitic steels (e.g. EUROFER, CLAM) as well as the development of anti-corrosion and anti-permeation coatings. Presently, two different coatings are under evaluation in EU BB project: Al-based corrosion barriers-electrochemical ECX process developed at KIT (Germany) and Al2O3 coating deposited by PLD proposed by IIT-ENEA (Italy). R&D activities are requested in order to characterise the coatings at relevant temperature, HT partial pressure, gamma and neutron irradiation flux.

Several R&D activities are on-going for the LLE chemistry purification. Indeed, He production would cause problems to T inventory and neutron shielding, a dedicated strategy has to be developed in order to avoid accumulation of He gas inside BB and to remove He from LLE. The development of gas saturator with cold traps has been conceived as possible solution to remove activated products (e.g., Hg and Po). Corrosion, heat transfer and Tritium transport are heavily influenced by MHD effects. A better comprehension of these phenomena would be greatly beneficial for the whole design of LLE loops.

Dedicated computational tools and experimental activities are mandatory to obtain a full understanding of all the mentioned phenomena, creating a database in support of reactor and components design.

REFERENCES

[1] HARMS A.A., et al., Principles of Fusion Energy: An Introduction to Fusion Energy for Students of Science and Engineering, ed. World Scientific Publishing Co., London (2000).

[2] AIELLO, G., et al, Development of the Helium Cooled Lithium Lead blanket for DEMO, Fusion Engineering and Design **89** (2014) 1444−1450.

[3] MARTELLI, E., et al., Advancements in DEMO WCLL breeding blanket design and integration, Int. J. Energy Res. **21** (2017)

[4] RAPISARDA, D., et al., Conceptual Design of the EU-DEMO Dual Coolant Lithium Lead Equatorial Module, IEEE Transactions on Plasma Science **44** 9 (2016).

[5] KONYS, J., et al., Flow rate dependent corrosion behaviour of Eurofer steel in Pb–15.7Li, Journal of Nuclear Materials **417** (2011) 1191−1194.

[6] MARTELLI, D., et al., Design of a new experimental loop and of a coolant purifying system for corrosion experiments of EUROFER samples in flowing PbLi environment, Fusion Engineering and Design **124** (2017).

[7] SMOLENTSEV, S., et al., MHD thermofluidic issues of liquid-metal blankets: Phenomena and advances, Fusion Engineering and Design **85** (2010) 1196−1205.

[8] POHORECKI, W., et al., Tritium production rate in HCLL TBM: Conception of a measurement system with application of liquid scintillation technique, Fusion Engineering and Design **88** (2013) 2492−2496.

[9] CARELLA, E., et al., Tritium modelling in HCPB breeder blanket at a system level, Fusion Engineering and Design **124** (2017).

[10] URGORRI, F.R., et al., Preliminary system modelling for the EUROfusion water cooled lithium lead blanket, Fusion Science and Technology **71** (2017) 444−449.

[11] KOSAK, M., et al., Helium bubble formation in Pb-16Li within the breeding blanket, Fusion Engineering and Design **124** (2017).

[12] EBOLI, M., et al., Post-test analyses of LIFUS5 Test#3 experiment, Fusion Engineering and Design **124** (2017).

[13] GARCÍA FERRÉ, F., et al., Advanced Al_2O_3 coatings for high temperature operation of steels in heavy liquid metals: a preliminary study, Corrosion Science **77** (2013) 375−378.

[14] CARMONA GAZQUEZ, M., et al., Al_2O_3 coating as barrier against corrosion in Pb-17Li, Fusion Engineering and Design **124** (2017).

[15] SCHULZ, B., Thermophysical properties of the Li(17) Pb(83) alloy, Fusion Engineering and Design **14** (1991) 199−205.

[16] STANKUS, S.V., et al., An Experimental Investigation of the Density and Thermal Expansion of Advanced Materials and Heat–Transfer Agents of Liquid–Metal Systems of Fusion Reactor: Lead–Lithium Eutectic, High Temperature **44** (2006) 829−837.

[17] TINCANI, A., UTILI, M., Conceptual Design of DCLL PbLi Loop with auxiliaries/ implementation of preliminary design of DCLL PbLi loop – status 2016, EFDA_D_2ND2PX v. 1.0 (2017).

[18] UTILI, M., Preliminary design of HCLL/WCLL PbLi loops, EFDA_D_2MUJWT v. 1.0 (2016).

[19] GARCINUNO, B., RAPISARDA, D., DCLL TES Conceptual Design Flow Diagram and Operation Points/Consolidated conceptual design of DCLL TES, EFDA_D_2MPZ6D (2017).

[20] GARABEDIAN, P.R., Design of the DEMO Fusion Reactor Following ITER, J Res Natl Inst Stand Technol. **114** (2009) 229−236.
[21] RAO, J.S., SANKAR, H., Developments in Heat Transfer, Intech Open (2011).
[22] MISTRANGELO, C., BÜHLER, Electro-magnetic flow coupling for liquid metal blanket applications, Fusion Engineering and Design **109–111** (2016) 1452−1457.
[23] BÜHLER, L., MISTRANGELO, C., Magnetohydrodynamic flows in breeder units of a HCLL blanket with spatially varying magnetic fields, Fusion Engineering and Design 88 (2013) 2314−2318.
[24] BORGSTEDT, H., GRUNDMANN, M., The influence of liquid PbLi eutectic on the mechanical properties of structural materials, Fusion Eng. Des. **6** (1988) 155−158.
[25] SANNIER, J., et al., Corrosion of austenitic and martensitic stainless steels in flowing Pbl7Li alloy, Fusion Eng. Des. **14** (1991) 299−307.
[26] KONYS, J., et al., Corrosion behaviour of EUROFER steel in flowing eutectic Pb–17Li alloy, J. Nucl. Mater. **329−333** (2004) 1379−1383.
[27] MALANG, S., SMITH, D., Modeling of liquid metal corrosion/deposition in a fusion reactor blanket, ANL/FPP/TM-**192** (1984).
[28] BUCENIEKS, L., et al., Investigation of corrosion phenomena in EUROFER steel in PbLi stationary flow exposed to a magnetic field, Magnetohydrodynamics **42** (2006) 237−251.
[29] KONYS, J., et al., Comparison of corrosion behaviour of EUROFER and CLAM steel in flowing Pb-15.7Li, J. Nucl. Mater. **455** (2014) 491−495.
[30] WULF, S.E., et al., Comparison of coating process in the development of aluminium-based barriers for blanket applications, Fusion Engineering and Design **89** (2014) 2368−2372.
[31] GARCÍA FERRÉ, F., ORMELLESE, M., DI FONZO, F., BEGHI, M.G., Advanced Al2O3 coatings for high temperature operation of steels in heavy liquid metals: a preliminary study, Corrosion Science **77** (2013) 375−378.

WATER CHEMISTRY CHALLENGES AND R&D GUIDELINES FOR WATER COOLED SYSTEMS OF DEMO PB-LI BREEDER BLANKET

A.BARON-WIECHEC, R.BURROWS, A.DEL NEVO, C.HARRINGTON, R HOLMES, A.HOJNA, E.LO PICCOLO, E.SURREY, R.TORELLA, S.WALTERS
Centre for Fusion Energy,
Culham, UK

Abstract

The aim of this section is to present work done by participants of R&D sub-topics on water chemistry and corrosion study under the EU DEMO Water Cooled Lithium Lead Breeding Blanket (WCLL BB) project. The selection of light water reactor (LWR) water chemistry would enable the exploitation of valuable existing knowledge from the global LWR fleet in terms of water quality conditioning, control, and purification technologies. However, some specific parameters of the DEMO plant, such as the water radiolysis induced by 14 MeV neutrons, the rapid plasma burning and dwell cycle, presence of tritium in the coolant, and an unknown effect of the very high magnetic fields (4–8 T) required to confine the plasma, may have significant effects on the water chemistry, and needs to be considered during the design phase.

1. INTRODUCTION

It is anticipated that by 2050 a demonstration fusion reactor, DEMO will have been commissioned, capable of delivering several hundred megawatts of electrical energy to the grid and breeding fuel to close the power plant fuel cycle [1]. This requires that a design solution featuring low activation materials, an efficient cooling system and tritium extraction system, together with full consideration of other aspects (safety, materials qualification etc.), be developed in an integrated manner from the outset. One such design concept centres around the Water Cooled Lithium Lead (WCLL) breeder blanket and, as part of this, there is a need to develop a basis of water chemistry guidelines for the first-of-a-kind power plant based on fission industry experience, modelling, virtual engineering and new technologies [2–4]. To highlight R&D challenges facing water coolant chemistry for DEMO, this paper describes briefly the main elements of the DEMO concept and WCLL BB design, including the main structural material foreseen for BB piping, Eurofer-97. We then summarise current developments on water chemistry, recent developments of modelling codes (PACTITER and FACSIMILE) and their experimental validation, and list open questions and knowledge gaps identified so far. The work presented here has been carried out through the DEMO BB project package implemented under EUROfusion consortium [5]. The concept of the nuclear power plant and breeder blanket is presented in Fig.1.

The DEMO fusion power plant is a tokamak reactor. A central solenoid is used to induce the current required to control the plasma; however, such a current can only be induced via this means for a limited period of time. A dwell period in between pulses allows the central solenoid, and other essential systems, to be recharged. As a result, pulsed operation is an unavoidable factor in design of the power plant and for the heat transfer system will require an understanding of the water coolant behaviour under such unusual conditions. It is hoped that the length of the pulse could be extended to reach 8 hours with 15 minutes to recharge, however currently the operational concept assumes a burn time of around 2 hours followed by a half hour dwell. The pulsed operation of the tokamak is a non-trivial issue for WCLLBB and requires water chemistry optimisation [6,7].

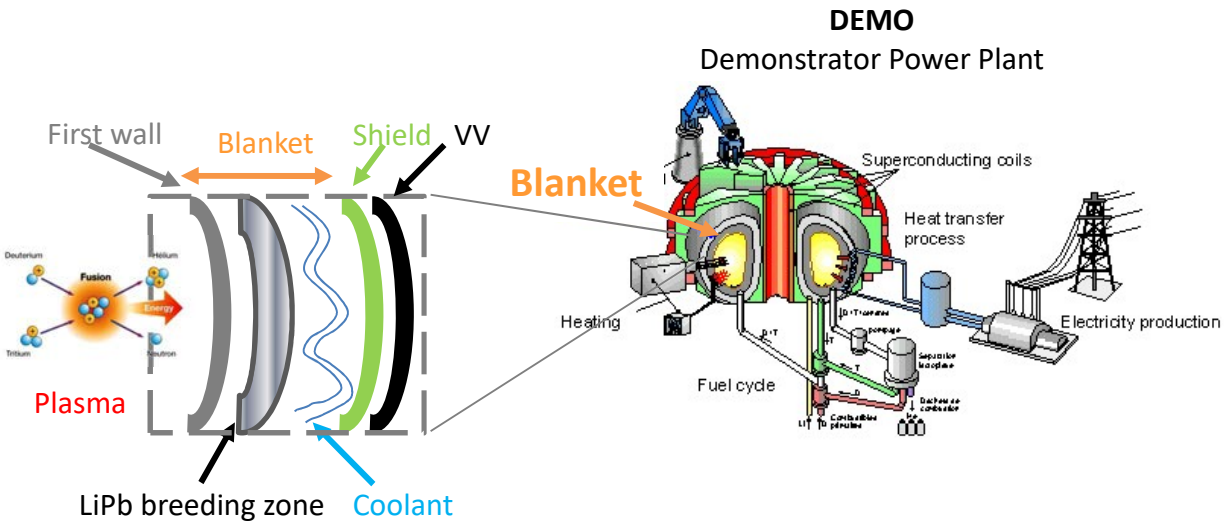

FIG. 1. Demonstrator Power Plant DEMO [44] and concept of Breeder Blanket.

2. DEMO WATER COOLED BREEDER BLANKET CONCEPT (DEMO WCLL BB)

The BB is a major system as its design impacts the plant design, safety, and cost of electricity. The water cooled lithium-lead breeder blanket (WCLL BB), one of four concepts currently under conceptual design, is a promising option for the European DEMO design, [8]. A concept of the DEMO breeder blanket is shown in Fig 2. The system is complex and requires development of an effective combination of materials, manufacturing and cooling technologies, within an integration envelope of neutronics, thermo-mechanical, fluid-dynamical and safety aspects. Sufficient identification of all requirements is crucial and dialog at an early stage of conceptual DEMO BB design between designers, materials scientists, chemists and safety authority is vital for the success of the project [9–12]. The breeder blanket (BB) comprises the in-vessel system with a primary scope to produce (breed) tritium and remove nuclear heat of the plasma for electricity production. The BB is also required to provide shielding of the vacuum vessel and other equipment from direct heating and the neutron flux.

The liquid lithium-lead eutectic acts as the breeder-multiplier, it flows at low velocity and low temperature (i.e. about 330℃) through the main body of the breeder blanket modules. A secondary loop contains pressurized water which provides cooling of the structure and heat transfer to the power conversion system (PCS) and the energy storage system (ESS) by means of water cooling tubes in the breeding zone. The WCLL BB is based on the Multi-Module-Segment concept, for detailed information regarding the conceptual design please refer to [10].

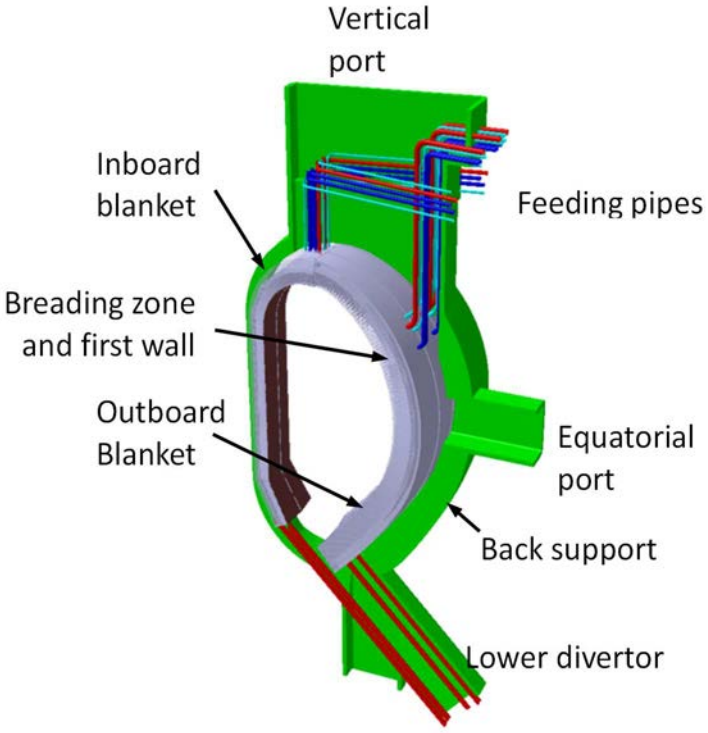

FIG. 2. DEMO segmentation [44].

3. EUROFER-97 CORROSION BEHAVIOUR

A few classes of functional materials have been identified for construction of the blanket module cooling. A central driver is for the material to have a reduced susceptibility to neutron activation. There is currently very limited choice of structural materials fulfilling all the requirements (i.e. low activation, good thermo-mechanical properties). Eurofer-97 (ferritic-martensitic steel) is chosen as a baseline material [13–15]. Relatively large work programmes have been carried out to establish the corrosion resistance of Euroder-97 in water and in liquid LiPb [16–18]. However, there is only limited data regarding irradiation assisted corrosion and T permeation in Eurofer and anti-corrosive surface treatment. Irradiation damage to material microstructure brings a number of modifications which alter the intrinsic properties of the material, degrading the mechanical performance and in consequence the corrosion resistance of the material. The lifetime irradiation of materials during operation in DEMO is assumed to reach 100 dpa. The corrosion processes of concern depend on many interdependent variables such as coolant velocity, coolant chemical composition, flow distribution in the complex geometries of the cooling systems, presence of large temperature gradients and stresses from fabrication, joins/welds or service. Material performance might impact significantly on the concept of the cooling/breeding systems [19]. The effects of tritiated water on materials are relatively well described. In some facilities, the inner surfaces of piping or vessels in contact with tritiated water corroded more than expected, indicating that a change of water condition might be induced. Tritium decays with the emission of a beta particle. The energy released decomposes water with the production of non-negligible concentrations of oxidising radiolytic products (e.g., hydrogen peroxide) which may influence the electrochemical potential of the system [for example 19–21]. The interaction of water radiolysis products with surfaces in corrosion processes in fission environment has been reported by many workers [for example 22–24] and the general mechanisms by which radiolytic processes can enhance corrosion in aqueous solutions is relatively well understood. The radiolytic production of ions, radicals and molecular products (e.g. H+, e-aq, OH, H, H2, HO_2, H_2O_2) follows defined yields which are dependent on temperature and radiation type and energy. However, to date, no significant work has been carried out on aqueous enhanced corrosion susceptibility or hydrogen diffusivity of irradiated materials and joints in environments relevant to DEMO, such as specific water chemistries, elevated temperatures, and large applied magnetic fields. There are only a few facilities in Europe dedicated to corrosion studies in the fusion environment (for example in CEA in France, PICOLO in Germany or at a test loop at the University of Latvia) and they address corrosion issues on a semi-industrial scale. The knowledge gap has been recognised and some preliminary results will be published at 13th International Symposium on Fusion Nuclear Technology (ISFNT) proceedings, held in Kyoto, Japan, at the time of writing this document [25]. Corrosion therefore remains one of the challenges for the cooling system modules in future fusion devices such as

DEMO. Extensive experience over many decades in the fission power industry has demonstrated that water chemistry is one of the most important and effective approaches for corrosion control. Fusion does not have such an asset and modelling is one way to develop adequate water chemistry.

4. WATER CHEMISTRY

The chemistry programme for DEMO is under development; however, a reasonable expectation is that it might be based on the chemistry for ITER with some additional extrapolations. The optimal water coolant chemistry will be a balance between achieving the primary goals of assuring materials integrity, minimising radiation doses and reducing waste, within constraints imposed by the peculiarities of fusion power plant operation such as various phases of operation or power transients or accident scenarios, [26].

The proposed DEMO water coolant chemistry is driven from expertise in the LWR fleet and its most common designs, namely the Pressurised Water Reactor (PWR), Water-Water Energetic Reactor (VVER) and Boiling Water Reactor (BWR). The water chemistry regimes for these plants have evolved considerably since their initial designs were introduced in the 1950s. The overall aims remain the same, however, and are based on maintaining the integrity of the primary coolant circuit components and fuel clad materials, as well as lowering the radiation fields as much as possible. There are elements of PWR, VVER and BWR chemistry regimes that can be taken into consideration when developing chemistry guidelines for the DEMO WCLL. Table 1 summarise some of the typical characteristics related to coolant chemistry based on a current knowledge of LWR (light water reactors) [for example 27-30] and recent reviewed of a concept design of DEMO BB [8].

The face velocity in the WCLL flow channels is not very high however this with combination of magnetic fields may presents some additional corrosion related issues specific to these regimes. Flow assisted corrosion (FAC) can occur when the water chemistry produces a soft corrosion layer which can be removed at an increased rate, by either enhanced mass transport of sparingly soluble corrosion products, or due to physical removal. Consequently, the surface is unable to accrue a thick protective layer and does not passivate, so maintaining the initial peak corrosion rates. It is currently unclear whether Eurofer-97 may suffer FAC, more detailed analysis of a morphology and adhesion of oxide layer on Eurofer-97 is required.

TABLE 1. CHARACTERISTICS RELATED TO COOLANT CHEMISTRY BASED ON LWR FLEET AND RECENT REVIEWED OF A DESIGN OF DEMO BB

	PWR/VVER	BWR	DEMO
Coolant conditions			
Pressure, /bar	155	75	155
Temperature , ˚C	285-325	275-285	285-325
Irradiation	Thermal neutron spectrum	Thermal neutron spectrum	14MeV neutrons
Component life	60+ years	60+ years	5 years
Operation	12 to 24 month fuel cycles	12 to 24 month fuel cycles	2 to 8 hour burn dwell cycles
Coolant flow, m/s	15 (depends on reactor size)	depends on reactor size	2-5
Presence of magnetic fields	no	No	yes

Effect of the water radiolysis from the neutron flux is not sufficiently understood. It is assumed that the neutron flux at positions within the blanket module is in order of 5x1014 n/cm2/s. The blanket attenuates the flux which decreases to 2×10^{12} $n\cdot cm^{-2}\cdot s^{-1}$ at the back of the module. Reactor coolant radiolysis could be suppressed by means of injection of hydrogen, ammonia or hydrazine. Some authors suggest that adding less than 1 ml/kg of hydrogen needs to be sufficient [30 and reference there], although this may not be adequate to suppress radiolysis in areas where hydrogen depletion may occur, notably due to nucleate boiling or areas of reduced flow. Based on experience from fission plant, a target concentration range in the region of 25–35 ml/kg has been suggested.

The review of corrosion and radiolysis by Torella et al. [31] and Burrows et al. [32] indicated DEMO WCLL chemistry would involve high purity water with hydrogen addition. Review of compounds used to achieve an optimised water chemistry and its relevance in fission and fusion is summarise in table 2. The target dissolved

hydrogen concentration is considered to be around 10.0 Nml/kg (normal ml hydrogen per kg coolant) with control of pH of around 8.0 imposed by lithium hydroxide of a few mg/kg and deoxygenation to around 1 μg/kg achieved by hydrazine (N2H4) addition.

Additionally, Torella et al. note that the experimental programme at CV-Řež will consider pH control options based on three possible systems, (borate, ammonia, lithium hydroxide) with the conclusion that the lithium hydroxide water chemistry offers the best compromise in terms of avoiding neutron depletion due to reactions with boron or nitrogen atoms. The optimum chemistry would be 1 to 2 mg/kg lithium hydroxide to give a pH of 8 at 300 °C. Further, the experiments at CV-Řež will use a dissolved hydrogen concentration of around 10 Nml/kg, and oxygen removal by hydrazine treatment to obtain a residual oxygen concentration of 1 μg/kg.

The current, preliminary water chemistry defined for the DEMO power plant is presented in table 3. Some further preliminary considerations have also been made by NNL [32] and also CSM [33] who consider that DEMO target pH of 8.0 and minimum lithium hydroxide level may need a further underpinning. It is suggested that pH of 7.2 may be more suitable based on current experience from PWR chemistry.

TABLE 2. REVIEW OF COMPOUNDS USED TO ACHIEVE AN OPTIMISED WATER CHEMISTRY AND ITS RELEVANCE IN FISSION AND FUSION [32,33]

	Purpose for fission	Relevance to DEMO WCLL
Boric acid/Borate	Reactivity control, with higher concentrations at the start of a cycle	Not present as reactivity control not required
Lithium hydroxide or potassium hydroxide	Alkalising agents for pH control, particularly to balance effect of boric acid addition	Necessary but concentration may be lower. Not subject to the same upper concentration limits arising from fission reactor fuel clad
Hydrogen, ammonia, or hydrazine	reducing agents to supress the concentration of oxygen and hydroxide free radicals for corrosion mitigation	Necessary but optimum concentration of H and effect on Eurofer-97 requires further experimental work
Oxidising species	Concentrations minimised for stress corrosion cracking (SCC) control	Requirements will be the same or similar
Impurity Levels	Concentrations minimised for stress corrosion cracking (SCC) control	Requirements will be the same or similar
Zinc injection and noble metal addition	Reduce radiation fields through reduction in corrosion production generation, and mitigation against SSC	Use of depleted zinc seems the most relevant
Other developments e.g. titanium dioxide or methanol addition	alternatives to zinc and noble metal addition	Possibly relevant depending on progress with other mitigators

TABLE 3. EXAMPLE TABLE PRELIMINARY WATER CHEMISTRY OF DEMO WCLL BB.

Water	Demineralised
Temperature	300-320
Oxygen	<10 μg/kg
Hydrogen	10 ml/kg
LiOH	0-2 mg/kg
pH_T	5.7-8.0
Conductivity*	As low as possible
Flow rate	2 m/s

* Make-up water conductivity, or coolant degassed after-cation (DGAC) conductivity

Recent review of water chemistry by NNL reviewed the choice and suggested that the pH needs to be controlled to above 7 but that there may be drivers for a control band below 8. A need for a higher hydrogen control band was also noted, so mitigate against possible hydrogen stripping in localised areas of boiling. The need to control specific aggressive impurities was also highlighted. A set of technical bases, drivers and control measures was outlined for each chemistry parameter to assist in the development of a chemistry programme for DEMO WCLL.

Apart from the radiolysis, activation of the coolant could be another operational issue for the water cooled breeder blanket concept. Neutrons of 14 MeV energy created from the DT reaction in burning plasma when reaching the coolant will induce a nuclear reaction with 16O. The short-lived Nitrogen isotope 16N is formed in the 16O(n,p)16N nuclear reaction. Although 16N has a half-life of only 7.1 s it emits radiation at 6.1 and 7.1 MeV [34, 39].

Another specific of the fusion power plant mentioned earlier is the pulsed mode operation. It requires water chemistry optimisation, in particular to minimise solubility transients and reduce transport and deposition of corrosion products. Large solubility transients, either across the temperature gradient in the heat transfer zone, or between the pulse and dwell phases will tend to promote deposition of corrosion products, which can lead to increase in soluble and particulate activation products in the coolant. Thicker deposits can lead to heat transfer impairment and ultimately pressure differentials. Modification and underpinning of the water chemistry regime is expected to continue as part of the developing chemistry programme. This will facilitate translation of technical requirements across to the plant as the coolant circuit is not yet fully designed with a detailed layout and the final structural materials and fabrication methods are still being developed. Even the most elegant water chemistry regime from anti-corrosion and radiolysis suppression point of view must be consistent with effective extraction of T from the coolant.

5. CORROSION AND RADIOLYSIS CODES FOR WCLL BB SYSTEM

An extensive review of corrosion and radiolysis codes is available in [31]. Currently, 2 codes: corrosion code PACTITER (used and developed by CMS) and radiolysis code FACSIMILE (used and developed by NNL) are being considered for DEMO WCLL BB. PACTITER is based on the PACTOLE code used for estimating the behaviour of corrosion products within PWR primary circuits and specifically, the source term arising from their activation in the core neutron flux.

The PACTITER code is assumed to be used for WCLL BB conditions analysis and predictions, and it is aim of the project partners, namely CMS and CV-rez, to validate the predictive models for corrosion processes, as the code libraries do not include Eurofer. The recent development of the code allows simulation of corrosion product production analysis in continuous mode and in pulse mode. Recent results of preliminary validation of the code carried out by CMS and CV-REZ showed good agreement between modelling and experimental results [11].

A radiolysis model has been developed based on an existing water radiolysis code implemented within the FACSIMILE package. This model applies high temperature radiolysis and speciation reaction schemes based on extrapolated “g”-values for high energy neutrons. The requirement to extrapolate simultaneously in two variables (temperature and neutron energy) from the best available experimental data introduces significant uncertainties which have been addressed initially with sensitivity analyses. The code accommodates the DEMO pulse-dwell cycle and considers the addition of varying levels of hydrogen in a homogeneous volume. Initial estimation of the efficiency of hydrogen in suppressing radiolysis throughout the circuit used a pseudo-one-dimensional adaptation of the code.

6. SUMMARY, PROSPECT AND OPEN QUESTIONS

Through a technology transfer exercise between the fission and fusion technology areas of expertise, NNL, CMS, CV-Rez, ENEA and UKAEA (CCFE) have contributed to a review of radiolysis and corrosion in the WCLL system of a fusion power plant. A better understanding of cross-dependencies between Eurofer-97 corrosion behaviour, water coolant chemistry and plant operation regime will allow development of monitoring techniques and effective chemistry control suitable for fusion power plant.

Corrosion and radiolysis modelling codes, like PACTITER and FACSIMILE must be validated against the final plant conditions. Some important unknown input data for modelling, for example a degree of porosity and adherence of corrosion product to the surface of the Eurofer-97 are still missing. The codes, widely applied and validated by the fission industry, extrapolate the concentration of oxidising species produced by radiolysis under 14 MeV neutron flux from data available for fission regime. The feasibility of this approach still must be assessed. The codes also do not take in to account corrosion mechanism other than uniform corrosion. Control of feedwater impurities, hydrogen dosing and buffering of the water must be more deeply studied, keeping in mind that even the most elegant water chemistry composition must allow water processing and tritium extraction.

To add uncertainty to the above, recent observations by W.G. Luscher et.al. [35] indicate enhanced tritium permeation in materials in working reactors, which is not observed for ex-situ tritium permeation and retention study. In-situ tritium permeation measurements obtained from the TMIST-2 experiment have indicated that in-reactor tritium permeation is enhanced by a factor of ~2 to 5 relative to the ex-reactor tritium permeation predicted by Le Claire et al. [36]. In addition, the permeation data revealed ~p0.5 pressure dependence over a broad range of pressures, which suggests that permeation is diffusion-limited instead of surface-limited, even at very low tritium partial pressures. This is a particularly important observation because it suggests that in-reactor tritium permeation does not become surface limited at low pressures, which has been observed in ex-reactor studies. The open question is whether neutron or gamma radiation enhance tritium permeation through structural materials, and how the variable pressure and temperature is affecting the process? For fusion technology it might become an issue.

None of the existing codes simulating corrosion of materials in fusion environment take in to account magnetic field effect or streaming potential in Eurofer-97 pipes. Similarly, transport and accumulation of corrosion products in areas of variable magnetic field is not accounted for and has not been studied. The main magnetic field in DEMO is in the toroidal direction with a design value of 5.67 T on the plasma toroidal axis. However, this field varies with a 1/r dependence of the radial distance, leading to different fields of around 9T on the inboard blanket and 4T on the outboard blanket.

High-level recommendations are set out below as to the areas which require further investigation in chemistry regime:

- Establish the suitability of different alkalising agents that could be used (e.g., lithium hydroxide, potassium hydroxide) and their compatibility with Eurofer-97.
- Determination of the optimum pHT control band in order to minimise corrosion of Eurofer-97, corrosion product release rate and corrosion product solubility gradients through the plant.
- Investigation of effect of short term chemistry transients, particularly associated with start-up and shutdown conditions, and definition of plant control action levels.
- Investigation of high fluence neutron irradiation effects, particularly with regard to possible irradiation assisted corrosion mechanisms.
- Investigation of the suitability of different reducing agents that could be used (e.g., hydrogen, ammonia, hydrazine) and their compatibility with Eurofer-97.
- Determine the SCC susceptibility of Eurofer-97 under various concentrations of oxygen and aggressive species (e.g., chloride, fluoride, sulphate) and the efficiency of inhibition due to increase in pH.
- Determine the effects of various concentrations of cationic or complexing species (e.g., calcium, magnesium, aluminium, sodium and silica) on Eurofer-97, in particular in terms of the effect on corrosion product morphology and crud deposition.
- Determination of the separate or combined effects of depleted zinc injection, noble metal (Pt/Rh) chemical and titanium dioxide addition on Eurofer-97 under relevant LWR chemistry regimes.

— Assess the extent of any effect of the very high magnetic fields at the breeder blanket location on corrosion within the water coolant circuit.
— Translate the considerations above to relevant design development in related DEMO plant, such as the alternative first wall design.

It is recognised that the chemistry programme needs to be considered a live document to be updated in tandem with the plant design and the developing technical basses.

REFERENCES

[1] EFDA, "Fusion Electricity: A roadmap to the realisation of fusion energy," Document JG12.356, 2012.
[2] SURREY, E., PORTON, M CABALLERO, A., DAVENNE, T., FINDLAY, D., et al., Fusion Engineering and Design Volume 89, Issues 9–10, October (2014) 2108–2113.
[3] PORTON, M., AKTAA, J., BACHMANN, C., FERNANDEZ, P., KALSEY, M., et al., Fusion Science and Technology **66** (2014).
[4] FEDERICI, G., BIEL, W., GILBERT, M.R., KEMP, R., TAYLOR, N., et al., Nuclear Fusion **57** (2017).
[5] BOCCACCINI, L., "Breeding Blanket Project: Project Management Plan", EFDA_D_2MDAMJ EUROfusion (2016).
[6] TODD, T.N., CLARKE, R., KALSI, H., KOVARI, M., MARTIN, A., et al., The Key Impacts of Pulsed Operation on the Engineering of DEMO, CCFE-R **17** (2010).
[7] KOVARI, M., HARRINGTON, C., JENKINS, I., KIELY, C., Review Article for Proceedings of the Institution of Mechanical Engineers, Part A: Journal of Power and Energy: Converting energy from fusion into useful forms, Journal Ref: CCFE-PR **70** (2013).
[8] BOCCACCINI, L.V., AIELLO, G., AUBERT, J., BACHMANN, C., BARRETT, T., et al., Objectives and status of EUROfusion DEMO blanket studies Fusion Engineering and Design **109–111** (2016) 1199–1206.
[9] DEL NEVO, A., GIAMMUSSO, R., DI PIAZZA, I., VILLARI, R., MARTELLI, E., et al., WCLL Design Report 2015 - CAD, neutronic, thermo-hydraulics and thermomechanical analyses, DM-D-R-203 ENEA (2016)
[10] DEL NEVO, A., MARTELLI, E., AGOSTINI, P., ARENA, P., BONGIOVÌ, G., et al., Villari Fusion Engineering and Design **124** (2017).
[11] TORELLA, R., LO PICCOLO, E., BEONE, T., Corrosion, H2O radiolysis and H2O chemistry analysis report activities in 2016, EUROfusion, WPBB-DEL-BB-3.3.1-T002-D001 (2017).
[12] DI MAIO, P.A., ARENA, P., BONGIOVÌ, G., CHIOVARO, P., DEL NEVO, A., et al., Fusion Engineering and Design **109–111** (2016) 227–231.
[13] FERNANDEZ, P., LANCHA, A., LAPENA, J., SERRANO, M., HERNANDEZ-MAYORAL, M., "Reduced Activation Ferritic/Martensitic Steel Eurofer'97 as Possible Structural Material for Fusion Devices, Metallurgical Characterisation on As-Received Condition and after Simulated Service Conditions", IT/1048 CIEMAT, Madrid (2004).
[14] GAGANIDZE, E., PETERSEN, C MATERNA-MORRIS, E., DETHLOFF, C WEISS, O., et al., Mechanical properties and TEM examination of RAFM steels irradiated, Journal of Nuclear Materials **417** 93 (2010).
[15] ZHANG, T., VIEH, C WANG, K., DAI, Y., Irradiation-induced evolution of mechanical properties and microstructure of Eurofer 97, Journal of Nuclear Materials **450** (2014).
[16] VAN DYCK, S., BOSCH, R.W., Stress corrosion susceptibility of ferritic-martensitic stainless steels for fusion applications in high temperature water, EUROCORR 2001 (Proc. Int. Conf. Riva del Garda 2001).
[17] VAN DYCK, S., BOSCH, R.W., Environmentally assisted cracking of Eurofer 97 in water, Fusion Engineering and Design **75** (2005).
[18] LAPENA, J., BLAZQUEZ, F., GOMEZ BRICENO, D., FERNANDEZ, P., DFN/ME-35/IE-01 CIEMAT (2001).
[19] JOSHI, K.S., et al., Journal of Physics : Conference series **390** (2012) 012038.
[20] BELLANGER, G., et al., Corrosion Science **36** (1994) 545–564.
[21] BELLANGER, G., et al., J. Nucl. Mater. **374** (2008) 20–31.
[22] BOYD, W., et al., Radiation Physics and Chemistry **15** (1980) 177.
[23] ELLIOT, J.A., Atomic Energy of Canada Ltd report AECL 11073 (1994).
[24] BOYD, A.W., et al., Radiation Physics and Chemistry **15** (1980) 177.
[25] BARON-WIECHEC, A., ISFNT 2017 (Proc. Int. Conf. Kyoto, 2017).
[26] ONR, "Chemistry of Operating Civil Nuclear Reactors", NS-TAST-GD-088 (2017).
[27] JACQUIER, H., "Chemistry Evaluation in French EDF Nuclear Power Plants," International Conference on Water Chemistry of Nuclear Reactor Systems (Proc. Int. Conf. Sapporo, 2014).

[28] EPRI, “Review of VVER Primary Water Chemistry and the Potential for its Use in PWRs: Potassium Hydroxide and/or Ammonia Based Water Chemistries”, Document 1003382.
[29] ZMITKO, M., “Primary Coolant Technology and Experience in VVER Units”, 14th International Conference on the Properties of Water and Steam (Proc. Int. Conf. Kyoto 2004).
[30] BURROWS, R. HOLMES, R., WALTERS, S., “Chemistry program review and experimental support Developments for the European DEMO fusion power plant breeder blanket water coolant circuit”, document NNL 14284 (2017).
[31] TORELLA, R., LO PICCOLO, E., BEONE, T., “Corrosion, H2O radiolysis and H2O chemistry analysis report activities in 2015”, EUROfusion, WPBB-DEL-BB-3.3.1-T002-D001 (2016).
[32] BURROWS, R., HARRINGTON, C., BARON-WIECHEC, A., WARREN, A., “Development of Conceptual Water Chemistry Guidelines for Water Coolant Circuits of a Demonstration Fusion Power Reactor”, Nuclear Plant Chemistry (2016).
[33] CSM, “CSM open question for corrosion assessment”, Ref. EX10332/06/09/01.
[34] BIENLEIN. J.K., KALSCH, E., The half-life of N16, Nuclear Physics **50** (1964) 202.
[35] LUSCHER, W.G., Journal of Nuclear Materials **437** (2013) 373–379.
[36] LE CLAIRE, A.D., J. Nucl. Mater. **122–123** (1984) 1558–1559.
[37] FISHER, U., CRISTESU, I., PERESLAVSTEV, 1st IAEA Workshop on Challenges for Coolants in Fast Neutron Spectrum Systems (Workshop material, 2017, Paper No. O-8) IAEA, Vienna (2017).
[38] KURTZ, R.J., 1st IAEA Workshop on Challenges for Coolants in Fast Neutron Spectrum Systems (Workshop material, 2017, Paper No. O-8) IAEA, Vienna (2017).
[39] KONISHI, S., 1st IAEA Workshop on Challenges for Coolants in Fast Neutron Spectrum Systems (Workshop material, 2017, Paper No. O-14) IAEA, Vienna (2017).

PRESSURIZED HELIUM AS COOLANT OF FUSION REACTOR BREEDING BLANKETS: A FOCUS ON THE PURIFICATION TECHNOLOGIES

I. RICAPITO, J. GALABERT
Fusion for Energy,
Barcelona, Spain

A. AIELLO, A. TINCANI
ENEA,
Bologna, Italy

Y. POITEVIN
Fusion for Energy,
Saint Paul-lez-Durance, France

Abstract

Pressurized He is one of the candidate coolants for the breeding blanket of future fusion reactors as per the European Fusion Roadmap [1]. As a matter of fact, two out of the four DEMO breeding blanket under development in Europe are cooled down by He at 8 MPa: they are the Helium Cooled Lithium Lead (HCLL) and Helium Cooled Pebble Bed (HCPB) concepts. In the Dual Cooled Lithium Lead (DCLL) concept, mainly developed in USA, the breeding blanket structural material is also cooled down by pressurized He. Among the R&D and design activities aimed at demonstrating that pressurized He is an effective coolant for fusion application, the development of a system with the main function to keep under control the tritium concentration and impurities level in the He coolant is of basic importance: the Coolant Purification System (CPS), directly connected with the He coolant, accomplishes these functions in normal operation. This paper first recalls the pros and cons related to the use of pressurized He as primary coolant, clarifying the reasons why a high-performance CPS is needed. Then the paper describes the current CPS design baseline [2] as foreseen for HCLL and HCPB Test Blanket Systems (TBS), derived from the corresponding breeding blanker concepts, focusing on the proposed technologies and operative conditions, as well as the on the main challenges and required R&D activities.

1. INTRODUCTION

Use of pressurized helium as primary coolant for fusion application is a challenging technology, even if not new in the nuclear environment. In fact, there has been a limited but significant experience in the past with fission reactors cooled down by He at a pressure close to 20 bar (Dragon Project-UK, Peach Bottom-USA, Fort St. Vrain-USA), extracting a thermal power not exceeding 800 MW. Further studies have been carried out more recently in the frame of the development of gen. IV fission reactors. Since some decades He pressurized at 8 MPa has been proposed as primary coolant for different concepts of breeding blankets of a fusion reactor. Use of He at so high pressure extracting a thermal power higher than 2 GW requires a strong effort which justifies the intense R&D carried out in many European labs. Essentially, Pros and Cons of the pressurized He technology can be summarised as follows:

— PROS:
  (i) Full compatibility with materials also at high temperature;
  (ii) As a consequence of the point A., there is the potential for high plant efficiency;
  (iii) No radiation effects;
  (iv) No chemical reactivity in case of accident;
  (v) No neutron absorption.
— CONS:
  (i) High pumping power required;
  (ii) Compared with water or liquid metals, He coolant requires much bigger heat exchange surfaces and consequently bigger cooling system volume;
  (iii) Reduced technological maturity (i.e. He circulator) at high power scale;
  (iv) Permeated tritium from the breeding modules into the coolant generates a significant tritium partial pressure with the consequent tritium permeation into the cooling system vault which, depending on the conditions, can exceed the limits imposed by the nuclear authorities;

(v) Potential high leakage rate (tritiated He) into the cooling system vault with the consequent tritium contamination.

Issues I and J can be radically mitigated keeping low and under control the tritium partial pressure in He in normal operation. This can be achieved by:

— The minimization of the tritium source, the tritium permeation into the coolant [3], [4].
— The operation of a system, directly connected to the primary coolant, able to extract tritium at high rate and efficiency: this is the "Coolant Purification System" (CPS).

2. CPS FUNCTIONS AND MAIN TECHNOLOGIES

The main functions of the Coolant Purification System in a He cooled breeding blanket are:

— To extract tritium permeated from the breeding blanket module into the He coolant;
— To route the extracted tritium in suitable form to the downstream tritium processing systems;
— To remove continuously the generated impurities from the He coolant.

As shown in Fig. 1 for HCLL-TBS, CPS is connected not only with HCS (He Cooling System) but also with other systems belonging to the TBS and to the Tritium Plant. CPS is fed by a small portion of the He flow-rate in the HCS. The extracted tritium is sent in concentrated form to the tritium accountancy (TAS) and then to TEP (Tokamak Exhaust Processing System) for the final purification. The removed impurities are sent to Detritiation System (VDS). Both TEP and VDS belong to the Tritium Plant.

A three-step process is foreseen for CPS in HCLL and HCPB-TBS: i) oxidation of Q_2 (Q= H, D, T) and CO; ii) trapping and recovery of oxidized species; iii) removal of impurities.

The technologies selected during the conceptual design phase of HCLL and HCPB-TBS to accomplish the CPS functions and implement the three-stage process are summarized here below.

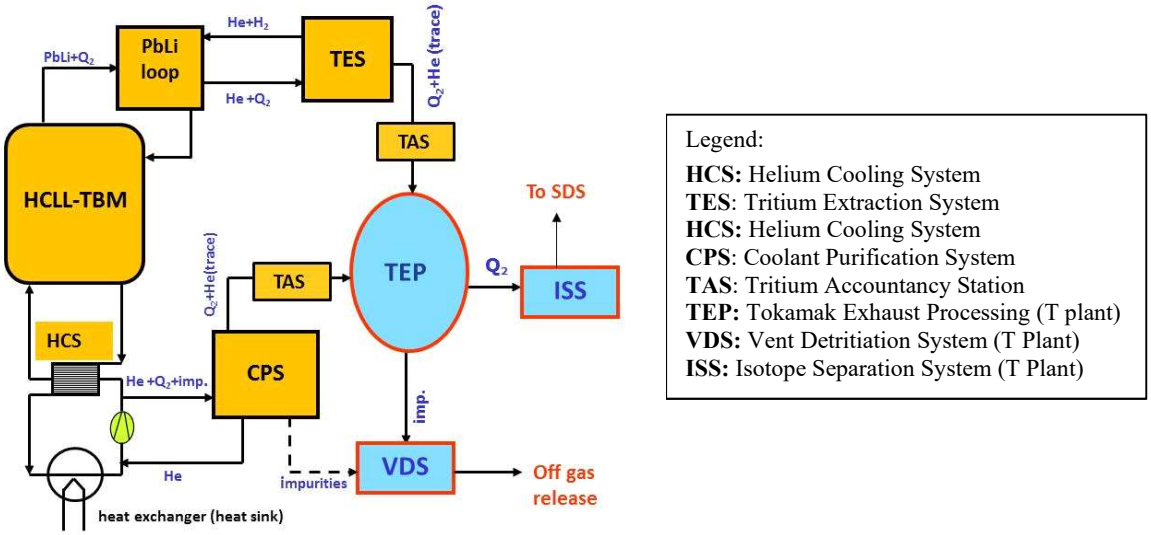

FIG. 1 HCLL-TBS block diagram.

— Oxidation: the conversion of Q_2 to Q_2O and, of CO to CO_2 is accomplished by a Cu oxide reactor working at 250 °C in normal operation [5]. The Cu oxide reactor can be regenerated using a purge gas of N_2 or He with a low oxygen content (1-2%) to avoid excessive temperature increase.

— Q_2O Trapping: this function is implemented by a TSA (Temperature Swing Adsorption) with 13X zeolite as adsorbent material. TSA consists of two adsorbent beds operated in parallel, one working in adsorption at room temperature and high pressure and the other one regenerated at high temperature and lower pressure, in a counter-flow configuration. Once the regeneration process is over, the main flow stream is switched towards the regenerated column, while the bed in parallel saturated by Q_2O is driven to the regeneration cycle for its desorption from the adsorbent material. The net effect of the TSA is to deliver a gas stream concentrated in Q_2O to TAS for tritium accountancy.
— Concentrated Q_2O reduction to Q_2: reduction of Q_2O into Q_2 is needed to assure reliable tritium accountancy, avoiding Q_2O adsorption on the piping wall connecting the CPS to the Tritium Plant where TAS (Tritium Accountancy Station) is assembled. The selected technology is currently based on the use of the SAES Getter material St909 alloy (Zr-Fe-Mn alloy) with a theoretical conversion performance of 30-40 torr Lt of oxygen/g of alloy, corresponding to 27 mg of O_2 absorbed per gram of alloy. The main issue of this technology is that this material cannot be regenerated. This implies the replacement of the reducing bed at the end of its lifetime with the consequent problems related to the maintenance tasks.
— Impurity Removal: for this function the technology of heated getter has been selected as reference solution. The getter material, based on a Zr alloy, is operated at a temperature of around 400°C. It removes O_2, CO, CO_2, N_2 at an overall concentration of 10 vppm, forming almost irreversible chemical bonds. An impurity removal efficiency of 90% is guaranteed by the supplier for this set of impurities. This material cannot be regenerated and, then, the same consideration done for the reducing bed applies also in this case.

3. CPS PROCESS DESCRIPTION

With reference to the simplified process flow-diagram in fig. 2, the CPS process can be described as it follows:

— A slip stream is extracted by CPS downstream the HCS He compressor;
— The slip stream is routed to the heat economizer EC where the temperature rises to 250 ˚C;
— The gas stream enters the catalytic oxidizers OX where Q_2 and CO are oxidized to Q_2O and CO_2, respectively;
— The gas stream is cooled down to nearly room temperature before entering the two-beds TSA for Q_2O and CO_2 extraction;
— Detritiated He is then heated to 400 ˚C and then passed through an heated getter where inorganic impurities (essentially O_2, CO, CO_2, N_2) are removed;
— Detritiated and purified He is routed back to the inlet of the main HCS circulator, after being cooled down through the economiser EC;
— Tritium adsorbed in TSA in form of HTO is desorbed through the regeneration loop of the CPS, with the saturated adsorbent bed operated at around 300 ˚C under a small He flow at low pressure. The reducing bed RB converts Q_2O into Q_2 in the stream. After a further cooling stage, the concentrated Q_2 (with HT) is sent to the Tritium Plant.

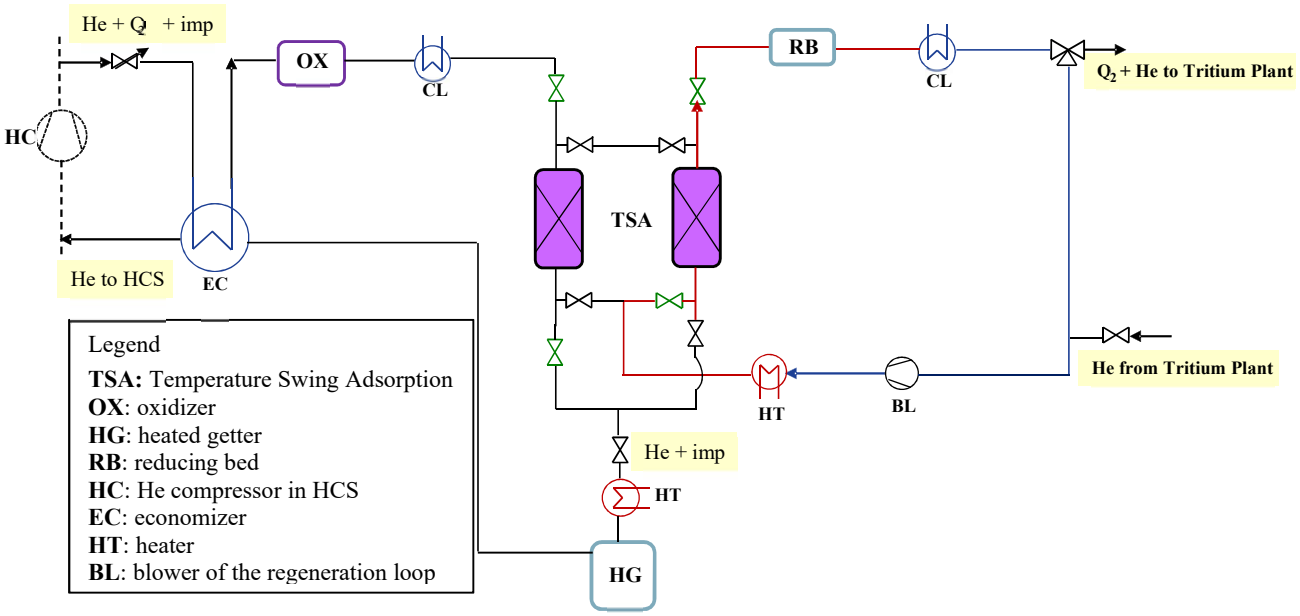

FIG. 2 CPS Process Flow Diagram.

The He flow-rate Γ_{CPS} to be processed by CPS in order to keep a tritium specific activity C_{TO} in He coolant is a function of the tritium permeation rate from the blanket, of the CPS tritium extraction efficiency and of C_{TO} itself. Γ_{CPS} can be calculated by tritium mass balances in the coolant, between the TBM inlet and outlet, and in the node A as reported in fig.3.

— Tritium mass balance in HCS:

$$\Gamma C_o^T = \Gamma C_i^T + P \tag{1}$$

— Tritium mass balance in the node A:

$$\Gamma C_o^T + \Gamma_{cps} C_u^T = \left(\Gamma + \Gamma_{cps}\right) \cdot C_i^T \tag{2}$$

where:

— C_i^T tritium concentration at HCS inlet;
— C_o^T tritium concentration at HCS outlet;
— C_u^T tritium concentration at CPS outlet;
— P tritium permeation rate from the blanket.

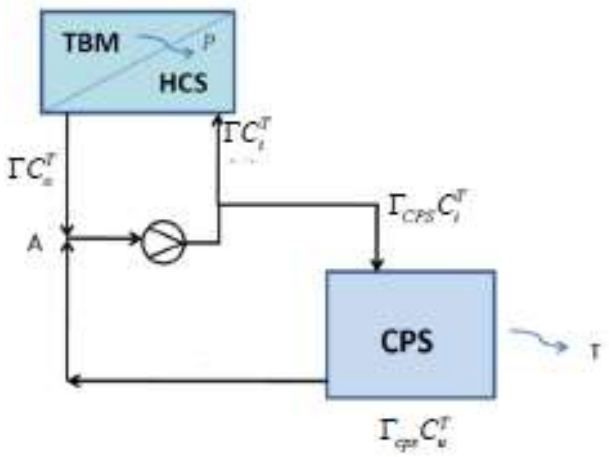

FIG. 3 CPS connection with HCS.

Having defined the CPS tritium extraction efficiency as:

$$\eta_{cps} = \frac{C_i^T - C_u^T}{C_i^T} \tag{3}$$

Γ_{CPS} can be calculated as:

$$\Gamma_{cps} = \frac{\Gamma P}{\eta_{cps}\left(\Gamma C_0^T - P\right)} \tag{4}$$

In case of HCLL-TBS, assuming a steady state tritium concentration in the coolant of 2.5E-02 Pa, a tritium permeation rate from the breeding region of the TBM into the main coolant of 5.7 mg/day (as per the preliminary results from tritium transport model in HCLL-TBS) and a CPS tritium extraction efficiency of 98%, the flow-rate to be processed by CPS is 580 Nm^3/h. The two values of tritium concentration in the coolant and CPS throughput are the results of iterations carried out to have low tritium contamination the ITER cooling system vault while ensuring a CPS of reasonable dimension and easy to integrate in ITER.

The main operating conditions and performance parameters of HCLL-CPS during normal operation are summarized in Table 1.

TABLE 1. HCLL-CPS OPERATIVE CONDITIONS IN NORMAL OPERATION

Processed He mass flow-rate (Nm^3/h)	580
Fraction of the total He coolant flow-rate (%)	2.2
CPS tritium extraction efficiency (%)	95
He pressure at CPS inlet (MPa)	8.1
Total CPS pressure drops (MPa)	0.9
He temperature at CPS inlet (˚C)	90
He temperature at CPS outlet (˚C)	70
Maximum temperature in the loop (˚C, heated getters)	400

The selected material for the CPS piping and components is AISI 316L. In order to satisfy the requirement of high tightness, the use of welding joints has to be implemented in the design at the maximum possible extent. However, when strictly needed, flanged joints with metallic C or energized C gasket rings are a suitable option.

4. Challenges and R&D needs

The following points can be considered as summary of this paper:

— Use of pressurized He as primary coolant of the breeding blanket of fusion reactors requires keeping low tritium partial pressure during normal operation (< 0.1 Pa). This is needed to avoid unacceptable tritium permeation and leakages into the reactor cooling vault.
— This low tritium partial pressure in He coolant can be achieved by the operation of an efficient CPS accompanied by tritium permeation barriers which have the function of reducing the tritium permeation into the He coolant from the breeding blanket modules.
— Intense R&D is needed to develop tritium permeation barriers with high performance (Permeability Reduction Factor >10) in relevant geometry and operative conditions. The objective to reduce the tritium permeation rate into the coolant of at least one order of magnitude appears necessary to keep the CPS throughput at a reasonable level in view of the scale-up to DEMO.
— For the proposed CPS process the biggest challenge is to find an efficient reducing bed material which can be fully regenerated, in alternative to the current Zr-Fe-Mn alloy (SAES getter ST-909).
— In view of the scale-up to DEMO, it would be important to find alternatives to the CPS process described here, going in the direction of simplification and of more flexible technologies.

REFERENCES

[1] ROMANELLI, F., at al., Fusion Electricity A roadmap to the realisation of fusion energy, EFDA (2012)
[2] AIELLO A., et al., Finalization of the conceptual design of the auxiliary circuits for the European test blanket systems, Fusion Engineering and Design **96-97** (2015).
[3] DEMANGE, D., et al., Tritium management and anti-permeation strategies for three different breeding blanket options foreseen for the European Power Plant Physics and Technology Demonstration reactor study, Fusion Engineering and Design **89** (2014) 1219–1222.
[4] RICAPITO, I., et al., Current design of the European TBM systems and implications on DEMO breeding blanket, Fusion Engineering and Design **109–111** (2016) 1326–1330.
[5] LIGER, K., et al, HCLL and HCPB coolant purification system: design of the copper oxide bed, Fusion Engineering and Design **86** (2011) 1859–1862.

MOLTEN SALTS CHARACTERISTICS UNDER IRRADIATION IN FISSION RELATED SYSTEMS

V. IGNATIEV
National Research Center, Kurchatov Institute,
Moscow, Russia

Abstract

The radiation chemistry of molten fluorides is traced mainly from their development as fuels / coolants in molten salt reactor (MSR) programs in different countries with important factors in their selection being discussed. Key molten salt characteristics under irradiation such as transmutation reactions; fission products (FP's) behaviour (including noble gases and tritium, soluble stable compounds, noble and semi noble metals); operational constrains (e.g. solubility of metal trifluorides and tellurium) and uncertainties features are explained as they relate to the behaviour of molten fluorides fuel system. Issues deals with the preparation of initial fuel; contamination possibilities; fuel maintenance options and methods, such as removal of gaseous Xe and Kr, addition of actinides, maintaining the desired Redox potential (e.g. UF3 / UF4 ratio etc.), removal of in adherent oxide contamination thorium addition, removal of noble and semi noble metals are described. It is concluded that while much is known about molten salt fluorides fuel / coolant salt behaviour under irradiation, which can be used effectively to reduce the amount of the research and development required for future fast spectrum systems. Some significant questions need to be addressed.

1. INTRODUCTION

Today R&D studies are on-going in order to verify that fast spectrum MSR systems satisfy the goals of Gen-IV reactors in terms of sustainability, non-proliferation, safety and waste management. Recent MSR developments in the Russian Federation on the 1000 MWe molten-salt actinide recycler & transmuter (MOSART) and in Europe on the 1400 MWe molten-salt fast reactor (MSFR) address the concept of large power units with a fast neutron spectrum in the core without graphite moderator. The main characteristics of the MOSART and MSFR designs are given in Table 1. Summary times and possible methods for FP removal and actinides recycling in MOSART and MSFR are presented in the Table 2.

Even in the homogeneous core, where removal times for soluble FP's are long enough, taking away of neutronic poisons is, of course, the primary purpose of fuel processing. TRU nuclides and the lanthanide FP's are recovered by selective extraction to liquid Li-Bi alloy. All actinides are immediately returned to fuel circuit. The "consideration done demonstrated the potential of the MSFR and MOSART as systems with flexible configurations and fuel cycle scenarios which can operate within technical limits with different loadings and make up based on TRUs (from spent LWR fuel with MA/TRU ratio up to 0.45) as special actinide transmuter, as self-sustainable system (CR=1) or even as a breeder (CR>1)" [1].

The US is working on solid fuel FHR (Fluoride-salt-cooled High temperature Reactor) as well as liquid fuelled MCFR (Molten Chloride salt Fast Reactor).

China in co-operation with US and Australia is working on FHR and TMSR (Thorium Molten fluoride Salt thermal Reactor) graphite moderated designs.

TABLE 1. MAIN CHARACTERISTICS OF THE MOSART AND MSFR DESIGNS

Fuel circuit	MOSART	MSFR
Fuel salt, mole%	$LiF\text{-}BeF_2\text{+}1TRUF_3$ $LiF\text{-}BeF_2\text{+}5ThF_4\text{+}1UF_4$	$78.6LiF\text{-}12.9ThF_4\text{-}3.5UF_4\text{-}5TRUF_3$ $77.5LiF\text{-}6.6ThF_4\text{-}12.3UF_4\text{-}3.6TRUF_3$
Temperature, ^oC	620-720	650-750
Core radius/height, m	1.4/2.8	1.13/2.26
Core specific power, W/cm^3	130	330
Container material	High Ni-Mo alloy	High Ni-W alloy
Removal time for soluble FPs, yrs	1-3	1-3

TABLE 2. SUMMARY TIMES AND METHODS FOR FP'SREMOVAL AND ACTINIDES RECYCLING IN MOSART AND MSFR

Element	Time	Method
Kr, Xe	50 s	Sparging with He
Zn, Ga, Ge, As, Se, Nb, Mo, Ru, Rh, Pd, Ag, Tc, Cd, In, Sn, Sb, Te	2-4 hrs	Partial plating on surfaces, removal to off-gas system, limited filtering
$^{233}U,^{234}U,^{235}U,^{236}U,^{237}U$	10-15 days	Fluorination
Zr, ^{233}Pa	1-3 yrs	
Ni, Fe, Cr	1-3 yrs	
Pu, Am, Cm, Np	1-3 yrs	Reductive extraction;
Y, La, Ce, Pr, Nd, Pm, Gd, Tb, Dy, Er	1-3 yrs	
Sm, Eu	1-3 yrs	
Sr, Ba, Rb, Cs	5-10 rs	

2. FISSION AND ITS CONSEQUENCES

In MSR fragments produced on fission of a heavy atom originate in energy states and with ionization levels far from those normally considered in chemical reactions. When the fission occurs in a well mixed molten-salt liquid medium, these fragments must come to a steady state (The rapid radioactive decay of many species further complicates an already complex situation) as commonly encountered "chemical entities because they quickly lose energy through collisions with the medium. The valence states that these chemical species assume are presumably defined by the requirements that (i) cation - anion equivalence be maintained in the molten-salt medium; and (ii) redox equilibria be established between the melt and the surface layers of the container metal. The FP cations must satisfy the fission-product anions plus the fluoride ions released by disappearance of the fissioned atom" [2].

ORNL studies indicated that the summation of the products of fission yield and stable valence for each species might be as low as three per fission event. Accordingly, fission of UF4 (releasing 4F- + 0.015 (Br- + I-) per fission) would be intrinsically oxidizing to metallic alloy. Fission of PuF3 and other TRUs trifluorides probably would be nearly neutral in this regard. Maintenance of a small fraction of the uranium in the fuel as UF3 was successfully adopted to preclude corrosion from fission of 235UF4 in the MSRE. A properly maintained redox potential in the fuel salt apparently will prevent any untoward immediate consequences of the "fission event and will permit grow-in of the FP's in valence states defined by the redox potential.

3. EFFECTS OF RADIATION

When fission occurs in a molten fluoride solution, both electro-magnetic radiations and particles of very high energy and intensity originate within the fluid. Local overheating is almost certainly not important in a MSR where turbulent flow causes rapid intimate mixing. Moreover, the bonding in molten fluorides is completely ionic. Such a mixture, with neither covalent bonds to rupture nor a lattice to disrupt, needs to be quite resistant to radiation. Nevertheless, because there plausibly exists a radiation level sufficiently high to dissociate a molten fluoride into

metal and fluorine" [3] (this would occur even though the rate of recombination of Lio and Fo needs to be extremely rapid), a number of tests of the possibility were made.

Many irradiation tests with fuel salts were conducted at ORNL and KI. These tests strongly suggested that the F2 generation had not occurred at the high temperature (up to 1200°C) but had occurred by radiolysis of the mixture in the solid state. "F2 evolution at 35°C corresponded to about 0,02 molecules per 100 eV absorbed, could be completely stopped by heating to 100 °C or above, and could be reduced by chilling to -70°C. The F2 evolution resumed, usually after a few hours, when temperature was returned to 35 to 50°C.

These and subsequent experiences, including operation of the 8MWe MSRE at US ORNL, strongly indicate that radiolysis of the molten fuel at reasonable power densities is not a problem. It seems unlikely, though it is possible, that MSR fuels will evolve F2 on cooling. If they do, arrangements must be made for their storage at elevated temperature until a fraction of the decay energy is dissipated" [2].

4. CHEMICAL BEHAVIOR OF FP'S

For molten salt fuels, FP's could be grouped by the three broad classes: i) the soluble at salt redox potential FP's; ii) the noble metals; and iii) the noble gases.

4.1. Noble-gas FP's and Tritium

Krypton and xenon (which is an important neutron absorber) form no compounds under conditions existing in a MSR. Moreover, these gases are only very sparingly soluble in molten fluoride mixtures. As with all noble gases "their solubility increases with temperature and with diminishing size of the gaseous atom, while the heat of solution increases with increasing atomic size. This low solubility is a distinct advantage because it enables the ready removal of krypton and xenon from the reactor by sparging with helium. The relatively simple sparging system of the MSRE served to remove more than 80% of the 135Xe, and far more efficient sparging was proposed for the new MSR designs. Stripping of the noble gases from the reactor after a short residence time avoids the presence of their radioactive daughters in the fuel" [2].

If fuel / coolant salt is based on LiF and BeF2 the high flux of energetic neutrons will transmute lithium (6Li(n,α) 3H; 7Li (n,nα)3H) and beryllium (9Be(n,2nα), and to a lesser extent fluorine (19F(n,17O)3H). The problem posed by transmutation of Li and Be are basically similar to those encountered in the fission of UF4 in MSR, i.e., approximately one fluorine atom per fission is free to oxidize or corrode the container.

The transmutation of lithium is essential for production of tritium. This tritium will originate in principle as 3HF; however, with appreciable concentrations of UF3 present, this 3HF will be reduced largely to 3H2. Some of this 3H2 would be removed, along with krypton and xenon, by sparging with helium. However, the extraordinary ability of hydrogen isotopes to diffuse through hot metals will permit a large fraction of the 3H2 to penetrate the primary heat exchanger to enter the secondary coolant.

4.2. FP's with soluble stable compounds.

Rubidium, caesium, strontium, barium, yttrium, the lanthanides, and zirconium all form quite stable fluorides that are relatively soluble in fuel salts. Bromine and iodine would be expected to appear in the fuel as soluble Br and I, particularly in the case where the fuel contains an appreciable concentration of UF3. Analyses for 131I "showed that a large fraction of the iodine was present in the fuel and that 131I deposited on metal or graphite surfaces in the core region. However, material balances for 131I were generally low. It is possible that some of the precursor, 131Te (25 min), was volatilized and sparged with the krypton and xenon. Further, 131I produced by decay of 131Te in complex metallic deposits (as in the heat exchanger) may not have been able to return to the salt.

4.3. Noble and semi noble FP's

Some fission-product metals (Ge, As, Nb, Mo, Ru, Rh, Pd, Ag, Cd, Sn, and Sb) have fluorides that are unstable toward reduction by fuel mixtures with appreciable concentrations of UF3; thus, they must be expected to exist entirely in the elemental state in the reactor. Selenium and tellurium were also expected to be present as elements within the reactor circuit, and this behaviour was generally confirmed during operation of the MSRE" [2].

Precipitation on the metal surface (most of which is in the heat exchanger) will be quite insufficient to impede fuel flow, but radioactive decay of the deposited material contributes to heat generation during reactor shutdown.

Operation of the MSRE did produce one untoward effect of FP's. These studies implicated fission-product tellurium as responsible for the embrittlement of the metal surface exposed, and subsequent work has confirmed this. Later work at ORNL and KI strongly suggest that (1) if the molten fuels were made to contain as much as 2-5% of the uranium as UF3, the tellurium would be present as Te2- and (2) in that form, tellurium is much less aggressive.

5. OPERATIONAL CONSTRAINTS

The actinide (including UF3) and lanthanide trifluorides are moderately soluble in molten LiF-BeF2, LiF-ThF4, LiF-ThF4-UF4 and LiF-BeF2-ThF4-UF4 mixtures. The data on solubility in molten salt fluorides appear to follow a linear relationship within the experimental accuracy of the measurements when plotted as logarithm of molar concentration of actinide trifluoride vs. 1/T(K). If more than one such trifluoride is present, they crystallize as a solid solution of all the trifluorides on cooling of a saturated melt. If so, the total (lanthanide plus actinide) trifluorides in the reactor might possibly exceed their combined solubility.

Recently, the joint solubility of PuF3 and CeF3 in the 873-1023K temperature range, was measured for 78LiF-7ThF4-15UF4 and 72.5LiF-7ThF4-20.5UF4 melts (see Table 3). "In this case, logarithms of the molar concentration of CeF3, PuF3 as well as (CeF3 + PuF3) vs. 1/T (K) in the studied ternary melts LiF-UF4-ThF4 are not linear. Near the liquidus temperature for 78LiF-7ThF4-15UF4 and 72.5LiF-7ThF4-20.5UF4 salts, the CeF3 significantly displace plutonium trifluoride at their joint dissolution. This suggests that the use of CeF3 additives in the fuel LiF-ThF4-UF4-PuF3 salt can provide effective removal for PuF3" [4].

6. FUEL MAINTENANCE

In general, to achieve fuel maintenance, (i) the fuel must be delivered to and into the reactor in a proper state of purity and homogeneity; (ii) the fuel must be sufficiently protected from extraneous impurities; (iii) sound procedures must exist for addition and recycling of the actinides required; and (iv) provision of the required redox potential in the system.

For a fast Th-U MSR that propose chemical reprocessing to remove FP's, the required fuel maintenance operations also include (i) continuous removal (by the sparging and stripping section of the reactor) of fission-product krypton and xenon; (ii) addition of U and TRUs to replace that lost by burnup; (iii) in situ production of UF3 to keep the redox potential of the fuel at the desired level; (iv) recycling of all actinides; (v) removal of soluble FP's (principally rare earths); they probably also include (vi) isolating 233 Pa from the region of high neutron flux during its decay in order to hold neutron absorption in these materials to acceptably low levels; (vii) removal of inadvertent oxide contaminants from the fuel; in addition, they may include (viii) addition of ThF4 to replace that lost by transmutation or stored with fuel removed from the operating circuit; and (ix) removal of a portion of the insoluble noble and semi noble FP's. Each of these is discussed briefly below.

TABLE 3. JOINT SOLUBILITY OF PUF_3 AND CEF_3 IN LIF-THF_4-UF_4 FUEL SALTS, MOLE%

Temperature, K	72.5LiF-7ThF_4-20.5UF_4		78LiF-7ThF_4-15UF_4	
	PuF_3	CeF_3	PuF_3	CeF_3
873	0.35±0.02	1.5±0.1	1.45±0.7	2.6±0.1
923	4.5±0.2	2.5±0.1	5.6±0.3	3.6±0.2
973	8.4±0.4	3.7±0.2	9.5±0.5	4.8±0.3
1023	9.4±0.5	3.9±0.2	10.5±0.6	5.0±0.3

6.1. Preparation of initial fuel

"Initial purification procedures for the MSR present no formidable problems. Nuclear poisons (e.g., boron, cadmium, or lanthanides) are not common contaminants of the constituent raw materials. All the pertinent compounds contain at least small amounts of water, and all are readily hydrolysed to oxides and oxyfluorides at elevated temperatures. The compounds LiF and BeF_2 generally contain a small quantity of sulphur as sulphate ion. Uranium tetrafluoride commonly contains small amounts of UO_2, UF_5, and $U0_2F_2$

Purification procedures used to prepare materials in many laboratory and engineering experiments have treated the mixed materials at high temperature (usually at 600 °C) with gaseous H_2-HF mixtures and then with pure H_2 in equipment of nickel or copper. The HF-H_2 treatment serves to (1) reduce the U^{5+} and U^{6+} to U^{4+}, (2) reduce sulphate to sulphide and remove it as H_2S, (3) remove Cl^- as HCl, and (4) convert the oxides and oxyfluorides to fluorides. Final treatment with H_2 serves to reduce FeF_3 and FeF_2 to insoluble iron and to remove NiF_2 that may have been produced during hydro fluorination. To date, all preparations have been performed in batch equipment, but continuous equipment has been partially developed" [2].

Purification of the bulk of the fuel would presumably be conducted on LiF-BeF_2-ThF_4-UF_4 mixtures containing perhaps 85 to 90% of the required UF_4 and on molten Li_3UF_7 to provide the additional uranium necessary to bring the fuel to the critical and operating concentration.

Such a purification procedure can provide a sufficiently pure and completely homogeneous fuel material for initial operation of the reactor.

6.2. Contamination possibilities

"Though the fuel material can be supplied and introduced into the reactor in sufficiently pure form, contamination of the fuel is possible from several sources:

- Other reactor materials. The graphite reflector can contain a large quantity of CO_2, CO, and H_2O by virtue of its porosity and internal surface. Outgassing of the reflector by pumping at reduced pressure and elevated temperature is necessary and sufficient to prevent contamination of the fuel by oxide ion from reactive gases from this source. Oxide films on the structural metal can also contaminate the fuel by oxide ion, and, as described previously, the dissolved Fe^{3+}, Fe^{2+}, and Ni^{2+} can be responsible for subsequent metal corrosion. A small (100-ppm) concentration of Cr^{2+} in the fuel as a consequence of reaction of the metal with the fuel cannot be avoided. However, in the absence of extraneous oxidants, the reaction is very slight, and the presence of Cr^{2+} is completely innocuous. Grow-in of the FP's is also unavoidable, as is the presence of a relatively small steady-state concentration of $^3H_2$.
- Atmospheric contamination. Reaction of the MSR fuel mixture with oxygen is relatively slow, but reaction with water vapor is more rapid" [2]. Treatment of the initial fuel charge with anhydrous HF-H_2 mixture during its preparation reduces the O^{2-} concentration to innocuous levels, and similar treatment of contaminated fuel would serve to remove the O^{2-}. Such treatment might never be required, but in the MSR, simple equipment needs to be included that is capable of treatment to remove oxide ion needs to inadvertent contamination occur.
- Contamination of fuel by secondary coolant. Intermixing of the fuel and the secondary coolant salts, as caused by leaks in the primary heat exchanger, would be an important consideration. The MSR design assured a slightly higher pressure on the coolant side so that most leaks would be of coolant into fuel. Such a leak, however small, needs to be recognized at once because of the marked reactivity loss caused by admission of boron into the fuel. "Small leaks of coolant into the fuel system probably pose no safety problems. However, additional study of the mixing of these fluids in realistic geometries and in flowing systems is needed before we can be certain that no potentially damaging situation could arise as a consequence of a sudden major failure of the heat exchanger. The fluoroborate secondary coolant apparently will contain small quantities of oxygenated species and some species containing hydroxyl ions. These would be capable of precipitating oxides from the fuel if the coolant were mixed with fuel in large amounts, but the effects would be trivial compared with other effects noted previously. These substances in the secondary coolant, however, appear to have a nontrivial and beneficial effect on MSR performance. This beneficial effect is the apparent ability of the secondary coolant to scavenge tritium and convert it to recoverable water-soluble form" [3]. US ORNL studies "suggested that oxide-bearing and protonated (e.g., BF_3 OH-) species were present in the molten NaF-$NaBF_4$ mixture proposed as the secondary coolant; the hypothesis was that exchange reactions might offer a mechanism for holdup of tritium in this mixture. Small-scale experiments seemed to show that deuterium diffused through a thin metal tube into such mixtures was retained by the melt but that exchange with OH- was not the responsible mechanism" [2]. Further studies are clearly necessary; once the mechanism is established, the performance of the system might be improved. Means for replenishment of the active agent must be established, and improved means for recovery and ultimate disposal of the tritium must be developed.
- Removal of krypton and xenon. Stripping of krypton and xenon makes possible their continuous removal from the reactor circuit by the purely physical means of stripping with helium. Such a stripping circuit would remove an appreciable (but not a major) fraction of the tritium and a small (perhaps very small) fraction of the noble and semi noble FP's as gas-borne particulates. In addition, the stripper would remove BF_3 if leaks

of secondary coolant into the fuel were to occur. None of these removals (except possibly the last) appreciably affects the chemical behaviour of the fuel system.

— Fuel chemical processing. In MSRs, from which xenon and krypton are effectively removed, the most important FP's poisons are among lanthanides which are soluble in the fuel. Also, the trifluoride species of AnF_3 and the rare earth's are known to form solid solutions so, that in effect, all the LnF_3 and AnF_3 act essentially as a single element. In combination of all trifluorides, AnF_3 solubility in the melt is decreased by lanthanides accumulation. Since actinides must be removed from the fuel solvent before rare earth's FP's the MSR must contain a system that provides for removal of all actinides from the fuel salt and their reintroduction to the fresh or purified solvent. This fuel processing system can be based principally on three types of operations: removal of uranium from fuel salt by fluorination; selective removal of protactinium, TRUs, rare earths, and other FP's from the salt by extraction into molten bismuth; and the hydrogen reduction of UF_6 to UF_4 in the presence of the processed fuel carriers. The chemical basis on which the processing system is founded is well established; however, only small engineering experiments have been carried out to date, and a considerable engineering effort remains.
— "Partial removal of noble and semi noble metals. The behaviour of these insoluble fission-product species, as indicated previously, is not understood in detail. If they precipitate as adherent deposits on the DMSR heat exchanger, they would cause no particularly difficult problems. However, should they form only loosely adherent deposits that break away and circulate with the fuel, they would be responsible for appreciable parasitic neutron captures" [3]. To the extent that they circulate as particulate material in the fuel, insoluble fission-product species could probably be usefully removed by a small bypass flow through a relatively simple Ni based-wool filter system. Presumably, such a system would need to have a reasonably low pressure drop and probably would need to consist of sections in parallel so that units whose capacity was exhausted could be reasonably replaced.
— Addition of actinides. It will apparently be necessary, assuming the fuel volume changes from these additions or other causes do not require removal of any fuel to storage. Developing and demonstrating methods of addition of solid UF_4 (or proper mixtures of UF_4 plus UF_3) should be possible. These will be inherently more complex (and radioactively dirty) and stating which of the options would be preferred is not presently possible. If making a few additions of plutonium and thorium to the reactor fuel during its lifetime is necessary, then adding it as a liquid containing ^7LiF -ThF_4 and ^7LiF -PuF_3 mixtures should be possible. A possibility would be a melts containing about 70LiF-30ThF_4 and 80LiF-20PuF_3 (in mole %) melting respectively near 600°C and 740°C. Alternatively, a procedures presumably could be developed for addition of solid PuF_3 and ThF_4.
— Maintaining the desired UF_3/UF_4 ratio. Operation of the MSRE demonstrated that in situ production of UF_3 could be accomplished readily and conveniently be permitting the circulating fuel to react in the pump bowl with a rod of metallic beryllium suspended in a cage of Hastelloy-N. This technique could be adapted for use in other MSR designs; beryllium reduction would be desirable if the fissionable and fertile uranium additions are to be made as Li_3UF_7.

7. SUMMARY, CONSTRAINTS, AND UNCERTAINTIES

It is obvious from the discussion above that use of molten fluorides as fuel and coolant for a fast reactor system of energy production and incinerator type faces a number of formidable problems. Several of these have been solved, and some seem to be well on the way to solution. But it is also clear that some still remain to be solved:

— Additional experiments are necessary to establish exactly what fraction of the uranium may be present as UF3 without deleterious chemical reactions of the UF3 with other materials within the primary reactor system;
— Details of behaviour of the noble and semi noble FP's are still poorly known;
— The technology necessary to limit to acceptable levels the rate at which tritium is released from MSR is required;
— Presently, we do not know whether:
  i. Treatment to remove inadvertent contamination by oxide will be necessary;
  ii. Addition of uranium to the MSR fuel will be done by use of 7Li3UF7;
  iii. The oxidative effect of fission is near 1 oxidative equivalent per mole of uranium fissioned;
  iv. The removal of noble and semi noble metal from MSR fuel will be desirable.

The molten salts have many desirable properties for application in fast reactor systems, and it seems likely that – given sufficient development time and money - a successful burner system could be developed.

REFERENCES

[1] SERP, J., et al., “The molten salt reactor (MSR) in generation IV: Overview and perspectives”, Progress in Nuclear Energy (2014).

[2] OAK RIDGE NATIONAL LABORATORY, web.ornl.com

[3] AMAZON SIMPLE STORAGE SERVICE, moltensalt.org.s3-webiste-us-east-1.amazonaws.com

[4] IGNATIEV, V., SURENKOV, A., Materials Performance Molten Salts, Comprehensive Nuclear Materials **5** (2012) 221–250.

MODELLING OF THE CONTAMINATION TRANSFER IN NUCLEAR REACTORS: THE OSCAR CODE - APPLICATIONS TO SFR AND ITER

F. DACQUAIT, J.B. GÉNIN, L. BRISSONNEAU
CEA,
Cadarache, F-13108 Saint-Paul Lez Durance, France
Email: frederic.dacquait@cea.fr

Abstract

Predicting the radioactive contamination of nuclear reactor circuits, being a significant challenge for plant designers and operators for more than 40 years, the CEA has developed the OSCAR code to simulate the contamination transfer in the PWR primary system. In the same way, activated corrosion products in the ITER primary heat transfer system and in the SFR primary system can be a major concern as contributors to the radioactive source term. Although the design and operating conditions of these reactors are different from those of PWRs, an application of the OSCAR code to SFRs, OSCAR-Na, and another one to ITER, OSCAR-Fusion, have been developed to simulate the behaviour of corrosion products thanks to the modularity of the OSCAR code.

1. INTRODUCTION

Predicting the radioactive contamination of nuclear reactor circuits is a significant challenge for plant designers and operators. The major stakes are to decrease personnel exposure to radiations, to optimize plant operation, to limit activity of wastes and to prepare decommissioning. To address this challenge, the French strategy has been focusing on performing experiments in test loops representative of Pressurized Water Reactor (PWR) conditions, measuring the PWR contamination and developing a simulation code namely OSCAR (Outil de Simulation de la Contamination en Réacteur – tool of Simulation of Contamination in Reactor). The OSCAR code has been developed by the CEA in collaboration with EDF and AREVA NP for more than 40 years. It has resulted from the merging of two former codes [1]: PACTOLE for Activated Corrosion Products (ACPs) and PROFIP for fission products and actinides [2]. Thus, the OSCAR code has been designed to predict the contamination transfer in PWR reactor coolant systems.

In the same way, ACPs in the Primary Heat Transfer System (PHTS) of the International Thermonuclear Experimental Reactor (ITER) and in the primary system of Sodium-cooled Fast Reactors (SFRs) can be a major concern as contributors to the radioactive source term of potential released activities to the environment in case of accident and to the Occupational Radiological Exposure (ORE) during the normal operation and decommissioning. Although the design and operating conditions of these reactors are different from those of PWRs, an application of the OSCAR code to SFRs, so-called OSCAR-Na, and another one to ITER, so-called OSCAR-Fusion, have been developed to treat the behaviour of corrosion products thanks to the modularity of the OSCAR code.

After a presentation of the OSCAR code, the specificities of OSCAR-Fusion and OSCAR-Na are described. Issues and R&D needs related to the modelling of the ACP transfer in these nuclear reactors are proposed.

2. THE OSCAR CODE

The process governing the ACP contamination of a PWR primary system involves many different mechanisms that react with each other. The source term is the uniform corrosion of metallic alloys, which leads to the formation of an oxide layer. This oxide layer limits ion diffusion but does not eliminate them: ions are directly released in the primary coolant. Ions, generated by oxide dissolution as well, are transported by the coolant. When the coolant becomes supersaturated in corrosion products, ions precipitate on the walls or on particles in the bulk. Particles are also generated by erosion processes. Transported by the primary coolant, particles are deposited on the walls. Two types of ACP formation coexist. On the one hand, the activation of corrosion products occurs when they are deposited on the under-neutron flux surfaces. On the other hand, the corrosion of structural materials under neutron flux is accompanied by a direct release of ACPs. Then, ACPs transported by the coolant contaminate the primary and auxiliary systems. The OSCAR code is devoted to model this phenomenology, which is common to other types of nuclear reactors.

2.1 Transfer modelling

The OSCAR code modelling is based on a control volume approach; briefly:

— The systems are discretized into as many control volumes or regions as necessary, defined according to their geometric, thermal-hydraulic, neutronic, material and operating characteristics.
— Six media can be defined in each control volume: metal, inner oxide, outer oxide/deposit, particles, ions and filter (ion exchange resins and particle filter).
— The following elements Ni, Co, Fe, Cr, Mn, Ag, Zn and Zr and their corresponding radioisotopes can be taken into account.
— A system of mass balance equations is calculated for each isotope (stable and radioactive) in each medium of each region using the following equation:

$$\frac{\partial m_i}{\partial t} = \sum_{Source} J_m - \sum_{Sink} J_m \quad (1)$$

where mi is the mass of the isotope (i) in a given medium [kg], t is the time [s] and J_m is the mass flux between 2 media, 2 regions or 2 isotopes [kg·s^{-1}].

The main transfer mechanisms taken into account are corrosion-release, dissolution, precipitation, erosion, deposition, convection, purification, activation and radioactive decay. The first five mechanisms are described hereafter.

Corrosion of the base metal causes the formation of an inner oxide layer (mainly a chromite), of an outer oxide (a ferrite + metal Ni° or NiO in general) and a direct ion release into the bulk. The corrosion and release rates [kg·s^{-1}] are given by:

$$J_{Cor}^{elt} = V_{Cor} \cdot S_w \cdot \alpha_{met}^{elt} \quad (2)$$

$$J_{Rel}^{elt} = V_{\mathrm{Re}l} \cdot S_w \cdot \alpha_{rel}^{elt} \quad (3)$$

where V_{Cor} and V_{Rel} are the surface corrosion and release rates [kg·m^{-2}·s^{-1}] calculated by an empirical model as a function of chemistry, temperature and material (or by a power law, logarithmic law or constant value per stage), S_w is the wet surface area [m²], α_{met}^{elt} is the element fraction in the metal and α_{rel}^{elt} is the element fraction involved in the release.

Dissolution of an oxide occurs when the concentration of a soluble species in the coolant is lower than its equilibrium concentration. The dissolution flux of the element elt, J_{dissol}^{elt} [kg·s^{-1}] may be written:

$$J_{dissol}^{elt} = \frac{S_w}{1/h + 1/V_{dissol}} \cdot (C_{equil}^{elt} - C^{elt}) \quad (4)$$

where h is the mass transfer coefficient of ions in the fluid [m·s^{-1}], V_{dissol} is the dissolution velocity (dissolution surface reaction rate coefficient) [m·s^{-1}], C_{equil}^{elt} is the equilibrium concentration of the element elt [kg·m^{-3}] and Celt is the bulk concentration of the element elt [kg·m^{-3}].

The equilibrium concentration of each chemical element and the oxide speciation are calculated by the OSCAR chemistry module, PHREEQCEA (a version of the PHREEQC code [3] extended to the PWR temperature range) in combination with a thermodynamic database developed by the CEA [4]. PHREEQCEA determines the composition of the ideal solid solution (mixed oxides and any pure solid phases possibly in excess) and the equilibrium concentration of each element in relation to the chemical conditions (pH, H2, O2), the coolant temperature and the masses of the metallic element of the outer oxide/deposit or the inner oxide in each control volume.

Soluble species precipitate when their concentration in the coolant reaches their equilibrium concentration. The expression of the precipitation flux is similar to that of the dissolution flux.

Erosion of a deposit results from the coolant friction forces. The erosion flux, Jeros [kg·s^{-1}], is given by:

$$J_{eros} = \frac{E}{\Psi} \cdot m_{erod} \tag{5}$$

where E is the erosion coefficient [s^{-1}] based on [5] model and depending on the shear stress at the wall and the dynamic viscosity of the coolant, Ψ is the erosion resistance [-] and m_{erod} is the mass of the deposit that can be eroded [kg].

Deposition rate of particles takes into account turbulent diffusion [6], sedimentation, thermophoresis and boiling deposition [7]. The deposition flux, J_{depos} [kg·s^{-1}], may be expressed as follows:

$$J_{Deposition} = S_w \cdot V_{depos} \cdot C^{part} \tag{6}$$

where V_{depos} is the deposition velocity of particles [m·s^{-1}] and C_{part} is the particle concentration in the fluid [kg·m^{-3}].

2.2. Calibration and Validation

As the dissolution velocities and the erosion coefficient are not well known in PWR conditions, they are calibrated.

The validation of the OSCAR code is based on a large operating experience feedback unique in the world: the so-called EMECC campaigns (about 400 campaigns of the γ surface activity measurements in 72 different PWRs in France and abroad since 1971 using the EMECC device [8, 9].

The last version of OSCAR, OSCAR V1.4, is validated in power operating and cold shutdown conditions for PWR primary and auxiliary systems (e.g. Figure 1, thus covering a large range of chemical and thermo-hydraulic conditions (water temperature from 20°C to 350°C, laminar and turbulent, reducing and oxidizing, alkaline and acid conditions).

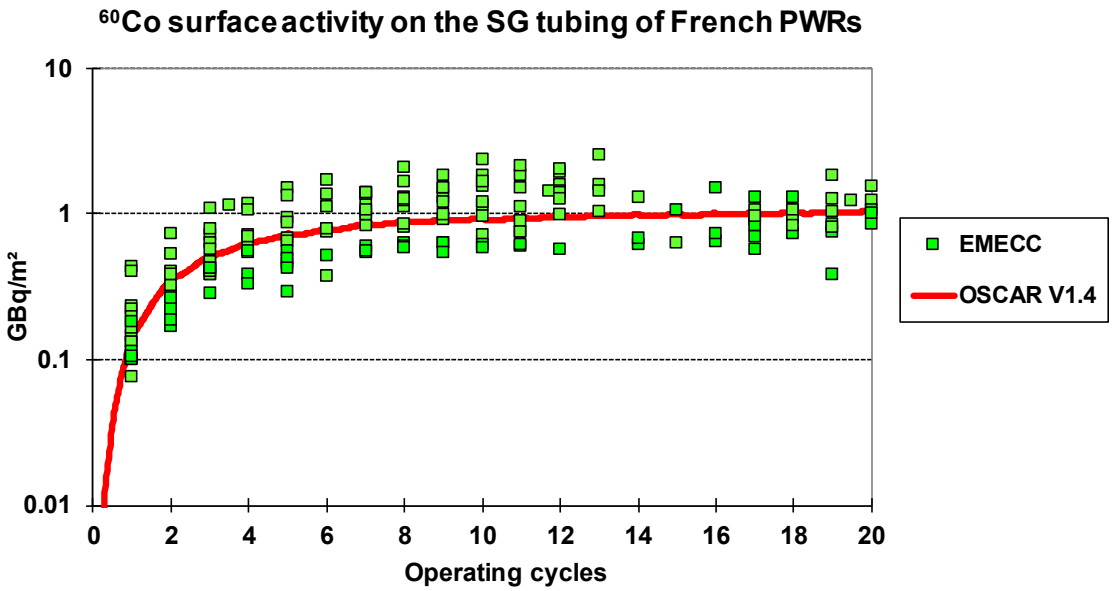

FIG. 1: Comparison EMECC measurements in French PWRs/OSCAR V1.4 calculation of a typical PWR – 60Co surface activity on the steam generator tubing.

3. OSCAR APPLICATION TO ITER: OSCAR-FUSION

The PHTSs (IBED, NBI, VV) of the ITER Tokamak Water Cooling System (TCWS) are also subject to contamination by ACPs. Indeed, a part of these systems are under neutron flux and their materials (mainly stainless steel and copper alloy) corrode.

Thanks to similarities between ITER PHTSs and PWR primary and auxiliary systems, mainly the coolant, since 1995 the PACTOLE code and then the OSCAR code has been used to calculate the ACP contamination transfer in the ITER PHTSs. Nevertheless, some differences, mainly the presence of CuCrZr alloy for the plasma facing components and the neutron flux, involved adaptations of PACTOLE and OSCAR, called PACTITER [10] and OSCAR-Fusion respectively. OSCAR-Fusion is currently the reference version, in particular thanks to its powerful chemistry module PHREEQCEA.

3.1. Transfer modelling

As the coolant of ITER PHTSs and PWRs is the same, the transfer modelling of the OSCAR-Fusion code is the same as the one of the OSCAR code (see section 2.1).

Cu data were added in PHREEQCEA thermodynamic database based on an experimental campaign performed by CEA to obtain Cu solubility data for ITER divertor PHTS conditions [11]. The three following nuclear reactions involving Cu, found to be the most important ones for safety and ORE analysis, were then included in OSCAR-Fusion: $^{63}Cu(n, \gamma)^{64}Cu$; $^{65}Cu(n, 2n)^{64}Cu$; $^{63}Cu(n, \alpha)^{60}Co$. For the other most important corrosion products (Ni, Fe, Co, Cr and Mn), the activation rates were calculated by considering the ITER fast neutron flux.

3.2. Calibration and validation

In order to get realistic values of release rates, experiments were carried out using the CEA CORELE loop in thermohydraulic and chemical operating conditions envisaged for ITER PHTS [10].

Nevertheless, the validation of OSCAR-Fusion is based on the validation of OSCAR, which covers a large range of conditions (see section 2.2).

As for the ITER PHTSs, OSCAR-Fusion can be used to predict the ACP contamination transfer in the water cooling system of DEMO (DEMOnstration power station) or of other nuclear fusion reactors.

3.3. Issues and R&D needs

In addition to the “Corrosion issues in thermonuclear fusion reactors and facilities” detailed by N. Baluc [12], the following issues and R&D needs related to the ACP transfer and its modelling in a simulation code such as OSCAR-Fusion can be highlighted:

— Simulation of the pulsed mode within a reasonable time for each ACP whatever their radioactive half-life (short or long). The pulsed mode is a succession of burn, hot and cold stand-by, baking and shutdown phases (about 400,000 burn phases of 400s over about 20 a).
— Validation of OSCAR-Fusion against experiments in ITER/DEMO PHTS conditions.
— Optimization of the cooling water chemistry conditioning for each PHTS and each operating phase. The water chemistry specification of each PHTS for plasma operation is based on the Boiling Water Reactor water chemistry, which is mainly controlled by its cation conductivity [13], rather than on the PWR water chemistry, which is mainly controlled by its pH and H_2 concentration, for instance [14].
— Determination of the corrosion rates of the different materials (stainless steels, Cu alloys and the impact of Cu swirls, RAFM steel) in the different conditions.
— Assessment of the impact of manufacturing processes (surface finish) of the materials, which is a key parameter for the contamination level [15].
— Assessment of the impact of the corrosion at different material junctions like CuCrZr and stainless steels.
— Assessment of the fraction or the quantity of ACP deposit released from the loop after a large LOCA.

4. OSCAR APPLICATION TO SFR: OSCAR-NA

The OSCAR-Na code has been developed to calculate the contamination by corrosion products in the primary circuit of SFRs [16].

In SFRs, contamination of the primary circuit is due to the release of radioactive nuclides produced in the reactor core by neutron reactions on the constituent elements of the stainless-steel fuel cladding and subassembly wrappers. Due to both bulk corrosion (i.e. surface loss) of the activated cladding and preferential release of highly soluble elements, a small fraction of the radionuclides is released into the flowing sodium and deposits throughout the primary circuit. This leads to contamination of the piping and components such as primary pumps or Intermediate Heat eXchangers (IHX). The main radio-contaminants are ^{54}Mn and ^{60}Co.

4.1. Transfer modelling

The OSCAR-Na code is based on the OSCAR code. For each region and each isotope considered, a mass balance is calculated in the sodium and in the metal. The modelling assumes that the transfer between steel and sodium is primarily by solution and precipitation of metallic elements, rather than by particle detachment and particle deposition.

The solution/precipitation model at the steel/sodium interface is based on mass transfer theory [17]. The mass flux Φ between sodium and steel is obtained by equating the fluxes at both sides of the interface:

$$\Phi = D \cdot \left.\frac{\partial C}{\partial x}\right|_{x=0} + u \cdot C_i = K^{eff} \cdot \left(\frac{C_i}{\beta} - C'\right) \tag{7}$$

where C and C' are the nuclide concentration (g/m^3) in the steel and bulk sodium, respectively (the subscript i indicating interfacial values at $x = 0$). In OSCAR-Na, C' is calculated through a complete mass balance around the primary circuit, and C_i is obtained by numerical solving of the general diffusion equation in the steel:

$$\frac{\partial C}{\partial t} = D \cdot \left(\frac{\partial^2 C}{\partial x^2}\right) + u \cdot \frac{\partial C}{\partial x} - \lambda \cdot C + R \tag{8}$$

with eq. (7) as boundary condition at the interface (λ is the decay constant of the considered radionuclide, and R is the rate of production by neutron activation).

Thus, the main parameters of the model are, for each element:

— D (m^2/s): diffusion coefficient in the austenitic stainless steel. A higher diffusion coefficient can also be considered in the ferrite layer which forms near the steel surface due to nickel depletion.

— K^{eff} (m/s): effective mass transfer coefficient between interface and bulk sodium. It corresponds to the limiting value between the diffusion rate through the sodium laminar boundary layer (k) and the dissolution or precipitation rate (k_a) at the interface: $K^{eff} = \frac{k \cdot k_a}{k + k_a}$.

— β: dimensionless chemical partition coefficient. It is related to the concentration $C'_{éq}$ in the sodium at equilibrium with the steel surface by $C'_{éq} = C_i / \beta$. For a pure element, β varies inversely with respect to the solubility.

— u (m/s) is the interfacial velocity or moving rate of the sodium/steel interface, due to dissolution and precipitation. It is positive or negative in case of bulk corrosion (dissolution) or bulk deposition (precipitation) respectively.

The other transfer models considered in the OSCAR-Na code (convection, purification, neutron activation and radioactive decay) are the ones of the OSCAR code for PWR.

The OSCAR-Na code uses a numerical method for solving the diffusion equation in the steel and the complete mass balance in sodium for all elements, allowing the calculation of the metal/sodium interface shifting and of the flux of each element through this interface.

4.2. Calibration and validation

The key parameters (D, K^{eff}, β and u) of the solution/precipitation model have been assessed from a literature review or adjusted to match some experimental data.

The simulation of the French SFR reactor PHENIX using OSCAR-Na was able to assess the correct amount of contamination and the correct contamination profiles on heat exchanger surfaces for ^{54}Mn, ^{58}Co and ^{60}Co radionuclides, compared with measurements (see Fig. 1, further details in [16]). In addition, the simulation of tests performed in the STCL loop confirms OSCAR-Na modelling ability to calculate weight losses due to corrosion of 316 SS in sodium circuits (see [18]).

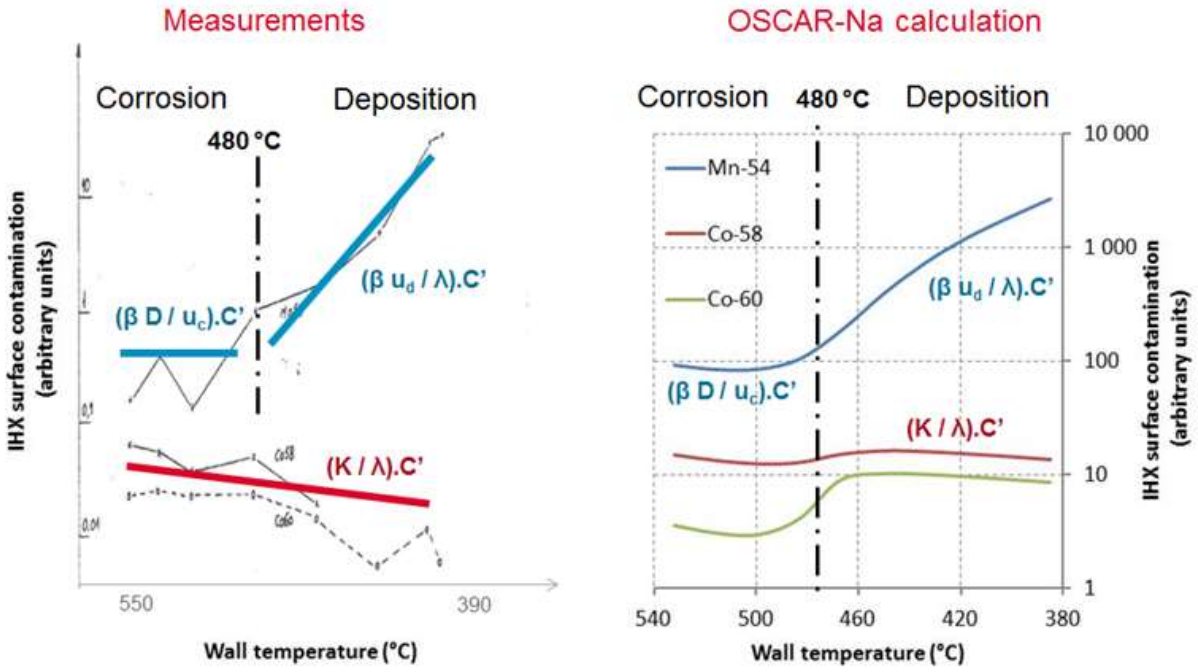

FIG. 2. Comparison measurements/OSCAR-Na calculation - PHENIX reactor IHX contamination [16].

4.3 Issues and R&D needs

In addition to the "Corrosion issues in sodium-cooled fast reactor (SFR) systems" detailed by E. Yoshida and T. Furukawa [12], the following issues and R&D needs related to the contamination transfer and its modelling in a simulation code such as OSCAR-Na can be highlighted:

- Obtaining of data on oxide equilibrium concentrations (only pure element solubility in sodium are known) and on co-precipitation.
- Obtaining of further data on diffusion coefficient in steel.
- Assessment of the impact of the ACP transfer under particle form.
- Carrying out of further OSCAR-Na validation work against operating experience with SFRs and experimental loops.
- Modelling of the contamination by fission products.

ACKNOWLEDGEMENTS

The authors are thankful to Luigi Di PACE from ENEA for his valuable suggestions on issues and R&D needs for ACP transfer in fusion reactor water cooling systems.

REFERENCES

[1] BEAL, S.K., Deposition of particles in turbulent flow on channel or pipe walls, Nuclear Science and Engineering **40** 1–11.
[2] BESLU, P., LEUTHROT, C., PACTOLE-PROFIP: two codes allowing prediction of the contamination of PWR primary circuits, Revue Générale Nucléaire (1990) 552–554.
[3] CLEAVER, J. W., YATES, B., Mechanism of Detachment of Colloidal Particles from a Flat Substrate in a turbulent Flow, Journal of Colloid and Interface Science **3** (1972).
[4] DACQUAIT, F., GUINARD, L., BARDET, F., BRETELLE, J.L., ROCHER, A., "Low primary system contamination levels in some French PWRs", Nuclear Plant Chemistry Conference (Proc. Int. Conf. Jeju Island, 2006, Paper No. 17).
[5] DACQUAIT, F., FRANCESCATTO, J., BROUTIN, F., GENIN, J.B., BENIER, G., YOU, D., RANCHOUX, G., BONNEFON, J., BACHET, M., RIOT, G., "Simulations of corrosion product transfer with the OSCAR V1.2 code", Nuclear Plant Chemistry Conference (Proc. Int. Conf. 2012).
[6] DI PACE, L., TARABELLI, D., YOU, D., Development of the PACTITER code and its application to the assessment of the ITER Divertor cooling loop corrosion products, Fusion Technol. **34** (1998) 733–737.
[7] DI PACE, L., DACQUAIT, F., SCHINDLER, P., BLET, V., NGUYEN, F., PHILIBERT, Y., LARAT, B., Development of the PACTITER code and its application to safety analyses of ITER Primary Cooling Water System, Fusion Engineering and Design **82** (2007) 237-247.
[8] EIMECKE, R., ANTHONI, S., "Ensemble de Mesure et d'Etude de la Contamination des Circuits (EMECC)", 7th International Conference on Radiation Shielding (Proc. Int. Conf. Bournemouth, 1998).
[9] FERON, D., Nuclear corrosion science and engineering, Woodhead Publishing, 2012.
[10] FERRER, A., Modélisation des mécanismes de formation sous ébullition locale des dépôts sur les gaines de combustible des Réacteurs à Eau sous Pression conduisant à des activités volumiques importantes, PhD thesis, Université de Strasbourg, 2013.
[11] FRUZZETTI, K., GARCIA, S., LYNCH, N., REID, R., "BWR and PWR chemistry operating experience and perspectives", Nuclear Plant Chemistry Conference (Proc. Int. Conf. Sapporo 2014, Paper No. 10095).
[12] GENIN, J.B., MARTEAU, H., DACQUAIT, F., BÉNIER, G., FRANCESCATTO, J., BROUTIN, F., NGUYEN, F., GIRARD, M., NOIROT, L., MAILLARD, S., MARELLE, V., BOULORÉ, A., YOU, D., PLANCQUE, G., RANCHOUX, G., BONNEFON, J., BONELLI, V., BACHET, M., RIOT, G., GRANGEON, F., "The OSCAR code package: a unique tool for simulating PWR contamination", International Conference on Water Chemistry of Nuclear Reactors Systems (Proc. Int. Conf Quebec 2010).
[13] GÉNIN, J.B., BRISSONNEAU, L., GILARDI, T., BENIER, G., OSCAR-Na V1.3: a new code for simulating corrosion product contamination in SFR, Metallurgical and Material Transactions **3E** (2016) 291–298.
[14] GÉNIN, J.B., BRISSONNEAU, L., "Validation Against Sodium Loop Experiments of Corrosion Product Contamination Code OSCAR-Na", International Conference on Fast Reactors and Related Fuel Cycles: Next Generation Nuclear Systems for Sustainable Development (Proc. Int. Conf. Yekaterinburg, 2017).
[15] GOPALAPILLAI, B., CURD1, W., PLOYHAR, S., DELL'ORCO, G., CHANG, K.-P., LI, F., SOMBOLI, F., PETROV, A., GUPTA, D., KUMAR, A., Design features of ITER Cooling Water Systems to Minimize Environmental Impacts, An International Journal of the American Nuclear Society **61** (2012) 113–118.
[16] PARKHURST, D. L., APPELO, C. A. J., Description of Input and Examples for PHREEQC Version 3 - A Computer Program for Speciation, Batch-Reaction, One-Dimensional Transport, and Inverse Geochemical Calculations, US Geological Survey, Denver (2013).
[17] PLANCQUE, G., YOU, D., BLANCHARD, E., MERTENS, Y., LAMOUROUX, C., "Role of chemistry in the phenomena occurring in nuclear power plants circuits", International Congress on Advances in Nuclear power Plants (Proc. Int. Conf. Nice, 2011).
[18] POLLEY, M.V., SKYRME, G., An analysis of radioactive corrosion product transfer in sodium loop systems, Journal of Nuclear Materials **75** (1978) 226–237.

MODELING THE RELEASE OF RADIONUCLIDES FROM IRRADIATED HEAVY LIQUID METALS

A. AERTS
Chemistry and Conditioning Programme, Belgian Nuclear Research Centre,
Boeretang, Belgium

Abstract

The approach towards modelling the source term of released radioactive materials from heavy liquid metal used as coolant and spallation target is reviewed. Accurate prediction of this source term is necessary to establish new HLM-based reactors and accelerator driven systems. To this aim, an extended approach for equilibrium modelling of the primary coolant and cover gas is proposed, based on the Gibbs energy minimization technique coupled to databases of thermochemical properties. It is indicated which properties are missing in available databases. Several topics for future research and development are proposed, in order to improve the current release models.

1. INTRODUCTION

The prevention of the release of radioactive products into the environment is a primary objective in the design of nuclear installations. The protection of the public against the consequences of an accidental release of radioactive material relies on correct operation of a series of barriers under normal operating and accidental conditions. In water cooled systems, these barriers include the fuel matrix, the fuel cladding, the reactor coolant pressure boundary and the primary containment [1].

The quantity and chemical nature of the released material is called the “source term”. This term must be known as accurately as possible, in order to determine the short and long term health and environmental effects of a release. In water cooled reactors, the source term and its radiological consequences after accidents are primarily caused by fission products initially released from the fuel [2]. The release of fission products from fuel is well understood and can be predicted reliably. However, the source term that reaches the environment is also strongly affected by retention by other barriers such as the containment, as well as by physicochemical processes occurring in the coolant.

The development of next generation nuclear systems entails the use of coolants other than water and heavy liquid metal (HLM) based reactor technology with liquid lead or lead-bismuth eutectic (LBE) coolant is seen as one of the more promising approaches [3]. The lead fast reactor is one of the generation IV concepts and lead-bismuth is foreseen in critical fast reactors as well as subcritical, accelerator driven systems (ADS).

The retention of radioactive material in heavy metal coolants strongly differs from that in water. It is generally considered that heavy liquid metals form a good barrier for fission product release and therefore have a significant mitigating effect on the source term [4–5]. In addition to their different retention properties, heavy metal cooled systems also lead to the production of a number of radioactive elements not typically encountered in water cooled reactors. Both LBE and Pb will contain activated impurities and corrosion products after irradiation. Importantly, significant amounts of polonium will form when LBE is used as coolant [6]. When the heavy metal is also used as spallation target in ADSs, a broad range of additional radioactive elements is formed [7]. Since all these elements are formed in the primary coolant, the accurate assessment of the retention properties of the coolant in such HLM based systems is a critical step in the determination of the source term.

As an example the calculated coolant activation in the MYRRHA ADS at end of life [8] is given (Fig.1). MYRRHA is a fast spectrum research reactor (50-100 MWth) under design at the Belgian Nuclear Research Centre [9]. It is an accelerator driven system (ADS) with a proton accelerator of 600 MeV, a spallation target and a multiplying core with MOX fuel. As LBE is used both as primary and coolant and spallation target, the retention of both fission and coolant activation (including spallation) products needs to be assessed. The presence of spallation and activation products in the primary coolant, next to potential ingress of fission products from damaged fuel, makes systems such as MYRRHA perhaps one of the most complex liquid metal nuclear systems from a coolant chemistry point of view.

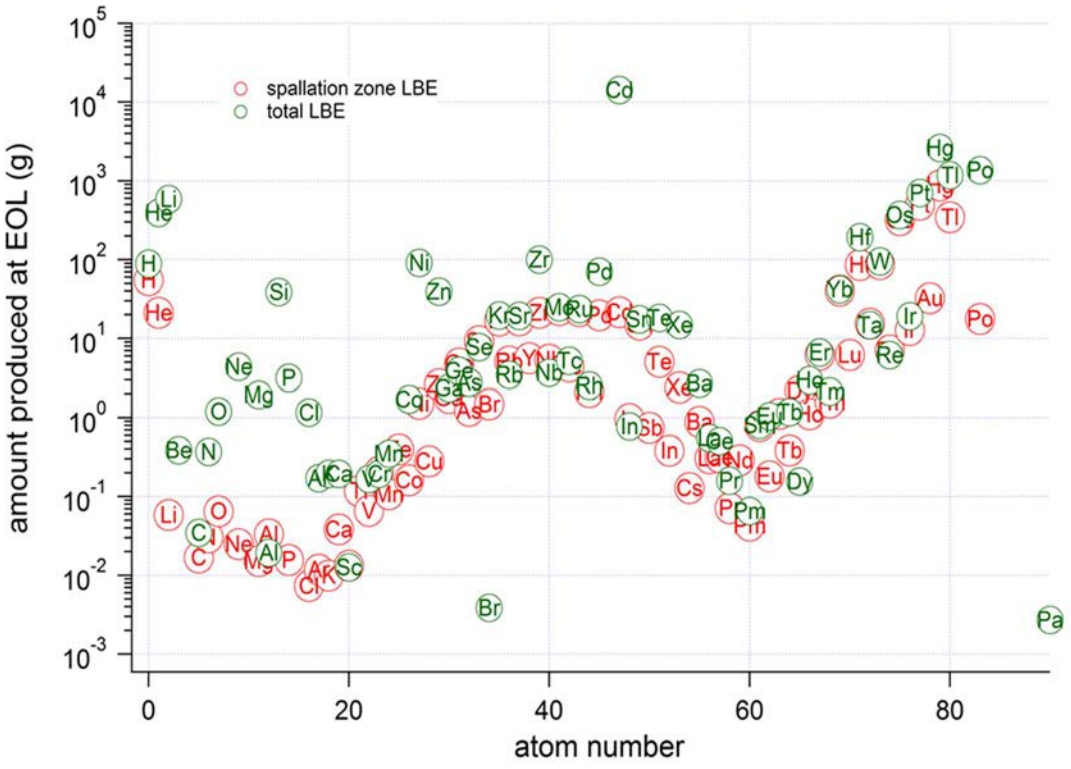

FIG. 1. Calculated inventory of radionuclides produced in the primary LBE of MYRRHA at end of life (EOL). The total inventory in the primary LBE is given by the green markers.

In MYRRHA, about 30 of the elements formed by coolant activation may individually cause unacceptably high off-site doses to the public if one adopts the assumption that they are released completely from the coolant during an accident. Examples of such elements are polonium (formed by bismuth activation), silver (mainly formed by activation of cadmium impurity in LBE) and mercury (formed by spallation).

It is clear that the assumption that these 30 elements are released completely from the LBE leads to an extremely unrealistic assessment of the source term. In reality, these elements interact chemically with the LBE coolant, with each other, with the cover gas and with various surfaces in the primary system, leading in most cases to a significant retention and therefore reduction of their release.

In view of their potential contribution to the dose, the quantification of the retention capability of LBE for these elements is crucial in safety assessments of new reactor systems, and therefore required to obtain a license. This quantification is not a trivial task, given the multitude of chemical interactions and phase transformations that these elements may undergo under various normal operation and accident conditions [10].

In the following, we briefly discuss the state-of-the-art regarding the calculation of the release of radionuclides from LBE and Pb and discuss its limitations. Based on recent work in the frame of the MYRRHA project and European projects funded by the European Union (see e.g. [11–13]), suggestions for future R&D are made with the aim to improve and extend the current capability to model radionuclide release from heavy liquid metals.

2. RADIONUCLIDE RETENTION IN HEAVY LIQUID METALS

Chemical equilibria between radioactive elements or their chemical compounds form the basis of any release analysis, as they determine the thermodynamic driving forces.

In only a few cases, these chemical equilibria can be approximated by simple laws. Noble gases can be assumed to be completely released from the LBE/Pb at equilibrium. The validity of this assumption in LBE has been confirmed by analysis of release measurements during the integral experiments ISOLDE and MEGAPIE [10,14,15].

In most cases, however, chemical interactions of the radioactive element with LBE/Pb, with other impurities in LBE/Pb, with compounds in the cover gas and with various surfaces have a large influence on the extent at which a given radionuclide is released. As a result, the released amounts are frequently much lower than complete. Transport processes and chemical reaction kinetics further govern the timing of the release.

Although in safety analyses one could in principle make the conservative assumption of complete release, this assumption in many cases leads to unacceptable radiological consequences. Therefore, the release needs to be quantitatively known.

As a first approximation, one can assume for source term calculations that the release of radioactive elements from LBE/Pb is governed by an equilibrium that effectively exists between a single, highly diluted dissolved species and a single vapor species. The partial pressure of the radioactive element is then given by Henry's law, using a simple correlation for the Henry constant K_h, which only depends on temperature T, and the concentration of the dissolved element in the LBE. In the 2015 edition of the OECD-NEA handbook on HLM technology, such correlations are recommended for a selection of elements including Pb, Bi, Po, Hg, Cd, Tl, I and Cs dissolved in LBE (and Pb). These correlations, typically of the form $\log K_h = A/T+B$, were derived from analysis of existing experimental results and theoretical considerations [10,16–17].

The number of experiments as well as the experimental conditions from which the correlations were determined are typically limited. This means that it is difficult to assess the reliability of the correlations and as well as to justify any extrapolation outside of the measured conditions.

Experimental results obtained in conditions other than dry inert or reducing cover gas are especially scarce. Based on the existing empirical correlations, it is therefore impossible to reliably assess the influence of water on the release of a given radioactive element. Also, the influence of chemical properties of the coolant such as its dissolved oxygen concentration on the release of a dissolved component cannot be predicted. Yet these conditions need to be studied for the assessment of release in large LBE and Pb based nuclear reactors or ADSs as such systems are equipped with oxygen control systems and in accidental situations may have water coming in contact with the primary coolant. Several experiments have already shown that these conditions and parameters do have an effect. For example, there are reports of increased polonium release from LBE in contact with water [18–19]. The influence of the concentration of dissolved oxygen in LBE on polonium release has been suggested in a recent study [20]. For most other elements, such studies do not exist.

On the other hand, the simplified OECD-NEA recommended correlations have been shown to be conservative in that they typically overpredict observed release in several larger scale, integral experiments such as MEGAPIE (an overview can be found in [10]). However, it is important to note that in these experiments, the LBE has experienced a narrow range of conditions only, which does not encompass the variety of conditions that may occur in the larger HLM nuclear reactors or ADSs currently under design. Accidental conditions involving for example substantial water ingress have not been encountered in MEGAPIE.

3. EXTENDED APPROACH TOWARD RELEASE MODELING

In order to predict release in large and complex LBE/Pb based nuclear installations, there is a need for improved models. The first step is to improve equilibrium modelling by extending the number of interactions that can occur in the coolant of nuclear installations as well as in the cover gas into which radionuclides are first released.

The method of choice for complex equilibrium calculations involving many phases and species is the Gibbs energy minimization method (GEM). Assuming all compounds that are involved in a certain process are known, the reliability of such GEM calculations is strongly dependent on the availability and accuracy of thermochemical data (free energies) of each species. Such data can be measured experimentally or estimated by advanced simulations [21].

In the frame of licensing and engineering design of the MYRRHA accelerator driven system, a GEM-based global approach towards prediction of the retention of elements in LBE was initiated. In contrast to previous recommendations [10], the approach takes into account much more interactions of radioactive impurities with Pb and Bi, with the main stable dissolved impurities (oxygen, corrosion products, …) and with each other. Three categories of thermochemical data were used. The two first categories comprise the properties of pure condensed phases and gaseous species, respectively, which are to large extent known and are compiled in existing thermochemical databases such as [22]. An important exception here is the element polonium, for which thermochemical properties were derived from experimental and theoretical results (mostly quantum chemical)

obtained within the frame of the MYRRHA R&D programme and previous and ongoing European projects (e.g. FP7 SEARCH, H2020 MYRTE). The third category are the thermochemical properties of the dissolved elements. Here, many data for LBE are lacking, but a preliminary database for all elements could be compiled based on available information from literature of binary systems with either Pb or Bi, and from analysis of experimental results. With these thermochemical properties, the chemical composition at equilibrium in MYRRHA was calculated by the GEM method. The approach allows quantification of the release and chemical speciation of each element in LBE and has been used recently in support of the licensing of the MYRRHA ADS.

Several simulations could quantitatively reproduce experimental release data under inert or reducing conditions, such as those of Se, Te, Hg and Cd from LBE. This adds confidence that the modelling approach and assumptions are valid. The improved physicochemical description also increases confidence in extrapolations outside the range in which experimental data were collected. From the results, the contribution of these elements to the source term could be derived.

The modelling approach further allows to assess the influence of e.g. water on the release. For example, an increased release of dissolved tellurium in specific humid conditions was predicted, similar to experimental observations of polonium. In case of tellurium, thermochemical properties of the involved compounds are much better known than for polonium. Such a simulation with tellurium thus hinted at which homologous polonium species could be responsible for the increased release. The properties of the missing polonium species are currently being calculated theoretically.

Thus, the results of GEM simulations indicated where possible issues may arise, in that way further pointing out the direction of future research. This is especially helpful, because without such information, the number of possible experiments would be impractically large. In summary, to improve release calculations from LBE and Pb, the following specific R&D needs were identified:

— Thermochemical properties of gaseous polonium molecules, especially compounds with oxygen and hydrogen by analogy with tellurium. These can be obtained by quantum chemistry simulations.
— Experimental determination of the thermochemical properties of dilute dissolved fission products and spallation products in Pb and especially in LBE. Crucial are iodine and caesium.
— Significant increase in the number of experimental release data in presence of water vapor and with better control of dissolved as well as gaseous oxygen.
— Dedicated experiments to investigate several potentially important (non-equilibrium) phenomena such as interactions between Cs and I and effects of oxide layers on free surfaces on release.
— Additional integral experiments under irradiation, focused on the chemistry of radionuclides in the coolant, which have chemical conditions representative for those expected in a reactor during normal operation and especially during accidents.
— Experimental measurement of the adsorption behaviour of dissolved radionuclides from LBE and of gaseous radionuclide compounds on structural materials.
— Concurrently, an R&D effort needs to be initiated to couple the equilibrium models to transport models.

4. CONCLUSIONS AND OUTLOOK

Simplified approaches for the evaluation of the release of radionuclides from LBE and Pb are available in literature. These approaches have been proven to be successful and conservative in several cases, but also present strong limitations when release from complex, large heavy liquid metal-based reactors and accelerator driven systems needs to be evaluated. A first step to improve these simple approaches is based on an extension of the number of interactions of radionuclides in the primary coolant and cover gas coupled to Gibbs energy calculations for calculation of chemical equilibrium. This modelling approach has been successful to predict experimental results accurately, and clearly shows which additional research is needed in order to improve the accuracy and range of applicability of the results.

ACKNOWLEDGEMENTS

This work is supported by the Belgian government through the MYRRHA project and the European Commission under the Horizon 2020 programme (MYRTE Project No. 662186). The author thanks Jörg Neuhausen for critically reviewing this manuscript.

REFERENCES

[1] BURKART, K., LIBMANN, J.; STOIBER, C.; ARO, I.; SCHOBER, C., Regulatory control of nuclear power plants. Regulatory control of nuclear power plants, https://www.iaea.org/ns/tutorials/regcontrol/assess/assess3213.htm

[2] KONINGS, R. J. M.; WISS, T.; BENES, O., Predicting material release during a nuclear reactor accident, Nat. Mater. **14** (2015) 247–252.

[3] LOCATELLI, G., MANCINI, M., TODESCHINI, N., Generation IV nuclear reactors: Current status and future prospects, Energy Policy **61** (2013) 1503–1520.

[4] TARANTINO, M., CINOTTI, L.; ROZZIA, D., Lead-cooled fast reactor (LFR) development gaps, Technical Meeting to Identify Innovative Fast Neutron Systems Development Gaps, IAEA, Vienna (2012).

[5] HUMMEL, D.W., "Source Term Evaluation for Advanced Small Modular Reactor Concepts", 4th International Technical Meeting on Small Reactors (ITMSR-4) Ottawa, 2016.

[6] PANKRATOV, D. V; EFIMOV, E. I.; TOSHINSKII, G. I.; RYABAYA, L. D., Analysis of the Polonium Hazard in Nuclear Power Systems with Lead--Bismuth Coolant, At. Energy **97** (2004) 559–563.

[7] ZANINI, L., DEMENTJEV, S.; GRÖSCHEL, F., LEUNG, W., MILENKOVIC, R., THOMSEN, K., WAGNER, W., WOHLMUTHER, M., CHENG, X.; CLASS, A., KONOBEYEV, A., AGOSTINI, P., MELONI, P., DAVID, J.-C., LETOURNEAU, A., LERAY, S., PANEBIANCO, S., CACHON, L., LATGÉ, C., ROUBIN, P., GUERTIN, A., THIOLLIERE, N., DIERCKX, M., Experience from the post-test analysis of MEGAPIE, J. Nucl. Mater. **415** (2011) 367–377.

[8] STANKOVSKIY, A.; VAN DEN EYNDE, G., Source term calculation for MYRRHA fast spectrum facility, SCK-CEN internal report (2012).

[9] ABDERRAHIM, H., Contribution of the European Commission to a European Strategy for HLW Management Through Partitioning and Transmutation, in Nuclear Back-end and Transmutation Technology for Waste Disposal, (NAKAJIMA, K., Ed.) Springer Japan (2015).

[10] FAZIO, C., Handbook on Lead-bismuth Eutectic Alloy and Lead Properties, Materials Compatibility, Thermal-hydraulics and Technologies, Nuclear Energy Agency - Organisation For Economic Co-operation And Development, Paris (2015).

[11] MAUGERI, E. A.; NEUHAUSEN, J.; EICHLER, R.; DRESSLER, R.; RIJPSTRA, K.; COTTENIER, S.; PIGUET, D.; VOEGELE, A., SCHUMANN, D., Adsorption of volatile polonium and bismuth species on metals in various gas atmospheres: Adsorption of volatile polonium and bismuth on gold, Radiochim, Acta **104** (2016).

[12] GONZALEZ PRIETO, B.,MARINO, A., LIM, J., ROSSEEL, K., MARTENS, J., RIZZI, M., NEUHAUSEN, J., DEN BOSCH, J., AERTS, A., Use of the transpiration method to study polonium evaporation from liquid lead-bismuth eutectic at high temperature. Radiochim. Acta **102** (2014).

[13] RIJPSTRA, K., DEYNE, A.V., MAUGERI, E.A.; NEUHAUSEN, J.; WAROQUIER, M.; SPEYBROECK, V. VAN; COTTENIER, S., Ab initio study of the trapping of polonium on noble metals, J. Nucl. Mater. **472** (2016) 35–42.

[14] THIOLLIERE, N., ZANINI, L., DAVID, J. C., EIKENBERG, J., GUERTIN, A., KONOBEYEV, A. Y., LEMAIRE, S., PANEBIANCO, S., Gas Production in the MEGAPIE Spallation Target, Nucl. Sci. Eng. **169** (2011) 178–187.

[15] ZANINI, L., ANDERSSON, M., EVERAERTS, P.; FALLOT, M.; FRANBERG, H.; GROESCHEL, F.; JOST, C.; KIRCHNER, T., KOJIMA, Y.; KOESTER, U.; LEBENHAFT, J.; MANFRIN, E.; PITCHER, E.; RAVN, H.; TALL, Y.; WAGNER, W., WOHLMUTHER, M., Volatile Elements Production Rates in a Proton Irradiated Pb/Bi Target, AIP International Conference on Nuclear Data for Science and Technology (Proc. int Conf. 2005) **769** (2005) 1525–1528.

[16] JOLKKONEN, M., Report on Source Term Assessment for XT-ADS and the lead cooled EFIT -- EUROTRANS D1.62/64 (2009).

[17] JOLKKONEN, M., WALLENIUS, J., Report on source term assessment for the ETDR (ALFRED) (2013).

[18] BUONGIORNO, J., LARSON, C., CZERWINSKI, K. R., Speciation of polonium released from molten lead bismuth. Radiochim, Acta **91** (2003) 153–158.

[19] LARSON, C. L.: Polonium extraction techniques for a lead--bismuth cooled fast reactor, Polonium extraction techniques for a lead--bismuth cooled fast reactor, MIT (2002).

[20] GONZALEZ PRIETO, B., LIM, J., ROSSEEL, K., MARTENS, J. A., AERTS, A., Polonium evaporation from liquid lead--bismuth eutectic with different oxygen content, J. Radioanal. Nucl. Chem. **1** (2015).

[21] VAN YPEREN-DE DEYNE, A., RIJPSTRA, K., WAROQUIER, M., VAN SPEYBROECK, V., COTTENIER, S., Binary and ternary Po-containing molecules relevant for LBE cooled reactors at operating temperature, J. Nucl. Mater. **458** (2015).

[22] BARIN, I., Thermochemical Data of Pure Substances, Wiley (1995).

ACTIVATION CHARACTERISTICS OF THE FUSION POWER PLANT COOLANTS HE, WATER, PB-LI AND ASPECTS OF TRITIUM EXTRACTION TECHNIQUES

U. FISCHER, P. PERESLAVTSEV
Karlsruhe Institute of Technology, Institut für Neutronenphysik und Reaktortechnik,

I. CRISTESCU
Karlsruhe Institute of Technology, Institut für Technische Physik,

Eggenstein-Leopoldshafen, Germany

Abstract

This paper presents the activation characteristics of the helium, water and Pb-Li coolants when employed in the HCPB, DCLL and WCLL DEMO power plants. Related activation analyses were performed on the basis of coupled MCNP transport and FISPACT inventory calculations using 3D DEMO models developed within the PPPT programme. The He coolant shows a very low activity level with no emission of gamma radiation. The water coolant shows a very high activity and gamma radiation level during plant operation and shortly after shut-down due to the radionuclide ^{16}N generated from ^{16}O. This results in a permanent γ-radiation source in the entire water loop during plant operation. The Pb-Li coolant acts also as breeder material and thus shows a high activity level due to the tritium generated. Without considering tritium, the activation level is significantly lower and is dominated by Pb activation products. The generation (and potential release) of ^{210}Po is of serious concern requiring possibly the continuous extraction of the Bi produced from the irradiated Pb-Li. Furthermore, some aspects of the tritium extraction from the considered coolants are presented. Tritium will be produced in large amounts in the Pb-Li coolant which serves also as tritium breeding material. Small quantities may be present in the helium or the water coolant due to permeation processes. A preliminary evaluation as far as tritium permeation in the WCLL, HCLL, HCPB and DCLL is concerned is introduced. A critical review of the technologies that have the potential for the industrialization at DEMO conditions and the features of the implementation in the coolant systems is presented as well.

1. INTRODUCTION

Helium gas, water and the liquid metal Pb-Li are the primary coolants considered for the heat extraction in future Fusion Power Plants (FPP). Within the European Power Plant Physics and Technology (PPPT) program of the EUROfusion Consortium [1], four blanket concepts utilizing these coolants are under development for a DEMOnstration power plant: the Water cooled Lithium Lead (WCLL), the Helium Cooled Pebble Bed (HCPB), the Helium Cooled Lithium Lead (HCLL) and the Dual Coolant Lithium Lead (DCLL) [2].

The activation of the coolants by neutron induced activation reactions on coolant constituents, impurities and possible corrosion products affects the safety during operation and maintenance of the plant as well as the processing and management of the activated materials including a possible re-use or the final disposal in a repository. It is thus required to have an assessment of the activation inventories produced in the FPP as well as the resulting radiation hazard potential.

The first part of the paper is devoted to the activation characteristics of the helium, water and Pb-Li coolants when employed in the HCPB, HCLL, DCLL and WCLL DEMO power plants. The related activation analyses were performed on the basis of coupled MCNP transport and FISPACT inventory calculations using 3D DEMO models developed for the blanket design and optimization analyses within the PPPT program. Activation results are reported and discussed including possible measures to reduce the radiation hazard.

The second part of the paper addresses aspects of the tritium extraction from the considered coolants. Tritium will be produced in large amounts in the Pb-Li coolant which serves also as tritium breeding material. In the helium or the water coolant, small amounts of tritium may be present, mainly due to permeation processes. A preliminary evaluation of the extraction techniques is provided as far as tritium permeation in the WCLL, HCLL, HCPB and DCLL is concerned. The paper concludes with a critical review of the technologies which show the potential for the industrialization at DEMO conditions and the features of the implementation in the coolant systems.

2. COOLANT ACTIVATION CHARACTERISTICS

The activation characteristics are assessed for the coolants helium gas, water and the liquid metal eutectic alloy Pb-15.7Li as employed in the designs of the HCPB, WCLL and DCL DEMO fusion power plants developed within the PPPT programme.

2.1. DEMO blanket concepts

The development of the EU breeder blanket concepts for DEMO is conducted within the PPPT programme of EUROfusion. The considered blanket concepts include three liquid metal based blankets, utilizing the eutectic alloy Pb-15.8Li as breeder material (HCLL, WCLL, DCLL) and a solid breeder blanket (HCPB) with Li_4SiO_4 pebbles as breeder and beryllium as neutron multiplier. The HCPB and HCLL blankets employ high pressure helium gas (8 MPa) as coolant, the WCLL blanket utilizes water at 15.5 MPa for the cooling. The DCLL blanket concept, on the other hand, employs helium (8 MPa) for the cooling of the blanket steel structures, including the highly loaded first wall, while the Pb-Li breeder is directly cooled by circulating the Pb-Li liquid metal to the heat exchanger. In this work, we consider the HCPB, the WCLL and the DCLL for the activation analyses of the helium, water and Pb-Li coolants, respectively.

Fig. 1 shows a CAD model of DEMO, along with the main reactor parameters, used as basis for the blanket design and the activation analyses. To this end, specific models of the blanket modules, derived from the engineering CAD models of the HCPB, HCLL, DCLL and WCLL blanket concepts, are inserted into the empty spaces reserved for the blanket [3]. This process is detailed on the example of the HCPB DEMO in the next section.

The DEMO blanket design is based on the Multi Module Segmentation (MMS) scheme with typically 6 to 8 modules arranged in poloidal direction in a torus segment on either side of the plasma chamber. The "modules are attached to a Back Supporting Structure (BSS) that acts as mechanical support and hosts the main manifolds for the coolant and the Tritium carrier. The space available in radial direction for the breeder blanket, including first wall (FW), breeder zone, manifold and blanket support structure, is about 80 cm and 130 cm, inboard and outboard, respectively. As a common design feature of the FW, a 2 mm thick tungsten armour is assumed" [2]. Fig. 2 shows the modules designed for the HCPB, DCLL and WCLL breeder blankets.

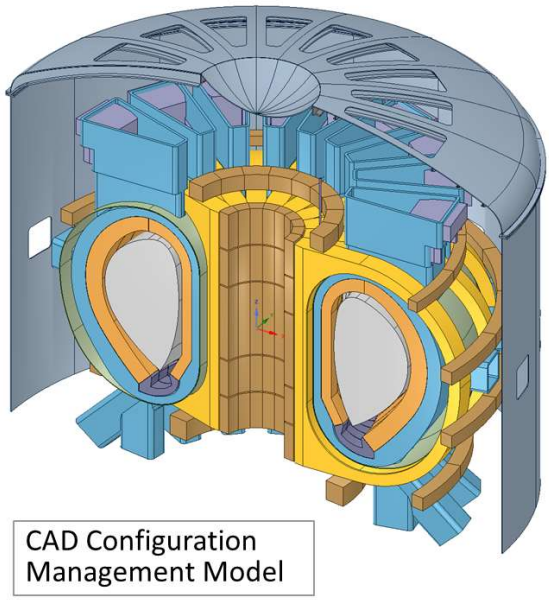

"EU DEMO1 2015"

Main reactor parameters	
No. of TF coils	18
Major radius [m]	9.072
Minor radius [m]	2.927
Aspect ratio	3.1
Plasma elongation, κ_{95}	1.59
Plasma triangularitry, δ_{95}	0.33
Average neutron wall loading [MW/m^2]	1.05
Fusion power [MW]	2037
Net electric power [MW]	500

$\Rightarrow$ *18 torus sectors of 20°*

FIG. 1. EU DEMO Baseline model and parameters.

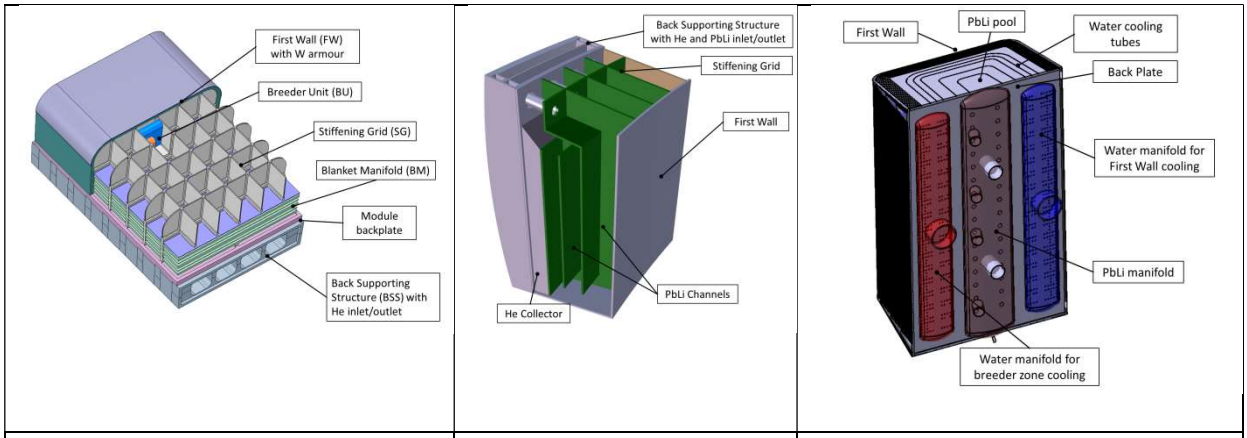

HCPB	DCLL	WCLL

FIG. 2. HCPB, DCLL and WCLL breeder blanket modules developed for DEMO (2015) [3].

2.2. Computational approach

Coupled neutron transport – activation calculations are performed to provide the activity inventories of the considered coolants at the specified locations in DEMO and decay times after shut-down. KIT's computational scheme linking the MCNP Monte Carlo code [4] and the FISPACT inventory code [5] through automated interfaces (see Fig. 3) is used for these calculations. This approach enables the use of full and detailed 3D models of DEMO as developed for the design analyses of the blanket concepts (see Fig. 4 for HCPB model). JEFF-3.1 nuclear data are used in the MCNP transport calculations, and EAF-2010 activation cross-section data in the FISPACT inventory calculations.

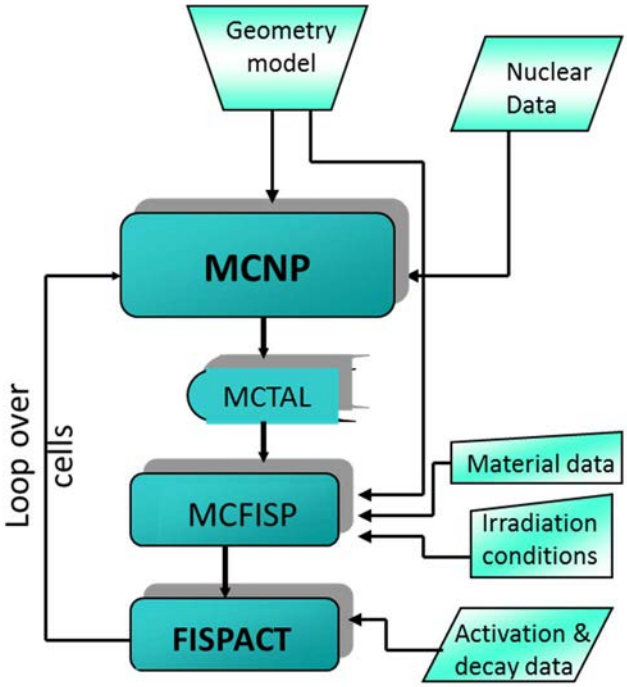

FIG. 3. Computation scheme for coupled MCNP transport – FISPACT inventory calculations [8].

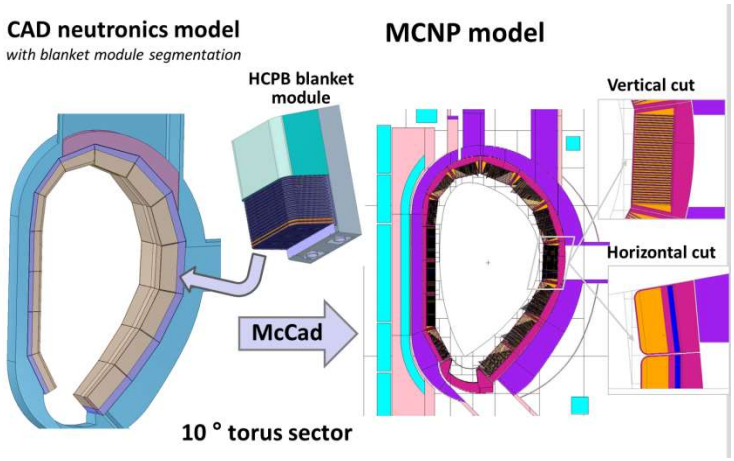

FIG. 4. MCNP model of the HCPB DEMO as generated from underlying CAD models and used with the coupled MCNP-FISPACT calculations [9].

The first computation step provides the neutron flux spectra, calculated with MCNP in 175 energy groups at the specified locations (geometry/material cells). In this work, we consider the central outboard blanket module (BM) which is subjected to the highest neutron wall loading, approximately 1.3 MW/m2. For the He gas and the water coolants in the HCPB and the WCLL blankets, respectively, the first wall (FW) of the BM is selected where the coolants are irradiated at the highest neutron flux levels. For the DCLL with the Pb-Li coolant, the selected location is the front channel of the BM. Here the neutron flux is averaged over the poloidal height of the BM and a radial depth of 5 cm.

The second computation step consists of a series of nuclide inventory calculations with the FISPACT code using the neutron flux spectra provided by the preceding MCNP calculation. In this work the inventory calculations are limited in each case (HCPB, WCLL, DCLL) to one location (geometry cell) and material (He, water and Pb-Li, respectively) as described above. Thus, no loop over the geometry cells and materials is required as indicated in Fig. 3.

The inventory calculations require as input the elemental material composition and the irradiation history. For the He coolant, pure helium is considered with its natural isotopic abundancies (1.38 appm ^{3}He, 99.999862 at% ^{4}He). Potential impurities are at extremely low levels and are considered not significant with regard to activation issues. For the water coolant, pure water is considered with a conservatively estimated amount of steel corrosion products of 20 g in 200 tons of water and the elemental composition shown in Table 1. For the Pb-Li eutectic alloy, the material specification shown in Table 2, provided by F4E for the procurement of Pb-Li [6], is used.

The irradiation scenario assumed for the activation calculations is based on the operation scheme specified for DEMO. The scheduled operation runs over 20 calendar years (CY) at an average availability of 30%. This results in a total DEMO plant lifetime of 6 full power years (FPY). Two operation phases are assumed: The first phase will run over 5.2 CY and reach 1.57 FPY. This phase assumes the deployment of a so-called starter blanket with a maximum displacement damage accumulation of 20 dpa in the steel of the first wall. (The second phase will last 14.8 CY (4.43 FPY) and employ another blanket that can withstand at least 50 dpa).

TABLE 1. ELEMENTAL COMPOSITION OF THE CORROSION PRODUCTS ASSUMED IN THE WATER COOLANT

Element	wt%
Fe	75.8078
Ni	7.6774
Co	0.0351
Cr	14.8827
Mn	1.4281
Cu	0.1689

TABLE 2. ELEMENTAL COMPOSITION OF THE PB-17.8LI EUTECTIC ALLOY, INCLUDING IMPURITIES AND TRAMP ELEMENTS [6]

Element	**wt% [10^{-2}g/g]**	**Element**	**wt% [10^{-2}g/g]**
Li	0.62	Mo	0.005
Ag	0.001	Ni	0.005
Cu	0.001	V	0.005
Nb	0.001	Si	0.01
Pd	0.001	Al	0.01
Zn	0.001	Bi	0.02
Fe	0.005	Sn	0.02
Cr	0.005	W	0.02
Mn	0.005	Pb	Balance

The irradiation scenario assumed for the activation calculations is based on the operation scheme specified for DEMO. The scheduled operation runs over 20 calendar years (CY) at an average availability of 30%. This results in a total DEMO plant lifetime of 6 full power years (FPY). Two operation phases are assumed: The first phase will run over 5.2 CY and reach 1.57 FPY. This phase assumes the deployment of a so-called starter blanket with a maximum displacement damage accumulation of 20 dpa in the steel of the first wall. (The second phase will last 14.8 CY (4.43 FPY) and employ another blanket that can withstand at least 50 dpa).

The irradiation scheme used in this work represents the first DEMO operation phase with a continuous operation over 5.2 years (CY) minus 10 days at 30% of the nominal fusion power followed by 10 days pulsed operation with 48 pulses of 4 hours at full power and 1-hour dwell time in between.

2.3. Results presentation and discussion

Fig. 5 compares the specific activities calculated for the He, water and Pb-Li coolants when irradiated in the HCPB, WCLL and DCLL DEMO, respectively, as specified above. Fig. 5a shows the specific activities in units of Bq/kg. The mass densities of the coolants at the given operation conditions amount to 4.92 kg/m3, 725 kg/m3, and 9540 kg/m^3, respectively. The specific activities, accordingly converted into units of Ci/m^3, are shown in Fig. 5(b). It is revealed that Pb-Li shows the highest activation level, even without considering tritium generated in the Pb-Li breeding material. The He activation level is lowest and only due to the tritium produced on the minor ^{3}He isotope. The activation level of water is high at the short term, and thus during plant operation, and very low afterwards. A more detailed discussion of the observed behaviour is given in the following sub-sections.

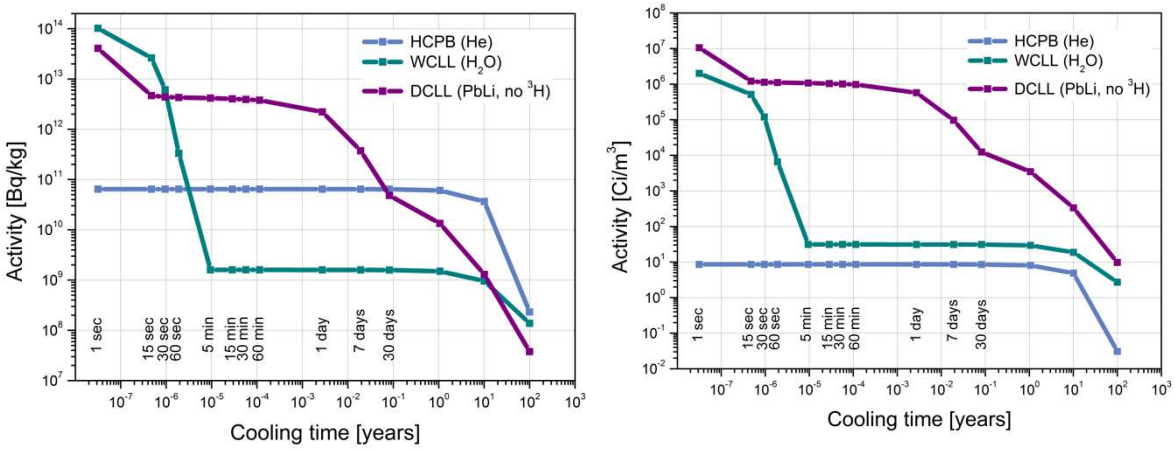

FIG. 5. (a) Specific activity of the He, water and Pb-Li coolants as function of the cooling time in Bq/kg; (b) same in Ci/m^3.

2.3.1. Helium gas in the HCPB DEMO

The activity of the He coolant is only due to tritium generated through the ^{3}He(n,p)^{3}H reaction from the minor ^{3}He isotope (1.38 appm natural abundancy). The resulting activity level for the HCPB DEMO is at 6.4×10^{10} Bq/kg (see Fig. 6) which translates into a specific activity of 0.35 Ci/m^3. Tritium decays to ^{3}He via β^- decay ($T_{1/2}$=12.3 y) with no emission of γ-radiation.

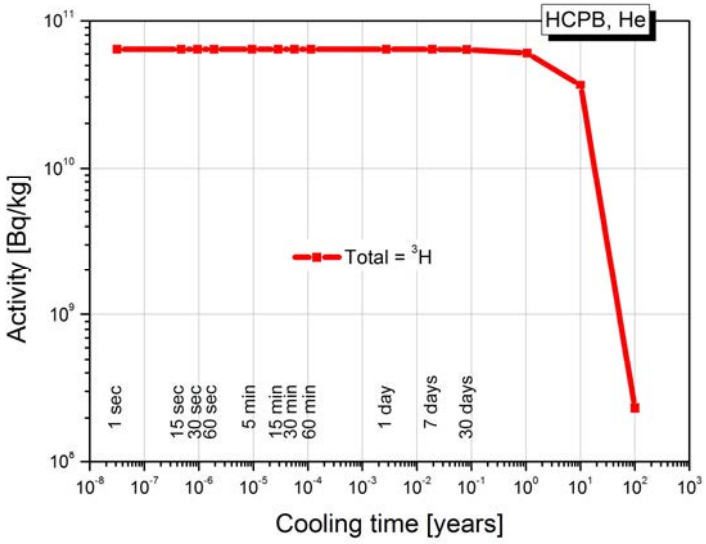

FIG. 6. Specific activity [Bq/kg] of the He coolant in the HCPB DEMO as function of the cooling time.

2.3.2. Pb-Li in the DCLL DEMO

Pb-Li serves both as breeder material and coolant in the DCLL DEMO. The activity is thus dominated by the tritium generated in the $^{6}Li(n,\alpha)t$ breeding reaction in Pb-Li (Fig. 7(a)). Tritium is externally extracted from the Pb-Li for the refuelling of the (D-T) plasma. Suitable extraction techniques are discussed in section 3.3 below. We thus consider the activation characteristics of the Pb-Li coolant without tritium, as shown in Fig. 7(b). The activity level is significantly lower (several orders of magnitude) and is dominated by Pb activation products, notably ^{207m}Pb ($T_{1/2}$= 0.8 s) and ^{203}Pb ($T_{1/2}$=51.9 h) at short times, and ^{204}Tl ($T_{1/2}$=3.78 y) at longer times, see Fig. 7(b).

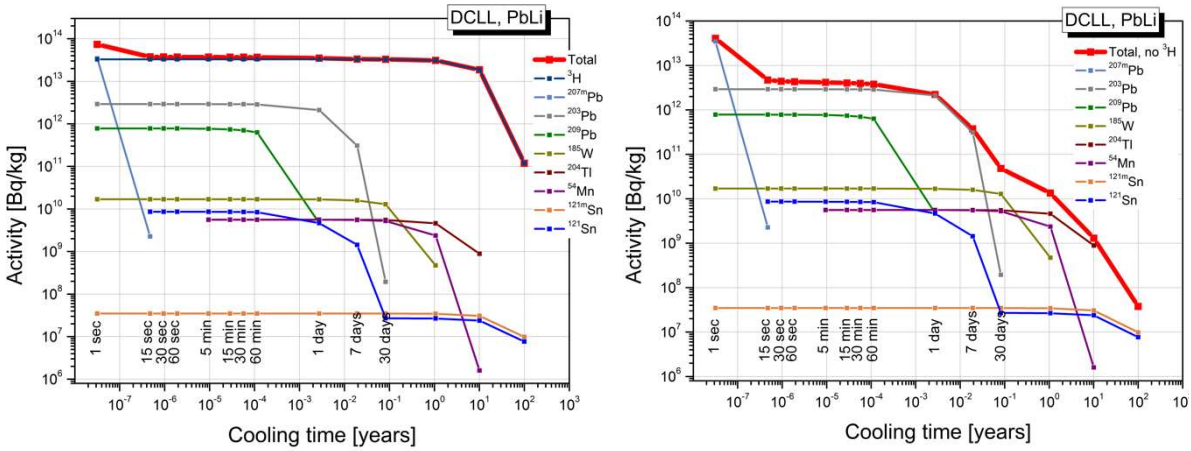

FIG. 7. (a) Specific activity of Pb-Li in the DCLL DEMO as function of the cooling time with tritium; (b) same without tritium.

2.3.3. Water in the WCLL DEMO

The activity level in the water coolant, shown in Fig. 8, is very high at short times due to the generation of the short-lived β^--active radionuclide ^{16}N ($T_{1/2}$= 7.13 s) via the reaction $^{16}O(n,p)^{16}N$. This applies accordingly during plant operation times and results in a permanent γ-radiation source of the circulating water inside and outside the irradiation zone. (As a consequence, the water pipes need to be properly shielded in the entire water loop). After the decay of ^{16}N, the activity drops to a very low level (around 10^9 Bq/kg) due to small amounts of ^{3}H and ^{14}C produced form ^{2}H and $^{16,17}O$, respectively.

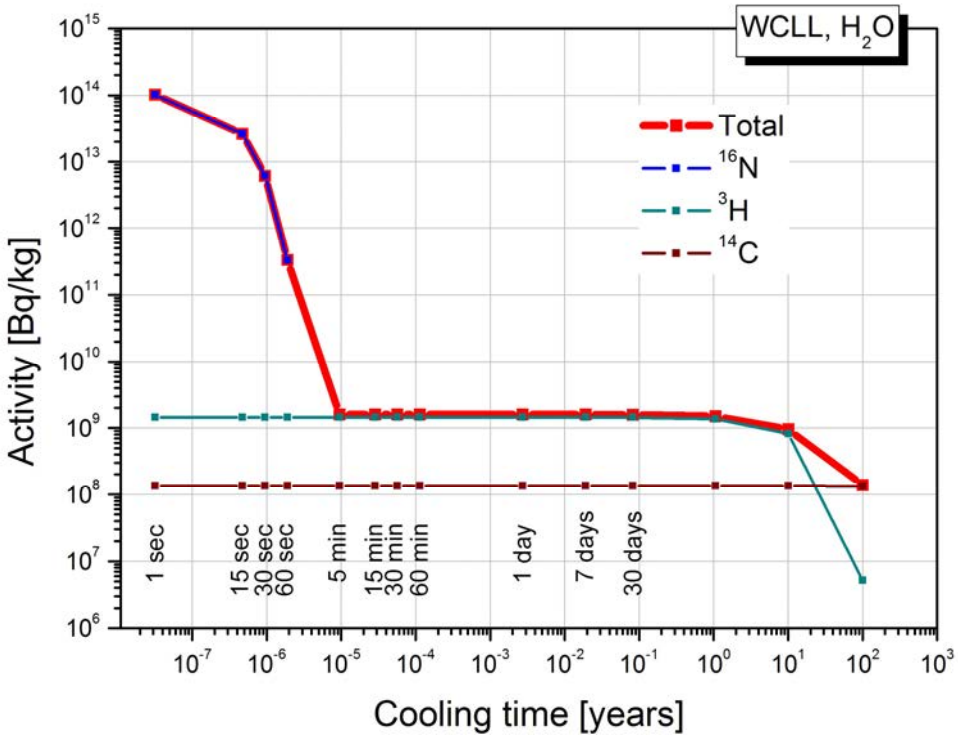

FIG. 8. Specific activity [Bq/kg] of the water coolant in the WCLL DEMO as function of the cooling time.

2.3.4. Contact gamma dose rates

The contact gamma dose rate is provided with the FISPACT calculation for the approximation of a semi-infinite slab arrangement of the activated material. Thus, this approximation does not take into account the real geometry, as employed in the coupled transport-activation calculation, nor the transport of the emitted decay photons through the actual material configuration.

Fig. 9 shows this contact gamma dose rate for the water and the Pb-Li, activated in the WCLL and the DCLL DEMO, respectively. Figs. 10 a and b show the breakdown into individual radionuclide contributions for the Pb-Li and the water coolant. (It is recalled that the activation of the He coolant in the HCPB DEMO does not result in gamma radiation due to the fact that the activity is only due to the tritium which decays without emission of gammas).

The dose rate level is highest for the activated water at short cooling times due to the ^{16}N radionuclide emitting high energy gammas of 6.13 and 7.12 MeV. With the decay of ^{16}N, the contact gamma dose rate of the water coolant drops to a low level below the recycling limit of 10 mSv/h. At these cooling times, it is dominated by the activated corrosion products assumed to be present in the water (20 g ACP in 200 tons of water, see section 2.2). The gamma dose rate level of the radionuclide ^{17}N ($T_{1/2}$= 4.17 s), generated in the water via the reaction ^{17}O(n,p)^{17}N, is comparatively low (see Fig. 9(b)). The presence of ^{17}N in the water coolant is an issue of serious concern since it emits delayed neutrons (β^-n decay) which activate the coolant pipes outside the irradiation zone.

The dose rate level of the Pb-Li coolant, activated in the DCLL DEMO, is at a high level, although lower than the activated water at short times and during the plant operation. The dose rate is dominated at short cooling times (less than one month) by the Pb activation products and afterwards by radionuclides generated from the specified impurities, in particular ^{54}Mn. Contributions from ^{210}Po, generated through the reaction & decay sequence ^{208}Pb(n,γ)^{209}Pb(β^-)^{209}Bi(n,γ)^{210}Bi)(β^-) ^{210}Po, to the contact gamma dose rate are not significant. The related (severe) radiation hazard arises from the release of gaseous Po and a potential inhalation of this strong a α-radiation emitter.

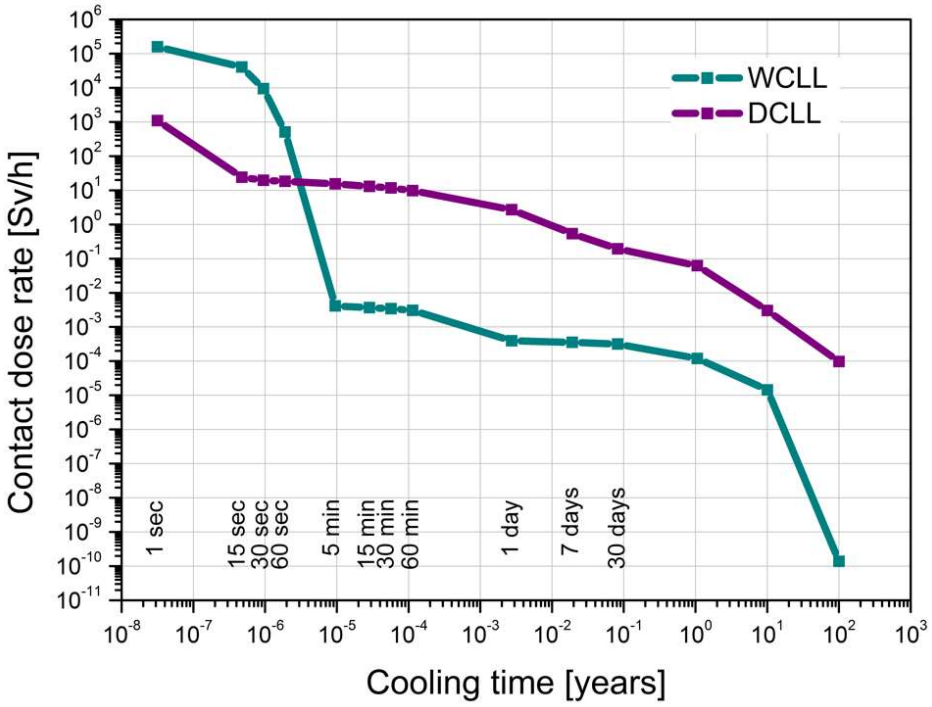

FIG. 9. Contact gamma dose rate for the water and the Pb-Li coolant activated in the WCLL and DCLL DEMO, respectively, as provided by FISPACT with the semi-infinite slab approximation.

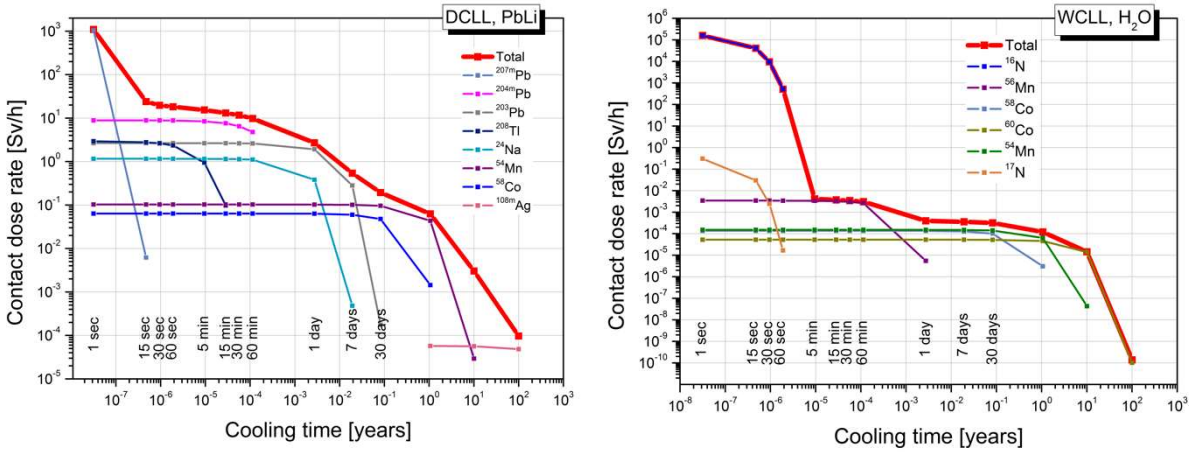

FIG. 10. (a) Contact gamma dose rates as function of cooling time as provided by FISPACT with the semi-infinite slab approximation for Pb-Li activated in the DCLL DEMO; (b) same for WCLL DEMO.

2.3.5. Conclusion on activation characteristics

Activation characteristics of the coolants helium, water and Pb-Li were assessed as employed in the European designs for a water cooled lithium-lead (WCLL), a helium cooled pebble bed (HCPB) and dual coolant lithium-lead (DCLL) based DEMO fusion power plant. The results are summarized as follows:

— The He coolant shows a very low activity level which is only due to the tritium generated from the minor ^{3}He isotope (1.38 appm natural abundancy). There is no emission of gamma radiation from the activated He coolant.
— The water coolant shows a very high activity and gamma radiation level during plant operation and shortly (few minutes) after shut-down due to the radionuclide ^{16}N generated from ^{16}O. This results in a permanent γ-

radiation source of the water circulating inside and outside the irradiation zone during the plant operation and requires the water pipes to be properly shielded in the entire water loop. At longer cooling times the activity and gamma dose rate levels are low due to the tritium generated in the water and the activated corrosion products (ACP) assumed in the water. Further consideration needs to be given to the tritium permeating into the water, the ACP, the radiolysis and the water chemistry affecting the activation behaviour of the water and the resulting radiation hazard.

— The Pb-Li coolant acts also as breeder material. The activity level is thus very high and dominated by the tritium generated in the $^{6}Li(n,\alpha)t$ breeding reaction. The activity level of Pb-Li without considering tritium is significantly lower and is dominated by Pb activation products. The activity and dose rate levels during operation and at shut-down are though comparatively high. Further consideration needs to be given to ACPs, produced in the Pb-Li loop, for which no assessment is available so far. The generation (and potential release) of the strong α-radiation emitter ^{210}Po is another concern for Pb-Li requiring possibly the continuous extraction of the Bi produced from the irradiated Pb-Li.

3. ASPECTS OF TRITIUM EXTRACTION TECHNIQUES FOR WATER, HE AND PB-LI

The optimisation of the heat transfer at the level of the breeder blanket (BB) and the steam generator (SG) has as a consequence that large surface area with thin walls operated at high temperatures are required. Therefore, the tritium permeation from the BB to the steam generator is favourable and consequently a significant amount of tritium may be released into the environment.

The commonly accepted tritium losses originating from the BB shall be maintained below a target value of 0.6 g/y. As a reference it is considered that the reactor including the inner fuel cycle needs to maintain the total tritium losses below the 1 g/y limit. In various studies, a maximum tritium release from the blanket of 2 mg/d (about 20 Ci/d) has been considered. This reference is more than five orders of magnitude lower than the production rate of about 360 g/d.

In order to mitigate the amount of tritium release into the environment, two main strategies are under development that shall work in a balanced manner:

— The enhancement of the efficiency of the tritium extraction system (TES) at the level of breeder zone (BZ) and minimization at reasonable technical values of the tritium concentration in the coolants through the coolant purification system (CPS).
— The feasibility of implementing anti-permeation barriers at both BB and SG interfaces, made of ceramic coatings or “natural” oxide layers chemically controlled.

Significant developments have been achieved as far as tritium permeation modelling is concerned, covering the most relevant phenomena such as physical adsorption of molecules on high pressure side, dissociative absorption into metal (Sievert’s law), atomic diffusion by concentration gradient (Fick’s law), recombination at the low pressure side and the molecular desorption in the gas phase. The calculations have shown that the tritium inventories in the system loops reach the steady state in short time. For the case of the WCLL the steady state is reached in less than 10 hours as shown in Fig. 11 [7].

The reference data for the coolants flow-rates in the four blankets investigated for a DEMO reactor and the estimated tritium content in the coolants as a result of permeation from the breeding zone are summarized in the Table 3.

Aiming to keep the tritium release below the 0.6 g/y mainly due to the tritium permeation the throughputs of the coolant purification systems have been calculated. Significant efforts are made in order to establish the allowable tritium concentration in the coolant loops that keeps the tritium permeation in the steam generation loop below the reasonable allowable tritium threshold.

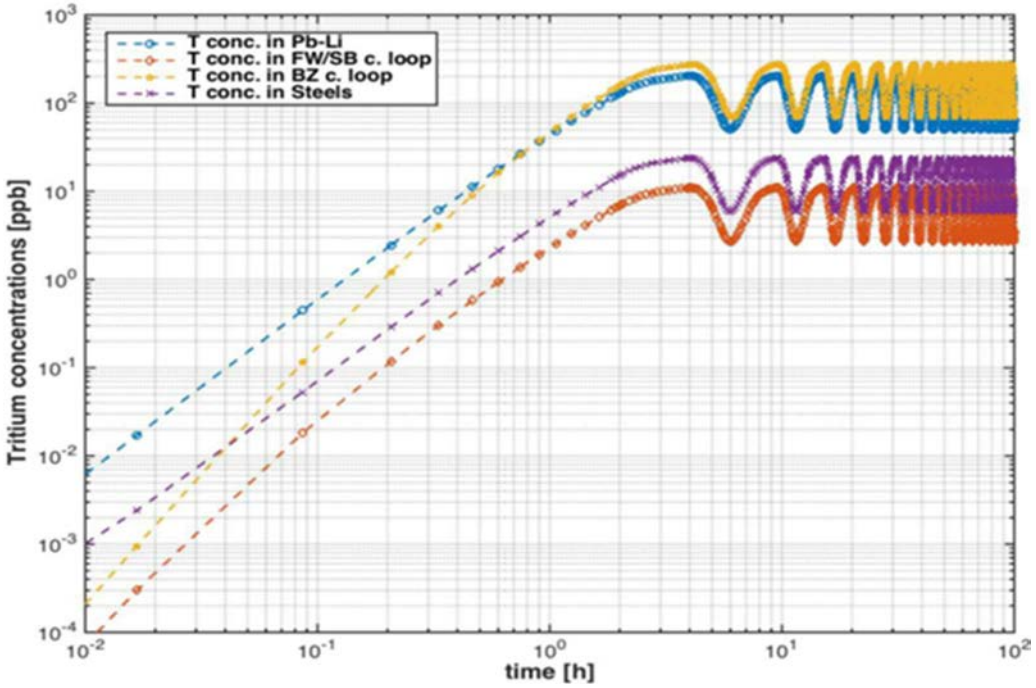

FIG. 11. Time evolution of tritium inventory in the WCLL systems.

TABLE 3. THE COOLANTS FLOW-RATES AND ESTIMATED TRITIUM CONTENT OF THE FOUR REFERENCE BB

Operation parameters	HCLL	HCPB	WCLL	DCLL
Coolant flow rate (kg/s)	2,400	2,400	10,561	26,466
T pressure in the coolants [Pa]	20-30	1-10	50-80	0.001-003

3.1. Evaluation of the technologies for tritium removal from water used in the WCLL

Technologies for tritium removal from tritiated water have been developed in the last decades, mainly focusing on tritium removal from the moderator of heavy water reactors. The technologies are based on a combination between the vapour phase catalytic exchange (VPCE), liquid phase catalytic exchange (LPCE), combined electrolysis catalytic exchange (CECE), direct electrolysis process followed by cryogenic distillation in order to enrich tritium up to 99%. The largest water detritiation facility with the throughput of 360 kg/h is still in operation at Darlington – Canada. The preliminary evaluation of the required flow-rate in the CPS of the WCLL gives a flow rate of 36,000 kg/h. For this very high throughput of a tritium removal facility, the only feasible technology can be water distillation under vacuum with heat pump as front end tritium enrichment. The tritium enriched water can be removed from the bottom of the water distillation column and further processed in a CECE system followed by full tritium recovery in the DEMO tritium plant. The block diagram of such configuration is shown in Fig. 12. In the case that the allowable tritium concentration in the cooling water will be in the ranges allowable for the operation of the CANDU reactors, the technology based on the CECE process followed by tritium recovery in the DEMO tritium plant offers the main benefits for implementation.

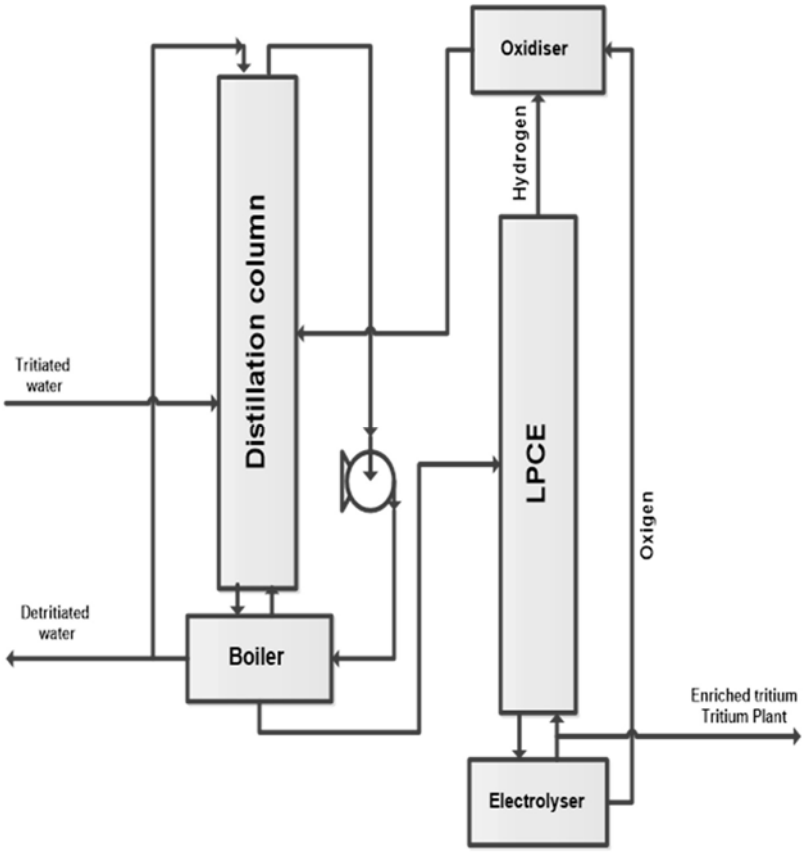

FIG. 12. Block diagram of the WDS for large throughput based on water distillation under vacuum and CECE process.

The throughput of the water detritiation facility for the WCLL strongly depends by the allowable tritium concentration in the cooling loop and the experience from the operation of the CANDU reactors may be used for the definition of the allowable tritium concentration in the loop.

3.2. Evaluation of the technologies for tritium removal from helium used in the HCLL and HCPB

In the evaluation of the possible technologies that have potential for industrialization in view of DEMO design and operation, the estimated throughput of the coolant purification system of 24 kg/s has been considered. Two technologies have been selected having in view the two possibilities of operation, continuous tritium extraction and batch mode tritium extraction. The following technologies have been investigated:

— Oxidation, trapping of tritiated water on a reactive molecular sieve bed followed by tritium recovery by isotopic exchange with swamping deuterium;
— Tritium recovery in permeation cascade.

Tritium recovery in a permeation cascade allows continuous tritium removal but the main drawback is that involves a significant amount of permeation stages, more than 20, with associated necessary components and hence is s very complex from the control system point of view. In addition, the complexity and the operation capacity of the components of such a system would require high energy consumption. Therefore, the tritium recovery based on tritium conversion to tritiated water is a preferable option. Such a system would require to be followed by isotopic exchange on reactive molecular sieve with deuterium and further processing in the DEMO Tritium Plant.

3.3. Evaluation of the technologies for tritium removal from LiPb used in the DCLL

The selection of the tritium extraction technology for the DCLL is strongly dependent by the required throughput capacity of the facility. The selected technology shall allow operation at throughputs up to the entire flow rate of

the cooling system that is approximately 26,500 kg/s. Therefore, several methods for tritium removal have been investigated and the most promising for the DEMO application are the followings:

— Gas Liquid Contactors (GLC);
— Permeation against vacuum (PAV);
— Regenerable getters;
— Droplets and Gas-liquid counter-current extraction tower or vacuum sieve tray (VST).

Significant efforts are ongoing related to the development of systems based on permeation against vacuum and vacuum sieve trays processes that have potential for application at DEMO requirements. These methods are preferable mainly due to the interface with the DEMO tritium plant where the tritium shall be recovered from the carrier gas, if any. In the case of the GLC, the tritium separation from the carrier gas requires a large separation system with significant impact on the energy consumption. The modelling of the tritium transport in the "vacuum chambers" of the VST and PAV and the definition of the requirements for the vacuum systems in view of qualification for tritium service are the main challenges of the two processes.

3.4. Conclusions on tritium extraction techniques

Significant efforts were made to enhance the tritium transport and permeation models aiming to accurate predict the tritium concentration and inventories in the coolants;

The experimental data base for tritium permeation to coolants in DEMO like operation conditions is very limited and the experimental procedures are not well harmonized;

The selection/development of the tritium removal technologies from coolants strongly depend on the allowable tritium concentration in the coolants that is the main issue from the licensing point of view. The lessons learned from the licensing and the operation of the CANDU reactors can be used as reference for defining allowable tritium concentration in the coolants. Available detritiation technologies provide a good basis for the development of the tritium removal process from the coolants of WCLL, HCLL and HCPB blankets; as far as DCLL is concerned, the technologies are under development and the validation at relevant DEMO operation conditions shall be the priority for the upcoming years.

ACKNOWLEDGMENTS

This work has been carried out within the framework of the EUROfusion Consortium and has received funding from the Euratom research and training programme 2014-2018 under grant agreement No 633053. The views and opinions expressed herein do not necessarily reflect those of the European Commission.

REFERENCES

[1] FEDERICI, G., et al., Overview of the design approach and prioritization of R&D activities towards EU DEMO, Fusion Engineering and Design **109–111**(2016) 1464-1474.
[2] BOCCACCINI, L.V. et al., Objectives and status of EUROfusion DEMO blanket studies, Fusion Engineering and Design **109–111** (2016) 1199–1206.
[3] FISCHER, U., et al., Neutronic performance issues of the breeding blanket options for the European DEMO fusion power, Fusion Engineering and Design **109-111** (2016).
[4] X-5 Monte Carlo Team, MCNP – A general Monte Carlo N-particle Transport Code, Version 5, LA-UR-03-1987, Los Alamos National Laboratory (2003).
[5] SUBLET, J.-Ch., et al., The FISPACT-II User Manual, CCFE-R **11** (2015).
[6] ZMITKO, M., Technical specification for the EFDA Article 7 contract EFDA/05-998 on "Procurement of the Pb-Li eutectic alloy for EBBTF facility and for dedicated neutronics experiment" (2009).
[7] UTILI, M. et al. Internal report EFDA_D_2L3AE6.
[8] CHEN, Y., FISCHER, U., Rigorous MCNP based shutdown dose rate calculations: Computational scheme, verification calculations and applications to ITER, Fusion Eng. Design **63-64** (2002)107.
[9] FISCHER, U. et al., Methodological approach for DEMO neutronics in the European PPPT programme: Tools, data and analyses, Fusion Eng. Design **123** (2017) 26-31.

OUR RECENT EXPERIMENTAL CHALLENGES ON FLIBE OR FLINABE COOLANT FOR FUSION APPLICATIONS AND RELATED JAPANESE RESEARCH

S. FUKADA
Dept. of Advanced Energy Engineering Science, Kyushu University,
Fuooka

A. SAGARA
National Institute for Fusion Science,
Toki

N. YUSA, H. HASHIZUME
Dept. of Quantum Science and Energy Engineering, Tohoku University,
Sendai

Japan

Abstract

This paper was presented at the First IAEA Workshop on Challenges for Coolants in Fast Neutron Spectrum Systems, 5–7 July 2017, IAEA Headquarters, Vienna, Austria. Applications of mixed fluoride molten salts such as Flibe ($0.67LiF+0.33BeF_2$, Li_2BeF_4) or Flinabe ($xLiF+yNaF+(1-x-y)\ BeF_2$) to fusion reactor blankets under high-energy neutron flux are proposed and several R&D issues are discussed here.

1. INTRODUCTION

The molten salts of Flibe or Flinabe are considered as not only one of the most promising tritium breeders for fusion reactors but also U, Pu or Th fuel solvents or coolants for fission reactors operated at higher temperatures. Molten Flibe is a chemically stable material having the advantages of higher tritium breeding ratio >1, lower electric conductivity resulting in low MHD effect, low vapor pressure (0.24Pa at 600^{o}C), good heat conductivity and moderate Pr number to mitigate heat impact as a coolant [1,2]. However, since the melting point of Flibe is comparatively high (459^{o}C) [3] and it becomes corrosive with an increase in temperature, its operating range of structural materials is limited. The Flinabe mixed molten salt is expected as its replacement, which has a melting point around 300^{o}C while keeping other properties almost unchanged [4-6]. Thus, Flibe or Flinabe is adopted as the blanket material for a conceptual design of the Force Free Helical Reactor (FFHR) in NIFS of Japan [7]. In addition, there are some growing expectations for some molten salts as heat-transfer mediums of solar power storage operated at high temperature [8].

Flibe or Flinabe, on the other hand, has disadvantages of higher hydrogen isotopes permeability and consequently high possibility in tritium leakage through tubing to the secondary coolant when it is applied to a fusion reactor blanket. In addition, there is possibility in that highly corrosive TF is generated in the molten salts under neutron irradiation conditions. Therefore, it becomes important to control the redox potential of the molten salts during operation. In addition, the increase of turbulent viscous force due to thermal stratification of the molten salt under strong magnetic force needs to be mitigated when it's applied to FFHR. In this presentation, our several experimental trials to control the redox potential of Flibe and to suppress hydrogen isotope permeation through the fluoride molten salts are introduced. Our previous three experiments are introduced here in short:(i) the redox control by a Be rod immersed in Flibe, (ii) tritium (T) release from neutron irradiated Flibe by inert gas purge with addition of H_2 and (iii) test of a new candidate of hydrogen-absorbing metals of solid Ti particles mixed in Flibe or Flinabe in order to suppress the H isotope permeation. Experimental apparatus including molten salts was set up, and the released gas components were measured. The results are introduced in short.

Although several physical or chemical properties such as the binary or tertiary phase diagram, melting point, viscosity, thermal conductivity, thermal capacity, H isotope diffusivity and solubility of Flibe or Flinak were determined previously, it becomes more important to predict those of new candidates such as Flinabe or other molten salts as a coolant. The research group in Tohoku University evaluated several properties of different molar fractions of Flinabe mixtures using molecular dynamics (MD) numerical simulation. In addition, possibility is discussed that molten salts are used to transmute minor actinides contained in spent fuels of nuclear fission reactors. Thus, recent Japanese works relating with Flibe or Flinabe experiment and numerical calculations are

introduced along with works made for the FFHR conceptual design in NIFS. Advantages of Flibe or Flinabe in combination with supercritical CO_2 secondary coolant are introduced as one of the most promising blanket candidates for fusion reactors [7].

2. NUCLEAR REACTION BETWEEN NEUTRON AND FLIBE AND TRITIUM RELEASE FROM MOLTEN SALT

It is considered that the Li_2BeF_4 molten salt has an ionic tetrahedral structure of BeF_4^{2-} (or $Be_2F_7^{3-}$) and 2 Li^+ atoms [9]. The BeF_4^{2-} ions may be almost independent of contiguous ions in the molten salt. Similarly, $LiNaBeF_4$ is also composed of BeF_4^{2+}, Li^+ and Na^+ ions. When Flibe is disposed to neutron irradiation, high-energy T nuclei generated are slowed down by elastic scattering with interstitial atoms. Finally, T is present in any state among the thermally stable molecular forms of T^-Li^+, T^+F^- and T^0H^0. Li nuclei of ^6Li and ^7Li in Flibe and Flinabe work for T generation, and ^9Be ones do for neutron breeding through the (n,2n) reaction. Other nuclei of ^{19}F and ^{23}Na show low neutron absorption cross-section less than 10^{-2} or 1 barn even at the thermal neutron spectrum region [10].

Just after 14MeV neutron irradiation to Flibe (also to Flinabe), there are three possibilities in that the two reactions of ^7Li (n,αn')T and $^9Be(n,2n)2^4He$ occur in MeV neutron regions and that of $^6Li(n,\alpha)^3T$ does in the thermal neutron region after neutron slowing down by elastic scattering [10]. According to the previous experiment by Moriyama *et al*. [11,12], the chemical form of generated T is around ten percent of T^- (LiT in molecular form), around 1% of T^0 (HT) and the rest of T^+ (TF). The percentage of HT is drastically increasing with the addition of 1%H_2 in He purge gas. Terai *et al*. certified experimentally that the change of the T chemical form is attributed by the chemical exchange reaction on Flibe surfaces ($TF+H_2 \rightarrow HT+HF$) [13,14]. We also determined quantitatively tritium release rates from neutron irradiated Flibe as shown in Fig. 1, where the rate of T released after thermal neutron irradiation in a nuclear fission reactor is well simulated by the analytical equations based on the transient T^+ diffusion in Flibe and the linear isotopic exchange rate on surfaces [15].

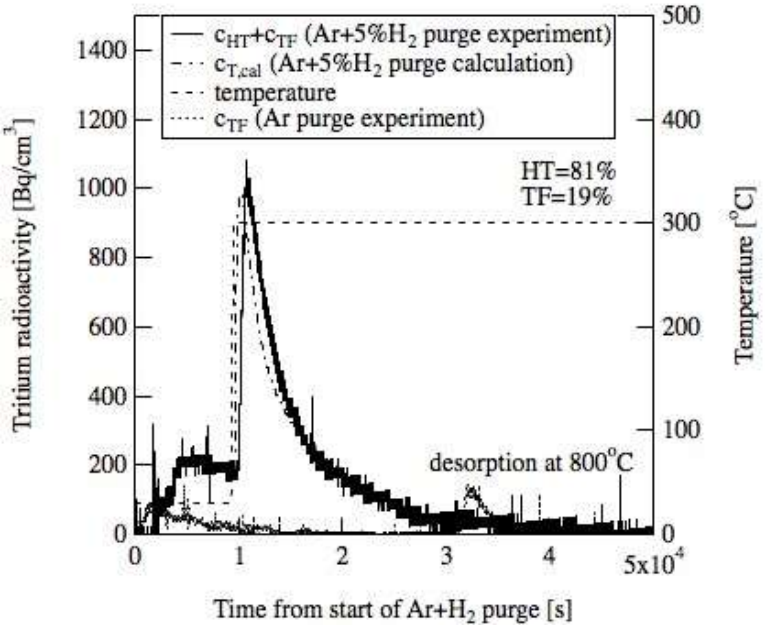

FIG. 1. Rate of tritium release from thermal neutron irradiation to Li_2BeF_4 molten salt in the 5%H_2+Ar purge gas [14].

The isotopic exchange reaction is described as $TF+H_2 \rightleftarrows HT+HF$. The main molecular form of released tritium is HT, and a small part of it is released in a form of TF in a similar way to the above previous experimental data. It is proved that the addition of 1% H_2 is sufficient for the isotopic exchange reaction proceeds in the right direction. The present results give assurance for the prediction of quantitative T release from a Flibe blanket under neutron irradiation to He sweep gas. The release rate is rapid and proceeds even at lower temperature. When no H_2 is included in the purge gas, the T release rate is extremely delayed, and the desorption temperature is increased [15], which is not shown in the figure.

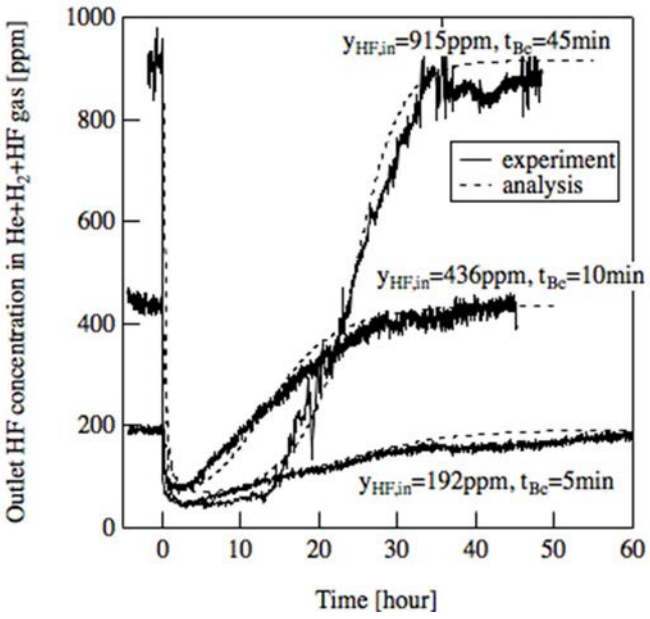

FIG. 2. Redox control of Flibe immersed in Flibe, where the broken lines are determined using the T diffusivity in Flibe and a linear rate constant for the isotopic exchange [21].

3. CONTROL OF REDOX POTENTIAL

When atomic T is generated in Flibe or Flinabe molten salts under neutron irradiation, the initial molecular form of T is TF. Since the fluoride ions have higher corrosive properties, the chemical state needs to be controlled to reduced one. The redox control reaction is described as follows: M +nTF = MF_n +(n/2)T_2. The candidates for the redox agent are Be, Ce, Eu and so on. Experiment using molten Flibe was performed using a Be rod for a redox agent under the collaboration work of Japan-US Program of Irradiation/Integration Test for Fusion Research-II, Jupiter-II [16-21]. The specified concentration of HF included in He purge is continuously bubbled through Flibe, and the eluted HF concentration is detected at the outlet of Flibe molten salt. At the same time a Be rod is immersed into Flibe during the specified time period of t_{Be}. Fig. 2 shows that the HF concentration is maintained at low one for the specified immersion time period of t_{Be}. Be atoms dissolved in Flibe reacts with HF immediately, and the HF concentration in elution gas is maintained at very low values. The control time continues until the Be immersion time has finished. The following assumptions are set for the simulation: (i) linear Be dissolution rate into the Flibe, (ii) constant diffusivity of T in Flibe and (iii) linear surface exchange reaction rate on the interface between Flibe and He purge. Good agreement is obtained between experiment and calculation.

Similarly, Suzuki *et al.* also determined the T release rate from neutron irradiated Flibe with the Be redox control [14], and they summarized their data in terms of the mass-transfer coefficient. Its value is k_{Flibe}=9.1x10^{-6} m/s taking into consideration of diffusion and isotopic exchange on surfaces. Judging from the relation between k_{Flibe} and D_{Flibe}, $k_{Flibe} = D_{Flibe}/\delta_{Flibe}$, where δ□□□□□ is the thickness of the diffusion boundary layer in Flibe, its value is consistent with our diffusion data.

4. HYDROGEN ISOTOPE PERMEATION THROUGH MOLTEN SALTS

Tritium generated in Flibe or Flinabe blanket diffuses from the molten salt bulk through heat-transfer tubes to the secondary coolant. If each permeation path is arranged ideally in the one-dimensional direction, the overall T atom permeation flux j_T at a steady state is described as follows [22-25]:

$$j_T = \frac{D_{Flinabe}K_{Flinabe}}{\delta_{Flinabe}}\left(p_{H,bulk} - p_1\right) = \frac{D_{Monel}K_{Monel}}{\delta_{Monel}}\left(\sqrt{p_1} - \sqrt{p_2}\right) = \frac{D_{gas}}{\delta_{gas}RT}\left(p_2 - p_{L,bulk}\right) \quad (1)$$

where D_k and δ_k in each medium mean the diffusivity and boundary layer thickness, $p_{H,bulk}$, p_1, p_2 *and* $p_{L,bulk}$ do the bulk T pressure in Flinabe, the upstream, downstream surfaces and the bulk one in purge gas, where the subscript k means any of Flinabe, Monel tube and the secondary gas. Fig. 3 shows comparison of the overall H_2 permeation flux between experiment and calculation, where the molten salt is Flinabe, the tertiary cylindrical tubes are made

of Monel 400 and the secondary fluid is Ar. In addition, the Henry's law is assumed for the H_2 solubility in Flinabe and the Sieverts' law for the H solubility in the Monel. Even if the overall permeation flux is affected by H_2 diffusion in Flinabe and H one in the metallic tube, the two permeation resistances can be separated by using the above relationship. Thus, the diffusivity and permeability of H isotope atoms in the molten salt can be estimated quantitatively. The fluoride molten salt has lower hydrogen isotope solubility, but higher permeability compared with other T breeder candidates. When the fluoride molten salt is under fluidized conditions, the rate-determining step changes from diffusion in molten salt to that in tube wall depending on temperature, the upstream H_2 pressure and molten salt velocity. Comparison of permeability, diffusivity and solubility among Flibe, Flinak (0.465LiF+ 0.115NaF+0.42KF, m.p.=454ºC), Fnabe (0.5NaF+0.5BeF_2, $NaBeF_3$, m.p.=376ºC) and Flinabe (0.333LiF+0.333NaF +0.333BeF_2, $LiNaBeF_4$, m.p.=315ºC) were made previously [22,25]. Fig. 3 shows comparison of diffusivity between Flibe and Flinak. The temperature ranges are from 400ºC to 600ºC for Flinabe or Fnabe and from 500ºC to 600ºC for Flibe or Flinak.

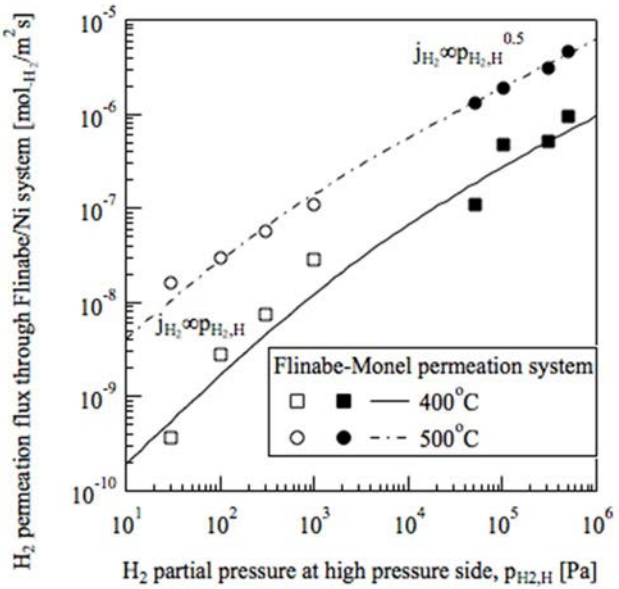

FIG. 3 Steady-state permeability through Flinabe ($LiF+NaF+BeF_2$ equimolar mixture) and Monel 400 conjugated system [22].

It is important information to guess the microscale diffusion path of T in the molten salts. If tritium is present as T^+ in molten salts, its path may be deeply related with self-diffusivity of F^-. It is known that the self-diffusivity of F^- ion is controlled by the rotation-exchange mechanism, which includes rotation inside the BeF_4^{2-} ion complex and F^- ion exchange between the contiguous ions. The latter has larger activation energy of 128kJ/mol [26]. The activation energy corresponds to the T diffusivity in redox non-controlled Flibe. Then T atoms diffuse inside Flibe with a form of TF. On the other hand, T in the redox-controlled Flibe diffuses through it with a form Li^+T^- in a low concentration region and HT in a higher H isotope concentration. Then the activation energy is well correlated by the diffusivity of general alkali halide ions in molten salts. The activation energy of the latter diffusion is comparatively small (=40-50 kJ/mol). The solubility of the molecular H isotopes (H_2, D_2 and T_2) in these molten salts along with those of HF and DF were discussed in our previous paper [25].

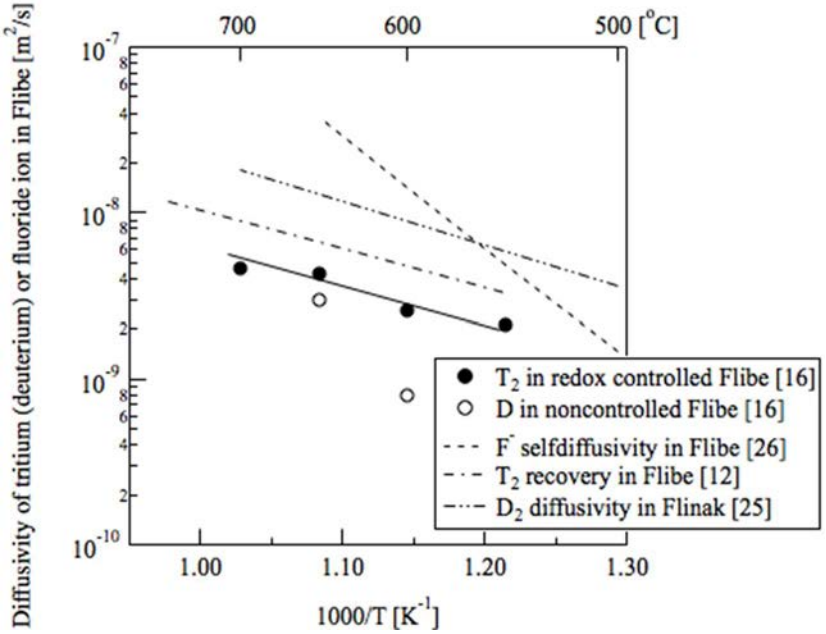

FIG. 4. H isotope diffusivity in Flibe and Flinak. [22].

5. PERMEATION PROTECTION BY HYDROGEN ABSORBING METALS

The H isotope molecule solubility of Flibe or Flinabe molten salts is very low. The equilibrium T_2 pressure in a self-cooled liquid blanket with a thermal output of 1 GW is estimated as 10^3 Pa for Flibe compared with10^{-6} Pa for $Li_{17}Pb_{83}$ or 10^{-13} Pa for Li [24]. The T partial pressure generated in the molten salts under neutron irradiation becomes the highest among the three. Consequently, it is important to control T permeation through the molten salt inside fusion blankets. Since oxide coating on tubing is an efficient method to reduce T permeation rates through various kinds of tubing materials, the permeation reduction factors of various kinds oxides were summarized previously [27]. On the other hand, another idea of mixing of H isotope absorbing metals with the molten salt was proposed and test experiment was carried out in NIFS [7,28,29]. We also set up a tertiary cylindrical Monel 400 (0.65Ni+0.33Cu+0.02Fe alloy) tubes for the H permeation experiment, and H isotope permeation rates through Flibe and Flibe+Ti systems were experimentally determined. The average diameter of Ti particles is 45μm, and 0.5wt% Ti is mixed in Flibe. It is clarified how the overall H_2 permeability is delayed by mixing with Ti particles included in Flibe. The details of the H_2 permeation experiment are described in the reference [30].

Fig. 5 shows an example for the history of the transient H_2 permeation through the Flibe or Flibe+Ti system. Constant pressure of H_2 is introduced into the upstream part at time zero, and the H_2 pressure increase in downstream is determined. Immediately after the H_2 introduction, permeation starts increasing in the Flibe/Monel system. The time delay is well predicted by the diffusion delay time defined by $l^2/6D_{Flibe}$. On the other hand, when Ti particles are mixed in Flibe, it works as a H absorber. After sufficient time elapsing, the steady-state permeation has been achieved. The transient H_2 permeation history is well reproduced by the analytical solution based on the transient diffusion equation in the Flibe+Ti/Monel system. When Ti particles are included in Flibe, the delay time becomes larger. The experimental H_2 history is in good agreement with the analytical equation that takes into consideration of diffusion in Ti particles along with Flibe and Monel walls. The calculation details are described in the reference [30]. The steady-state permeation rate of the system including Ti is almost consistent with the Flibe/Monel one. This is because diffusion inside Ti particles controls the overall permeation process when the plateau pressure of the Ti-H_2 system is lower than the outlet H_2 detection limit.

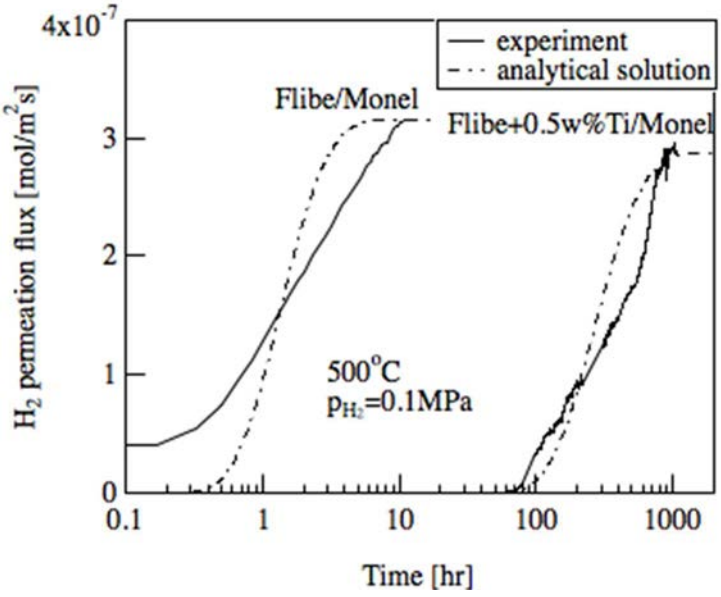

FIG. 5. Overall H_2 permeation flux through Flibe and Flibe+0.5wt%Ti system [30].

6. PREDICTION OF MOLTEN SALT PROPERTIES

The phase diagrams of the LiF-BeF_2 and LiF-NaF-BeF_2 systems were determined previously [4], and several numerical predictions were presented using thermodynamic data [32,33]. Whereas the low melting point of Flinabe implies that it would overcome the issue on temperature window in designing blanket systems using Flibe, actually there is not so much information on physical properties of Flinabe. Thus, most studies have assumed that its heat-transfer performance is the same as, or very similar to, that of Flibe to discuss the applicability of Flinabe to self-cooled liquid blanket systems. In contrast, measuring the physical properties of Flinabe suffers from several technical difficulties such as toxicity of Be, purification, and high operating temperature. To address this issue, studies have been performed to evaluate the physical properties of Flinabe with the aid of molecular dynamics simulations using a polarizable ion model [34-36]. Specifically, the studies evaluated dependence of the density, specific heat, viscosity, and thermal conductivity of Flinabe on the composition at several temperatures. The results of the studies were in good agreement with experimental results reported in literatures. Subsequent evaluations revealed that the low melting point does not necessarily lead to a wide design window for a reactor because of an exponential increase in the Pr number of Flinabe at low temperature. Another study has proposed adding heavier elements, such as Cs and Sr, to Flibe or Flinabe to improve their physical properties [37]. Molecular dynamics simulations would contribute to evaluate suitable compositions, including suitable elements to add, of molten salts.

7. FLUORIDE MOLTEN SALT AS HEAT-TRANSFER FLUID

Various properties of molten salts as heat-transfer fluid are summarized in the IAEA internship report [9]. Various types of heat-transfer rates in molten salts have been correlated in terms of the heat-transfer coefficient. Since the Pr number of Flibe is around 20-30, the previous heat-transfer data of turbulent flow are expected to be well correlated by the Dittus-Boelter equation of $Nu = 0.023Re^{0.8}Pr^{0.4}$ for heating in circular tubes. Previously a Flibe simulant heat-transfer salt (HTS, $0.53KNO_3$+$0.4NaNO_2$+$0.07NaNO_3$) was tested in the Jupiter-II [38]. A new coolant test loop of Flinak is mocked up in NIFS [39], and the heat transfer and magnetic effects on molten fluoride flows due to a large helical coil are investigated intensively.

An effect of the strong magnetic force on the Flibe simulant fluid of aqueous 0.3-0.4 KOH solution is observed as increase of the thermal stratification due to turbulent suppression [40]. Several experimental attempts for turbulent proportion were tested successfully using the Flibe simulant [41,42].

8. APPLICATIONS OF MOLTEN SALT TO NUCLEAR TRANSMUTATION OF MINOR ACTINIDES

To enhance the economic efficiency of fusion reactors in their early stage, recent studies have proposed a double-strata nuclear fuel cycle utilizing fusion reactors to transmute minor actinides contained in spent fuels of fission

reactors [43,44]. The studies intend to install minor actinides in the molten salt blanket to transmute the minor actinides using fast neutrons generated by fusion reactions. The volumetric ratio of the minor actinides is kept to be much lower than those discussed in earlier studies as hybrid reactors to request small modification of the present designs of fusion reactors. Numerical studies on the basis of Monte Carlo neutron transport simulations and burn-up calculations have confirmed that a helical-type fusion reactor having a fusion output of 1 GW enables to transmute approximately 350 kg of minor actinides every year while keeping the fission power caused by the transmutation below 130 MW. The studies also revealed that the heat density of the fission reactions is as low as 7 W/cm^3, which is less than 1/10 of the heat density generated at the core of typical pressurized water reactors and thus leads to less difficulty in heat removal. Subsequent evaluation demonstrated that introducing fusion reactors with a total output of 5 GW would decrease the inventory of minor actinides in Japan.

9. FFHR DESIGN WORK

NIFS has launched the Fusion Engineering Research Project (FERP) in preparation for DEMO by starting the redesign of the helical type reactor FFHR-d1 under the self-ignition state of Q=∞ [7]. In the first round, the main parameters were selected [45]. The major radius of the helical coils is 15.6 m, the toroidal field is 4.7 T, the plasma volume is 2,000 m^3, and the fusion power is 3 GW. The second round is to prepare the detailed three-dimensional (3D) design of the superconducting magnet support structures, and 3D neutronics analyses, where the diverter targets can be efficiently shielded from fast neutrons. With the help of inboard WC shield and outboard ferritic steel + B_4C shield, the fast neutron flux becomes $2x10^{10}$ n/cm^2s in the coil winding region in the inboard side. The maximum neutron wall loading is estimated to be 2.0 MW/m^2. A new Flinabe blanket mixed with metal powder is adopted. The calculated net TBR is 1.18 with a ^6Li enrichment ratio of 90%. Fabrication of helical coils by connecting half-helical-pitch segments of 100 kA-class $YBa_2Cu_3O_7$ (YBCO) high temperature superconductors is proposed as a promising method. Also, in progress is improvement of the first round of the core plasma design, ignition start-up analyses, and fuelling scenario. The pellet fuelling condition is accommodated below the ratio of the penetration depth to the minor radius of 0.3 with the pellet injection velocity at 1.5 km/s. As a consequence, a multi-path strategy on FFHR- d1 has been introduced with different versions of FFHR designs [7] and intensive LHD experiments [46], where design flexibility is expanded to include sub-ignition with options for “before demo, compact, and component-test”. At present the power generation system combining 1st loop of Flinabe with 2nd loop of supercritical CO_2 [39] is designed in new FFHR. The reasons why the supercritical CO_2 is selected as the secondary coolant operated at 480ºC/350ºC and 20MPa are that operating temperature conditions are proper and higher heat-transfer performance or thermal efficiency is expected [47]. In addition, there is possibility in that the T_2 pressure or chemical potential in the secondary CO_2 coolant is reduced by the reaction of $CO_2+4T_2 \rightarrow CT_4+2T_2O$ and CT_4 is readily removed from the stream without permeation through tubing.

10. CONCLUSIONS

— Main coolants and its behaviour under radiation: The targeted coolant is Flibe or Flinabe, which is not affected by γ irradiation but generates corrosive TF under neutron irradiation by the $^6Li(n,\alpha)^3T$.
— Range of use of the coolants under irradiation (limiting constraints): The coolant can be used between 350-700ºC for Flinabe (V-4Vr-4Ti) or 500-700ºC for Flibe regardless of irradiation. The redox control is necessary under neutron irradiation. It has been confirmed to convert TF to T_2 in Flibe by Be. The γ-ray shielding is necessary if MeV order γ-ray is generated.
— Major issues (present state of knowledge, experimental verification, lacking evidence R&D strongly required): Reduction of T leakage through Flibe or Flinabe is important to use it under high-energy neutron irradiation conditions for nuclear fusion or fission safety. One experimental trial is to include nanoscale powder of hydrogen-absorbing metal such as Ti in the molten salt along with various permeation barriers by oxide coating. Another one is to select the primary Flinabe/secondary supercritical CO_2 coolant. T will be removed in a chemical form of CT_4 in CO_2.
— Which coolant is adequate for each environment: Flibe or Flinabe can be used as self-cooled breeder and also for minor actinides transformer from nuclear fission reactor fuel processing using high-energy neutron fluence in Flibe. There is possibility in that the secondary coolant is supercritical CO_2 flow.

10.1. Radiation chemistry, radiolysis

— Main effects for the different coolants: Although Flibe or Flinabe is a chemically stable fluoride mixture, corrosion on surrounding materials is the main effect. The redox control can suppress the effect.
— Limits of use (temperature window, irradiation limits, susceptibilities to materials): The melting point of Flibe ($2LiF+BeF_2$) is 459ºC or that of Flinabe ($0.31LiF+0.31NaF+0.38BeF_2$) is 305ºC.

— Examples: Since less radioactive materials are generated except for T, limitation of Flibe or Flinabe for coolant is small.

10.2. Activation, Species production, Computational models

— Main effects for the different coolants: Prediction of physical or chemical properties for different compositions of fluoride molten salts such as Flinabe can be made based on MD calculations.
— Limits of use: Correct MD parameters have been presented, although the parameters of the tetrahedral ion combinations of BeF_4^{2-} may not been sufficient.
— Examples (experimental experiences): There are less experimental data for the tertiary component fluorides such as LiF+NaF+BeF_2.

10.3. Coolant processing and handling procedures

— Kind of processes and examples (limitations, scaling issues, ….): Although Pr number of Flibe or Flinabe at the composition is around 20, the values are increased exponentially with the increase of the BeF_2 composition. The permeability of T through Flibe or Flinabe is high, T leakage to the secondary coolant through heat exchange tubes needs to be suppressed.
— Major difficulties found (purification, resources): Impurities such as Li_2O, BeO in Flibe or Flinabe can be removed by using HF and the chemical reactions of deoxidization or redox control are described as BeO+2HF→BeF_2+H_2O. If the fluoride molten salt is used for nuclear transmutation of minor actinides under high-energy neutron conditions, further purification is necessary along with γ-ray shielding.
— New approaches (processes to be improved): A new candidate of Ti powder mixed in the fluoride molten salt is proposed and partly tested experimentally in order to delay T permeation through the salt.

REFERENCES

[1] MACPHERSON, H.G., The molten salt reactor adventure, Nuclear Science and Engineering **90** (1985) 374-380.
[2] WILLIAMS, D.F., TOTH, L.M., CLARNO, K.H., "Assessment of candidate molten salt coolants for the advanced high temperature reactor", ORNL-TM-2006/12.
[3] ROMBERGER, K.A., BRAUSTEIN, J., THOMA, R. E., New electrochemical measurements of the liquidus in the lithium fluoride-beryllium fluoride system. Congruency of lithium beryllium fluoride (Li_2BeF_4), J. Phys. Chem. **76** (1972) 1154-1159.
[4] THOMA, R.E., Phase diagrams of binary and ternary fluoride systems, Advances in molten salt chemistry edited by J. Braunstein, G. Mamantov and G.P. Smith, **3** (1975) Plenum Press.
[5] NYGREN, R.E., Thermal modelling of the Sandia Flinabe (LiF-BeF_2-NaF) experiments, Fusion Sci. Technol. **47** (2005).
[6] BENES, O., KONINGS, R.J.M., Thermodynamic calculations of molten-salt reactor fuel systems, Molten salts chemistry from lab to applications edited by F. Lantelme and H. Groult, Elsevier (2013).
[7] SAGARA, A., TAMURA, H., TANAKA, T., YANAGI, N., MIYAZAWA, J., GOTO, T., SAKAMOTO, R., YAGI, J., WATANABE, T., TAKAYAMA, S., the FFHR design group, Helical reactor design FFHR-d1 and c1 for steady-state DEMO, Fusion Engng. Des. **89** (2014) 2114-2120.
[8] BAUER, T., PFLEGER, N., LAING, D., STEIMANN, W.D., ECK, M., KAESCHE, S., High temperature molten salts for solar power applications, Molten salts chemistry from lab to applications edited by F. Lantelme and H. Groult, Elsevier (2013).
[9] TOTH, L.M., BATES, J.B., BOYD, G.E., Raman spectra of $Be_2F_7^{3-}$ and higher polymers of beryllium fluorides in the crystalline and molten state, J. Phys. Chem. **77** (1973) 216-221.
[10] SHIBATA, K., KAWANO, T., NAKAGAWA, T., IWAMOTO, O., KATAKURA, J., FUKAHORI, T., CHIBA, S., HASEGAWA, A., MURATA, T., MATSUNOBU, H., OHSAWA, T., NAKAJIMA, Y., YOSHIDA, T., ZUKERAN, A., KAWAI, M., BABA, M., ISHIKAWA, M., ASAMI, T., WATANABE, T., WATANABE, Y., IGASHIRA, M., YAMAMURO, N., KITAZAWA, H., YAMANO, N., TAKANO, H., Japanese evaluated nuclear data library version 3 revision-3: JENDL-3.3, J. Nucl. Sci. Technol. **39** (2002) 1125-1136.
[11] MORIYAMA, H., OISHI, J., KAWAMURA, K., The effect of fusion neutron irradiation on tritium recovery from lithium salts, J. Nucl. Mater. **161** (1989) 197-203.
[12] OISHI, J., MORIYAMA, H., MAEDA, S., ASAOKA, Y., Tritium recovery from molten LiF-BeF_2 salt, Fusion Engng. Des. **8** (1989) 317-321.
[13] TERAI, T., In-situ tritium release behaviour from CTR liquid breeding materials under 14 MeV beutron irradiation", J. Nucl. Sci. Technol. **27** (1990) 667-670.
[14] SUZUKI, A., TERAI, T., TANAKA, S., "Tritium release behaviour from Li_2BeF_4 molten salt by permeation through structural materials," Fusion Engng Des. **51–52** (2000) 863-868.
[15] EDAO, Y., FUKADA, S., NOGUCHI, H., Tritium release from neutron-irradiated Flibe purged out by Ar-H_2 or Ar at controlled temperature, Fusion Sci. Technol. **55** (2009) 140-151.
[16] ANDERL, R.A., FUKADA, S., SMOLIK, G.R., PAWELKO, R.J., SCHUETZ, S.T., SHARPE, J.P., MERRILL,

B.J., PETTI, D.A., NISHIMURA, H., TERAI, T., TANAKA, S., Deuterium/tritium behaviour in Flibe and Flibe-facing materials, Journal of Nuclear Materials **329-333** (2004) 1327-1331.
[17] FUKADA, S., ANDERL, R.A., HATANO, Y., SCHETZ, S.T., PAWELKO, R.J., PETTI, D.A., SMOLIK, G.R., TERAI, T., NISHIKAWA, M., TANAKA, S., SAGARA, A., Initial studies of tritium behaviour in Flibe and Flibe-facing material, Fusion Engineering and Design **61-62** (2002) 783-788.
[18] FUKADA, S., ANDERL, R.A., PAWELKO, R.J., SMOLIK, G.R., SCHUETZ, S.T., O'BRIEN, J.E., NISHIMURA, H., HATANO, Y., TERAI, T., PETTI, D.A., SZE, D.K., TANAKA, S., Flibe-D_2 permeation experiment and analysis, Fusion Science and Technology **44** (2003) 410-414.
[19] FUKADA, S., ANDERL, R.A., TERAI, T., SAGARA A., NISHIKAWA, M., Diffusion coefficient of tritium through a molten salt Flibe blanket and evaluation of tritium leak from fusion reactor system, Fusion Science and Technology **48** (2005) 666-669.
[20] SIMPSON, M.F., SMOLIK, G.R., SHARPE, J.P., ANDERL, R.A., PETTI, D.A., HATANO, Y., HARA, M., OYA, Y., FUKADA, S., TANAKA, S., TERAI, T., SZE, D. K., Quantitative measurement of beryllium-controlled redox of hydrogen fluoride in molten salt, Fusion Engineering and Design **81** (2006) 541-547.
[21] FUKADA, S., SIMPSON, M.F., ANDERL, R.A., SHARPE, J.P., KATAYAMA, K., SMOLIK, G.R., OYA, Y., TERAI, T., OKUNO, K., HARA, M., PETTI, D.A., TANAKA, S., SZE, D.K., SAGARA, A., Reaction rate of beryllium ion for Flibe redox control, J. Nucl. Mater. **367-370** (2006) 1190-1196.
[22] NISHIUMI, R., FUKADA, S., NAKAMURA, A., KATAYAMA, K., Hydrogen permeation through Flinabe fluoride molten salts for blanket candidates, Fusion Engineering and Design **109-111** (2016) 1663-1668.
[23] NAKAMURA, A., FUKADA, S., NISHIUMI, R., Hydrogen isotopes permeation in a fluoride molten salt for nuclear fusion blanket, Journal of Plasma and Fusion Research **11** (2015) 25-29.
[24] FUKADA, S., MORISAKI, A., Hydrogen permeability through a mixed molten salt of LiF, NaF and KF (Flinak) as a heat-transfer fluid, Journal of Nuclear Materials **358** (2006) 235-242.
[25] OHMICHI, T., OHNO, H., FURUKAWA, K., Self- diffusion of fluorine in molten dilithium tetrafluoroberyllate, J. Phys. Chem. **80** (1976) 1628-1631.
[26] FUKADA, S., EDAO, Y., SAGARA, A., Effects of simultaneous transfer of heat and tritium through Li-Pb or Flibe blanket, Fus. Engng Des. **85** (2010) 1314-1319.
[27] REITER, F., FORCEY, K.S., GERVASINI, G., A compilation of tritium-material interaction parameters in fusion reactor materials, EUR 15217 EN (1993).
[28] YAGI, J., SAGARA, A., TANAKA, T., TAKAYAMA, S., MUROGA, T., Hydrogen solubility of the molten salt Flinak mixed with nano-Ti powder, Plasma and Fusion Research **11** (2016) 2405099.
[29] YAGI, J., SAGARA, A., WATANABE, T., TANAKA, T., TAKAYAMA, S., MUROGA, T., Hydrogen solubility in Flinak mixed with titanium powder, Fusion Engng Des. **98-99** (2015) 1907-1910.
[30] NISHIUMI, R., FUKADA, S., YAMASHITA, J., KATAYAMA, SAGARA, A., YAGI, J., Hydrogen permeation through fluoride molten salt mixed with Ti powder, Fusion Science and Technology **72** (2017) 747.
[31] FUKADA, S., NAKAMURA, N., A Zn or Fe particle bed to convert HF with traces of TF to HT, Journal of Radioanalytical and Nuclear Chemistry **261** (2004) 291-294.
[32] FURUKAWA, K., Application of ionic-liquid structure theory to geochemistry, J. Mineralogical Society of Japan **14** (2) (1980) 34-50.
[33] FUKADA, S., NAKAMURA, A., Estimation of melting points of mixed fluoride molten salts, Flinabe, Fusion Science and Technology **66** (2014) 322-336.
[34] SALANNE, M., ROTENBERG, B., JAHN, S., VUILLEUMIER, R., SIMON, C., MADDEN, P.A., Including many-body effects in models for ionic liquids, Theor. Chem. Acc. **131** (2012) 1143.
[35] SHISHIDO, H., YUSA, N., HASHIZUME, H., ISHII, Y., OHTORI, N., Evaluation of physical properties of the molten salt mixture flinabe for a fusion blanket system using molecular dynamics simulation, Fusion Science and Technology **68** (2015) 669-673.
[36] SHISHIDO, H., YUSA, N., HASHIZUME, H., ISHII, Y., OHTORI, N., "Thermal design investigation for a flinabe blanket system", Fusion Science and Technology, in press.
[37] HASHIZUME, H., YUSA, N., MATSUI, K., Feasibility study of Flibe blanket with Cs, Fusion Science and Technology **60** (2011) 523-527.
[38] TODA, S., CHIBA, S., YUKI, K., OMAE, M., SAGARA, A., Experimantal research on molten salt thermofluid technology using a high temperature molten salt loop applied for a fusion reactor Flibe blanket, Fusion Engineering and Design **63-64** (2002) 405-409.
[39] SAGARA, S., TANAKA, T., YAGI, J., TAKAHASHI, M., MIURA, K., YOKOMINE, T., FUKADA, S., ISHIYAMA, S., First operation of the Flinak/LiPb twin loop Orosh^{2}i-2 with 3T SC magnet, Fusion Science and Technology **68** (2015) 303-307.
[40] YOKOMINE, T., TAKEUCHI, J., NAKAHARAI, H., SATAKE, S., KUNUGI, T., MORLEY, N.B., ABDOU, M.A., Experimental investigation of turbulent heat transfer of high Prandtl number fluid flow under strong magnetic field", Fusion Sci. Technol. 52(3) (2007) 625-629.
[41] SATOH, T., YUKI, K., CHIBA, S., HASHIZUME, H., SAGARA, A., Heat transfer performance for high Prandtl and high temperature molten salt flow in sphere-packed pipes, Fusion Sci. Technol. **52** (2007) 618-624.
[42] TAKEUCHI, J., SATAKE, S., MORLEY, N.B., KUNUGI, T., YOKOMINE, T., ABDOU, M.A., Experimental study of MHD effects on turbulent flow of Flibe simulant fluid in circular pipe, Fus. Engng. Des. **83** (2008) 1083-1086.
[43] SHISHIDO, H., FURUDATE, Y., YUSA, N., HASHIZUME, H., Designing of a fusion blanket system using molten salt flinabe for transmutation of minor actinides, GLOBAL2015, Paris, France 2015/09/20-24.
[44] FURUDATE, Y., SHISHIDO, H., YUSA, N., HASHIZUME, H., Scenario construction of MA transmutation in Japan using fusion reactor, The 22nd Topical Meeting on the Technology of Fusion Engineering, Philadelphia, USA, 2016/08/21-25.

[45] SAGARA, S., GOTO, T., MIYAZAWA, J., YANAGI, N., TANAKA, T., TAMURA, H., et al., Design activities on helical DEMO reactor FFHR-d1", Fusion Engng. Des. **87** (2012) 594-602.
[46] MIYAZAWA, J., GOTO, T., MORISAKI, T., GOTO, M., SAKAMOTO, R., MOTOJIMA, G., et al., Direct extrapolation of radial profile data to a self-ignited fusion reactor based on the gyro-Bohm model, Fusion Engng. Des. **86** (2011) 2879–288.
[47] ISHIYAMA, S., MUTO, Y., KATO, Y., NISHIO, S., HAYASHI, T., NOMOTO, Y., Study of steam, helium and supercritical CO_2 turbine power generations in prototype fusion power reactor, Progress in Nuclear Energy **50** (2008) 325-332.

SODIUM COOLANT: ACTIVATION, CONTAMINATION AND COOLANT PROCESSING

C. LATGÉ
CEA, Nuclear Energy Division/Nuclear Technology Department,
Cadarache, France
Email: christian.latge@cea.fr

Abstract

Sodium is a coolant used for nuclear and solar applications, since many years, due to its very attractive properties. It is also used to study the dynamo effect, to get a better understanding of the magnetic field of the earth. In order to operate in reliable and safe conditions a Sodium Fast Reactor, it is necessary to master the quality of the coolant. The chemical control of sodium is performed versus the different chemical compounds: oxygen (corrosion control), hydrogen (detection of the sodium-water reaction), and to a less degree carbon (carburization, decarburization phenomena). Oxygen contributes to corrosion of the cladding steel and the activated corrosion products are transported from the core towards the components and mainly to the Intermediate Heat Exchangers, leading to their contamination. Moreover, other detrimental effects need to be avoided: plugging of narrow sections, loss of heat transfer efficiency in heat exchangers, contamination due to activated corrosion products and dosimetry. Oxygen and moisture are introduced mainly during handling operations; hydrogen is due to the aqueous corrosion of the Steam Generator Units and thermal decomposition of hydrazine, used to control the oxygen content in the water. The purification of oxygen and hydrogen is performed satisfactorily thanks to cold traps and due to very low solubility, nearly nil for temperatures close to the melting point, i.e. 97.8°C. It is also possible to get a very high purity thanks to getters. In steady-state operation, traces of tritium are produced from boron carbide and ternary fission of plutonium and fixed in the cold traps. Before repair operations, after sodium draining, it is necessary to clean-up the internal structures, wetted by residual sodium: efficient processes have been developed thanks to the reactivity of sodium with moisture. Some stress corrosion cracking phenomena can occur in presence of aqueous soda; therefore, it is necessary to avoid any presence of residual aqueous soda on components, gaps…by appropriate rinsing or drying processes. Additionally, the structures are decontaminated, using acidic baths, which transfer the contamination to the effluents. The large amounts of sodium used in a Sodium Fast Reactor are converted into sodium hydroxide, at the end of the reactor operation, during the decommissioning phase. A process, NOAH, has been developed in CEA Cadarache and applied successfully to convert the primary sodium from Rapsodie, PFR, KNK2 and Superphenix. It will be also the reference process for Phenix. Residual sodium remaining in the main vessel or intermediate loop can be converted into Na carbonate, avoiding any further potential interaction between sodium and humidity.

1. INTRODUCTION

The Generation IV will focus on fast reactors which are able converting a large part of uranium-238 into plutonium-239 while producing electricity. In this way, it will become possible to exploit more than 90% of natural uranium to generate electricity, rather than only 0.5 to 1% in light water reactors. The large quantities of depleted and reprocessed uranium available in France could be used to maintain the current electricity production for several thousand years. The worldwide availability of primary fissile resources could thus be multiplied by more than 50. The construction of fast reactors will also open the door to unlimited plutonium recycling (multi-recycling) by taking advantage of its energy potential.

Radioactive waste management is yet another challenge facing Generation IV reactors which involves reducing the volume and the inherent long term radioactivity of final waste. These reactors may in fact be capable of burning some of the long lived radioactive elements contained in radioactive waste: minor actinides (americium, neptunium, curium, etc.).

Several main objectives have been defined to characterise the future reactor systems that must be: sustainability, safety and reliability, proliferation resistant, ability to resist to external hazards, cost effectiveness.

During the forties, three coolants were considered: mercury (Hg), sodium-potassium eutectic (Na-K), and lead-bismuth (Pb-Bi) for sub-marines in former Soviet Union, but beginning of the fifties, sodium was already selected as the reference coolant. Currently the Sodium Fast Reactors (SFR), connected to the Grid, represents only 1369 MWe, with 3 Units (BN600, BN800 in Russia and FBTR in India). Three additional experimental SFRs are in operation: CEFR in China, JOYO in Japan and BOR-60 in Russia. One SFR (500 MWe) is under commissioning: PFBR in India. One SFR is under construction: MBIR in Russia. Currently Na is considered as the most mature liquid metal coolant worldwide, for the new SFRs projects, JSFR (Japan), PGSFR (Korea), CFR600 (China), FBR1-2 (India), ASTRID (France, Japan and Europe).

Despite its attractive properties, the choice of sodium induces challenges facing nuclear systems, related to design, material behaviour, operation, maintenance and decommissioning phase particularly due to the well-known

coolant reactivity, radiochemistry, and their consequences on operation, maintenance, and decommissioning phases.

Since sodium has a tendency to lose its external electron, it has very significant reducing characteristics, as do all the alkali metals. It reacts with oxygen and can induce a sodium fire. It reacts also exothermically with water, and potentially with violence, as a function of local conditions. Despite very strong care with regards the contact with air and water, thanks to protection devices and confinement, sodium contains various non-radioactive impurities either present from the start or introduced during operation. Sodium can be activated and/or contaminated by activated impurities already present in the coolant or generated during operation of the reactor or by fuel cladding ruptures. Sodium radio-contamination and mass transfer created in the system, interaction between Na bulk and cover gas for liquid coolants induces relevant issues for radiological impact assessment, operation, including maintenance, inspection and handling, etc. The occurrence of activated corrosion products (ACP) generates the need of a mass transfer model able to predict the distribution of radio-activated species and to estimate dosimetry and consequently requirements for cleaning and decontamination processes, required prior to inspection and repair or decommissioning. Several tools have been developed in the recent years i.e. OSCAR-Na in France for SFRs [7], [8]; tools for similar objectives for SFRs have been also developed in Russia, Japan or India. It is possible to control corrosion in liquid metal systems thanks to O control mainly by cold trapping. Tritium is also a key issue for SFRs, due to its ability to permeate through structural walls at high temperature (namely > 400°C): in order to satisfy the release authorizations, it is necessary to mitigate the diffusion towards environment by appropriate means i.e. by cold trapping, on intermediate loops.

To support the maintenance of SFRs, it was necessary to develop an efficient strategy, after sodium draining, to remove the residual sodium on components and decontaminate the surfaces of the structural material. These processes are not only useful for reactor operation but also for maintenance and for decommissioning

2. REACTOR OPERATION

2.1. Steady-state conditions

In the primary circuit, there are essentially:

— One source of discontinuous contamination by oxygen and hydrogen at the beginning of the cycle, due to the fuel assemblies handling, which provides metallic oxides, less thermodynamically stable than sodium oxide, according to Ellingham diagram.
— One continuous source of hydrogen coming from the intermediate circuits, by permeation through the Intermediate heat exchangers, and in a much less extent from ternary fissions.

Thus, oxygen and hydrogen constitute the major contaminants of sodium, generating potentially large amounts of impurities in sodium.

The respective solubility's of oxygen and hydrogen are very low; the solubility reaching a value around nil, near the melting temperature i.e. 97.8°C (this is a property specific to sodium, in comparison with other liquid metals, used as coolants).

For oxygen, Noden law [1]:

$$\log_{10}[O(ppm)] = 6.250 - \frac{2444.5}{T(K)} \quad (1)$$

For hydrogen, Whittingham law [2]:

$$\log_{10}[H(ppm)] = 6.467 - \frac{3023}{T(K)} \quad (2)$$

Oxygen contributes to corrosion of steel and the activated corrosion products are transported from the core towards the components and mainly to the Intermediate Heat Exchangers, leading to their contamination. All the elements constitutive of steel (iron, Cr, Ni, Mn, C) are susceptible to be dissolved in sodium. Nevertheless, this phenomenon, which depends on diffusion near the interfaces, remains very weak because the diffusion coefficients of the components of steel are very low. Corrosion kinetics depends on sodium physical parameters

(temperature and flow rate) and sodium chemistry (mainly oxygen activity) and corrosion models have been established [3]. Even if it is generally taken into consideration, this “generalized” corrosion is only significant for temperatures higher than 544°C and for oxygen contents above 5 ppm. Therefore, it is generally considered that a SFR requires to be operated with an oxygen content below 3 ppm, in normal operation, to limit the corrosion, consequently the contamination and associated dosimetry during handling or repair operations. O content can be estimated with a plugging-meter or measured with an electrochemical oxygen-meter.

In the intermediate loops, hydrogen content has to be maintained as low as possible (< 0.1 ppm), in order to allow a fast detection of water ingress and to avoid subsequent sodium-water interaction.

Two main sodium purification processes have been developed with regards to oxygen and hydrogen control:

— Cold trapping [4] based on the crystallization of Na_2O and NaH, by lowering the sodium temperature below the saturation temperature and thus creating the optimal conditions for Na_2O and/or NaH nucleation and growth on a steel packing distributed in an auxiliary cooled vessel. Cold trapping (Fig 1) is the worldwide process used for sodium purification in the Sodium Fast Reactors, due to its undeniable advantages:
  i. The two most important impurities in a SFR, oxygen and hydrogen, can be trapped in the same component;
  ii. The highest efficiency can be obtained with optimized designs of cold traps, (efficiency: ratio between the effective decrease of concentration between inlet and outlet and the maximum decrease i.e. the difference between the inlet concentration and the solubility at the coldest point of the cold trap);
  iii. The highest capacity can be also obtained with optimized designs, (capacity: maximum amount of impurities trapped in the cold trap);
  iv. The cold trap can be regenerated by extracting solely the packing or by in-situ appropriate treatment (dissolution of impurities in hot sodium, chemical process).
— Hot trapping or “getter” operation [6] “based on the capacity of the chosen material (i.e. zirconium-titanium alloy for oxygen) to oxidize when it is placed in the presence of sodium containing some amount of dissolved oxygen.

This last process is generally chosen for small sodium volumes to be purified and when the risk of Na2O dissolution by loss of cooling function in the cold trap is unacceptable. As example, the $Zr_{0.87}$-$Ti_{0.13}$ alloy has been qualified for hot trapping in an irradiation loop for Phenix: kinetics and optimized operating conditions have been established for further use:

$$V = 41.26 \times 10^{-3} \times \exp(-40.3 \times 10^{3} / RT) \cdot [O] \ kg(O) \cdot h^{-1} \cdot m^{-2} \quad (3)$$

where V is the oxygen purification rate of ($mol.h^{-1}$), T designates the hot trap temperature (K), R Boltzmann’s constant ($J \cdot mol^{-1} \cdot K^{-1}$), [O] the oxygen content in ppm” [22].

For hydrogen trapping, “hydride” traps (i.e. yttrium) could be also be set-up but, due to their very low potential capacity and reversibility, their application for large sodium volumes has never been foreseen.

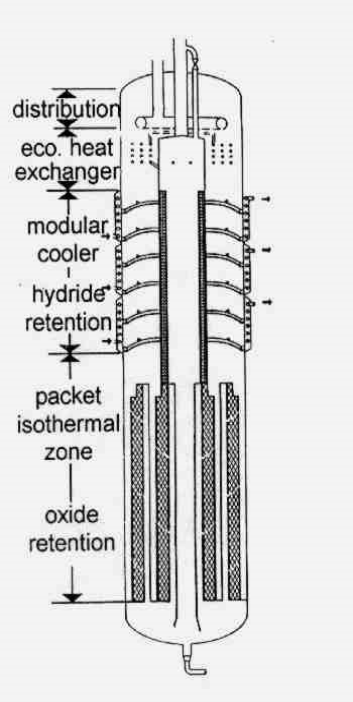

FIG. 1. Superphenix Cold trap (PSICHOS concept) [5].

2.2. Incidental conditions

When a sodium water reaction occurs, there is one discontinuous source of hydrogen, sodium hydroxide and potentially Na2O and NaH crystallized products. This reaction is strongly exothermic (162 kJ/mole of Na) and extremely fast. For these reasons, sodium water interaction which can occur in the Steam Generator Units is considered as an important issue and safety means are developed and implemented to mitigate this event.

A contamination of residual amount of sodium by air and moisture, after draining, prior to handling and/or repair operation, can also occur and induce deleterious effects, mainly due to stress corrosion cracking induced by aqueous soda [9].

In both cases, due to the pollution of sodium, it is necessary to perform a purification campaign, with the cold trap. After measurement of the impurities content (O and H), using a plugging-meter, the cold point of the cold trap is set-up, below the plugging temperature, creating the right conditions to promote the crystallization of impurities in the cold trap internals and consequently the purification of the sodium [10,11].

Oil from mechanical pumps, used as lubricant, can be introduced in the sodium. This event occurred in the primary sodium of PFR reactor. It is mitigated by filtering the solid particles produced by the interaction of oil with sodium and by venting the cover gas, polluted by methane and other organic gases.

3. REACTOR MAINTENANCE

3.1. Cleaning process

The reactivity of sodium with water is commonly used for the development of cleaning processes for structural material wetted with sodium. The amount of residual sodium is estimated up to 30mm on the vertical walls and up to 1mm on the flat horizontal surfaces; these values can be influenced by the wetting characteristics of the structure.

The main reactions involved in the process are the following ones:

$$Na_{(s)} + H_2O_{(l)} \rightarrow NaOH_{(s)} + 1/2\ H_{2(g)} \quad (4)$$

$$Na_2O_{(s)} + H_2O_{(l)} \rightarrow 2NaOH_{(s)} \quad (5)$$

$$NaH_{(s)} + H_2O_{(l)} \rightarrow NaOH_{(s)} + H_{2(g)} \quad (6)$$

The cleaning operation must remove the residual sodium and consequently eliminates a part of the contamination dissolved in sodium, like ^{137}Cs, in addition to ^{22}Na. Cleaning operation is often followed by a so-called "decontamination" process, aimed to reduce the dosimetry induced mostly by the activated corrosion products (^{60}Co, ^{54}Mn…) deposited on the surface and in the first nanometres of the structural material. It is based on the use of an acidic bath: the reference process used in France is the SPm process, which uses sulphuric acid and phosphoric acid. This process [12] is not detailed in this paper, focused on processes involving sodium.

A large operational feedback from the cleaning of large components has been gathered during the PHENIX operation: Intermediate heat exchangers (IHX) and primary pumps (Fig 2). The reference process used in PHENIX, after several improvements, consists in:

— Installing the drained component in the cleaning pit;
— Bubbling carbon dioxide in the demineralized water localized in the pit's lowest part. Thanks to bubbling, the gas becomes humid and the water vapor reacts with the residual sodium. The process is controlled, thanks to the continuous monitoring of the hydrogen content, in the gaseous effluent's discharge line (steady-state value: 1%), temperature, to avoid caustic corrosion (able to induce stress corrosion cracking above 80°C)) and pressure, to avoid any air ingress in the pit.
— Rinsing with water spray;
— Inspection after cleaning: the component is removed from the pit and inspected, to check absence of any significant amount of residual sodium, before immersion in water.

This process has been successfully operated during the last 15 years of the Phenix operation. On Superphenix, the cleaning process was slightly different from Phenix, based on water spray. The operational feedback was also very positive.

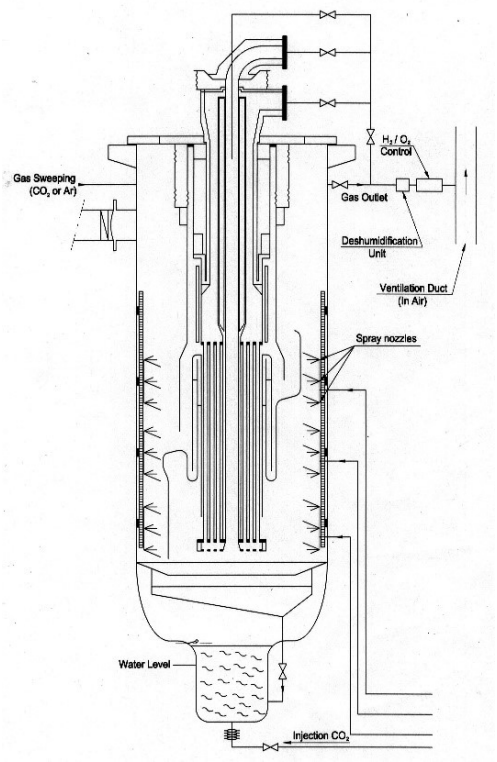

FIG. 2. IHX cleaning in a PHENIX Cleaning pit [19].

3.2. Cold trap regeneration

Several processes can be applied for the cold trap regeneration (regeneration means that the operator intends to reuse the cold trap), among them:

— Thermolysis: after sodium draining, the cold trap is heated up in order to induce the thermal decomposition of sodium hydride and consequently production of tritiated hydrogen. A secondary reaction between hydrogen and sodium oxide can occur at low temperature, from 100°C, which produces NaOH. Two regeneration operations were carried out in France on a cold trap in Phenix, in 1979 and 1984. The feedback is recalled in [13]. The same process was more recently applied to cold traps of Superphenix.
— Dissolution of sodium oxide and hydride in liquid sodium followed by adequate extraction.

In Japan Mitsubishi Heavy Industries Ltd) proposed in 1988 a process based on the dissolution of NaH followed by the extraction of H^2 from Na surface swept by argon [14]. The process efficiency is poor, mainly due to the too small free surface of Na.

In Russian Federation, RIAR developed a process based on the circulation of hot sodium, which circulates through the cold trap. Extraction of hydrogen is ensured by circulation of sodium in a vacuumed regeneration chamber having the developed surface for hydrogen desorption from free sodium surface and sodium oxide deposition on plates [15].

In France, CEA Cadarache developed the PRIAM process (Fig. 3) [13], based on the circulation of hot sodium through the cold trap, which induces the dissolution of sodium oxide and sodium hydride. Hydrogen and tritium are extracted thanks to permeators, equipped with nickel membranes, put under secondary vacuum, then trapped as metallic hydrides. Oxygen is trapped alone by an auxiliary cold trap, which can be treated by a treatment process only dedicated to sodium oxide. This last process has been selected for EFR project.

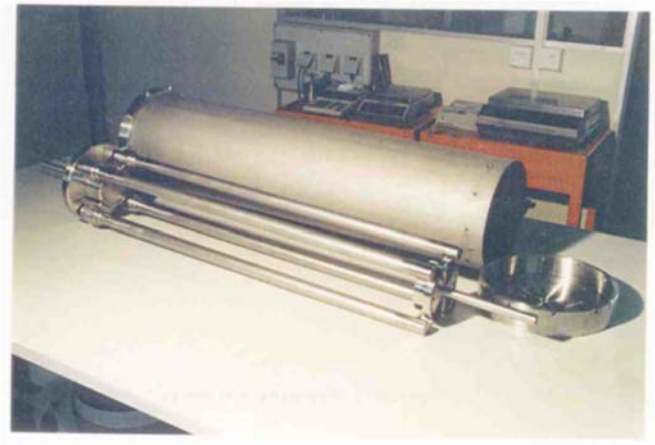

FIG. 3. PRIAM process for the Cold Trap regeneration [20].

4. REACTOR DECOMMISSIONING

The sodium reactivity with water can be used for the development of the sodium conversion process of large amounts of sodium into sodium hydroxide, at the end of the reactor life, during the decommissioning phase. A process, called NOAH, has been developed in CEA Cadarache and applied successfully to convert the primary sodium from Rapsodie, PFR and Superphenix. Currently NOAH is also the reference process for Phenix and the treatment unit is being built. NOAH process is based on the interaction between Na and water (Fig. 4) [16].

Sodium is injected in a vessel, filled of water, thanks to a “metering” pump which pushes continuously the sodium through a nozzle. It is spread out into small droplets, thanks to the water flow arriving in front of the nozzle, inducing large turbulence in this reactive zone. The resulting sodium hydroxide dissolves in the water, producing aqueous soda. In steady-state conditions, the water contents 10moles/litre of sodium hydroxide. Due to its dispersion in water and consequently large chemical interaction area, reaction kinetics is very fast. Na conversion

takes place in very safe conditions because there are only a few grams of Na involved in the reaction at any time: the total inventory of sodium in the system never exceeds a few grams and it is possible to end the reaction only a few seconds after sodium pump shut-down. The aqueous soda is recirculated and goes through a heat exchanger, allowing extracting the heat produced by the sodium-water interaction. The aqueous soda is evacuated continuously from the vessel, via an overflow and a lateral branch connection without letting gaseous waste through. Hydrogen produced is dried thanks to a separation process, including various steps, i.e. sintered filters, then it is lastly diluted in the ventilation duct exhaust air stream in a proportion of less than 1% by volume in the ventilation flow after mixing (factor of 4 relative to the 4% inflammability limit). It is dehumidified in order to remove the contamination carried out by the water steam. Hydrogen content is measured continuously in order to follow the overall reactive process.

The aqueous soda is collected in a dedicated storage tank then several options are open:

— Neutralization by means of acid i.e. hydrochloric acid, to form an aqueous saline solution, then released to the river or sea after further decontamination.
— Cementation and production of concrete blocks.
— Re-use to neutralize acidic effluents in reprocessing plant.

The NOAH process has been continuously improved; the operational feedback from the previous large applications at industrial scale is excellent. No major equipment failures and no safety issues occurred.

A conversion process for EBR2 sodium bulk, based on the same principle as NOAH process (Na-water reaction) has been designed, built and operated by Argonne National Laboratory to produce caustic solution then to convert it into sodium carbonate after combination with carbon dioxide.

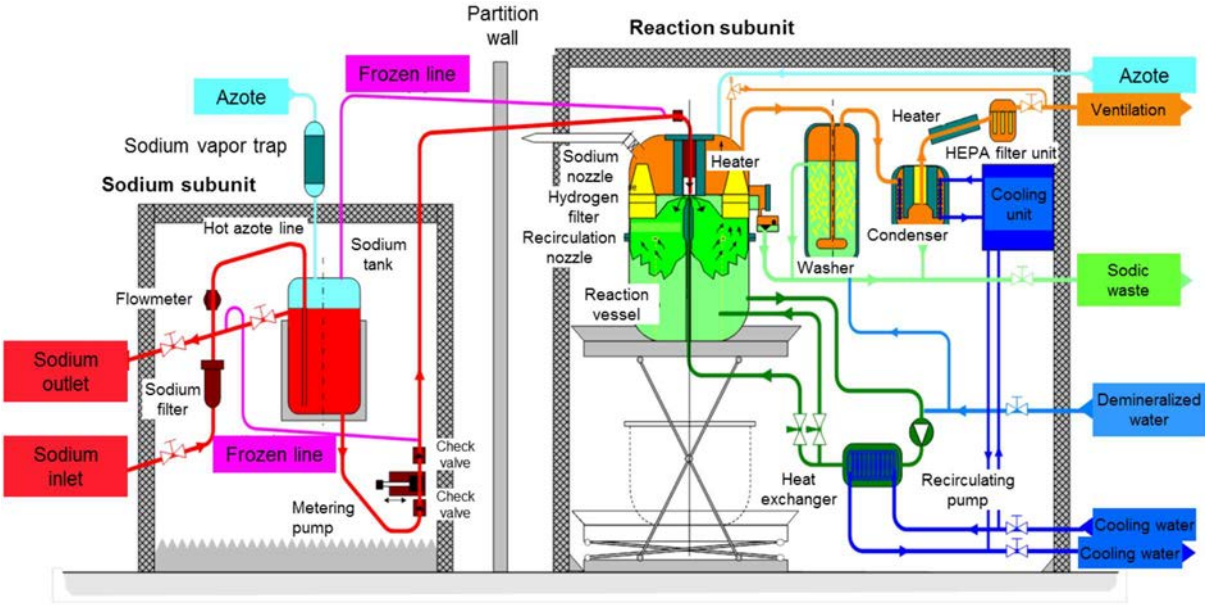

FIG. 4. NOAH Process [21].

After draining, some residual amounts of sodium remain in the main vessel, large piping, or tanks. A new process, named carbonation, has been developed to convert it into sodium carbonate Na_2CO_3.

$$Na_{(s)} + H_2O_{(g)} \rightarrow \frac{1}{2} H_{2(g)} + NaOH_{(s)} \quad (7)$$

Then:

$$2NaOH_{(s)} + CO_{2(g)} \leftrightarrow Na_2CO_{3(s)} + H_2O_{(g)} \quad (8)$$

$$Na_2CO_{3(s)} + CO_{2(g)} + H_2O_{(g)} \leftrightarrow 2\ NaHCO_{3(s)} \quad (9)$$

The main basic characteristics of this process are the following ones:

— Hydrogen production is linked to the quantity of sodium treated and allows to follow the reaction rate
— H_2O content is monitored to limit the amount of hydrogen produced,
— Temperature is controlled to avoid water condensation and potential local direct interaction between condensed water and metallic sodium,
— CO_2 is introduced in excess in order to avoid any soda formation.

A solid Na_2CO_3 layer is produced above the sodium, with large volume expansion, which facilitates the gas ingress through the carbonate layer (Fig. 5). Kinetics has been established in CEA. Even if the basic process is well mastered, it is necessary to carry out additional experimental tests with mock-ups representing some specific geometry, in order to demonstrate the full accessibility of all parts of the Na retentions.

FIG. 5. Carbonation process: sodium converted into sodium carbonate.

This process has been successfully applied in France in Superphenix for the Fuel Storage Drum in 1988, then improved for various applications pumps and vessels in Superphenix, Phenix secondary loops in 2015. It has been applied successfully for the treatment of residual sodium in the primary vessel of Superphenix; it will be applied in the near future for the treatment of residual sodium in the primary vessel of Rapsodie and Phenix.

During reactor operation, cleaning pits have been used extensively to clean up the residual amount of sodium, located on some specific components, prior to their inspection and repair (see paragraph 3 Maintenance).

Specific & new cleaning units has to be developed during decommissioning operations to have a treatment process for some specific components, loaded with sodium compounds: pure sodium, sodium oxide, sodium hydride. The most representative of these components is the cold trap, loaded with sodium compounds. Several processes can be applied for their final treatment:

— Thermolysis as it was described in paragraph 3 (Maintenance), with improved procedures, followed by WVN process (Water Vapor & Nitrogen). This process used by AREVA, on Superphenix secondary cold traps, mainly loaded with sodium hydride contaminated by tritium. For such application, it is necessary to master the hydrogen production and associated tritium balance.
— Alcohol cleaning, after Na draining, has also been investigated in the past, due to the low reaction rate between sodium and heavy alcohol (i.e. ethylcarbitol), diluted in an inert organic fluid. This method was never implemented, due to the production of tritiated organic waste, and, moreover, after the occurrence of accident close to Rapsodie reactor, occurred in 1994 March 31st [17], then in KIT in 1996 March 8th [18], using heavy alcohol to clean-up the residual sodium located in a storage tank.
— Water cleaning, after Na draining, by introduction of steam with an inert carrier gas (nitrogen). The reaction rate can be monitored theoretically by controlling the water content (dew point) in the carrier gas; nevertheless, due to the very high reactive surface (crystals spread out in the packing) and due to the complex geometry of the internals, it is rather impossible to guaranty a continuous and safe process.

— Carbonation, after Na cleaning, by introduction of water vapor and carbon dioxide in the cold trap,
— Without preliminary draining phase, cutting into slices with a saw, then cleaning with a water spray in a cleaning pit dedicated to large pieces of components, packed into a basket under inert gas: to support the Phenix decommissioning, a hydrolysis facility, named ELA, has been designed and is currently qualified in CEA Cadarache (Fig. 6).

FIG. 6. PEELA facility [21].

5. SUMMARY

In this paper we have described the main processes linked to the use of sodium as a coolant for Sodium Fast Reactors. Most of them are also relevant for other applications of sodium, such as solar applications, study of dynamo phenomena.

Thanks to these developments, sodium coolant technology is well mastered: sodium purification was never considered as a key issue during steady state operation and purification campaigns necessary to deal with the main pollutions i.e. sodium-water reaction or air ingress. Cleaning operations are currently used in Sodium Fast Reactors, operated since many years. All specific processes required for the decommissioning of SFR_s have been developed and applied at industrial scale.

REFERENCES

[1] NODEN, J.N., A general equation for the Solubility of O2 in liquid Sodium British Report RB/B/N 2500 (1972).
[2] WITTINGHAM, A.C., An equilibrium and kinetic Study of the liquid Sodium Hydrogen Reaction, Journal of Nuclear Materials **60** (1976).
[3] MASSE, F., ROUVIÈRE, G., Activation, corrosion and contamination in Fast Breeder Reactors validation of models with experimental data, Material behaviour and physical chemistry in Liquid Metal Systems 2 (BORGSTEDT, H.U., Ed.), Plenum Press (1993).
[4] LATGÉ, C., "Sodium quality control", International Conference on Fast Reactors (Proc. Int. Conf. Kyoto, 2009).
[5] LATGÉ, C., LAGRANGE, M., SURANITI, M., RICARD, J.B., "Development of a new cold trap concept for Fast Breeder Reactors", 4th LIMET Conference (Proc. Int. Conf. Avignon, 1988).
[6] LATGÉ, C., SELLIER, S., Oxidation of zirconium-titanium alloys in liquid sodium: validation of a hot trap, determination of the kinetics, Material behaviour and physical chemistry in Liquid Metal Systems 2 (BORGSTEDT, H.U., Ed.), Plenum Press (1993).
[7] GENIN, J.B., BRISSONNEAU, L., "Validation Against Sodium Loop Experiments of Corrosion Product Contamination Code OSCAR-Na FR17", (Proc. Int. Conf. Yekaterinburg, 2017).

[8] GÉNIN, J.B., BRISSONNEAU, L., GILARDI, T., OSCAR-Na: A New code for Simulating Corrosion Product Contamination in SFR, Metallurgical and Material Transactions E **3E** (2016) 291-298.
[9] BLAT-YRIEIX, M., et al., "Feedback from Stainless Steels Corrosion Related Issues during Maintenance Operation in Sodium Fast Reactor: SCC in caustic solution and Intergranular Corrosion by Acid Solution FR17", Conference Yekaterinburg, Russian Federation (2017).
[10] LATGÉ, C., GILARDI, TH., KHATCHERESSIAN N., "Sodium Purification Systems: requirements, tools and qualification strategies", (Proc. Int. Conf. Pamir, 2014).
[11] KHATCHERESSIAN, N., LATGE, C., JOULIA, X., GILARDI, TH., MEYER, X., "Modelling of Cold Traps for Sodium Purification in Fast Reactors", ESCAPE 22 (Proc. Int. Conf. United Kingdom, 2012).
[12] MASSE, F., RODRIGUEZ, G., "Cleaning and decontamination: experimental feedback from Phenix", https://inis.iaea.org/collection/NCLCollectionStore/_Public/31/040/31040844.pdf?r=1&r=1
[13] LATGÉ, C., "A new process for the removal of impurities in the cold traps of liquid metal fast reactors", Technical Committee meeting on Sodium Removal & Disposal from LMFBRs in normal operation and in the framework of decommissioning (Proc. Int. Conf. France, 1997).
[14] YOSHIKAWA, K., et al., "Experimental study on cold trap regeneration using sweep gas method", Fourth International Conf. on Liquid Metal Engineering and Technology (Proc. Int. Conf. France, 1988).
[15] YU, J., PRIVALOV, V., SHTYNDA, J., Liquid metal coolant impurities cold trap regeneration method, Russian Federation Patent N° 153476; Bulletin Izobreteniy N17 284.
[16] ROGER, J., LATGÉ, C., RODRIGUEZ, G., "Transformation of sodium from the RAPSODIE fast breeder reactor into sodium hydroxide", 3rd International Conference of the European Community on Decommissioning of Nuclear Installations (Proc. Int. Conf. Luxemburg, 1994).
[17] MARMONIER, P., DEL NEGRO, R., "Information about the accident occurred near Rapsodie", Annual Meeting of the International Working Group on Fast Reactors, IAEA, Vienna (1996).
[18] MINGES, J., CHERDRON, W., SCHUTZ, W., "Short report of an accident during sodium clean-up with Ethyl Carrbitol in a storage tank of a research facility", Technical Committee meeting on Sodium Removal & Disposal from LMFBRs in normal operation and in the framework of decommissioning (Proc. Int. Conf. France, 1997).
[19] RODRIGUEZ, G., et al., Description and identification of difficulties arising from the application of a cleaning process in operating conditions for the treatment of components used on liquid metal fast reactors (LMFR), Waste Management **21** (2001) 357-362.
[20] LATGÉ, C., "A new process for the removal of impurities in the cold traps of fast breeder reactors", IAEA-IWGFR: Sodium removal and disposal from LMFR's in normal operation and decommissioning, (Proc. Int. Conf. France, 1997).
[21] LATGÉ, C., BERTE, M., Contaminated Sodium disposal: The NOAH Process Revue Générale Nucléaire **2** (1998).
[22] ROUAULT, J., "Sodium Fast Reactor Design: Fuels, Neutronics, Thermal-Hydraulics, Structural Mechanics and Safety", Handbook of Nuclear Engineering (2010).

ALLEGRO GAS-COOLED FAST REACTOR HELIUM MANAGEMENT

M. SOUKUPOVÁ, L. BĚLOVSKÝ
ÚJV Řež,
Husinec
Email: monika.soukupova@ujv.cz

J. BERKA, M. JANÁK
UCT,
Prague

Czech Republic

Abstract

ALLEGRO is a helium cooled experimental fast reactor, which is currently under development by the consortium V4G4 Centre of Excellence (V4G4 CoE) (Czech Republic, Hungary, Poland and Slovakia) associated with France.

1. INTRODUCTION

The main purpose of ALLEGRO is:

- Demonstration of viability of the gas-cooled fast reactor (GFR) technology in pilot scale;
- Testing of innovative carbide-based refractory GFR fuels in the start-up oxide core driver;
- Qualification of other GFR-specific technologies such as components of the primary circuit, helium-related systems, fuel handling etc.

The current pre-conceptual stage of development by the V4G4 CoE (based on the 75 MWt concept presented by CEA in 2009) is mainly focused on: A) Oxide fuel driver core with six experimental positions and B) Coolability of the core in accident conditions by using (semi)passive decay heat removal system.

Concerning the auxiliary systems, ÚJV Řež is responsible within the V4G4 CoE for development of helium-related technologies. ÚJV Řež cooperates in this field with its daughter company Research Centre Řež (RC Řež) as well as with the University of Chemistry and Technology (UCT) in Prague and other industrial partners. The current efforts are focused onto assessment of feasibility of a recovery system for the helium leaked into the guard vessel and helium-tight seals testing. Besides this topic ÚJV & RC Řež devote their attention also to primary gas management (purification of primary helium) and behaviour of materials in impure helium at elevated temperatures.

1.1. Recovery of helium from GFR guard vessel using membrane separation

The primary circuit of the current concept of ALLEGRO is enclosed in a gas-tight guard vessel (GV – a metallic pressure boundary around the primary circuit filled with 0.1MPa nitrogen). The helium leaked from the pressurized boundaries of the primary circuit into the guard vessel can potentially be recovered from the nitrogen-helium GV atmosphere back to the helium storage system. This feature would make the future GFRs (including ALLEGRO) much less dependent on the helium market. A question arises, whether this idea is technically (and economically) feasible. Preliminary analysis identified a membrane separation as potentially the most suitable technology. The current efforts thus concentrate on both the separation method and the proposed (pre-conceptual) technical solution. The system is based on multi-cycle semipermeable membrane separation. Up to cca 95 % helium purity can be reached by this process, while the final purification is planned to be performed by other methods (e.g. by using a pressure swing adsorption technology). A membrane-based recovery system was developed, tested on laboratory scale (Fig.1) and a first concept of the recovery system was proposed for the conditions of ALLEGRO (Fig. 2).

FIG. 1. Membrane module PRISM® used for tests in the testing device.

Currently, "membrane separation technologies use a hollow-fibber membrane consisting of porous polymer fibbers coated with a separation layer.

A porous fibber has a complex asymmetric structure, with the polymer density increasing towards the fibber external surface.

The application of porous support layers with asymmetric structure allows separating gases under high pressures (up to 6.5MPa). The thickness of the fibber gas separation layer does not exceed 0.1μm, ensuring a high relative permeability of gases across the polymer membrane" [1].

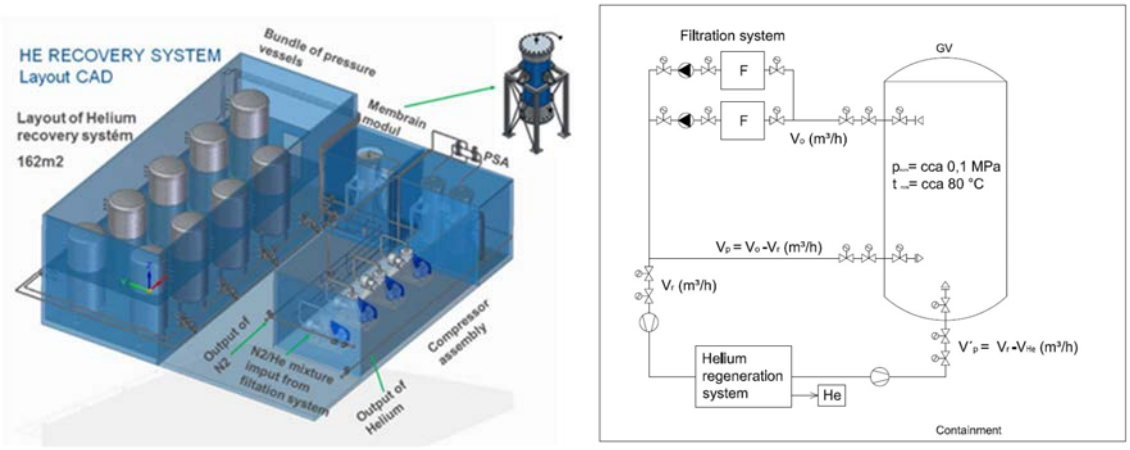

FIG. 2. Proposed concept of the recovery system for ALLEGRO.

1.2. Future plans in He recovery

In the future, we intend to replace a polymeric membrane with a borosilicate membrane. It seems that we would develop and test our own borosilicate membrane for He regeneration. The construction of helium recovery system will be done in both on a large and on a small scale. In order to acquire the best results, the flow rate of gas inlet mixture is estimated at 200 L/min (on a large scale). In Figure 3 pre-conceptual scheme of helium recovery system is shown. The simulation of He recovery is as follows. Helium and nitrogen feed, considered as majority component from the GV atmosphere, are mixed and flow through the heat exchanger and membrane module.

Permeate travels across the membrane and buffer tank. The permeate may be stored in storage tanks #1 & #2 or recirculate, if needed. The retentate returns to the membrane module through both the buffer tank and heat exchanger. The retentate may be stored in the storage pressure tank #3.

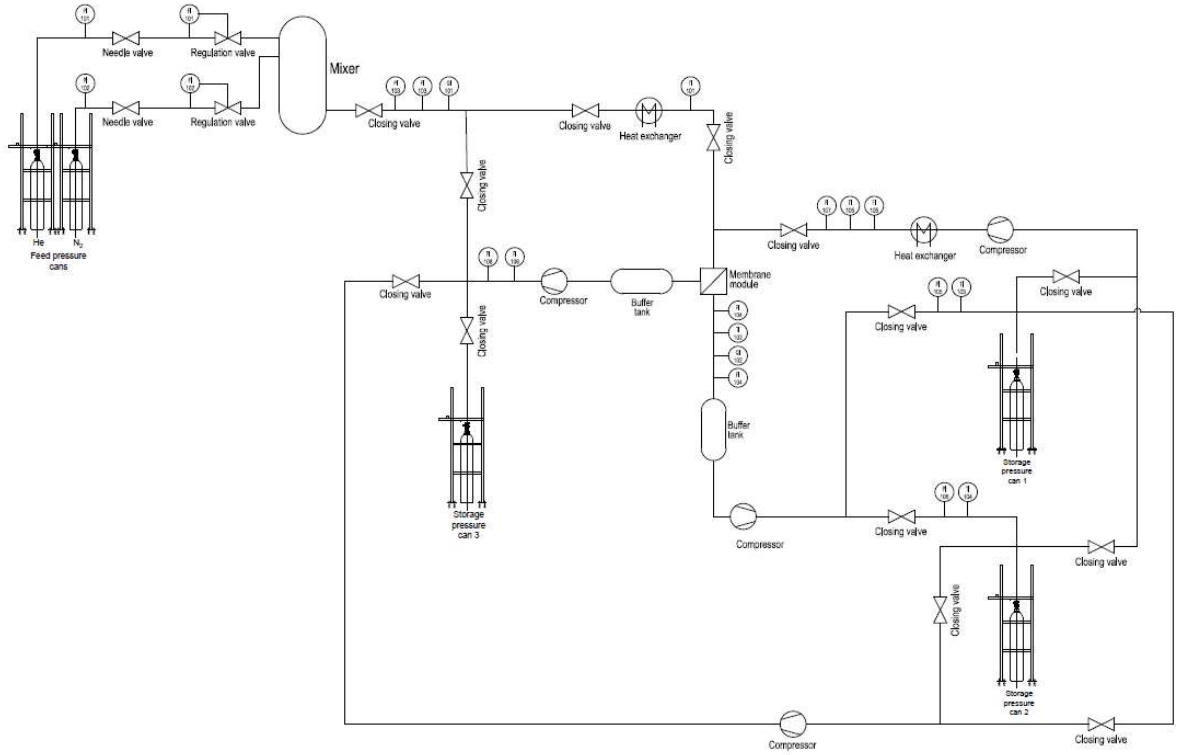

FIG. 3. Pre-conceptual scheme of experimental helium recovery system.

1.3. He seal development

The He recovery system test loop provides good opportunity to develop and test new types of the He-tight seals, because the total leakage of the He from the system depends among others on the tightness of flange joints. The development of the seals consists of many stages from the design proposal to the final seals (see Fig. 4). The samples of material used for the seal were tested at CV Řež in the High Temperature Helium Loop (HTHL) in order to determine the material behaviour in the He atmosphere under the extreme conditions.

Seal with mica foil in combination with expanded graphite seal was selected and tested. To verify the tightness and thus the design of the seals, the primary circuit conditions (700 °C, 6.5 MPa) were chosen in the test loop. The experiment lasted for 7 days. Figure 5 shows the seal after testing.

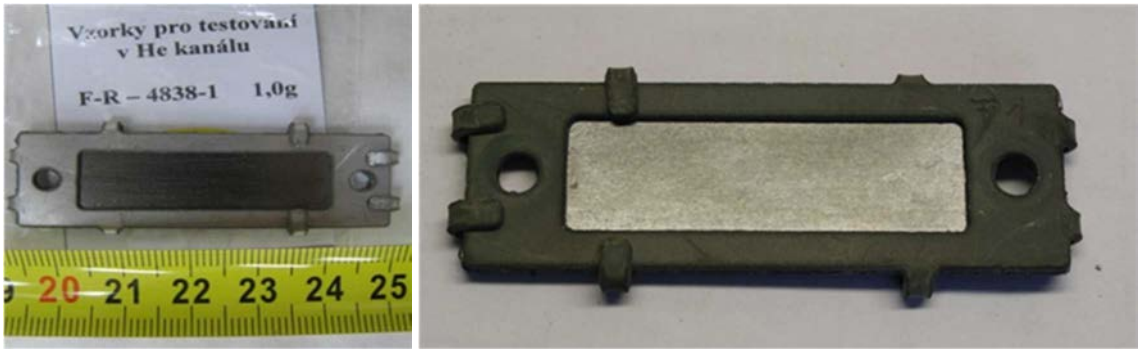

FIG. 4. Seal test - Seal F1 before (left) and after (right) testing in HTHL loop (700°C/He).

1.4. Helium purification

As ALLEGRO will use pin-type fuel, the primary helium purification system must be ready to manage potential contamination of the primary coolant from the tested fuel, when an unexpected important leakage occurs. Even relatively short lived gaseous fission products such as Xe and Kr (Figure 6) need to be rapidly removed from the primary coolant. For this purpose, various carbon absorbers were tested and their capability to adsorb Xe and Kr at various temperatures was determined.

FIG. 5. The seal after the test.

Except Xe and Kr, the removal of the ordinary impurities from the primary helium such as e.g. H_2, O_2, H_2O, CO, CO_2, CH_4, NO_x is being mastered for ALLEGRO using the methods used in HTR primary helium purification system (see e.g. reference [2] for more information) such as mechanical filters, molecular sieves, oxidation beds and adsorption on activated carbon at low temperature. Except the dedicated separate effect facilities, the HTHL at RC Řež is being used for integral experiments in the area – see citations [3-5] for more details. See Fig. 7 for examples of results.

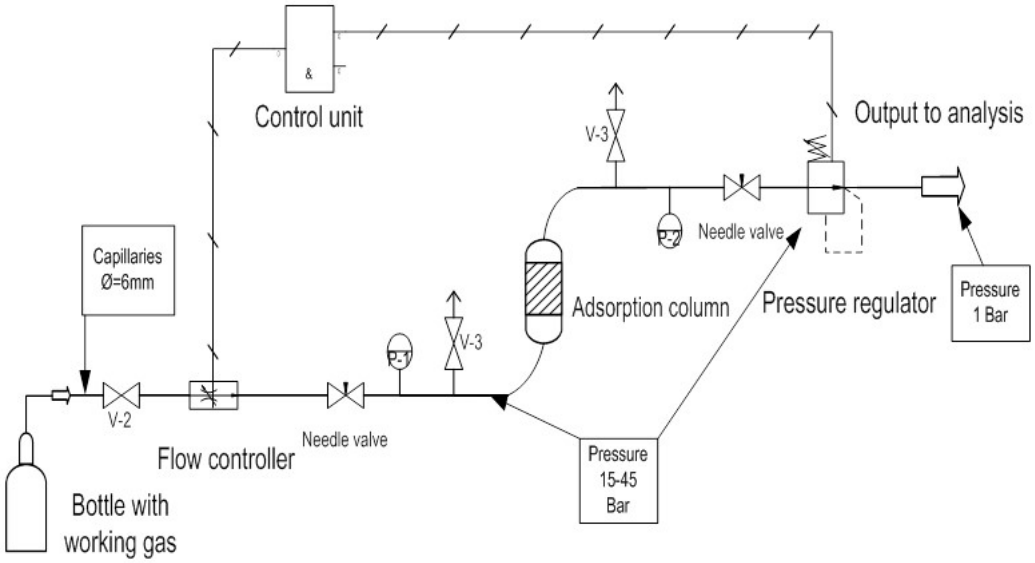

FIG. 6. Xe, Kr adsorption test equipment scheme.

2. MATERIAL TESTING IN IMPURE HELIUM ENVIRONMENT AT ELEVATED TEMPERATURES

One of the most important topics is also testing and evaluating of properties & degradations of materials in impure helium at elevated temperatures for high temperature helium cooled reactors. For these activities several experimental facilities were used including the HTHL loop. The main operational parameters of the loop are: Gas pressure 3–7 MPa, temperature in the test section 25 – 900 °C, gas flow 12 – 38 kg h^{-1} (for limited time the gas flow could be even lower than the mentioned lower limit). The gas in the loop needs to consist of helium with only minor impurities (H_2, H_2O, CO, CO_2, N_2, O_2, CH_4) in concentrations up to approximately 500 vppm.

Investigation into mechanical properties of ceramics Lunit 73 (C610), Luxal 203 (C799), AG 202 (C795) after log-term exposure in high temperature helium environment (up to 900 °C) was carried out. Within the program several metallic alloys were also tested – e.g. stainless steel 316L, ferritic steel P91, alloy 800 H with weld join and several types of high temperature nickel alloys.

With regard to metallic materials which were tested so far, stainless steel 316 L proved to be resistant to impure helium even at 750 – 760 °C. However, mechanical properties of this steel changed after exposure at high temperature. Fracture toughness of steel P91 almost did not change after exposure at high temperature. These materials are not designed for long term operation at such high temperatures; however, these materials could be used e.g. for not mechanically stressed parts of experimental devices or colder parts. Mechanical properties of Alloy 800 H after exposure at high temperature were not tested. According to obtained results, corrosion resistance of Alloy 800H at high temperature of impure helium seems to be worse compared to other tested materials. A part of results of this research had been already published – see Refs [6–9] for more details.

With reference to tested ceramic materials, corundum base ceramics seems to be better material as an insulator of heating elements for high temperatures than commonly used cordierite ceramics.

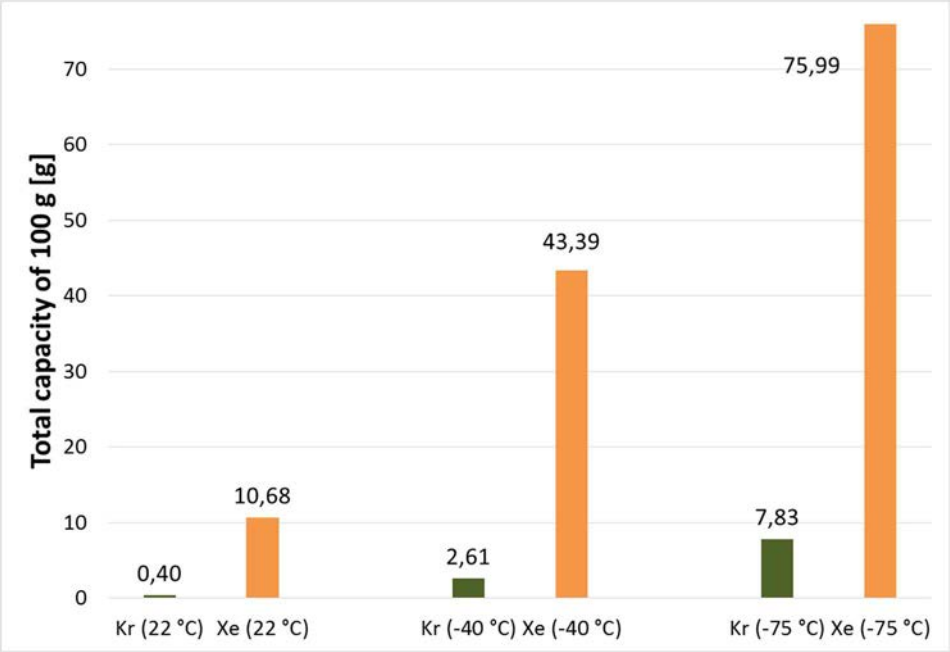

FIG. 7. Xe, Kr adsorption adsorbents capacities as function of temperature.

3. ONGOING AND PLANNED R&D ACTIVITIES

Further R&D activity is ongoing at ÚJV group on GFR issues related to helium coolant. Except the small demonstration unit for the He recovery from nitrogen-helium mixture, helium loops HTHL 1 & 2 for material research and S-ALLEGRO loop for GFR/ALLEGRO core coolability in accident conditions are either under operation or under commissioning.

ACKNOWLEDGEMENT

The work has been so far supported mainly by the Technology Agency of Czech Republic projects TA03010849, TA03020850, TA04021546 and TH02020578.

REFERENCES

[1] GRASYS, grasys.com
[2] YAO, M.S., WANG, R.P., LIU, Y.Z., HE, X.D., LI, J., The helium purification system of the HTR-10, Nucl. Eng. Des. **218** (2002) 163–167.
[3] BERKA, J., MATĚCHA, J., ČERNÝ, M., VÍDEN, I., SUS, F., HÁJEK, P., New experimental device for VHTR structural material testing and helium coolant chemistry investigation – High Temperature Helium Loop in NRI Řež, Nucl. Eng. Des. **251** (2012) 203–207.
[4] MATĚCHA, J., BERKA, J., SUS, F., ČERNÝ, M., LENGYEL, J., TEKÁČ, V., Testing of analytical and purification methods for HTR helium coolant, Nucl. Eng. Des. **251** (2012) 208–215.
[5] BERKA, J., HLINČÍK, T., VÍDEN, I., HUDSKÝ, T., VÍT, J., The design and utilization of a high temperature helium loop and other facilities for the study of advanced gas-cooled reactors in the Czech Republic, Prog. Nucl. Energy **85** (2015) 156–163.
[6] BERKA, J., VILÉMOVÁ, M., SAJDL, P., Testing of degradation of alloy 800 H in impure helium at 760 °C, J. Nucl. Mater. **464** (2015) 221–229.
[7] KUNZOVÁ, K., BERKA, J., SIEGL, J., HAUŠILD, P., Effect of thermal exposure in helium on mechanical properties and microstructure of 316L and P91, J. Nuc.l Mater. **472** (2016) 47–54.
[8] MARUŠÁKOVÁ, D., BUBLÍKOVÁ, P., BERKA, J., VÁVROVCOVÁ, Z., BURDA, J., Microstructural analysis of 800H steel exposed at test operation in HTHL by using FIB-SEM and HRTEM techniques, Appl. Sur. Sci. **416** (2017) 379–384.
[9] BERKA, J., KALIVODOVÁ, J., Testing of high temperature materials within HTR program in Czech Republic, EPJ Nuclear Sci. Technol. **2** (2016) 1–7.

EUROPEAN SPALLATION SOURCE ERIC – TARGET HELIUM COOLING

P. NILSSON, U. ODÉN
European Spallation Source,
Lund, Sweden
Email: ulf.oden@esss.se

Abstract

In ESS, a 5 MW proton beam will hit a tungsten target to generate neutrons by spallation. A large part of the proton power, about 3 MW, will be deposited as heat in the helium cooled target material - tungsten. For the purpose of investigating various aspects of cooling with helium, an experimental system has been constructed at Lund University, Department of Energy Sciences.

1. INTRODUCTION

By a booster compressor, a helium flow of about 3 g/s is circulated in a closed loop. The system is designed for 10 bar and above 400 C. The test vessel is equipped with a flow tube with the rectangular internal cross section 2 mm x 10 mm. This flat and narrow cross section is typical for the cooling flow in the ESS-target. The flow forms a jet perpendicularly onto a material sample of a coin shape with a diameter of 20 mm and a thickness of 3 mm. This coin shaped sample is submerged in a holder with the top surface flush with the holder surface. Below the sample there is a ceramic heater, which heats the sample from below.

One purpose of the test is to investigate the erosion of the oxidized sample surface by the impinging flow under the same conditions as in the ESS target. This experiment simulates the target operation environment, where pre-heated pure helium at about 200 C impinges on and cools the tungsten that is volumetrically heated by the proton beam. The samples are investigated with Scanning Electron Microscopy (SEM) at three different stages sequentially. First SEM pictures are taken of two pre-oxidized samples with their similar and specific surface structure and composition. Then the samples are exposed to the test conditions for 5 hours in the ETHEL vessel and a second set of SEM pictures are taken at the same positions on the sample surface. After that, the samples were exposed to the helium flow for 5 hours more and then an additional 15h. A third and a fourth set of SEM pictures was taken. The four SEM pictures at each position of the sample surface are compared visually. Some image analysis techniques have also been tested in an effort to locate and possibly quantify differences, i.e. measure the erosion rate.

Based on these pictures the conclusion is that the experiment could not reveal any dust formation what so ever with in the experiment basis. The erosion rate is by that 0 μm in this experiment, see Fig. 1.

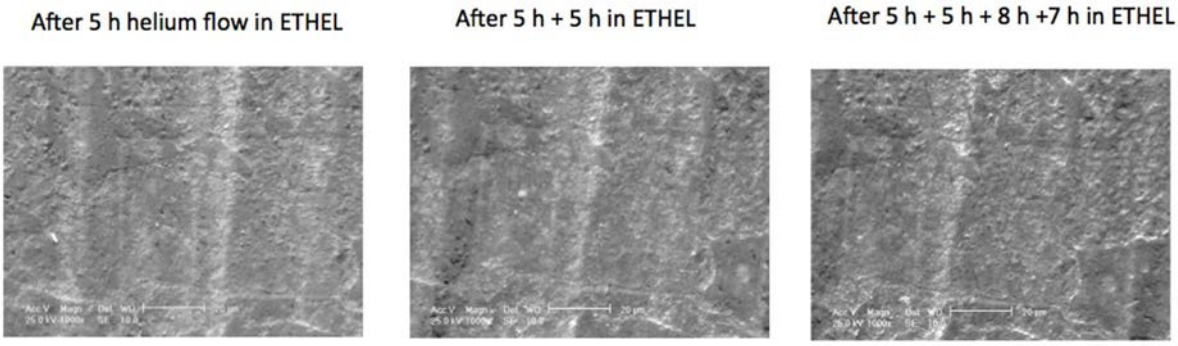

FIG. 1 ETHEL Pictures.

A particle production estimation is performed based on the ETHEL test, existing literature and in-house calculations. Looking at the picture some protruding features are recognized. The features are estimated to be (5 μm)^3= 125 μm^3. Some pictures have about 10 of these features. If you assume that this is the surface structure in general, and to make a conservative estimation, all of them are in some way eroded from the surface you can estimate a dust formation. These estimates will give an erosion amount of about 0,1 kg.

The calculation is, features volume x tungsten density x total tungsten surface / SEM surface:

$$1250\times10^{-18}m^3\times19300\ kg/m^3\times43m^2\times10^4m^{-2} \sim 0.1\ kg \quad (1)$$

The test samples are pre-oxidized in 500°C He with 0,5% oxygen during 1h. Compared to the steady state operational condition this is far beyond the oxygen requirements in the Helium Cooling Loop. During operation, the Helium is purified to 0,00001% (10 ppmV) oxygen. Taking this level into account the pre-oxidized test samples roughly could be compared to a five-year in operation tungsten brick. The 0.1 kg of particles derived from the eroded features is comparable to 20 g/y.

The ETHEL experiment could not display any erosion from the surface, neither from the tungsten itself nor the tungsten oxides on the surface. To still make a conservative estimation of the dust production the hypothesis is that all the oxides will in some way leave the tungsten surface and produce dust.

The tungsten will be operated in helium with a restricted amount of oxygen impurities. The following calculation assumes that all the oxygen is used for oxidization of the tungsten surface, which also is a conservative assumption.

In the absence of a helium purification system, the pure industrial helium typically has an oxygen impurity level of 5 appm, and the estimated leak rate of the primary cooling loop is 1 g/h. Under the ESS helium coolant loop conditions, the release of tungsten via the erosion of the oxide layer is estimated to be 10 g/year, even in the absence of purification system.

The estimated 10 g/y correspond to an erosion rate of 0.01μm/y. This is a considerably lower number than the number assumed in the TDR (10 μm/y). The number given in the TDR is however not taken into account the very low oxygen amount in the Helium Loop as in the calculation above.

If the hypothesis is correct, that there will just be dust formation coming from the oxide layer, the calculated 10 g/y seems reasonable and still conservative. We believe this estimation is conservative and mature enough to form the baseline input to the Preliminary Safety Analysis Report. ESS are preparing for a test regarding transportation of aerosols from oxidized tungsten to increase the knowledge about aerosol transport and to get release fractions from oxidized tungsten. A test setup shall be built to perform the experiments. This setup consists of the following main components, see Fig. 2 below:

— Test vessel;
— Controlled air supply;
— Controlled steam supply;
— Release path piping, including horizontal as well as vertical sections and wall cooling;
— Exit sample filter.

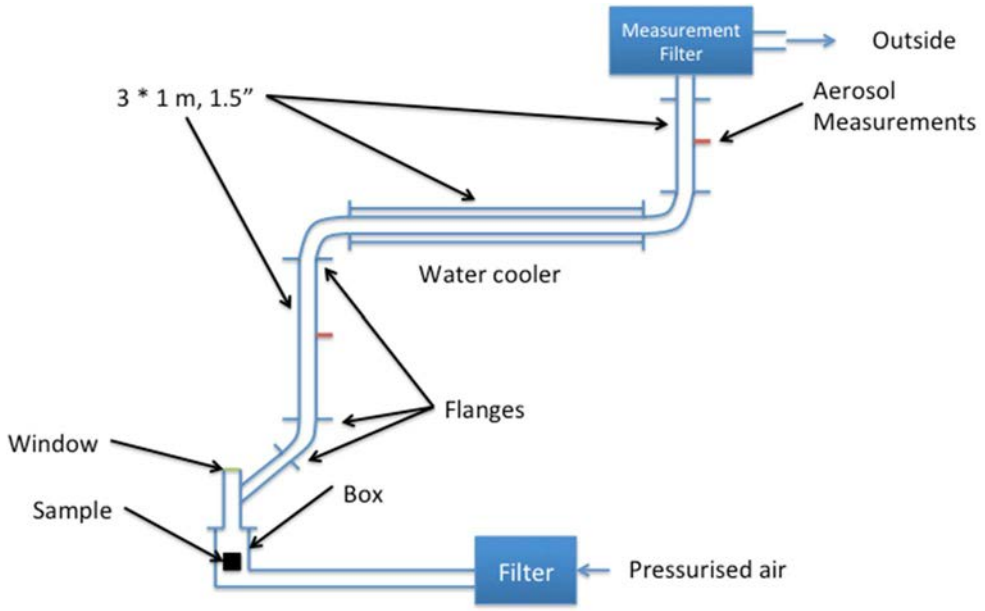

FIG. 2. Sketch of test setup.

The parts in contact with the air/steam need to be made of stainless steel. The test vessel is sketched in Fig. 3. A number of tests will be performed to conclude results according to Tables 1–2.

TABLE 1. TEST OBSERVABLES

Observables
Mass remaining in solid
Mass on filter
Size distribution

Test conditions according to Table 2.

TABLE 2. TEST CONDITIONS

Cases (examples)	
Velocity:	0.5 and 5 m/s
Humidity:	Air and Steam
Cooling:	No Water and Water

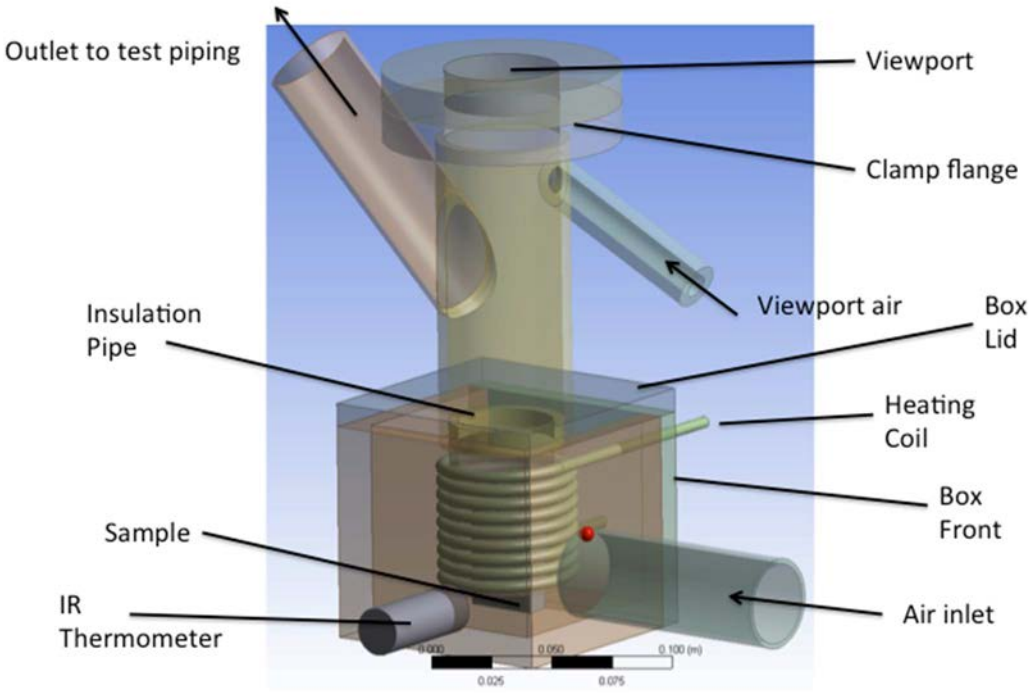

FIG. 3. Sketch of test vessel

DEVELOPMENT OF METHODOLOGY TO DETERMINE PBLI ACTIVATION IN DEMO BREEDING BLANKETS

M. GARCÍA, J.P. CATALÁN, R. GARCÍA, J. SANZ
UNED, Dept. of Energy Engineering,
Madrid, Spain
Email: maurigarciac@ind.uned.es

Abstract

A Computational System (CS), able to predict the activation of the PbLi flowing in the loops of the DCLL nuclear fusion blanket concept of the EUROfusion program, is presented. This CS is capable to take into account the main features of the loops; that is, the residence time of the PbLi (the time per cycle when the PbLi is being irradiated inside the breeding blanket), the different neutron spectra at different positions of the blanket, the extraction of the tritium in the Tritium Extraction System (TES), the purification of the PbLi in the Purification System (PS) and the accumulation of Activated Corrosion Products (ACP) during the functioning of the facility. A preliminary study of the DCLL PbLi loop concept has been addressed, finding significant differences in relevant quantities related to safety, maintenance and waste management when considering realistic residence time instead of continuous irradiation. The CS is also intended to be easily adaptable to the HCLL and WCLL loop concepts.

1. INTRODUCTION

Within the EUROfusion consortium activities, planned to the design of a Demonstration Fusion Power Reactor (DEMO), there are 4 blanket concepts under development: the Helium Cooled Pebble Bed (HCPB), the Helium Cooled Lithium Lead (HCLL), the Water Cooled Lithium Lead (WCLL) and the Dual Coolant Lithium Lead (DCLL) [1]. In the DCLL concept, the eutectic Pb–15.8Li alloy enriched to 90% in Li-6 is used as neutron multiplier, tritium breeder and carrier. The PbLi travels along pipe loops entering and leaving the Breeder Blanket (BB) modules located inside the Vacuum Vessel. These loops have several missions: i) to take the tritium produced inside the BB to the TES, ii) to remove generated impurities and activated corrosion products (ACP) in the PS, iii) to produce gravitational draining of the BB modules, iv) to maintain the PbLi in liquid state, and v) to transport the blanket heat to the steam generators [2]. The PbLi is activated by neutron irradiation inside the BB, undergoing decay along the rest of the loop and mass extractions in the TES and PS. The radioactive inventory generated in the PbLi plays a major role related to the design of the TES and PS, to the planning of maintenance and waste management activities and with regard to the consequences of an accidental loss of flow in the loop.

In this work, we design and apply a CS to face, in a realistic way, the activation of the PbLi alloy in the DCLL concept. The consideration of both the different neutron spectra irradiating the PbLi along the BB and the residence time of the alloy inside the BB, has a big impact over the activation prediction. Previous works performed by colleagues of the University of Wisconsin-Madison and the Idaho National Engineering and Environmental Laboratory, have pointed out the relevance of considering the residence time, instead of a continuous irradiation, in order to obtain a reliable activation of the moving alloy in the ARIES-AT conceptual fusion power plant [3], [4]. Our approach provides a CS able to estimate, at any position of the loop, and for any time during machine operation or after shutdown, significant quantities related to safety, maintenance and waste management activities. Specifically, it predicts i) the radioactive inventory in the PbLi, ii) the gamma sources in relevant components for maintenance planning, iii) the decay heat, iv) the amount of consumed lithium, v) the inventory of activated corrosion products (ACP) and vi) waste management related quantities. Other relevant quantities can be easily estimated, as the helium concentration and mass inventory. The CS has the capability of dealing with the different spectra and intensities of the neutrons irradiating the PbLi along the breeding blanket (BB), being also intended to be easily adaptable to the HCLL and WCLL BB systems.

The CS is preliminary applied to a simplified DCLL loop which takes into account the PbLi entering and leaving the BB, as well as the operation of the TES, being the remainder systems currently available in the CS as PS functioning and the ACPs evaluation, not considered. We focus on some safety, maintenance and waste management related responses, comparing the impact of considering realistic residence time instead of continuous irradiation.

2. LAYOUT OF THE DCLL PBLI LOOPS

The design of all the systems of the PbLi loops for the DCLL, WCLL and HCLL concepts is continuously under development. We use here the last design of the DCLL blanket and loop systems. The whole reactor is composed

by a repeated 20 degrees sector in which there are 3 Outboard (OB) segments and 2 Inboard (IB) segments. Each of the segments has 8 blanket modules. The number of blanket modules per sector is 16 for the IB and 24 for the OB. Therefore, the total number of blanket modules in the reactor is 720 (288 IB + 432 OB). Figure 1 shows a scheme of the blanket configuration and PbLi circuits inside the reactor [5].

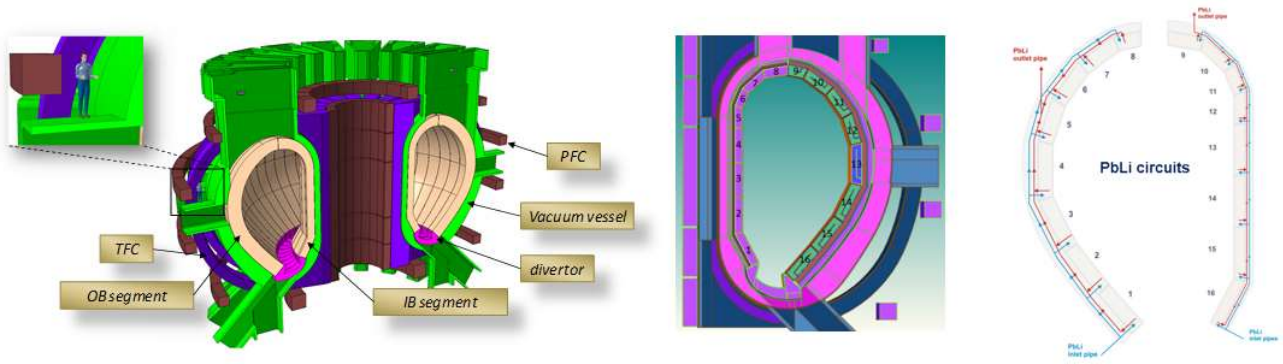

FIG 1. (a) DEMO reactor [13]; (b) 16 breeder modules (8 IB and 8 OB); (c) PbLi circuits (starting from left to right) [14].

The current design of the DCLL loops considers 3 loops feeding 288 modules of the IB and 9 loops feeding 432 modules of the OB, being all the 12 loops almost identical. Figure 2 shows the layout of one PbLi loop of DCLL blanket with the different systems and components: piping and valves, Storage Tank, Expansion Tank, Pumping System, TES, Electrical Heater, Heat Exchanger, Instrumentation and Heating Systems. The total PbLi volume for the whole reactor inside the BB for the OB and IB are respectively 603 and 183 m^3. The flow rates per loop are 2149 and 1957 Kg/s for the OB and IB are respectively [6].

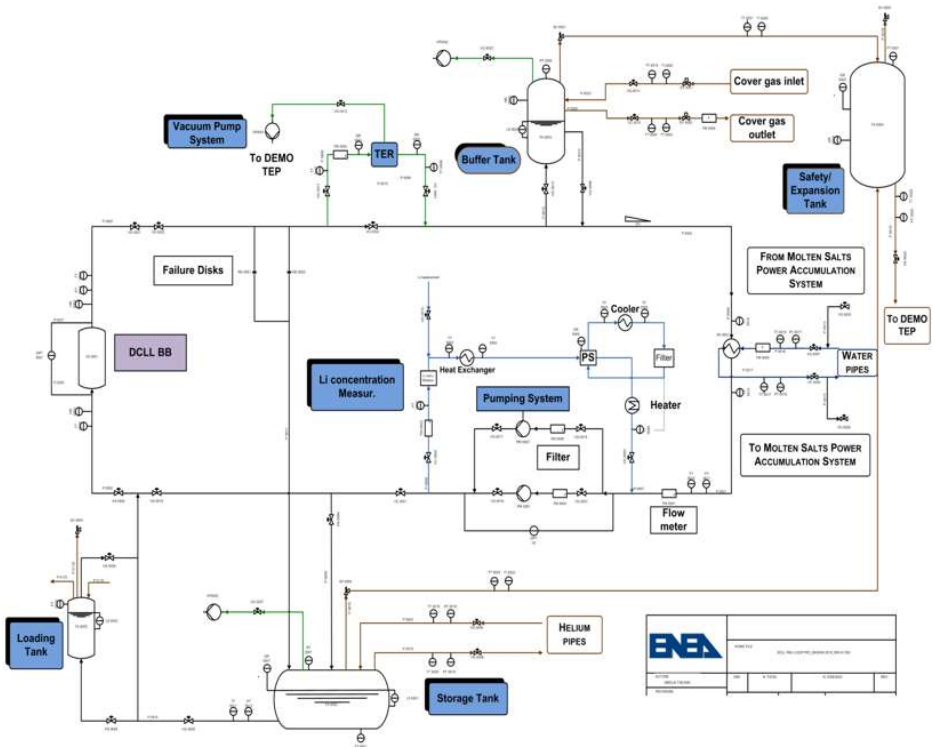

FIG. 2. Layout of the DCLL PbLi loop [15].

During normal operation, after the exit of the BB, the PbLi alloy enters in the TES, which is placed in the hot part of the loop. The PbLi mass flow rate managed by TES can be modified from 1% to 100%. An expansion tank is

placed after the TES in order to compensate thermal expansion of PbLi and to allow the release of Helium generated inside the blanket. Then, the PbLi passes through the heat exchanger and come out at the temperature of 300°C, and thus goes to the pumping system placed in the cold part of the loop. After the pump a portion of the eutectic alloy is sent to the PS (about 1% in the current design) that it placed as a by-pass line of the pump. After that, the PbLi flows to enter to the blanket. Figure 3 shows a scheme of the movement of the PbLi inside the BB; only one module is shown, being the remainder (a total number of 8 for the IB and 8 for the OB in each segment) similar in shape with differences in total volume and size [6].

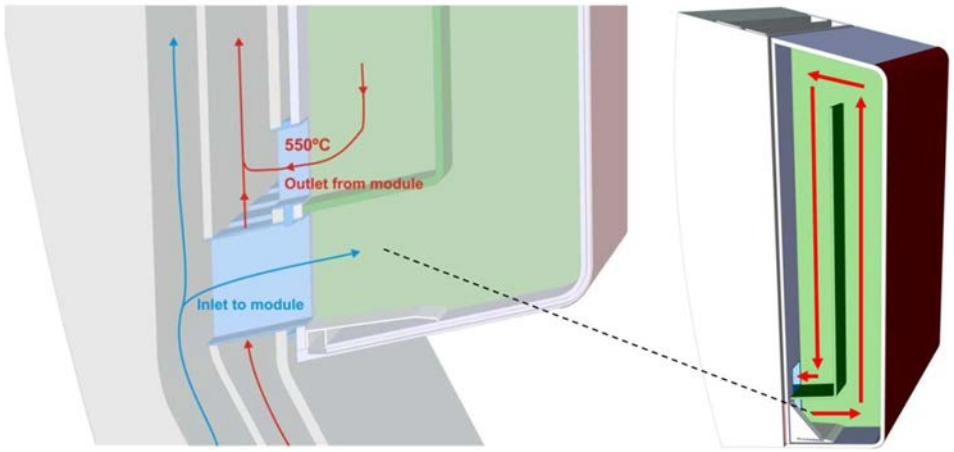

FIG. 3. Description of PbLi movement inside each of the modules of the BB [16].

3. METHODOLOGY

The CS makes use of the following computational packages: i) MCNP5 [7] code for the calculation of the neutron fluxes irradiating the PbLi inside the BB, ii) ACAB [8] activation code for the calculation of the inventory and related quantities generated in the PbLi, and iii) a set of scripts to manage the appropriate inputs to be delivered to and from ACAB, at any time of the simulation. The neutron transport libraries are JEFF-3.1.1 [9] and FENDL (3.0 and 2.1) [10] being the activation calculations performed using the EAF-2007 library [11].

We define t_{in} as the time per cycle when the PbLi is irradiated inside the BB, and t_{out} when the PbLi is not irradiated and it is flowing along the pipes and systems outside the BB, being the total time of a cycle $t_{in}+t_{out} = t_{cycle}$. For any of the cycles simulated, the nuclide inventory at the end of t_{in} calculated by ACAB is given as input to ACAB for the t_{out} period, being the inventory at the end of this "cooling" step the input for the next cycle. During the t_{out} of all the cycles, any nuclides can be extracted simulating the: i) extraction of tritium at the TES and ii) extraction of mass at the PS. Additionally, it is possible to continuously feed the PbLi alloy with the expected ACPs released from the systems both inside and outside the BB, in order to calculate the accumulation of the ACPs in the systems of the loops. It is worth noting that both t_{in} and t_{out} can be divided in any number of intervals to consider different neutron spectra inside the BB, and circulation times among systems outside the BB, respectively. The CS can provide any of the abovementioned quantities at any time; that is, related to any number of cycles. Additionally, for any selected cycle, it is possible to obtain the evolution of the quantities during the cycle as well as after machine shutdown, being the last relevant for maintenance and waste management purposes.

4. PROBLEM DESCRIPTION: FIRST APPLICATION OF THE CS

We have applied the CS in a simplified loop of the PbLi in the DCLL concept that considers some of the capabilities of the CS. This simplified loop takes into account the following: i) the 100% of the PbLi enter in the TES (where some tritium is extracted), and ii) after leaving the TES the PbLi enters into the blanket. This scheme is repeated for all the simulated cycles. A number of 265 cycles per day which means a total value of 326 seconds per loop is chosen based on the last available design of the DCLL loops. For this value, that is $t_{cycle} = 326$ seconds, we define the "fraction of residence time" as $t_{in}/(t_{in}+t_{out})$. The values of the fraction of residence time under consideration in this study are: 0.85, 0.75 and 0.50. With regard to the efficiency of the TES, values of 0.6 and 0.8 are analysed (that is, removal of 60 % and 80 % of the tritium in each cycle, respectively) based on the expected performance of this system.

The expected pulsed scheme for irradiation in DEMO (9 pulses of 2 hours each one per day), is considered [12]. This effect is taking into account using a "pulse factor" of (9X2 hours)/(24 hours) = 0.75, which will also multiply the t_{in}, providing the total time of irradiation "t_{irrad}" per cycle. Despite of the longer lifetime of functioning, we will use a maximum time of 1 month as a first reasonable time for the analysis of the realistic irradiation scenario. For the irradiation of the PbLi in the BB, we will use the average neutron flux at the PbLi position for the equatorial OB module (#13 of the Figure 1). This spectrum has the higher intensity compared to the remainder modules, being the spectra for all of them very similar. Despite of using here only one neutron spectrum, the CS is able to handle several neutron spectra taking into account the different properties of the neutron fluxes inside the BB.

We focus on the consequences of considering a realistic irradiation scheme instead of a continuous irradiation profile. This comparison also considers different values for two relevant variables currently not fixed in the design and are expected to have an important impact in the activation of the PbLi: i) the residence time of the PbLi in the BB, and ii) the efficiency of the TES. The remainder features of the loops, as ACP quantification, mass extraction at the PS and extended irradiation times will be considered in a future work.

5. RESULTS

Table 1 shows the variables and quantities under analysis. Using the t_{cycle} equal to 326 seconds, the residence time of 85% means a time of irradiation "t_{irrad}" of 326 X 0.85 X 0.75 = 208 seconds, being 0.85 the percentage of residence time and 0.75 the abovementioned "pulse factor". For residence factors of 0.75 and 0.50 we obtain t_{irrad} values of 183 and 122 seconds respectively. The current conceptual design of the DCLL loop is close to a t_{irrad} = 0.75.

TABLE 1. DCLL PBLI PARAMETERS UNDER ANALYSIS

<table>
<tr><th>Time of functioning</th><th>Residence time (%) and t_{irrad}</th><th>TES efficiency (%)</th><th>Response functions</th></tr>
<tr><td>326 seconds (1 cycle)</td><td>100; continuous</td><td rowspan="2">60</td><td rowspan="4">Activity, Decay Heat, Contact Dose Rate, Tritium inventory</td></tr>
<tr><td>1 hour (11 cycles)</td><td>85; 208 seconds</td></tr>
<tr><td>1 day (265 cycles)</td><td>75; 183 seconds</td><td rowspan="2">80</td></tr>
<tr><td>1 month (7951 cycles)</td><td>50; 122 seconds</td></tr>
</table>

5.1. Activity and Decay Heat

Table 2 shows the specific Activity (Bq/cc) and Decay Heat (W/cc) calculated just after the last irradiation of the corresponding cycle. As example, the value of the specific Activity for 1 hour and t_{in} = 0.85 means the specific activity just after the exit of the cycle 11 (a total time of 1 hour), considering a cycle of 208 seconds inside the BB, and 118 (326 – 208) seconds outside the BB. As it can be seen, there are not significant differences when continuous irradiation is considered instead of realistic scheme. In addition, very similar values are found for the 3 residence times, being identical the values for TES 0.8 and 0.6.

TABLE 2. ACTIVITY AND DECAY HEAT AFTER IRRADIATION: COMPARISON WITH CONTINUOUS IRRADIATION SCHEME

	Specific Activity (Bq/cc)				Specific Decay Heat (W/cc)			
	continuous	**t_{in} = 0.85**	**t_{in} = 0.75**	**t_{in} = 0.50**	**continuous**	**t_{in} = 0.85**	**t_{in} = 0.75**	**t_{in} = 0.50**
1 cycle	$1.663 \cdot 10^{11}$	$1.657 \cdot 10^{11}$	$1.657 \cdot 10^{11}$	$1.655 \cdot 10^{11}$	$4.278 \cdot 10^{-2}$	$4.274 \cdot 10^{-2}$	$4.273 \cdot 10^{-2}$	$4.270 \cdot 10^{-2}$
1 hour	$1.677 \cdot 10^{11}$	$1.669 \cdot 10^{11}$	$1.667 \cdot 10^{11}$	$1.662 \cdot 10^{11}$	$4.299 \cdot 10^{-2}$	$4.289 \cdot 10^{-2}$	$4.286 \cdot 10^{-2}$	$4.279 \cdot 10^{-2}$
1 day	$1.757 \cdot 10^{11}$	$1.716 \cdot 10^{11}$	$1.708 \cdot 10^{11}$	$1.690 \cdot 10^{11}$	$4.356 \cdot 10^{-2}$	$4.325 \cdot 10^{-2}$	$4.318 \cdot 10^{-2}$	$4.301 \cdot 10^{-2}$
1 month	$2.046 \cdot 10^{11}$	$1.756 \cdot 10^{11}$	$1.744 \cdot 10^{11}$	$1.713 \cdot 10^{11}$	$4.398 \cdot 10^{-2}$	$4.351 \cdot 10^{-2}$	$4.341 \cdot 10^{-2}$	$4.315 \cdot 10^{-2}$

Figure 4 shows the evolution, after the shutdown of the reactor, of specific Activity and Decay Heat after different irradiation schemes considering t_{in} = 0.75 and TES = 0.8. From the results, we conclude that there is a difference, for any of the times considered, between the continuous and real-cycles case, which makes widen for longer cooling times due to the responsible radionuclides. This fact reinforces the significance of consider a realistic irradiation profile instead of continuous irradiation.

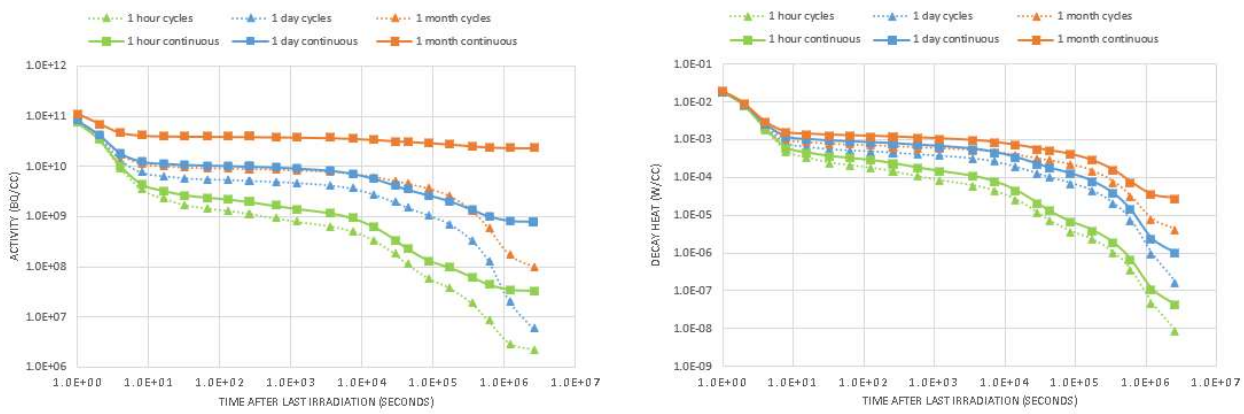

FIG. 4. Activity (left) and Decay Heat (right) evolution after shutdown (tin = 0.75; TES = 0.8).

5.2. Contact Dose Rate

It is now investigated the effect of the previous accumulated irradiation over the CDR evolution after the shutdown of the reactor. This analysis is very relevant in order to evaluate waiting times for a safe manual maintenance of systems and components. Figure 5 shows the evolution after shutdown of the CDR for different irradiation scenarios.

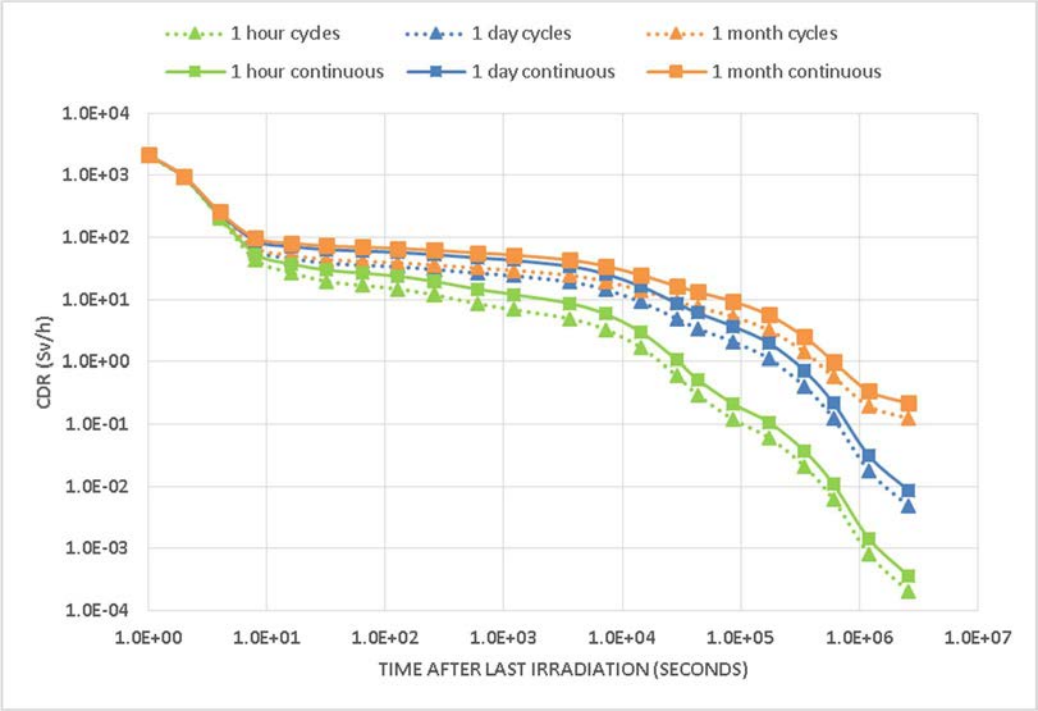

FIG. 5. CDR evolution after shutdown for different irradiation schemes (tin = 0.75; TES = 0.8).

As can be seen, for longer irradiation times, the CDR undergoes a lower decreasing when cooling time increases, due to the higher half-life of the responsible radionuclides, being very similar the results using continuous irradiation compared to the real irradiation scheme for the three cases analysed. CDR values at shutdown are very similar for the analysed scenarios, being identical the values for TES 0.8 and 0.6, since tritium does not contribute to the CDR.

5.3. Tritium inventory

The amount of tritium produced and carried by the alloy along the systems and pipes of the PbLi loop is a key value related to the performance of the reactor and the TES, and for safety purposes. Figure 6 shows the amount of tritium in the alloy, after the end of the analysed cycle and after exit of the TES. Because of the half-life of the tritium (12.3 years) compared to the maximum functioning time considered (1 month), the three cases without extraction can be also considered as the total tritium production, being, as expected, linear with the irradiation time. It is worth noting that, for the cases considering the TES, a “saturation” of the tritium content in the alloy is observed after 1 hour of functioning, which is a significant conclusion also for the quantity of tritium to be extracted at the PS.

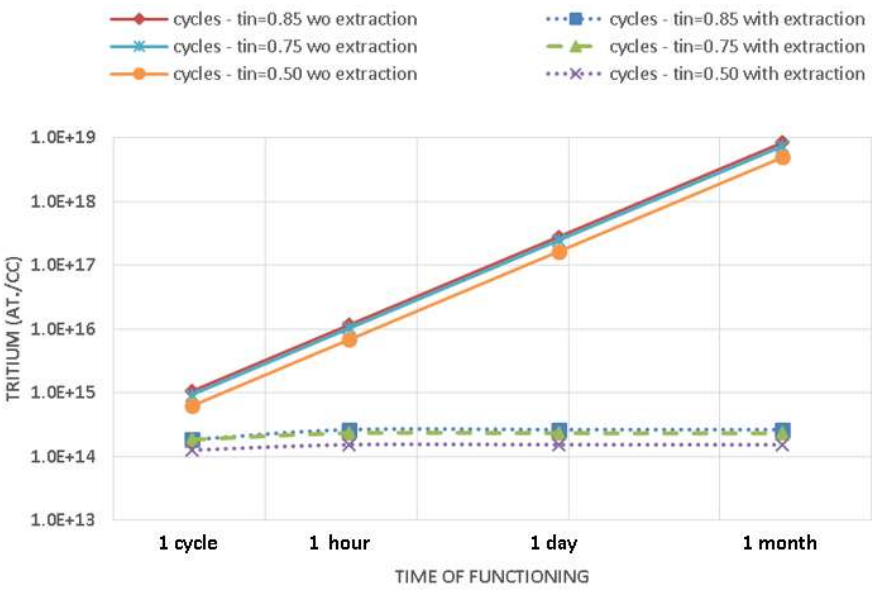

FIG. 6. Tritium concentration in the alloy (TES = 0.8): comparison with and without tritium extraction.

6. CONCLUSIONS

A CS capable of predicting the PbLi activation in the loops of the DCLL DEMO fusion reactor is presented. The significance of this CS lies in the fact that it is currently able to consider all the features of the loops relevant for activation related quantities, as the different spectra irradiating the alloy inside the BB, realistic residence times, material extractions and purifications, and ACPs accumulation.

We perform an application of the CS to a simplified DCLL loop, focusing on the effect of considering a realistic instead of a continuous irradiation scheme, and for relevant quantities related to safety, maintenance and waste management. In this sense, we have observed that in some cases (mainly for activity), it is very important to consider the realistic residence time of the loops instead a continuous irradiation profile, which reinforces the relevance of the CS presented in this work. This analysis has been done for a maximum functioning time of the system of 1 month, equivalent to 7951 cycles, which is shorter than the expected lifetime of the alloy but is significant in order to obtain some preliminary conclusions about the importance of considering real residence times and continuous extractions of the PbLi along the cycles. In a future work, we will apply the CS over a more realistic irradiation spectrum inside the BB, longer times of functioning closer to the expected lifetime of the systems, the accumulation of ACPs, and the performance of the PS.

ACKNOWLEDGEMENTS

The views and opinions expressed herein do not necessarily reflect those of the European Commission. This work has been performed within the framework of the Safety and Environment Project (WPSAE) implemented under the EUROfusion Consortium. It has been also partially supported by the Spanish MINECO (Ministerio de Economía y Competitividad) under Programa Estatal I+D+I-Retos, Proyecto ENE2015-70733-R, and the Programa de Actividades I+D de la Comunidad de Madrid under TECHNOFUSION(II)-CM, S2013/MAE-2745 Project.

REFERENCES

[1] BOCCACCINI, L.V., et al., Objectives and status of EUROfusion DEMO blanket studies. Fusion Engineering and Design **109–111** (2016) 1199–1206.
[2] UTILI, M., et al., Preliminary design of DCLL LiPb loops. EFDA_D_2ML9BZ v1.1. Internal EFDA Report (2016).
[3] HENDERSON, D., EL-GUEBALY, L., WILSON, P., ABDOU, A., Activation, Decay Heat, and Waste Disposal Analysis for ARIES-AT Power Plant, Fusion Technology **39** (2001).
[4] PETTI, D., MERRILL, B., MOORE, R., LONGHURST, G., EL-GUEBALY, L., MOGAHED, E., HENDERSON, D., WILSON, P., ABDOU, A., Safety and Environment Assessment of ARIES-AT, Fusion Technology **39** (2001).

[5] PALERMO, I., et al. Optimization process for the design of the DCLL blanket for the European DEMOnstration fusion reactor according to its nuclear performances, Nuclear Fusion **57** (2017) 076011.
[6] REUNGOAT, M., et al., Preliminary 3D CAD modelling of DCLL PbLi loop. EFDA_D_2MW4UA v1.1. Internal EFDA Report (2016).
[7] X-5 MONTE CARLO TEAM, MCNPTM, A General Monte Carlo N-Particle Transport Code. Version 5. Tech. Rep. LA-CP-03-0245, Los Alamos National Laboratory, MCNP 5 (2005).
[8] SANZ, J., CABELLOS, O., GARCÍA-HERRANZ, N., 'ACAB 2008: Activation Code V2008', Nuclear Energy Agency NEA Data Bank, NEA-1839 (2008).
[9] The JEFF-3.1.1 OECD (2009) NEA Nº 6807.
[10] LOPEZ ALDAMA, D., TRKOV, A., INDC (NDS)-467 (2004).
[11] FORREST, R.A., The European Activation File: EAF-2007 neutron-induced cross section library (2007).
[12] RAPISARDA, D., FERNÁNDEZ, I., PALERMO, I., Update of the DCLL System Requirements and Interface, EFDA_D_2MWDHS v1.1. Internal EFDA Report (2017).
[13] FERNANDEZ-BERCERUELO, I., "CAD related aspects", 3rd Monitoring Meeting DCLL BB, PbLi Technologies, EUROfusion, CIEMAT, Spain (2017).
[14] RAPISARDA, D., "The DCLL design", 3rd Monitoring Meeting DCLL BB, PbLi Technologies, EUROfusion, CIEMAT, Spain (2017).
[15] UTILI, M., et al., "Breeding Blanket Project", DCLL BB meeting, PbLi Technologies, EUROfusion, CIEMAT, Spain (2017).

4. SUMMARY OF COOLANT CONFINING STRUCTURES

Y. Dai (Paul Scherrer Institut, Switzerland)

In this section, the main issues tackled are related to materials performance in fast neutron irradiation environments, which include the internal damage induced by irradiation inside structural materials such as displacement damage, transmutation products, particularly helium and hydrogen, and external damage induced by coolants, e.g. the irradiation assisted stress corrosion cracking (IASCC). Several experts from different countries provided a brief overview on the following aspects.

— Radiation damage produced by neutrons has been a hot topic for nuclear materials since many years in the past. In this TECDOC it is just briefly reviewed by using the results of studies on ferritic/martensitic (FM) steels irradiated with fission neutrons to high dpa levels (>50 dpa).
— Helium and hydrogen induced embrittlement effects are very important for materials in fusion and accelerator/spallation applications, also in fission case where e.g. stainless steels are used. In the accelerator/spallation case, a large amount data has been obtained in the SINQ Target Irradiation Program (STIP), while for the fusion materials the challenges still exist, although great efforts have been devoted by the community for more than half century, due to the lack of 14 MeV neutron sources.
— The compatibility of materials with various coolants is a rather complicated issue. In this section, materials/coolant interactions and materials property changes by the interaction, are briefly reviewed, with emphasis of the applications where liquid Li, Pb, and Pb eutectics ($Pb_{83}Li_{17}$ and $Pb_{45}Bi_{55}$) used as coolants.

These issues have been in the core of many international nuclear materials R&D programs. They will remain as the main topics in the future, because a good basic understanding or even some necessary data are still missing. The difficulties are still the same as before:

— Lack of irradiation sources,
— Lack of proper techniques for in-situ irradiation experiments,
— Post-irradiation examination of radioactive materials, and
— High costs and time consumption related to these experiments.

Ion irradiation experiments and computer simulations are largely applied nowadays, but, with many limitations (e.g. surface effects, damage rate effects, etc.). For the fusion materials, facilities like IFMIF-DONES are certainly necessary for understanding the synergistic effects of displacement damage, H and He and achieving necessary database for lifetime assessment of fusion reactors.

It needs to be mentioned that, to increase the strength of materials, especially the creep resistance at high temperatures, various materials with nano-sized oxide particle dispersion strengthening (ODS) have been developed and studied. The manufacture, welding, mechanical testing, irradiation, testing rules, and corrosion experiments, as well as computer simulation studies of ODS FM steels have been carried out in Japan, China, USA and Europe. Some irradiation experiments demonstrate a better radiation damage resistance of ODS materials. However, the neutron irradiation data are still rare and the effects of the texture grain structure, welding etc. need to be well investigated. Therefore, in this TECDOC the ODS materials are not in focus.

NEUTRON IRRADIATION AND HELIUM EFFECTS IN RAFM STEELS

E. GAGANIDZE, C. DETHLOFF, J. AKTAA
Karlsruhe Institute of Technology, Institute for Applied Materials,
Eggenstein-Leopoldshafen, Germany

Abstract

The influence of the irradiation temperature and damage dose on the microstructure and mechanical properties of EUROFER97 and other RAFM steels have been extensively studied at KIT and by other European laboratories in the frameworks of neutron irradiation campaigns. We give the assessment of the degradation of the mechanical properties of RAFM steels under different irradiation conditions up to damage doses of 70 dpa. The role of the irradiation temperature on the embrittlement of RAFM steels will be addressed. The influence of the helium effects on the mechanical properties will be discussed in addition on the base of in-house and international experiments imitating helium production by applying boron doping technique under fission reactor irradiations or by utilizing spallation proton irradiation. The recommendations on the operating temperature range for the FW and BB components will be given on the base of the analysis of the displacement damage and helium effects.

1. INTRODUCTION

The 8-9%Cr Reduced Activation Ferritic/Martensitic (RAFM) steels are primary candidate structural materials for the First Wall (FW) and Breeding Blanket (BB) components of future energy generating Fusion Reactors (FR) [1]. The RAFM steel class is developed in the course of the systematic optimization of conventional 8-12% Cr-MoVNb ferritic/martensitic steels by exchanging the radiologically undesirable elements Mo, Nb and Ni with radiologically favourable elements W, Ta, Ti in order to achieve low activation [2]. Its European representative is EUROFER97 with a nominal composition of Fe-8.91Cr-1.08W-0.48Mn-0.20V-0.14Ta-0.006Ti-0.12C. The in-vessel components of FR will be exposed to high neutron and thermo-mechanical loads. Although the advanced RAFM steels exhibit clearly better neutron irradiation resistance than the commercial martensitic alloys, the performance of these materials under neutron irradiation suffers due to the degradation of the microstructure as a consequence of evolution of displacement damage and due to generation of gaseous transmutation products e.g. helium, see Refs [3,4] and references therein.

2. NEUTRON IRRADIATION EFFECTS

The mechanical properties of EUROFER97 and other advanced RAFM steels have been thoroughly investigated in several irradiation programmes [5–12]. The irradiation temperature plays a crucial role on the mechanical properties of RAFM steels, see Fig. 1. The low temperature neutron irradiation at temperature Tirr ≤340°C up to 16.3 dpa leads to a strong increase of the ductile-to-brittle-transition-temperature (DBTT) [7,13,14], whereas the irradiation at or above 350°C results only in a slight degradation of the DBTT [7,13]. Similar to the behaviour of the impact properties, the investigation of the tensile properties after neutron irradiations in HFR, Petten [8] and BOR-60, Dimitrovgrad [14] revealed strong material hardening at low irradiation temperatures (Tirr ≤ 340°C). The irradiation hardening was considerably reduced at Tirr = 350°C and is nearly negligible at irradiation temperatures of 400–450°C [8]. Such a strong suppression of embrittlement and hardening indicates substantial recovery of the displacement damage at elevated temperatures.

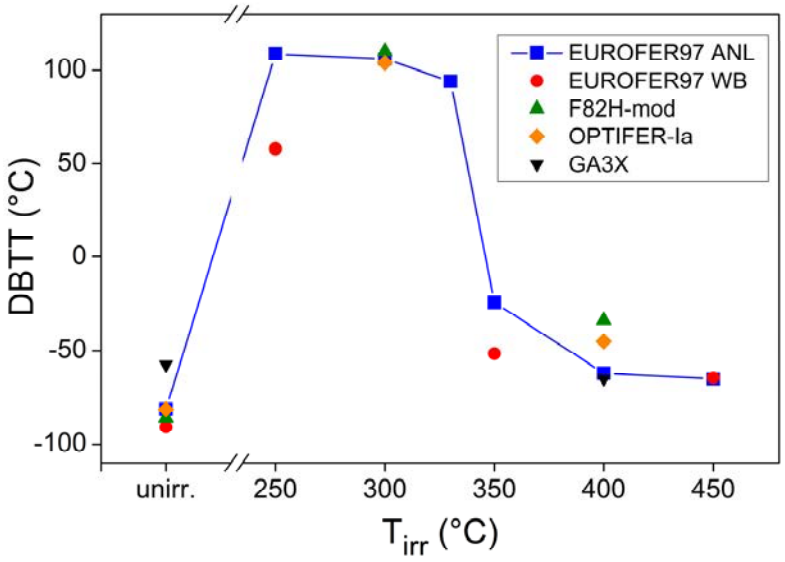

FIG. 1. DBTT vs. irradiation temperature for selected RAFM steels after irradiation in HFR, Petten to a volume average damage dose 16.3 dpa. For comparison, the results obtained in the unirradiated conditions are also included. The data point at Tirr = 330°C is obtained after irradiation in BOR-60 reactor to 15 dpa. The figure is reproduced from [3].

Irradiation induced low temperature hardening is accompanied by a strong reduction of the strain hardening capability closely correlated with nearly vanishing uniform elongation [3,8]. Suitable adaptation of the design rules is thus mandatory in order to make use of the substantial amount of the total elongation retained after low temperature irradiation up to 70–80 dpa, see Ref. [3] and references therein.

Fig. 2 shows the evolution of the neutron irradiation induced embrittlement (measured in impact tests) with dose for EUROFER97 and other RAFM steels at irradiation temperatures 300–337°C. A steep increase of the DBTT with damage dose is observed below about 15 dpa, see [3] and references therein. With further increasing the dose the embrittlement rate is decreased and clear tendency towards saturation is observed at the achieved damage doses of 70–80 dpa, see Ref. [3]. A qualitatively similar evolution with irradiation dose was found for the irradiation induced low temperature hardening characterized by significant reduction of the hardening rate and tendency towards saturation at the achieved damage doses of 70–80 dpa [3, 15].

The investigation of the radiation defect microstructure after neutron irradiation at low irradiation temperatures (300°C ≤ Tirr ≤ 340°C) up to 32 dpa identified the dislocation loops and black dots (interstitial defect clusters) as the dominant hardening sources for EUROFER97 [16], [17]. Furthermore, the study of the dislocation loops in EUROFER97 after irradiation to 16.3 dpa at multiple temperatures 250–450°C showed remarkable reduction of dislocation loop density at irradiation temperatures of 350°C and above [18]. These observations are in a good qualitative agreement with the temperature dependence of the irradiation induced embrittlement and hardening. Due to the close correlation between embrittlement and hardening, the low temperature embrittlement is frequently referred to as hardening dominated embrittlement in contrast to the non-hardening embrittlement measured in specimens with helium contents approx. above 50 appm [19–21].

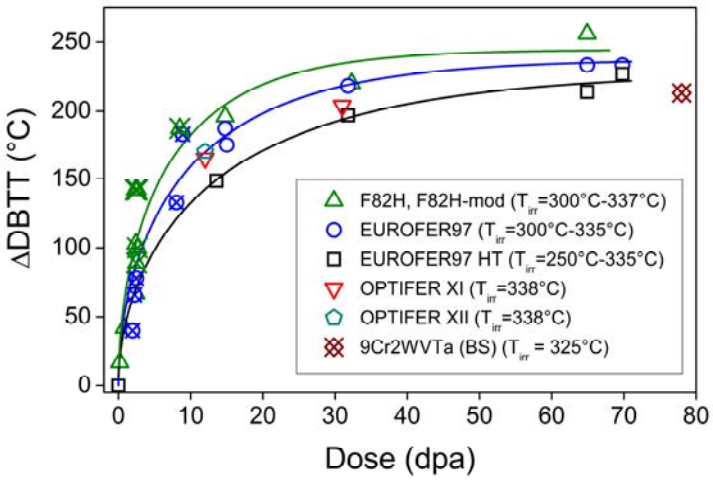

FIG. 2. Irradiation shifts in the DBTT as a function of dose for EUROFER97 and other RAFM steels. The figure is reproduced from [3].

The post-irradiation heat treatment at 550°C for 3h was found to lead to strong recovery of the impact and tensile properties of EUROFER97 and F82H steels after irradiation to 65-70 dpa at 335°C, indicating recovery of the displacement damage to a large extent [15].

3. HELIUM EFFECTS

Gaseous transmutation products such as helium and hydrogen produced under neutron irradiation are believed to further degrade the performance of the RAFM steels. Due to the absence of material irradiation facilities with fusion reactor relevant neutron spectrum the helium effects are frequently studied by different simulation techniques including but not limited to boron doping technique [7, 9, 21–25] and spallation target irradiation [26, 27].

At KIT boron doped EUROFER97 based model steels were developed with different contents of natural boron and separated ^{10}B-isotope [28]. Irradiations in HFR, Petten [7, 22–24] and BOR-60 [9, 11, 21] were performed in order to study the influence of the generated helium on the microstructure and mechanical properties of RAFM steels. It is the 10B isotope which transmutes under absorption of the thermal neutron to produce lithium and helium. Due to variations in the boron content from 10 wppm of natural boron up to 1120 wppm ^{10}B-isotope helium contents between 10 and 5580 appm have been realized. The study revealed however strong degradation of the microstructure of the model steel with 1120 wppm boron, characterized by a presence of high density of coarse (up to few µm large) Fe, Cr and B rich precipitates [28]. The boron distribution in 83 wppm ^{10}B doped model alloy was found to be predominantly homogeneous [3]. Due to these reasons, only generated helium contents up to about 430 appm He were considered for the assessment of the helium effects on the mechanical properties. The DBTT measured in the impact tests was found to be very sensitive to the produced helium contents [15, 21], whereas only minor influence of helium on the tensile properties was observed in [24].

The helium effects on the DBTT were found to strongly depend on the irradiation temperature [23], see Fig. 3. A large additional embrittlement measured in boron doped model steels in comparison with baseline EUROFER97 is attributed to helium. It has to be emphasized that helium effects are substantially reduced at elevated irradiation temperatures for the same produced helium contents (both for ADS2 and ADS3). This behaviour is attributed by the authors to rather different evolution of the helium microstructure at different irradiation temperatures in a given model steel. Indeed, the low temperature neutron irradiation was shown in [15, 22] to lead to homogeneous nucleation of the helium bubbles in the steel matrix with some minor fraction nucleated at the grain boundaries. On the other hand, bubble nucleation was found to be predominantly heterogeneous with majority of the bubbles nucleated at line dislocations after irradiation at 450°C, see [22]. At Tirr ≤350°C and up to 420 appm He, the helium embrittlement rate between 0.5 and 0.6°C/appm He was estimated from the boron doping experiment [3]. This embrittlement rate is slightly higher than the embrittlement rate of 0.4°C/appm He obtained in [25] at Tirr = 250°C up to 300 appm He by applying boron doping technique. At Tirr = 450°C the helium embrittlement rate of about 0.25°C/appm He is estimated up to 420 appm He in [3]. Fig. 4 shows the dose evolution of the helium embrittlement at low irradiation temperatures (250–350°C) obtained by the analysis of the DBTT of boron doped

steels after irradiation in HFR, Petten and BOR-60 reactors [15]. A progressive embrittlement with produced helium amount is observed up to 430 appm He.

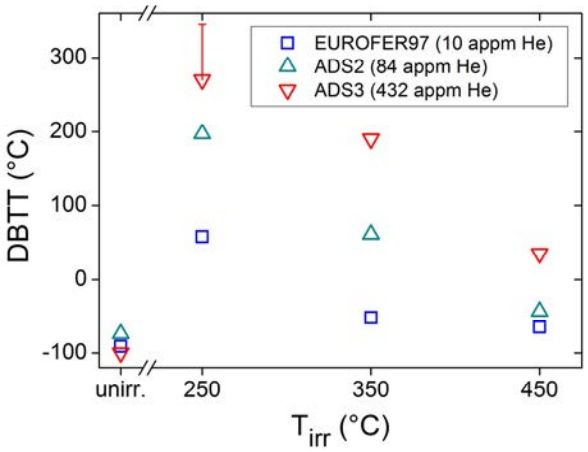

FIG. 3. DBTT vs. irradiation temperature for boron-doped and base EUROFER97 steels after irradiation in HFR reactor to about 16.3 dpa from [23]. For comparison the results in the unirradiated conditions are also included.

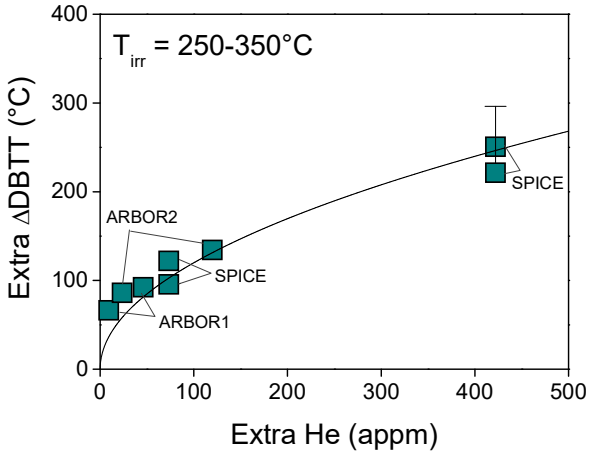

FIG. 4. Helium induced extra embrittlement vs. extra helium amount for irradiated boron doped steels at irradiation temperatures between 250 and 350°C [15]. The line is a model description of the data [15]. Figure 3b is reproduced from [15].

The main limitation of the boron doping technique is the metallurgical effects of the alloying element boron which limits the application of this technique to the boron content below 100 wppm. Furthermore, dedicated control of the thermal neutrons will be required in order to control helium to dpa ratio which was not kept constant in the above boron doping experiments. The effect of transmutation by-product lithium cannot be clearly assessed in this type of experiments either. Due to above limitations an overestimation of the helium effects is expected.

Spallation neutron and proton irradiation is another technique frequently used for the study of helium effects in EUROFER97 and other RAFM steels [26, 27]. Besides, this simulation technique implying irradiation of the sample with spallation neutrons and protons has some limitations. Particularly, very high helium to dpa ratio of about 70 appm/dpa and variation of irradiation temperature due to periodic variation of intensity of the proton beam have to be emphasized.

At irradiation temperatures below 380°C the DBTT shift of EUROFER97 due to synergy of helium and dpa effects under spallation target irradiation was shown to linearly increase with helium concentration up to 1600 appm [26, 27]. The embrittlement due to 18 dpa and 1400 appm helium was about 600°C. After accounting for the displacement damage induced low temperature embrittlement due to 18 dpa from Fig. 2, the helium embrittlement

under spallation target irradiation was estimated to be about 410°C for 1400 appm [3], which corresponds to the helium embrittlement rate of 0.3°C/appm He at Tirr ≤3 80°C. The helium induced embrittlement rate of only 0.13–0.15°C/appm He was estimated, however, for 600 appm He at Tirr ≤ 380°C.

4. DESIGN LIMITS DUE TO DPA AND HELIUM EFFECTS

The impact of the dpa and helium effects on the design briefly summarized below was assessed by the authors in [3]. The low temperature (Tirr ≤ 335°C) neutron irradiation induced strong hardening and correlated embrittlement imposes a low application temperature limit for EUROFER97 [7, 8, 13]. Only minor embrittlement and hardening observed at irradiation temperatures of 350°C and above indicates considerable healing of the displacement damage in EUROFER97 [7, 8, 13]. Therefore, EUROFER97 is highly suited for fusion reactor design with the operating temperature range 350–550°C for the FW and BB structures [3]. The helium effects will further limit the application of EUROFER97. By assessment of helium embrittlement between 0.15 and 0.25°C/appm He on the base of helium simulation experiments, and by considering fusion relevant helium to dpa ratio of 10 appm He/dpa, helium effects were estimated to be tolerable up to a damage dose of at least 40 dpa [3]. Summarizing the above assessment, the application temperature range and dpa and He limits for EUROFER97 are proposed between 350 and 550°C, 40 dpa, and 400 appm He, respectively [3].

At low irradiation temperatures (Tirr < 350°C) it is the dpa damage which mainly limits the mechanical performance of RAFM steels. The displacement damage effects can be largely recovered through application of post irradiation annealing. The helium effects, however, cannot be recovered as shown in [11]. By utilizing post irradiation annealing for the recovery of dpa effects at low irradiation temperatures in FW and BB structures and for fusion reactor relevant helium to dpa ratio of 10 appm He/dpa, the helium effects were assessed to be tolerable up to a damage dose of at least 40 dpa on the basis of spallation proton irradiation experiments [3].

5. SUMMARY

Displacement damage and helium effects expected under fusion irradiation conditions are assessed on the base of neutron irradiation experiments on EUROFER97 and other RAFM steels. Helium effects are estimated on the base of simulation techniques including boron doping experiments and spallation target irradiations. Application temperature range and dpa and helium limits are proposed for the FW and BB components to be made of EUROFER97 steel.

Availability of the irradiation facilities with fusion reactor relevant neutron spectrum, e.g. IFMIF, is mandatory for detailed investigation of synergetic effects of displacement damage and transmutation products. The effect of helium accelerated swelling excluded from the above assessment due to absence of reliable experimental data needs to be in addition studied under relevant helium and dpa production rates.

REFERENCES

[1] LINDAU, R., SCHIRRA, M., First results on the characterisation of the reduced-activation-ferritic-martensitic steel EUROFER, Fus. Eng. Des. **58–59** (2001) 781–785.

[2] MOESLANG, A., DIEGELE, E., KLIMIANKOU, M., LAESSER, R., LINDAU, R., et al., Towards reduced activation structural materials data for fusion DEMO reactors. Nuclear Fusion **45** (2005) 649–655.

[3] GAGANIDZE, E., AKTAA, J., Assessment of neutron irradiation effects on RAFM steels. Fusion Engineering and Design, Fus. Eng. Des. **45** (2013) 118–128.

[4] TANIGAWA, H., GAGANIDZE, E., HIROSE, T., ANDO, M., ZINKLE, S.J., et al., Development of benchmark reduced activation ferritic/martensitic steels for fusion energy applications. Nucl. Fusion **57** (2017) 92004.

[5] LUCON, E., CHAOUADI, R., DECRÉTON, M., Mechanical properties of the European reference RAFM steel (EUROFER97) before and after irradiation at 300 °C, J. Nucl. Mater. **329– 333** (2004) 1078–1082.

[6] RENSMAN, J., NRG irradiation testing: Report on 300°C and 60°C irradiated RAFM. EFDA TW2-TTMS-001a D6 and TW2-TTMS-001b D12, Nuclear Research and consultancy Group (NRG), 2005.

[7] GAGANIDZE, E., DAFFERNER, B., RIES, H., ROLLI, R., SCHNEIDER, H.-C., et al., Irradiation Programme HFR Phase IIb (SPICE), Impact testing on up to 16.3 dpa irradiated RAFM steels, Forschungszentrum Karlsruhe, 2008.

[8] MATERNA-MORRIS, E., MÖSLANG, A., SCHNEIDER, H.-C., Tensile and low cycle fatigue properties of EUROFER97-steel after 16.3 dpa neutron irradiation at 523, 623 and 723 K, J. Nucl. Mater. **442** (2013) 62–66.

[9] PETERSEN, C., Post irradiation examination of RAF/M steels after fast reactor irradiation up to 33 dpa and < 340°C (ARBOR 1), Karlsruher Institut für Technologie, 2010.
[10] ALAMO, A., BERTIN, J.L., SHAMARDIN, V.K., WIDENT, P., Mechanical properties of 9Cr martensitic steels and ODS-FeCr alloys after neutron irradiation at 325 °C up to 42 dpa, J. Nucl. Mater. **367– 370** (2007) 54–59.
[11] GAGANIDZE, E., PETERSEN, C., Post irradiation examination of RAFM steels after fast reactor irradiation up to 71 dpa and <340 °C (ARBOR 2), Karlsruhe Institute of Technology, KIT Scientific Report 7596, 2011.
[12] HENRY, J., AVERTY, X., ALAMO, A., Tensile and impact properties of 9Cr tempered martensitic steels and ODS-FeCr alloys irradiated in a fast reactor at 325 °C up to 78 dpa, J. Nucl. Mater. **417** (2011) 99–103.
[13] GAGANIDZE, E., SCHNEIDER, H.-C., DAFFERNER, B., AKTAA, J., High-dose neutron irradiation embrittlement of RAFM steels, J. Nucl. Mater. **355** (2006) 83–88.
[14] PETERSEN, C., AKTAA, J., DIEGELE, E., GAGANIDZE, E., LÄSSER, R., et al., Mechanical Properties of Reduced Activation Ferritic/Martensitic Steels after European Reactor Irradiations, Poc. of 21st IAEA Fusion Energy Conference, Chengdu, China, 2006.
[15] GAGANIDZE, E., PETERSEN, C., MATERNA-MORRIS, E., DETHLOFF, C., WEIß, O. J., et al., Mechanical properties and TEM examination of RAFM steels irradiated up to 70 dpa in BOR 60, J. Nucl. Mater. **417** (2011) 93–98.
[16] WEISS, O.J., GAGANIDZE, E., AKTAA, J., Quantitative characterization of microstructural defects in up to 32 dpa neutron irradiated EUROFER97, J. Nucl. Mater. **426** (2012) 52–58.
[17] DETHLOFF, C., GAGANIDZE, E., AKTAA, J., Review and critical assessment of dislocation loop analyses on EUROFER 97, Nuclear Materials and Energy **15** (2018) 23–26.
[18] KLIMENKOV, M., MATERNA-MORRIS, E., MÖSLANG, A., Characterization of radiation induced defects in ERUOFER97 after neutron irradiation, J. Nucl. Mater. **417** (2011) 124–126.
[19] RIETH, M., DAFFERNER, B., RÖHRIG, H.-D., Embrittlement behaviour of different international low activation alloys after neutron irradiation, J. Nucl. Mater. **258–263** (1998) 1147–1152.
[20] YAMAMOTO, T., ODETTE, G., KISHIMOTO, H., RENSMAN, J.-W., MIAO, P., On the effects of irradiation and helium on the yield stress changes and hardening and non-hardening embrittlement of ~8Cr tempered martensitic steels: Compilation and analysis of existing data, J. Nucl. Mater. **356** (2006) 27–49.
[21] GAGANIDZE, E., PETERSEN, C., AKTAA, J., Study of helium embrittlement in boron doped EUROFER97 steels, J. Nucl. Mater. **386–388** (2009) 349–352.
[22] MATERNA-MORRIS, E., MÖSLANG, A., SCHNEIDER, H.-C., ROLLI, R., Microstructure and tensile properties in reduced activation 8-9% Cr steels at fusion relevant He/dpa ratios, dpa rates and irradiation temperatures, Proc. of 22nd IAEA Fusion Energy Conference, Geneva, Switzerland, 2008.
[23] GAGANIDZE, E., AKTAA, J., The effects of helium on the embrittlement and hardening of boron doped EUROFER97 steels, Fus. Eng. Des. **83** (2008) 1498–1502.
[24] MATERNA-MORRIS, E., MOESLANG, A., ROLLI, R., SCHNEIDER, H.-C., Effect of helium on tensile properties and microstructure in 9%Cr-WVTa-steel after neutron irradiation up to 15 dpa between 250 and 450 °C, J. Nucl. Mater. **386–388** (2009) 422–425.
[25] WAKAI, E., OKUBO, N., ANDO, M., YAMAMOTO, T., TAKADA, F., Reduction method of DBTT shift due to irradiation for reduced-activation ferritic/martensitic steels, J. Nucl. Mater. 398 (2010) 64–67.
[26] DAI, Y., WAGNER, W., Materials researches at the Paul Scherrer Institute for developing high power spallation targets, J. Nucl. Mater. **389** (2009) 288–296.
[27] DAI, Y., HENRY, J., TONG, Z., AVERTY, X., MALAPLATE, J., LONG, B., Neutron/proton irradiation and He effects on the microstructure and mechanical properties of ferritic/martensitic steels T91 and EM10, J. Nucl. Mater. **415** (2011) 306–310.
[28] MATERNA-MORRIS, E., KLIMENKOV, M., MÖSLANG, A., The influence of boron on structural properties of martensitic 8-10%-steels, Materials Science Forum **730–732** (2013) 877–882.

HE AND H EFFECTS ON STRUCTURAL MATERIALS IN FUSION AND ACCELERATOR DRIVEN SYSTEMS

Y. DAI
Paul Scherrer Institut,
Villigen, Switzerland

Abstract

In the last two decades, various structural materials were irradiated in the targets of the Swiss spallation source (SINQ). Of the particular interest to develop high power spallation sources for both neutron science and ADS applications, austenitic steels, tempered martensitic steels, Ni- and Al-based alloys have been extensively investigated. Post-Irradiation Examinations (PIE) include mechanical testing using tensile, bend, impact, small punch testing techniques and microstructural analysis employing Transmission Electron Microscopy (TEM), Positron Annihilation Spectroscopy (PAS) and Atom Probe Tomography (ATP). The specimens used for PIE are with irradiation doses up to about 20 dpa and helium (He) concentrations up to about 1800 appm, in the temperature range of 60–500°C. The results of mechanical tests demonstrate pronounced embrittlement effect when the He concentration is above about 500 appm. Meanwhile, additional hardening effect is observed, which can be attributed to high-density He bubbles of 1-2 nm in diameter.

1. INTRODUCTION

"High power (~1 MW or higher) spallation targets have been developed for different attractive applications, such as in advanced spallation neutron sources for neutron scattering science and technology, or in Accelerator Driven Systems (ADS) for nuclear waste transmutation. In such targets, both target and structural materials are exposed to intensive irradiation of high energy protons and spallation neutrons. Since spallation reactions induced by high energy protons can produce He and H and other transmutation elements at very high rates, the behaviour of materials used in spallation targets is expected to be much different from that observed from materials irradiated in fission reactors. Therefore, the damage induced by spallation irradiation cannot be simply simulated by fission neutron irradiation experiments. To establish a necessary database for the R&D of high-power spallation targets, the SINQ Target Irradiation Program (STIP) has been run since 1998 with broad international collaboration" [1]. In the past 20 years, seven irradiation experiments were done, in which more than 8000 samples of various metals and ceramics were irradiated to doses up to 30 dpa (in iron) and 2400 appm He in the temperature range of 80–600°C.

He and H effects have been among the important materials issues for fusion reactors for several decades. In fusion reactors, the first wall blankets are exposed to irradiation of 14 MeV neutrons, which produces He and H at rates of about 11 appm He/dpa and 40 appm H/dpa, respectively. However, since there is no 14 MeV neutron source available for irradiation experiments, studies of He and H effects on fusion materials rely essentially on simulations using ion irradiations, which cannot obtain useful mechanical data of bulk materials. In this respect, the spallation irradiation may contribute to the understanding of He and H effects for fusion materials.

2. RETENTION OF H IN DIFFERENT MATERIALS IRRADIATED IN STIP

The behaviour of H in different materials can be very different. The retention and release of H in some materials irradiated in STIP were analysed by using the Thermal Desorption Spectroscopy (TDS) technique [2–4]. As an example, Fig. 1 presents the TDS analysis of gas release of a sample of Tempered Martensitic (TM) steel F82H and a sample of Zircaloy-2. The samples are discs of 3 mm in diameter and 0.25 mm in thickness. The F82H sample was irradiated at temperature around 400°C to 20.3 dpa. The calculated H content is 7650 appm. The Zircaloy-2 sample was irradiated at about 160°C to 25.8 dpa. The calculated H content is 4750 appm. In Figure 1 one can see two clear differences: i) the release peaks of H and its isotopes of F82H are much lower than that of the Zircaloy-2, although the calculated H content of the F82H sample is higher; ii) the H peak temperature of the F82H sample is lower. For the F82H sample, since H release starts at about 200°C, it is understandable that the H was largely released during irradiation at 400°C, while for the Zircaloy-2 sample it remained in the sample because of low irradiation temperature.

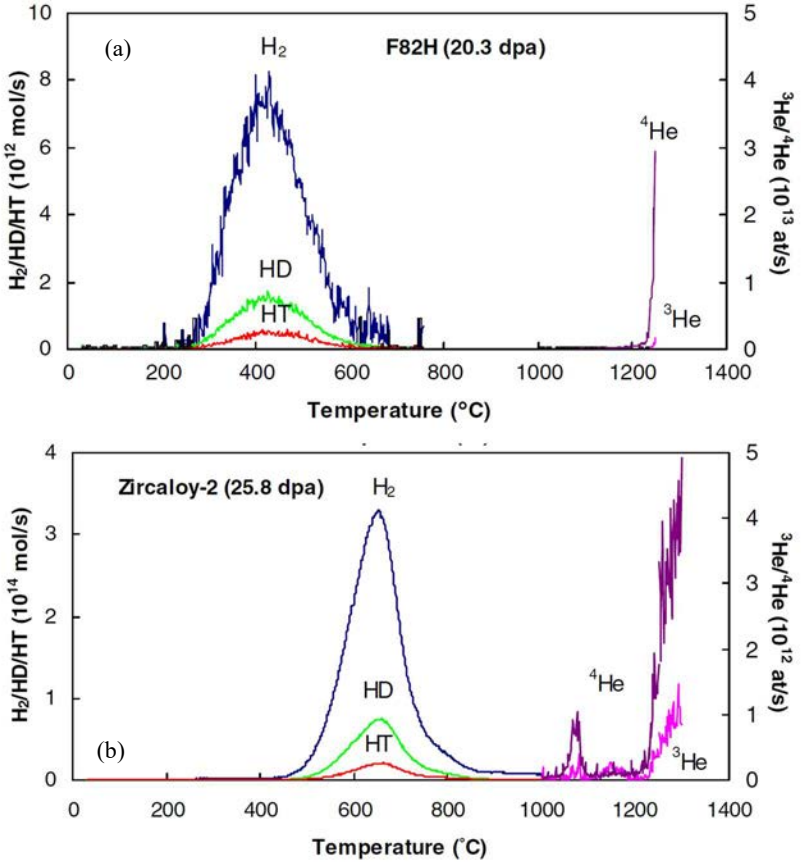

FIG. 1. (a) Gas release versus temperature for a F82H samples irradiated in STIP-II [3]; (b) SS316LN samples.

The gas concentration and release measurements were conducted on four alloys: SS316LN, F82H, Zircaloy-2 and AlMg3, and nine pure metals: Al, Ti, Fe, Ni, Cu, Nb, Ta, Au and Pb [3,4]. The results demonstrate that Ti, Nb and Ta behave similarly to Zircaloy-2, with high H retention. The H content measured from the samples of these materials is even much higher than the calculated values. This implies that the samples of these materials absorbed a large amount of H released from other samples irradiated in the rod. For the other materials the measured H content is lower than the calculated values. The ratio between the measured and the calculated values depends strongly on irradiation temperature. Figure 2 presents the ratio values derived from the results of SS316LN and F82H steels. The temperature dependence can be clearly seen.

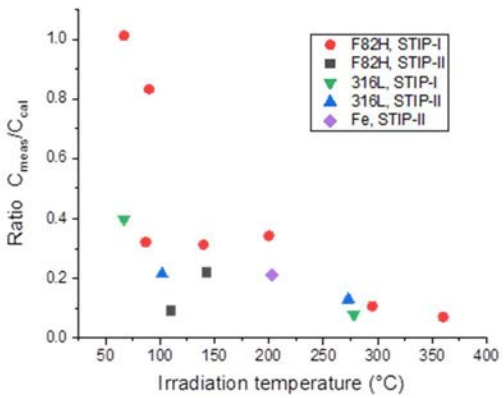

FIG. 2. The ratio between measured and calculated H contents in the F82H and SS316LN specimens irradiated in STIP-I and STIP-II

The H content of samples irradiated in STIP can only be known by TDS measurement. The calculated values are essentially not applicable. Therefore, in the publications of STIP results the H contents of the specimens are normally not given unless the evidence of H induced effects is significant. In the following sections it will demonstrate that H should not play an important role like He in the irradiation-induced changes of mechanical properties of the steels irradiated in STIP.

3. HE EFFECTS ON DIFFERENT MATERIALS IRRADIATED IN STIP

Due to the high production rate of He in any material used in accelerator/spallation systems, the irradiation-induced microstructural and mechanical changes exhibit significant differences from that of fission neutron irradiations, particularly when He concentration is above 500 appm. In this section, some examples will be given to demonstrate the differences.

3.1 He effects on irradiation-induced microstructural changes of TM steels

TM steels are promising candidate materials for various nuclear applications. They are the dominant materials in every STIP irradiation experiment. The major difference between the microstructure of TM steels after spallation and fission neutron irradiations is the formation of helium bubbles. In TM steels irradiated with fission neutrons at temperatures below 400°C, the nanometric defect clusters and dislocation loops are the main features. In the same TM steels after spallation irradiation, besides the nanometric defect clusters and dislocation loops, tiny bubbles are observed in samples irradiated to doses above 10 dpa/500 appm He at temperatures above 180°C [5,6]. Figure 3 is an example showing the bubble structure in a F82H sample irradiated to 9.8 dpa/550 appm He at 185°C. The size of visible bubbles is about 1 nm. Similar bubble structures have been also observed in austenitic steels, but at temperatures slightly higher than that of TM steels at the same irradiation dose [7].

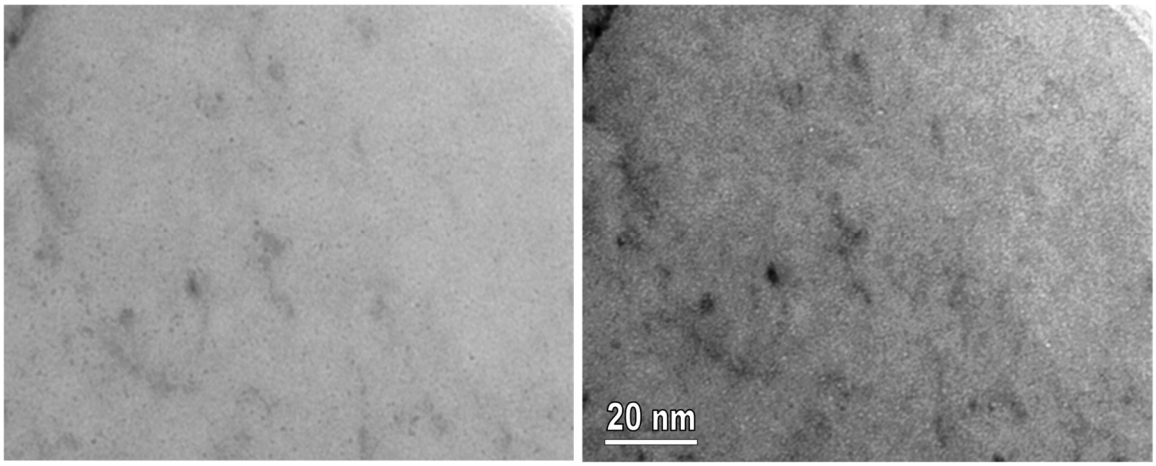

(a) (b)

FIG. 3. (a) Over-focused bright-field image of a F82H sample irradiated to 9.8 dpa, 550 appm at 185±20 C in STIP-II; (b) under-focused image.

3.2 He effects on mechanical properties of steels

Compared to He embrittlement effect observed at high temperatures above 600°C [8], He embrittlement effect on materials in the low temperature regime (<~400°C) is even more pronounced. He embrittlement effect has been detected in all materials irradiated in SINQ targets after mechanical testing. Figure 4 is a collection of tensile test results which shows the elongation versus irradiation dose for TM steel samples irradiated in SINQ targets at 350°C and below and tested at room temperature. At doses above about 15 dpa these samples exhibit brittle behaviour. The samples were either broken in the elastic regime or at a total elongation < 1–2%. The fracture mode was either cleavage or cleavage and intergranular mixed type [9,10]. At higher test temperatures up to the irradiation temperature of the samples, the ductility did not recover much. It needs to be noted that after neutron irradiation at the similar irradiation dose (>15 dpa) and temperature (~300°C), the same TM steels still exhibit > 5% total elongation in general [12,13].

Besides the embrittlement effect, He may introduce additional hardening due to the formation of high-density small (1–3nm) bubbles. The hardening effect manifests at > 400°C, where little or no hardening effect observed in TM steels after neutron irradiation [14], or > ~10 dpa, where the hardening of neutron irradiated TM steels saturates [10].

As shown in Fig. 2, the H content of high dose samples irradiated at > ~250°C is low. However, these samples manifest strong embrittlement and hardening effects. This implies that H needs to not play an important role like He in the synergistic effects observed in steels irradiated at elevated temperatures.

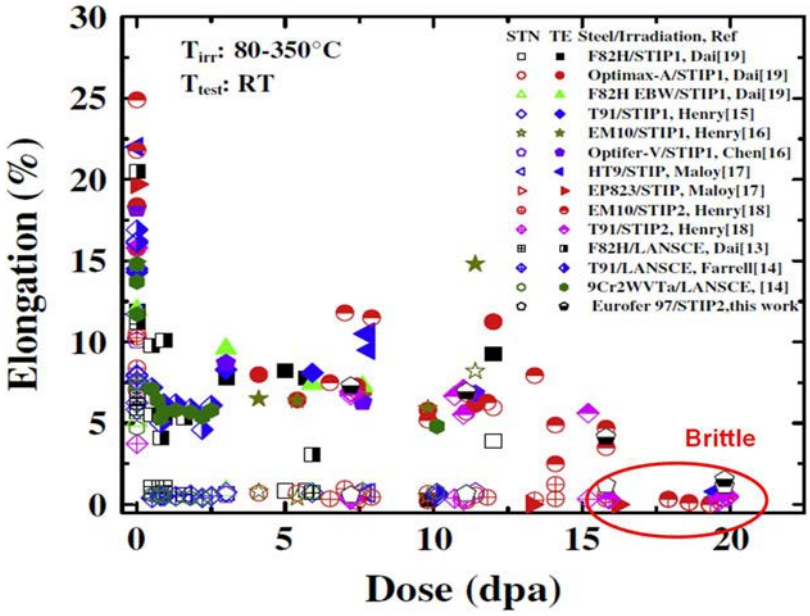

FIG. 4. Elongation versus irradiation dose for TM steel samples irradiated in SINQ targets at 350°C and below and tested at room temperature.

4. STUDY OF H AND HE EFFECTS WITH ION IRRADIATIONS

Since He and H effects are highly important for fusion materials, it is very popular to study the effects by using low energy (mostly <5 MeV) proton or alpha ion irradiations. Despite of some advantages of ion irradiations, there are several fatal limitations for simulating neutron irradiation with ion irradiation, include: i) unrealistic high damage or implantation rates; i) shallow damage depths and the proximity of free surfaces; iii) non-uniform depth profile of damage production and helium/hydrogen concertation; iv) inability for measuring bulk properties. Due to the unrealistic high damage or implantation rates, the formation and evolution of defect clusters, loops or bubbles/cavities in ion irradiation cases may be greatly different from that in neutron or spallation irradiations. Without proper modelling it is difficult to get a correct interpretation of the experimental results.

REFERENCES

[1] DAI, Y., BAUER, G., Status of the first SINQ Irradiation Experiment, J. Nucl. Mater. **296** (2001) 43; DAI, Y., WAGNER, W., Materials researches at the Paul Scherrer Institute for developing high power spallation targets, Journal of Nuclear Materials **389** (2009).

[2] DAI, Y., FOUCHER, Y., JAMES, M.R., OLIVER, B.M., Neutronics calculation, dosimetry analysis and gas measurements of the first SINQ target irradiation experiments, J. Nucl. Mater. **318** (2003) 167.

[3] OLIVER, B.M., DAI, Y., CAUSEY R.A., Helium and hydrogen release measurements on various alloys Irradiated in SINQ, J. Nucl. Mater. **356** (2006) 148.

[4] OLIVER, B., DAI, Y., Helium and hydrogen measurements on pure materials irradiated in SINQ Target 4, J. Nucl. Mater. **386–388** (2009) 383.

[5] JIA, X., DAI, Y., VICTORIA, M., The impact of irradiation temperature on the microstructure of F82H martensitic/ferritic steel irradiated at a proton and neutron mixed spectrum, J. Nucl. Mater. **305** (2002) 1.
[6] JIA, X., DAI, Y., Microstructure of the F82H martensitic steel irradiated in STIP-II up to 20 dpa, J. Nucl. Mater. **356** (2006) 105.
[7] HAMAGUCHI, D., DAI, Y., Microstructural Study of EC 316LN and its Welds Irradiated in SINQ Target-3, J. Nucl. Mater. **343** (2005) 262.
[8] SCHROEDER, H., BATFALSKY, P., J. Nucl. Mater. **117** (1983) 287.
[9] HENRY, J., AVERT, X., DAI, Y., PIZZANELLI, J.P., Tensile behaviour of 9Cr-1Mo martensitic steel irradiated up to 20 dpa in a spallation environment, J. Nucl. Mater. **377** (2008) 80.
[10] DAI, Y., HENRY, J., TONG, Z., AVERTY, X., MALAPLATE, J., et al., Neutron/proton irradiation and He effects on the microstructure and mechanical properties of ferritic/martensitic steels T91 and EM10, J. Nucl. Mater. **415** (2011) 306.
[11] HENRY, J., AVERTY, X., ALAMO, A., Tensile and impact properties of 9Cr tempered martensitic steels and ODS-FeCr alloys irradiated in a fast reactor at 325 _C up to 78 dpa, J. Nucl. Mater. **417** (2011) 99.
[12] MATERNA-MORRIS, E., MÖSLANG, A., SCHNEIDER, H.-C., Tensile and low cycle fatigue properties of EUROFER97-steel after 16.3 dpa neutron irradiation at 523, 623 and 723 K, J. Nucl. Mater. **442** (2013) S62.
[13] ALAMO, A., HORSTEN, M., AVERTY, X., MATERNA-MORRIS, E.I., RIETH, M., Mechanical behaviour of reduced-activation and conventional martensitic steels after neutron irradiation in the range 250±450°C, J. Nucl. Mater. **283–287** (2000) 353.
[14] TONG, Z., DAI, Y., The microstructure and tensile properties of ferritic/martensitic steels T91, Eurofer-97 and F82H irradiated up to 20 dpa in STIP-III, J. Nucl. Mater. **398** (2010) 43.

MATERIALS ISSUES FOR LIQUID METAL COOLANT NUCLEAR SYSTEMS

T. MUROGA
National Institute for Fusion Science,
Toki
Email: muroga@nifs.ac.jp

M. KONDO
Institute of Innovative Research, Tokyo Institute of Technology,
Tokyo
Email: kondo.masatoshi@lane.iir.titech.ac.jp

Japan

Abstract

This paper overviews materials issues for some of the nuclear systems using liquid metals as coolants, including: (i) materials/coolant interactions (mainly materials aspects); (ii) materials property change by the interaction; (iii) system dependent materials issues; (4) radiation effects. Emphasis is placed on the similarities and differences in the issues for Li, Pb-Li and Pb coolants. The main target systems are Li/V-alloy and Li/Reduced Activation Ferritic/Martensitic (RAFM) Fe-Cr-W based steel fusion blankets, Li targets for the International Fusion Materials Irradiation Facility (IFMIF) with a RAFM nozzles and back-plates, Li-Pb/RAFM fusion blankets and Pb/Fe-Cr steels for advanced fast reactors and Accelerator Driven Systems (ADS).

1. INTRODUCTION

A variety of liquid metals are used or planned to be used in nuclear systems such as blankets and divertors of fusion reactors, present and advanced fast reactors, and accelerator-based nuclear systems. The materials issues highly depend on physical, chemical and fluid flow characteristics of the coolants as well as materials composition and structure. Figure 1 summarizes liquid metals used in nuclear systems in the past, ongoing and under-planning programs.

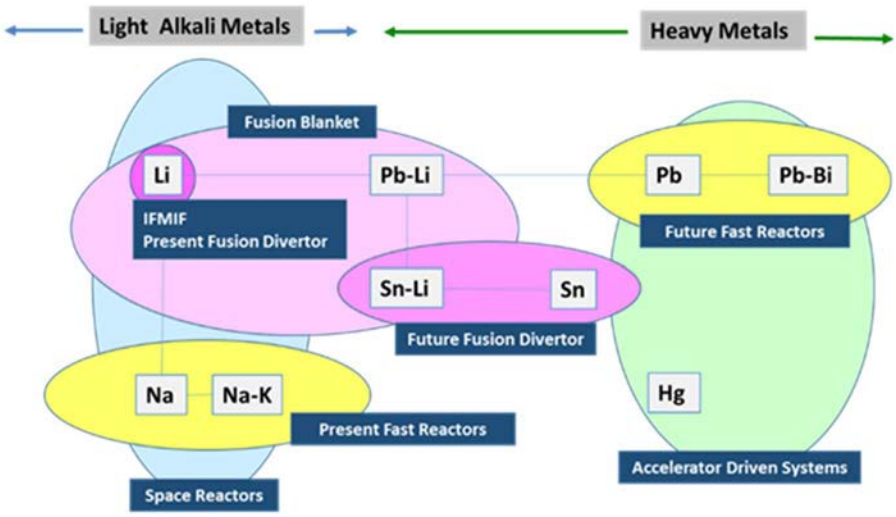

FIG. 1. Use of liquid metals in nuclear systems.

This paper overviews materials issues for some of the nuclear systems using liquid metals as coolants, including (i) materials/coolant interactions (mainly materials aspects); (ii) materials property change by the interaction; (iii) system dependent materials issues; (iv) radiation effects.

In this report, emphasis will be placed on the similarities and differences in the issues for Li, Pb-Li and Pb coolants. The main target systems are Li/V-alloy and Li/RAFM Fe-Cr-Mo based steel fusion blankets, Li targets for IFMIF

with a RAFM nozzles and back-plates, Li-Pb/RAFM fusion blankets and Pb/Fe-Cr steels for advanced fast reactors and ADS. Materials issues with Sn-Li and Sn for fusion divertor application will also be covered.

2. LIQUID LI SYSTEMS

Vanadium alloys (V-4Cr-4Ti) are candidate low activation structural materials [1]. V-4Cr-4Ti cannot be used in oxidizing conditions as it is requiring oxidation protection treatments. Combination with Li coolants realize highly efficient compact blankets, free from oxidation issue. Static exposure test of V-4Cr-4Ti in Li showed that loss of O and pick-up of N and C take place by exposure to static liquid Li [2]. Loss of O and pick up of N result in softening and hardening, respectively. Comparative test of the corrosion in different Ti levels showed that Ti in V-4Cr-4Ti interacts with N, limiting N diffusion to bulk [3]. Mechanical property change is moderate once N level is controlled. Weight loss is also small.

Li-RAFM combination is a conservative option of fusion blanket at lower operation temperature. Generally, corrosion in Ni-free steels is small. However, N impurity in Li enhances Cr dissolution by forming Li-Cr-N [4]. Carbon transfer may be an issue if materials with different C affinity is used side-by-side (softening by loss of carbon) [5].

In liquid Li blankets, ceramic insulator coating is necessary for the purpose of mitigating Magnetohydrodynamic (MHD) pressure drop. Most of the insulator ceramics are unstable in the extremely reducing Li condition. Er_2O_3 and Y_2O_3 are the limited candidates and being investigated [6]. Among the issues for the coatings are robustness and lifetime.

IFMIF needs >15 m/s free surface flow with stable thickness of ±1 mm at ~300°C [7]. Corrosion of the nozzle and back-plate can disturb the flow. A test Li loop named ELTL (Oarai, Japan) were carried out and stable flow was maintained for 3800 hours. Simulated high speed flow tests (Lifus-6) with nozzles showed < 0.001 mm corrosion with 30 wppm N after 4000 hours operation [8]. Thus, once the N level is maintained in a low level, corrosion of the nozzles would not be any issue. Then high dose neutron irradiation effect on the back-plate, which is subject to higher neutron flux than that for the samples in the test cell is the major issue.

3. PB AND PB-BI INTERACTIONS WITH STEELS

Pb and Pb-Bi are candidates for Lead-Cooled Fast Reactor (LFR) and ADS. For both Pb and Pb-Bi, solubility of Ni is much higher than that of Cr and Fe [4]. Cr have higher affinity to O than Pb and thus natural oxide (Cr_2O_3) can protect corrosion if Pb is saturated with O. Corrosion of steels is known to be strongly influenced by the oxygen activity in Pb or Pb-Bi.

— Low O: Uniform dissolution and Pb(Bi) penetration into interfaces.
— High O: Thick oxide scale formation and spalling off.

Thus, corrosion loss of steels in Pb/Pb-Bi melts can be minimized substantially by maintaining the oxygen concentration in the liquid metal in the optimal range.

Mechanical property changes of steels exposed to Pb and Pb-Bi (Lead Bismuth Eutectic) is also strongly influenced by the oxygen activity. In low oxygen potential, wetting of the surfaces accelerate mechanical property degradation especially for ferritic steels [9].

As a possible solution to eliminate the corrosion, Al_2O_3 Forming Steels, steels alloyed with 1–4% Al, are promising candidates as robust corrosion resistant alloy at high O level of Pb (Bi).

4. Pb-Li/RAFM FUSION BLANKET

A variety of Pb–Li/RAFM fusion blankets have been proposed and designed, e.g. Dual Coolant Lead Lithium (DCLL), Dual Functional Lithium Lead (DFLL), Helium Cooled Lithium Lead (HCLL), Water Cooled Lithium Lead (WCLL), Lead Lithium Ceramic Breeder (LLCB). Materials issues vary with design, some requires insulating insert/coating. The interfaces of RAFM are summarized as follows:

— DCLL, DFLL: Pb–Li/RAFM/He, Pb–Li/SiC (insert);
— HCLL: Pb–Li/RAFM/He;

— WCLL: Pb–Li/RAFM/water;
— LLCB: Pb–Li/RAFM/Solid Breeder, Pb–Li/insulator coatings.

Pb–Li corrosion has an intermediate or combined character of Li and Pb corrosion. Natural oxide layer (Cr_2O_3) is not stable. The incubation followed by linear increase in corrosion depth reported by the flowing loop tests suggests that dissociation of the natural oxide layer takes place during the incubation. Al (rich phase) coating or bulk alloying with Al, forming stable Al_2O_3 in contact with Pb–Li, is a possible protection method. However, further effort is necessary for optimization (e.g. avoiding Li–Al–Fe compound formation).

It is to be noted, the Pb–Li eutectic point still has some uncertainty. Compositional deviation from the eutectic points can change the property as follows.

— Pb-rich: more Pb like corrosion:
  (i) Fe solution, Pb penetration into interfaces;
— Li-rich: more Li like corrosion:
  (i) Cr dissolution by N attack;

Thus, the stoichiometry control is critically important [10].

Corrosion–Erosion tests of RAFM in flowing conditions of Pb–Bi, Pb–Li and Li show the following different characteristics of surface corrosion.

— Pb–Bi: Penetration to Prior Austenitic Grain (PAG) boundaries, Packet Boundaries and Block Boundaries;
— Li: Penetration to Lath Boundaries by reaction with carbides on the boundaries;
— Pb–Li: Combined characteristics of the above two cases.

Thus, control of PAG boundaries can be effective for controlling Pb–Bi corrosion, and control of carbides on lath boundaries can be effective for controlling Li corrosion [11,12].

5. Sn, Sn–Li: A NEW INTEREST FOR FUSION DIVERTOR APPLICATION

Sn–Li was a candidate fusion blanket coolant because of its moderate tritium solubility etc. [13] The solubility of tritium in Li is too high, making the removal of tritium from Li difficult, and that in Pb–Li is too low, inducing leakage of tritium during the transportation as a critical issue.

Liquid metals have been considered as plasma-facing materials for withstanding very high thermal loading. Li has been used for the present plasma test facilities mainly for pumping of hydrogen (isotopes), contributing enhancement of core plasma performance. Sn–Li and Sn attract attention for future fusion divertor application mainly because of its low vapor pressure (small contamination of plasma) [14].

However, the corrosion data of Sn/Sn–Li are limited. Since the oxidation potential of SnO is close to that of PbO, similar corrosion control strategy may be applied both to Pb–Li/Pb and Sn–Li/Sn. A preliminary study showed severe Sn penetration to steels. Impact of Sn/Li ratio, O and N impurities need to be assessed [15].

6. RADIATION-RELATED ISSUES

Neutron/proton irradiations can change liquid metal/container interactions via microstructural changes, grain boundary segregation/degradation, damaging on protective layers, and so on. Irradiation test of a ferritic/martensitic steel (T91) in Pb–Bi showed that at 723 K, impact of radiation in Lead Bismuth Eutectic (LBE) on tensile property is small. But, at 623 K, both liquid metal embrittlement and radiation embrittlement appeared [16]. Upper temperature edge of the liquid metal and radiation embrittlement may be close with each other [17]. Their synergism is, however, not clear and controversial.

7. SUMMARY OF MATERIALS ISSUES FOR LI, PB/PB–LI/PB–BI, AND SN/SN–LI SYSTEMS

Figure 2 schematically shows coolant materials interaction and possible controlling procedures. In addition of chemical control of coolant (O, N, Pb/Li), the following techniques are being explored:

a) Ti enrichment (stable nitrides) and Y_2O_3, Er_2O_3 coating for Li and Li-rich Pb–Li.
b) Al, Si, Cr bulk or surface enrichment and coating with Al_2O_3, Cr_2O_3 for Pb-rich Pb–Li, high O, Pb and Pb–Bi.
c) Plating with Nb, Mo W, Ta (low solubility elements) for low O, Pb and Pb–Bi. It needs to be noted, that these methods cannot be applied to high O, Pb and Pb–Bi.

It needs to be noted, that the interactions are strongly subject to coolant flow rate, temperature, temperature gradient and stress.

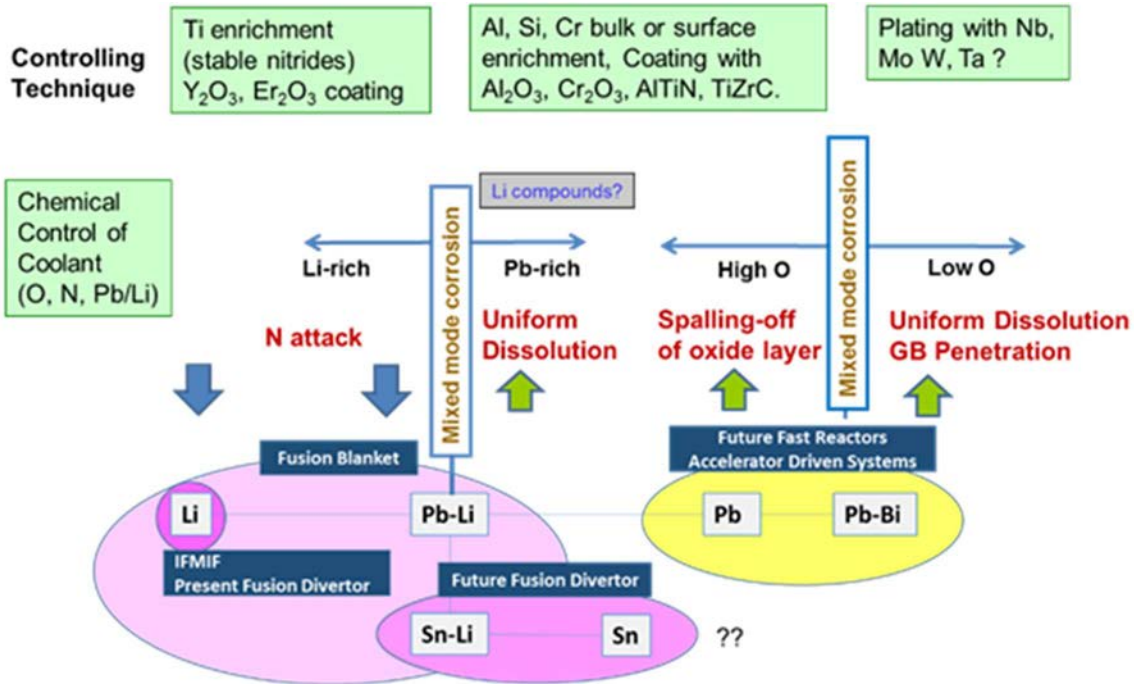

FIG. 2. Schematic representation of coolant materials interaction and possible controlling procedures.

8. CONCLUSION

In liquid metal coolant systems, different corrosion mechanisms arise in different conditions, such as uniform dissolution, matrix and boundary penetration, nitrogen enhanced dissolution, oxide layer formation and spalling off, and so on. Materials aspects for improving the compatibility are:

a) Surface engineering: pre-deformation, pre-oxidation (if Cr_2O_3 is stable), surface alloying and their combinations.
b) Plating/coating of corrosion-resistant materials.
c) For these cases, robustness is an issue especially if they are used in flowing conditions.
d) Bulk compositional change, such as Al_2O_3 forming alloys.

This is robust but needs new database such as manufacturing and joining technology, basic mechanical property including stability, radiation effects and licensing scenario. Microstructural control (e.g. grain size and carbides distribution).

It needs to be noted, that the corrosion mitigation measures need to not deteriorate the functional role of the material (e.g. tritium permeation, electrical insulation/conduction, thermal conduction).

Liquid metal embrittlement and radiation embrittlement, both of which have strong (in some case similar) temperature dependence, and their possible synergism influence the system operation conditions.

In the mission-oriented materials development shown above, international collaboration is essential for cross-checking the development strategy and constructing necessary database for timely development and licensing.

REFERENCES

[1] MUROGA, T., CHEN, J.M., CHERNOV, V.M., KURTZ, R.J., LE FLEM, M., J. Nucl. Mater. **455** (2014) 263–268.
[2] NAGASAKA, T., MUROGA, T., LI, M., HOELZER, D.T., ZINKLE, S.J., et al., Fus. Eng. Des. **81** (2006) 307.
[3] YELISEYEVA, O.I., FEDIRKO, V.N., CHERNOV, V.M., ZAVIALSKY, L.P., J. Nucl. Mater. **283–287** (2000) 1282.
[4] LYUBLINSKI, I.E., EVTIKHIN, V.A., YU, V., KRASIN, V.P., PANKRATOV, J. Nucl. Mater. **224** (1995) 288–292.
[5] XU, Q., KONDO, M., NAGASAKA, T., MUROGA, T., SUZUKI, A., Fus. Eng. Des. **83** (2008) 1477–1483.
[6] MUROGA, T., PINT, B.A., Fusion Engineering and Design **85** (2010) 1301–1306.
[7] KONDO, H., KANEMURA, T., FURUKAWA, T., HIRAKAWA, Y., KNASTER, J., Fus. Eng. Des. **109–111** (2016) 1759–1763.
[8] KNASTER, J., FAVUZZA, P., Fus. Eng. Des. **118** (2017) 135–141.
[9] GORSE, D., AUGER, T., VOGT, J.-B., SERRE, I., WEISENBURGER, A., et al., J. Nucl. Mater. **415** (2011) 284–292.
[10] KONDO, M., ISHII, M., HISHINUMA, Y., TANAKA, T., NOZAWAD, T., et al., Fus. Eng. Des. (2017) in press.
[11] KONDO, M., TAKAHASHI, M., SUZUKI, T., ISHIKAWA, K., HATA, K., J. Nucl. Mater. 343 (2005) 349–359.
[12] KONDO, M., TAKAHASHI, M., TANAKA, T., TSISAR, V., MUROGA, T., Fus. Eng. Des. 87 (2012) 1777–1787.
[13] KANG, Y., TERAI, T., J. Nucl. Mater. 329–333 (2004) 1318–1321.
[14] MIYAZAWA, J., GOTO, T., OHGO, T., MURASE, T., YANAGI, N., et al., IAEA FEC, Kyoto, 2016.
[15] KONDO, M., ISHII, M., MUROGA, T., Fus. Eng. Des. **98–99** (2015) 2003.
[16] VAN DEN BOSCH, J., COEN, G., BOSCH, R.W., ALMAZOUZI, A., J. Nucl. Mater. **398** (2010) 68–72.
[17] LONG, B., DAI, Y., BALUC, N., J. Nucl. Mater. **431** (2012) 85–90.

THERMODYNAMIC CONSIDERATIONS ON CHEMICAL INTERACTIONS BETWEEN LIQUID METALS AND STEELS

M. KONDO
Tokyo Institute of Technology,
Tokyo
Email: kondo.masatoshi@lane.iir.titech.ac.jp

C. PARK, T. NOZAWA
National Institute for Quantum and Radiological Science and Technology,
Chiba

K. SASAKI
Hirosaki University,
Hirosaki

M. TAKAHASHI
Osaka University,
Osaka

Y. HISHINUMA, T. TANAKA, T. MUROGA
National Institute for Fusion Science,
Toki

Japan

B. MATOVIC
Vinca Institute of Nuclear Science,
Belgrade, Serbia

Abstract

Material compatibility between liquid metals and steels is one of the important issues for the development of nuclear reactors. The corrosion behaviours of steels in liquid lead (Pb) and liquid Lead Bismuth Eutectic (LBE), which are candidate coolants of fast reactors, are strongly influenced by oxygen dissolved in the liquid metals. The corrosion is caused through a dissolution of the steel compositions such as iron (Fe) and chromium (Cr) into the liquid metals when the oxygen potential is lower than that required for a formation of protective oxide layers on the steels. The dissolution type corrosion is mitigated by the formation of oxide layers, when the oxygen potential of the liquid metals is adequately controlled. Some additional elements such as aluminium (Al) and silicon (Si) can improve the corrosion resistance of steels due to the formation of compact oxide layers. The corrosion of steels in liquid lithium (Li), which is candidate target material of fusion neutron source, is negligibly small when its purity is high. However, the corrosion is promoted by oxygen and nitrogen dissolved in the liquid Li owing to the formation of unstable chemical compounds such as Li–Cr–O and Li–Cr–N. The oxygen potential in the liquid Li is quite low. Therefore, the surfaces of the steels are never oxidized. The corrosion behaviours of steels in liquid Pb–^{16}Li, which is candidate tritium breeder of fusion reactors, are influenced both by the corrosion features of liquid Li and liquid Pb. The oxides are hardly formed on the steels, since the oxygen potential of the Pb–^{16}Li alloy is low. The corrosion is caused thorough the dissolution of steel compositions into the liquid alloy. The dissolution-type corrosion is then promoted by the nitrogen in the alloy as the similar way to the corrosion in liquid Li.

1. INTRODUCTION

Liquid lead (Pb) and lead bismuth eutectic alloy (Pb–Bi) are candidate coolants for fast reactors [1]. Liquid lithium (Li) and liquid lead-lithium alloy (Pb–Li) are promising fluids as tritium breeders of fusion reactors. Liquid tin (Sn) that has extremely low vapor pressure [2] is considered as a plasma facing fluid of a liquid wall divertor concept [3]. The material compatibility of these fluids with structural and functional materials is critical issue. The corrosion characteristics of steels and ceramic materials have been investigated.

It is known that some non-metal and metal impurities (e.g., oxygen, nitrogen, hydrogen and carbon), which are dissolved in the liquid metals, strongly influence on the corrosion behaviours of the materials. The chemical potential of oxygen has the large influence on the material compatibility in a liquid Pb–Bi. The steels were severely corroded in the flowing Pb–Bi due to a dissolution type corrosion and a severe corrosion-erosion, when the oxygen potential of the Pb–Bi was low [4]. The severe corrosion behaviours could be mitigated at a high oxygen potential

condition according to the formation of protective oxide layers that worked as a barrier for the dissolution type corrosion [5]. The relationship between the oxygen potential and the corrosion behaviours were summarized in the diagram that is called as 'Gorynin diagram' [6]. However, only limited types of oxides can survive in a liquid Li because of the extremely low oxygen potential in the melt [7]. The study on searching the stable oxides that can be used as the corrosion barrier and the tritium permeation barrier in the liquid Li has been performed.

Cross cutting discussions on corrosion interactions between the liquid metal coolants and the structural materials for various nuclear reactors were taken place in the 1st IAEA Workshop on "Challenges for Coolants in Fast Neutron Spectrum Systems: Chemistry and Materials". The purpose of the present study is to review recent research findings on the corrosion interactions and summarize the thermodynamic considerations on the non-metal impurities dissolved in the liquid metals. This report also introduces an impurity mixing in fabrication procedures of liquid Pb–Li alloys.

2. CHEMICAL POTENTIALS OF OXYGEN IN LIQUID METALS

The chemical potentials of oxygen in liquid metals Pb, Sn and Li 'ϕ' are expressed as follows:

$$\phi_{O,Pb} = \Delta G_{f,\mathrm{PbO}} + RT\ln\left(\frac{C}{Cs}\right) \text{ [kJ.mol-1]} \quad (1)$$

$$\phi_{O,Sn} = \frac{1}{2}\Delta G_{f,\mathrm{SnO_2}} + RT\ln\left(\frac{C}{Cs}\right) \text{ [kJ.mol-1]} \quad (2)$$

$$\phi_{O,Li} = \Delta G_{f,\mathrm{Li_2O}} + RT\ln\left(\frac{C}{Cs}\right) \text{ [kJ.mol-1]} \quad (3)$$

where c is the oxygen concentration [wt%], c_s is the oxygen solubility [wt%], $\Delta G_{f,MO}$ is the Gibbs free energy of formation of oxides of the fluids [kJ/mol], R is the gas constant (8.314×10^{-3} [kJ/K/mol]) and T is the temperature [K].

The oxygen potentials of liquid binary alloys such as Pb-Bi and Pb-17Li are also expressed in the same way. Then, the chemical activity of their chemical composition must be taken into account. The previous studies indicated that the liquid Pb-Bi formed only PbO in the oxidation procedure at the oxygen saturation conditions [8], and Bi was not involved at all. Then, the oxygen potential in the liquid Pb-Bi is expressed as [9]:

$$\phi_{O,Pb-Bi} = \Delta G_{f,\mathrm{PbO}} - \overline{\Delta G_{\mathrm{Pb(Pb-Bi)}}} + RT\ln\left(\frac{C}{Cs}\right) \text{ [kJ.mol-1]} \quad (4)$$

$$\overline{\Delta G_{\mathrm{Pb(Pb-Bi)}}} = 1.59 \text{ [kJ.mol-1]} \quad (5)$$

where $\overline{\Delta G_{\mathrm{Pb(Pb-Bi)}}}$ is the excess Gibbs energy of mixing Pb into Pb–Bi.

It was indicated that Li_2PbO_3 was formed in the liquid Pb–17Li when it was oxidized [8]. However, the information about the Gibbs free energy for the formation of the ternary oxides has not been made clear. This Gibbs free energy for the formation may be close to that of Li_2O. The oxygen potential in the liquid Pb–17Li, where $\overline{\Delta G_{\mathrm{Li(Pb-17\ )}}}$ is the excess Gibbs energy of mixing Li into Pb–17Li [10], is expressed as follows:

$$\phi_{O,Pb-17} = \Delta G_f \mathrm{Li_2O} - 2\overline{\Delta G_{\mathrm{Li(Pb-17Li)}}} + RT\ln\left(\frac{C}{Cs}\right) \text{ [kJ.mol-1]} \quad (6)$$

$$\overline{G_{\mathrm{Li(Pb-17Li)}}} = -60.122 + \frac{1778.2}{T} \text{ (713<T[K]<1013) [kJ.mol-1]} \quad (7)$$

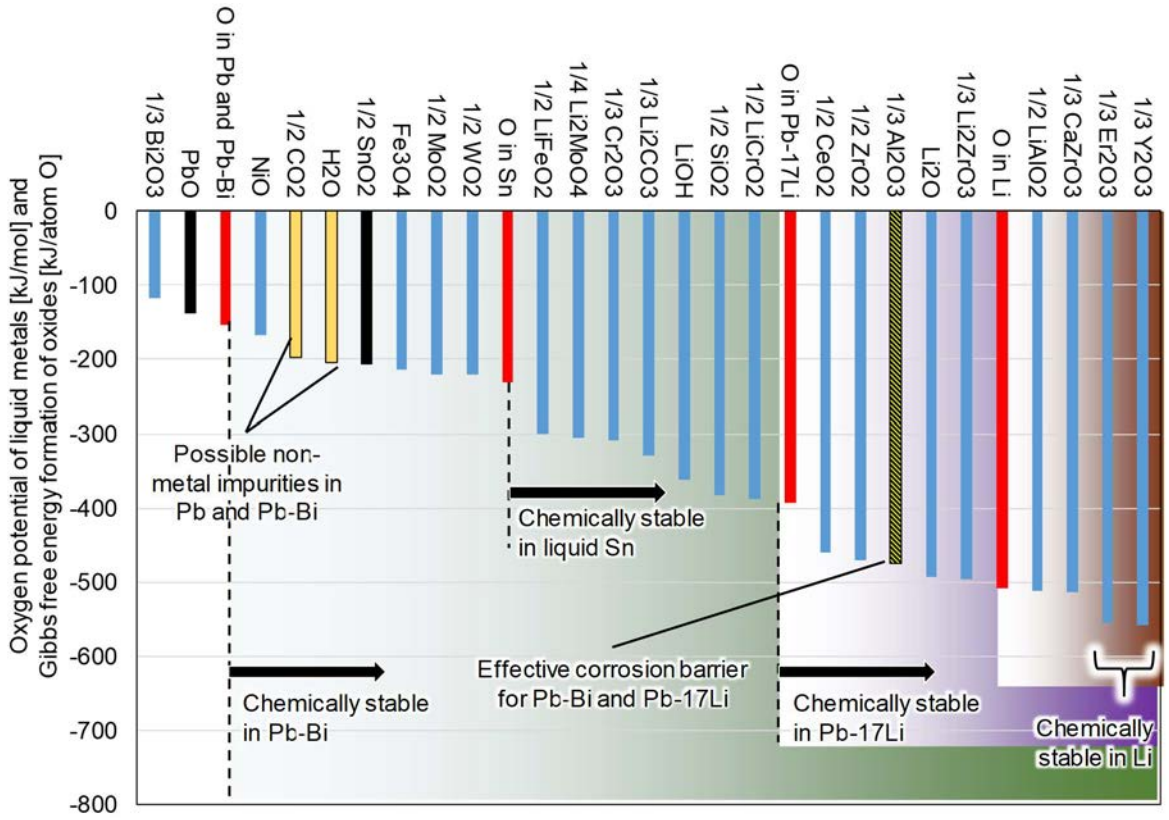

FIG. 1. Chemical potential of oxygen in liquid Pb–Bi, Pb–^{17}Li and Li, and chemical stabilities of various oxides at 800 K (527ºC).

Figure 1 shows the oxygen potential of the liquid metals Sn, Pb–Bi (Pb), Pb–17Li and Li when their oxygen concentration is one-tenth of their solubilities as C/Cs = 0.1. The Gibbs free energy for formation of various oxides are also shown in Fig. 1. The oxygen potential in the liquid Pb–Bi is can be controlled at a relatively high region by means of the gas injection method [4] and the mass exchanger method [11]. Then, various oxides may be chemically stable in the liquid Pb–Bi. The oxide layers such as Fe_3O_4, $(Fe, Cr)_3O_4$ and Cr_2O_3 were formed on the steel surfaces in the liquid Pb–Bi [5]. The Si and/or Al rich oxide layers that had a compact structure revealed an excellent chemical and structural stability. These layers were effective to protect the steel surfaces in the flowing Pb–Bi [12, 13]. The oxygen potential of the liquid Sn is also relatively high. However, the effectiveness of the oxide layers as the corrosion barrier against the alloying type corrosion [14, 15] has not been made clear so far.

The oxygen potential of the liquid Pb–^{17}Li is much lower than that of liquid Pb and Pb–Bi, because the Li composition in the alloy reduce the oxygen potential. Then, only limited number of oxides can survive in these liquid metals. It was reported that aluminium oxide (Al_2O_3) might be stable in the liquid Pb–^{17}Li [16]. The oxygen potential of the liquid Li is extremely low. The compatibility of erbium oxide (Er_2O_3) and yttrium oxide (Y_2O_3) that are theoretically stable in the liquid Li have been investigated [7, 17].

Ceria (CeO_2) has good chemical stability as shown in Fig. 1. The ceria-based materials have become one of the most important ceramic materials [18], and the applications in the field of energy production have been studied. Nanostructured ceria-based coatings revealed a protectiveness against high temperature oxidation on AISI 304 steel [19]. The high-performance coating may be also effective for the corrosion mitigation in the liquid metal conditions. However, the ceria-based materials were not studied for fusion reactor materials. The study on material compatibility of ceria-based material may be important for the development of the functional materials of nuclear reactors.

The oxygen potential of the liquid metals Pb, Sn, Pb–Bi and Pb–^{17}Li can be measured by solid electrolyte oxygen sensors. For example, the marital of the sensor is Y_2O_3 stabilized ZrO_2 (YSZ) [11] and is chemically stable in these liquid metals as shown in Fig. 1. The oxygen potential of the liquid Li is lower than that for the formation of the solid electrolyte ceramics. Then the sensor is reduced in the liquid Li. Therefore, the measurement of the oxygen potentials in the liquid Li by the solid electrolyte sensor is not easy.

3. CORROSION OF STEELS PROMOTED BY DISSOLVED OXYGEN AND NITROGEN IN LIQUID LI

The effect of oxygen and nitrogen on the corrosion of steels in the liquid Li has been studied. The corrosion in the liquid Li was promoted by both the oxygen [20] and the nitrogen [21] dissolved in the melt. The corrosion promotion by dissolved oxygen might be caused by the formation and the dissolution of unstable ternary oxides (Li–Metal–O). The information on this reaction is still limited. However, the chemical reactions between Li oxide (Li_2O) and the steels were reported in the previous literature on the compatibility issues of ceramic breeders [22]. The oxide scales of Li_5FeO_4, $LiCrO_2$ and $Li_2Ni_8O_{17}$ were formed between the Li_2O and the steels. The possible reactions for the formation of unstable oxides in the liquid Li are expressed as follows:

$$5Li + 4OLi + Fe \rightarrow Li_5FeO_4 \quad (8)$$

$$Li + 2OLi + Cr \rightarrow LiCrO_2 \quad (9)$$

The similar reactions must be caused also in the liquid Pb–^{17}Li. However, the intensity needs to be much smaller than that in the liquid Li due to the small chemical activity of Li in the liquid Pb–^{17}Li. The oxygen concentration in the liquid Li was reduced by the use of Er metal powders as an additive to decrease the oxygen concentration [23]. The corrosion promotion must be suppressed by the reduction of oxygen in the liquid Li.

The concentration of nitrogen in the liquid Li can be measured by an ammonia extraction method [24]. Figure 2 shows the nitrogen potential in the liquid metals and the Gibbs free energy for formations of various nitrides. Nitrogen is inert gas. It is known that nitrogen chemically dissolves in the liquid Li. The chemical potentials of nitrogen in liquid Li and Pb–^{17}Li are expressed as follows:

$$\phi_{N,Li} = \Delta G_f Li_3N + RT\ln\left(\frac{C}{Cs}\right) \text{ [kJ.mol-1]} \quad (10)$$

$$\phi_{N,Pb-17} = \Delta G_f Li_3N - 3\overline{\Delta G_{Li(Pb-17Li)}} + RT\ln\left(\frac{C}{Cs}\right) \text{ [kJ.mol-1]} \quad (11)$$

The corrosion reactions between Li with nitrogen and steel compositions (i.e. Fe and Cr) were proposed in the literature [13] as follows:

$$2Li_3N + Fe \rightarrow Li_3FeN_2 + 3Li \quad (12)$$

$$5Li_3N + Cr \rightarrow Li_9CrN_5 + 6Li \quad (13)$$

The Gibbs free energy for formation of the ternary compounds, Li_3FeN_2 and Li_9CrN_5, are not shown in Fig. 2, because these values are not made clear. However, it was made clear that Cr was selectively depleted from the steel surface in the liquid Li, when the nitrogen concentration was high. The depletion was promoted when the nitrogen concentration in the liquid was high [21]. The Gibbs free energy for formation of Li_9CrN_5 might be smaller than that of Li_3FeN_2. The nitrogen concentration was also measured by the ammonia extraction method.

The dissolved nitrogen promoted the corrosion of steels also in liquid Pb–Li alloys [25]. The liquid Pb, Pb–Bi and Sn do not form their nitrides. Therefore, the dissolution of nitrogen in these liquid metals must be negligibly small in these liquid metals.

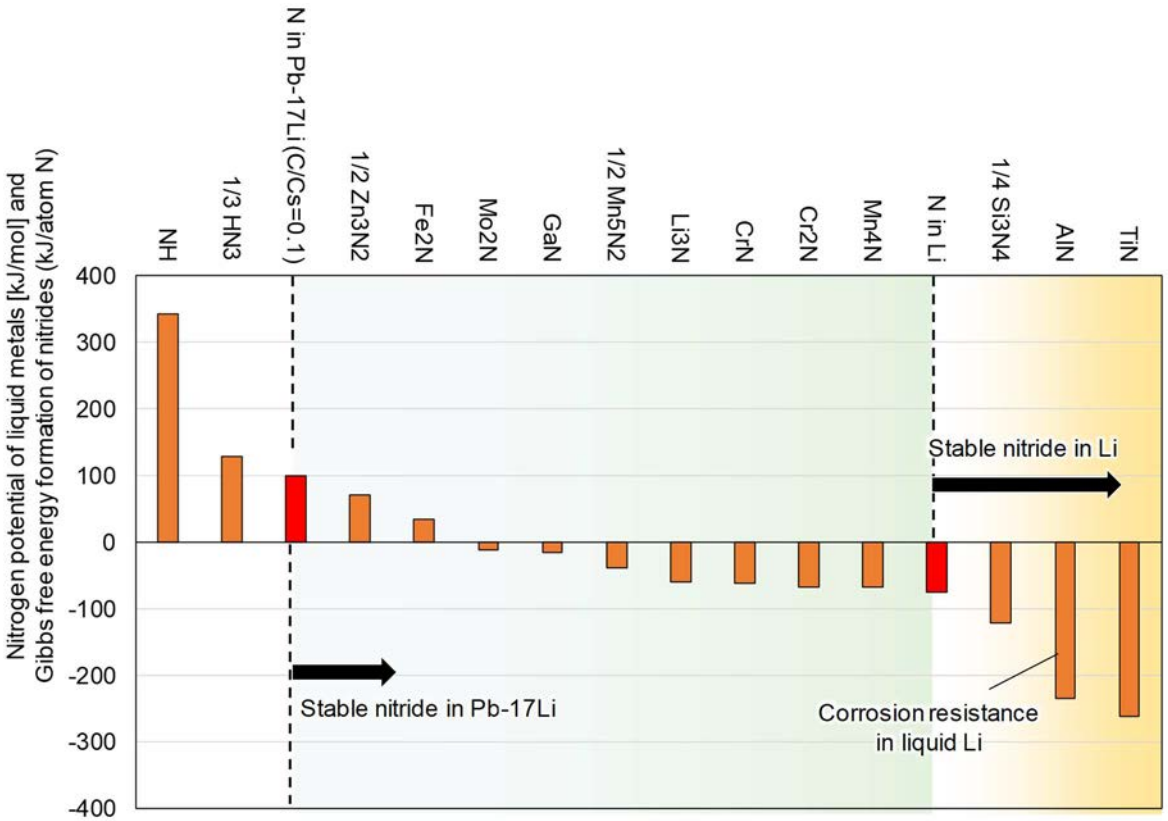

FIG. 2. Chemical potential of Nitrogen in liquid Li and Pb–17Li, and chemical stabilities of various nitrides at 800 K (527ºC).

The aluminium nitride (AlN) revealed excellent corrosion resistance in liquid Li at 673 K and 773 K [7,17], though the information on the compatibility of nitrides in the liquid Li and Pb–17Li are still limited. The corrosion resistance of the AlN is reasonable based on the thermodynamic considerations in Fig. 2.

4. CHEMICAL POTENTIAL OF CARBON IN LIQUID METALS AND DECARBURIZATION OF STEELS

Figure 3 shows the chemical potential of carbon in liquid metals and the Gibbs free energy for formation of various carbides. It was made clear that the RAFM steel JLF-1 (Fe–9Cr–2W–0.1C) caused the phase transformation from martensite to ferrite on the surface in the liquid Li [27]. The phase transformation of the steel was caused by the decarburization in the liquid Li. The carbon potential of the liquid Li was controlled by the cold trap [27] and the container material [28]. The carbon potential in the liquid Li was controlled at extremely low condition, when the potential was in the equilibrium state for the formation of Nb_2C by the use of the container made of Nb. Then, the depletion of carbon from the steel surface into the liquid Li and the phase transformation of the JLF-1 steel was promoted. Then, the degradation of the mechanical properties was advanced from the steel surface.

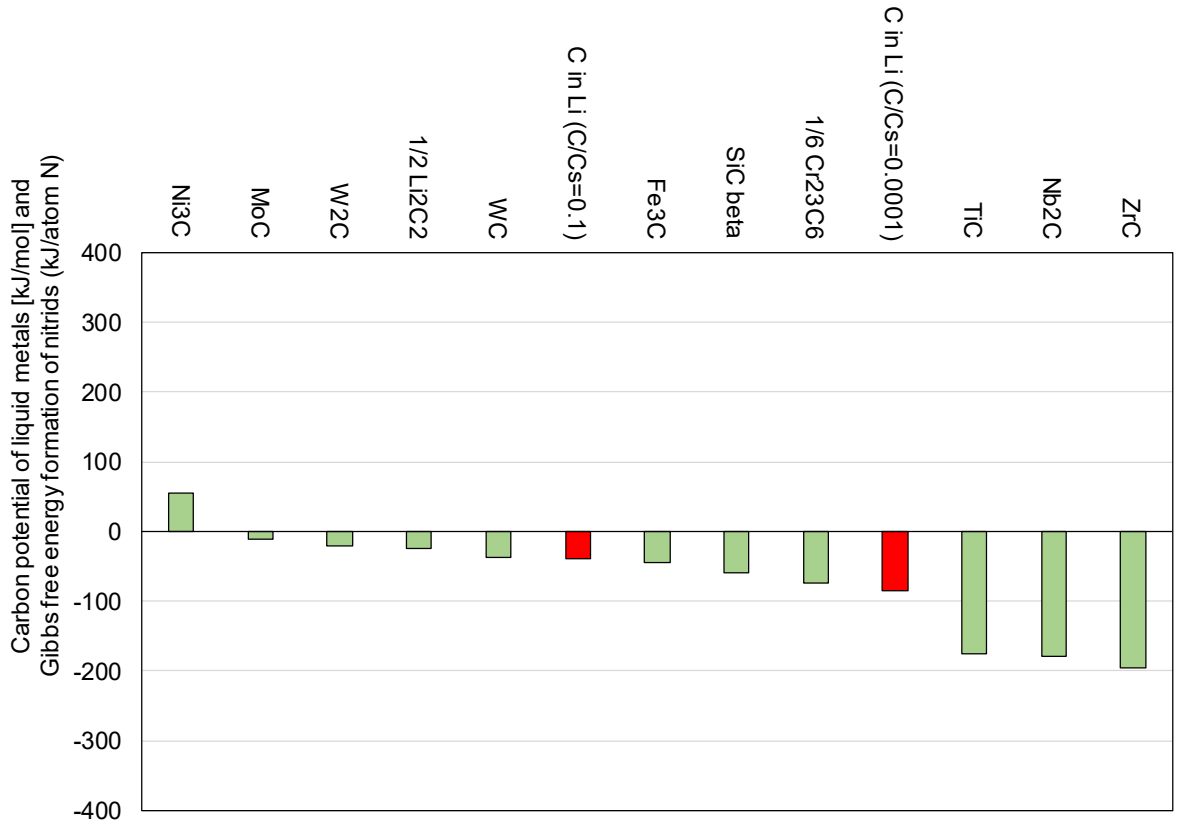

FIG. 3. Chemical potential of carbon in liquid Li and chemical stabilities of various nitrides at 800 K (527°C).

5. NON-METAL IMPURITIES IN LIQUID PB-LI ALLOYS

The information on the impurities in liquid Pb–Li alloys is still limited. However, it was found that some impurities were dissolved in the fabrication procedure of the alloy. Some unexpected chemical reactions between the Li and the impurities were caused in the fabrication procedure [28]. The impurities in the law materials for the alloy fabrications were analysed by the metallurgical analysis and the temperature programmed desorption analysis [29]. The metal Pb, which was used as a low material for the alloy fabrication, initially had a layer of PbO on the surface. The PbO layer absorbed non-metal impurities (e.g. H_2O and CO_2) as follows;

$$PbO + H_2O \leftrightarrow Pb(OH)_2 \quad (14)$$

$$PbO + CO_2 \leftrightarrow PbCO_3 \quad (15)$$

These non-metal impurities were chemically stable in the metal Pb. These impurities reacted with Li in the fabrication procedure as follows;

$$PbO + 2Li \rightarrow Pb + Li_2O \quad (16)$$

$$4Li + H_2O \rightarrow 2Li_2O + 2LiH \quad (17)$$

$$2Li + H_2O \rightarrow LiOH + LiH \quad (18)$$

$$LiOH + 2Li\ (Pb\text{-}Li) \rightarrow Li2O + LiH \quad (19)$$

$$6Li + CO_2 \rightarrow 2Li_2O + 2Li_2C_2 \quad (20)$$

Then, the Li was selectively oxidized and did not have the contribution as the alloying composition in the Pb–Li alloys. In the same time, Li_2O and other impurities dissolved in the alloys.

6. SUMMARY

The oxygen potentials of liquid metals were estimated and compared with the Gibbs free energy for formation of various oxides. The oxide layers and the ceramic coatings available as the corrosion barriers in the liquid metals were summarized. The effect of dissolved oxygen on the corrosion behaviours of steels in the liquid metals were also summarized. The effect of nitrogen and carbon dissolved in the liquid Li and Pb–Li alloys on the corrosion behaviours of steels were summarized based on the thermodynamic considerations.

REFERENCES

[1] ALEMBERTI, A., SMIRNOV, V., SMITH, C. F., TAKAHASHI, M., Overview of lead-cooled reactor activities, Progress in Nuclear Energy **77** (2014) 300-307.

[2] KONDO, M., NAKAJIMA, Y., Boiling points of liquid breeders for fusion blankets, Fus. Eng. Des. **88** (2013) 2556–2559.

[3] MIYAZAWA, J., GOTO, T., MURASE, T., OHGO, T., YANAGI, N., et al., Conceptual design of a liquid metal limiter/divertor system for the FFHR-d1, Fus. Eng. Design **125** (2017) 227–238.

[4] KONDO, M., TAKAHASHI, M., SUZUKI, T., ISHIKAWA, K., HATA, K., et al., Metallurgical study on erosion and corrosion behaviours of steels exposed to liquid lead–bismuth flow, J. Nucl. Mater. **343** (2005) 349–359.

[5] KONDO, M., TAKAHASHI, M., SAWADA, N., HATA, K., Corrosion of Steels in Lead–Bismuth Flow, J. Nucl. Sci. Technol. **43** (2005) 107–116.

[6] GORYNIN, I.V, KARZOV, G.P., MARKOV, V.G., LAVRUKHIN, V.S., YAKOVLEV, V.A., Structural Materials for Power Plants with Heavy Liquid Metals as Coolants, Proc. of HLMC1999 (1999) 120–124.

[7] NAGURA, M., KONDO, M., SUZUKI, A., MUROGA, T., TERAI, T., Experimental Study on Corrosion of Ceramic Materials in Natural Convection Lithium Loop, Fusion Science and Technology **52** (2007) 630–634.

[8] M. KONDO, N. OKUBO, E. IRISAWA, A. KOMATSU, N. ISHIKAWA, Oxidation characteristics of lead-alloy coolants in air ingress accident, Energy Procedia **131** (2017) 386–394.

[9] MULLER, G., HEINZEL, A., SCHUMCHER, G., WEISENBURGER, A., Control of oxygen concentration in liquid lead and lead–bismuth, J. Nucl. Mater. **321** (2003) 256–262.

[10] HUBBERSTEY, P., SAMPLE, T., Thermodynamics of the interactions between liquid breeders and ceramic coating materials, J. Nucl. Mater. **248** (1997) 140–146.

[11] KONDO, M., TAKAHASHI, M., MIURA, K., ONIZAWA, T., Study on control of oxygen concentration in lead–bismuth flow using lead oxide particles, J. Nucl. Mater. **357** (2006) 97–104.

[12] KONDO, M., TAKAHASHI, M., Corrosion resistance of Si- and Al-rich steels in flowing lead–bismuth, J. Nucl. Mater. **356** (2006) 203–12.

[13] HEINZEL, A., KONDO, M., TAKAHASHI, M., Corrosion of steels with surface treatment and Al-alloying y GESA exposed in lead–bismuth, J. Nucl. Mater. **350** (2006) 264–70.

[14] KONDO, M., ISHII, M., MUROGA, T., Corrosion of steels in molten gallium (Ga), tin (Sn) and tin lithium alloy (Sn–20Li), Fus. Eng. Des. **98–99** (2015) 2003–2005.

[15] HEINZEL, A., WEISENBURGER, A., MULLER, G., Corrosion behaviour of austenitic steel AISI 316L in liquid tin in the temperature range between 280 and 700 °C, Materials and Corrosion **9999** (2017) 1–7.

[16] PINT, B.A., The effect of coatings on the compatibility of Fe–Cr steels with Pb–Li, J. Nucl. Mater. **417** (2011) 1195–1199.

[17] SAWADA, A., SUZUKI, A., TERAI, T., Lithium compatibility of insulator coatings fabricated by RF sputtering method, Fus. Eng. Des. **81** (2006) 579–582.

[18] MATOVIC, B., DOHCEVIC-MITROVIC, Z., RADOVIC, M., BRANKOVIC, Z., BOSKOVIC, S., et al., Synthesis and characterization of ceria based nanometric powders, Journal of Power Sources **193** (2009) 146–149.

[19] AADHAVAN, R., SURESH BADU, K., Impact of structure and morphology of nanostructured ceria coating on AISI 304 oxidation kinetics, Applied Surface Science **411** (2017) 219–226.

[20] KONDO, M., TAKAHASHI, M., TANAKA, T., TSISAR, V., MUROGA, T., Compatibility of reduced activation ferritic martensitic steel JLF-1 with liquid metals Li and Pb–17Li, Fus. Eng. Des. **87** (2012) 1777–1787.

[21] TSISAR, V., KONDO, M., XU, Q., MUROGA, T., NAGASAKA, T., et al., Effect of nitrogen on the corrosion behaviour of RAFM JLF-1 steel in lithium, J. Nucl. Mater. **417** (2011) 1205–1209.

[22] FINN, P.A., BREON, S.R., CHELLEW, N.R., Compatibility study of solid ceramic breeder materials, J. Nucl. Mater. **103–104** (1981) 561–544.

[23] NAGURA, M., SUZUKI, A., TERAI, T., Corrosion prevention of Er2O3 by O control in Li, J. Nucl. Mater. **417** (2011) 1210–1213.
[24] SAKURAI, T., YONEOKA, T., TANAKA, S., SUZUKI, A., MUROGA, T., Control of the nitrogen concentration in liquid lithium by the hot trap method, J. Nucl. Mater. **307–311** (2002) 1380–1385.
[25] KONDO, M., ISHII, M., HISHINUMA, Y., TANAKA, T., NOZAWA, T., et al., Metallurgical study on corrosion of RAFM steel JLF-1 in Pb-Li alloys with various Li concentrations, Fus. Eng. Des. **125** (2017) 316–325.
[26] XU, Q., KONDO, M., NAGASAKA, T., MUROGA, T., NAGURA, M., Corrosion characteristics of low activation ferritic steel, JLF-1 in liquid lithium in static and thermal convection conditions, Fus. Eng. Des. **83** (2008) 1477–1483.
[27] XU, Q., KONDO, M., NAGASAKA, T., MUROGA, T., YELISEYEVA, O., Effect of chemical potential of carbon on phase transformation and corrosion of JLF-1 steel in a static lithium, J. Nucl. Mater. **394** (2009) 20–25.
[28] NAKAJIMA, Y., KONDO, M., NOZAWA, T., Study on fabrication method of lithium alloys with metal grains, Fusion Eng. Des. **98–99** (2015) 2009–2014.
[29] KONDO, M., NAKAJIMA, Y., TANAKA, T., NOZAWA, T., YOKOMINE, T., Experimental study on chemical behaviours of non-metal impurities in Pb, Pb-Bi and Pb-Li by temperature programmed desorption mass spectrometer analysis, Plasma Fusion Res. **11** (2016) 2405076.

5. SUMMARY OF INTERFACES

V. Ignatiev (National Research Center, Kurchatov Institute, Russian Federation)
J. Konys (Karlsruhe Institute of Technology, Germany)

Fundamental knowledge about the deterioration of structural materials in the presence of liquid lead (Pb), Lead Bismuth Eutectic (LBE) and eutectic Pb–Li is essential for the construction and safe operation of fission and fusion reactors to be built in the near future as well as industrial-scale fast neutron reactors in the long term. Given that the structural materials are metallic, i.e. steels, elements of the solid metal will dissolve in the liquid metal, depending on the liquid metal chemistry. Depending on whether this mass transfer affects the metallic elements in proportion to their concentration in the solid material or is selective for specific constituents, the result is either a recession of the material surface or development of a near-surface depletion zone. Both reduce the thickness of the cross section capable of bearing the mechanical load acting on the material and may compromise other functions the material needs to fulfil as part of its service in the plant. Furthermore, a liquid metal in immediate contact may cause weakening of a solid metallic material beyond the thinning of the cross section that resulted from dissolution. A prominent example is the so-called Liquid Metal Embrittlement (LME) that occurs for specific combinations of liquid metal and solid metallic material, especially at low temperature and simultaneous action of mechanic stress in the solid material.

The key challenges, achievements and open issues have been identified as follows:

— In liquid sodium, corrosion phenomena, including liquid metal embrittlement are considered under control (authentic SS). In liquid lead and its alloys, corrosion issues may need mitigation strategies (steels). More investigations in liquid lithium (embrittlement & dissolution) are required.
— Oxygen addition to liquid lead and its alloys allow the use of steels up to 450°C. Localized corrosion hinders the use at higher temperatures. At temperatures above 450°C advanced mitigation strategies are required. Alumina forming steels or surface layers are one promising option. Insoluble coatings like alumina by Pulsed Laser Deposition (PLD) process is another option.
— Removal of moisture, metal chlorides, and other oxidizing impurities from all molten salt types are mandatory.
— Development of the understanding of synergistic effects of high temperature creep, molten salt corrosion and radiation damage on material performance has been achieved.
— Mapping of appearance of Stress Corrosion Cracking (SCC) as function of hydrogen content and test temperature is possible.
— For corrosion mitigation, aluminization by pack cementation and Al_2O_3 coatings by PLD have been developed but require demonstration under irradiation at relevant conditions.
— Tritium permeation reduction by a factor up to 10^5 at laboratory conditions by means of nanoceramic coatings was achieved, while for a fusion DEMO about 1000 is required, but behaviour under irradiation is still lacking.
— Regarding the investigations of oxide nanoceramics at extreme radiation levels (in fast reactor neutron spectrum), a corrosion resistance and mechanical stability following a 150 dpa irradiation could be shown.
— The SCC resistance testing of SUS310S has shown that SUS310S is less susceptible than SUS316L under ITER-Test Blanket Module (TBM) water conditions.
— The effect of nitrogen in Pb–Li alloys on the steel corrosion was newly discovered at Tokyo Institute of Technology.
— More modelling and simulation for proven and optimized corrosion mitigation measures is needed for all heavy liquid metal environments.
— Complementary validation of models calls for neutron irradiation facilities to study synergistic effects of the materials behaviour under relevant conditions (e.g. neutron spectrum, flux, temperature, magnetic field, etc.).
— Studies of the kinetics of the boundary diffusion of tellurium in candidate alloys and of the mechanism of their tellurium intergranular embrittlement need to be carried out under non-

isothermal conditions simulating the operation mode in the fuel circuit of the MSR. The metallurgy properties of these alloys need to be studied in more detail and especially under irradiation.

Currently, several ongoing or planned projects intend to address and overcome the knowledge gaps in order to meet the near-term R&D needs for coolants for fission and fusion environments. Some examples of ongoing/planned projects include:

— 14 MeV neutron sources are being built worldwide in the USA and China for materials testing, validation of nuclear data and numerical tools, blanket testing, etc. In particular, EU is working on an accelerator-based neutron source International Fusion Material Irradiation Facility–DEMO-Oriented Neutron Source (IFMIF-DONES) and also Japan is planning a facility based on a similar technology. All are aiming to provide irradiation data for the qualification of materials for the EU DEMO.
— At CAS-INEST China, several test systems are operated and are being build (CLEAR-series) to investigate the feasibility and credibility of reactor design options for future lead-cooled ADS, lead fast reactor and hybrid systems.
— Additionally, at ENEA, Italy and at CAS-INEST, China, large-scale loops are being operated to investigate the corrosion behaviour of Reduced Activation Ferritic/Martensitic (RAFM) steels in flowing PbLi in the presence of a fusion-relevant magnetic field. Furthermore, both labs are looking on the impurity management in PbLi by introducing Fe-trapping in their loop systems.
— At J-PARC, Tokai-mura, Japan evaluates the coupling of their existing linear accelerator with a subcritical LBE target (TEF-T) and the erection of a small reactor-like facility (TEF-P), operated with small amounts of minor actinides, to study the physics of such systems.
— Within the framework of the EUROfusion consortium, at KIT (Germany), PICOLO, ENEA LIFUS and IIT (Italy), and Rez (Czech Republic), comprehensive investigations on the corrosion behaviour in flowing PbLi and coating development for tritium permeation and corrosion reduction are being conducted.

CORROSION OF STRUCTURAL MATERIALS BY LIQUID METALS USED IN FUSION, FISSION AND SPALLATION

D. FÉRON, J.-L. COUROUAU
Den-Service de la Corrosion et du Comportement des Matériaux dans leur Environnement,
CEA – Université,
Paris – Saclay, France
Email: Damien.feron@cea.fr

Abstract

Liquid metals (lithium, sodium, lead and its alloys Pb-Li or Pb-Bi) are used as coolants for fusion, fission or spallation reactors due to their thermal and nuclear properties. However, these liquid metals are corrosive when they come into contact with solid metallic materials. Preserving structural alloys (no- and low alloyed steels, stainless steels, nickel-based alloys) in contact with these liquid metals requires the knowledge of the corrosion phenomena that may occur: mainly liquid metal embrittlement and general corrosion with mass transfers within the heat transfer circuit. Liquid metal embrittlement is a particular case of stress corrosion cracking in liquid metals which results in a decrease of the toughness or the ductility of the structural materials in association with a brittle fracture surface. Wetting, temperature, stress and strain rates, solid and liquid metal compositions are key factors. General corrosion mechanisms in liquid metals are governed by thermodynamics and may be divided into two main phenomena: (i) reaction with impurities, oxygen mainly (and other soluble interstitial elements such as carbon, nitrogen, hydrogen and boron); and (ii) dissolution of alloying elements which is function of their solubility in the liquid metals. Liquid metal chemistry is then a key parameter for general corrosion of structural materials. As the solubility is generally decreasing with temperature, mass transfer plays an important role in non-isothermal systems with dissolution in the hottest section and precipitation in the coldest parts of the circuits.

1. INTRODUCTION

Coolants required for use in advanced nuclear energy systems such as Fast Neutron Reactors (FNRs), Fusion reactors and Accelerator Driven system (ADS) need specific properties: high heat transfer coefficients are required since the power density in these systems is significantly higher than the previous generation of nuclear reactors. The operating temperatures are also higher in order to increase the efficiency of these systems, so their coolants need to have high liquidus range. Liquid metals with high thermal conductivity, high boiling point and adequately high specific heat meet these requirements, even at low pressures. The coolant of FNRs need to possess low neutron absorption cross section and be a poor moderator for achieving high neutron economy and for sustaining the hard neutron spectrum. Liquid sodium has been the coolant of choice for FNRs while liquid lithium or Pb–17Li alloy is considered as tritium breeder coolant in fusion systems. Liquid lead and Lead–Bismuth Eutectic (LBE) alloy are the candidate coolants for neutron breeder of ADS as well as for FNRs. The main thermo-physical properties of these liquid metal coolants are compared with those of water in Table 1.

In these advanced nuclear energy systems, controlling corrosion due to liquid metals stands as a major challenge. Corrosion of structural materials by liquid sodium, lithium, lead or its alloys may act according to various mechanisms [1, 2, 3, 4]: (i) intergranular penetration of the liquid metal into the solid and embrittlement of the solid by the liquid; (ii) formation of intermetallic compounds; (iii) reaction with dissolved impurities (oxygen, carbon, nitrogen); (iv) dissolution of the solid into the liquid metal. Moreover, in presence of a thermal gradient, dissolution–deposition phenomena may occur between hot and cold areas. This may generate materials degradation in hot areas, deposition or even plugging in cold areas.

For this overview of main corrosion phenomena of structural materials (mainly steels and stainless steels) focus will be put on liquid metal embrittlement (§2), oxidation (§3) and dissolution (§4).

TABLE 1. THERMO-PHYSICAL PROPERTIES OF LIQUID METAL COOLANTS COMPARED TO WATER [1, 2, 4]

Property	Coolant					
	Sodium	**Lithium**	**Pb–Li**	**Pb**	**LBE**	**H_2O**
Melting Point (K)	371	453.5	507	600.5	398	273
Boiling Point (K)	1156	1620	-	2018	1901	373
Density Kg/m^3 at 773 K	845	487	9486	10520	10150	0.99 at 323 K
Thermal conductivity at 773K (W/(K.m)	68.8	53.5	17	17.1	14.2	0.67 at 323 K
Heat capacity kJ/(kg, K) at 773 K	1.269	4.212	0.187	0.150	0.146	1.339 at 323 K
Vapour pressure (Pa) at 773K	2 at 573 K	0.08	0.002	0.002	0.0024	101325 Pa at 373 K

2. LIQUID METAL EMBRITTLEMENT

Liquid metal embrittlement (LME) is the reduction in the elongation to failure that can be produced when normally ductile solid metals are stresses while in contact with liquid metal [5]. In other terms, a ductile solid metal or alloy experiences a loss, which might be drastic, in the tensile elongation when exposed to liquid metal. This phenomenon stands as a major issue for metallic alloys exposed to liquid metals. It is specific to a pair solid/liquid metal. Main LME factors include:

— Wetting which is a prerequisite to LME. Pre-exposure at high temperature is often necessary to get a good wetting of the liquid metal on the solid alloy. For instance, after a pre-exposure at 550°C during 1000 h in liquid lithium, austenitic and ferritic steels exhibit some susceptibility at 200–250°C in liquid lithium [6].
— Temperature: generally, LME is more important around the melting point and decreases when temperature increases. For instance, with the T91 steel (a 9% Cr martensitic steel) in a stagnant liquid Pb or LBE, the "tensile tests revealed an embrittlement of the material, more pronounced at low temperature, that disappears as the temperature is raised above 450°C [7, 8]. This behaviour is explained by the reduction of the surface energy of the bare metal induced by the adsorption of the liquid metal. When the steel is submitted to low cycle fatigue tests in presence of the liquid Pb–Bi eutectic at 300°C, its lifetime is significantly reduced compared to tests performed in air" [7].
— Irradiation: on susceptible materials, LME is enhanced by irradiation. For instance, LBE embrittlement effects on ferritic/martensitic (FM) steels have been studied by conducting slow-strain-rate tensile (SSRT) testing on T91 and F82H ferritic steels either in argon or in liquid LBE after irradiation to doses up to about 20 dpa. Tests in argon revealed significant irradiation-induced hardening and embrittlement effects (loss of ductility) as compared to the un-irradiated ones. Tests in LBE showed additional embrittlement effects induced by LBE, which increased with irradiation-induced hardening. As a consequence, the fracture strain of irradiated specimens was reduced to a very low level of about 2–3% [9].
— Solid metal microstructure and liquid metal impurities are also important parameters for LME susceptibility [1, 2, 3].

"It is generally considered that exposure of ferritic and austenitic steels to pure liquid sodium (with a low impurity content), under constant-load test conditions, does not produce a major effect on the rupture strength of these steels [2, 10, 11]. Moreover, regarding stainless steels containing nitrogen (added to steel to improve its mechanical properties at high temperature, and, so, its resistance to failure), such as those of 316L(N) grade, they display comparable times to failure under creep in pure sodium and air, as shown on Fig. 1" [22]. However, some creep-stressed specimens of AISI 304 austenitic steel when exposed to pure liquid sodium at 550°C presented reduced time to rupture and strain to rupture, associated with the last period of the creep rupture life, the range of tertiary creep [12]. The intergranular cracks were observed in the deformed parts of the specimen and are thought to be related to decarburization of the specimen. Accordingly, the same grade of steel presented a slight reduction of the ductile area in association with intergranular brittle fracture in area of high plastic deformation where martensitic transformation (γ to α') occurred in relation with very fine microstructure [13].

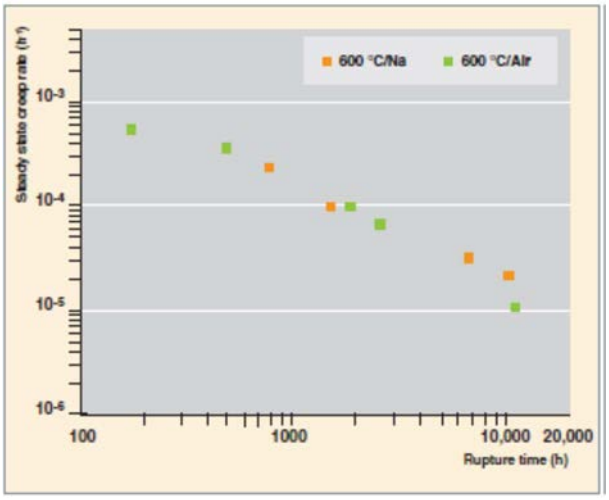

FIG. 1. Influence of the surrounding environment (air/sodium) on the time to rupture of a stainless steel at 600°C. In sodium, this time to rupture is comparable to that obtained in air at the same temperature [4].

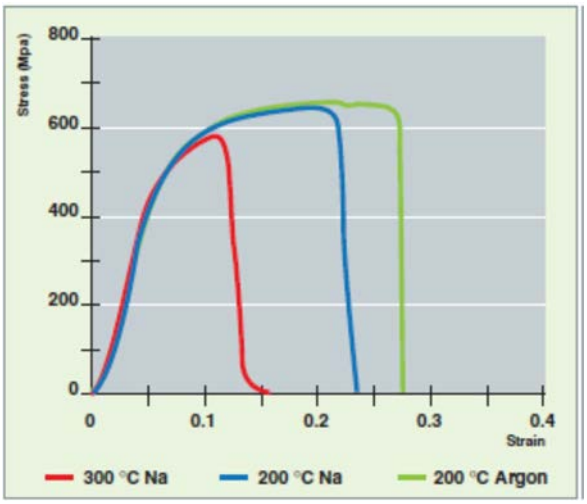

FIG. 2. Stress-strain curves relating to a low-alloy steel in sodium and argon at 200°C and 300°C, at 10^{-6} s^{-1} [4].

"With impurity concentrations typical of sodium-cooled reactors, a certain susceptibility of unalloyed or low-alloy steels (up to 9% chromium) can be observed during the very severe slow strain rate tensile tests, at temperatures between 200°C and 400°C, as displayed on Figure 2 for a low-alloy steel [9]. As evidenced by the observations carried out, microstructure and non-metallic impurities present in the alloy have a great impact on these phenomena of embrittlement by liquid sodium. At higher temperatures, a sharp change of behaviour can be seen, so that embrittlement by liquid sodium no longer seems to ever take place" [10–11, 22].

Accidents (e.g. water or air leaks) may increase impurity concentration in liquid sodium and may lead to cracking, even if it is not a LME phenomenon: sodium hydroxide (NaOH) causes stress corrosion cracking (SCC) in both ferritic and austenitic steels in liquid sodium contaminated by NaOH, if its concentration, temperature and stress are sufficiently high [14]. "In addition, stress corrosion cracking phenomena may occur owing to the presence of aqueous sodium hydroxide when the component, covered by a residual sodium film, is contaminated by moisture, with local generation of aqueous sodium hydroxide. At temperatures higher than 80°C for ferritic steels, and higher than 110°C for austenitic steels, transgranular cracking may take place very rapidly. Such temperatures may occur during facility preheating" [22] after repair, and then during sodium filling. It is therefore required to avoid any residual presence of aqueous sodium hydroxide on components, especially in gaps and clearances of structures and circuits, which is obtained through relevant washing and drying procedures [4, 14].

In summary, regarding the susceptibility liquid metal embrittlement of structural materials (i.e. the diminution of strain or of the maximum stress before rupture):

— Ferritic & martensitic steels, including ODS materials, are susceptible to LME in lead and its alloys (PbLi and PbBi) and some (low) susceptibility is observed in sodium and lithium at low temperatures [15].
— Austenitic stainless steels exhibit some susceptibility at low temperatures in liquid lithium and a low or negligible susceptibility in liquid lead and its alloys.
— No susceptibility has been observed in liquid sodium on austenitic steels. However, recent studies on both austenitic and ferritic/martensitic steels have shown that by increasing the oxygen activity in liquid sodium, a degradation of mechanical properties is observed, which was dependent also on other parameters (exposure time and temperature, wetting condition) [16, 17].

Other types of cracking may be observed, mainly in liquid sodium, due to the formation of sodium hydroxide during pollution periods (like during shutdowns).

3. OXIDATION

The corrosion process will depend on the thermodynamic data which indicate the products to be formed. According to thermodynamics, reactions between elements from the solid alloy (iron, nickel, chromium) and dissolved species (oxygen, carbon, nitrogen) in the liquid metal can be predicted depending of the activity or the chemical potential of the dissolved species [1, 2, 3, 4, 18]. For oxygen, which is the more common impurity, the formation of oxides solid compounds is given by predominance thermodynamic diagram called Ellingham diagram. This diagram represents the equilibrium oxygen partial pressure of metal oxidation reactions, as shown in Figure 3. Following this diagram, it is not possible to form iron, nickel neither chromium oxides in liquid lithium, and in liquid lead-lithium. But in lead and in lead-bismuth eutectic (the BiO/Bi reaction is not represented in Figure 3 but it is above the PbO/Pb equilibrium), metallic oxides (Fe, Cr, Ni) can be formed if the oxygen content is high enough in liquid sodium, sodium oxide Na_2O is more stable than NiO, magnetite Fe_3O_4 and even chromium oxide below 500°C. Only ternary oxides like $NaCrO_2$ are more stable than sodium oxide and can be formed if the oxygen content is high enough.

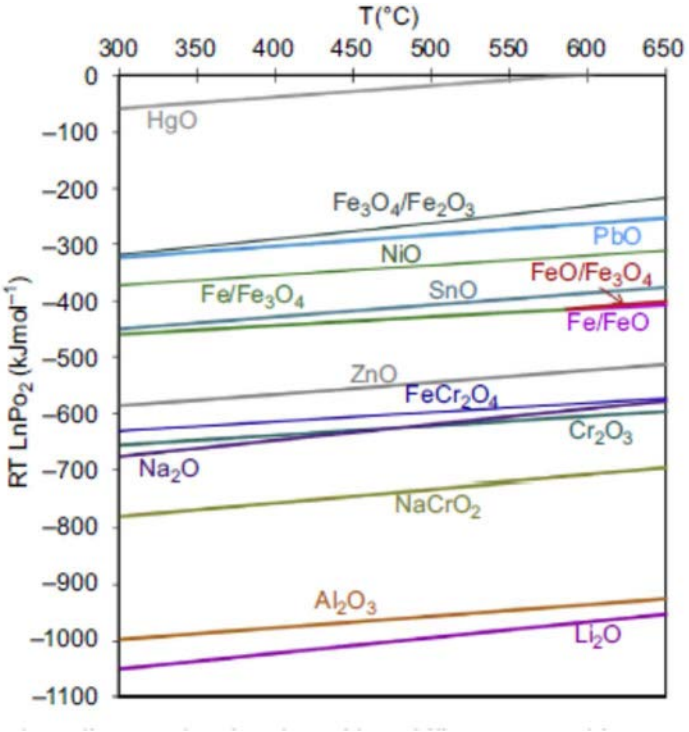

FIG. 3. Ellingham diagram showing metal oxide stability as function of oxygen potential and temperature [1, 2, 4, 18].

In lead and lead–bismuth alloy, one way of protecting materials against corrosion "lies in the in situ formation of a protective oxide layer on the surface of materials (austenitic or martensitic steels). Such a layer can be formed on the solid's surface by finely controlling the dissolved oxygen content, while avoiding lead oxide precipitation within the liquid metal. Yet, only through a strict control and accurate measurements of the oxygen content in the whole facility can this method prove to be successful. Ensuring the good behaviour and resistance of these oxide layers first requires understanding their formation mechanism, then modelling the oxidation kinetics in order to predict long term steel behaviour under given conditions" [22]. Martensitic steels Fe–9Cr were particularly investigated in as much as they are considered as the candidate material for the spallation target window in hybrid reactors. In all the cases, a duplex oxide layer is seen to form on contact with steel (Figure 4): it consists of an internal layer of Fe–Cr spinel on which a magnetite outer layer is superposed on contact with the liquid alloy. The nature of these two layers is identical whatever the test temperatures may be (between 470°C and 600°C).

So, controlling the dissolved oxygen content in liquid lead alloys is of key importance for creating the thermodynamic conditions required for the formation of a protective oxide layer on the structural steel surface, consisting of iron and chromium oxides. "The formation of this layer is much alike the in-situ building of a barrier against material transfer, which significantly reduces diffusion of alloying elements (especially, iron) towards the liquid. Yet, a strict control of the oxygen content in the whole facility is the condition required for this method to be fruitful. Moreover, dissolved oxygen activity has to be controlled within relatively narrow operating limits (Figure 5), so as to reach an oxygen content not only higher than the threshold value for the formation of iron and chromium oxides, i.e. the condition required for protecting structures, but also lower than lead oxide (PbO) solubility, that results in precipitation of solid crystals likely to be deposited on heat exchanger walls or to plug narrowed passage sections partially or even fully" [19, 22].

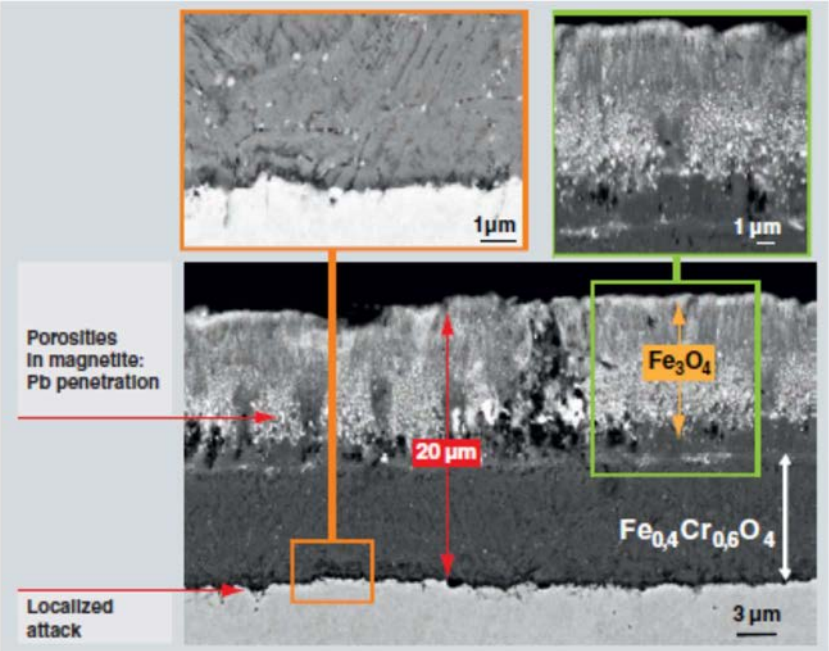

FIG. 4. Backscattered-electron image of a cross-section of a steel (T91) immersed for 3600 hours into oxygen-saturated Pb–Bi alloy at 470°C [4].

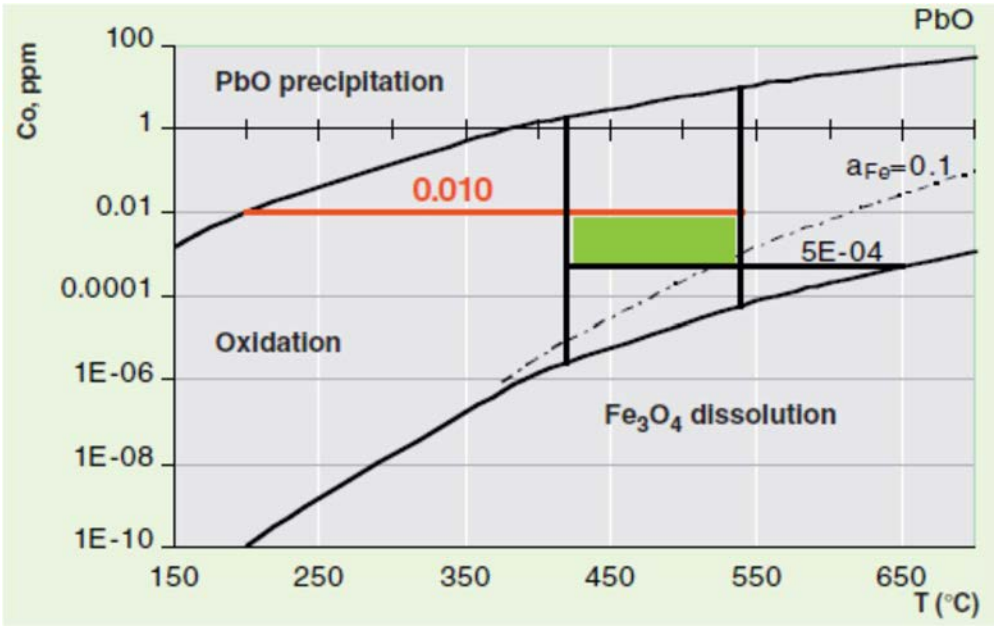

FIG. 5. Allowable range of oxygen concentration (Co in ppm) for the lead-bismuth eutectic of primary coolant (420–540°C). The allowable area is represented by the green section, circumscribed by the vertical (cold and hot collector temperature) and horizontal lines that stand for the threshold concentrations in equilibrium with lead oxide formation at the coldest wall temperature (200°C–10^{-2} ppm) with iron oxide dissolution at the hottest wall temperature of the system (650°C–5.10^{-4} ppm) [3, 4].

In liquid sodium, uniform corrosion rates increase with the oxygen activity, which indicates that the ternary oxide layer, if formed, has no protective effects. Uniform corrosion rates up to 500 µm per year has been observed at 650°C with 25 to 50 ppm of oxygen on austenitic stainless steel (316L type). The corrosion rate of austenitic steels in liquid sodium between 450°C and 700°C is estimated to be proportional to oxygen concentration in the range 5 to 100 ppm. The exact mechanism at play in this oxygen enhanced dissolution is still to fully elucidate, though the intermediate formation of Na–Cr–O and Na–Fe–O complexes were hypothesized since the 70ies to justify the straight increase of the iron solubility with the oxygen content [20, 21]. In any case, the policy to maintain the oxygen content to the lowest achievable level, typically lower than roughly 10 wppm, make the corrosion rates almost negligible on the long term in liquid sodium systems below 550°C.

The behaviour of structural materials under oxidizing conditions (with high dissolved oxygen) can be summarized as follow:

— In lead and lead bismuth alloy, the formation of oxides may have protective properties and high chromium steels improve the corrosion resistance, but a strict range of oxygen concentrations needs to be followed in order to avoid dissolution of the oxides and precipitation of lead oxide. Mitigation includes protective coatings (typically Al_2O_3) or steels with some aluminium content to form a self-healing protective layer.
— In liquid sodium, the corrosion rates increase with dissolved oxygen, though the full understanding of the effect of oxygen is still to be completed; the efficient oxygen control in reactor systems makes uniform corrosion rates low and not critical.
— No oxidation of iron, chromium, nickel occurs in liquid lithium neither in lead-lithium due to the low oxygen activity in these liquid metals.

4. DISSOLUTION

In liquid metals, the dissolution of a solid metal can occur when: (i) the oxides forms by the liquid metal (or alloy) are more stable than those formed from the solid metal (it is what happens in liquid lithium or lead-lithium); (ii) if the oxygen concentration is lower than the required concentration needed to form oxides from the solid metals, like it may happen in sodium, lead or lead–bismuth. The solubility of the main alloying elements becomes a key parameter for the behaviour of solid metals in liquid metals. As shown in table 4, nickel is the most soluble element whatever is the liquid metal. So, nickel base alloys will not be suitable for these environments.

TABLE 2. SOLUBILITY OF THE MAIN ALLOYING ELEMENTS AT 500°C (SELECTED DATA COMING FROM REFERENCES 2, 3, 9 & 11 / LARGE SCATTERING BETWEEN AVAILABLE DATA)

Liquid metal	Fe (ppm)	Cr (ppm)	Ni (ppm)
Lithium	4	4	200
Sodium	0.2	0.005	1
Lead	0.8	0.1	5,000
Lead–Bismuth	5	50	50,000
Lead–Lithium	1	10	3,000

"General corrosion mechanisms of austenitic steels in liquid sodium were investigated in the 70s–80s and described in the literature devoted to this topic. They consist in a dissolution of the surface elements in steel (Fe, Cr, Ni, Mn), in contact with sodium, followed by their transfer and deposition, or diffusion, on the reactor structures. This deposition phenomenon represents the main vector of contamination of reactor structures by activated corrosion products. The dissolution phase can be divided into successive time steps" [22] including:

(a) The dissolution of austenite which occurs mainly at temperatures higher than 550°C and consists in a selective dissolution of nickel present in the austenitic phase.
(b) The formation of a ferritic layer linked to the preferential dissolution of the nickel present in steel from the outer austenitic layer which causes steel to be ferritized. This ferritic layer is also dissolved, but at a slower rate, in liquid sodium (iron and chromium are also soluble in sodium to a lesser extent than nickel).
(c) A steady state regime is reached when the thickness of the ferrite layer has reached its threshold value; the rates of alloying element dissolution and diffusion towards sodium correspond with a 'stoichiometric corrosion' of austenite, i.e. the relative quantities of metallic elements dissolved correspond with those of the initial alloy, as shown in Figure 6.

In pure sodium (i.e. oxygen concentration lower than e.g. 5 ppm), corrosion corresponds with a dissolution of metallic elements in liquid sodium, as expressed here above. If temperatures are not too high (e.g. up to 550 °C), this phenomenon is relatively slow, corrosion is therefore limited.

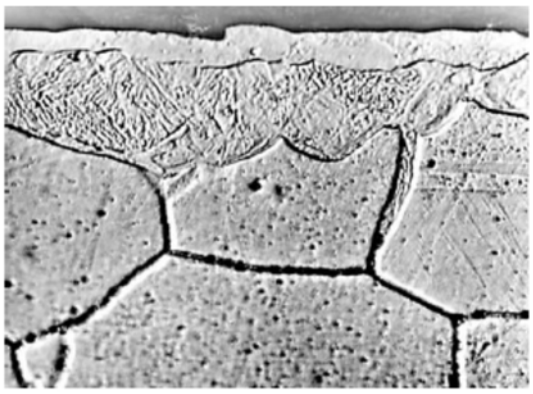

FIG. 6. General corrosion of an austenitic stainless steel in liquid sodium with low oxygen content (< 5 wppm, presumably 650°C, 8 m.s^{-1}, 8000 h, and grain of 25–50 µm). The picture shows the emergence of a ferritic film at the surface (Ferrite/Ferr).

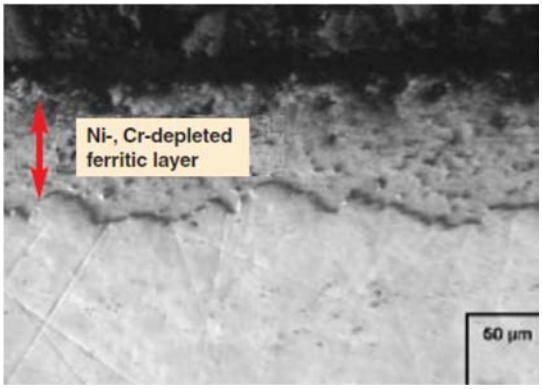

FIG. 7. General corrosion of an austenitic steel after immersion for 3000 hours at 500°C into liquid Pb–Bi with a low oxygen content (7×10^{-8} wt. %) [4].

Corrosion studies have evidenced that in the case of pure lithium and Pb–17Li alloy, corrosion occurs as a dissolution phenomenon; regarding pure lead and Pb–Bi alloy, the corrosion mechanism varies according to the dissolved oxygen content in liquid metal: for oxygen concentrations lower than a critical minimum content needed to form oxides with solid metal alloying elements, corrosion takes place as a dissolution phenomenon, just as in lithium, Pb–17Li alloy or liquid sodium with low oxygen content.

Regarding 316L stainless steel, it undergoes a selective dissolution in these liquid metal environments as in liquid sodium: owing to the very high solubility of nickel in lead and lead alloys, it is preferentially dissolved, thereby inducing the formation on the steel surface of a ferritic porous layer consisting of a network of channels filled with liquid alloy (Fig. 7). Analyses have evidenced a very high depletion in nickel, chromium and manganese, as well as an iron enrichment [4].

In "Pb–17Li alloy, pure lead, as well as in Pb–Bi alloy (when the dissolved oxygen content is low), use of uncoated steel-316L is limited to moderate temperatures (below 350°C approx.), at which it does not undergo significant dissolution. So is it for ferritic/martensitic steels, and strictly in flow velocity ranges which do not induce high corrosion rates" [22]. If temperatures are higher (above 350°C approx.), steel dissolution rates become unacceptable, and materials protection need to be considered in order to ensure their corrosion resistance. This protection can be achieved either by outer coatings, or through liquid alloy chemistry (oxygen and formation of an oxide protective layer) for lead or lead–bismuth.

The behaviour of structural materials under reducing conditions (with low dissolved oxygen) can be summarized as follow:

— Preferential dissolution of nickel occurs under reducing conditions and leads to avoid nickel base alloys in most cases.
— In lead and its alloys (Pb–Li and Pb–Bi), the dissolution rates are more often too high above 350–400°C for ferritic and martensitic and austenitic steels. Mitigation measures include coatings.
— In liquid sodium, acceptable corrosion rates are observed up to 650°C in low oxygen content on ferritic and austenitic steels but more investigations are needed for long term behaviour and modelling.
— In liquid lithium, other alloys like vanadium and niobium alloys are under consideration.

5. CONCLUSIONS AND OUTLOOK

Among the corrosion issues which have not been detailed here above, two need to be mentioned: (i) carburation/decarburation, nitruration/denitruration, which occurred at high temperature – typically above 550°C, and (ii) transfer processes which include dissolution in hot parts of the circuit and precipitation in the colder parts and which have major influence in non-isothermal systems leading to the issue of contamination by radioactive species (54Mn, 60Co). These corrosion issues need to be included together with LME, oxidation and dissolution phenomena when the choice of structural materials need to be done.

In conclusive remarks, it could be outlined that:

— In liquid sodium, corrosion phenomena, including liquid metal embrittlement, are considered under control in expected environmental conditions (low oxygen, maximum temperature of 550°C/600°C). Mechanisms and modelling are still needed for long term issues.
— In liquid lead and lead-bismuth, corrosion issues need mitigation strategies which are under development.
— More investigations are needed in liquid lithium either regarding mitigation or other alloys like vanadium or niobium alloys.

ACKNOWLEDGEMENTS

The authors would like to thank CEA-Den for the authorization of reproducing part of the text and the above figures from the e-den monograph on corrosion and alteration of nuclear materials (from Ref. [4]).

REFERENCES

[1] YVON, P., Structural materials for Generation IV nuclear reactors, Woodhead publishing, Cambridge (2017).
[2] FÉRON, D., Nuclear corrosion science and engineering, Woodhead publishing, Cambridge (2012).
[3] Handbook on lead-bismuth eutectic alloy and lead properties, materials compatibility, thermal-hydraulics and technologies, EAN-NEA, OECD publications, Paris (2007).
[4] FÉRON, D., RICHET, C., Corrosion and alteration of nuclear materials, CEA-Den, Editions Le Moniteur, Paris, (2010).
[5] NICHOLAS, M.G., OLD, C.F., Review liquid metal embrittlement. Journal of Materials Science **14** (1979) 1 – 18
[6] BORGSTEDT, H.U., GRUNDMANN, M., The fracture of austenitic and martensitic steel in liquid lithium. Nuclear Engineering and Design **3** (1986) 273-286.
[7] LEGRIS, A., Vogt, J.-B., VERLEENE, A., SERRE, I., Wetting and mechanical properties, a case study: Liquid metal embrittlement of a martensitic steel by liquid lead and other liquid metals. Journal of Materials Science **40** (2005) 2459 – 2463.
[8] AUGER, T., SERRE, I., LORANG, G., HAMOUCHE, Z., GORSE, D., et al., Role of oxidation on LME of T91 steel studied by small punch test. Journal of Nuclear Materials **376** (2008) 336–340.
[9] LONG, B., DAI, Y., BALUC, N., Investigation of liquid LBE embrittlement effects on irradiated ferritic/martensitic steels by slow-strain-rate tensile tests. Journal of Nuclear Materials **431** (2012) 85–90.
[10] HILDITCH, J.P., HURLEY, J.R., SKELDON, P., TICE D.R., "The liquid metal embrittlement of iron and ferritic steels in sodium", Corrosion Science **37** (1995) 445–454.
[11] SKELDON, P., HILDITCH, J.P., HURLEY, J.R., TICE D.R, The liquid metal embrittlement of 9Cr steel in sodium environments and the role of non-metallic impurities", Corrosion Science **36** (1994) 593–610.
[12] BORGSTEDT, H.U., MATHEWS, C.K., Applied chemistry of the alkali metals. Plenum Press, New-York (1987).
[13] BARKIA, B., AUGER, T., COUROUAU, J.L., BOURGON, J., Multiscale investigation of crack path and microstructural changes during liquid metal embrittlement of 304L austenitic steel in liquid sodium. Corrosion Science **127** (2017) 213–221.
[14] BORGSTEDT, H.U., CHAMPEIX, L., "Corrosion in fast breeder reactors", EFC publication N°1, The Institute of Metals, London, (1989).
[15] KIMURA, A., KASADA, R., KOHYAMA, A., KONISHI, S., ENOEDA, M., et al., Ferritic steel-blanket systems integration R&D—Compatibility assessment, Fusion Engineering and Design **81** (2006) 909–916
[16] HÉMERY, S., AUGER, T., COUROUAU, J.L., BALBAUD-CÉLÉRIER, F., Liquid metal embrittlement of an austenitic stainless steel in liquid sodium. Corrosion Science **83** (2014) 1–5.
[17] BARKIA, B., AUGER, T., COUROUAU, J.-L., BOURGON, J., Wetting by liquid sodium and fracture path analysis of sodium induced embrittlement of 304L stainless steel. Journal of Materials Research **33** (2017) 121–129.
[18] BALBAUD-CELERIER, F., MARTINELLI, L., Phénomènes de corrosion dans les métaux liquides. Techniques de l'Ingénieur, Paris, COR640 V1, (2017).
[19] COUROUAU, J.L., ROBIN, R., Chemistry control analysis of lead alloys systems to be used as nuclear coolant or spallation target. Journal of Nuclear Materials **335** (2004) 264–269.
[20] WEEKS, J.R., ISAACS, H.S., A general model for the corrosion of steels in high velocity sodium (JANSSON, S.A., Ed.), Presented at the Chemical aspects of corrosion and mass transfer in liquid sodium, The metallurgical Society of the American Institute of Mining, Metallurgical, and Petroleum Engineers, New-York (1973) 207–222.
[21] KOLSTER, B.H., Mechanism of Fe and Cr transport by liquid sodium in non-isothermal loop systems. Journal of Nuclear Materials **55** (1975) 155.
[22] HAL-CEA,
hal-cea.archives-ouvertes.fr

CORROSION IN PB-ALLOY COOLED NUCLEAR REACTORS AND ADVANCED MITIGATION MEASURES

A. WEISENBURGER, G MÜLLER
Karlsruhe Institute of Technology,
Institute for Pulsed Power and Microwave Technology,
Karlsruhe, Germany
Email: Alfons.weisenburger@kit.edu

Abstract

Liquid Pb and PbBi are among the promising coolants for reactors operating in fast neutron spectrum. Beside its excellent neutronic properties, Pb and PbBi offer improved safety features. But, deficient compatibility of structural materials with the liquid metals especially at higher temperatures is a major challenge to be solved for the use of Pb and PbBi cooled fast nuclear systems like MYRRHA, BREST and others at time under consideration. The major driving force for corrosion attack is the solubility of steel alloying elements like Ni, Fe and Cr in the HLM. Addition of oxygen to the HLM to provide in-situ formation of protective oxide scales is the mitigation mechanism of choice but limits the operating temperature window. Ferritic steels are not considered at present due to their susceptibility to liquid metal embrittlement. The use of austenitic steels of 316-type is limited to temperatures below 450°C due to corrosion attack. Even at this temperature localized corrosion was observed at oxygen concentrations in the HLM of about 10^{-7} wt%. Beside composition and crystal structure, imperfections like twin boundary seems to impact the compatibility of the steel in HLM. To enlarge the operation window of HLM cooled nuclear reactors advanced mitigation measures are under investigation since several years. Alumina forming surface alloyed layers and bulk materials are one option to increase the operating temperature window to 600°C by increasing the corrosion resistant in oxygen containing liquid metals. Fully corrosion resistant coatings like alumina, TiN or W are additional possible options, but require the integrity of the coating at all operating conditions, which is less stringent for the protection methods that rely on in-operation forming capabilities.

1. INTRODUCTION

Liquid Pb and PbBi are among the promising coolants for reactors operating in fast neutron spectrum. Beside its excellent neutronic properties, Pb and PbBi offer improved safety features. But, deficient compatibility of structural materials with the liquid metals especially at higher temperatures is a major challenge to be solved for the use of Pb and PbBi cooled fast nuclear systems like MYRRHA, BREST and others at time under consideration.

The major driving force for corrosion attack is the solubility of steel alloying elements like Ni, Fe and Cr in the HLM (heavy liquid metal). Addition of oxygen to the HLM to provide in-situ formation of protective oxide scales is the mitigation mechanism of choice but limits the operating temperature window. Numerous experiments with ferritic and austenitic steels in recent years [1] allowed to define the possible operating ranges regarding temperature and oxygen content for both class of steel. Ferritic steels are not considered at time due to their susceptibility to liquid metal embrittlement. The use of austenitic steels of 316 type is limited to temperatures below 450°C due to corrosion attack. Even at this temperature localized corrosion was observed at oxygen concentrations in the HLM of about 10^{-7} wt% [2]. Beside composition and crystal structure, imperfections like twin boundary seems to impact the compatibility of the steel in HLM [3]. To enlarge the operation window of HLM cooled nuclear reactors advanced mitigation measures are under investigation since several years [1]. Alloying of strong oxide formers like Al into steel surfaces can shift the operating temperature window to 600°C and even higher [4]. FeCrAlY surface layers and bulk materials are one further option to increase the corrosion resistant in oxygen containing liquid metals [5]. Both methods rely on the in-situ oxidation capability of the modified or changed material. Fully corrosion resistant coatings like Alumina [6], TiN or W are additional possible solutions options, but require the integrity of the coating at all operating conditions, which is less stringent for the protection methods that rely on the in-situ forming capabilities.

This presentation will give an overview on involved corrosion (dissolution and oxidation) mechanisms and will discuss some of the advanced mitigation strategies (surface alloying and coating and new advanced alumina forming bulk materials) required for reliable long term operation at higher temperatures for HLM cooled fast reactors.

2. STEEL CORROSION IN LIQUID PB-ALLOYS

Compatibility of materials with Pb is mainly driven by the temperature dependant solubility of the alloying elements in the liquid Pb. Ni, Mn, Al and Si have substantial solubility of up to some wt% at 550°C as shown in Figure 1[1]. The main elements of steel, Fe and Cr, are less soluble but still some 10^{-5} wt% can't be neglected.

Practically insoluble are refractory alloys like W, Mo and Ta and most ceramics. Therefore, Ni containing metals like austenitic steels suffer more from dissolution attack than Ni free f/m steels like T91. However, mechanical tests performed in liquid Pb-alloy exhibit the susceptibility of f/m steels to LME [8, 9]. Therefore, f/m steels are beside their improved corrosion resistance and higher irradiation stability not considered any longer in the design of fast reactors cooled with Pb-alloys. To mitigate dissolution any direct contact between the steel and the liquid Pb needs to be avoided. The most appropriate method is the in-situ oxidation by dissolved oxygen [10]. The oxygen concentration is determined by the operating temperature range of the reactor (see Figure 2). PbO formation to avoid any related coolant channel blockage at the low temperature side and avoiding of corrosion attack on the other side limit both the temperature and the oxygen content. But, the limit by the Fe3O4 formation line as indicated in Figure 2 was shown to be too low [3]. E.g. at 450° 10^{-8} wt% dissolution attack was reported [1].

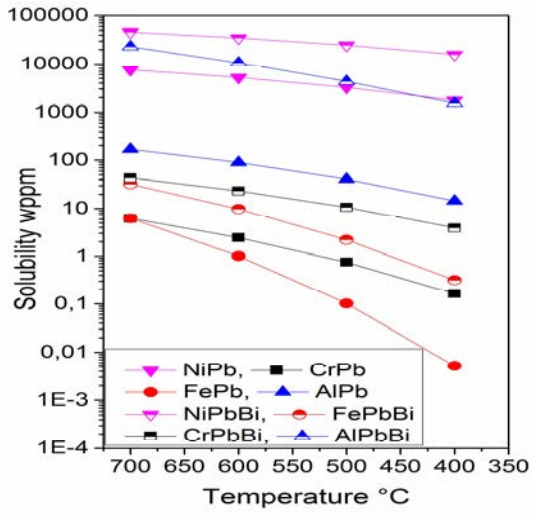

FIG. 1. Solubility of main Ni, Cr, Fe and Al in Pb and PbBi as function of temperature.

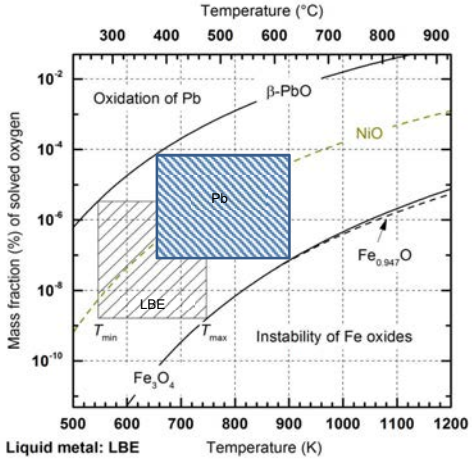

FIG. 2. Operating window in terms of oxygen content and temperature of Pb alloy cooled nuclear reactors.

The general corrosion mechanism for both coolants, Pb and PbBi, the dissolution of Ni accompanied by penetration of Pb into the steel matrix, is equivalent. However, the rate of dissolution and the resulting temperature and oxygen concentration limits might differ. Below 430°C, the maximum temperature of the reactor vessel of a Pb cooled fast reactor, even in LBE no dissolution attack was observed as long as the oxygen content is sufficiently high for the formation of oxide scales. In Pb an improved behaviour of the steels can be expected. However, if the oxygen concentration drops to low values even at this temperature dissolution attack will become an issue. The use of austenitic steels of 316 type is limited to temperatures below 450°C due to corrosion attack [1]. But, even at this

temperature localized corrosion was observed at oxygen concentrations in the HLM of about 10^{-7} wt% [2]. Beside composition and crystal structure, imperfections like twin boundary seems to impact the compatibility of the steel in liquid metals [3]. In dedicated dissolution experiments the preferential attack at those sides was clearly shown [11].

3. ADVANCED MITIGATION MEASURES

To enlarge the operation window of HLM cooled nuclear reactors advanced mitigation measures are under investigation since several years [1]. Three different advance mitigation measures are presented: (i) Insoluble ceramic coatings like TiN; (ii) Al2O3 and formation of alumina scales during operation either by surface alloying or by new developed bulk alloys like AFA-steels; (iii) MAXPHASE materials [12]. Evaluation criteria based on requirements are beside corrosion resistant up to 600°C at least the stability regards delamination for the coatings and the self-healing capability of the alumina formers. The latter is in any case the preferential one. Insoluble coatings were applied by many different methods including HiPIMS and RF-Sputtering and pulsed laser deposition (PLD). The first two method are already industrial and applied to generate TiN and AlTiN coatings on steel. Corrosion resistance was proven in tests at 550°C for 1200 h. Irradiation experiments in contact with PbBi performed at PSI Switzerland exhibit the brittle behaviour on such coatings especially under combined load of corrosion, irradiation and strain [1]. The PLD-process, still on lab scale, allows the coating of steels by amorphous alumina scales with nano-scaled alumina precipitates [6, 7]. The coating showed beside the expected good corrosion resistance in first test promising stability against delamination and also against irradiation. All methods relying on coatings have inherently no self-healing capability. If the coating has a defect the underlying base steel will be attacked. This aspect requires new strategies for service and maintenance. Mitigation measures that rely on the formation of alumina scale during operation have the advantage of being capable to heal scratched or re-new destroyed protective scales. Alloying of strong oxide formers like Al into steel surfaces or alloying of FeCrAlY surface layers can shift the operating temperature window to 600°C and even higher see figure 3[4]. The surface alloying is achieved by the so called GESA-process using an intense pulsed electron beam to alloy by surface melting a previously applied coating into the steel surface. New advanced alumina forming bulk materials like FeCrAl or AFA-steels or alumina forming HEA (high entropy alloys) use the same protection method of in-situ alumina formation [5, 13]. Minor additions of reactive elements like, Hf, Zr, Y and others foster the alumina formation in liquid Pb-alloys. The last option is a new class of materials called MAXPHASES [13]. The two MAX-phase materials Ti_3SiC_2 and Ti_2AlC ("tested at 550°C, 650°C and 700°C up to 10000 h in LBE with 10^{-6} and 10^{-8} wt% oxygen) exhibit strong influence of the secondary phases on corrosion. The major phase of both showed oxide scale formation at all conditions, while secondary phases rich in Al and Si exhibit locally interaction with the liquid metal, not surprisingly knowing the high solubility of pure Al and Si in liquid lead alloys. Single phase MAXPHASEs have a high potential to mitigate any corrosion attack" [16].

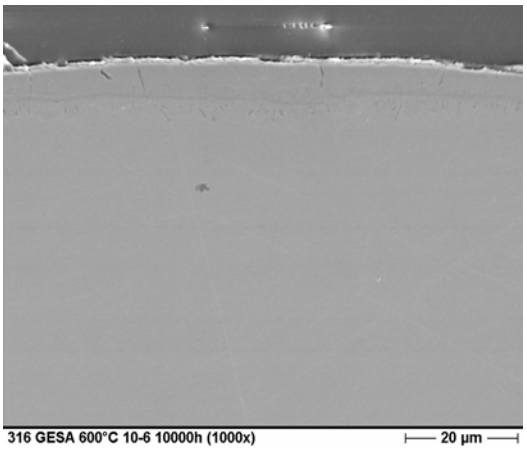

FIG. 3. 316L steel surface alloyed with Al.

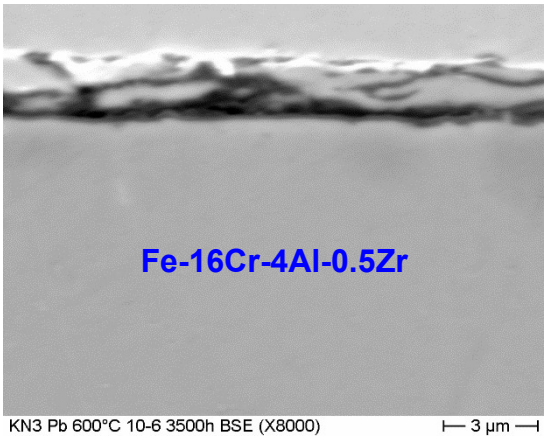

FIG. 4. FeCrAl with minor addition of Zr exposed to Pb at 600°C for 3500 h (un-effected).

As mentioned above, LME of f/m steels have excluded these steels from being considered as structural material in a Pb-alloy cooled reactor. One option to re-introduce the f/m steel T91 can be the surface alloying with aluminium. The influence of the coolant in creep strength test was negligible in case of surface aluminized T91 compared to the steel in the as-produced state (Fig. 5) [14].

Beside pure corrosion combined effects like erosion-corrosion in combination with high flowing velocities or fretting-corrosion are investigated. Fretting-corrosion is a specific type of wear occurring at fuel claddings and heat exchanger tubes. Fretting wear can lead to fuel clad penetration at the T91 and 15–15Ti steel of more than 10% of wall thickness already after 150 h at a frequency of 10 Hz [14]. Both steels show in addition a strongly increased wear with increasing temperature. The surface aluminized T91 steel has a superior resistance against fretting wear. Loads above 75N and amplitudes below 15 µm combined with surface aluminizing seems to be safe parameters.

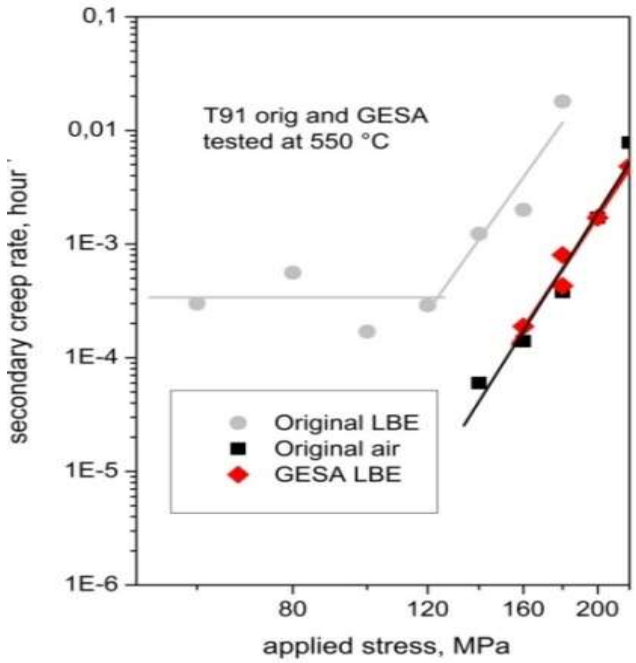

FIG. 5. Secondary creep rate in LBE and Air-threshold stress [14].

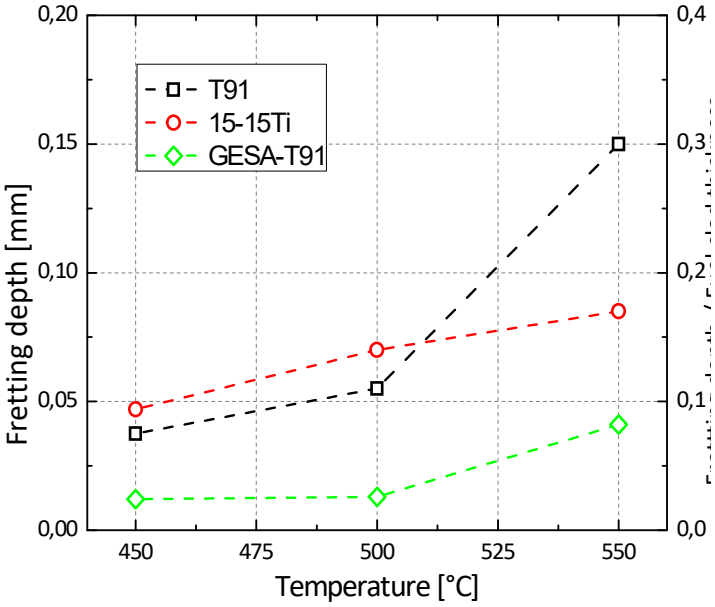

FIG. 6. Fretting damage as function of temperature [15].

4. SUMMARY, CONCLUSION AND OUTLOOK

— Solubility, oxygen potential, dissolution and oxidation kinetics are key parameters for material compatibility.
— Austenitic steels of 316L-type can be used in the temperature range up to 450°C if oxygen is ~10^{-6} wt%.
— Localized corrosion is one key issue and yet not fully understood.
— Advanced corrosion mitigation strategies are required for Pb-alloy cooled nuclear reactors. Alumina forming surface alloy or steels can mitigate corrosion and even deteriorating effects of coolant on mechanical properties.
— At present several EERA-JPMN and H2020 projects started to evaluate advanced corrosion mitigation strategies.

REFERENCES

[1] ORGANISATION FOR ECONOMIC CO-OPERATION AND DEVELOPMENT, Handbook on Lead-bismuth Eutectic Alloy and Lead Properties, Materials, Compatibility, Thermal hydraulics and Technologies, Edition, OECD, NEA (2015)
[2] TSISAR, V., SCHROER, C., WEDEMEYER, O., SKRYPNIK, A., KONYS, J. Nucl. Mater. **468** (2016) 305–312.
[3] HOSEMANN, P., FRAZER, D., STERGAR, E., LAMBRINOU, K., Scripta Materialia **118** (2016) 37–40.
[4] MÜLLER, G., HEINZEL, A., KONYS, J., SCHUMACHER, G., WEISENBURGER, A., et al., J. Nucl. Mater. **335** (2004) 163–168.
[5] WEISENBURGER, A., JIANU, A., DOYLE, S., BRUNS, M., FETZER, R., et al., J. Nucl. Mater. **437** (2013) 282–292.
[6] GARCIA FERRE, F., ORMELLESE, M., DI FONZO, F., BEGHI, M.G., Corrosion Science **77** (2013).
[7] GARCIA FERRE, F., MAIROV, A., IADICICCO, D., VANAZZI, M., DI FONZO, F., Corrosion Science **77** (2013).
[8] ERSOY, F., GAVRILOV, S., VERBEKEN, K., J. Nucl. Mat. **472** (2016) 171–177.
[9] VAN DEN BOSCH, J., BOSCH, R.W., SAPUNDJIEV, D., ALMAZOUZI, A., J. Nucl. Mat. **376** (2008) 322–329.
[10] WEISENBURGER, A., SCHROER, C., JIANU, A., HEINZEL, A., KONYS, J., et al., J. Nucl. Mat. **415** (2011) 260
[11] LAMBRINOU, K., CHARALAMPOPOULOU, E., VAN DER DONCK, T., DELVILLE, R., SCHRYVERS, D., J. Nucl. Mat. **490** (2017) 9–27.
[12] HEINZEL, A., WEISENBURGER, A., MÜLLER, G., J. Nucl. Mat. **482** (2016) 114–123.
[13] JIANU, A., FETZER, R., WEISENBURGER, A., DOYLE, S., MUELLER, G., J. Nucl. Mat. **470** (2016) 68–75.
[14] WEISENBURGER, A., JIANU, A., AN, W., DEL GIACCO, M., HEINZEL, A., et al., J. Nucl. Mat. **431** (2012) 77–84.
[15] DEL GIACCO, M., WEISENBURGER, A., MUELLER, G., J. Nucl. Mat. **450** (2014) 225–236.
[16] WEISENBURGER, A., LANG, F., MÜLLER, G., "Material and experimental issues related to the use of liquid metals as heat transfer media for CSP tower receivers", AIP Publishing (2018).

CORROSION OF STRUCTURAL MATERIALS IN MOLTEN CHLORIDE AND FLUORIDE SALTS

S. RAIMAN
Oak Ridge National Laboratory,
Knoxville, USA
Email: Raimanss@ornl.gov

Abstract

The molten salt reactor is attracting renewed interest lately, both from government and from private industry. Among the challenges which must be resolved before deployment of a working MSR is the identification of structural materials that resist degradation by molten salt.

1. SUMMARY

Hastelloy-N, developed for the Aircraft Reactor Experiment and used in the Molten Salt Reactor Experiment, was found to have acceptable chemical compatibility in fuel-containing fluoride salt for short operating lifetimes, but was susceptible to degradation at longer lifetimes and in more aggressive salt environments. Further, it was found to have poor mechanical properties at high temperatures, and was susceptible to embrittlement under irradiation, and cracking due to tellurium [1]. This operational experience suggests that the development of new materials and new techniques for corrosion mitigation are needed to allow for safe and economic operation of MSRs. Extensive work was done at Oak Ridge National Laboratory in the 1960s and 1970s using thermal convection loops to study corrosion of structural materials in fluoride salts [2–6]. The loops employed a design (shown schematically in Figure 1) in which one side of the loop was heated, while the other side was not. This served to both drive the flow of the loop, and to more accurately recreate the conditions in a reactor. The work is well summarized by Koger [7], Ignatiev and Surenkov [8], and Sridharan and Allen [9]. The Oak Ridge researchers (as well as others [10–12]) reported that the primary mechanism of alloy degradation in molten fluoride salts is selective dissolution of chromium from the alloy into the salt. It was found during loop testing that samples in the hot side of the loop lost mass due to chromium dissolution, while samples in the cold side gained mass due to deposition of chromium from the hot side.

In addition to thermal convection loops, static testing is also widely employed [10, 13–15]. Static tests can be conducted in an open crucible with a (usually inert) cover gas, or in a sealed capsule. Without imposing a thermal gradient on flowing salt, the specimen and the salt will reach equilibrium, so static tests are less predictive than loop experiments. However, capsule and crucible experiments can be used for comparing materials and for targeted corrosion studies to investigate specific phenomena in salt and alloys. Figure 2 shows the capsule testing setup used at Oak Ridge National Laboratory. Coupons are anchored to the lids of molybdenum capsules, filled partially with salt, evacuated, and welded shut. The molybdenum inner capsules are then sealed within stainless steel outer capsules and heated in a furnace.

When considering materials for molten salt systems, an important parameter is the stability of the metallic halide forms of the alloying constituents. The Ellingham diagram shown in Figure 2 shows the stability of several Cl compounds relevant to MSR structural materials. From the diagram, Chromium forms a relatively stable chloride when compared to nickel, molybdenum, and iron (The hierarchy of fluoride stability is similar to chlorides). Therefore, in a corrosive halide, chromium is the mostly likely alloy constituent to dissolve into the salt.

With these stabilities in mind, the materials most commonly used with molten salts are nickel-based alloys, since nickel is relatively stable as a metal in contact with halide salt. Several studies are available comparing nickel alloys [4, 16]. Candidate materials are generally low in chromium, and often include molybdenum additions, such as Hastelloy-N. Stainless steels have also been widely studied in fluoride salts [3, 17]. Iron based alloys have not shown good compatibility in salt compared to nickel alloys, but interest remains due to the relatively low cost and wide availability of iron-based alloys compared to nickel alloys.

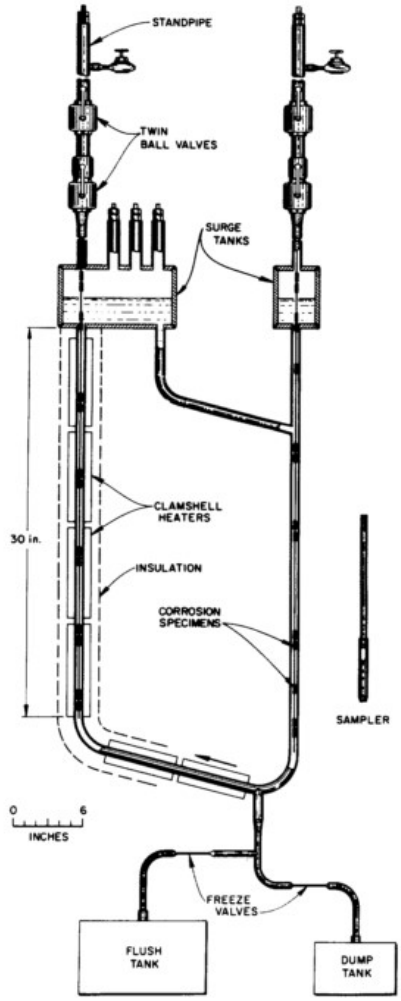

FIG. 1. Schematic drawing of a thermal convection loop used for corrosion studies in molten fluoride at Oak Ridge National Laboratory. Reproduced from Ref.[6].

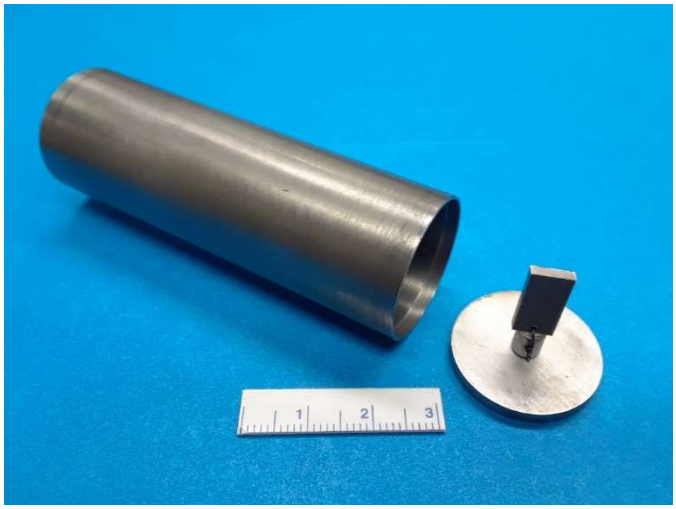

FIG. 2. An open molybdenum capsule with a corrosion coupon attached to one lid. The capsule is filled with salt, welded shut, and then sealed within a stainless-steel outer capsule. The scale shown in the image is in cm.

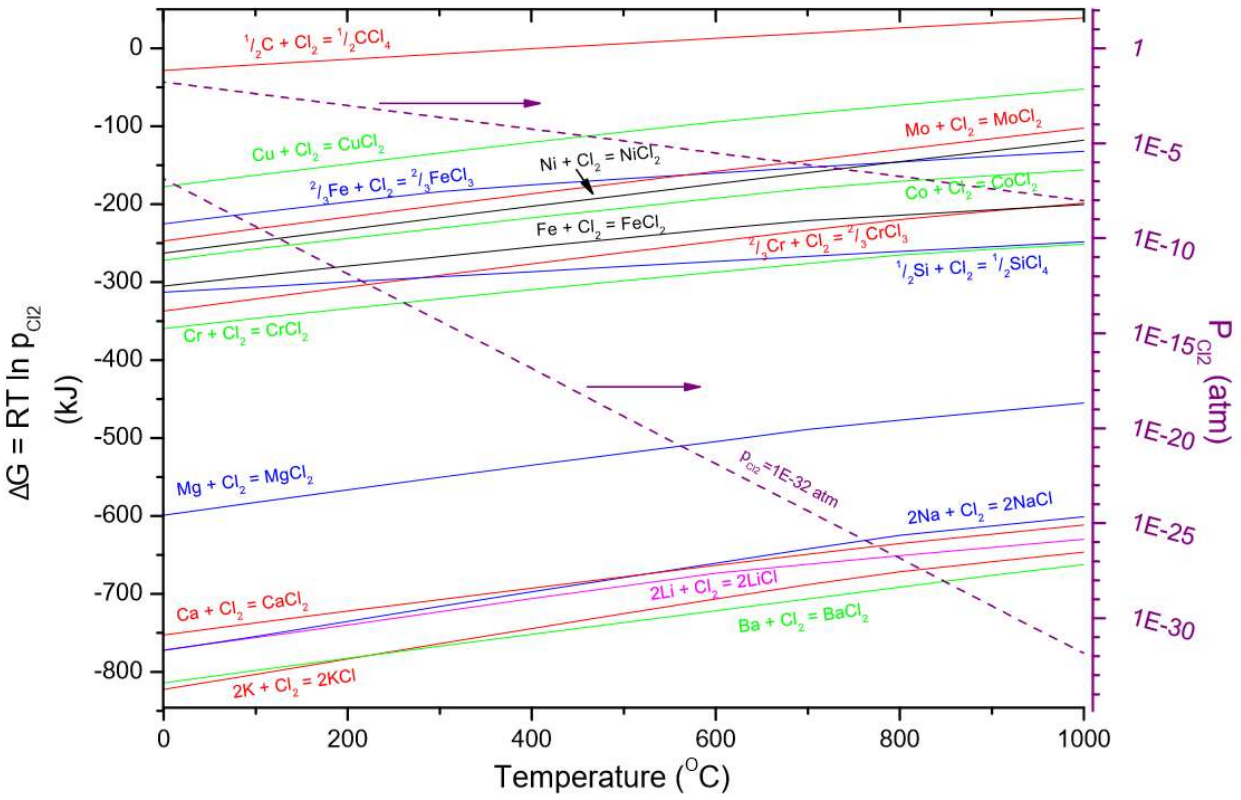

FIG. 3. Ellingham diagram of chlorides relevant to molten chloride reactors. Reproduced from Ref. [15].

2. CURRENT CHALLENGES

With renewed interest in molten salt reactors, several challenges lie ahead. Among them is the lack of data on material compatibility in chloride salts. Since the MSRE and other early MSR designs mostly utilized fluoride salts, there is a relatively large body of corrosion data on materials in fluoride salts. Since chloride fast reactors have only recently gained favour, corrosion data on alloys in Cl salts is very limited. Cl salts have previously need used for metal processing, and some data is available [18–21], but it varies in quality and applicability to MSRs (largely due to the impurity control required for MSR salts, which is not required for metal processing). Chloride salts have also been studied as a heat storage medium for concentrated solar power, as a higher temperature alternative to nitrate salts, and several works on corrosion of structural materials in chloride salts are available [14, 22, 23]. A primary disadvantage of these studies is that they do not include potential fuel salts, and they do not consider the effect of radiation on materials properties or salt chemistry.

Another challenge is the lack of modelling capability for molten salt corrosion. While experimental studies can be used to empirically predict materials performance within defined parameters, computational modelling is required to accurately predict material performance over a wide range of conditions, time scales, and material compositions. Unfortunately, the field of corrosion is lacking in predictive modelling capability. Even for light water reactors, physics-based predictive models for materials degradation do not exist, outside of a limited set of tools based on phenomenological data.

Calculation of Phase Diagrams (CALPHAD) codes have proven to be useful tool for making thermodynamic predictions and have already been used for calculating phase equilibria in salts. However, the calculation of phase equilibria relevant to alloy-salt interactions requires fundamental thermodynamic parameters such as Gibbs free energies and solubilities which can only be obtained from experimental data and are not fully described in molten fluoride and are even less complete in molten chlorides. Beyond thermodynamic modelling, true predictive capability will require the development of multi-physics models which incorporate corrosion kinetics with radiation and salt chemistry.

A third major challenge is the difficulty and long lead times inherent in the development of new materials for use with molten salt. Research and development of new materials can be a long process, and thorough testing is expensive and can take many years. In addition to being chemically compatible with molten salt, new materials must possess sufficient mechanical strength at high temperature, adequate creep life, and satisfactory radiation tolerance. Testing for all these properties requires a sustained multi-faceted R&D effort.

Additionally, a knowledge gap exists regarding the effect of fission products on material corrosion. Experience with the MSRE showed that tellurium production led to cracking of structural Hastelloy-N during reactor operation [1]. Current efforts are underway to predict fission product concentrations over reactor lifetimes, and this data will be useful for designing testing environments for material compatibility.

REFERENCES

[1] KEISER, J.R., Status of Tellurium-Hastelloy N Studies in Molten Fluoride Salts, ORNL/TM-6002, United States (1977).

[2] J.H. DEVAN, R.B. EVANS, Corrosion behaviour of reactor materials in fluoride salt mixtures, ORNL/TM-0328, United States (1962) 1–39.

[3] KEISER, J.R., DEVAN, J.H., LAWRENCE, E.J., Compatibility of molten salts with type 316 stainless steel and lithium, J. Nucl. Mater. **85–86** (1979) 295–298.

[4] KEISER, J.R., MANNING, D.L., CLAUSING, R.E., Corrosion resistance of some Nickel-Base Alloys to Molten Fluoride Salts Containing UF4 and Tellurium, in: Molten Salts, The Electrochemical Society, New York (1976) 315–328.

[5] DISTEFANO, J.R., DEVAN, J.H., KEISER, J.R., KLUEH, R.L., EATHERLY, W.P., Materials considerations for molten salt accelerator-based plutonium conversion systems, ORNL/TM-12925, United States (1995).

[6] KEISER, J.R., Compatibility studies of potential molten salt breeder reactor materials in molten fluoride salts, ORNL/TM-5783, United States (1977).

[7] KOGER, J.W., Evaluation of Hastelloy N Alloy After Nine Years Exposure to Both a Molten Fluoride Salt and Ait at Temperatures from 700 to 560C, ORNL TM 4189, United States (2017).

[8] IGNATIEV, V., SURENKOV, A., Alloys compatibility in molten salt fluorides: Kurchatov Institute related experience, J. Nucl. Mater. **441** (2013) 592–603.

[9] SRIDHARAN, K., ALLEN, T.R.R., Corrosion in Molten Salts, Elsevier Inc. (2013).

[10] OLSON, L.C., AMBROSEK, J.W., SRIDHARAN, K., ANDERSON, M.H., ALLEN, T.R., Materials corrosion in molten LiF–NaF–KF salt, J. Fluor. Chem. **130** (2009) 67–73.

[11] ZHENG, G., HE, L., CARPENTER, D., SRIDHARAN, K., Corrosion-induced microstructural developments in 316 stainless steel during exposure to molten Li2BeF4(FLiBe) salt, J. Nucl. Mater. **482** (2016) 147–155.

[12] LIU, M., ZHENG, J., LU, Y., LI, Z., ZOU, Y., YU, X., ZHOU, X., Investigation on corrosion behaviour of Ni-based alloys in molten fluoride salt using synchrotron radiation techniques, J. Nucl. Mater. **440** (2013) 124–128.

[13] ZHENG, G., HE, L., CARPENTER, D., SRIDHARAN, K., Corrosion-induced microstructural developments in 316 stainless steel during exposure to molten Li2BeF4(FLiBe) salt, J. Nucl. Mater. **482** (2016) 147–155.

[14] GOMEZ-VIDAL, J.C., TIRAWAT, R., Corrosion of alloys in a chloride molten salt (NaCl-LiCl) for solar thermal technologies, Sol. Energy Mater. Sol. Cells. **157** (2016) 234–244.

[15] AMBROSEK, J., Molten Chloride Salts for Heat Transfer in Nuclear Systems, University of Wisconsin (2011).

[16] SHANKAR, A.R., KANAGASUNDAR, A., MUDALI, U.K., Corrosion of nickel-containing alloys in molten LiCl-KCl medium, Corrosion. **69** (2013) 48–57.

[17] ZHENG, G., KELLEHER, B., CAO, G., ANDERSON, M., ALLEN, T., SRIDHARAN, K., Corrosion of 316 stainless steel in high temperature molten Li2BeF4 (FLiBe) salt, J. Nucl. Mater. **461** (2015) 143–150.

[18] MISHRA, B., OLSON, D.L., Molten salt applications in materials processing, J. Phys. Chem. Solids **66** (2005) 396–401.

[19] SANDNES, E., HAARBERG, G.M., MARTINEZ, A.M., OSEN, K.S., TUNOLD, R., Anode Processes on Carbon in Chloride Melts with Dissolved Oxides, Molten Salts Chemistry and Technology, John Wiley & Sons, Ltd (2014) 17–25.

[20] POLOVOV, I.B., TRAY, M.E., CHERNYSHOV, M.V., VOLKOVICH, V.A., VASIN, B.D., REBRIN, O.I., Electrode Processes in Vanadium-Containing Chloride Melts, (n.d.).

[21] C.A.C. SEQUEIRA, Electrodeposition of Ti from K2TiF6 in NaCl-KCl-NaF Melts, Molten Salts Chemistry and Technology, John Wiley & Sons, Ltd (2014) 287–294.

[22] VIGNAROOBAN, K., PUGAZHENDHI, P., TUCKER, C., GERVASIO, D., KANNAN, A.M., Corrosion resistance of Hastelloys in molten metal-chloride heat-transfer fluids for concentrating solar power applications, Sol. Energy **103** (2014) 62–69.

[23] KRUIZENGA, A.M.A., Corrosion Mechanisms in Chloride and Carbonate Salts, Livermore, SAND2012-7594, United States (2012) 34.

ADVANCED NUCLEAR REACTOR MATERIALS RESEARCH IN AUSTRALIA: HIGH TEMPERATURE PROPERTIES, RADIATION EFFECTS AND CORROSION BEHAVIOUR

O. MURÁNSKY, L. EDWARDS
Australian Nuclear Science and Technology Organisation,
Lucas Heights, Australia
Email: Ondrej.muransky@ansto.gov.au

Abstract

The Australian Nuclear Science and Technology Organisation (ANSTO) and its predecessor, the Australian Atomic Energy Commission has a long history in nuclear-based research and development. This is continuing through Australia's recent membership of the Generation IV International Forum (GIF). As Australia's implementing agent within GIF, ANSTO is focussing the majority of its research on nuclear materials engineering including structural performance evaluations in complex nuclear environments, advanced manufacturing, and system reliability assessment. Although this work concentrates on the Molten Salt Reactor (MSR) and Very High Temperature Reactor (VHTR) systems most of the research outcomes are applicable to a wide range of advanced nuclear reactor systems.

1. INTRODUCTION

With increasing global population and the threat of global warming linked to greenhouse gas emissions (as noted in the Paris Climate Agreement), it is vital that development continues to investigate sustainable, low-emission power generating systems. Nuclear-based energy systems produce low greenhouse emissions per MW of generated electricity and are well-suited for base-load power generation. However, since Fukushima there are still prevalent concerns over the safety and reliability of light water reactor systems. The next generation (Gen IV) of nuclear-based power generation systems is addressing the safety concerns by incorporating inherent safety features (e.g. passive cooling) that prevent fuel meltdown such as in the Fukushima, and Three Mile Island accidents. One of the most promising concepts of these reactors is the MSR design. The MSR system has attracted worldwide interest owing to its inherent safety, high efficiency of fuel utilization and low production of nuclear waste [1,2].

MSR research was first established in the 1950s and 1960s at ORNL and was re-vitalised when chosen as one of the six the most promising reactor systems by the GIF. Although initial progress on the MSR system since then has been relatively slow, there been a very substantial increase in interest in recent years. The community of national nuclear laboratories, university researchers and large nuclear companies that have typically led research and development of advanced reactor systems have been joined by an ever increasing number of small and medium sized private companies worldwide including many dedicated to the design and deployment of MSR-based system [3]. The vast majority of these are start-ups and in an era where many large public Nuclear Companies find market conditions challenging, they collectively have attracted very significant amounts of private capital and some governmental support. However, these developments have been accompanied by a dilution and diminution of the traditional nuclear supply chain capability worldwide. For these new advanced reactor concepts and systems, most of which are MSR-based systems, to succeed lower cost, agile, nuclear manufacturing chains capable of reaping the benefits of manufacturing scale need to be developed. However, it is important to recognize that these issues are common to all potential advanced reactor systems and, as such, present a key opportunity for cross-platform and cross research entity collaboration. Indeed, this is a common problem in many regulated industries, e.g. oil and gas, maritime and aerospace, and there is very significant global advanced manufacturing R&D effort looking at how high quality, lower cost safety critical components can be produced. Furthermore, the costs of assessing the Technological Readiness Level (TRL) of emerging technologies are high and as advances are very rarely linked to one reactor concept or company the area is highly fertile for large scale cross sector collaboration.

The rapid development and deployment of MSR systems in common with many other advanced rector systems is hindered by the development and standardisation of suitable structural materials. These materials are expected to withstand a combination of challenging operation conditions present in MSR systems: (i) high temperature; (ii) radiation; and (iii) molten salt [4–7]. Therefore suitable structural materials have to exhibit a combination of unique properties [6]: high temperature strength, microstructure stability, creep resistance, radiation resistance, fatigue resistance, minimum tritium retention, low activation, and corrosion resistance. Most of these requirements apply to any structural material used in any type of nuclear reactor however the molten-salt corrosion in MSR systems is partially challenging [4–6, 8]. This is due to the fact that unlike the oxide corrosion products, which are formed on the surface of alloys in oxygen-containing environment (air, water), the corrosion products forming in molten-salt environment (e.g. metallic fluorides) are unstable and easily dissolvable in the molten salt [9]. Hence, the

corrosion resistance of structural materials for MSR systems is directly dependent on the thermodynamic-driven dissolution of formed corrosion products [10].

Over the past decades, a number of nickel-based alloys (Hastelloy-N, GH3535, MONICR, Alloy-NM, HN80, EM-721) [4, 6, 11–13] have been developed specifically for application in MSRs. However, their high cost has severely limited their application and in turn hindered the development and deployment of MSR systems. In addition, the time required to qualify these new materials in design codes such as ASME III Subsection NH, RCC-MRX and the UK code R5 can take decades, thus imposing further delays to the deployment of MSR technology.

Informed by this background ANSTO has developed a portfolio of nuclear materials engineering research activities that are intended to support a wide range of MSR concept designs. This has included a collaborative Joint Research Center (JRC) with the Shanghai Institute of Applied Physics (SINAP) that was initiated by a major grant to both parties from the Australia-China Science Research Fund in 2012. SINAP has recently finished the design of a liquid-fuel MSR [13], and through a $3.3 billion investment from the Chinese government, will begin prototype construction of two molten salt reactors in the Gobi Desert (northern China). The mission of the ANSTO/SINAP collaboration is to conduct fundamental studies on the performance of materials in simulated Molten Salt Reactor (MSR) environments. To date we have focussed on high temperature creep, creep-fatigue damage, radiation damage and corrosion of nickel alloys and graphite. This paper summarises the current published progress in these areas.

2. ALLOY DEVELOPMENT

SINAP and ANSTO researchers have worked on the characterisation of the Ni–SiC [14, 15] and NiMo–SiC [16, 17] composites with varying amount of SiC (0.5–2.5 wt.%) for applications in MSR systems. These novel materials were developed by SINAP and are prepared by powder metallurgy route consisting of (i) high-energy ball milling of initial powder mixtures (mechanical alloying); (ii) spark plasma sintering (1150°C/50 MPa); (iii) rapid cooling; (iv) high temperature annealing; and (v) water quenching. The microstructural analysis revealed that the Ni–SiC composites consist of Ni-matrix and unreacted SiC nano-particles, while the microstructure of NiMo–SiC composites is more complex consisting of NiMo matrix, Mo_2C agglomerates, Ni_3Si nano-precipitates, and unreacted SiC nano-particles from the initial powder mixture. It has been shown [16, 17] that these newly developed materials have superior strength, but limited ductility. The strength of these materials stems from the combination of various strengthening mechanisms: dispersion strengthening (SiC), precipitation strengthening (Ni_3Si), solid-solution strengthening (Mo in NiMo matrix), and Hall-Patch strengthening (matrix grain refinement). On the other hand, the low ductility is likely the consequence of porosity present in the materials.

3. HIGH TEMPERATURE CREEP

The structural integrity, lifetime and ultimately the cost-effectiveness of power generating systems is directly dependent on the expected lifetime of its high temperature components in service. This is defined by the creep resistance of the employed materials. Creep damage is a significant problem for high temperature reactor components, which for MSR systems are expected to be around 700°C. GH3535 alloy developed by the Center of Thorium Molten Salt Reactor System, Chinese Academy of Science is intended to be used in Chinese MSR systems currently under development. Understanding the creep damage of the GH3535 alloy is therefore essential for determining the lifetime of a component in service and overall economy of MSR systems. Shrestha et al. [18] performed a number of creep tests at different temperatures (650, 700 and 750°C) under applied loads between 85 and 380 MPa. Based on the obtained results it has been determined that the maximum allowable design stress of the GH3535 alloy at 700°C is 35 MPa according to the ASME BPVC guidelines. This stress is above the operating stresses expected in the MSR system. In addition, the formation of secondary precipitates along the grain boundaries was observed during the creep testing. The chemical analysis revealed that these precipitates contain Ni, Mo, Cr, Si and C. The combination of microscopy and diffraction techniques revealed that secondary precipitates are M12C type precipitates [18, 19], while the primary precipitates found in as-received material as well as in the GH3535 welds are M6C type [19, 20].

4. RADIATION DAMAGE

Neutron irradiation research programmes are complicated, time consuming and, since they require large capital nuclear infrastructure, are very expensive. Indeed, there is arguably a shortage of reactors with fast neutron fluxes large enough to produce the radiation damage seen in nuclear structural materials over the expected lifetime of operational Gen IV reactors. Hence, the majority of the initial radiation damage science on new materials is usually undertaken using ion irradiation. Although a new alloy or process is highly unlikely to be qualified for reactor use

through ion irradiation studies alone, the technique provides fast irradiation times and, importantly, usually does not significantly activate the sample. It is these features that are the key reasons for its increasing popularity. A variety of ion species can be used as seen by the work described below.

Reyes et al. [21, 22] studied the effect of krypton irradiation (100 dpa) at elevated temperature (450°C) on the microstructure of GH3535 alloy using TEM and molecular dynamics modelling. This study revealed that two different types of dislocation loops were formed in the alloy – the first ½<100> (unfaulted loops) being away from pre-existing dislocations, whilst the second lying in {111} plane being closer to pre-existing dislocations. Molecular dynamics simulations indicated that unfaulted ½<100> dislocation loops may be formed in the collision cascades region during cascade relaxation. Whilst the observed dislocation loops on {111} planes form near pre-existing ½<110> edge dislocations by absorption of atoms from the collision cascade, leaving behind 1/3{111} Frank loops, which could act as a nucleation site for 1/6<112>{111} dislocations.

Huang et al. [23] studied the effect of nickel ion irradiation (0.5, 2, 12 dpa) at room and elevated temperature (600°C) on the microstructure of GH3535 alloy weld metal using XRD, TEM and nano-indentation. It was shown that nickel ion irradiation leads to formation of clusters or dislocation loops. Their size did not change with dose, while their number increased gradually. These irradiation-induced defects were found in both the matrix and also along pre-existing dislocations. There was clearly a lower density of irradiation-induced defects in samples irradiated at elevated temperatures. It is believed that this is due to the higher diffusion rate of defects at elevated temperature. In addition, Huang et al. [23] have shown that ion irradiation leads to hardening of the material and that, as expected, this effect is more pronounced when the samples are irradiated at room temperature.

Although it is important to know and understand the microstructural changes that cause radiation damage, measurement of its effect on the mechanical properties of irradiated components and structures is of critical importance for any successful reactor design. This is one the main deficiencies of ion irradiation since the transmission of ions into materials is orders of magnitude smaller than the penetration of neutrons. Thus, unless very expensive near relativistic accelerators are used, ion irradiation depth in samples is limited. To counteract this issue research is ongoing into the measurement of mechanical properties using small ion-irradiated samples. Reichardt et al. [24] studied the effect of helium ion irradiation on Ni single crystals using in-situ micro-tensile testing. The obtained results clearly show that the fracture strength is proportional to damage dose. While the un-irradiated sample did not fracture even at 57% of strain, the sample irradiated to 10 dpa showed first rupture at a strain of about 1.7% and failed completely at about 26%. The sample irradiated to 19 dpa showed first rupture at a strain of about 2.2% and complete fracture at about 22.5%. The increase in strength was found to be almost linear with dose with the hardening/dose slope determined to be 230–240 MPa/dpa.

5. MOLTEN SALT CORROSION

As mentioned above, the lifetime of a component in service in MSR systems is strongly influenced by the corrosion resistance of the material. Chinese-developed GH3535 alloy and NiMo–SiC composites are designed to withstand molten salt corrosion. ANSTO and SINAP researchers studied the corrosion resistance of these alloys in FLiNaK molten salt at different temperatures. Yang et al. [25] have studied the corrosion resistance of NiMo–SiC composites containing varying amount of SiC in FLiNaK salt at 650°C (200 h exposure). It has been found in Ref. [25] that the thickness of the corrosion layer and the material mass loss of these power-metallurgy prepared NiMo–SiC composites during the corrosion testing was directly proportional to the volume fraction of the Mo_2C, which was found to be proportional to the SiC content in the initial powder mixture. Zhu et al. [26, 27] studied the corrosion resistance of GH3535 alloy with and without helium ion irradiation damage in FLiNaK salt at 750°C (200 h exposure). It was found that helium bubbles act as nucleation sites for corrosion cavities resulting in significantly accelerated corrosion of ion-irradiated material in comparison to non-irradiated material. The corrosion cavities also coalesce with helium bubbles leading to the formation of large corrosion voids in the microstructure thus significantly extending the corrosion-affected layer. Interestingly, it was also found that the corrosion-induced cavities act as defect sinks and absorb the radiation-induced helium bubbles, leading to the absence of large helium bubbles in the corrosion-affected layer.

Apart from studying the molten salt corrosion of structural alloys, SINAP and ANSTO researchers studied infiltration of FLiNaK molten salt into different nuclear graphite (IG-10, 2114, G1, NBG-18, G2) under inert gas pressure (20 h and 100 h exposure). Zhoutong at al. in Ref. [28] clearly showed that that Chinese-developed G2 graphite displays the smallest weight gain suggesting the least FLiNaK salt infiltration. This work further shows the trend of increasing graphite weight gain during the molten salt exposure due to salt infiltration with increasing pressure gas pressure, while the increasing the exposure time from 20 h to 100 h had minimal effect.

6. SUMMARY

This paper reports aspects of Australia's research on advanced nuclear reactors systems related to its GIF membership. ANSTO, including through a major collaboration with SINAP, has undertaken research on candidate structural materials for MSR-based systems. The main focus of the research has been the development of new materials, and degradation of materials in service conditions (high temperature, radiation, and molten salt). The intent of this work has been to reduce impediments to the design, and deployment of novel MSR power-generation systems.

REFERENCES

[1] WALDROP, M.M., Nuclear energy: Radical reactors, Nature **492** (2012) 26–29.
[2] DOLAN, T.J., Molten Salt Reactors and Thorium Energy (DOLAN, T.J., Ed.), Woodhead Publishing (2017).
[3] BRINTON, S., The Advanced Nuclear Industry (2015), https://www.thirdway.org/report/the-advanced-nuclear-industry
[4] IGNATIEV, V., SURENKOV, A., Corrosion phenomena induced by molten salts in Generation IV nuclear reactors, Structural Materials for Generation IV Nuclear Reactors (2017) 153–189.
[5] IGNATIEV, V., SURENKOV A., Material Performance in Molten Salts, Reference Module in Materials Science and Materials Engineering (2016).
[6] YOSHIOKA, R., KINOSHITA M., SCOTT I., Materials, Molten Salt Reactors and Thorium Energy (DOLAN, T.J., Ed.), Woodhead Publishing (2017) 189–207.
[7] ZHU, H., et al, High temperature corrosion of helium ion-irradiated Ni-based alloy in fluoride molten salt., Corrosion Science **91** (2015) 1–6.
[8] PATEL, N.S., PAVLÍK V., BOČA M., High temperature Corrosion Behavior of Superalloys in Molten Salts – A Review, Critical Reviews in Solid State and Materials Sciences **42** (2017) 83–97.
[9] YE, X.-X., et al., The high temperature corrosion of Hastelloy N alloy (UNS N10003) in molten fluoride salts analysed by STXM, XAS, XRD, SEM, EPMA, TEM/EDS, Corrosion Science **106** (2016) 249–259.
[10] OLSON, L.C., et al., Materials corrosion in molten LiF–NaF–KF salt, Journal of Fluorine Chemistry (2009) 67–73.
[11] YIN, H., et al., Effect of CrF3 on the corrosion behaviour of Hastelloy-N and 316L stainless steel alloys in FLiNaK molten salt, Corrosion Science **131** (2018) 355–364.
[12] OUYANG, F.-Y., CHANG C.-H., KAI J.-J., Long term corrosion behaviours of Hastelloy-N and Hastelloy-B3 in moisture-containing molten FLiNaK salt environments, Journal of Nuclear Materials **446** (2014) 81–89.
[13] ZHANG, D., Generation IV concepts, Handbook of Generation IV Nuclear Reactors (2016) 373–411.
[14] HUANG, H., et al., Effect of Milling Time on the Microstructure and Tensile Properties of Ultrafine Grained Ni–SiC Composites at Room Temperature, Journal of Materials Science and Technology **31** (2015) 923–929.
[15] HUANG, H.F., et al., Mitigation of He embrittlement and swelling in nickel by dispersed SiC nanoparticles, Materials and Design **90** (2016) 359–363.
[16] YANG, C., The effect of milling time on the microstructural characteristics and strengthening mechanisms of NiMo-SiC Alloys prepared via powder metallurgy, Materials **10** (2017)
[17] YANG, C., et al., On the origin of strengthening mechanisms in Ni-Mo alloys prepared via powder metallurgy, Materials and Design **113** (2017) 223–231.
[18] SHRESTHA, S.L., et al., Creep resistance and material degradation of a candidate Ni–Mo–Cr corrosion resistant alloy, Materials Science and Engineering **674** (2016) 64–75.
[19] LIU, T., et al., Effect of Long term Thermal Exposure on Microstructure and Stress Rupture Properties of GH3535 Superalloy, Journal of Materials Science and Technology **31** (2015) 269–279.
[20] BHATTACHARYYA, D., et al., Characterization of complex carbide-silicide precipitates in a Ni-Cr-Mo-Fe-Si alloy modified by welding, Materials Characterization **105** (2015) 118–128.
[21] DE LOS REYES, M., et al., Defect evolution in a NiMoCrFe alloy subjected to high-dose Kr ion irradiation at elevated temperature, Journal of Nuclear Materials **474** (2016) 155–162.
[22] DE LOS REYES, M., et al., Microstructural evolution of an ion irradiated NiMoCrFe alloy at elevated temperatures, Materials Transactions **27B** (2014) 428–433.
[23] HUANG, H., et al., Temperature dependence of nickel ion irradiation damage in GH3535 alloy weld metal, Journal of Nuclear Materials **497** (2017) 108–116.
[24] REICHARDT, A., et al., In situ micro tensile testing of He+2 ion irradiated and implanted single crystal nickel film, Acta Materialia **100** (2015) 147–154.
[25] YANG, C., et al., On Molten Salt Corrosion of NiMo-SiC Alloys, 2018 (in preparation).
[26] ZHU, H., et al., High temperature corrosion of helium ion-irradiated Ni-based alloy in fluoride molten salt, Corrosion Science **91** (2015) 1–6.
[27] ZHU, H., et al., Effects of bubbles on high temperature corrosion of helium ion-irradiated Ni-based alloy in fluoride molten salt, Corrosion Science **91** (2017) 184–0193.
[28] HE, Z., et al., Molten FLiNaK salt infiltration into degassed nuclear graphite under inert gas pressure, Carbon **84** (2015) 511–518.

STRESS CORROSION CRACKING BEHAVIOR OF SUS316L AND SUS310S IN FUSION RELEVANT ENVIRONMENTS

Y. HUANG
Graduate School of Energy Science, Kyoto University

A. KIMURA
Institute of Advanced Energy, Kyoto University
Email: Kimura@iae.kyoto-u.ac.jp

Kyoto, Japan

Abstract

A brief background and current status of researches on Stress Corrosion Cracking (SCC) in hydrogenated hot water were delivered. Recent studies often dealt with water chemistry on maintaining structural integrity of aging reactors and available works on SCC in hydrogenated hot/pressurized water were summarized. The effect of dissolved-hydrogen content on SCC draws much attention in past decade. Also, searching the root cause of irradiation-assisted SCC continues. The two factors — dissolved-hydrogen and irradiation — were being considered critical in fusion relevant environment.

1. INTRODUCTION

Stress Corrosion Cracking (SCC) is one of major degradation issues in Pressurized Water Reactor (PWR) and Boiling Water Reactor (BWR). Since the first SCC incident reported by Coriou in 1959 [1], numerous inducing factors have been recognized. A common solution is replacing with more corrosion-resistant alloys. Water purification and water chemistry optimization are another approach. In PWR, lowering Dissolved-Oxygen (DO) and raise boron concentration have been implanted. In BWR, hydrogen injection and subsequent noble metal chemical addition have been applied. SCC incidents gradually decreased in past score. Recent studies focus on adequate Dissolved-Hydrogen (DH) margin in PWR's primary water environment. Results reveal that DH amount affects SCC behaviours. Brittle fracture was found on specimens tested at relatively higher DH amount. However, relationship between DH amount and fracture severity indicator (ex: time-to-failure, %IGSCC) scatters. On the other hand, fracture features resemble Hydrogen-Induced Cracking (HIC) in gaseous hydrogen environment. Within this field, a number of works point out that increasing Ni content can reduce HIC susceptibility [2–5]. Light water is responsible to bring heat energy away from plasma-facing components. 316L Stainless Steel (SS) has been considered as one of candidate structural materials for fusion reactors [6–13]. It faces some potential issues and challenges under fusion environment with unique design and operating conditions of the systems. For instance, in testing blanket modules, tritium permeates into coolant and forms TH/T2 gases. These shapes a water environment resembles hydrogenated hot/pressurized water and casts shadows on structural integrity. This document briefly reviews background and current status of researches on SCC in hydrogenated hot/pressurized water.

2. BACKGROUNDS OF STRESS CORROSION CRACKING

SCC involves three major factors: the susceptible material, the tensile stress and the corrosive environment. It is regarded as a synergetic interaction of metallurgical, mechanical and electrochemical aspects. Crack initiates as stress intensity surpasses critical threshold, KISCC; and propagates with nearly constant crack velocity. The velocity may be accelerated as propagation enters into final stage until catastrophic fracture. Fracture mode could be intergranular (IG), transgranular (TG) or their mixed mode. In PWRs and BWRs, SCC occurs on many internal components such as reactor pressure vessel penetration heads, heat exchangers, core shrouds and recirculation pipes.

2.1 Material aspects

In material aspects, sensitization is major cause of IGSCC. Sensitization is a phenomenon that describes a steel with downgraded corrosion resistance being sensitive to corrosive environments due to insufficient Chromium (Cr) content to form continuous passive layer on steel surface [14]. Cr are consumed by Cr carbide formation during inadequately applied welding or heat-treating process. Some works show that sensitization occurs at low-temperature region (573–698 K) as well. Adding carbide stabilizer such as Titanium (Ti), Niobium (Nb) and Tantalum (Ta) reduces degree of sensitization. 321 (Ti added) and 347 (Nb+Ta added) stainless steels had been proved effective. Reducing carbon content below 0.03% is another solution; low-carbon grade stainless steels such as 304L and 316L have been widely applied among reactors. Recent concerns have been focused on the SCC in

solution-annealed materials in which no sensitization nor irradiation-induced local change in microstructures was involved. A systematic research on the SCC in solution-annealed materials is necessary especially for the cases of SCC in water with a lower electrical potential.

2.2 Tensile stress aspects

In tensile stress aspects, structural load and residual stress are two major causes. Residual stress comes from heat treating, welding process or Cold Work (CW). Where CW includes surface grinding and bulk cold-deformation. Welding has workpieces experiencing uneven thermal cycles such as weld pool container and pool periphery. This results in microstructure distortion and multi-layered microstructure different from original weld and base metal. Extensive SCC incidents have been reported within this heat-affected zone. Nb-rich precipitates and Cr carbide are being considered an initiation site of inter-dendritic SCC. CW-produced hardened layer near surface also affects SCC susceptibility [15–19]. It has been reported that SCC occurs on heavy cold worked components. A number of researches indicated HV270~300 could be a threshold of SCC occurrence [20, 21]. However, the cause of CW related issues remains unsolved.

Appropriate heat treatment and welding technique improvement are ways to solve stress related issues. Solution-annealing heat treatment is proven effective to annihilate residual tensile stress. Shot peening [22], water jet peening [23] and laser peening [24] are able to decrease the degree of tensile stress state and create compressive stress state on component surface. Developments in welding technique aim at reducing overall heat input while keeping similar quality. A common method is changing design to lessen required welding process. Advanced technique such as last pass heat sink welding can create residual stress state in welds. High energy beam welding technique, such as laser beam welding and electron beam welding, are having higher energy density than traditional technique. They are capable of achieving rapid thermal cycle in a welding process, minimizing degree of sensitization; range of heat-affected zone and thermo-induced microstructural changes.

2.3 Environment aspects

In environment aspects, electrochemical corrosion potential (ECP) is an important indicator. It reflects overall redox reaction on steel surface at equilibrium state. It can indicate the aggressiveness of water environment. Oxidants such as hydrogen peroxide and oxygen in water shapes a corrosive environment and increases ECP on steels. Aggressive species such as chloride ions and sulphate ions are known detrimental [25]. Flow-accelerated cracking is prone to occur on piping and often accompanied with wall thinning. Temperature also affects ECP and corrosion behaviour. It has been demonstrated that corrosion accelerates as temperature increases simulated hot/pressurized water [26–31]. Nonetheless, several research works reported that corrosion rate (or other fracture severity indicator) reached a local maximum rather than a monotonic increase [32–35]. Experiments of these works were conducted in oxygenated or hydrogenated hot and/or pressurized water environments. This scattering could be due to the difference between testing specimens, testing equipment and analysis methods.

2.3.1. Water chemistry

In typical BWR environment, normal water chemistry contains 200 ppb DO with ECP around +100 mVSHE. To reduce oxidant level and to lower corrosion potential, hydrogen was injected into feedwater to modify water chemistry. This technique is known as hydrogen water chemistry (HWC). Hydrogen injection significantly reduces crack growth rate (CGR) [36].

SCC are suppressed when corrosion potential reaches ‘protection potential’ of -230 mVSHE [37]. Recombination effectiveness, however, relies on gamma-radiation in down comer, of which the design varies from plant to plant, no standard HWC is applicable. Alternation between normal and hydrogen water chemistry lead to a 60Co concentration increase and radiation build up [38]. Further, its coverage region is limited, leaving steam region unprotected [39, 40]. Increasing H_2 injection amount to expand coverage causes 16N increase in main steam lines. Noble metal chemical addition (NMCA) is later introduced to improve the efficiency of recombination process and to expand coverage region. Pt compounds are able to adhere to wetted area, including components in steam phase. Online NMCA is also developed which allows addition during full-power operation.

In PWR, primary water contains 1000 ppm Boron as H_3BO_3 for reactivity control and 2 ppm Lithium as LiOH for pH control (at the start of a cycle). Similar to BWR, highly oxygenated water chemistry in early developing stages caused extensive SCC on steam generator tubes (where original mill-annealed Inconel 600 is replaced with thermal treated Inconel 690). Water purification and hydrogen injection alleviates corrosions. Recent water chemistry suggests a DH content ranging from 25-50 cc.(STP)/kg H_2O (often abbreviated as cc/kg, depending on plant

design) to prevent SCC [41]. As a result, primary water possesses a lower corrosion potential. Besides, Boron and Lithium concentration shift pH value, which affects Fe/Fe ion equilibrium boundary and corrosion resistance of steel as well.

2.4. Irradiation-assisted Stress Corrosion Cracking

Irradiation is a unique factor. Neutron radiation displaces atoms, creating vacancy and self-interstitial atom pairs with cascade damages. Defects reform into void and cavities or assist in forming dislocation loops and precipitates. Precipitates may preferentially form at dislocations or grain boundaries. Defects unbalance element concentration within metal matrix. For instance, Cr has higher diffusivity and higher exchange frequency with voids. Voids deplete Cr adjacent to grain boundaries and form a Cr-depleted zone. On contrary, Ni and Si enrichment occur near grain boundary. This phenomenon is called radiation-induced segregation (RIS). Defects such as He void/bubble and dislocation loop structures change mechanical properties, deformation mechanisms and increase IGSCC susceptibility. Macroscopically, swelling, radiation hardening, dislocation channelling and reduced fracture elongation have been identified. Threshold of SCC falls around 1021 neutron fluence (n/cm^2, $E > 1$ MeV), approximating to 1 dpa (typical for BWR conditions). Threshold of typical PWR conditions is around 3 dpa. For a 20-year life extended PWR, this number can reach 1023, exceeding 100 dpa [42]. Proposed mechanisms to explain the role of radiation include radiolysis, grain boundary Cr-depletion and local deformation. Radiolysis increases hydrogen peroxide and oxygen concentration. Oxidizing conditions favours IGSCC occur on sensitized austenitic stainless steels. Next, the relationship between Cr content at grain boundary and %IG seems obscure at low Cr levels. But as Cr level increases, data become clear and suggests that higher Cr content contributes to higher IASCC resistance. Third, it is suggested that local deformation such as dislocation channelling plays role in IASCC as well [43, 44].

2.5. Stress Corrosion Cracking mechanisms

So far, several models are applicable to certain metal-environment systems. From electrochemical viewpoint, SCC is being controlled by anodic-cathodic reactions at crack-tip. Anodic reaction involves metal dissolution process. The developed film rupture/slip-dissolution model is most widely accepted. In this model, passive film covers surface and crack tip. Crack growth stops and reactivates until sufficient build up of the crack tip strain to rupture passive film. Crack advances intermittently, leaving striations (crack-arrest mark) on fractured surface. This film rupture-dissolution-repassivation cycle is further developed by Ford and Andresen via field experiences and empirical formula [45]. The Ford–Andresen film rupture model well predicts CGR of alloys in BWR. Macdonald proposed Coupled Environment Fracture Model (CEFM) basing on electron charge conservation [46]. The two models well describe behaviour of IGSCC but rules out TGSCC.

Products of cathodic reaction depend on oxygen and hydrogen concentration at crack-tip. Hydrogen may produce during reaction. Proposed mechanisms include hydrogen-enhanced decohesion (HEDE) [47] and hydrogen-enhanced localized plasticity (HELP) [48]. The core concept of HEDE mechanism is that localized hydrogen weakens metal-metal bonding strength at or near crack-tip by decreasing electron-charge density between metal-metal atoms. The HELP mechanism is based on experiments carried out over a range of strain rates and temperatures. Hydrogen in a solid-solution decreases the repulsive stress field between dislocations and the activation energy barrier for a dislocation to move. This results in an increased amount of deformation within localized region and a reduced ductility in macroscope. In short, for HIC to occur, hydrogen must be transported to and being trapped at certain potential degradation sites.

2.6. Stress Corrosion Cracking studies in hydrogenated hot/pressurized water

Recent studies centre on PWSCC CGR behaviour in hydrogenated hot/pressurized water. The relationship between DH content and Ni/NiO phase stability draws much attention. However, results vary from work to work. Table 2 is the summary of available studies.

Take 316L stainless steel. Furutani reported that %IGSCC of CW 316 increased as DH content increased [56]. Choi tested AS316L and found that CGR at 50 cc/kg was higher than at 25 cc/kg. The CGR of warm-rolled 316L was higher than as-received one [55]. However, Meng found a monotonic decrease on 28% CW 316NG [20]. Zhong tested heavy and moderate CW 316 steel at 325ºC. He reported a minimum strain at 15 cc/kg [57]. Fukumura examined non-sensitized 316 SS and found a minimum CGR at 30 cc/kg, 583K [58]. Available data in hot water is limited. Nono tested CW 316L in hydrogenated hot water via SSRT method. He reported a brittle fracture was found on solution-annealed 316L at DH = 0.4 ppm, 561 K [59]. Andresen's simulation on A82

suggests a CGR peak at Ni/NiO boundary. Peak shifts from 4 to 15 cc/kg as temperature from 563 to 616 K. He also calculated DH content at different temperature on Ni/NiO boundary, as shown in Table 2 [57].

TABLE 1. CALCULATED DH CONTENT AT DIFFERENT TEMPERATURE ON NI/NIO BOUNDARY

Temperature, ℃	Dissolved H_2, ppb	Dissolved H_2, cc/kg
250	137	1.53
274	253	2.83
288	362	4.05
300	491	5.5
325	928	10.4
340	1357	15.2
360	2267	25.4

TABLE 2. SUMMARY OF RESEARCHES RELATES TO HYDROGENATED HIGH TEMPERATURE WATER. (1) A600/A82/A182: ABBR. OF ALLOY 600/82/182, A.K.A. INCONEL 600; FILLER METAL 82/182. MA: MILL-ANNEALED. TT: THERMAL-TREATED. CW: COLD WORK. NG: NUCLEAR GRADE. AS: AS-RECEIVED. SA: SOLUTION-ANNEALED. (2) CGR: CRACK GROWTH RATE. SSRT: SLOW-STRAIN RATE TEST. (3) NUMBER IN BRACKET IS THE DH CONTENT WHERE PEAK LOCATES (4) UNIT: KELVIN (5) UNIT: CC. STP/KG H2O

Author	Materials[(1)]	Method[(2)]	Behavior[(3)]	Peak temp.[(4)]	DH Range[(5)]	Ref.
Totsuka	A600	CGR	peak (50)	633		[49]
Labousse	MA-A600		peak (40/35/25)	633/611/563		[29]
Molander	A600	CGR	peak (27)			[50]
Fukumura	CW20%-A600	CGR	peak (0.5ppm)	563	0-2.7 (ppm)	[51]
Yamada	CW20%-TT690	CGR	peak (30)	633	0-45	[35]
Andresen	A82	simulation	peak (16/10/5)	616/598/563		[52]
PNNL	A182	CGR	peak (12)	598		[53]
Bruemmer	A82	CGR	peak (8)	611	1-35	[53]
Furutani	CW 316	CGR	increase	593	0-30	[54]
Meng	CW316NG	CGR	decrease	593	0.16-50	[16]
Zhong	CW316	SSRT	minimum (15)	598	5-50	[55]
Choi	AS316L	CGR	increase	613	25/50	[56]
Fukumura	SA316	SSRT	minimum (30)	583	15-45	[31]

3. CONCLUSION AND OUTLOOK

The above section briefly delivers the background of SCC and current state of SCC studies in light water reactor. Solutions to SCC — replacement with more corrosion-resistant alloys, manufacture quality control and water chemistry optimization — have been applied. Efforts continue to search the root cause of IASCC and SCC on steels in hydrogenated hot/pressurized water. Our recent works have revealed that hydrogen played important role in SCC progress.

ITER's special design and its PWR-like operating conditions shape a unique water environment. Tritium permeation may form tritiated water and TH/T2 gaseous bubbles. Behaviors of these species resemble that of DH in water. Further, intensified neutron fluence not only enhances radiolysis but also damages steel. To ensure the structural integrity, tritium recovery and water chemistry optimization need to be applied. The importance of radiation and effect DH needs to be much more addressed.

REFERENCES

[1] CORIOU, H., GRALL, L., LE GALL, Y., VETTIER, S., Corrosion sous contrainte de I'Inconel dans L'eau a haute temperature, North Holland Publishing Co., Amsterdam (1959) 161–9.
[2] CASKEY, G.R., Hydrogen compatibility handbook (1983).
[3] YOKOGAWA, K., FUKUYAMA, S., Hydrogen environment embrittlement of materials for hydrogen energy service, Chugoku National Industrial Research Institute (CNIRI) (1996).
[4] HAN, G., HE,J., FUKUYAMA, S.,YOKOGAWA, K., Effect of strain-induced martensite on hydrogen environment embrittlement of sensitized austenitic stainless steels at low temperatures, Acta Mater. **46** (1998) 4559–4570.
[5] ZHANG, L., WEN, M., IMADE, M., FUKUYAMA, S., YOKOGAWA, K., Effect of nickel equivalent on hydrogen gas embrittlement of austenitic stainless steels based on type 316 at low temperatures, Acta Mater. **56** (2008) 3414–3421.
[6] GOHAR, Y., BAKER, C.C., ATTAYA, H., BILLONE, M., CLEMMER, R.C., et al., Water cooled Solid-Breeder Blanket Concept for ITER, Fusion Technol. **15** (1989) 864–870.
[7] KIMURA, A., MATSUBARA, S., MISAWA,T., Hydrogen Induced Cracking in Type 316 Stainless Steels for International Thermonuclear Experimental Reactor, Mater. Trans. **34** (1993) 1097–1105.
[8] TAVASSOLI, A.A.F., Assessment of austenitic stainless steels, Fusion Eng. Des. **29** (1995) 371–390.
[9] LORENZETTO, P., GIERSZEWSKI, P., SIMBOLOTTI, G., A European proposal for an ITER water cooled solid breeder blanket, Fusion Eng. Des. **27** (1995) 423–429.
[10] LORENZETTO, P., HELIE, M., MOLANDER, A., Stress corrosion cracking of AISI 316LN stainless steel in ITER, J. Nucl. Mater. **233–237** (1996) 1387–1392.
[11] BELOUS, V., KALININ, G., LORENZETTO, P., VELIKOPOLSKIY, S., Assessment of the corrosion behaviour of structural materials in the water coolant of ITER, J. Nucl. Mater. **258–263** (1998) 351–356.
[12] TSURU, D., TANIGAWA, H., HIROSE, T., MOHRI, K., SEKI, Y., et al., Achievements in the development of the Water Cooled Solid Breeder Test Blanket Module of Japan to the milestones for installation in ITER, Nucl. Fusion **49** (2009) 65024.
[13] KAWAMURA, Y., TANIGAWA, H., HIROSE, T., ENOEDA, M., SATO, et al., Progress of R&D on water cooled ceramic breeder for ITER test blanket system and DEMO, Fusion Eng. Des. **109** (2016) 1637–1643.
[14] MCGUIRE, M., Austenitic Stainless Steels, Stainl. Steels Des. Eng. (2008) 69–78.
[15] TOLOCZKO, M.B., ANDRESEN, P.L., BRUEMMER, S.M., "SCC crack growth of cold-worked type 316 ss in simulated bwr oxidizing and hydrogen water chemistry conditions", 13th Int. Conf. Environ. Degrad. Mater. Nucl. Power Syst., Whistler, British Columbia (2017).
[16] MENG, F., LU, Z., SHOJI, T., WANG, J., HOU HAN, E., et al., Stress corrosion cracking of uni-directionally cold worked 316NG stainless steel in simulated PWR primary water with various dissolved hydrogen concentrations, Corros. Sci. **53** (2011) 2558–2565.
[17] PARAVENTI, D.J., MOSHIER, W.C., "The effect of cold work and dissolved hydrogen in the stress corrosion cracking of alloy 82 and alloy 182 weld metal", 12th Int. Conf. Environ. Degrad. Mater. Nucl. Power Syst. – Water React (2005).
[18] CHEN, J., LU, Z., XIAO, Q., RU, X., HAN, et al., The effects of cold rolling orientation and water chemistry on stress corrosion cracking behaviour of 316L stainless steel in simulated PWR water environments, J. Nucl. Mater. **472** (2016) 1–12.
[19] LOZANO-PEREZ, S., YAMADA, T. TERACHI, T., SCHRÖDER, M., ENGLISH, C.A., et al., Multi-scale characterization of stress corrosion cracking of cold-worked stainless steels and the influence of Cr content, Acta Mater. **57** (2009) 5361–5381.
[20] KATAYAMA, Y., TSUBOTA, M., SAITO, Y., "Effect of the plastic strain level quantified by EBSP method on the stress corrosion cracking of L-grade stainless steels", 12th Int. Conf. Environ. Degrad. Mater. Nucl. Power Syst. – Water React. (2005) 31–38.
[21] CHIANG, M.F., YOUNG, M.C., HUANG, J.Y., Effects of hydrogen water chemistry on corrosion fatigue behaviour of cold-worked 304L stainless steel in simulated BWR coolant environments, J. Nucl. Mater. **411** (2011) 83–89.
[22] SAGAWA, W., AOKI, T. ITOU, T., ENOMOTO, K., HAYASHI, E., et al., Stress corrosion cracking countermeasure observed on Ni-based alloy welds of BWR core support structure, Nucl. Eng. Des. **239** (2009) 655–664.
[23] HIRANO, K. ENOMOTO, K., HAYASHI, E., KUROSAWA, K., Effects of Water Jet Peening on Corrosion Resistance and Fatigue Strength of Type 304 Stainless Steel, J. Soc. Mater. Sci. **45** (1996) 740–745.
[24] SANO, Y., OBATA, M., KUBO, T., MUKAI, N., YODA, M., et al., Retardation of crack initiation and growth in austenitic stainless steels by laser peening without protective coating, Mater. Sci. Eng. **417** (2006) 334–340.
[25] GORDON, B., GARCIA, S., Technical Basis for Water Chemistry Control of Igscc in Boiling Water Reactors (2011) 2061–2076.
[26] FORD, F.P., POVICH, M.J., The Effect of Oxygen Temperature Combinations on the Stress Corrosion Susceptibility of Sensitized Type 304 Stainless Steel in High Purity Water, Corrosion **35** (1979) 569–574.
[27] ANDRESEN, P.L., Effects of Temperature on Crack Growth Rate in Sensitized Type 304 Stainless Steel and Alloy 600, Corrosion **49** (1993) 714–725.
[28] AGRAWAL, A.K., WELCH, G.A., BEGLEY, J.A., STAEHLE, R.W., Stress Corrosion Cracking of Sensitized Type 304 Stainless Steel in High-Purity Water, Corrosion **78** (1978) 1–8.
[29] LABOUSSE, M., DÉFORGE, D., GRESSIER, F., TAUNIER, S., Optimization of the dissolved hydrogen level in pwr to mitigate stress corrosion cracking of nickel alloys, Int. Coop. Gr. Environ. Assist. Crack (2012).
[30] ARIOKA, K., Influence of Temperature, Hydrogen and Boric Acid Concentration on IGSCC Susceptibility of Unsensitized 316 Stainless Steel, J. Inst. Nucl. Saf. Syst. **9** (2002) 116–123.

[31] FUKUMURA, T., TERACHI, T., ARIOKA, K., Influence of Temperature and Water Chemistry on IGSCC Susceptibility of SUS316 in High temperature Water, J. Inst. Nucl. Saf. Syst. **11** (2004) 143–152.
[32] LU, Z., SHOJI, T., TAKEDA, Y., ITO, Y., KAI, A., et al., Transient and steady state crack growth kinetics for stress corrosion cracking of a cold worked 316L stainless steel in oxygenated pure water at different temperatures, Corros. Sci. **50** (2008) 561–575.
[33] SYUNJI, S., NAKAJIMA, N., TAKAO, M., Stress Corrosion Cracking of Stainless Steel in PWR Primary Water (Japanese), J. Inst. Nucl. Saf. Syst. **15** (1996).
[34] ARIOKA, K., KANESHIMA, Y., YAMADA, T., Influence of Grain Boundary Sliding and Carbide Precipitation on IGSCC Susceptibility of SUS 316 under Hydrogenated High Temperature Water, J. Inst. Nucl. Saf. Syst. **10** (2003) 125–135.
[35] YAMADA, T., AOKI, M., MIYAMOTO, T., ARIOKA, K., SCC growth behaviour of cold worked alloy 690 in high temperature water－Dependence of test temperature, dissolved hydrogen in water, grain boundary carbide and chemical composition－, J. Inst. Nucl. Saf. Syst. **21** (2014) 133–143.
[36] ANDRESEN, P.L., MORRA, M.M., IGSCC of non-sensitized stainless steels in high temperature water, J. Nucl. Mater. **383** (2008) 97–111.
[37] BILANIN, W., CUBICCIOTTI, D., JONES, R.L., MACHIELS, A.J., NELSON, L., et al., Hydrogen water chemistry for BWRs, Prog. Nucl. Energy **20** (1987) 43–70.
[38] LIN, C.C., SMITH, F.R., COWAN, R.L., Effects of hydrogen water chemistry on radiation field buildup in BWRs, Nucl. Eng. Des. **166** (1996) 31–36.
[39] BWRVIP-62NP: BWR Vessel and Internals Project Technical Basis for Inspection Relief for BWR Internal Vessel and Internals Project Internal Components with Hydrogen Injection, Technical Report, Electronic Power Research Institute (2014).
[40] HORN, R., GORDON, G.,FORD, F., COWAN, R., Experience and assessment of stress corrosion cracking in L-grade stainless steel BWR internals, Nucl. Eng. Des. **174** (1997) 313–325.
[41] WOOD, C.J., 5.02 - Water Chemistry Control in LWRs A2 - Konings, Rudy J.M. BT - Comprehensive Nuclear Materials, Elsevier, Oxford (2012) 17–47.
[42] ZINKLE, S.J., WAS, G.S., Materials challenges in nuclear energy, Acta Mater. **61** (2013) 735–758.
[43] JIAO, Z., WAS, G.S., Impact of localized deformation on IASCC in austenitic stainless steels, J. Nucl. Mater. **408** (2011) 246–256.
[44] WAS, G.S., FARKAS, D., ROBERTSON, I.M., Micromechanics of dislocation channelling in intergranular stress corrosion crack nucleation, Curr. Opin. Solid State Mater. Sci. **16** (2012) 134–142.
[45] Ford, F.P., ANDRESEN, P.L., Development and use of a predictive model of crack propagation in 304/316L, A533B/A508 and Inconel 600/182 alloys in 288^0C water, The Metallurgical Society Inc, United States (1988)
[46] MACDONALD, D.D., URQUIDI-MACDONALD, M., A coupled environment model for stress corrosion cracking in sensitized type 304 stainless steel in LWR environments, Corros. Sci. **32** (1991) 51–81.
[47] ORIANI, R.A., The diffusion and trapping of hydrogen in high purity aluminium, Acta Matallurgica. 18 (1970) 147–157.
[48] BIRNBAUM, H.K., SOFRONIS, P., Hydrogen-enhanced localized plasticity-a mechanism for hydrogen-related fracture, Mater. Sci. Eng. **176** (1994) 191–202.
[49] TOTSUKA, M., NISHIKAWA, Y., NAKAJIMA, N., Influence of Dissolved Hydrogen and Temperature on Primary Water Stress Corrosion Cracking of Mill Annealed Alloy 600, Corros. **6** (2002) 1–11.
[50] MOLANDER, A., JENSSEN, A., NORRING, K., KO, M., ANDERSSON, P.O., "Comparison of PWSCC initiation and crack growth data for Alloy 600", VGB NPC'08 Water Chem. (Proc. Int. Conf. Berlin, 2008).
[51] FUKUMURA, T., TOTSUKA, N., Effect of Dissolved Hydrogen Concentration on PWSCC Crack Growth Rate of Alloy 600 at 290℃, J. Inst. Nucl. Saf. Syst. **17** (2010) 122–129.
[52] ANDRESEN, P., HICKLING, J., AHLUWALIA, A., WILSON, J., Effect of H2 on mitigation of PWSCC in nickel alloys, in: Optim. Dissolved Hydrog. Content PWR Prim. Cool., Tohoku University, Sendai, Japan (2007).
[53] BRUEMMER, S.M., VETRANO, J.S., TOLOCZKO, M.B., "Microstructure and SCC Crack Growth of Nickel-Base Alloy 182 Weld Metal in Simulated PWR Primary Water", 13th Int. Conf. Environ. Degrad. Mater. Nucl. Power Syst., Whistler, British Columbia (2007) 1–11.
[54] FURUTANI, G., NAKAJIMA, N., KONISHI, T KODAMA, M., Stress corrosion cracking on irradiated 316 stainless steel, J. Nucl. Mater. **288** (2001) 179–186.
[55] ZHONG, X., BALI, S.C., SHOJI, T., Effects of dissolved hydrogen and surface condition on the intergranular stress corrosion cracking initiation and short crack growth behaviour of non-sensitized 316 stainless steel in simulated PWR primary water, Corros. Sci. **118** (2017) 143–157.
[56] CHOI, K.J., YOO, S.C., JIN, H.H., KWON, J., CHOI, M.J., et al., Crack growth behaviour of warm-rolled 316L austenitic stainless steel in high temperature hydrogenated water, J. Nucl. Mater. **476** (2016) 243–254.
[57] ANDRESEN, P. CHOU, P., "Effects of Hydrogen on SCC Growth Rate of Ni Alloys in BWR Water", 15th Int. Conf. Environ. Degrad. Mater. Nucl. Power Syst. - Water React. (2011) 2039–2059.

BARRIERS AND COATINGS FOR CORROSION MITIGATION MATERIALS ISSUES IN HEAVY LIQUID METAL COOLED SYSTEMS

M. ANGIOLINI, P. AGOSTINI, S. BASSINI, F. FABBRI, M. TARANTINO
ENEA,
Rome
Email: Massimoemilio.angiolini@enea.it

F. DI FONZO
Istituto Italiano di Tecnologia,
Milano

Italy

Abstract

The assessment of structural materials able to withstand the operating conditions represents the most critical challenge in the development of innovative nuclear systems cooled by heavy liquid metals (HLMs), such as Lead-cooled Fast Reactor (LFRs). HLMs have many unique nuclear and thermo-physical properties, in particular low neutron moderating power, very high boiling point, and chemical inertness with water and fuel which can offer a large flexibility for the safe design of LFR-Gen IV reactors. On the other hand, the contact with lead or lead alloys exposes the materials to severe degradation according to various mechanisms, non-passivating oxidation, dissolution of the alloys components and liquid metal embrittlement. The development of a chromium rich oxide layer on the steel surface that acts as physical barrier to further oxidation in most environments, is not effective in HLM at high temperature and above 450~500° C severe corrosion attacks are observed in both austenitic and F/M steels, with the formation of thick not protective oxide layers, internal oxidation and dissolution of the steel in the coolant. The dissolutive process, if not counter-acted, proceeds at the speed of 200 microns/year at a temperature of 550°C for a typical austenitic steel exposed to liquid lead at concentration of 10^{-7} wt% oxygen. F/M steels in contact with HLM suffer liquid metal embrittlement (LME) i.e. a loss of ductility when tested in traction in HLM environment in the temperature range 200–450°C. The protection by oxides more stable than chromium oxide in HLM and namely alumina is at present the most viable approach to operate the conventional steels in HLM at high temperature.

1. INTRODUCTION

The HLM technology applications to the nuclear energy started in the first half of the last century in the Soviet Union where nuclear systems cooled by Lead–Bismuth Eutectic (LBE) were developed and deployed for the submarine propulsion. Recently there was a renewed attention to the HLM coolants for the realization of accelerator driven systems (ADSs) and LFRs as their advantageous characteristics have gradually become recognized. HLMs have many unique nuclear and thermo-physical properties, in particular low neutron moderating power, very high boiling point, and chemical inertness with water and fuel which can offer a large flexibility for the safe design of LFR-Gen IV reactors

One of the main limiting factor for the development of the HLM cooled systems is the corrosion of the structural steels. Corrosion occurred as a technological issue for HLM cooled reactors since their first application, regarding the eutectic lead-bismuth alloy used for Alfa class Soviet submarines. Several phenomena are involved to this regard, such as non-passivating oxidation, leading to thick and unstable oxide layers and dissolution of the steel constitutive elements.

The dissolution of the alloying elements of structural steels is the most intensive and rapid corrosive process. The most sensitive element to this phenomenon is nickel but also chromium and iron show a certain solubility in heavy metals melts. The dissolutive process, if not counter-acted, proceeds at the speed of 200 μm/y at a temperature of 550°C for a typical austenitic steel exposed to liquid lead at concentration of 10^{-7} wt% oxygen [1].

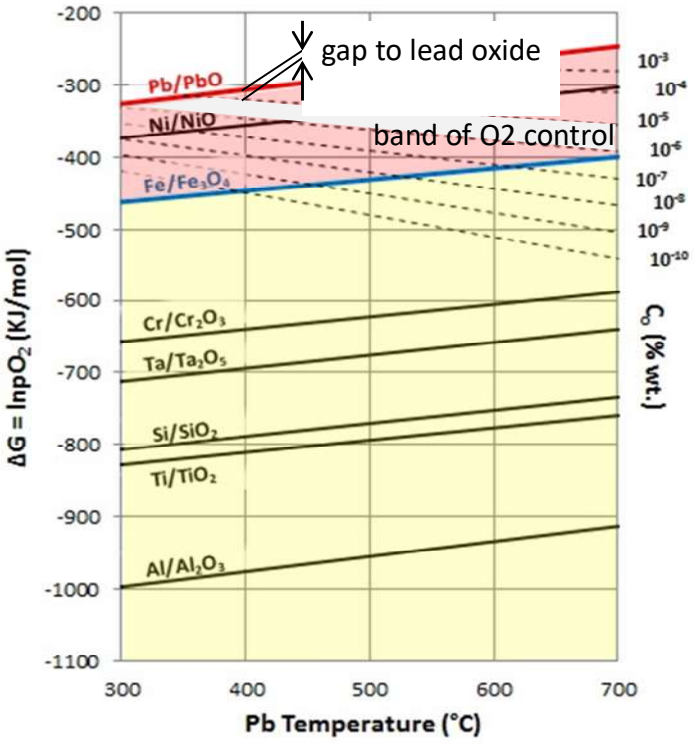

FIG. 1. Ellingham diagram.

The operation under controlled oxygen content and low temperature (450–480°C) conditions in order to keep low oxidation levels (Active Oxygen Control, AOC), has proven to be effective in handling corrosion issues by promoting the formation of a thin passivating oxide film on the steels surface, so reducing steel corrosion and coolant contamination. AOC was the solution devised by the Russian designers in the sixties for the Alfa class submarines reactors and proved to be very practical and efficient at their operational temperature. It consisted in dissolving oxygen in the liquid metal and keeping its concentration lower than the value at which lead oxide precipitates but high enough to allow the formation of the protective oxides, mainly a chromium rich spinel, on the stainless-steel surface. To this purpose, by means of suitable control systems, a dissolved oxygen content, between 10^{-5} wt% and 10^{-6} wt%, was kept within the heavy liquid metal. The higher oxygen concentration is set below the level at which precipitation of solid led oxide occurs; the lower level of oxygen content allows, at any operational temperature, the formation of magnetite, the less stable oxide among those constituting the protective layer. Fig. 1 illustrates in a simplified manner, by using the Ellingham diagram, the concentration limits for the oxygen dissolved for a LFR reactor following the approach adopted for Alfa class submarines. Note that the lower level of oxygen content allows, at any operational temperature, the formation of magnetite, the less stable oxide among those constituting the protective layer while the upper level is set to prevent the formation of lead oxide.

2. MATERIALS ISSUES IN HLM

Chromium is the major element added to the steels to improve their corrosion properties and stainless steels contain at least 11% wt of chromium. The ability of stainless steel to resist corrosion at high temperature relies on the formation of a compact, slow-growing protective layer by the selective oxidation of chromium; the protective behaviour being the result of slow transport of ions and electrons through the thickness of the oxide, decreasing further oxidation of the material. In general it has been shown that above temperatures around 450~500°C, depending on the steel considered and on the working conditions, the operation in HLM under control of the oxygen concentration is not effective in keeping a thin passivating surface layer and all the steels tested to date demonstrated to suffer oxidation corrosion issues: another, faster mode of oxidation starts, characterized by the growth of a non-protective dual layer scale, made of an inner chrome rich layer and an outer iron oxide, accompanied by dissolution of oxygen into the metal and internal oxidation [2]. The inner and outer layers are reported as an iron chromium spinel and magnetite, respectively.

Oxidation experiments on 9% wt Cr ferritic/martensitic steel using 18O tracers have shown that the inner chrome rich layer grows inward in contact with the steel surface, while the outer magnetite layer grows outward in contact with the molten metal [3]. Regardless of the differences in the test conditions and materials used, there is a common agreement about the growth of the scale (i.e. the two sub-layers) with parabolic kinetics indicating, a diffusion-controlled growth where the diffusion of the iron cations through the oxide is the rate determining factor [3–7]. Since lattice or grain boundaries diffusion of oxygen through the oxide layers is too slow to account for the observed growth kinetic, it is supposed an oxygen transport mechanism via pores, nano-channels or cracks produced by the stress field in the growing film, filled with the liquid metal and the oxygen dissolved therein, acting as fast diffusion path to bring oxygen from the bulk liquid metal to the Fe–Cr spinel-steel interface [3, 6]. Several investigations report about the presence of lead in the oxide layer and demonstrated by elemental analysis via EDS, GD-OES and SIMS. The detection of the lead in the oxide has been used to support the presence of nano-channels in the oxide layer [3].

On the other hand, the above-mentioned microstructural features have never been observed and, on the contrary, their existence seems to be excluded by impedance spectroscopy measurements [8]. Some authors report the presence of lead-iron mixed oxides, lead-bismuth-iron mixed oxides and bismuth-iron mixed oxides after XRD analysis of the oxide layer [9–12]. Extra XRD peaks non indexable as Fe-Cr spinel or magnetite are reported in [7]. TEM investigations carried out on D9 steel samples exposed to LBE, reveal that what was believed to be a duplex oxide layer, is actually a more complicated structure formed by more distinct oxide layers [13].

A research line that received little or no attention by the research community, is that the mechanisms accounting for the oxidation corrosion at high temperature in HLM may be associated to the precipitation/incorporation of complex oxides of iron and chromium with lead and bismuth, during the growth of the scale. The pseudo-binary phase diagram precipitation of the systems $PbO–Fe_3O_4$ and $PbO-Cr_3O_4$ [14, 15] has eutectic points around 760°C, so the corrosion oxidation in the temperature range of interest cannot be attributed to the formation of low melting complex compounds. However, it must be considered that the complex oxides can give rise to defective structures [16] that can account for the high diffusion rate of oxygen through the oxide. In addition, the small volumes involved make difficult the careful identification of the corrosion products and the contamination by other steel constituents, giving rise to a more complicated oxide with unknown behaviour, cannot be excluded. Another important point is the possibility that complexes oxides may have high solubility in HLM so leading to a continuous removal of the oxide layer and depletion of the passivating element from the substrate.

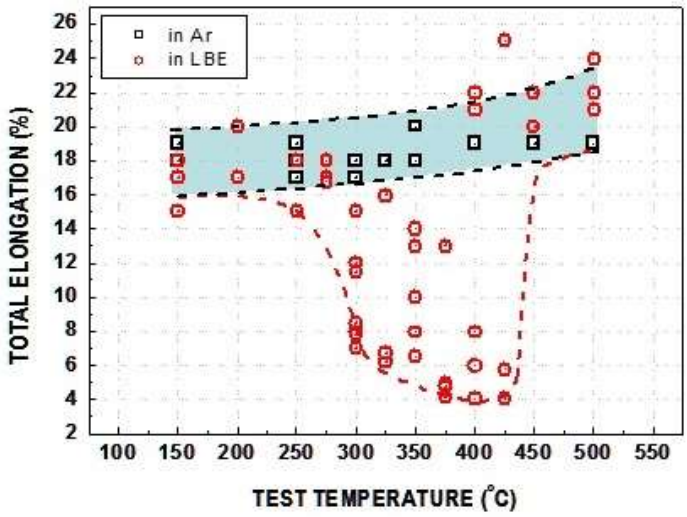

FIG. 2. Total elongation versus testing temperature for the HT760 specimens tested in Ar gas and LBE [17].

Another important issue regarding the compatibility of the structural steels with HLM coolants is the LME. F/M steels as well as many alloys with body centred structure are reported to suffer a loss of ductility when exposed to molten lead alloys. The experimental results on liquid lead alloys embrittlement of F/M steels exclude the effect of corrosion and point out that, on the contrary, the effect manifests itself when no oxidation processes are in place (low oxygen concentration) so making possible an intimate contact between the heavy liquid metal and the steel. According to the results obtained in the last few years LBE embrittlement effect on ferritic martensitic steels has

been observed in a certain temperature range, the so-called 'ductility-trough'. The ductility-trough of the system LBE-T91 is from its melting point to around 450°C [17].

Due to the LME issues F/M steels, despite exhibiting a number of attractive features when used as structural materials in nuclear environment, especially in terms of swelling resistance, thermal conductivity and thermal expansion coefficient, have been excluded from the list of the candidate materials for the realization of HLM cooled systems and replaced in the prototype design by austenitic steels.

3. MATERIALS FOR LEAD COOLED SYSTEMS

In order to simplify the control process that, for a thermodynamic machine of significant dimensions, also requires a continuous measurement of the thermal stratification, it could be appropriate to maintain oxygen level next to the upper limit to prevent metal dissolution everywhere. As the upper limit of oxygen corresponds to the formation of lead oxides, at the lower temperature (400°C) an extremely accurate control of the oxygen content is necessary, since the gap in oxygen concentration to form lead oxide is very narrow, as can be seen in Fig. 1, and, PbO formations could plug the coolant channels. The two conflicting needs to ensure the formation of the layer of chromium and iron oxides and to prevent the formation of lead oxides, require a sophisticated control through very fine adjustment of the coolant chemistry. For a reactor pool volume larger than 100 cubic meters, it appears difficult to maintain accurate control of the coolant chemistry in order to keep the oxygen concentration in the limits allowed to inhibit corrosion. For such reason some recent LFR designs intend to assign corrosion control rather than to the AOC, to the operation of the reactor at high temperatures and low oxygen concentrations and the careful selection of materials, either by special alloys or by surface treatment.

The current design of the lead cooled ALFRED reactor foresees operating the reactor with an oxygen content well below the saturation limit at the coldest temperature of the coolant (400°C), so eliminating the risk of lead oxide precipitation in the whole system. This option exposes the steels to severe corrosion/dissolution issues in the regions of the reactor operated at temperatures above 450°C. The core structures are at temperatures higher than the above-mentioned limits at which oxidation is not protective and the corrosion processes cannot be neglected; due to the small thickness of the cladding tubes, additional protection measures must be put in place. In the short term the most viable solution is the use of the special steels developed so far and assign the protection from the HLM corrosion to protective surface treatments. The base material is kept retaining the mechanical properties aimed to guarantee the integrity against stresses and irradiation. The surface material/treatment is added to complement the base material with the corrosion resistance. This approach has the obvious advantage of using materials with known properties already codified in the regulations [18].

The above arguments do not apply to the HLM cooled systems that foresee and allow operations at temperatures below the limits at which corrosion issues occurs and for which the adoption of the AOC is considered sufficient to guarantee safe operations of the machine. Nevertheless, corrosion/erosion is expected for the components that face the HLM flux at high velocity like the pumps impellers.

4. COATINGS

In this context, in Italy at ENEA were promoted studies to identify suitable protective coatings for a Lead cooled fast reactor. The main target of the research was the development of a suitable material for the fuel claddings that, based on the present design is operated at 550° and so represent the main challenge for this kind of reactors. The reference material was the 15–15 Ti steel (AIM-1) used in sodium cooled fast reactors, due to its already proven good performance in high temperature, fast neutrons environment. The 15–15 Ti steel, like other austenitic steels, is prone to liquid metal corrosion in HLM, although less intense then 316L steel [1]. The corrosion protection coating of such steel appeared the most practical solution to preserve the thermomechanical and swelling performance and to enhance its corrosion resistance.

The qualification of this approach consisted of corrosion test, scratch tests and thermal shocks to verify adherence, mechanical tests and thermal cycling tests to verify compliance with the substrate even in plastic condition and finally heavy ions irradiations to simulate the behaviour under fast neutrons flux.

From the fabrication point of view of coatings for the cladding, it is required that, the coating deposition process happen without any temperature increase. This prescription is necessary since the swelling resistant austenitic steels of the class 15–15 Ti are metastable by design and an high temperature treatment could lead to important microstructural changes with the loss of the performance under neutron irradiation. This constraint ruled out the adoption of diffusion coating techniques that imply the exposure to high temperatures for times of the order of

hours to allow for the formation of the diffusion layer over the steel surface. Low temperature, with T < 700°C, pack cementation FeCrAl depositions have been tried but with poor results in term of thickness of the diffused layer and surface roughness.

The candidate coatings/surface treatments can be divided in two classes, inert coatings and self-passivating coatings. In the first case the protection is provided by a compound with high stability in the environment, in the second case the protection is provided by the precipitation of a stable compound by reaction with the environment that passivates the surface.

Beyond the corrosion resistance in HLM, the coating must have good adhesion and mechanical compatibility with the substrate, low swelling property and a stable microstructure under neutron irradiation up to elevated doses. The self- healing i.e. ability to regenerate by reaction with the environment in case of scratch or surface failure is a further requirement.

In order to render the surface passive, the compounds that form by the reaction with the environment must form a compact, slow growing layer with low conductivity and diffusion coefficients of metal ions and oxygen. In addition, must have a melting temperature largely above the operative one, low partial pressure of sublimation, must be insoluble in the environment and mechanical compatibility with the substrate.

The first coating systems considered was a self-passivating tantalum coating deposited by chemical vapour deposition. Ta coatings are widely used to protect the steels in aggressive environments. Tantalum oxide according to the diagram in Fig.1 has lower free energy of formation than the chromium oxide at all temperatures and has been considered a potential good candidate but testing in molten lead at various oxygen concentrations Ta developed a flaky and porous oxide layer permeable to oxygen (Fig. 3). After 1000 h of exposure the coating was nearly completely oxidised and upon further exposure the steel surface was exposed to the lead.

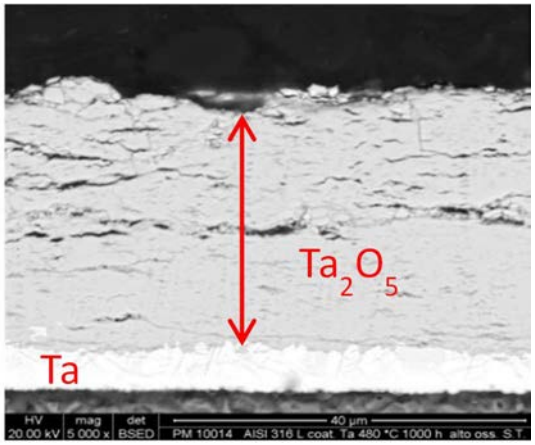

FIG. 3. Ta coating on 316 L Steel after 1000 hours exposition in static Pb at 480°C.

Looking at the Ellingham diagram in Fig.1, one can immediately observe that aluminium oxide Al_2O_3 is an extremely stable compound and Al rich alloys are known to develop self-passivating layers at high temperature in most environments. Preliminary testing in molten lead at various temperatures and concentrations showed that FeCrAl compounds have outstanding corrosion properties in the lead environment so it was started the development of ceramic alumina coatings and metallic alumina forming coatings.

4.1 Passivating coatings

Among the overlay metallic coatings, FeAl and FeCrAl showed excellent behaviour in oxygen rich liquid lead and after 5000 hours of exposure in the CHEOPEIII loop at the ENEA laboratories, FeAl specimens showed an outstanding performance with no corrosion nor erosion attacks (Fig. 4). Coatings have been produced via several techniques, namely magnetron sputtering, High Velocity Oxy Fuel and Arc-PVD and pack cementation. Long term tests in flowing lead and thermal creep experiments in molten lead are under way. Nevertheless, apart from corrosion and thermal creep, other issues still need to be addressed. Among them, the most important is the resistance to the displacement damage induced by irradiation, swelling, irradiation creep, stability of the

microstructure, changes in mechanical properties and adhesion strength. To protect the core structural materials, the coatings must retain their properties after neutron irradiation up to a dose of 100 dpa that is the dose at which the fuel element is replaced for reprocessing. The 100 dpa dose is estimated to be suffered by the cladding after 3 years irradiation in the core of the ALFRED reactor. In order to assess the performance of FeCrAl coatings under neutron irradiation, an ion irradiation campaign has been started at the National Laboratories of the Istituto Nazionale di Fisica Nucleare (INFN).

4.2 Ceramic coatings

The experimental campaign on ceramic coatings was mainly focused on the deposition of Al_2O_3 coatings by pulsed laser deposition (PLD). The PLD technique uses high power laser pulses to melt, evaporate and ionize material from the surface of a target of the material to be deposited so producing a plasma plume that expands at high speed to re-condense on a substrate where the coating growth occurs. The Al_2O_3 coatings produced by PLD developed by the Istituto Italiano di Tecnologia in collaboration with ENEA at present represent the most promising option to protect the core components (mainly cladding and spacer grids) by the corrosion. PLD is a relatively simple technology that allows to grow thin films of a wide range of materials. The deposition conditions can be adjusted to obtain different coating microstructures, varying from fully dense and compact to columnar and porous [19].

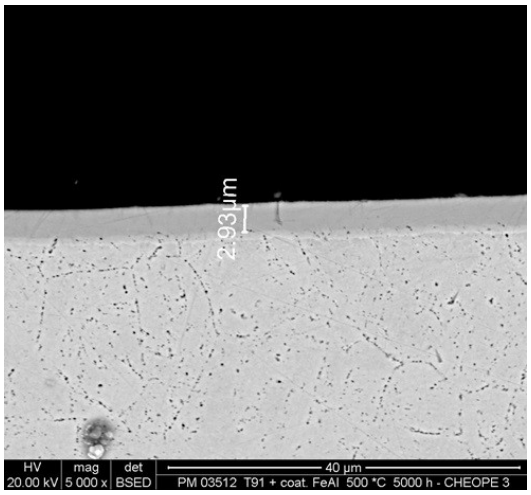

FIG.4. FeCr coating on T91 Steel after 5000 hours exposition in flowing Pb at 500°C.

Fully dense and compact Al_2O_3 coating grown by PLD on various steels have been obtained by tailoring the deposition process to attain an advanced nanocomposite which consists of a homogeneous dispersion of ultra-fine nanocrystalline domains (6 ± 4 nm) in an amorphous alumina matrix (Fig. 5), with the desired properties [20]. Some of the main features of this material are an ensemble of metal-like mechanical properties (E = 195 ± 9 GPa, ν = 0,29 ± 0,02) and enhanced plastic behaviour, full compactness and strong adhesion, as well as a relatively high hardness (H = 10 GPa) [19, 20].

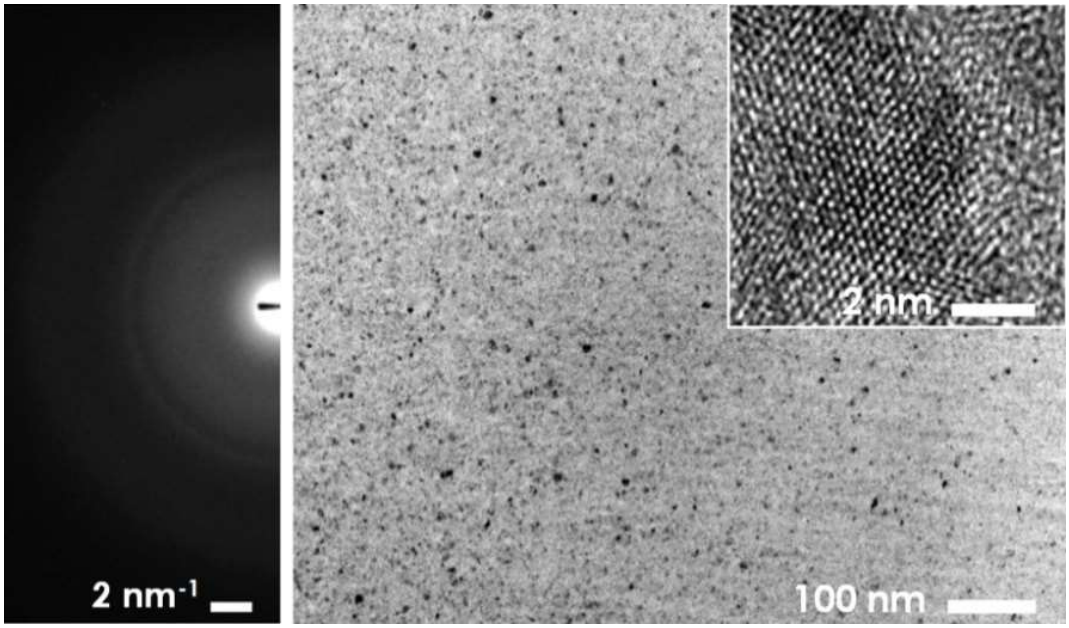

FIG.5. Microstructure of the Al_2O_3 coatings showing homogeneous dispersion of randomly oriented crystalline Al_2O_3 nanodomains in an amorphous Al_2O_3 matrix, as shown in the electron diffraction patterns on the left.

The Al_2O_3 barriers have been tested for protecting the steels up to 600°C in stagnant HLMs with outstanding results [21]. Long term (>10.000 hours) tests in flowing Lead and thermal creep experiments on coated 15–15 Ti tubes and plates are in progress. The performance of the Al_2O_3 nanocomposites under irradiation have been investigated via heavy ion irradiations during several experiments at various doses up to 150 dpa at 600°C. Irradiations have been carried out at the JANNUS-Saclay platform on bilayers FeCrAlY buffer + Top Al_2O_3 on 15–15 Ti and the doses were 20, 40, and 150 dpa. The energy of the ions has been chosen in order to obtain the maximum displacement damage at the interface with the substrate. Such high levels of radiation damage approach or even exceed the damage exposures foreseen for the ALFRED reactor. In Fig. 6 a, b, c, d it is shown the evolution of the microstructure increasing the irradiation dose. These images indicate that increasing the irradiation dose, a fully nanocrystalline structure is developed followed by grain growth. The average grain size increases from 6 ± 4 nm to 101 ± 56 nm at 20 dpa, 153 ± 62 nm at 40 dpa and 293 ± 85 nm at 150 dpa. The crystalline phases present in the irradiated nanoceramic are γ - Al_2O_3 up to 40 dpa, and both γ - Al_2O_3 and α -Al_2O_3 at 150 dpa. Some voids are present at the interface with the steel substrate and in the FeCrAlY bonding layer. It is important to outline that the irradiation did not induce any loss of adhesion or delamination effects at the thin film-substrate [9]. The ion irradiations are part of a broader irradiation project which includes irradiation experiments on coated steel samples by fast neutron flux up to high doses.

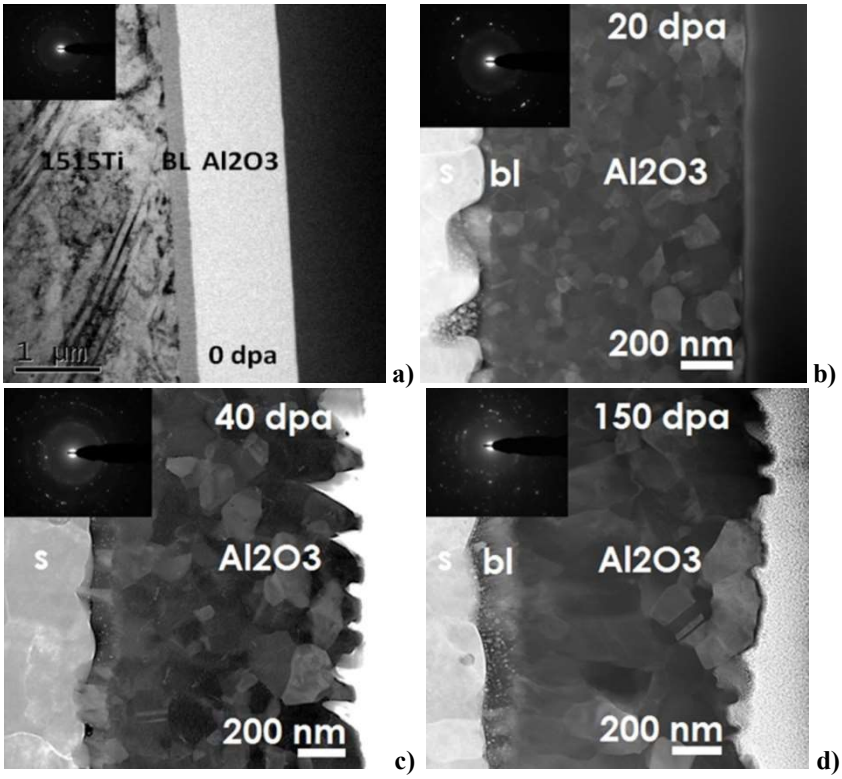

FIG.6. TEM micrographs (diffraction pattern in the insets) showing the microstructural evolution during ion irradiation: as-deposited (a) after20 dpa (b), 40 dpa (c) and 150 dpa (d) at 600 °C.

5. FINAL REMARKS

LFR systems offer great promise in terms of the potential for providing cost effective, simple and robust fast reactor concepts that are essential to long term sustainability of the nuclear energy option.

Recent efforts, particularly in the development of the ALFRED concept, have gone a long way toward verifying the advantages of lead cooled systems. Further advancements need to be done, but overall, the prospects continue to appear very positive.

Corrosion of structural materials in lead is one of the main issues for the design of LFRs. A larger effort has been dedicated to short/medium term corrosion experiments in both stagnant and flowing LBE. A few number of experiments have been carried out in pure Pb resulting in a lack of knowledge particularly on medium/long term corrosion behaviour in flowing lead. Experiments confirm that corrosion of steels strongly depends on the operating temperature and amount of dissolved oxygen. It has been demonstrated that generally, in the low temperature field, e.g. below 450°C, and with an active oxygen control system (AOC), ferritic/martensitic and austenitic steels build up a stable oxide layer which behaves as a barrier against leaching of steel elements providing thereby effective corrosion protection.

For higher temperature application, the strategy developed for the ALFRED reactor, “aims to work with an oxygen concentration in the coolant much lower than the saturation limit at the minimum operating temperature of the reactor (lower than 3.2×10^{-5} % wt, which is the saturation limit at the re-fuelling temperature of 380°C). In particular, the preferred oxygen concentration range will be between 10^{-6} and 10^{-8} % wt. in order to reduce the chance of Pb oxides formation even in case of local heterogeneities and potential deviations” [22].

The selected oxygen concentration range is positioned slightly below than the ‘active oxygen’ range required to ensure both no coolant contamination and passivation of conventional steels. As a matter of fact, this oxygen concentration range can, in principle, guarantee the self-protection of the structures exposed to the lowest temperatures (e.g. the reactor vessel at about 400°C) but not the other structures exposed to higher temperatures. However, since the passivation method is not completely effective for structures exposed above 480°C (due to the loss of protectiveness of the oxide layer), the use of other protection strategies is mandatory even in presence of a

sufficient amount of oxygen in the liquid metal. Concerning that, the protection strategy followed consists in using coatings, which have the advantage to protect the structure while maintaining mechanical and irradiation properties of the steel substrate (in particular, swelling and creep property for fuel cladding tubes).

The most promising coating for this goal consists in amorphous Al_2O_3 with nano-crystalline inclusions obtained by PLD. Differently from pack cementation technique, PLD technique allows to deposit the coating even at room temperature, thus preventing micro-structural modifications in the steel. From the point of view of the mechanical behaviour, the compatibility between steels and PLD-Al_2O_3 coating is remarkable: the nano-dispersed amorphous structure gives to the coating mechanical properties similar to those of the steel substrate and enhanced wear resistance. Moreover, the chemical compatibility of the coating with the liquid lead is excellent and corrosion is not expected in the low oxygen concentration in practice achievable in liquid Pb.

Assessment of 15–15 Ti (AIM-1) with Al_2O_3 PLD coating is in progress, including preliminary (and very promising) irradiation tests with heavy ions at high dpa, and flowing lead corrosion tests at different temperature and oxygen content into the melt.

ACKNOWLEDGMENT

Most of this work is being performed in the frame of the EERA JPNM pilot projects MOSEL, MOLECOS, CERBERUS and STAR-TREK. The authors wish to acknowledge the support from the H2020 GEMMA project under the umbrella of the EERA JPNM.

REFERENCES

[1] EJENSTAM, J., SZAKALOS, P., Journal of Nuclear Materials **461** (2015) 164–170.
[2] MULLER, G., HEINZEL, A., KONYS, J., SCHUMACHER, G., WEISENBURGER, A., et al., Journal of Nuclear Materials **335** (2004) 163-168.
[3] MARTINELLI, L., BALBAUD-CELERIER, F., TERLAIN, A., DELPECH, S., SANTARINI, G., et al., Corrosion Science **50** (2008) 2523.
[4] MARTINELLI, L., BALBAUD-CELERIER, F., TERLAIN, A., BOSONNET, S., PICARD, et al., Corrosion Science **50** (2008) 2537.
[5] MARTINELLI, L., BALBAUD-CELERIER, F., SANTARINI, G., PICARD, G., Corrosion Science **50** (2008) 2549
[6] ZHANG J., LI, N., Oxidation of Metals **63** (2005) 353.
[7] MULLER, G., SCHUMACHER, G., ZIMMERMANN, F., Journal of Nuclear Materials **278** (2000) 85.
[8] CHEN, X., STUBBINS, J.F., HOSEMANN, P., BOLIND Journal of Nuclear Materials **398** (2010) 172─179.
[9] MAITRE, A., FRANÇOIS, M., PODOR, R., GACHON, J.C., Materials Science Forum **1141** (2004) 461─464.
[10] QUANQIANG, S., JIAN, L., HE, L., ZHENGUO, Y., WEI, W., WEI, Y., YIYIN, S., KE, Y., Journal of Nuclear Materials **457** (2015) 135.
[11] YELISEYEVA, O., TSISAR, V., BENAMATI, G., Corrosion Science **50** (2008) 1672.
[12] TSISAR, V., YELISEYEVA, O., Materials at High Temperatures **24** (2007) 93.
[13] HOSEMANN, P., DICKERSON, R., DICKERSON, P., MALOY, S.A., Corrosion Science **66** (2013) 196─202.
[14] DIOP, I., DAVID, N., FIORANI, J.N., PODOR, R., VILASI, M., Thermochimica Acta **510** (2010) 202─212.
[15] COCCO, A., Annali di Chimica **45** (1955) 737─753.
[16] ARTEM, M., ABAKUMOV, J., HADERMANN, S., BALS, I., NIKOLAEV, V., et al. Angew. Chem. **118** (2006) 6849.
[17] LONG, B., TONG, Z., GRÖSCHEL, Z., Journal of Nuclear Materials **377** (2008) 219─224.
[18] WEISENBURGER, A., SCHROER, C., JIANU, A., HEINZEL, A., KONYS, J., et al., Soler Crespo Journal of Nuclear Materials **415** (2011) 227.
[19] DI FONZO, F., TONINI, D., LI BASSI, A., CASARI, C.S., BEGHI, M.G., et al. Contro, Appl. Phys. A **93** (2008) 765─769.
[20] GARCÍA FERRÉ, F., BERTARELLI, E., CHIODONI, A., CARNELLI, D., GASTALDI, D., et al., Acta Mater. **61** (2013) 2662─2670.
[21] GARCIA FERRÉ, F., ORMELLESE, M., DI FONZO, F., BEGHI, M.G., Corrosion Science **77** (3013) 375─378.
[22] AMS DOTTORATO, amsdottorato.unibo.it

CORROSION PHENOMENA INDUCED BY COOLANT, BLANKET AND FUEL SALTS: FOCUS ON STAINLESS STEELS AND HIGH NICKEL ALLOYS

A.I. SURENKOV, V.V. IGNATIEV, V.S. UGLOV
National Research Center,
Kurchatov Institute,
Moscow, Russia
Email: Surenkov_al@rrcki.ru

Abstract:

For all molten salt reactor (MSR) designs, materials selection is a very important issue [1–6]. This paper summarizes results, which led to selection of materials for MSRs in the Russian Federation. Different forced and natural loops operated in reactor and laboratory conditions with following molten salt mixtures: LiF-NaF-BeF_2+PuF_3, LiF-BeF_2-UF_4, LiF-BeF_2-ThF_4-UF_4 were tested in the Russian Federation. These non-isothermal corrosion tests were done with stainless steels (12H18N10T, EP-164) and high nickel alloys developed for MSR in the Russian Federation (HN80M-VI, HN80MTY, HN80MTW, etc.) including those developed in USA (Hastelloy–N), Czech Republic (MONICR) and France (EM-721) in the temperature range from 600 up to 800°C and mechanical loads on specimens up to 80 MPa [4–12]. To control the redox potential of the fuel and coolant salts containing beryllium and uranium, as well as, ways to maintain it at a predetermined level, special devices and methods, including molten salt clean up, were developed. Operating experience with corrosion loops has demonstrated good capability of the 'nickel–molybdenum alloys fluoride salt fuelled by UF_4 and PuF_3+cover gas' system up to 750°C. Tellurium corrosion of Ni-based alloys in stressed and unloaded conditions studies was also tested in different molten salt mixtures at temperatures up to 750–800°C also with measurement of the redox potential. HN80MTY alloy with 1% added Al and Ti is the most resistant to tellurium intergranular cracking of Ni-base alloys under study. A brief description is given of the container material work in progress.

1. INTRODUCTION

Materials research in support of the MSR concept in USA led to the development of a nickel-based alloy, Hastelloy-N, which was the main constructional material of MSRE and ensured the success of the experiment [1–3]. According to the results of Hastelloy-N tests, two problems were noted: (i) the alloy was embrittled under the action of helium, which is formed from 10B and nickel by nuclear reactions; (ii) the diffusion of the fission product of tellurium into the alloy along the grain boundaries led to its intergranular corrosion [2]. The development of the fourth generation MSR concepts required solving these problems and creating alloys of increased heat resistance, radiation and corrosion-mechanical durability when operating at temperatures up to 800°C. The compositions of these alloys are given in Table 1.

2. CORROSION CHEMISTRY

Metal fluorides that make up salt formulations are stronger compounds than the fluorides of metals entering into structural alloys. In terms of the decrease in the energy of the formation of fluorides, the metals are arranged in the series Li> Na> K> Be> Th> U3+> Zr> U4+> Al> V> Ti> Mn> Cr> Nb> Fe> Co> Ni> Mo> W [6, 13, 14]. Therefore, the fluorides of the melt do not enter into the oxidation reaction of metals contained in the alloy. When there are VF_2, TiF_2, CrF_2, FeF_2, NiF_2, HF in the melt, there are reactions:

$$nMe^1(s) + mMe^2F_n(d) \leftrightarrow nMe^1F_m(d) + mMe^2(s) \quad (1)$$

TABLE 1. CHEMICAL COMPOSITION OF NICKEL ALLOYS

Element	Hastelloy-N, INOR-8	Hastelloy-NM, 1976	Hastelloy -N, (UNS10003)	MONICR	HN80-MT	HN80-M-VI	HN80-MTY, (EK-50)	HN80-MTW	EM-721
Cr	7.52	6–8	7	6.85	7.02	7.61	6.81	7.0	5.7
Mo	16.28	11–13	16	15.8	12.1	12.2	13.2	9.35	0.07
Ti	Ti + Al	─	Ti + Al	0.026	1.72	0.001	0.93	1.68	0.13
Al	0.5 max	─	0.5 max	0.02	_	0.038	1.12	_	0.08
Fe	3.97	0.1	4 max	2.27	<0.33	0.28	0.15	<0.33	<0.05
Mn	0.52	0.15–0.25	0.8 max	0.037	<0.1	0.22	0.013	<0.1	0.086
Nb	─	1–2		<0.01	_	1.48	0.01	_	_
Si	0.5	0.1	1.0 max	0.13	<0.05	0.040	0.040	<0.05	0.065
W	0.06	─	0.5 max	0.16	_	0.21	0.072	5.5	25.2
Cu	0.02	─	0.35 max	0.016	<0.01	0.12	0.020	<0.1	_
Zr	─	─		0.075	_	─	─	_	_
B	<0.01	0.001		<0.003	<0.001	0.008	0.003	<0.0005	<0.0005
S	0.004	0.01		0.003	<0.001	0.002	0.001	<0.001	<0.0002
P	0.007	0.01		0.003	<0.001	0.002	0.002	0.02	<0.005
C	0,05	0.05	0. 06 max	0.014	0.04	0.02	0.025	<0.0035	<0.002

─ The elements were neither added to the melt nor determined.

Where $Me^1(s)$ are the metals included in the structural material: $Me^2(d)$ -metal, the fluoride of which is present in the melt as a dissolved impurity. The rate of such a reaction depends strongly on the thermodynamic activity of Me^1 in the solid solution of the structural material and on the solubility in the salt melt of the fluorides formed on its surface. For a number of metals that are included as alloying elements in the structural material (such as Al, Ti, V, Nb), the thermodynamic activity in nickel alloys or the solubility of the fluorides formed is small. Therefore, in spite of the great affinity of these metals for fluorine, reactions of the type (1) with their participation practically do not proceed. Only the reactions of reduction of fluorides of iron, nickel and hydrogen fluoride with chromium, which has a high activity in nickel alloys, are realized. These reactions, in poorly purified melts from fluorides of iron, nickel and hydrogen fluoride can lead to significant initial corrosion [6]. Hydrogen fluoride and oxygen appear in the melt as result of the interaction of the components of fluoride melts with impurities of water vapor by reactions of the type:

$$UF_4 + 2H_2O \leftrightarrow UO_2 + 4HF \quad (2)$$

$$ZrF_4 + 2H_2O \leftrightarrow ZrO_2 + 4HF \quad (3)$$

$$BeF_2 + H_2O \leftrightarrow BeO + 2HF \quad (4)$$

Therefore, the presence of moisture and oxides in the structural material (oxide films of nickel, copper, molybdenum, etc.) on its surface in contact with the fluoride salt is extremely undesirable. In this case, the reactions presented below will occur, followed by oxidation of chromium and iron in the alloy:

$$2NiO + ZrF_4 \rightarrow 2NiF_2 + ZrO_2 \quad (5)$$

$$NiO + BeF_2 \rightarrow NiF_2 + BeO \quad (6)$$

$$2NiO + UF_4 \rightarrow NiF_2 + UO_2 \quad (7)$$

The development of effective methods for purification of melts of fluoride salts from impurities of water and its accompanying oxygen (hydro fluorination), as well as from metal fluoride impurities (reduction by hydrogen, beryllium or electrolysis) were successfully implemented on loops in ORNL [15–19] and then at NRC KI [6–11].

2.1 Chromic corrosion of structural materials and control of the oxidation-reduction state of melts of fluoride salts

In the melt with the fuel component of UF_4, the corrosion of the alloys proceeds according to the reaction:

$$2UF_4\ (d) + Me\ (s) \leftrightarrow UF_3\ (d) + MeF_2\ (d) \quad (8)$$

where chromium is most vulnerable than Fe, Ni or Mo. Reaction (8) is reversible, therefore in the fuel circuit with a constant temperature gradient, chrome from the hot zone will be transported and deposited in the cold zone, forming a mechanism of continuous corrosion. The initiating factor of mass transfer is the dependence of the equilibrium constant of the reaction (8) Cr with UF_4 on the temperature, the value of which increases with the temperature in the exponential dependence and is determined by the relation:

$$Kp = (XUF_3 / XUF_4)^2 \times (XCrF_2 / A_{Cr}) \quad (9)$$

where Xi are the molar concentrations of the corresponding components; ACr - the diffusion activity of chromium for the Hastelloy-N alloy was measured and the empirical temperature dependences for the equilibrium constant (9) of the reaction (8) in the fuel salt based on the LiF–BeF_2 solvent was obtained Baes and Koger [13–14].

During circulation, the uniform concentration of CrF_2, UF_4 and UF_3 is maintained throughout the non-isothermal circuit. The sections of the circuit with a 'balance' temperature at which the chromium concentration at the surface of the alloy become equal to the concentration in the core of the salt flow by the reaction (9) come into thermodynamic equilibrium with the melt and there is no corrosion in them. At sections of the circuit, the temperature of which is above this balance temperature, the equilibrium is shifted towards the removal of chromium from the alloy surface by oxidation to CrF_2, followed by its dissolution in the fuel salt. On sections of the circuit, the temperature of which is below the balanced one, the reverse process is going on.

The speed of selective corrosion of chromium is controlled by two kinetic parameters (by analogy with heat transfer): (i) the diffusion rate of chromium in the solid alloy to its surface (the diffusion coefficient of chromium in the solid alloy); and (ii) the mass transfer of chromium from the surface to the molten salt stream [14]. The rate of corrosion loss of the Cr mass of the structural material is determined by both parameters. By the relation (9), the equilibrium concentration of CrF_2 in the salt melt increases in proportion to the square of the ratio of the molar concentration of uranium in the tetravalent state (UF_4) to its molar concentration in the trivalent state (UF_3). By changing the uranium ratio [U(IV)]/ [U(III)] downward and maintaining at an acceptable level, it is possible to minimize the rate of corrosion of the alloy in the fuel salt, and thus control the rate of its corrosion. Reduction of diffusion activity of Cr in solid alloys also increases its corrosion resistance. The diffusion coefficients of chromium in the solid alloy (DACr) and in the molten salt (DSCr), the uranium ratio [U (IV)] / [U (III)] and the chromium concentration in the melt, the chromium ACr activity for the Hastelloy-N alloy and the equilibrium constants Cr (9) for the reaction (8) were obtained during the operation of some loops in the ORNL [13–19].

It is possible to calculate the rate of chromium corrosion using these data, by the diffusion-kinetic model [14]. Studies of corrosion processes in nickel alloys and stainless steels are performed on loops with natural and forced circulation of fluoride melts in NRC KI [4–11, 22, 30–33] and ORNL [1–3,13–19] on the MSRE reactor [1]. The most representative results are summarized in Tables 2, 3 and 4. Our estimates of the Hastelloy-N corrosion rate in fuel salts are in good agreement with the experimental data for testing the alloy in NCL-16, NCL-21A, FCL-2b (ORNL) and Te3 (NRC KI). However, the rate of corrosion of Hastelloy-H in MSRE was 5 times higher than the calculated rate. This is because the reactor worked for a long time at a high redox potential (U (VI)/U (III) ≈ 200–500) and, as analysis of the content of corrosion products showed, not only chromium, but also iron was oxidized in the alloy [17]. The increased corrosion rate in MSRE was caused by the oxidation of the Hastelloy-N alloy by free fluorine formed in the fuel salt as a result of the fission of UF_4, a significant amount of which remained in the melt after its treatment with a reducing agent (metallic beryllium was introduced into the melt). Nevertheless, the rate of uniform corrosion of Hastelloy-H in MSRE was at an acceptable level of 8 μm/year.

Experimental data on the rate of corrosion of nickel alloys of the Inconel 601 type showed that it is proportional to the chromium content in them and considerably exceeds the value for Hastelloy-N alloy. For stainless steels, the corrosion rate is more than an order of magnitude higher than that of the Hastelloy-H alloy, since the base is iron, which is second only to chromium in oxidation. According to the ORNL test data [15] in NCL-1258 and NCL-22 loops and NRC KI test data [30–33] (C1 and C2, see Table 3), the corrosion intensity strongly depends on the composition of alloying additives in stainless steel. The results show that the possibilities of stainless steels as candidate materials of MSR are limited to a limiting operating temperature of 650°C, and their service life for different compositions of fluoride salts will be determined by the composition of steel and salt melt.

2.2 Tellurium intergranular corrosion of nickel alloys and development of nickel alloys with enhanced corrosion-mechanical resistance.

The key task in the development of the structural alloy of MSR is to solve the problem of tellurium intergranular corrosion (IGC). In MSRE tests, the Hastelloy-H alloy was significantly exposed to tellurium corrosion and radiation embrittlement. Therefore, the alloy was modified. Reducing the concentration of Mo up to 12% and Si to 0.1%, as well as the addition of Ti to 2% to form fine-grained forms of carbides in the alloy, resulted in a good resistance to helium embrittlement.

The alloying of the Nb alloy from 1% to 2% gave good resistance to destruction by tellurium. However, all the alloying variants of Ti and Nb alloy both individually and collectively did not provide the required resistance to tellurium and radiation embrittlement of the alloy at a temperature of 700°C, as a result of which its working temperature was reduced to 650°C [2, 24–29].

The effect of the oxidation-reduction state of the fuel salt on the intensity of tellurium IGC nickel-based alloys was found in ORNL [28, 29] during testing of Hastelloy-N samples with 71.7LiF–16BeF_2–12ThF_4–0.3UF_4 containing additives of chromium telluride. It was shown that the dependence of the intensity of the tellurium cracking of the alloy (parameter K is the number of cracks multiplied by their average depth in microns) from the oxidation-reduction state of the melt, characterized by the ratio of the concentrations of oxidized and reduced forms of uranium [U(IV)]/[U (III)], has a threshold character. As a result, the problem of the tellurium corrosion of nickel alloys in fluoride fuel salts can be solved by maintaining the ration [U(IV)]/[U(III)] below 60.

TABLE 2. INTEGRAL RESULTS OF CORROSION TESTS ON ORNL LOOPS WITH MELTS OF FLUORIDE SALTS

Test loop	Structural material	Molten salt, % mole	Fluid test conditions				T_{alloy} °C	Corr. rate μm/yr
			Circulation mode	T_{max} °C	ΔT_{max} °C	Exposure hrs		
NCL-1258	Stainless steel S-304L	70LiF-23BeF_2-5ZrF_4-1UF_4	Natural convection	688	100	6100 79400	688 688	53 26
NCL-22	Stainless steel S-316	71.7LiF-16BeF_2-12UF_4-0.3ThF_4	Natural convection	650	110	4298	650	23
NCL-16	Hastelloy–N Hastelloy–N, mod. Ti≤0.5	66.5LiF–34BeF_2-0.5UF_4	Natural convection V=2.5cm/s	704	170	28000	660 675 700	1.0(1.0*) 0.5 0.9
MSRE	Hastelloy –N	65LiF-29.1BeF_2-5.0-Zr F_4-0.9UF_4	Fuel circuit circuit	654	22	21800	654	8.0(1,6*)
		66LiF–34BeF_2	Coolant circuit	580	35	26100	580	no
NCL-15A	Hastelloy –N	73LiF-2BeF_2-5ThF_4	Natural convection V=0.7cm/s	677	55	35400	677	1.5
NCL-21A	Hastelloy –N Hastelloy–N, mod. 1%Nb	71.7LiF-16BeF_2-12ThF_4-0.3UF_4	Natural convection V=1 cm/s $U^{4+}/U^{3+}\approx10^4$	704	138	10009 1004	704 704	3.5 (3.1*) 3.7
NCL-23	Inconel 601	71.7LiF-16BeF_2-12ThF_4-0.3UF_4	Natural convection V=1 cm/s, $U^{4+}/U^{3+}\approx40$	704	138	721	704	≥34
NCL-24	Hastelloy–N, mod. 3.4%Nb	68LiF-20 BeF-11.7ThF-0.3UF_4	Natural convection	704	138	1500	704	2.5
FCL-2b	Hastelloy –N Hastelloy–N mod. 1%Nb	71.7LiF-16BeF_2-12ThF_4-0.3UF_4	Forced convection V=2.5–5 m/s $U^{4+}/U^{3+}\approx100$	704	138	4309 2242	704 704	2.6(2.5*) 0.4
FCL-2	Hastelloy –N	92NaBF4-8NaF	V=2.3 m/s V=6.2 m/s	620	170	5100 5100	620 620	12 16
LDRD	Hastelloy –N	46.5LiF-11.5NaF-42KF	Natural convection	815	566	3048	815	5

* - Calculated value for the diffusion-kinetic model

When developing Russian alloys for MSR, the main tasks were to enhance their resistance to tellurium intergranular corrosion and selective chromium corrosion, by complex alloying with elements (Ti, Nb, Al, V, W, Re, Y), suppressing their diffusion activity in the alloy and developing methods for reducing redox-potential of the melt. To this end, devices have been developed and methods for controlling the oxidation-reduction potential

for various compositions of fluoride salts containing beryllium and uranium have been developed, as well as methods of maintaining it at a given acceptable level. To this end, devices have been developed and methods for controlling the oxidation-reduction potential for various compositions of fluoride salts containing beryllium and uranium have been developed, as well as methods of maintaining it at a given acceptable level. As a result of complex studies, the HN80MTY (EK-50) alloy with enhanced corrosion-mechanical resistance to tellurium and radiation embrittlement and chromium corrosion was developed at NRC KI for MSR. The composition of which and a number of its modifications is given in TABLE 1.

Corrosion data on the resistance of Russian alloys obtained on loops in NRC KI in comparison with the Hastelloy-N (UNS10003), EM-721, MONICR alloy are given in Tables 3 and 4 [20, 21, 23].

TABLE 3. INTEGRAL RESULTS OF CORROSION TESTS IN NRC KI WITH MELTS OF FLUORIDE SALTS

Loop	Salt, in mole %	Specimens material	T_{max} °C	ΔT °C	Duration hr	Corrosion rate, μm/yr
Solaris	46.5LiF-11.5NaF-42KF	12H18N10T HN80MT	620	20	3500	250 22
KI C1 KI C2 KI C3	92$NaBF_4$-8NaF	12X18H10T EP - 164 HN80MT	630 630 630	100 100 100	1000 1000 1000	250 50 12
KI F1 KI F2	71.7LiF-16BeF_2-12ThF_4-0.3UF_4+Te	HN80MT HN80MTY	750 750	70 70	1000 1000	3.0 6.0
KI M1	66LiF- 34BeF_2+UF_4	12H18N10T	630	100	500	20
KURS-2	66LiF -34BeF_2+UF_4	12H18N10T	750	250	750	25
NCL-1	15LiF-58NaF-27BeF_2 +PuF_3	HN80M-VI HN80MTY MONICR	700	100	1600	5 5 19
KI Te1	15LiF-58NaF-27BeF_2 +Cr_3Te_4	HN80M-VI HN80MTY MONICR	700	10	400	3 3 15
KI Te2	75LiF-5BeF_2-20ThF_4 +(0.27-2.1) UF_4 + Cr_3Te_4 Average value [U(VI)/U(III)] = 5	HN80M-VI HN80MTY HN80MTW EM -721	730 735 735 735	40	250	29 57 28 10
KI Te3	73LiF -27BeF_2+ 2.0UF_4 +Te(metal) Average value [U(VI)/U(III)] =42	Hastelloy- N HN80MTY HN80MTW EM -721	760	40	256	21(20*) 8 12 22
	73LiF -27BeF_2+ 2.0UF_4 +Te(metal) Average value [U(VI)/U(III)]=85	Hastelloy- N HN80MTY HN80MTW EM- 721	800 780 800 800	40	248	45(56*) 52 63 55

* - Calculated value for the diffusion-kinetic model

The effect of the oxidation-reduction state of the fuel salt on the intensity of tellurium IGC nickel-based alloys was found in ORNL [28, 29] during testing of Hastelloy-N samples with 71.7LiF-16BeF_2-12ThF_4-0.3UF_4 containing additives of chromium telluride. It was shown that the dependence of the intensity of the tellurium cracking of the alloy (parameter K is the number of cracks multiplied by their average depth in microns) from the oxidation-reduction state of the melt, characterized by the ratio of the concentrations of oxidized and reduced forms of uranium [U(IV)]/[U (III)], has a threshold character. As a result, the problem of the tellurium corrosion of nickel alloys in fluoride fuel salts can be solved by maintaining the ration [U(IV)]/[U(III)] below 60.

When developing Russian alloys for MSR, the main tasks were to enhance their resistance to tellurium intergranular corrosion and selective chromium corrosion, by complex alloying with elements (Ti, Nb, Al, V, W, Re, Y), suppressing their diffusion activity in the alloy and developing methods for reducing redox-potential of the melt. To this end, devices have been developed and methods for controlling the oxidation-reduction potential for various compositions of fluoride salts containing beryllium and uranium have been developed, as well as methods of maintaining it at a given acceptable level.

To this end, devices have been developed and methods for controlling the oxidation-reduction potential for various compositions of fluoride salts containing beryllium and uranium have been developed, as well as methods of maintaining it at a given acceptable level. As a result of complex studies, the HN80MTY (EK-50) alloy with enhanced corrosion-mechanical resistance to tellurium and radiation embrittlement and chromium corrosion was developed at NRC KI for MSR. The composition of which and a number of its modifications is given in Table 1.

Corrosion data on the resistance of Russian alloys obtained on loops in NRC KI in comparison with the Hastelloy-N (UNS10003), EM-721, MONICR alloy are given in Tables 3 and 4 [20, 21, 23].

3. SUMMARY

Structural materials recommended for fuel and intermediate circuit MSR are special Ni–Mo alloys with low chromium concentration. The composition of the reference Hastelloy-N alloy was optimized by researchers in ORNL (USA) for corrosion resistance (in the gaseous atmosphere and in molten fluorides), for radiation resistance and mechanical properties at high temperature.

It is shown, that the redox potential of salt is a key parameter in the corrosion of MSR constructional materials. A redox-buffer pair (for example in a fuel salt ratio (UF4/UF3) can control chemical corrosion. For individual cooling salt compositions (46.5LiF–11.5NaF–42KF), such redox-buffer pair needs to be matched.

New materials are developed and tested in the Russian Federation, China (Ni–Mo–Cr alloys), France (Ni–W–Cr alloys). The Russian nickel alloy HN80MTY, doped with Ti and Al, is the most resistant to intergranular tellurium cracking when tested with molten salts of Li, Th, U/F and Li, Be, Th, U/ F up to a temperature of 800°C and with a redox-potential salt [U(IV)]/[U(III)] having a value of ≤100.

Detailed studies of the kinetics of the boundary diffusion of tellurium in candidate alloys and the mechanism of their tellurium intergranular embrittlement needs to be carried out under nonisothermal conditions simulating the operation mode of the fuel circuit of the MSR. The metallurgy and properties of these alloys need to be studied in more detail in the future and especially with regard to the resistance to irradiation and the possibility of manufacturing the required assortment of materials.

TABLE 4. TEST DATA OF TELLURIUM IGC NICKEL ALLOYS IN NRC KI

Conditions for corrosion testing of alloy samples				Mechanical properties after exposure, T = 20 C			Parameters of IGC	
Composition of salt, % mol. [U(IV)]/[U(III)]	Alloy	T_{alloy} °C	Loading МПа	σ_B МПа	$\sigma_{0,2}$ МПа	δ %	Depth cracks Lmax, μm	Parameter K, pc × μm/cm
15LiF-58NaF-27BeF_2+Cr_3Te_4 243-hour exp. Ep = 1.18V-Relative to Be reference electrode	HN80M-VI	700	0	780	400	50	75	690
		700	80	800	370	50	125	1560
	HN80MTY	700	0	820	400	47	37	380
		700	80	815	410	53	75	880
	MONICR	700	0	760	515	53	44	3590
		700	80	Brittle fracture			220	>10000
70LiF-6,9BeF_2-20ThF_4-2,1UF_4 + Cr_3Te_4 Average value [U(IV)]/[U(III)] = 500	HN80M-VI	735	0				166	3360
		730	25	665	335	43	180	8300
	HN80MTY	735	0				68	1650
		735	25	760	400	45	80	1850
	HN80MTW	735	0				350	7060
		725	25	710	350	40	220	8400
	EM-721	735	0				434	6720
		735	25	595	350	28	390	9200
70LiF-6,9BeF_2-20ThF_4-2,1UF_4 + Cr_3Te_4 [U(IV)]/[U(III)]= 100	HN80M-VI	750	20	765	410	36	No IGC	
	HN80MTY	750	20	780	410	45±3	No IGC	
	HN80MTW	745	20	820	370	48	38	540
		745	0				34	480
	EM-721	750	20	810	370	52	No IGC	
71LiF-27BeF_2 - 2UF_4 +Te 248-hour exposure Average value [U(IV)]/[U(III)] =85	Hastelloy-N (UNS10003)	800	0	–	–	–	148	4490
	HN80MTY	800	0	715	270	48	32	670
		780		745	355	56	29	530
	Ni-12Mo-7Cr-1,0 Nb	800	0	815	340	50	290	3490
	Ni-12Mo-7Cr 0,5Ti-1,0 Nb	800	0	700	280	53	112	3280
	EM-721	800	0	700	310	50	286	5830
	HN80MTW	780	0	700	270	52	126	5820
71LiF-27BeF_2 - 2UF_4 +Te 250hour exposure Average value [U(IV)]/[U(III)] =60	Hastelloy- N (UNS10003)	750	0	–	–	–	69	3500
	HN80MTY	750	0	740	340	48	No IGC	
	HN80MT	730	0	860	380	44	No IGC	
	Ni-12Mo-7Cr-1,0 Nb	750	0	730	370	49	56	1330
	EM-721	750	0	710	340	33	117	3380
	EM-721	730	0	710	280	38	103	2370
	HN80MTW	750	0	770	310	48	No IGC	

REFERENCES

[1] HAUBENREICH, P.N., ENGEL, J.R., Experience with the molten-salt reactor experiment, Nuclear Applications and Technology **8** (2) (1970) 107–140.

[2] ENGEL, J., BAUMAN, H., DEARING, J., GRIMES, W., Mccoy, H., Development status and potential program development of proliferation resistant molten salt reactors, USAEC Report ORNL/TM-6415, Oak Ridge, USA.

[3] MANLY W.D., et al., Metallurgical problems in molten fluoride systems. Progress in Nuclear Energy **2** (4) (1979) 164–179.

[4] NOVIKOV, V.M., et al., Issledovanie korrozionnoy stoykosti konstrukcionnyh materialov dlya shidkosolevyh reaktorov. Voprocy Atomnoi Nauki i Tehkniki: Atomno - Vodorodnaya Energetika i Tehnologiya **3** (10) (1981) 74–76.

[5] NOVIKOV, V.M., IGNATIEV, V.V., FEDULOV V.I., CHEREDNIKOV, V.N., Molten Salt Reactors: Perspectives and Problems. Moscow, USSR: Energoatomizdat (1990).

[6] IGNATIEV, V.V., NOVIKOV, V.M., SURENKOV, A.I., FEDULOV, V.I., Institute of Atomic Energy The state of the problem on materials as applied to molten-salt reactor: problems and ways of solution, Preprint IAE-5678/11, Moscow (1993).
[7] IGNATYEV, V.V., NOVIKOV, V.M., SURENKOV, A.I., Testing loops with salt melts (out-of-core and in-core experimental studies), Preprint IAE-5307/4. Moscow (1991).
[8] IGNATIEV, V., FEYNBERG, O., SUBBOTIN, V., et al., Molten salt actinide recycler & transforming system without and with Th-U support: fuel cycle flexibility and key material properties, Annals of Nuclear Energy **64** (2014) 408–420.
[9] IGNATIEV, V., AFONICHKIN, V., FEYNBERG, O., MERZLYAKOV, A., SURENKOV, A., et al., Molten salt reactor: new possibilities, problems and solutions. Atomic energy **112** (2012) 157.
[10] IGNATIEV, V., SURENKOV, A., Corrosion phenomena induced by molten salts in generation IV nuclear reactors, Structural materials for generation IV nuclear reactors, Woodhead Publishing Series in Energy **106**, Elsevier, Amsterdam (2016).
[11] IGNATIEV, V., SURENKOV, A., Material Performance in Molten Salts, Reference Module in Materials Science and Materials Engineering, Elsevier (2016) 1–30.
[12] DELPECH, S., et. al., MSFR: M, "Oxfordaterial issues and effect of chemistry control", GIF Symposium (Proc. Int. Conf. Paris 2009).
[13] GRIMES, W.R., Molten salt reactor chemistry. Nuclear Applications and Technology **8** (1970) 137–155.
[14] EVANS, R. B., KOGER, J.W., DE VAN, J.H., Corrossion in Polythermal Loop Systems. II, Solid-State Diffusion Mechanism with and without liquid Film Effects, ORNL-4575, USA (1971).
[15] BAES, C.F., The chemistry and thermodynamics of molten salt reactor fuels, Journal Nuclear Materials **51** (1974) 149.
[16] KOGER, J.W., Alloy compatibility with LiF–BeF2 salts containing ThF4 and UF4, ORNL-TM-4286, USA (1972).
[17] KEISER, J.R. et al., Salt corrosion studies, ORNL-5078, USA (1975).
[18] HUNTLEY, W.R., KOGER, J.W., Forced-convection loop corrosion studies, ORNL-4832, USA (1973).
[19] BAMBERGER C.E., BAES C.F., Corrosion of Hastelloy N by fluoroborate melts, ORNL-4832, USA (1973).
[20] SHAFFER, J.H., Preparation of MSRE fuel, coolant and flush salt, ORNL-3708, USA (1964).
[21] AFONICHKIN, V., BOVET, A., IGNATIEV, V., et al., Dynamic reference electrode for investigation of fluoride melts containing beryllium difluoride, J. Fluor. Chem. **130** (2009) 83–88.
[22] JENKINS, H.W., MAMANTOV, G., MANNING, D.L., YOUNG, J.P., EMF and Volta metric Measurements on the U(IV)/U(III) Couple in Molten LiF-BeF2-ZrF4 J. Electrochem. Soc. **116** (1969) 1712–1714.
[23] IGNATIEV, V.V., et al., Intergranular tellurium cracking of nickel-based alloys in molten Li, Be, Th, U/F salt mixture, J. Nucl. Mater. **440** (2013) 243–249.
[24] AFONICHKIN, V., BOVET, A., SHISHKIN, V., Salts purification and voltammetric study of electro-reduction of U(IV) to U(III) in LiF-ThF4 melt, J. Nucl. Mater. **419** (2011)
[25] MCCOY, H.E., ORNL-4782, USA (1972).
[26] MCCOY, H.E., ORNL-4832, USA (1972).
[27] MCCOY, H.E., et al., Metallographic examination of samples exposed to tellurium-containing environments, ORNL-5078, USA (1972).
[28] MCCOY, H.E., et al., Development of modified Hastelloy, ORNL-5132, USA (1976).
[29] MCCOY, H.E., et al., Status of materials development for molten salt reactors, ORNL-TM-5920, USA (1978).
[30] KEISER, J.R., Status of tellurium-Hastelloy N studies in molten fluoride salts, ORNL-TM-6002, USA (1977).
[31] IGNATIEV, V.V., SURENKOV, A.I., Alloys compatibility in molten salt fluorides: Kurchatov Institute related experience, J. Nucl. Mater. **441** (2013) 583–591.
[32] IGNATIEV, V.V., et al., Investigation of the corrosion resistance of nickel –based alloys in fluoride melts, At. Energ. **101** (2006) 278–285.
[33] IGNATIEV, V.V., et al., Compatibility of selected Ni-based alloys in molten Li, Na, Be/F salts with PuF3 and tellurium additions, Nuclear Technology **164** (2008) 130−142.
[34] IGNATIEV, V.V., SURENKOV, A.I., GNIDOI, I.P., UGLOVV.S., KONAKOV, S.A., Experimental Study on Tellurium Corrosion of Nickel-Molybdenum Alloys with Ternary Molten Salt Fluorides of Lithium, Beryllium and Uranium, At. Energ. **120** (2016) 326–330.

6. SUMMARY OF SAFETY AND OPERATIONAL ASPECTS

G. Bruna (Institut de Radioprotection et de Surete Nucleaire, France)
R. Stieglitz (Karlsruhe Institute of Technology, Germany)

This summary provides a view on safety and operational aspects, as addressed in the summaries of coolant characteristics (see Section 3 of this TECDOC), coolant confining structures (see Section 4 of this TECDOC) and interfaces (see Section 5 of this TECDOC), because they are key cornerstones for licensing of a nuclear facility. Growing international nuclear safety requirements for operation and additional considerations for anticipated events demand more sophisticated approaches for nuclear safety demonstration. This section is divided into two blocks:

— Inventory control, accountancy and qualification procedures;
— Enveloping safety analysis.

The coolant selection is the most important choice for the designer to make, considering coolant chemical and thermophysical properties, which defines temperature and pressure of the primary circuit, interactions with the confining structural materials, leak detection approach and systems, size of the containment and the heat removal system design, among others.

Thanks to the long time operating experience, especially with regard to sodium-cooled reactors, a large know-how has been accumulated. For accelerator/spallation systems, there is also a certain operational experience available for different coolants for in-pile operation, while for fusion reactors it is mainly provided through experimental facilities currently in operation.

The focus in the recent years has been directed towards the fast neutron spectrum sodium cooled reactors in the commissioning or start-up phase in Russia, India and China. The progress as documented also in this TECDOC is in brief condensed in the article context of safety and operational aspects (in this Section 6) and concentrates mainly on rather specific aspects devoted to the real set-up and thereby critical near-term R&D issues are formulated:

— Impurity monitoring (including detection devices) and purification systems (their efficiency, tritium- transfer from primary to secondary side);
— Optimized operation procedures (cleaning methods, air dryers), inspection and control methods (non-intrusive instrumentation and monitoring devices), component designs (bellows, pumps, use of advanced materials for piping, insulation and heaters,) and operational sequences;
— Leak detection and fire extinguishing methods.

Fast neutron spectrum reactors must apply the same safety standards as light water reactors at all levels, so that the safety demonstration for the specific reactor design has to be supported by validated calculation tools (both probabilistic and deterministic) with adoption of suitable safety margins as prescribed by the regulatory bodies.

Regarding the liquid metal cooled fast reactors a homogenization of safety concepts starting from the design and incorporating decay heat removal systems is underway since decades. Nevertheless, the uncertainty bandwidth of the predictive capabilities of currently existing tools compared to LWR reactors is still considerable. Essentially lacking and therefore of near-term R&D interest are well instrumented experiments with the following features:

— Single effect tests at prototypical power densities to develop more refined physical models for transitional phenomena such as Departure of Nucleate Boiling (DNB-water, sodium) or flow regime transitions;

— For material and fuel at high burn-up and dpa ratios in the correct neutron spectrum to derive functional relations for life-time and accidental behaviour.
— Simulation of reactor relevant transients allowing for verification, validation as well as uncertainty assessment of integral codes and their models.

The knowledge base for fast neutron gas-cooled and water cooled applications especially under irradiation and at proto-typical power densities is not sufficient. Hence, a R&D strategy to be developed needs to aim to reduce the complexity of the computational models for safety analysis by means of conservative problem condensation in existing fast reactor safety codes and to verify and validate those condensed models by provision of an experimental data base. Such an approach is also followed in fusion for the DEMO/fusion power plant. Also, here mainly benchmark experiments are lacking at fusion typical operational parameters, geometry configurations or time scales.

The R&D efforts on inventory control, accountancy & qualification procedures are closely linked to the enveloping system analysis. The R&D projects underway concentrate mainly on reactor systems or accelerator projects being in built or near built phase or in the detailed design phase, since those are a subject to a licensing procedure. Internationally, collaborative R&D is underway in frame of the IAEA, Nuclear Energy Agency (NEA/OECD) as well as multi-/bilateral agreements. For fusion systems the safety analysis regarding to criticality accidents as occurring in fast reactors is obsolete, however, the safe decay heat removal has to be demonstrated. In this context synergies with fast reactor R&D are given for the different coolants. The accident initiators, however, differ substantially in fusion reactor from those in fast reactors and require adequate modelling efforts accompanied by experimental confirmation. Currently, many R&D activities focus around ITER, in which the all blankets concepts will be tested and thereby also first in-pile behaviour experience on coolants will be gathered.

CONTEXT OF SAFETY AND OPERATIONAL ASPECTS

G. BRUNA
Institut de Radioprotection et de Surete Nucleaire,
Fontenay-aux-Roses, France

Abstract

This short introduction outlines the specific importance of the coolant choice in the view of a safe, secure and economical operation of a fast neutron nuclear facility. Furthermore, it is discussed how the qualification of nuclear components and their operation is integrated in the regulatory framework, which forms the key to the enveloping safety analysis as an indispensable element for a nuclear safety demonstration.

1. INVENTORY CONTROL, ACCOUNTANCY & QUALIFICATION PROCEDURES

The coolant activation in fission and fusion energy production systems strongly depends on the nature of the coolant itself and the features of the systems, as well. It can be a either a minor or a major treat to the safe operation of the installations, depending on their design and characteristics. So that suitable procedures of cleaning/decontaminations are to be considered.

Several examples can be provided for fission reactors:

— In the Metal Cooled Reactors, the coolant can be poisoned by its-own activation by-products, as it is the case for Sodium isotopes engendered by the neutron capture in the Sodium Cooled Fast Reactors and for Polonium in the eutectic Lead-Bismuth Cooled Fast Reactors;
— In the Gas Cooled Reactors, the activation of the coolant depends both on the abrasion of the graphite structures and the presence of oxidants in the gas (mainly helium). The oxidation of graphite results in a wide range of gaseous products (CO, CO2, H2, etc.) depending on the oxidant;
— In the ADS (Accelerator Driven Systems) with proton incident energies up to the GeV-range, the coolant is contaminated by lots of tritium and activated target materials which are stripped-out the spallation source.

Major care merits the particular case of the Molten Salt Reactor (MSR) where the mixing of the fuel and the coolant engenders specific problems of filtering and cleaning-out the fission and capture by-products to allowing the system keep on operating with a reactivity swing close to zero.

Fusion reactors are affected by similar problems of coolant contamination. That is namely the case for Tritium. So that specific technologies are implemented to filter it out. This topic is addressed and widely discussed in the paper:

— I. Critescu, Tritium Transfer and Extraction from Water, He, and PbLi Coolants, which presents new technologies for extraction of Tritium from various coolants, including water, He and PbLi in fusion reactors. The paper accurately points-out that the selection of these technologies depends on the accuracy of the Tritium source definition and the threshold value for Tritium release to the environment. Ahead from the activation itself, it needs to be considered the problem of the dispersion of the contaminants in the coolant from the fuel which have to be detected and cleaned-out more or less continuously depending on the operation features and design constraints (e. g. assembly plugging in boxed assembly design).

The inventory control of coolant is a major challenge for both fission and fusion systems. The topic is widely addressed and investigated in the following papers:

— B. Babu, B.K. Nashine, P. Selveraj, “Twenty Years Experience in Handling Sodium Experimental Sodium Facilities”, which underlines the safety and operational experience gained over 20-year managing sodium facilities in the Indira Gandhi Centre for Atomic Research in Kalpakkam - India - and describes the improvements proposed for design and operation of the new ones.
— N. Kharitonova, “Some aspects of Coolant Chemistry Safety regulation at Russia’s NPP with Fast Breeder Reactors”, which summarizes the main elements in regulation of the FBR coolant chemistry and chemistry control in Russian Federation, pointing-out the key requirements for chemistry in the primary and secondary circuits of FBR, as well.
— B. Annop, S. Athmalingam, S. Raghupathy, P. Puthiyavinayagam, “Design Provisions for Sodium Inventory Control in FBR” (presented in the poster session), which addresses the monitoring of the sodium inventory in

the primary and secondary circuits of Indian reactors as well as the detection and handling of leaks in the decay heat removal system of pool-type sodium-cooled FBR.

2. CONTEXT OF SAFETY AND OPERATIONAL ASPECTS

The qualification of nuclear components is aimed at guaranteeing the safe and economical operation of electrical, electronic, electromechanical and mechanical equipment of the NPPs for postulated service conditions (including the normal and abnormal 'mild' environmental conditions and the 'harsh' accidental conditions as well).

From the regulatory viewpoint, the main objective of the component qualification process is the identification of the measures and practices which are to be adopted in the fabrication, installation, operation and control processes to enable the components of the NPPs operating in a safe way for the entire duration of their lifetime. Whenever that is allowed, these practices and measures need to be generalized and harmonized to allow an extended opportunity for licencing. These measures have to account for not only the construction and operation aspects but also for the decommissioning and dismantling, in a whole.

A specific topic could be devoted to piping, structures and other passive NPP components which, because of their own design and operational use, cannot undergo conventional qualification procedures. Accordingly, their qualification is to be achieved directly by design, construction, testing and inspection, according to applicable codes.

Among them we mention the passive safety systems, the reliability and operation domain of which are extremely hard to define, because the accidental environmental conditions, which are practically impossible to realize in the testing phase, have got a direct end deterministic impact on them. Unfortunately, no paper in the session addresses this very important topic.

3. ENVELOPING SYSTEM ANALYSIS MEANS TO SERVE A FILE FOR A SAFETY DEMONSTRATION, WHICH RELIES TO INTERNATIONAL STANDARDS

The safety demonstration has to show that the NNPs and any other nuclear installation - including cycle ones - are designed and operated in any circumstance, including incidental & accidental conditions, shut-down, decommissioning and dismantling, in compliance with safety rules established and shared by the national and / or the international Regulators and translated into practice through the application of acknowledged suitable codes, standards and practices. Historically, it needs to have considered a given set of initiators and transients included in the so-called Design Basis (DBA), the remainder, or Beyond Design Basis (BDB), being addressed as an overall load.

Currently, as an application of the lessons learned from the Fukushima events, according to the more and more demanding new trends and requirements in regulation (e.g., non-evacuation of neighbouring population, practical elimination of the consequences of transients with early releases), the DBA, is expanding to practically include all internal and external known initiators.

The safety demonstration has to rely upon both probabilistic and deterministic analyses, which - respectively - allow evaluating the contribution of the initiators to the risk and quantifying it. An extended evaluation and propagation of uncertainties [1] of any nature (systematic and epistemic, as well) is to be performed to evaluate the compliance with safety rules and a suitable estimation of the residual risk is to be also to be considered.

The definition of the safety case is to be achieved adopting adequate computation tools and chains, the verification of which needs to be achieved through comparison with analytical solutions and benchmarking, and the validation needs to rely upon wide and internationally acknowledged data base resulting from comprehensive and representative mock-up experiments. The topic is addressed in the following papers.

— For fission reactors:
  i. Bojanowska-Czajka, E. Chajduk, "Study of Processes Occurring under Regular Operation of Water and circulation Systems in Nuclear Power Plants with Suggested Actions Aimed at Upgrade of Nuclear Safety" (presented in the poster session) which addresses coolant purification aspects (evaluation of the efficiency of primary circuit decontamination devices and ion exchangers for cooling water) and more general safety topics such as the tightness of fuel rods and the search of suitable ways to reduce the dose rate to the workers.

— For fusion and hybrid systems:

ii. W. Hering, X.Z. Jin, E. Buelis, S. Perez-Martin, “Operation in the Helium cooled DEMO Fusion Power plant and Related Safety Aspects”, which analyses the heat transfer process in DEMO and provides with an accurate description of the heat transport and storage systems for extraction of the pulsed thermal power generated by the plasma and its conversion to electricity;

iii. B.V. Kuteev, I.V. Daniliv, A.V. Razmerov, Yu.S. Shpanski, “Choice of Coolants for DEMO-FNS Fusion-Fission Hybrid Facility”, which investigates the features of a selection of coolants and materials for the DEMO-FNS facility for the main coolant-using components such as the divertor, the first wall, the active core, the breeding blankets.

iv. Specific attention merits a paper presenting the advanced project for production of radioactive ion beams, which could end in several applications.

v. R. Augusto, P. Bricault, M. Delonca. M. Dierckx, L. Egoriti, A. Gottberg, D. Houngbo, T. Mendonca, L. Popescu, J.-P. Ramos, S. Rothe, T. Stora, S. Warren, “High Power Molten Target for the Production of Radioactive Ion Beams”, which presents a description of the advanced project of high-power targets for production of radioactive ion beams, and its possible applications.

As a general conclusion of the session, it has been pointed-out that the safety demonstrations of the advanced systems (including fusion and fission-fusion hybrid ones) needs to rely upon and profit from those of fission reactors in operation and/or under design. Search for convergence and harmonization of regulation and practices is recommended. That could be achieved through a common work gathering the OCDE-NEA and IAEA frameworks.

REFERENCES

[1] IVANOV, E., SARGENI, A., DUBOIS, F., BRUNA, G., “Best estimate plus uncertainty (BEPU): Why it is still not widely used”, ANS Best Estimate Plus Uncertainty International Conference (BEPU 2018) (Proc. Int. Conf. Real Collegio, Lucca, 2018).

TWENTY YEARS OF EXPERIENCE IN HANDLING SODIUM IN EXPERIMENTAL SODIUM FACILITIES

B. BABU, B.K. NASHINE, P. SELVARAJ
Indira Gandhi Centre for Atomic Research,
Kalpakkam, India

Abstract

Indira Gandhi Centre for Atomic Research at Kalpakkam, India has developed expertise in design, construction, commissioning and operation of high temperature sodium systems. The Centre is actively involved in the development and manufacture of sodium sensors and devices for in–sodium examination and development of instruments for measuring sodium flow, level and leak. Design validation is achieved through experiments in sodium using scaled down models. The major sodium test facilities include 5.5 MWt Steam Generator Test Facility (SGTF), Safety grade decay heat removal loop in sodium (SADHANA), Large Component Test Rig (LCTR), In Sodium Test facility (INSOT) and Sodium Water Reaction Test (SOWART) facility. The sodium facilities were constructed for full scale testing of the critical components of Proto type Fast Breeder Reactor (PFBR) in sodium and has been successfully operated for more than 70000 hours. Many experiments were conducted, and experiences gained during operation. The PFBR components were tested in sodium, qualified and installed in the reactor. The Operation is carried out based on approved technical specifications and by trained manpower. The purity of sodium was monitored periodically by plugging meter and maintained by continuous on-line operation of cold trap. Sodium sampling was done to assess the impurity content in the loop and carbon activity assessment was conducted by nickel foil equilibration method. Sodium & cover gas purity are well maintained for over two decades. The important concern arises from high chemical energy potential of sodium coolant and primarily sodium-air and sodium-water reactions. Devices and systems have been developed to effectively address these issues. A disadvantage of sodium is its chemical reactivity, which requires special precautions to prevent and suppress fires. There have been very few leak incidents with the maximum sodium leak of 2.8 kg which was from the sodium to air heat exchanger. Sodium systems have been operating for over two decades and their performance has provided very good operational experience feedback in large scale handling of sodium experience and provided sufficient confidence for the launch of sodium cooled fast breeder reactors in India. Satisfactory performance of the sodium systems and the successful handling of sodium during incidents & during interventions for maintenance & modifications have provided us sufficient mastery over sodium technology. The paper presents the safety and operation experience gained over twenty years of handling of sodium in the operation of sodium facilities and also the modifications /improvements proposed for the new facilities.

1. INTRODUCTION

Design, construction and operation of sodium cooled Fast Breeder Reactors form the second stage of Indian Nuclear Power Programme [1]. Research and development in sodium technology has commenced in IGCAR as early as 1970 in support of Fast Breeder Test Reactor (FBTR) and then for Prototype Fast Breeder Reactor (PFBR) [2]. To test and qualify the reactor components, instrumentation systems, pool hydraulics of the reactor and to master the various facets of sodium technology, many experimental facilities in sodium and water were designed, erected and operated in the various Engineering halls at the centre. These experimental facilities have made it possible to carry out research and development activities in the challenging areas of component development and testing, sodium technology, thermal hydraulics and sodium instrumentation. Critical components required for PFBR were designed, developed and their performance was evaluated at simulated reactor operating conditions and off normal conditions in these test facilities. Testing of prototype full scale shut down mechanisms, testing of fuel handling machines, studies on the model steam generator and testing and calibration of reactor worthy sodium sensors are some of the important studies that were completed successfully.

2. EXPERIMENTAL SODIUM FACILITIES

2.1 Large Component Test Rig

Large Component Test Rig **(**LCTR) (Fig. 1) was constructed to carry out full scale testing of large sized critical components of PFBR in sodium under simulated reactor operating conditions. This facility was commissioned in 1994 and the cumulative operating hours of the test facility is more than 70,000 h [3]. The facility is housed in a 43 m tall high bay building with two large storage tanks having a total sodium hold up 100 ton.

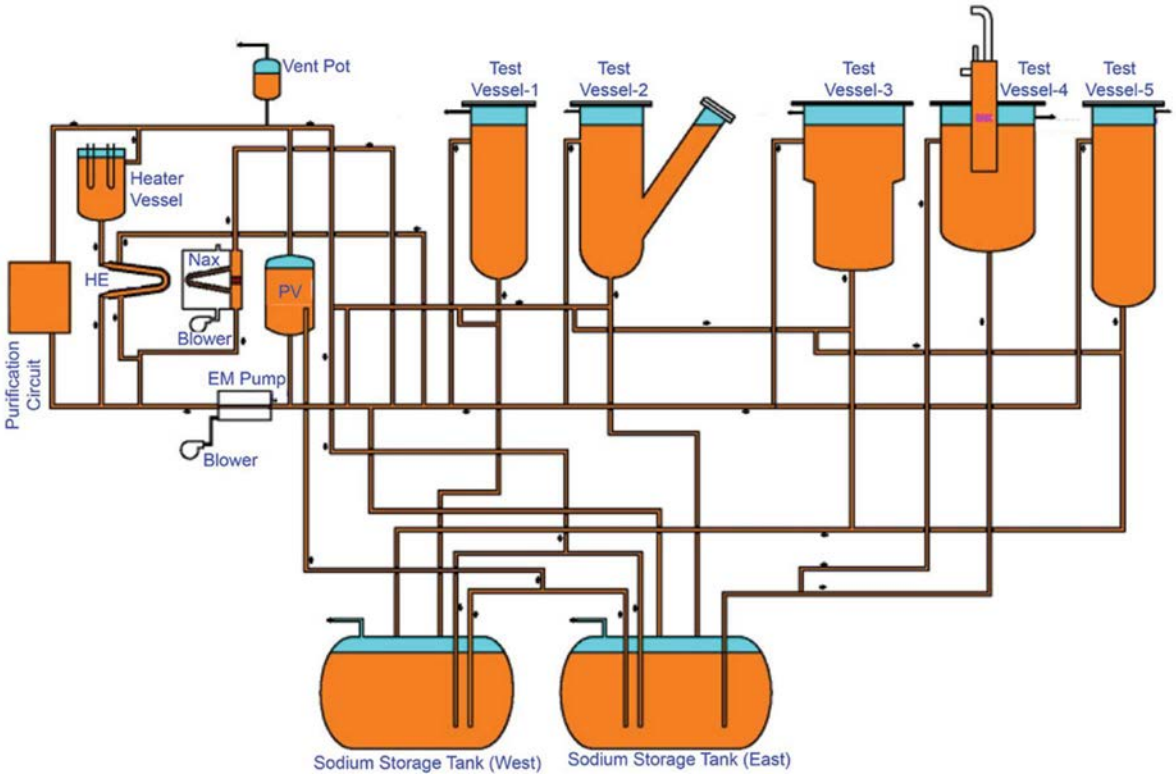

FIG. 1. Flowsheet of LCTR.

It consists of five test vessels of different capacities in which independent test conditions can be maintained, heater vessel with 200 kW immersion heaters, 150 kW sodium to air heat exchanger, air cooled cold trap, plugging indicator, Flat Linear Induction Pump for pumping requirements and sodium circulation, Permanent magnet flow meters for flow measurement etc. The pipe lines and components are provided with surface heaters, thermocouples and wire type leak detectors. MI type continuous and discontinuous level sensors are used in the test vessels. Sodium Aerosol detectors are utilized for detection of sodium fire in the loop area. A PLC based Data Acquisition and Control system is used for monitoring all the parameters in the control room. Leak collection trays are provided below the sodium containments to contain the leak. The maximum operating temperature of the test facility is 550°C and the maximum sodium flow rate is 20 m3/h. Material of construction of this test facility is Austenitic Stainless steel, grade 316. Major experiments carried out in LCTR include testing of under sodium ultrasonic scanner, calibration of sodium level probes, testing of fuel handling mechanisms, performance testing of in-sodium sensors and pumps, testing and qualification of prototype shutdown mechanisms.

2.2. Experiments in other sodium facilities

The other major experimental sodium facilities in operation are Steam Generator Test facility (SGTF), Experimental facility for Safety Grade Decay Heat Removal studies in Sodium (SADHANA), In-Sodium Test Facility (Creep loop and Fatigue loop) and Sodium Water Reaction Test Facility (SOWART). In order to cater to the research and developmental activities for future SFRs, a multipurpose sodium loop namely Sodium Facility for Component Testing (SFCT) and Sodium Technology Complex comprising of a large sodium facility, air testing station and sodium cleaning utility are also envisaged.

Experiments on Adjacent tube wastage studies at different steam leak rates, SG endurance test at rated conditions and Estimation of SG heat transfer area margin, Flow Induced Vibration studies of SG tubes, fatigue and creep experiments, Testing of Integrated Cold trap and Integrated Plugging Indicator, Development & Testing of in-sodium and cover gas hydrogen meter etc. are carried out in the other sodium facilities.

3. SODIUM LOOP OPERATION EXPERIENCE

3.1. Operation philosophy

The loop operation philosophy has been fine tuned and is followed meticulously as per an established sequence. This consists of loop filling, purification, and commencement of testing, completion of tests, dumping and removal of test chambers. The key operational sodium parameters monitored and maintained are the flow, temperature and purity [4].

The purity of the loop sodium was maintained consistently at reactor grade by continuous online purification using cold trap (CT). The cold point temperature of the CT was maintained at 393 ± 5K. The plugging runs were taken weekly to monitor and maintain the oxygen level less than 2 ppm. The performance of the CT is excellent with no plugging problem.

3.2. Impurities in sodium & purification

The impurities normally found in alkali metals include both metals and non-metals. Calcium is a particularly important impurity in sodium, arising from the electrolytic process itself. It is the impurities such as O, H and C which are of greater concern in the purification and handling of alkali metals. Because of the reactive nature of these metals, these impurities will ingress into sodium from air, moisture, Carbon-di-oxide, oils, and greases. Oxygen would thus be present not only as dissolved oxide, but also as a surface coating (solid oxide). Even though carbon solubility is low, carbon can be present as dispersed particulates.

The periodic sampling of loop sodium is carried out annually/ between test campaigns using the overflow type sodium sampler to analyse for the various metallic and non-metallic impurities. The impurity levels of oxygen, carbon and trace elements are determined by chemical analysis.

3.3. Sodium leak detection

Liquid sodium although best suited as fast reactor coolant, has certain undesirable properties like violent reaction with air / water that makes it difficult to handle. It requires a very efficient leak tight containment and specialized sensors to detect leak in the incipient stage itself to take safety measures. There are two ways by which the sodium leak is detected, namely -Sodium aerosol detection with the help of Sodium Ionisation Detector (SID) and Sodium leak detection with the help of leak sensors. SID (Fig. 2) serves to detect minute quantity of sodium leak and tests demonstrated that it can detect 1 mg of sodium per m3 (1 nanograms/cm3) of carrier gas instantaneously. Sodium leak sensors that utilize the good electrical conductivity of sodium are -wire type, spark plug type and Mutual Inductance type Leak Detector (MILD). Wire type leak sensors are used to find out the leak in the pipelines. Spark plug type leak detectors are used to detect the leak in sodium capacities, bellow sealed valves and double envelope. MILD works on the principle of decrease in mutual inductance between two coils when sodium surrounds it.

FIG. 2. Sodium Ionisation Detector (SID).

3.4. Minor sodium leak incidents

There have been very few leak incidents in LCTR. The maximum sodium leak was 2.8 kg which was from the sodium to air heat exchanger. The cause of the incident was due to failure of a finned tube to tube sheet weld joint. The other leak incidents have been due to failure of bellows from bellows sealed valves and the amount of sodium leaked was very minimum < 100 g. The leak from the bellows sealed valves were attributed mainly to stress corrosion of the bellows at the atmospheric side (leak port side) due to chloride environment or moisture, improper storage of valves in saline/moist atmosphere, or carburization of bellows.

3.5. Sodium fire and extinguishing methods

Sodium fire is characterised by short flame golden yellow in colour and dense white oxide smoke. Sodium when left open to atmosphere is oxidised spontaneously with the evolution of heat at room temperature. As sodium temperature increases, the rate of oxidation also increases, resulting in sodium catching fire, which is characterised by incandescent sparks with low flames. Sodium combustion is also very conspicuous by the large amount of white smoke evolved. Generally, the fire is extinguished by the application of dry chemical powder. Argon or nitrogen can be used to smother the fire burning in a container by flooding it. This method is slow and effective but is difficult in inaccessible areas. The method of oxygen starvation called blanketing is very effective with leak collection trays covered with corrugated sheets having small vent holes.

3.6. Handling of sodium components

The test vessel shall be kept at positive pressure and continuous argon purging is maintained during introduction and removal of components to eliminate the ingress of atmospheric air into the system. The cleaning of sodium exposed components such as stainless-steel pipes, valves, filters and other equipment are necessary for reuse of components and its safe storage. Cleaning methods involving chemical reactions could be dangerous and the resulting phenomena are complex. Alcohol and thermo fluid oil are used for removal of sodium from piping and small components like valves. Dry steam along with nitrogen purging is used for the sodium exposed components. The parts with very simple geometry like wide bore pipes or vessels may be cleaned directly by a jet of water. Large components can be cleaned by process of carbon di oxide bubbled through hot water.

4. SAFETY ASPECTS

— Operation of the rig is carried out based on approved technical specifications and by trained manpower;
— To avoid entry of water into the dump pit under conditions of inundation in the case of a severe cyclonic storm, 0.6 m height dyke is provided all around the storage tanks in dump pit;
— The dump tanks and all other sodium system components are of helium leak tight construction;
— The complete floor area inside the dump pit and side walls up to a height 2 metres are steel lined with 5 mm thick MS plate and all the joints between the plates are fully welded. This will avoid contact / reaction of sodium with concrete in the very unlikely event of sodium leak;

— Accumulation of small quantity of water over long periods under the MS liner is removed using a small pump. Water level in the sump is indicated by a level detector and in turn linked to a level alarm;
— All the test vessels are provided with over flow lines which are linked to dump tank;
— The test vessels are filled with major quantity of sodium and are operated at high temperature. Covered leak collection trays are provided below these capacities. This type of tray will collect the sodium leaking and will extinguish the fire by passive means;
— All the major capacities like sodium storage tanks and test vessels are provided with wire type leak detectors;
— Two types of fires have been considered, sodium metal fire and conventional fires and provisions are made to handle both the fires;
— The proper functioning of all the instrumentation systems, safety inter locks, dump valves, sodium leak detection system, diesel generator operation, Un Interrupted Power Supply (UPS) and battery banks are checked periodically as per operation procedure and technical specifications;
— All industrial hygiene and safety requirements as stipulated in the Atomic Energy (factories) rules are complied with during all operations in the sodium facilities.

5. IMPROVEMENTS PROPOSED FOR FUTURE FACILITIES

Based on the operating experience, the following feedback is considered for the design, construction, commissioning and operation activities of upcoming sodium facilities in Sodium Technology Complex:

— Material of construction is AISI 316 LN which is better compared to AISI 316;
— Storage tanks are planned to be vertical tanks due to easier design, low thermal shocks and easier supporting;
— Larger capacity cold trap for faster purification after experiments;
— The operating experience of EM Pumps (Annular Linear Induction Pump and Flat Linear Induction Pump) has been satisfactory and suggested to go for ALIP;
— Recommended to have a level probe in the priming vessel for the priming of the pump;
— Failure of 50 % of the heaters in vertical Heater Vessel (HV) had occurred after 15 years of operation. So, a vertical HV with additional heaters with dished ends will be suitable;
— Alternate dump paths for the large sodium capacities need to be provided;
— Mineral Insulated Sheathed heaters shall be used as surface heaters;
— Unbreakable bead type sleeves to be used to avoid spurious leak signals;
— At the outlet of the Plugging indicator blower, a smoke detector and sodium ionization flute pipe for aerosol detection is recommended;
— Periodical check of the leak port of bellows sealed valves for any blockage like foreign particles and cleaning the same, ensures prompt leak signal;
— Cleanliness shall be maintained to reduce the probability of blockage of the SID sampling flute holes and frequent surveillance/ cleaning of the flute pipes is necessary;
— Mutual Inductance type discrete sensors instead of Resistance Type Level Probes to be used;
— Air drier unit needs to be utilized in the compressed air circuit to reduce the moisture carryover to the solenoid actuated pneumatic valves;
— The Diesel Generator set shall be positioned at a higher elevation on a pedestal to take care of any revision in the design basis flood level in future.

Single crane in high bay lead to queuing of the experimental activities. Two cranes of different load carrying capacities are recommended for STC building.

6. CONCLUSION

LCTR was operated successfully for more than 20 years without any major incidents. The PFBR components were tested in sodium, qualified and installed in the reactor. There was lot of experience gained during the course of operation of LCTR. The feedback of the experience has been provided as input to the design of new test facility. The overall experience in operating the sodium loops at high temperature has given us the confidence to continue further experiments and design and commissioning of new sodium facilities.

REFERENCES

[1] RODRIGUEZ, P., BHOJE, S.B., The FBR program in India, Energy **23** (1998) 629–636.

[2] CHETAL, S.C., CHELLAPANDI, P., Indian fast reactor technology: Current status and future programme, Sadhand **38** (2013) 795–815.

[3] CHANDRAMOULI, S., KUMAR, SURESH, V.A., SHANMUGAVEL, M., PADMA, G., et al., Experimental Facilities for Performance Evaluation of Fast Reactor Components, Technical Meeting on Existing and Proposed Experimental Facilities for Fast Neutron System, IAEA, Vienna, Austria (2013).

[4] RAJASUNDARAM, P., VIJAYARAGHAVAN, S., CHANDRAN, T., SHANMUGAVEL, M., SHANMUGASUNDARAM, M., et al., Experience in long term operation of sodium loop for creep experiments in dynamic sodium at high temperature, Procedia Engineering **55** (2013) 842–849.

OPERATION OF THE HELIUM COOLED DEMO FUSION POWER PLANT AND RELATED SAFETY ASPECTS

W. HERING, X.Z. JIN, E. BUBELIS, S. PEREZ-MARTIN, B.E. GHIDERSA
Karlsruhe Institute of Technology,
Institute for Neutron Physics and Reactor Technology,
Karlsruhe, Germany
Email: Wolfgang.Hering@kit.edu

Abstract

The DEMO heat transfer and the power conversion systems (PCS) are both part of DEMO Balance of Plant (BOP). Since a tokamak operates in pulsed mode, a concept using an internal thermal energy storage system was elaborated to allow for flexible operation of the power plant also under dwell time conditions. As part of the Power Plant Physics and Technology (PPPT) conducted by the EUROfusion Consortium for the development of fusion energy, the balance of plant develops the necessary systems and interfaces to relevant DEMO systems to allow efficient energy production. This includes design adaptation and safety analyses in order to identify safety provisions to address issues not acceptable to licensing authorities. As an example, the proposed safety provisions for the integrity of the vacuum vessel (VV) are given. An outlook summarizes design development and safety investigations.

1. INTRODUCTION

The main aim of the paper is to give an overview of the operation of DEMO based on Helium Cooled Pebble Bed (HCPB) concept and to introduce the associated safety aspects. Furthermore, the needs of an electrical grid beyond 2050 have to be taken into account. As part of DEMO Balance of Plant (BoP) and Safety Analyses and Environment (SAE) activities, simulation models of the DEMO power plant are developed at KIT-INR for normal operation and accidental sequences. For BoP scoping calculations, the industrial tool EBSILON® is used to cope with feasibility studies and to simulate the Power Conversion System (PCS) [1]. For more detailed accidental analyses, for loss of coolant (LOCA) scenarios such as in-vessel, in-box and ex-vessel LOCAs, system codes RELAP5-3D and MELCOR are being applied; in future the French- German system code ASTEC will be used as well.

In that context, transport and conversion of heat, available from different sources such as Breeding Blanket (BB) including First Wall (FW), Divertor (DIV) and Vacuum Vessel (VV) for electricity generation has to be optimized. Furthermore, the utilization of any other additional energy source at suitable temperature, in order to avoid additional costs and efforts for cooling, becomes of interest also with respect to safety reasons. From the very beginning, the safety aspects are taken into account, thus defining different accidental scenarios and possible counter measures to ensure the integrity of the confinement barriers.

2. DEMO POWER PLANT DESIGN

In the simplified overview of the different subsystems of DEMO, the most important systems necessary to operate plasma in a tokamak are grouped on the left side, such as plasma heating, fuel (tritium) system, magnet systems, cryoplant and vacuum systems. The black lines indicate electrical power supply, the coloured show the connections to the tokamak and th dashed line show the power for charging the magnet during dwell time. On the right side, the heat to power conversion chain is shown consisting of the primary heat transfer system (PHTS), intermediate heat transfer and storage system (IHTS), and the power conversion system itself. If a thermal energy storage system (ESS) is integrated in the IHTS, power release to the grid in the dwell time is assured and, moreover, the FPP can act as a power sink in case of negative energy market prices. In such a case the dwell time can also be extended using the PCS only for in-house demand and the grid excess energy is stored into the ESS. All the systems on the left side of Figure 1, including the IHTS, are safety relevant.

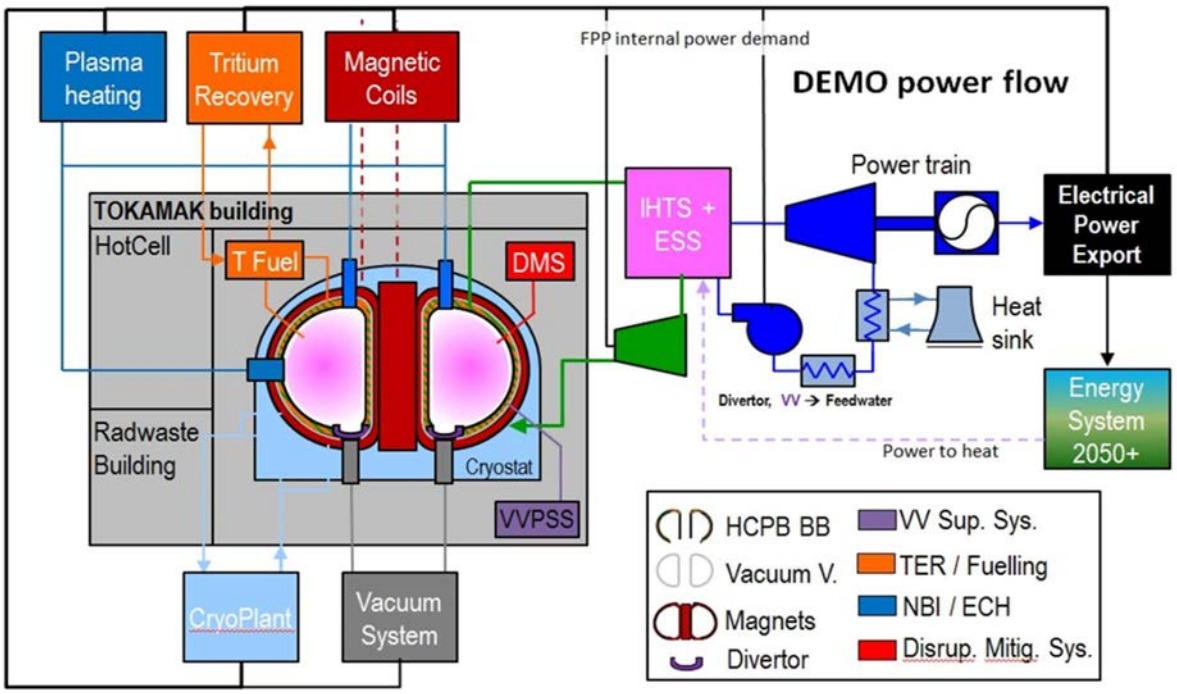

FIG. 1. Interaction of Balance of plant to the most important subsystems of DEMO.

3. HEAT TRANSFER CHAIN FOR HCPB

The DEMO BB PHTS (see Fig. 2), is subdivided into 9 loops: 3 loops, each supplying 6 inboard (IB) blanket sectors and 6 loops, each connected to 3 outboard (OB) blanket sectors [2]. Each PHTS loop has its own heat exchanger (HX) and two helium blowers to cope with blower failures to ensure 50% flow on failure. During pulse operation each IB PHTS transfers to the IHTS via a HX ~235 MW heat with a He mass flow rate of ~213 kg/s. In the same way each OB PHTS transfers ~303 MW heat at a mass flow rate of ~277 kg/s. In the ESS, energy is stored using solar salt (60% $NaNO_3$ + 40% KNO_3, Tm~220°C [5]) for dwell time operation.

The other three heat sources DIV-PFU (DIV-Plasma facing unit), DIV-Cassettes and VV shown in Fig. 2 operate with pressurized water at different power levels, system pressures and exit temperatures. Each of these heat sources has its own HX, a redundant water pump and a pressure control system. In order to ensure that the correct amount of heat is being transferred to the PCS and that the returning water to each of these 3 heat sources has its predefined parameters, feedwater flow around the 3 HXs is being split into a main flow and into a bypass flow [1]. This enables continuous operation of the PCS for any time of DEMO operation. The accumulated heat transferred to the feedwater system allows a heat-up from condenser temperature (~35°C) to app. 190°C as indicated in Fig. 2. Final heat-up to the steam generator entrance is done by live steam from HP turbine, to avoid freezing of the solar salt. In the future HITEC (53% KNO_3, 40% $NaNO_2$ 7% $NaNO_3$), a molten salt mixture with an operational range from 130°C to 550°C will be used to reduce live steam consumption.

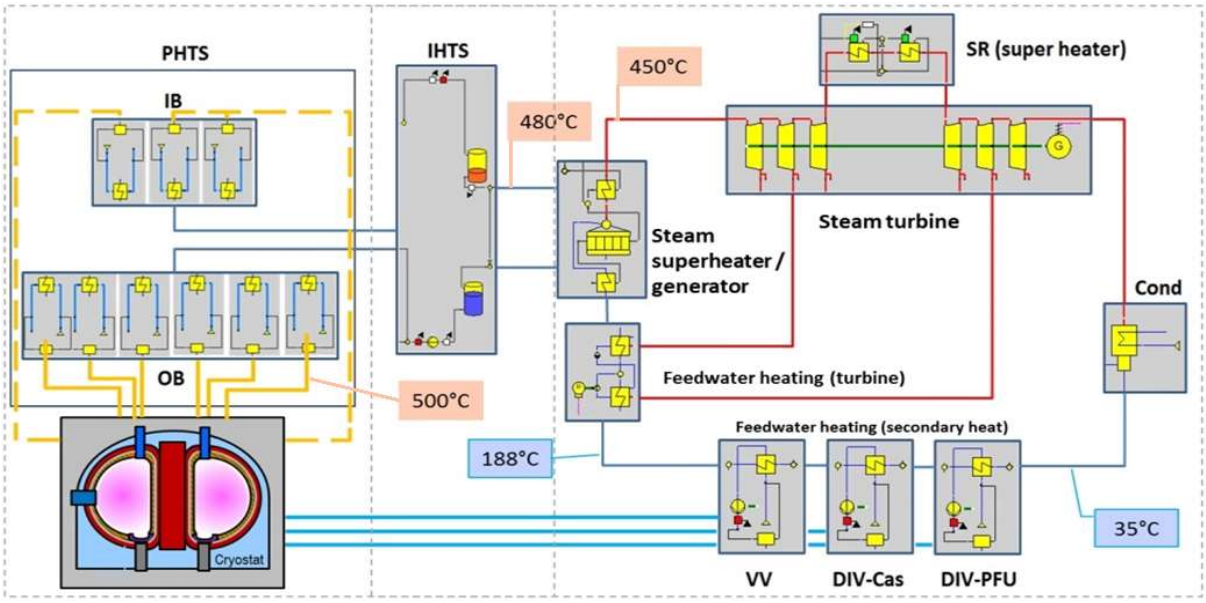

FIG 2. DEMO HCPB heat transfer chain composed of PHTS, IHTS, and PCS, including heat usage of diverter and vacuum vessel. Data are for the pulse phase operation [4].

In the PCS scheme (Fig. 2) two steam re-heaters are foreseen powered by solar salt from the ESS to operate during the dwell time. The simplified turbine schematic shown here is presently updated using experiences from a turbine manufacturer to come as close as possible to state-of-the-art.

For the situation in the dwell time (see Figure 3) the complete scheme of the EBSILON® simulation shows the complexity of the system developed so far. During dwell time only, the decay heat of app. 1% has to be removed from the BB segments. Also, the power from DIV and VV drop to app. 1MW each. This means that all power for feedwater heating, steam generation, and super-/re-heating has to be supplied by the ESS. For that purpose, 8000t of solar salt are necessary. The further development of the ESS relies on research performed in concentrated solar power (CSP) technology.

During dwell time, the gross power output is higher compared to pulse time, since the power of the PHTS blowers is significantly reduced. From the dwell time set up, we can learn that with an IHTS including an ESS, the loss of off-site power scenario can be eliminated practically, however substituting it with the LOFA in the IHTS. Since the IHTS is on ambient pressure and the storage technology is well proven by CSP facilities worldwide, that risk can be reduced by conventional techniques. On facility load, the energy stored in the ESS may last for several days, depending on systems activated. Despite of the fact, that the tritium concentration in the helium of the PHTS is rather small, the penetration through the heat transfer interface of the HX and the storage of tritium in the solar salt has to be investigated.

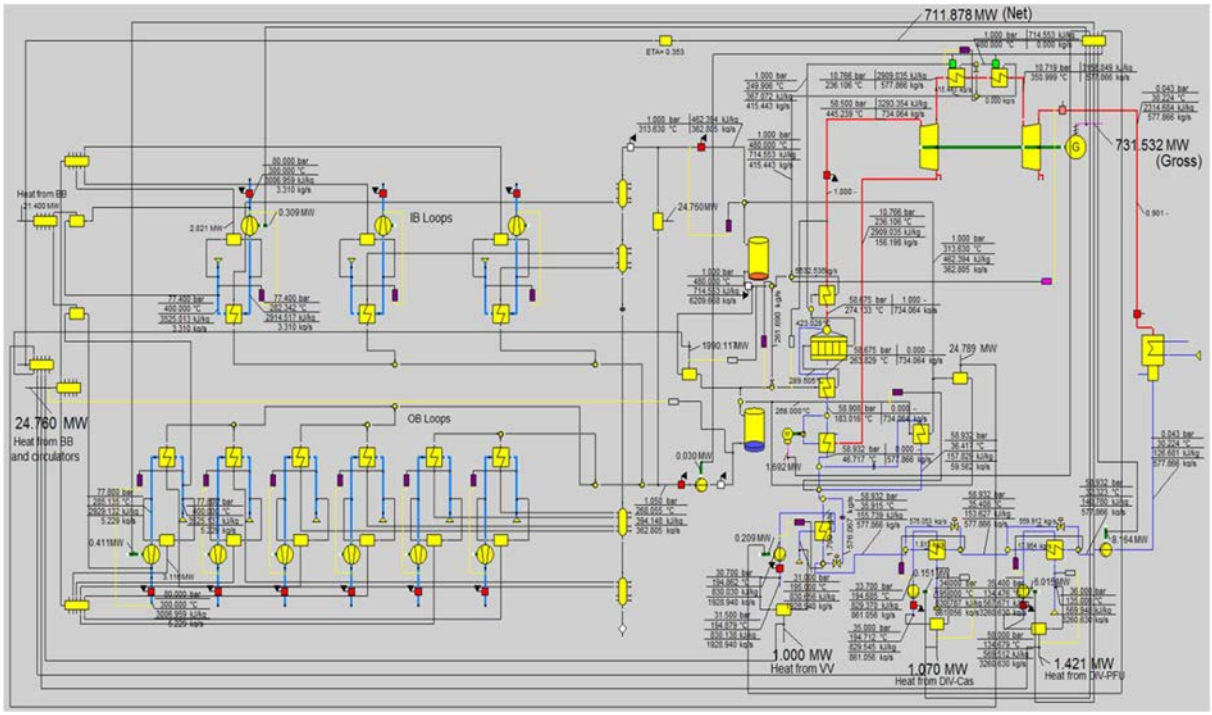

FIG. 3. Detailed power plant data computed by EBSILON® optimized for power output during dwell time [5].

4. SAFETY INVESTIGATION

Simulations to assess safety features of the PHTS and HCPB systems are performed with MELCOR for in-box and in-vessel LOCA taking place in one OB blanket module (BM) at the equatorial level [6]. The basic nodalisation scheme is shown in Fig. 4 right side with a representation of the discretisation of one outboard sector, which comprises three BB segments. The model of the affected BM, which is connected to the VV and suppression tank (ST) to address LOCA conditions correctly, is integrated in this loop (symbolised with blue box in FIG. in the middle segment). The rupture discs and bleed lines of safety system are simulated by simple valves.

Water cooled (WCLL) and helium cooled systems (HCPB, HCLL, DCLL) operate with high system pressure at 15.5MPa and 8MPa, respectively. The design pressure of the VV is at ~0.2MPa, the confinement pressure is significantly below 0.12MPa. The general consequences of any PHTS accident is a pressure increase either in the VV or in the tokamak confinement.

In case of a FW failure, the inventory of the destroyed FW segments and the connected PHTS loop ingress into the VV increasing the system pressure above the design limit. Rupture discs are installed to avoid such a situation, releasing the inventory into the VVPSS. Also, in case of divertor (DIV) leakage or ex-vessel damages of the PHTS the pressure increase inside the tokamak confinement has to be limited below safety pressure or design pressure limits.

The second important aspect is the prevention of the release of contaminated fluid i.e. tritium, Activated Corrosion Products (ACP), and/or dust to the environment. While steam can be condensed to reduce the pressure and volume, helium as a non-condensable gas requires an expansion volume (EV) to safely keep the inventory inside the facility.

Example: FW failure with subsequent VV failure. With the assumed relieve line sizes and a 0-D approach, only small leak sizes are tolerated by the VV. So, several relieve lines are necessary each supplied with 3-4 rupture discs, each in the size is limited to DN800! Nevertheless, the enthalpy, kinetic energy, and in case of water the latent heat of condensation have to be kept under control.

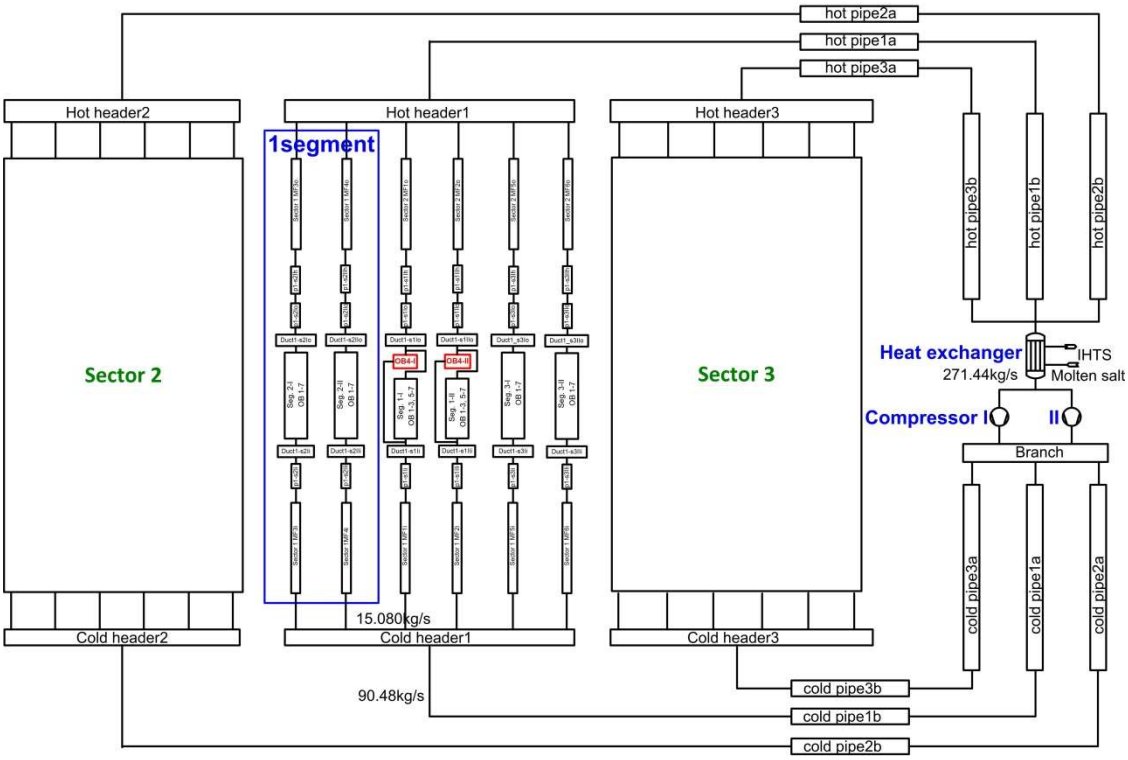

FIG. 4 MELCOR model for one OB loop of the PHTS [6].

Initially a very large EV made of concrete or steel was expected for the helium cooling option to store the helium after breach. Considerations revealed that such a structure has also to withstand high thermal loads and tensile stresses due to the pressure and temperature transients in case of FW failure. The basic idea behind the proposed concept is that it is not necessary to develop a dedicated pressure suppression system for water and Helium, separately. A single VVPSS (see Fig. 5) comprises a cooler for enthalpy reduction, in a pool scrubber to wash out ACPs and tritium and to reduce pressure level by water condensation and a subsequent expansion volume for helium. The cooler is necessary to reduce the superheating of the steam, so that the scrubber can work with shallow water (reduction of back pressure).

The EV is realized by inflatables used for intermediate helium storage in cryogenic systems. Modularisation can be adjusted to allow failure of one balloon without jeopardizing the release limitations to the environment. This seems feasible since the pool scrubber reduces the tritium and the ACP concentration in the helium. When that design is accepted as VVPSS/EV, detailed 1-D calculations will determine the necessary sizes, depending on realistic FW failures sized.

5. SUMMARY

A DEMO balance of power concept has been developed so that safety investigations can start and deliver insights into the safety margins in case of accidental situations. The BOP system has been designed and optimized to demonstrate that DEMO is able to cope with the challenges of the Energy system beyond 2050, where worldwide a substantial contribution of renewables is expected. The vision is that a FPP is a stabilization element in any energy system. Safety is included from the very first moment of the design especially with respect to safety provisions in order to work for elimination of risks.

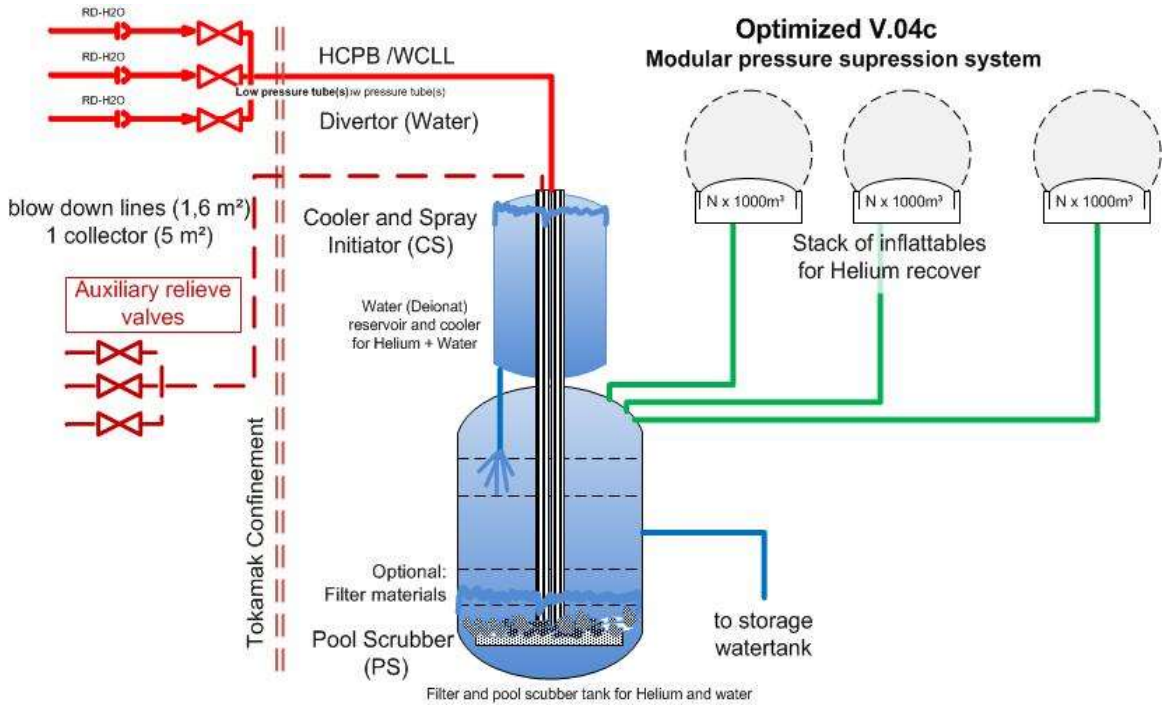

FIG. 5. Combination of vacuum vessel pressure suppression system and expansion vessel (HCPB) [8].

ACKNOWLEDGEMENT

This work has been carried out within the framework of the EUROfusion Consortium and has received funding from the Euratom research and training programme 2014-2018 under grant agreement No 633053. The views and opinions expressed herein do not necessarily reflect those of the European Commission.

REFERENCES

[1] BUBELIS, E., HERING, W., Final Report on Deliverable Conceptual designs of PHTS, ESS and PCS components for DEMO BoP with Helium cooled BB and water cooled BB concepts, KIT report No. INR-04/16, FUSION **485** (2016).

[2] BARUCCA, L., CIATTAGLIA, S., CHANTANT, M., DEL NEVO, A., HERING, W., "Status of EU DEMO Heat Transport and Power Conversion Systems", ISFNT (Proc. Int. Conf. Kyoto, 2017).

[3] Magnetic Fusion Energy from Experiments to Power Plants: Power Extraction, Woodhead publishing Series in Energy **99**, Elsevier (2016).

[4] HERNÁNDEZ, F.A., et. al., "Overview of the HCPB Research Activities in EUROfusion", 27th IEEE Symposium On Fusion Engineering (Proc. Int. Conf. Shanghai, 2017, Paper No.532).

[5] BUBELIS, E., HERING, W., PEREZ-MARTIN, S., "Conceptual Designs of PHTS, ESS and PCS Components for DEMO BoP with Helium Cooled BB Concept", ISFNT (Proc. Int. Conf. Kyoto, 2017).

[6] JIN, X.Z., "BB LOCA analysis for the reference design of the EU DEMO HCPB blanket concept", ISFNT (Proc. Int. Conf. Kyoto, 2017).

[7] FERNANDEZ, A.G., et. al., Thermal characterization of HITEC molten salt for energy storage in solar linear concentrated technology, J. Therm. Anal. Calorim. **122** (2015) 3–9.

[8] HERING, W., PEREZ-MARTIN, S., MAZZINI, G., Combined system VVPSS/EV, PPPT WPSAE Progress Meeting (2016).

SOME ASPECTS OF COOLANT CHEMISTRY SAFETY REGULATIONS AT RUSSIA'S NUCLEAR POWER PLANT WITH FAST REACTORS

N. KHARITONOVA, R. SHARAFUTDINOV
Scientific and Engineering Centre for Nuclear and Radiation Safety,
Moscow, Russian Federation
Email: kharitonova@secnrs.ru

Abstract

The basic directions of regulatory documents improvement in the part of requirements establishing to liquid metal coolants chemistry and chemistry control at NPPs with fast reactors in Russia are considered.

1. INTRODUCTION

The necessity to optimize the coolant chemistry regulations caused by the requirements to ensure the integrity of safety barriers on the routes of ionizing radiation and radioactive substances propagation into environment and to ensure the reliability and availability of the main plant structures, systems and components that have a bearing on safety is presented. The issues of establishing requirements to the development, justification and maintenance of chemical regimes are considered. The principles are listed on the basis of which the quality indicators of coolant and working environments of nuclear power plant safety-important systems are developed, established and maintained.

The information regarding basic safety requirements reflected in current regulatory documents that establish general requirements to quality of liquid metal coolants of fast reactors (NP-018-05, NP-001-15, NP-082-07) is provided. It is presented that key requirements to coolant chemistry of primary and secondary sodium of fast breeder reactors (BN) are the following ones:

— Minimization the construction materials corrosion in sodium to exclude a sodium contact with water and leaks of sodium;
— Providing the fire protection measures;
— Minimization of corrosion products mass transfer in sodium loop systems;
— Ensuring the control of sodium and shielding gas quality;
— Using primary and secondary sodium purification systems effectively to remove impurities;
— Providing the sodium clean up performance.

General requirements related with the technical process to ensure the proper quality of heavy liquid metal coolants (lead, lead-bismuth), which are of major importance for a reactor unit equipment safety ensuring, are considered. In particular, the following requirements are addressed:

— To exclude the slagging with lead oxides and corrosion products of structural materials of heat transfer surfaces of safety-important systems, as well as safety systems;
— To provide for the minimum corrosion of structural steels of equipment and pipelines in contact with lead coolant;
— To provide for the minimum deposits on the heat transfer surfaces of fuel rods, equipment and in pipelines of safety-important systems (including in gas systems);
— To provide for instrumentation devices to control the process correctness, equipment and pipelines integrity;
— To exclude the generation of hydrogen explosive concentrations in systems and equipment where the hydrogen accumulation is possible during operation.

Using of liquid metals as coolants of nuclear power plants makes it possible to create highly efficient power plants in nuclear power engineering [1]. Increasing the level of NPPs safety is largely determined by the level of optimization of physical and chemical processes in the system coolant- construction materials - impurities present in this coolant. The dependability of any equipment component of nuclear power plants is closely related to chemistry conditions (regimes) in which the equipment is operated (i.e. it is related to the environment or medium the equipment is in contact with). This environment is never absolutely pure liquid metal coolant, but always contained chemical additives or contaminated by corrosion products, gases, salts etc. To control the allowable -

from the safe nuclear power plant operation point of view - chemical additives or contamination level chemistry specifications have to be set up, as well as the means to maintain these specifications.

Russian Federal Rules and Regulations in the field of nuclear energy establish a number of requirements to chemistry at nuclear power plants (NPP) and to systems required for chemistry control. The basic safety requirements are reflected in the current regulatory documents that establish general requirements for the quality of coolants, including liquid metal for fast reactors:

— “General Safety Rules of Nuclear Power Plants” (NP-001-15);
— “Nuclear Safety Rules for Nuclear Plant Reactor Units” (NP-082-07);
— “Requirements to the Content of Safety Analysis Report for Nuclear Power Plants with Reactors on Fast Neutrons “(NP-018-05);
— “Rules for the Arrangement and Safe Operation of Equipment and Pipelines of Nuclear Power Plants" (NP-089-15).

The requirements of these normative documents are of a general nature and are limited to indications that:

(a) In design of NPP, it needs to be established (in Safety Analysis Report needs to be reflected) the requirements to the chemical regimes in the systems and elements of NPP, which needs to be observed during operation of NPP in order to maintain the integrity of physical barriers to the spread of ionizing radiation and radioactive substances into the environment (paragraph 3.1.19 of NP-001-15);
(b) In Technical Specifications of the NPP unit must be determined (established) operational limits and conditions for safe operation relating to control of the chemical regime (paragraph 4.1.3 of NP-001-15).

Some proposals to development of safety regulation for chemistry at NPP with regard to fast sodium reactors and to reactors with a heavy metal coolant are performed below.

2. CHEMISTRY CONTROL OF COOLANT FOR THE FIRST AND SECOND CIRCUITS OF FAST SODIUM REACTORS (BN)

The Russian experience in the development of reactors on fast neutrons with sodium coolant (BN-350, BN-600, BN-800) has been recognized as successful worldwide. The evolution of the BN-type power reactor began with the commissioning of the BN-350 unit in 1973. The Unit 3 on Beloyarsk NPP (BN-600) with a capacity of 600 MW was put into operation in April 1980 and is in operation up to the present time, and its operation has been extended to 2020. The stable operation of the Unit 3 of the Beloyarsk NPP with semi commercial reactor BN-600, as well as the commissioning at the Beloyarsk NPP the Unit 4 (commercial fast reactor BN-800 (800 MW (e)) with the fast neutron reactor in November 2016, was an important milestone in the development of LMFR technology. Current efforts with regard to LMFRs in the Russian Federation are directed towards improving safety margins.

Sodium, which has a low corrosive aggressiveness in relation to construction materials, ensures their high corrosion resistance during the whole lifetime of the NPP unit by minimizing corrosion and erosion-corrosive wear (FAC) processes in all operating modes. However, sodium has a high chemical activity to water and oxygen, which increases the importance of providing the fire protection measures.

Technical requirements to the quality of sodium of reactor purity for BN type reactors (BN-600, BN-800) are currently established by the industry standard OST 95 10582-2003, which applies to metallic sodium, used as a coolant for fast reactors, and establishes requirements for methods of impurity control.

The technical requirements of the standard OST 95 10582-2003 are established both for the period of delivery of sodium from the manufacturer and for the period of operation of the reactor (primary + secondary circuits).

The standard OST 95 10582-2003 defines the list of regulated impurities and their allowable content in sodium. Both on delivery and during operation is regulated the content (limit mass concentrations) of potassium, calcium, carbon, chlorides, nitrogen, iron, silicon, bismuth, barium, tin, oxygen, hydrogen in sodium and radionuclide 137Cs (specific activity is limited only by operation at the level of 185 M Bq / kg). The standard OST 95 10582-2003 provides that in the absence of sources of impurities and with constant analysis results (sampling and

automatic monitoring), the mass concentrations of chlorides, silicon, barium, nitrogen, potassium and calcium can be excluded from the list of controlled parameters.

Principles for conduct of primary and secondary chemistry for fast reactors (BN), used liquid metal sodium as a coolant are aimed at:

— Preventing the formation of sodium oxides and other compounds on the surface of primary equipment to avoid ingress of these compounds into the reactor core;
— Minimising the construction materials corrosion in sodium to exclude a sodium contact with water and leaks of sodium;
— Providing the sodium clean-up performance to remove oxides, hydrides, carbonates, etc. in the period of initial accumulation of coolant;
— Providing the fire protection measures;
— Using primary and secondary sodium purification systems effectively to remove impurities during the plant operation;
— Ensuring the control of sodium and shielding gas quality;
— Reducing the concentration of iodine and caesium radionuclides in sodium coolant.

BN third water chemistry control programmes are plant-specific programmes that protect the steam generators and other components of third circuit from corrosion-related damage and performance losses. They focus on the following:

— Minimising the deposits on heat exchange surfaces of steam generators, steam super heaters and on the flow-parts of the turbine;
— Reducing flow-assisted corrosion and corrosion product input into the steam generator;
— Maintaining turbine condenser reliability and leak-free;
— Reducing impurity intrusion sources such as resin fines;
— Using condensate purification systems to remove soluble and insoluble impurities;
— Using chemical treatments;
— Verifying high-quality makeup water.

3. GENERAL REQUIREMENTS FOR CONDUCT OF CHEMISTRY FOR FAST REACTORS, USED HEAVY LIQUID METAL COOLANTS (LEAD, LEAD-BISMUTH)

Heavy liquid metal coolants (HLMC) including lead-bismuth and lead make significant corrosion and erosion impact on construction steel elements. For example, liquid lead used in the reactor can contain suspended impurities, the content of which can vary due to corrosion of structural materials, erosion of oxide films, possible leaks in the steam generators, ingress of impurities into the primary circuit during repair work, etc. These impurities contained in the lead coolant can lead to the formation and accumulation of deposits on the surfaces of the heat exchange equipment, in the core and in the stagnant zones of the primary circuit. This can lead to a change in the thermal and hydrodynamic operating modes of the equipment [2].

The possible way to ensure the long term reliable operation of steels of the primary system components operating in contact with HLMC is to provide protective coating on the steel surface.

By now, for this purpose, Russian scientists have developed oxygen-based technology of structural steel surface passivation [3]. This technology implies formation of protective oxide films on the steel surface and assurance of their integrity during plant operation by maintaining specified oxygen potential of coolant (i.e. providing the concentration of oxygen in the coolant in a given range). In case of HLMC circuits operation without purposeful supply of dissolved oxygen to the coolant spontaneous deoxidization of coolant takes place down to the level, at which corrosion protection of structural steels cannot be provided.

Analysis of the current state of work on the technology HLMC3 shows the need to solve the following main tasks of heavy liquid-metal coolant technology (lead, lead-bismuth), fundamentally important for ensuring the safety of reactor plants:

— Ensuring the required purity of the coolant to maintain design limits and conditions specified in order to maintain the integrity of physical barriers in the path of ionizing radiation;
— Excluding the slagging with lead oxides and corrosion products of structural materials of heat transfer surfaces of safety-important systems, as well as safety systems;
— Providing the minimum corrosion of structural steels of equipment and pipelines in contact with lead coolant;
— Providing the minimum deposits on the heat transfer surfaces of fuel rods, equipment and in pipelines of safety-important systems (including in gas systems);
— Providing the instrumentation devices to control the process correctness, equipment and pipelines integrity;
— Excluding the generation of hydrogen explosive concentrations in systems and equipment where the hydrogen accumulation is possible during operation.

The normative documents on the chemical regimes of HLMC need to formulate the requirements for the technological procedures such as:

— Preparation of coolant (Pb-Bi or Pb) and filling of NPP circuits;
— Preliminary passivation of reactor plant elements before their installation;
— Passivation of the inner surface of the primary circuit of the reactor plant;
— Coolant technology concerning repair and refuelling procedures;
— Coolant purification and removal of impurities from the circuit surfaces during normal operation;
— Control of coolant oxidizing potential during operation of NPP with HLMC;
— Purification of cover gas in the liquid metal circuit.

The quality of the coolant is affected by the composition of the shielding gas (argon) in the gas cavity of the reactor before filling the primary circuit with a coolant and when operating the reactor. At present, the quality of argon is regulated by GOST 10157-79 “Argon gaseous and liquid. Technical specifications”. For the projected units with HLMC it is recommended to develop the quality standards for shielding gas. Criteria need to be formulated that define the requirements for:

— Means and methods for controlling the content of normalized impurities in a shielding gas;
— Purification systems of shielding gas in the HLMC circuit.

4. GENERAL PROPOSALS ON THE ESTABLISHMENT OF GENERAL REQUIREMENTS FOR THE ORGANIZATION OF THE CHEMICAL REGIME OF LIQUID METAL COOLANTS AT RUSSIA'S NPPS WITH FAST NEUTRON REACTORS

The chemical regime of LMC needs to be developed and maintained in such a way as to ensure:

— Integrity of physical barriers (fuel elements and the boundaries of the coolant circuit of the reactor);
— Corrosion resistance of construction materials of equipment and pipelines of systems important for safety throughout the lifetime of the NPP unit by minimizing corrosion and corrosion erosion processes under all operating conditions;
— Minimum amount of deposits on the surfaces of fuel elements, equipment and pipelines of NPP systems important for safety.
— Prevention of flammable gases accumulation in equipment and pipelines of NPP systems in explosive concentrations.

In order to ensure the radiation safety, the chemical regime of NPPs with LMC needs to help to reduce to a reasonably achievable level of radiation exposure to personnel caused by activated corrosion products forming deposits on the surfaces of equipment and pipelines of NPP systems and reagents to maintain the LMC chemical regime.

By analogy with the requirements for the NPP water chemistry [4] in normative documents for the LMC chemistry it is recommended to provide the following requirements:

— LMC chemistry control needs to include the correct application of the appropriate chemistry regimes for safety systems and safety related systems. The appropriate chemistry regime will depend on the design of the system and its construction materials;
— The control parameters selected need to be the most important LMC chemistry parameters for monitoring the LMC chemistry regime and monitoring for the presence of deleterious impurities. In addition to control values, expected values may also be specified for internal use by plant staff in order to avoid a chemistry parameter inadvertently exceeding its limit value;
— If a control parameter is outside its limit values, degradation of conditions for structures, systems and components may occur in the long term and may result in unavailability of safety systems. Thus, graded action levels may be specified in advance for control parameters; if deviations from these levels occur, corrective actions need to be initiated progressively within an acceptable period of time and further corrective actions need to continue to be applied until plant shutdown, if necessary;
— In addition, diagnostic parameters may be defined. These provide further information on the chemical status of the plant and can help to identify the reason for any deviation in the LMC chemistry regime.

5. CONCLUSIONS

The information is provided on the basic safety requirements reflected in the existing regulatory documents that establish general requirements for the quality of liquid metal coolants for fast reactors at NPP of the Russian Federation.

The reasonable practicality is shown for optimization of LMC chemistry regulation in the part of chemical regime concept choice, as well as the basic principles and criteria for ensuring the safety of NPP by development, establishment and providing of the chemical regime.

Reasonable practicality is shown to divide all liquid-metal coolants parameters (by analogy with water-chemistry) for control and diagnostic parameters and to specify the graded action levels in advance for LMC coolant control parameters. If a parameter exceeds its limit, appropriate actions need to be taken to recover its normal operating value within a specified time.

REFERENCES

[1] ARNOLDOV, M.N., KOZLOV, F.A., SOROKIN, A.P., “Physical chemistry and technology of liquid metal coolants. International Conference Thermal Physics of Fast Neutron Reactors”, (Proc. Int. Conf. Obninsk, 2014).

[2] INTERNATIONAL ATOMIC ENERGY AGENCY, Liquid Metal Coolants for Fast Reactors Cooled by Sodium, Lead, and Lead-Bismuth Eutectic, Nuclear Energy Series No. NP-T-1.6, IAEA, Vienna (2012).

[3] MARTYNOV, P.M., ASKHADULLIN, R.SH., ORLOV, JU.I., “Current issues and the tasks of heavy liquid-metal coolant technology for nuclear power plants (lead, lead-bismuth)”, TZHMT-2013 (Proc. Int. Conf. Obninsk, 2013).

[4] INTERNATIONAL ATOMIC ENERGY AGENCY, Chemistry Programme for Water Cooled Nuclear Power Plants, IAEA Safety Guide, SSG-13, IAEA, Vienna (2011).

DESIGN PROVISIONS FOR SODIUM INVENTORY CONTROL IN FAST BREEDER REACTORS

B. ANOOP, S. ATHMALINGAM, S. RAGHUPATHY, P. PUTHIYAVINAYAGAM
Indira Gandhi Centre for Atomic Research,
Kalpakkam, India
Email: anoop@igcar.gov.in

Abstract

Sodium is the most widely used coolant in fast breeder reactors. Sodium inventory control in the primary, secondary and decay heat removal circuits in Fast Breeder Reactors is necessary to ensure heat transfer from the core to ultimate heat sink under all operating states of the reactor. Quantity of sodium used in a reactor depends on many factors like pool type or loop type reactor, heat transfer capacity, number of loops in each circuit, configuration of the components in the loop, size of piping and components of the loop, operating parameters etc. The sodium inventories in the heat transport systems and connected loops are continuously monitored by level probes and leak detectors. Both automatic and manual actions are taken if any variation from the normal levels or sodium leak are reported. Engineered safety features are employed to limit the extent of sodium leakage. In case of reactor vessel leakage, sodium will be contained in the safety vessel to ensure heat transfer through the heat exchangers of secondary and decay heat removal circuits. In case of any leak in sodium to sodium heat exchanger tube, sodium from secondary / decay heat removal loops will enter into the primary sodium. Maintenance of proper sodium inventories in the systems is required for safe, efficient and economic operation of FBR. Hence, sodium inventory in all the sodium systems in FBR is to be controlled, monitored and recorded for accountability and to ensure availability of coolant for the process purposes.

1. INTRODUCTION

Sodium is the most widely used coolant in Fast Breeder Reactors (FBR) due to its availability, good thermal properties and neutron economy. Thermal power generated in the core is transported to the heat sink by circulating sodium in the heat transport loops. The normal heat sink is steam-water circuit connected to a turbo-generator plant in case of a power plant or to a simple condenser in case of experimental reactors without the intention of power generation. In addition to this, there can be a dedicated heat transport system for removal of decay heat from the reactor core to an ultimate heat sink, like atmospheric air, during unavailability of normal heat transport path. Usual medium of heat sink is either steam-water or air. In order to avoid adverse effects of direct mixing of heat sink medium to sodium in the reactor core, intermediate sodium heat transport loops needs to be employed between the primary sodium circuit and the heat sink medium, for transfer of thermal power. Sodium capacities of the heat transport systems have to be optimally decided to enable safe, efficient and economic operation of the nuclear reactor. Provisions would be normally incorporated in the design to enable maintenance of inventories in the sodium systems to the required level in a failsafe manner. The description of systems in this paper is mainly for a pool type reactor and the illustrative data provided is specific to a typical commercial scale fast breeder reactor.

2. SODIUM INVENTORY REQUIREMENT FOR SYSTEMS

Liquid sodium is the principal heat transport medium in Fast Breeder Reactors. Usually, a primary sodium circuit will transfer the heat generated in the reactor core to a secondary sodium circuit which in turn exchanges the thermal power to a heat sink like steam water system or air. There can be a dedicated decay heat removal (DHR) circuit or decay heat removal may be part of the other systems. In case of a dedicated DHR circuit, the decay heat from the core is removed by primary sodium and is exchanged to the intermediate DHR circuit for passing to the ultimate heat sink. Heat removal path during normal operation of the reactor is from primary sodium to steam water system through secondary sodium circuit. If the DHR circuit is a passive system, it enhances the reliability of decay heat removal following a reactor shutdown in the event of unavailability of heat transfer route through secondary and steam water system. The quantity of sodium used in the circuits varies depending on the type of reactor and configuration of the heat transfer loops. Table 1 indicates the proportion of sodium used in various loops in a typical pool type reactor. It can be seen that the pool type reactor uses large quantity of primary sodium filled in the reactor main vessel compared to that in the secondary circuit. There is not much difference in the quantities of sodium filled in the primary and secondary circuits in case of a loop type reactor. In addition to the sodium filled in the operating circuits in the plant, some quantity of sodium has to be kept in reserve for future uses.

TABLE 1. COMPARISON OF SODIUM USED IN CIRCUITS FOR A POOL TYPE REACTOR

Sodium circuit	Sodium quantity as percentage of total in all loops
Primary Sodium	70 – 75 %
Secondary sodium	20-25 %
Dedicated DHR	5-10 %

2.1. Primary Sodium

The quantity of sodium in a primary circuit in a reactor is mainly decided by whether it is pool type or loop type reactor. In the pool type reactor, major share of sodium inventory will be in primary circuit owing to the large size of reactor main vessel to accommodate the heat exchangers and sodium pumps of the circuit (Fig. 1). Heat transfer to the secondary circuit is enabled through a sodium to sodium Intermediate Heat Exchanger (IHX) while that to dedicated DHR circuit is through another Decay Heat Exchanger (DHX). Heat transfer part of both these heat exchangers are immersed in primary sodium. The height of the primary sodium in main vessel is decided by the height of inlet windows of these heat exchangers as well as the height of the fuel subassemblies. In fact, sufficient margin is given in height of primary sodium in main vessel above the IHX inlet window to avoid the possibility of cover gas entrainment in sodium which causes reactivity repercussions in the core. Hence, the primary sodium inventory is decided by the diameter of main vessel and height with margin for sodium level above IHX inlet window. Loss of primary sodium inventory in main vessel impedes heat removal through IHX as well as through DHX and engineered safety features are implemented to avoid this situation. The mean bulk sodium temperature varies under different operating conditions of the reactor. The sodium mass specified for the primary circuit is based on the density corresponding to the operating temperature. Sodium hold up in the purification circuit has to be considered in determining the initial quantity of sodium filled in the main vessel. In a loop type reactor, requirement of primary sodium quantity is comparatively much less than that for a pool type reactor.

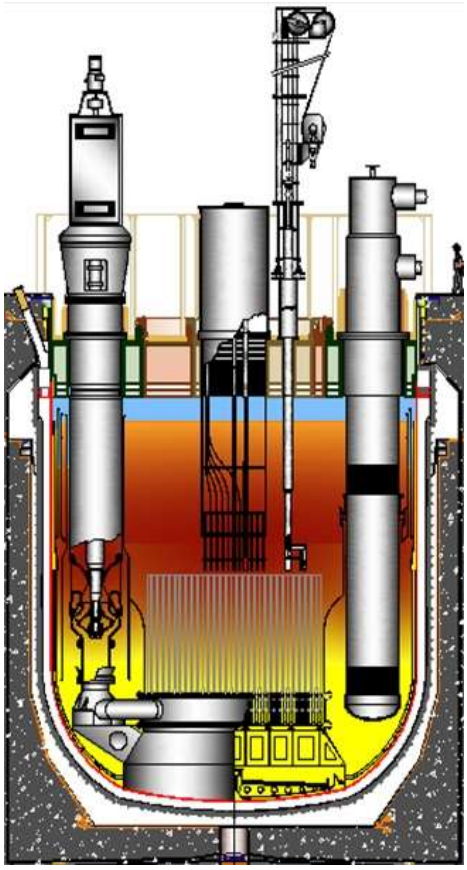

FIG. 1. Primary sodium in a pool type reactor [1].

2.2. Secondary Sodium

Sodium in econdary circuit transports heat from primary circuit in IHX and transfers it to steam water system in Steam Generator (SG). Refer Fig. 2 for the schematic of a typical secondary sodium circuit. The layout of secondary sodium circuit has to be selected from various combinations of options like provision of surge tank and position of pump in hot or cold leg of the loop and system sodium hold up varies for each case. Usually a surge tank has to be provided at the top most point of secondary sodium circuit, which allows thermal expansion /contraction in the system and absorbs pressure surges due to a large sodium water reaction incident in Steam Generator. The sizes of the components and piping are determined by the number of loops, the thermal power transferred through each loop and the number of heat exchangers and pumps for each loop. Sodium inventory in secondary circuit is decided by that filled in components and piping and sodium level maintained in the connected secondary sodium storage tanks to which sodium is drained. Quantities of sodium in the auxiliary circuits for fill and drain, purification and SG leak detection have to be considered in the initial filling in the secondary loops.

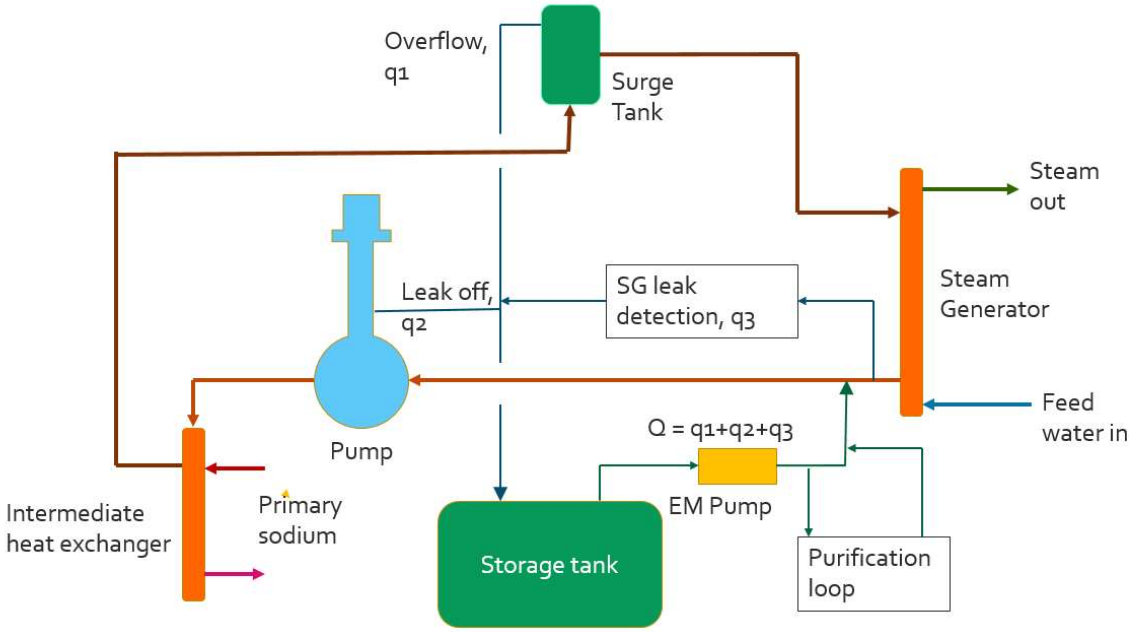

FIG. 2. Secondary sodium System (typical).

3. REGULATION OF INVENTORY

Sodium inventories in primary, secondary and dedicated DHR circuits are to be maintained and controlled at the required levels during all the states of reactor operation. The quantity of radioactive and non-radioactive sodium in the plant is regularly monitored and recorded for accountability. Decommissioning activities of the reactor are planned and designed, based on the active and inactive sodium inventories in the plant.

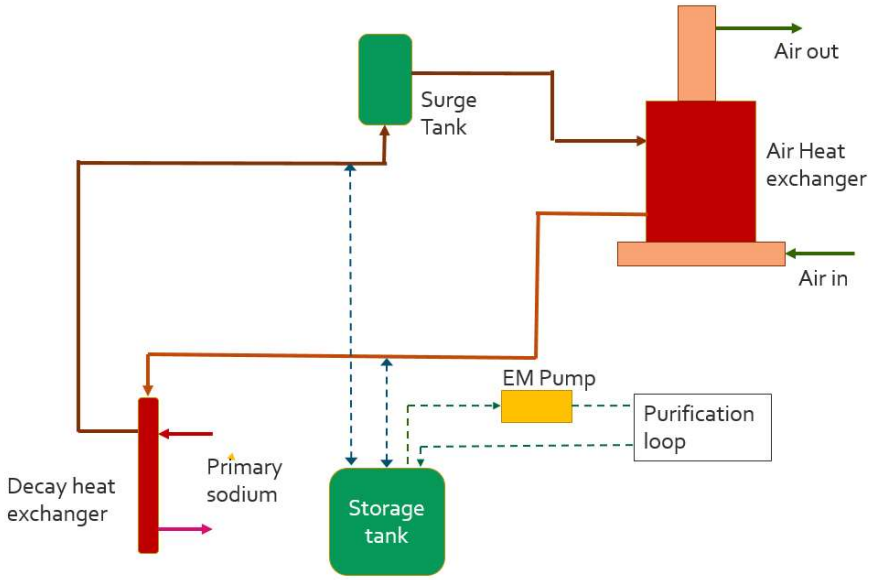

FIG. 3. Decay Heat Removal Circuit (typical).

3.1. Primary Sodium Circuit

Sodium levels in main vessel are measured by level probes of both continuous type and discontinuous type at many intervals. These level probes can be based on mutual inductance principle. Taking a comprehensive example of Prototype Fast Breeder Reactor (PFBR), sodium levels in the hot pool above the core, the cold pool on discharge side of IHX and primary sodium pump standpipe are at different elevations during operation of the pool type reactor. Two continuous level probes are used for level measurement in the hot pool as well as in the cold pool for redundancy. One continuous level probe is used in the pump standpipe. One discontinuous probe with three level switches are used in the hot pool. In case of any leak in IHX or DHX tubes, sodium from secondary sodium/DHR loop will enter the primary sodium as the pressure in the secondary and DHR circuit is more than the primary circuit. Secondary / DHR loop sodium leak into primary system through IHX or DHX is detected by the sodium level fall in secondary sodium storage tank or in expansion tank of DHR loop and also by level rise in primary sodium pool. One level switch is for highest level above the normal sodium level for detection of any leakage from secondary sodium circuit through IHX into primary sodium. Second level switch is for fill level of sodium during primary sodium filling and third switch is at the top of IHX inlet window to ensure sodium level available for circulation through IHX. Cold pool level probes are used for alarm and taking operator action if sodium level is below the fuel subassembly top during a primary sodium draining operation.

3.2. Secondary Sodium Circuit

Sodium has to be filled into the secondary loop piping and components from a storage tank. Sodium filled in the secondary sodium circuit is always connected to the storage tank during normal operation also. Secondary sodium inventory in the operating loop varies with respect to different operating conditions and is dynamically balanced to the requirement by controlling the flow into the loop from the storage tank and drain flow from the loop to the storage tank. The volume of the secondary loop remains almost fixed during the different operating conditions. The mass of the sodium in the loop varies depending upon operating temperatures. During operation of the secondary sodium circuit, there will be a continuous loss of inventory from the loop to the storage tanks due to leak of flow through secondary sodium pump seals and small sampling flow through SG leak detection system. In order to make up these losses, sodium is continuously fed into the secondary sodium loop by an electromagnetic (EM) pump which takes suction from the storage tank. For an effective control of inventory in secondary sodium loop, the EM pump injection rate is sufficiently excess to the total expected drain rate from the system considering all states of operation and the excess sodium injected into the loop is returned to the storage tank though the overflow pipeline of surge tank connecting to the storage tank. This ensures constant level in surge tank. Refer Fig.2 for the sodium inventory balancing in the secondary loop. A small quantity of sodium remains in the secondary storage tank to enable sodium circulation through the fill and drain lines. Mutual inductance type continuous level probe as well as discontinuous level switches are provided in the system tanks. Surge tank is at

the highest elevation in the system and level switches for high, normal and low levels are provided. In addition to the alarm annunciation, the high and low levels in surge tank will trip the secondary sodium pump. Low and fill level switches are provided in storage tank and low-level switch trips secondary sodium main pump and the EM pump. Any overall leak from the system is detected by continuous level probe in the storage tank when sodium is below the set point. Low and high level are provided in the pump tank. The discontinuous level switches give interlock to trip the sodium main pump.

3.3. DHR Circuit

Each loop of dedicated DHR circuit has to be filled from a storage tank of the loop. The sodium is filled in the loop up to the specified level in the expansion tank of the loop, which is situated at the highest elevation. Once filled, the loop can be isolated from the storage tank and sodium inventory in the loop has to be maintained. However, loss of sodium due to seat leakage through the isolation valves in the drain line has to be considered. Accordingly, before restarting the reactor after a fuel handling campaign, additional quantity of sodium is filled in the loop over the required level based on the expected sodium loss during the period between two fuel handling campaigns including the time required for DHR. Provisions are made in the loop to compensate if the loss of inventory is more than that expected. Volume of sodium in the expansion tank increases according to the volumetric expansion in the loop when the bulk temperature increases from filling temperature to the maximum operating temperature. Sodium inventory in the loop is monitored by mutual inductance type continuous and discontinuous level probes in the expansion tank. Three level switches are provided in expansion tank for low level, fill level and high level. Fill level is for stopping filling of the loop while low level indicates loss of inventory in the loop. Similar continuous and discontinuous level probes are provided in the DHR circuit storage tank.

4. PREVENTION AND MITIGATION OF SODIUM LEAK

Sodium inventory in the circuits has to be maintained for safe and uninterrupted operation of the sodium cooled fast breeder reactor. Sodium leak is the major cause for loss of inventory from the systems. Primary sodium is highly radioactive due to ^{24}Na, ^{22}Na isotopes and active corrosion and fission products. Hence, all the piping and components of primary sodium are provided with radiation shielding so as to restrict dose in the accessible locations within the limits. Any primary sodium leak can lead to consumption of additional Man-Rem. Leak in the unguarded pipelines and components can result in burning of sodium in atmospheric air. Part of the leaked sodium transforms into sodium aerosols constituted by sodium hydroxide and sodium carbonate. Sodium hydroxide, in particular, is very corrosive and can cause health hazards which has a Threshold Limit Value of 2.0 mg/m3 in air. Instrumentation provided in the plant monitors sodium inventory which takes automatic action and gives alarm for operator action on loss of inventory. The continuous and discontinuous level transmitters in the main vessel and sodium tanks helps to maintain the sodium inventory. Engineered safety features adopting defence in depth approach, forms the part of design to protect the plant from loss of coolant incidents.

4.1. Prevention of Leak

Stringent design and manufacturing procedures are followed for sodium systems of a fast breeder reactor. Primary and DHR sodium systems which are important for safety of the reactor belongs to Safety Class I and designed by detailed and vigorous process and mechanical analysis. The secondary sodium systems which are non-nuclear service also undergo detailed design analysis. All the possible combination of events which can lead to failure is considered for the system analysis. This qualifies the system in the design stage against extreme possible events. Material of construction selected for sodium systems are based on wide experience and service conditions expected. Stringent measures are adopted during fabrication and erection of sodium systems including proper quality control, qualification of fabrication procedure, all welded construction, volumetric and surface inspections, leak testing etc. All these measures in design and manufacturing make sodium systems highly reliable and less vulnerable to failure leading to loss of inventory.

4.2. Engineered Features for Mitigation of Loss of Inventory

The biggest advantage of a pool type reactor is that core is always submerged in the primary coolant. A safety vessel is provided outer to the reactor main vessel to contain sodium in case of a leak in main vessel. The inter space between main vessel and safety vessel is filled with nitrogen. The gap between safety vessel and main vessel is restricted such that even in case of a main vessel leak, the limited volume between main vessel & safety vessel restricts fall in sodium level such that sodium circulation through IHX and DHX is ensured. However, minimum gap between main vessel and safety vessel is decided by in service inspection requirements on outer surface of main vessel. Primary sodium is taken out of the pool only for purification through pipelines. Most of the equipment

and piping of the auxiliary circuits are kept at higher elevations such that sodium in the loop can be drained to the main vessel or storage tanks in case of a leak incident. In case of sodium leak in the system, the EM pump is tripped, argon is injected into the system to drain sodium from the loop. In case of a loop type reactor, a leak in the primary piping can lead to draining of sodium. In order to prevent loss of primary coolant from the reactor vessel due to any leak in the primary piping or components, syphon break arrangement is provided in the pipeline from the reactor such that sodium level in the reactor cannot be drained below the safe level.

In order to prevent sodium fire in a reactor building, all the sodium pipelines in the building have to be kept in guard pipe or steel cabins filled with nitrogen gas. The guard pipes act as a second boundary to the sodium main pipe and restricts the leakage of sodium. In case of large guard pipes, the leaked sodium is drained to leak collection tanks filled with inert nitrogen gas. Sodium piping without guard pipe are provided with leak collection trays for mitigation of sodium fire after a leak incident. If a sodium leak is detected, the particular loop is isolated from balance system and sodium is dumped from the loop. In case of a sodium water reaction in SG, the affected SG is isolated, and sodium is drained, and both shell side and tube side are maintained in inert atmosphere.

4.3. Leak Detection

The system needs to be designed for an early detection and mitigation of sodium leak and loss of inventory. Leak before break approach can be followed in the design of large piping and components to enable leak detection before catastrophic failure of the system. Sodium leak detectors are to be placed external to all sodium system piping and components which gives alarm in the main control room as well as local control centres seeking urgent operator action. Diverse leak detectors based on different principles will ensure reliability. Redundant spark plug leak detector (SPLD) and mutual inductance leak detector (MILD) can be provided at the bottom of inter space between main vessel and safety vessel for main vessel leak detection. Similar leak detectors are provided in bottom of reactor vault in which safety vessel is placed.

PLD and MILD type leak detectors can be provided in all the sodium piping with guard pipes. Wire type leak detectors are provided for the piping without guard pipe. Sodium aerosol detector can be provided near to the piping and components for leak detection. Continuous sampling of sodium at the outlet of all the steam senerators has to be done to detect hydrogen evolved due to any leak in SG tube bundle. There exist indirect methods for detection of leak in the sodium systems. In case of leak in the intermediate heat exchanger, the level fall in secondary sodium storage gives first indication of leak followed by a level rise in primary sodium level in main vessel. The leakage from the sodium loop to storage tank due to valve passing is overcome by continuous charging of EM pump for the secondary loop. The sodium leaking due to valve passing into storage tank of DHR loop can be detected by level rise in the tank.

However, there can be unavoidable minor loss of sodium from the system due to specific operations in the plant. During each refuelling campaign, the core subassemblies are replaced. Sodium will be sticking on the core subassemblies taken out of the reactor vessel during a refuelling campaign. Similarly, whenever sodium wetted components are taken out of the system and decontaminated for maintenance, system loses a small quantity of sodium. During sodium sampling for chemical analysis, a meagre quantity of sodium is taken out from the system in a sampler. Reserve sodium is maintained in the plant to make up the systems when sodium inventory in a loop is below the required level. The loss of inventory has to be made up by transferring reserve sodium into the system either using EM pumps or pressurization method.

4.4. Advances in Maintenance of Inventory

In-vessel sodium purification is an excellent option for reducing possibility of sodium leakage from main vessel in a pool type reactor and to reduce extensive radioactive primary piping outside the reactor vessel. The guard pipes on sodium piping can be extended to the maximum coverage to contain sodium leakage. Use of advanced material reduces the risk of failures in piping and components.

5. SUMMARY

The sodium inventory control and monitoring are important in the primary, secondary and DHR sodium circuits of FBR. Effective heat removal from the core can be impaired due to loss of sodium from the heat transport sodium circuits, which affects safety in operation of the reactor. Redundant and diverse instrumentation needs to be provided for monitoring sodium level in capacities and for early detection of any leak incident. Engineered safety features like guard vessels, syphon break etc. provide defence in depth against any leak of sodium coolant. The

sodium inventory control and accountability of radioactive and non-radioactive sodium is necessary for planning and design of decommissioning activities of the plant after the service life.

REFERENCES

[1] INTERNATIONAL ATOMIC ENERGY AGENCY, Status of Fast Reactor Research and Technology Development, IAEA-TECDOC-1691, IAEA, Vienna (2013).

CHOICE OF COOLANTS FOR DEMO-FNS FUSION-FISSION HYBRID FACILITY

B.V. KUTEEV, V.I. KHRIPUNOV, YU.S. SHPANSKIY
National Research Center,
Kurchatov Institute,
Moscow
Email: Kuteev_BV@nrcki.ru

I.V. DANILOV, A.V. RAZMEROV
JSC "NIKIET",
Moscow

Russian Federation

Abstract

Since 2010 the development of new facilities capable to accelerate implementation of currently available fusion technologies and to demonstrate an energy valuable level of power and neutron generation has been started in Russia. The analysis fulfilled has shown that tokamak based fusion neutron sources and fusion-fission hybrid facilities could solve these goals. However, intensive R&D activities are needed in the fields of steady state plasma operation and compatibility of tokamak systems with combined fusion and fission neutron environment. Fusion-Fission Hybrid Facility DEMO-FNS is considered in this strategy as a device qualified for demonstration of enabling technologies and allowing the proper choice of engineering solutions for a Pilot Hybrid Power Plant. This paper describes possible challenges and prospective options for coolants associated with DEMO-FNS operation.

1. INTRODUCTION

The DEMO-FNS Fusion-Fission Hybrid Facility is considered in Russia as a device supporting the further development of ITER-DEMO tokamak fusion line and innovative nuclear technologies for fission [1].

The superconducting tokamak DEMO-FNS has the major radius of 3.2 m, the aspect ratio A=3.2 and the ITER-like shaping but with a double null divertor configuration. The fusion power of the device is ~40 MW and fission power ~500 MW. The thermal loading on plasma facing components conditioned by conductive and radiative heat transfer may reach 10MW/m2. The 14 MeV neutron wall loading up to 0.2 MW/m2 and the volumetric heat generation due to fission reactions up to100 kW/l are expected. The device operation requires creation and maintenance of a fast neutron spectrum in active cores and thermal spectra in a tritium breeding blanket.

This paper describes challenges and prospective options for different coolants associated with DEMO-FNS systems operation. It has the following structure: section 2 is devoted to introduction to general design features of DEMO-FNS; section 3 presents the activation characteristics of candidate coolants; section 4 contains analysis of coolant options for major enabling systems; prospective coolants are addressed and presented in Section 5.

2. GENERAL DESIGN FEATURES OF DEMO-FNS

A cutaway view and basic engineering parameters of DEMO-FNS are given in Fig. 1. The device needs to produce 200 MW of electric power at least for its maintenance. Selection of coolants and materials for such facility is the start-up point for the device design. Tokamak enabling systems using coolants include the divertor, the first wall, the active core, blankets for tritium and fissile nuclides breeding. The device coolants operate in a wide range of temperatures from cryogenic 4-80 K in the magnetic system and thermal shield up to 100-500 °C in others.

Potential of coolants implementation in the integrated DEMO-FNS design is evaluated by plus (+) and minus (–) signs in the Table 1 indicating thermal loads and temperature ranges for operation conditions.

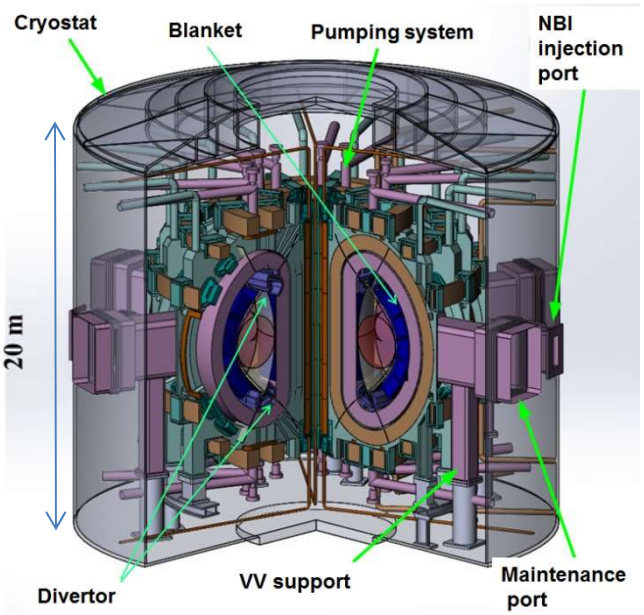

Aspect ratio	**R/a**	**3.2/1 m**
Toroidal magnetic field		**5 T**
Temperature: electron/ion		**11.5/10.7 keV**
Beta normalized	**β_N**	**2.1**
Plasma current	**I_{pl}**	**5 MA**
Neutron yield	**G_N**	**$1.3 \cdot 10^{19}$ s^{-1}**
Neutral injection power		**36 MW**
ECR heating power		**6 MW**
Discharge time		**5000 h**
Capacity factor		**0.3**
Life time		**30 year**
Consumed/ generated power	**P_C/P_G**	**200 MW**
Engineering	**$Q_{eng}=P_C/P_G$**	**1**

FIG. 1. DEMO-FNS cutaway view.

TABLE 1. COOLANT SELECTION

System	Loads	T-range, K	Potential coolants/Materials							
			Water	Heavy Water	Water-Steam Mixture	Orga-nic	He	CO2	Liquid Metals	Molten Salts
First Wall	5 MW/m2	300-500	+	-	-	-	-	+	-	-
Divertor	10 MW/m2	350-500	+	-	-	-	-	+	-	-
Vacuum Vessel	0.2 MW/m2	300-470	+	-	-	-	-	-	-	-
Active Core	85 kW/l	<550	∓	+	±*	-	-	+	-	-
T-Breeding Blanket	0.5 kW/l	<600	-	+	-	-	+	+	±	-
Fissile Breeding Blanket	1 kW/l	<550	-	-	-	-	+		-	+
Li-circulation	~1/h	<600	+	-	-	-	-	+	-	-
Magnets and Thermal Shield	~20 kW at 4 K	4-80	-	-	-	-	+	-	-	-
*) symbol ± - rather "yes" than "no"; symbol ∓ - rather "no" than "yes"										

A reduced 14 MeV-neutron wall loading of <0.2 MW/m2 as compared to a few MW/m2 value expected in forthcoming fusion reactors makes it possible implementation of available materials.

While ITER is aimed at realization of thermonuclear fusion the beam-plasma fusion will provide a comparable fraction of the fusion power in DEMO-FNS tokamak. The neutron wall loading in DEMO-FNS is lower than 0.7 MW/m2 in ITER. However, the lifetime neutron fluence at the first wall of this facility of ~2 MWy/m2 is significantly higher than that of ITER being below 0.3 MWy/m2 due to a higher duty factor of ~0.3. Reaching such duty factor requires implementation of lithium technologies for protection the tokamak divertor and first wall against erosion.

Additional neutrons and thermal power will be produced in the subcritical fissile active core (AC) and breeding blankets (BB). The fission and □-decay thermal power in the AC and BB of ~450 MW will be converted to electricity.

Compatibility of coolants with multiple enabling fusion and fission technologies integrated in DEMO-FNS is challenging.

3. ACTIVATION CHARACTERISTICS OF CANDIDATE COOLANTS

Mixed neutron spectra are formed in DEMO-FNS by plasma (fusion source), the active core (fission source) and blanket (neutron moderation and nuclear reactions). The spectra used in coolant activation analysis performed with [2, 3] are shown in Fig. 2. These spectra correspond to a Commercial Hybrid Power Plant (CHPP) with subcritical active core having the effective neutron multiplication factor keff =0.95 and the fusion neutron wall loading of 0.2MW/m2. It is clear that the spectrum in DEMO-FNS is close to that of fusion reactor and is much harder than fast reactor spectra.

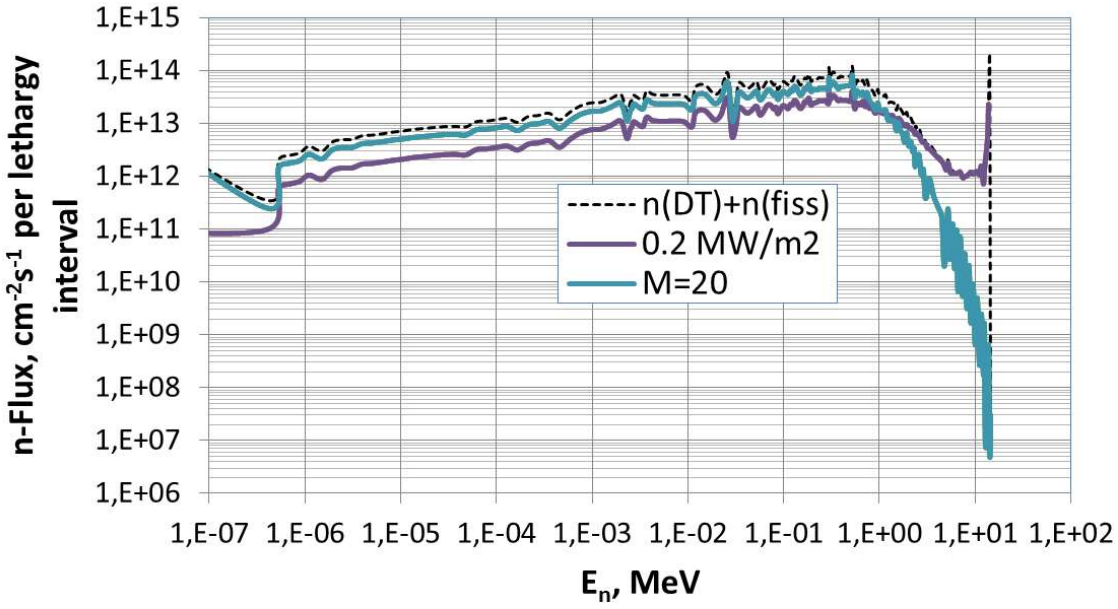

FIG. 2. Neutron spectra formed in the FW region by DT-fusion in plasma and fission in AC.

The results of activation analysis are shown in Fig. 3. The "fast neutron fluence was assumed to be ~4.4×1021cm-2 and the total neutron fluence ~1.3×1022cm-2 due to one year irradiation. The dominant isotopes responsible for the activity of candidate coolants in different cooling periods are indicated nearby the decay curves. Normal water, heavy water and superctrical carbon dioxide (S-CO_2) coolants are characterized by the lowest activation and the fast activity decay. The sodium (Na) activation via ^{24}Na and ^{22}Na prolongs by substantial tritium activity and finally by the ^{36}Cl-decay. The molten salts (MS) after irradiation have the highest tritium activity, however this property is positive for tritium breeding. The long term radionuclides generated from impurities become dominant after hundred years cooling. A characteristic time for 6Li burning is close to ~100 days, so blanket feeding by this isotope needs to be provided for T-breeding during prolong irradiation campaigns" [11].

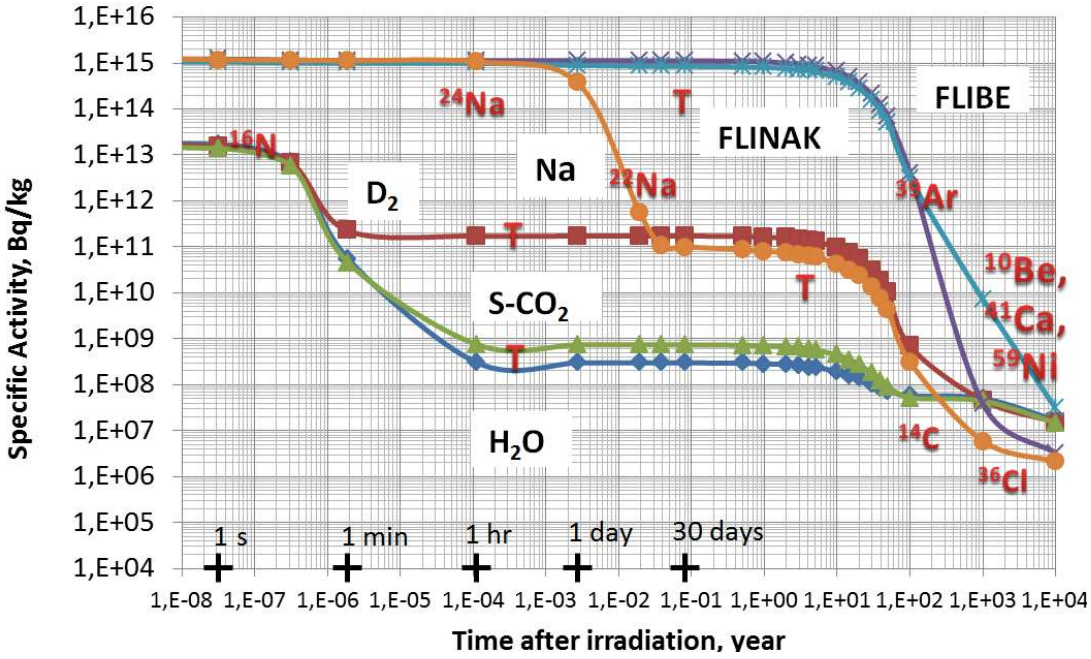

FIG. 3. Specific coolant activity after irradiation during 1 FPY in the CHPP spectra.

Decay curves presented in Fig. 4 show the lowest and comparable levels of specific afterheat for water and S-CO_2 as well as the highest levels for sodium and MS. The short term afterheat of oxygen containing coolants is provided by ^{16}N produced through $^{16}O(n,p)^{16}N$ reaction. ^{16}N-nucleus decays back to ^{16}O with $T_{1/2}$=7.12 s emitting particle with 2.7 MeV energy and high energy (4.6 MeV) gamma.

This delayed afterheat affects the design of the radiation shield for the primary circuit of coolant and opportunities for single-loop cooling system for energy conversion.

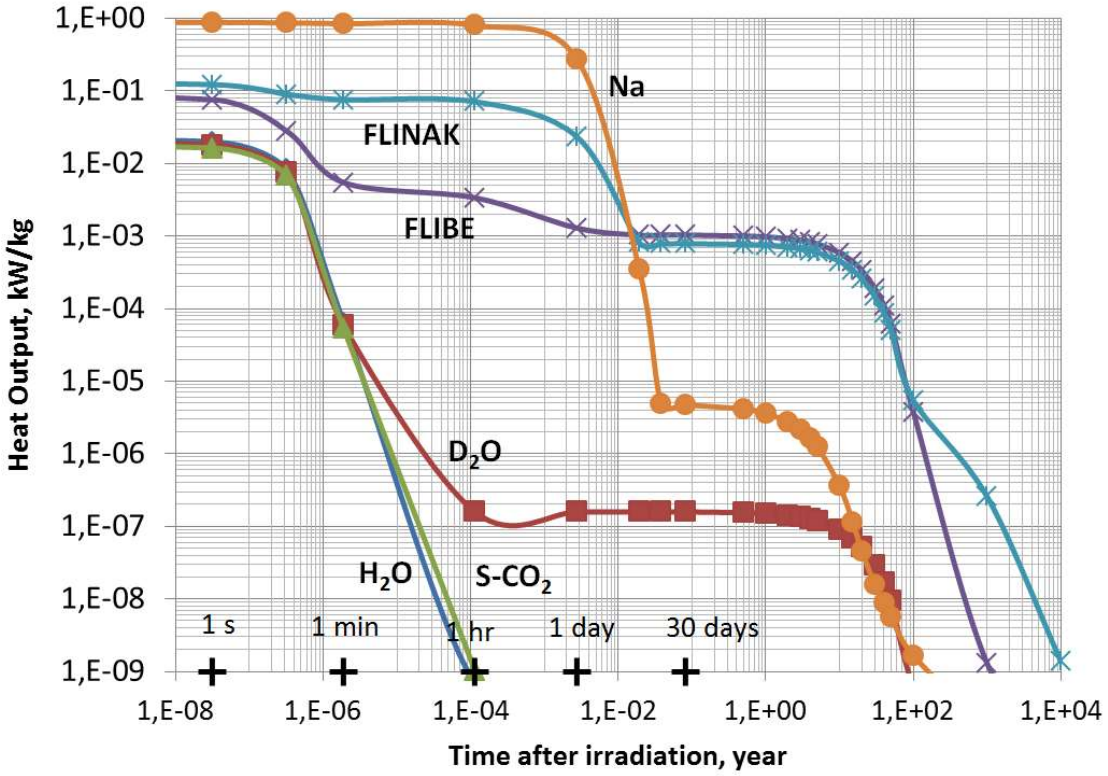

Fig. 4. Specific afterheat in coolants after irradiation during 1 FPY in CHPP spectra.

4. COOLANT OPTIONS FOR MAJOR ENABLING SYSTEMS

The first wall and divertor are subjected to high local heat loads coming from plasma up to 5/10 MW/m^2, respectively. The total power for those does not exceed 10% of the AC generated power. This allows using H_2O in the FW&D systems with the maximal temperature in the loop <500K which is similar to the ITER engineering solutions, which are well developed, experimentally tested and compatible with magnetic field [4]. Concerns remain associated with corrosion effects of the heat sink material CuCrZr, coolant-Li compatibility in accidents and softening neutron spectra. The "advantage of supercritical coolants in comparison with liquid coolants is the absence of a heat transfer crisis during boiling. However, in order to remove the heat flux of ~ 5 MW/m2 to achieve acceptable heat transfer coefficients, it is necessary to pump the S-CO_2 coolant with velocity of up to 100 m/s. At such velocities, the regimes with reduced heat transfer will not occur as was observed in [5]. In any case, additional computational and experimental R&D is required" [11].

The vacuum vessel of the device requires the operation temperature up to 470 K during cleaning procedures. A large volume and high mechanical stresses due to internal coolant pressure give a preference to H_2O for it.

The AC designed for minor actinides burning, high temperature heat and neutron production has neutronics characteristics: the best with S-CO2 coolant, the acceptable with water-steam mixture and marginal with pressurized water. Advantages of S-CO2 are the acceptable pressure 80 bar at 790 K, the hard neutron spectrum, low chemical activity and level of activation as well as fast afterheat reduction. This coolant may also simplify the energy conversion system to the one-loop option and reduce significantly the facility size due to compacter heat exchangers.

Recently the interest to S-CO_2 coolant started to grow up in applications for fusion [6-8] and fission [9, 10]. Energy conversion systems with 3-loops have been considered in these works very well correlating with our design. Schematic diagram of such system [10] is shown in Fig.5.

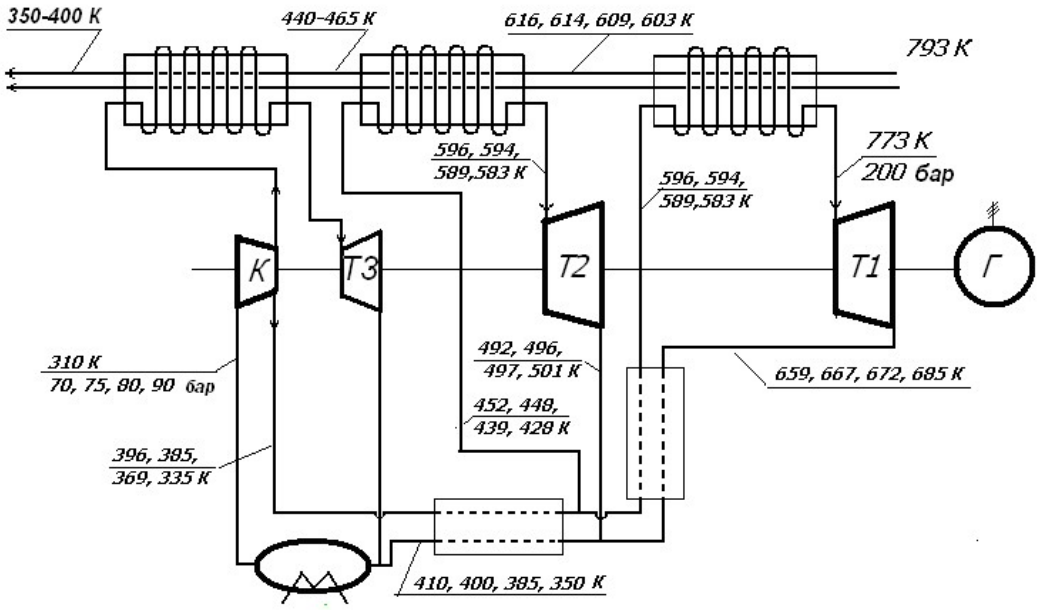

Fig. 5. Schematic diagram of the energy conversion system using S-CO2.

For the fertile breeding blanket, the neutron economy gives preferences to D_2O, CO2 and MS. Materials used in the MS tritium breeding blanket and in the He-cooled solid breeder blankets have acceptable characteristics due to a low level of specific heat power and the simplified extraction technology.

5. SUMMARY

Development of the DEMO-FNS device for testing of fusion and hybrid technologies is in progress being at the stage of transition from the conceptual to engineering designs. Sequentially, in 2013-2016 the designs of tokamak, a hybrid blanket and fusion and fission fuel cycles were integrated in the facility. The project is based on the available materials; however, it may require development of new materials for fusion and testing of components.

Integration of fusion and fission technological systems in one design with minimal set of coolants is under the design activity. The water coolant, water-steam mixture and super-critical CO2 are possible engineering solutions for DEMO-FNS with a broad list of final products including neutrons, energy, tritium and fissile nuclides.

General operation requirements define the minimal set of coolants used in the device. Those may include He for cryogenic systems and water/steam for enhanced heat flux (EHF) systems. Meanwhile, the heat transfer crisis and thermal-hydraulic instability remain significant issues for water-steam mixture. It is as well necessary to notice safety problems dealing with the compatibility of coolants and other technologies used in the device like Li-circulation technology. For light and heavy liquid metal coolants their specific features in hydrodynamics and heat transfer are important selection factors.

A few options are still under analysis like molte salt for FBB and TBB, supercritical CO_2 for the active core. Liquid metals and organic coolants are of a lower priority in our analysis due to magneto-hydrodynamic (MHD) effects (LM) and lack of principal advantages (OC).

REFERENCES

[1] KUTEEV, B.V., et al., Status of DEMO-FNS development, Nucl. Fusion **57** (2017).

[2] FORREST, R.A., The European Activation System: EASY-2007 Overview, EASY Documentation Series, UKAEA Fus 533, EURATOM/UKAEA Fusion Association the EASY-2010 Software NEA-1564/15 (2007).

[3] PACKER, L.W., SUBLET, J-CH., The European activation file: EAF-2010 Biological, Clearance and Transport Libraries, EASY Documentation Series CCFE-R (10)04, EURATOM/CCFE Fusion Association, Culham Science Centre, Abingdon Oxford-shire, United Kingdom, 2010.

[4] SERGEEV, V.YU., et al., Conceptual design of divertor and first wall for DEMO-FNS, Nucl. Fusion **55** (2015) 123013.

[5] KURGANOV, V.A., "Heat Exchange in Pipes at Coolant's Supercritical Pressures: Some Results of Scientific Research", 4th RNHTC (Proc. Int. Conf., 2006, Vol. 1, 74–83).

[6] ISHIYAMA, S., et al., Study of steam, helium and supercritical CO2 turbine power generations in prototype fusion power reactor, Progress in Nuclear Energy **50** (2008) 325–332.

[7] VESELY, L., et al., "Study of the cooling systems with S-CO2 for the DEMO fusion power reactor", SOFT (Proc. Int. Conf., 2016).

[8] LINARES, J., et al., Supercritical CO2 Brayton Power Cycles for DEMO Fusion Reactor Based on Dual Coolant Lithium Lead Blanket, EUROFUSION WPBOP–PR (15) 01 (2016).

[9] YU, H. et al., A Conceptual Study of a Supercritical CO2-Cooled Micro Modular Reactor, Energies **8** (2015).

[10] SUROVTSEV, I.G., et al., Application of supercritical carbon dioxide cycles in facilities for utilization of industrial heat, Science and Education, Bauman University Publishing, 2013.

[11] SHPANSKIY, Y., Progress in design of DEMO-FNS hybrid facility, Nuclear Fusion **59** (2019).

HIGH POWER MOLTEN TARGETS FOR THE PRODUCTION OF RADIOACTIVE ION BEAMS

J.P. RAMOS, M. DELONCA, F. BOIX PAMIES, T.M. MENDONÇA, T. STORA
CERN,
Genève, Switzerland
Email: joao.pedro.ramos@cern.ch, thierry.stora@cern.ch

Abstract:

A first loop prototype is expected to operate in the coming year online at CERN within the LIEBE project collaboration. Finally, a design of a compact spallation source made of tungsten and passive cooling with molten PbBi is investigated for operation at the ISAC facility in TRIUMF.

1. INTRODUCTION

The Isotope mass Separation Online (ISOL) method was introduced in the fifties and has since been developed in different facilities across the continents. ISOLDE at CERN has celebrated this year its fiftieth anniversary, the longest from other facilities [1]. From the first proof-of-concept experiment, a large uranium dioxide target of several kg was exposed to fast neutrons produced from a deuteron beam intercepting a beryllium target [2]. A large range of other targets, solid or liquid, and methods to convert an incoming ion beam into neutrons have been devised, prototyped and some are now routinely used. In all cases, careful heat management must be guaranteed throughout operation, where often a uniform high temperature must be provided for a fast release of condensable radioisotopes, and efficient cooling of parts of the production unit must be provided to prevent the decrease or losses of functionalities in the beam production process. In this report, we provide an overview of recent target developments where molten targets can be operated and isotope extracted online, a technique that we have used to measure phenomena and properties of the melts that where not yet determined previously.

2. MOLTEN METAL TARGETS

Molten targets are used at ISOLDE due to their high density, resistance to radiation damage and high diffusion coefficients characteristic of the liquid state. Beams of volatile isotopes, with half-lives in the order of minutes are usually extracted from these targets, due to their long release times. Even though the diffusion rates are high the diffusion distances are in the order of cm, contrarily to solid powder targets where there are in the order of micrometres.

Nowadays at ISOLDE metal liquid targets are mainly lead and tin, however in the past Lanthanum were also frequently used, completed with operation of PbBi Eutectic (LBE) prototypes. Apart from those a few other liquid prototype target materials were also tested at ISOLDE [3].

The molten targets at ISOLDE have experienced several upgrades over the last 50 years of operation mainly due to the change of the primary beam energy and intensity, which caused several failures of previous designs that could not cope with the beam upgrades [4]. The main changes in the liquid metal targets were done when ISOLDE moved from the quasi continuous Synchrocyclotron (SC - 600 MeV protons, 1.5x1011 ppp (protons per pulse), 100 Hz pulse frequency and 30 μs pulse length) beam to the highly pulsed Proton-Synchrotron-Booster (PSB – 1.4 GeV, 3.3E13 ppp, 0.4 Hz pulse frequency and 2.4 μs pulse length). This increased the instantaneous power deposition in the targets by 3 orders of magnitude to 10's GW, which causes severe thermal shocks and eventually damaged the units [4,5].

The Ion source and beam line operation requires high vacuum conditions (10^{-6} mbar) which are not compatible with the high vapor pressures of liquid metals. Furthermore, under pulsed conditions of the PSB pressure waves and splashes are created in the melt. To prevent these splashes and the vapours to reach the ion source, baffles and a temperature controlled helix was installed as a condensation element in the transfer line [4]. This device allowed a fast transfer of the less than femtomole quantities of isotopes to go through, and still prevent the mole quantities of the target vapours and splashes of liquid metal to reach the ion source.

The steering of the incoming proton beam was also changed. The beam was defocused to increase the beam size area by a factor 4, thereby reducing the energy density. By creating a time-staggered extraction of the proton bunches from the 4-ring PSB, where the pulses normally consist of 4 bunches sequentially spaced by 230 ns were

evolved into a pulse with 3 bunches spaced by 16 μs [6]. This not only avoids constructive interference between the different bunch-induced pressure waves but also spreads the energy deposition over time.

To accommodate better the thermal stresses, the cylindrical tantalum target oven, which also serves as a structural support, thickness was increased from 0.5 to 1 mm as well as significant changes to the proton beam window design and assembly [4]. All these changes together have significantly increased the lifetime of the liquid metal targets at ISOLDE, which are now used with no decrease of their performance even after several online operation periods.

Pulsed proton beam induced ageing was first identified at ISOLDE in the tantalum beam windows of the liquid lead targets at 720 °C where micro cracks along the grain boundaries and pit corrosion was caused by cavitation, as shown in Fig. 1. The very focused proton beam also caused cauliflower formations on Ta at high temperatures. Stress waves inducing plastic deformation caused severe permanent deformation of Ta rods that served as spallation neutron sources [5]. In a recent post-irradiation analysis of a LBE molten unit after 2 years of radioactive cooldown, the present molten metal target designs showed no signs of degradation [7]. It was seen that the Bi from the LBE migrated to the Ta forming a 1-2 μm thick layer at 950 °C (operation temperature) [7].

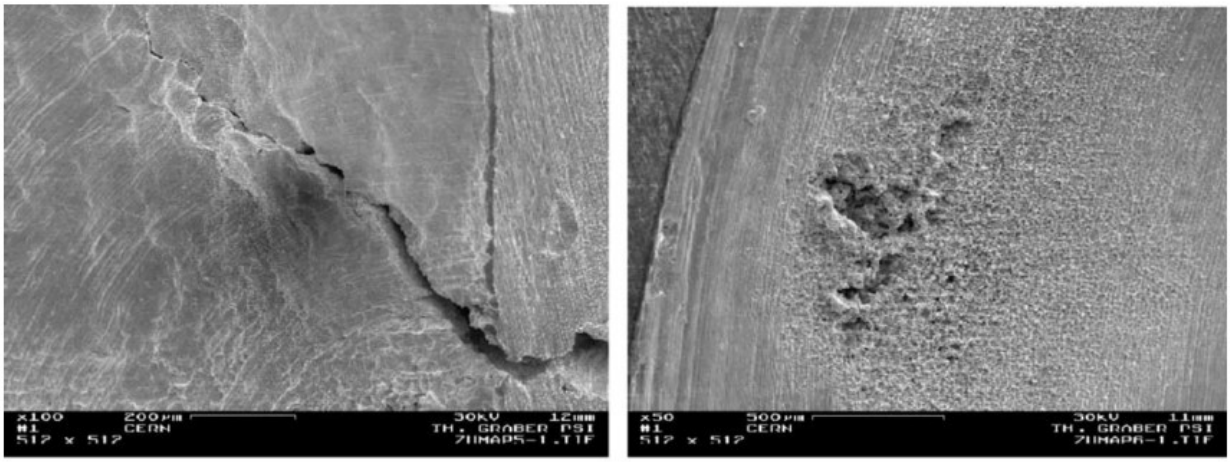

FIG. 1. (a) Inside of a Ta container operated with molten lead showing stress induced cracking; (b) corrosion by cavitation. Reproduced from Ref. [5].

3. MOLTEN SALT TARGETS

A molten salt loop target has been proposed to produce high rates of 18Ne for the beta beams project which ultimately would serve as a neutrino and antineutrino facility at CERN as reviewed in ref. [8]. Two molten salts have been selected and studied, NaF:ZrF4 (60:40 mol.%)[2] and NaF:LiF (39:61 mol.%)[3], due to their low melting point and high 18Ne production rates. The NaF:ZrF4 was discarded due to its high reactivity, notably with water vapours, and its high vapor pressure which didn't allow for safe operation as a target material. Both salts are highly hygroscopic so handling had to be done under an inert atmosphere [9].

To test the potential of the NaF:LiF salt for the beta beams project a static molten bath was selected to be operated at ISOLDE as a prototype target under direct proton irradiation [9]. A special age-hard able Ni-Mo-Cr alloy (Haynes242®) with high resistance to corrosion and high temperature strength was validated with thermo-mechanical simulations and used as target container and oven, where the connection to the ion source was made with stainless steel [10].

---

[2] Properties of $NaF:ZrF_4$ (60:40 mol.%): 500 °C melting point, 3.14 g/cm^3, 5 mmHg vapor pressure at 900 °C

[3] Properties of NaF:LiF (39:61 mol.%): 649 °C melting point, 2.75 g/cm^3, 0.1 mmHg vapor pressure at 900 °C

The target was irradiated with different proton beam time-structures and intensities in staggered mode (described in section 0) and at different temperatures (700 to 745 °C). The proton beam time-structure variations had more impact in the 18Ne release than the operation temperature. Carbon radioisotopes were also produced in high quantities from this target in the form of a molecule – xC16O. Since the target local environment is dominated by fluorine, it was expected that the carbon would be released dominantly as xC16Fx. The CO formation was attributed to the presence of oxygen in the target structural materials since water and oxygen were less than 1 ppm in the salt [9].

By modelling the release of isotopes of target materials fundamental properties, such as diffusion coefficients, can be estimated [11,12]. Using the models provided in ref. [11] a diffusion coefficient for Ne diffusion on NaF:LiF salt at 740°C was estimated to be 6.7x10-3 mm2/s. This Ne diffusion constant was similar to published noble gas diffusion data on molten salts and used to calculate release efficiencies for a loop where instead of a bath, a film of liquid or droplets would be used [13].

4. LIEBE - LIQUID LEAD BISMUTH EUTECTIC LOOP TARGET

Static bath molten metal targets suffer from isotope diffusion distances that are in the order of cm, which is detrimental of the extraction of short-lived isotopes (half-life below a few minutes) and from the difficulty to implement a cooling scheme when operated with high incoming beam powers. A LBE loop target has been proposed and tested offline for EURISOL for radioisotope production for 1GeV proton at 100 kW of beam power [14]. For online testing, a prototype has been designed and built to be tested at ISOLDE-CERN and named LIEBE – Liquid Eutectic PbBi target loop for EURISOL [13,15,16].

The LIEBE target shown on FIG. , has an irradiation chamber where the proton beam interacts with the LBE creating the isotopes. The irradiated LBE then quickly goes through a series of grids to form droplets in a diffusion chamber where the isotopes are rapidly released. The released isotopes will diffuse through the transfer line until they reach the ion source to be ionized, accelerated, mass separated and delivered to physics experiments. The droplets are then collected at the bottom of the diffusion chamber and the liquid is pumped back to the irradiation chamber, through a heat exchanger. The heat exchanger allows to cool the LBE to evacuate the deposited power from the primary proton beam and to allow a safe operation of the electromagnetic pump [13,15,16].

The achieved droplet size is very important for the release efficiency and yield of isotopes, since the shorter the diffusion length, the faster the isotope can escape the target material. The LIEBE was designed to create droplets of 400 μm using a stainless steel grid with 100 μm diameter laser-drilled holes [15]. To obtain such droplets the theory of breakup of liquid jets was studied, in order to have the right liquid velocity to be in the dripping formation regime, for 400 μm droplet size (Fig. 2(a)), the minimum size achievable with this concept [15,17]. The LIEBE prototype target will be tested offline this year (see Fig. 2(b)) and later online for isotope production.

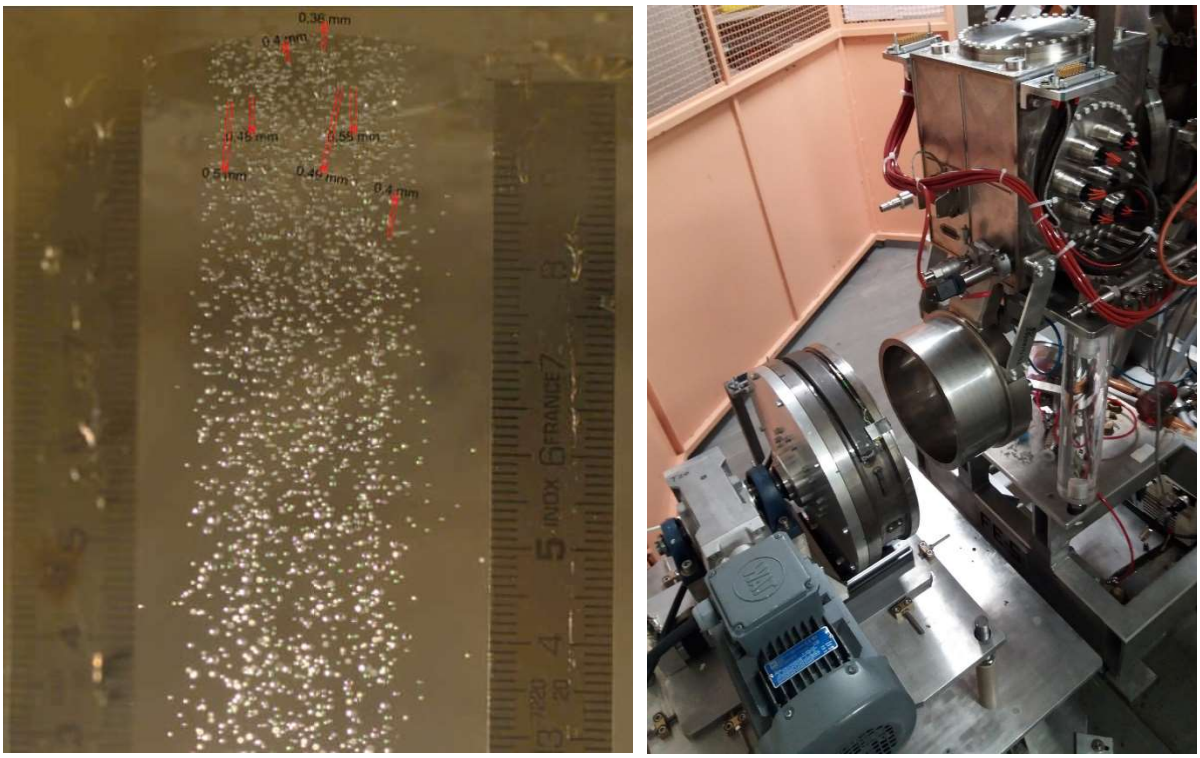

(a) (b)

FIG. 2. (a) Droplet shower tests for LIEBE [15] (reproduced from Ref. [15]); (b) LIEBE mounted in the ISOLDE offline separator for tests.

5. SPALLATION TARGETS FOR ISOTOPE PRODUCTION

The idea to use a spallation target from high energy beams to get fast neutrons to produce radioisotopes was proposed by J. Nolen back in 1993 [18]. The irradiation of a spallation source made of W, also known as neutron-converter at ISOLDE, produces fast neutrons that will interact with a secondary target producing pure neutron-rich fission fragments. These beams are of higher purity since when irradiating the uranium carbide directly with 1.4 GeV protons produces neutron-rich fission fragments but also the neutron-deficient ones as isobaric contaminations. The first neutron-converter to produce radioactive isotopes used at ISOLDE was operated in 2000 [19], and such type of targets are still in operation after some evolution of their design.

Since the neutron-converter is positioned very close to the secondary target, for high neutron fluxes, some of the scattered protons from the converter (see Fig. 3) still interact with the target, producing the undesired contaminations. The neutron-converter geometry was thus studied and optimized using simulation codes and a few concepts have been proposed [20,21] where one was tested successfully at ISOLDE [22].

To continue the work of the neutron-converter geometry optimization a collaboration was started between CERN, TRIUMF in Canada and SCK-CEN in Belgium. In this collaboration, the main purpose is to design a neutron converter concept for both low and high beam powers of 50kW. Since the targets to produce radioisotopes are replaced frequently, the concept must be compact, thus beam power deposition in the converter body up to 1 kW/cm3 can be achieved. The heat generated and the proximity of the secondary target at 2000 °C make the cooling of such device very challenging. Since the W thermal conductivity at high temperatures (2000 °C) is an inefficient heat transport mechanism the use of LBE capsules which would transport the heat away from the hot spot more efficiently could be used. These LBE capsules would conduct the heat away through natural convection, a concept which has yet to be tested. Furthermore, Cu is normally used to transport the heat from the W to a water-cooling circuit. In this case the W-Cu interface is important for a proper operation, where contact must be insured at all times, even when there are beam interruptions and extreme temperature gradients.

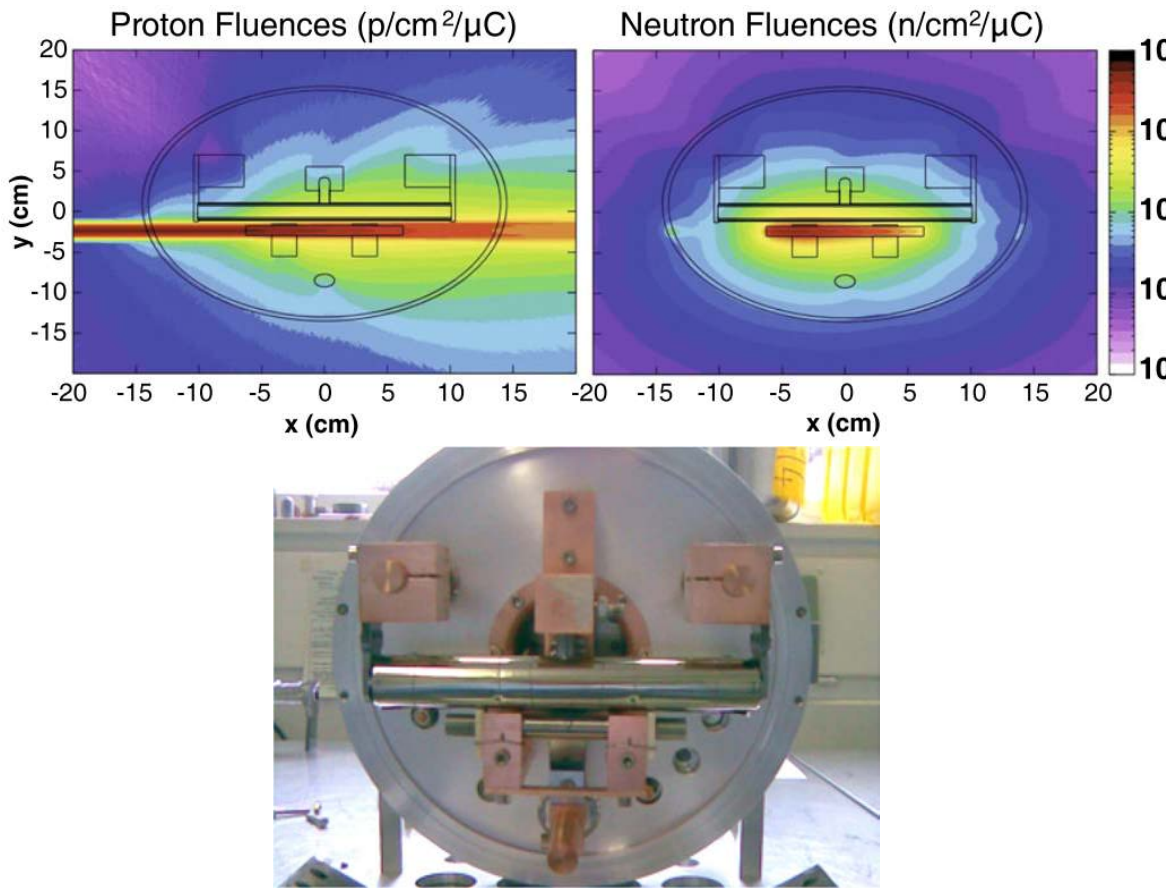

FIG. 3. Proton fluences (top left) and neutron fluences (top right), both reproduced from ref. [21], from a standard neutron converter target at ISOLDE (bottom). Reproduced from Ref. [23].

The ISOLDE facility can also be used to irradiate materials for diverse studies. In a recent irradiation, a tungsten slab from the European Spallation Source (ESS) has been irradiated inside of an ISOLDE target unit with 1.4 GeV, 1x1018 protons, an energy not too far from the one of the ESS (2.5 GeV). This was done in order to study the release fraction of iodine, an highly radiotoxic and volatile element, which can contaminate the He cooling circuit of the ESS [24].

On the cooling subject, generally oxide targets cannot be used with high beam powers due to their low thermal conductivity and inadequate mechanical properties. Graphite foils/carbide composites are usually used [25] to solve such problems but oxides, at high temperatures, are incompatible with graphite. A solution was found at CERN for alumina targets by creating a Al2O3-Nb foils composite. This was done by brazing 30% porous micrometric Al2O3 ceramics on 100 μm Nb foils with a reactive brazing alloy TA6V (86.2% Ti 10.2% Al, 3.6% V). A thermal conductance across the brazed surface of 10000 W/m2 K was achieved and the target was successfully operated at unprecedented high proton beam power at TRIUMF [26].

6. CONCLUSIONS

In this report, we have provided some details on the challenges and on the developments to operate targets for high beam powers. In particular, findings on ageing due to beam-induced cavitation were obtained, as well as first operation of molten salts under proton beam. Finally, original solutions must be proposed and tested to operate liquid metal targets and spallation neutron sources at 100kW and MW beam power for the online extraction of secondary radioisotope beams.

REFERENCES

[1] CATHERALL, R., ANDREAZZA, W., BREITENFELDT, M., DORSIVAL, A., FOCKER, G.J., et al., The ISOLDE facility, J. Phys. G Nucl. Part. Phys. **44** (2017) 94002.

[2] KOFOED-HANSEN, O., NIELSEN, K.O., Short-lived krypton isotopes and their daughter substances, Phys. Rev. **82** (1951) 96–97.

[3] GOTTBERG, A., Target materials for exotic ISOL beams, Nucl. Instruments Methods Phys. Res. Sect. B Beam Interact. with Mater. Atoms **376** (2016) 8–15.

[4] LETTRY, J., CATHERALL, R., CYVOCT, G., DRUMM, P., EVENSEN, A.H.M., et al., Release from ISOLDE molten metal targets under pulsed proton beam conditions, Nucl. Instruments Methods Phys. Res. Sect. B Beam Interact. with Mater. Atoms **126** (1997) 170–175.

[5] LETTRY, J., ARNAU, G., BENEDIKT, M., GILARDONI, S., CATHERALL, R., et al., Effects of thermal shocks on the release of radioisotopes and on molten metal target vessels, Nucl. Instruments Methods Phys. Res. Sect. B Beam Interact. with Mater. Atoms **204** (2003) 251–256.

[6] NOAH, E., BRUNO, L., CATHERALL, R., LETTRY, J., STORA, T., Hydrodynamics of ISOLDE liquid metal targets, Nucl. Inst. Methods Phys. Res. B. **266** (2008) 4303–4307.

[7] NOAH, E., BOUTELLIER, V., BRÜTSCH, R., CATHERALL, R., GAVILLET, D., et al., Post-irradiation analysis of the tantalum container of an ISOLDE LBE target q, J. Nucl. Mater. **431** (2012) 60–65.

[8] MENDONÇA, T.M., HODÁK, R., STORA, T., Opportunities for neutrino experiments at ISOLDE, J. Phys. Conf. Ser. **408** (2013) 12068.

[9] MENDONCA, T.M., HODAK, R., GHETTA, V., ALLIBERT, M., HEUER, D., et al., Production and release of ISOL beams from molten fluoride salt targets, Nucl. Instruments Methods Phys. Res. Sect. B Beam Interact. with Mater. Atoms **329** (2014) 1–5.

[10] CIMMINO, S., MENDONCA, T.M., MARZARI, S., STORA, T., Validation of electro-thermal simulation with experimental data to prepare online operation of a molten salt target at ISOLDE for the Beta Beams, Nucl. Instruments Methods Phys. Res. Sect. B Beam Interact. with Mater. Atoms **317** (2013) 426–429.

[11] KEDL, R.J., HOUTZEEL, A., Development of a Model for computing 135Xe migration in the MSRE, ORNL-4069, USA (1967).

[12] KIRCHNER, R., On the release and ionization efficiency of catcher-ion-source systems in isotope separation on-line, Nucl. Instruments Methods Phys. Res. Sect. B Beam Interact. with Mater. Atoms **70** (1992) 186–199.

[13] MENDONCA, T.M., "High Power Molten Targets for Radioactive Ion Beam Production: from Particle Physics to Medical Applications", 5th Int. Part. Accel. Conf., JACoW, (Proc. Int. Conf. Dresden, 2014).

[14] CORNELL, J., BLUMENFELD, Y., FORTUNA, G., Final report of the EURISOL Design Study (2005-2009) - A Design Study for a European Isotope-Separation-On-Line Radioactive Ion Beam Facility, GANIL, Caen, France (2009).

[15] DELONCA, M., Development of new target concepts for proton beams at CERN/ISOLDE, PhD Thesis, Université de Technologie Belfort-Montbéliard, 2015.

[16] HOUNGBO, D., BERNARDES, A.P., DAVID, J.C., DELONCA, M., KRAVALIS, K., et al., Development of a liquid Pb-Bi target for high-power ISOL facilities, Nucl. Instruments Methods Phys. Res. Sect. B Beam Interact. with Mater. Atoms **376** (2016).

[17] VAN HOEVE, W., GEKLE, S., SNOEIJER, J.H., VERSLUIS, M., BRENNER, M.P., et al., Breakup of diminutive Rayleigh jets, Phys. Fluids **22** (2010) 122003.

[18] NOLEN, J.A., A target concept for intense radioactive beams in the 132Sn Region, in: D.J. Morrissey (Ed.), Proc. Third Int. Conf. Radioact, Nucl. Beams, Editions Frontieres, East Lansing (1993) 111–114.

[19] CATHERALL, R., LETTRY, J., GILARDONI, S., KÖSTER, U., Radioactive ion beams produced by neutron-induced fission at ISOLDE, Nucl. Instruments Methods Phys. Res. Sect. B Beam Interact. with Mater. Atoms **204** (2003) 235–239.

[20] LUIS, R.F., Radiological protection and nuclear engineering studies in multi-MW target systems, PhD Thesis, Universidade de Lisboa, 2013.

[21] LUIS, R., MARQUES, J.G., STORA, T., VAZ, P., ZANINI, L., Optimization studies of the CERN-ISOLDE neutron converter and fission target system, Eur. Phys. J. A. **48** (2012) 90.

[22] GOTTBERG, A., MENDONCA, T.M., LUIS, R., RAMOS, J.P., SEIFFERT, C., et al., Experimental tests of an advanced proton-to-neutron converter at ISOLDE-CERN, Nucl. Instruments Methods Phys. Res. Sect. B Beam Interact. with Mater. Atoms **336** (2014) 143–148.

[23] STORA, T., NOAH, E., HODAK, R., HIRSH, T.Y., HASS, M., et al., A high intensity 6He beam for the β-beam neutrino oscillation facility, EPL Europhysics Lett. **98** (2012) 32001.
[24] JENSEN, M., Irradiation of prototype tungsten blocks for test of Halogen Release Fraction from the future ESS Helium cooled Tungsten Target. (WHALE project), Proposal for an Experiment to the ISOLDE and Neutron Time-of-Flight Committee, CERN, Geneva (2016).
[25] DOMBSKY, M., VICTOIRE, H., Method of forming composite ceramic targets, US Patent 7682664 B2, 2010.
[26] FERNANDES, S., BOUQUEREL, E., BRUNO, L., CATHERALL, R., GILES, T., et al., EURISOL Task 3 Deliverable Report - D3 - Online tests of a high power Al2O3 EURISOL Target Prototype, Geneva, 2009.

CONTRIBUTORS TO DRAFTING AND REVIEW

Aerts, A.	Belgian Nuclear Research Centre, Belgium
Angiolini, M.	Italian National Agency for New Technologies, Energy and Sustainable Economic Development, Italy
Anoop, B.	Indira Gandhi Centre for Atomic Research, India
Babu, B.	Indira Gandhi Centre for Atomic Research, India
Barbarino, M.	International Atomic Energy Agency
Baron-Wiechec, A.	Centre for Fusion Energy, United Kingdom
Bruna, G.	Institut de Radioprotection et de Surete Nucleaire, France
Dai, Y.	Paul Scherrer Institut, Switzerland
Dacquait, F.	French Alternative Energies and Atomic Energy Commission, France
El-Guebaly, L.	University of Wisconsin, United States of America
Féron, D.	French Alternative Energies and Atomic Energy Commission, France
Fischer, U.	Karlsruhe Institute of Technology, Germany
Fukada, S.	Kyushu University, Japan
Gaganidze, E.	Karlsruhe Institute of Technology, Germany
García, M.	National Distance Education University, Spain
Gonzalez de Vicente, S.M.	International Atomic Energy Agency
Hering, W.	Karlsruhe Institute of Technology, Germany
Huang, Y.	Kyoto University, Japan
Ignatiev, V.	National Research Center, Kurchatov Institute, Russian Federation
Kharitonova, N.	Scientific and Engineering Centre for Nuclear and Radiation Safety, Russian Federation

Kondo, M.	Tokyo Institute of Technology, Japan
Konys, J.	Karlsruhe Institute of Technology, Germany
Kriventsev, V.	International Atomic Energy Agency
Kuteev, B.V.	National Research Center, Kurchatov Institute, Russian Federation
Latgé, C.	French Alternative Energies and Atomic Energy Commission, France
Luis Hernandez, J.	International Atomic Energy Agency
Muránsky, O.	Australian Nuclear Science and Technology Organisation, Australia
Muroga, T.	National Institute for Fusion Science, Japan
Nilsson, P.	European Spallation Source, Sweden
Raiman, S.	Oak Ridge National Laboratory, United States of America
Ramos, J.P.	European Organization for Nuclear Research (CERN), Switzerland
Ricapito, I.	Fusion for Energy, Spain
Ridikas, D.	International Atomic Energy Agency
Soukupová, M.	ÚJV Řež, Czech Republic
Stieglitz, R.	Karlsruhe Institute of Technology, Germany
Surenkov, A.I.	National Research Center, Kurchatov Institute, Russian Federation
Utili, M.	Italian National Agency for New Technologies, Energy and Sustainable Economic Development, Italy
Weisenburger, A.	Karlsruhe Institute of Technology, Germany

Workshop

IAEA Headquarters, Vienna, Austria: 5–7 July 2017

Consultancy Meeting

IAEA Headquarters, Vienna, Austria: 2–4 July 2018

IAEA
International Atomic Energy Agency

No. 26

ORDERING LOCALLY

IAEA priced publications may be purchased from the sources listed below or from major local booksellers.

Orders for unpriced publications should be made directly to the IAEA. The contact details are given at the end of this list.

NORTH AMERICA

Bernan / Rowman & Littlefield

15250 NBN Way, Blue Ridge Summit, PA 17214, USA
Telephone: +1 800 462 6420 • Fax: +1 800 338 4550

Email: orders@rowman.com • Web site: www.rowman.com/bernan

REST OF WORLD

Please contact your preferred local supplier, or our lead distributor:

Eurospan Group

Gray's Inn House
127 Clerkenwell Road
London EC1R 5DB
United Kingdom

Trade orders and enquiries:

Telephone: +44 (0)176 760 4972 • Fax: +44 (0)176 760 1640
Email: eurospan@turpin-distribution.com

Individual orders:

www.eurospanbookstore.com/iaea

For further information:

Telephone: +44 (0)207 240 0856 • Fax: +44 (0)207 379 0609
Email: info@eurospangroup.com • Web site: www.eurospangroup.com

Orders for both priced and unpriced publications may be addressed directly to:

Marketing and Sales Unit
International Atomic Energy Agency
Vienna International Centre, PO Box 100, 1400 Vienna, Austria
Telephone: +43 1 2600 22529 or 22530 • Fax: +43 1 26007 22529
Email: sales.publications@iaea.org • Web site: www.iaea.org/publications

International Atomic Energy Agency
Vienna
ISBN 978–92–0–107820–9
ISSN 1011–4289